TOTAL SYNTHESIS OF COELICHELIN, COCHINMICIN I, AND COCHINMICIN V

By

Jade Charmaine Williams

Dissertation

Submitted to the Faculty of the

Graduate School of Vanderbilt University

in partial fulfillment of the requirements

for the degree of

DOCTOR OF PHILOSOPHY

In

Chemistry

January 31, 2022

Nashville, Tennessee

Approved:

Jeffrey N. Johnston , Ph.D.

Gary A. Sulikowski, Ph.D.

Steven D. Townsend, Ph.D.

Brian O. Bachmann, Ph.D.

Eric P. Skaar, Ph.D.

TABLE OF CONTENTS

LIST OF TABLES

LIST OF FIGURES

CHAPTER 1

TOTAL SYNTHESIS OF THE SIDEROPHORE COELICHELIN

1.1 Introduction

Iron is one of the most essential metal nutrients for organisms due to its critical role in cellular redox processes. Iron has been implicated in numerous electron-transfer processes in both prokaryotes and eukaryotes, including metabolism, proliferation, and microbial pathogenicity.[1] [2]

1.1.1 Significance of Iron in Host-Pathogen Interactions

Given the significant role that iron plays in many life-sustaining processes, there is a consistent struggle between microorganisms and their hosts for metal nutrients.[3] [4] [5] Host organisms have evolved various systems to acquire, steal, and limit iron sources from pathogens rendering the environment less hospitable for microbial growth. Likewise, pathogens have evolved in response to these advances in an effort to acquire iron in these deficient environments. This battle for metal nutrients has resulted in the evolution of elegant strategies by both host and pathogens to counteract the metal acquisition methods used by the opposition.

The generation of an iron-limited environment serves as the first line of defense against invasion by a microorganism. The process by which hosts restrict free iron available for pathogens is referred to as nutritional immunity. [6] There are several methods that hosts use to sequester iron thereby generating iron-deficient environments, which negatively impact bacterial growth and pathogenesis. One such method is through circulation of the protein transferrin (Tf), which binds iron effectively reducing the concentration of free-iron available to invading microorganisms.[7] [8] [9] [10]

Another method employed by hosts is through the production of lipocalin-2 (lcn2), also referred to as siderocalin, by neutrophils, macrophages, and epithelial cells.[11] [12] [13] [14] Lcn2 sequesters bacterial iron-siderophore complexes thus preventing uptake by microorganisms.[15] In response to this, pathogens have evolved chemically modified "mutated" siderophores which are incapable of sequestration by Lcn2 often referred to as stealth siderophores.[16] [17] For example,

enterobactin (**1.1**) is produced by enteric bacteria and can be sequestered by lcn2. Several strains also produce glycosylated variants of enterobactin, the salmochelins (**1.2**), which are not recognized by lipocalin-2 and can fulfill their role in bacterial iron acquisition (Figure 1). [18] [19] [20] *Yersinia pestis* produces the siderophore yersiniabactin as a mixed ligand type siderophore, also capable of evading sequestration by lcn2.[21] [22]

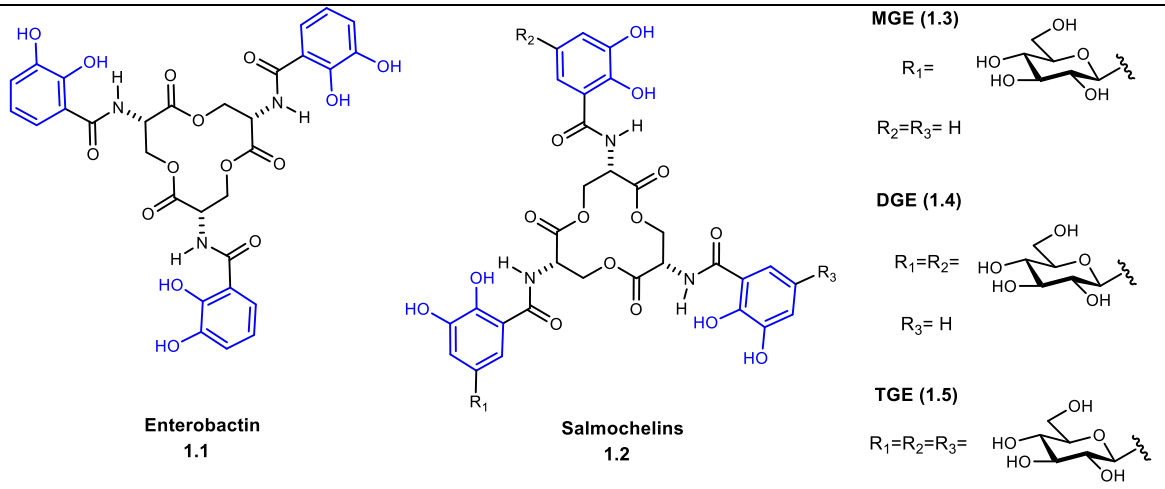

Figure 1. Glycosylation of enterobactin to afford stealth siderophores salmochelins.

Lactoferrin (Lf) is a third antimicrobial peptide which is produced by neutrophils and epithelial cells.[23] [24] [25] Lactoferrin is capable of binding two ferric ions in extracellular compartments. However, select microbes have evolved mechanisms to extract iron from Lf such as *Leishmania*.[26] [27] Further, pathogenic members of *Neisseriaceae* and *Pasterurellaceae* have evolved mechanisms for direct recognition of transferrin and lactoferrin proteins.[28] [29] Ferritin is another such iron storage protein, which is expressed in response to detected iron and cytokines.[30] [31] [32]

1.1.2 Methods for Iron Acquisition

There are a number of elegant mechanisms microorganisms utilize to acquire iron from their environments. Some microbes have evolved heme acquisition systems via secretion of proteins termed hemophores.[33] [34] However, these systems are limited in low heme availability. Functionally analogous to hemophores, select microbes secrete small-molecule iron chelators referred to as siderophores.[35] [36] [37] [38] [39] [40]

Siderophores refer to low molecular weight small molecules, which possess a high affinity for iron and are secreted by microorganisms in response to iron-deficient conditions. Following secretion and complexation with ferric iron, the siderophore-iron complex is recognized by receptors on the cell surface where it is internalized and utilized for various biological processes. It's been demonstrated that siderophore-defective bacterial strains are less effective pathogens in animal models of infection.[41] [42]

Some microorganisms have developed siderophore uptake systems to acquire exogenously produced siderophores, which is referred to as siderophore piracy.[43] These microbes are able to acquire and use siderophores produced by other microorganisms. These are referred to as xenosiderophores. This represents another strategy pathogens have evolved to acquire iron in deficient environments without having to expend metabolic energy producing their own small molecules.

1.2 Siderophores

Production of siderophores is intricately linked to several factors including the concentration of iron in the environment, pH, temperature, and the presence of other metal nutrients.[44] [45] Siderophores can be produced by bacteria, plants, and fungi. [46] [47] There have also been recent characterization of possible mammalian siderophores.[48]

1.2.1 Biosynthesis

Biosynthesis of siderophores occurs through two pathways: (1) non-ribosomal peptide synthetases (NRPS) and (2) NRPS-independent processes.[49] NRPSs are multienzyme complexes which assemble structurally diverse peptidic properties.[50] This diversity can be attributed to specialized domains which catalyze various modifications during assembly and elongation of the NRPS product. Non-ribosomal peptide synthetases can be comprised of adenylation (A), thiolation (T), condensation (C), and epimerization (E) domains. In many cases, there is also a domain, such as a thioesterase (TE) domain, which catalyzes cleavage of the product from the NRPS via intra- or intermolecular cyclization.[51] The method by which the product is cleaved

adds an additional component of structural diversity. Polyketide synthase (PKS) domains can also be incorporated into a NRPS/PKS hybrid synthetase, which provides for even greater structural variation through the incorporation of malonyl-derived building blocks. Alternatively, siderophores can be synthesized via NRPS-independent mechanisms. In these cases, siderophores are generated through concerted activity of aminotransferases, acyltransferases, aldolases, amino acid ligases, decarboxylases, and monooxygenases.[52]

1.2.2 Iron (III) Chelation Ability

Siderophores are characterized by their high affinity for iron and ability to acquire metal nutrients for microorganisms in iron limited environments. Many siderophores incorporate oxygen-rich ligands which have a high affinity for hard ferric ions.[53] [54] These iron-siderophore complexes often are most effective when containing three bidentate ligands allowing for octahedral coordination with the ferric iron. These thermodynamically stable iron chelates are accompanied by association constants of 10^{30} or higher. Many bacteria produce multiple siderophores, which can acquire iron under different conditions and evade detection by the host immune system.[55] An alternative theory is that microorganisms secrete "redundant" siderophores with non-classical functions.[56] Siderophores have been characterized as transporters of other metal nutrients, such as copper, manganese, molybdenum, vanadium, and zinc. [57] [58] [59]

1.2.3 Types of Siderophore Functional Groups

There exists a breadth of structural diversity in siderophores produced by microorganisms. To account for this diversity, siderophores are classified according to the functional groups involved in metal chelation (Figure 2).[60] Thus far, five structural classifications have been described: hydroxamates, catecholates, carboxylates, phenolates, and mixed ligands.

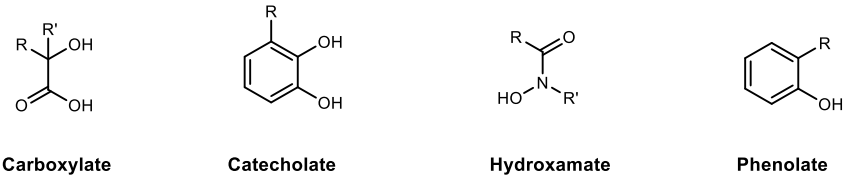

Figure 2. Functionality involved in siderophore iron chelation.

Siderophores containing hydroxamic acid moieties are termed hydroxamate type (Figure 3). Desferrioxamine is produced by *Streptomyces pilosu*s when grown under iron restriction.[61] [62] It is currently approved for clinical use in the treatment of iron-overload disorders such as hemochromatosis and β-thalassemia.[63] [64] [65] [66] [67] [68] While desferrioxamine represents an example of a linear hydroxamate type siderophore, there are a number of examples of cyclic hydroxamate siderophores such as fusarinine C produced by the fungus *Fusarium roseum*, putrebactin excreted by the Gram-negative bacterium *Shewanella putrefaciens*, and ferrichrome generated by the fungus *Ustilago sphaerogena*.[69] [70] [71] [72]

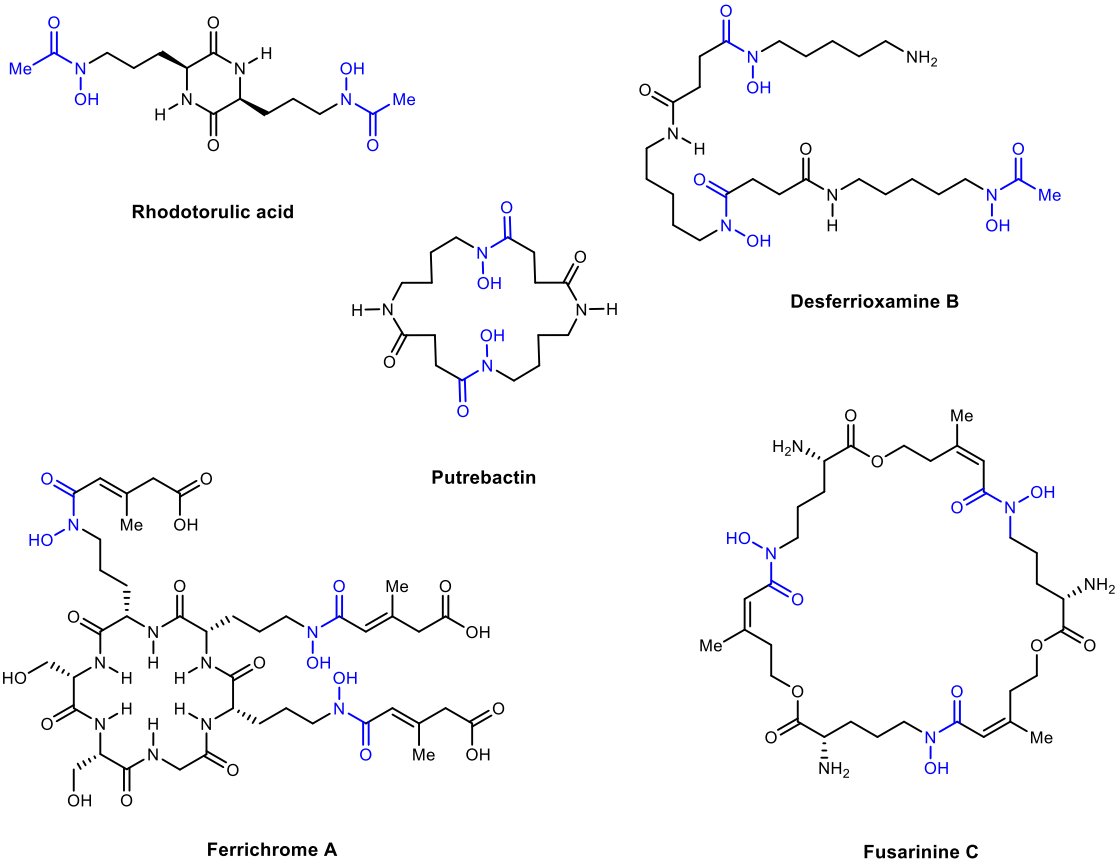

Figure 3. Select examples of hydroxamate type siderophores.

Siderophores which utilize alpha hydroxy carboxylates for metal chelation are deemed carboxylate type (Figure 4). *Staphylococcus aureus* produces the carboxylate type siderophore

staphyloferrin in response to iron restriction. [73] [74] [75] Rhizobactin is produced by *Rhizobium meliloti* and contains an unprecedented ethylenediamine group proposed to be involved in chelation. [76] Uniquely, *Erwinia chrysanthemi* produces achromobactin which features a cyclic hemiaminal. [77]

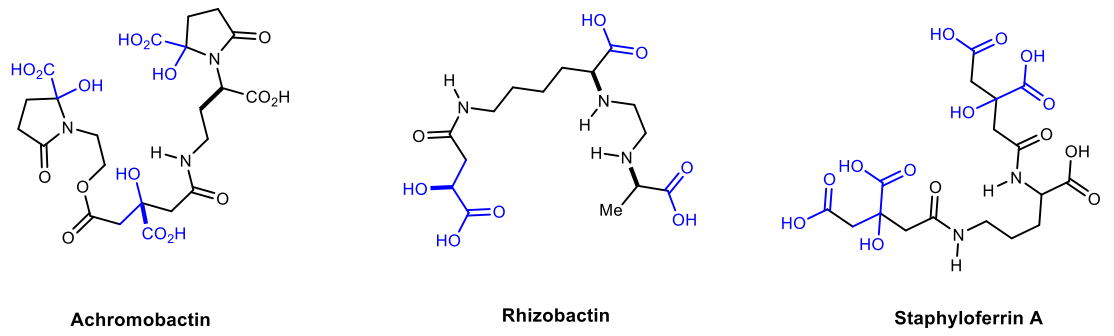

Figure 4. Select examples of carboxylate type siderophores.

Catecholate type siderophores use catechol functionality for iron chelation (Figure 5). Enterobactin represents a cyclic catecholate siderophore produced by *Salmonella typhimurium, Escherichia coli*, and *Bacillus subtilis.* [78] [79] [80] Uniquely, it can also serve as a xenosiderophore for many other species including *Pseudomonas*.[81] [82] There are also several examples of linear catecholate siderophores. Vibriobactin represents one such example produced by *Vibrio cholerae* and protochelin is another example secreted *by Azotobacter vinelandii*.[83] [84]

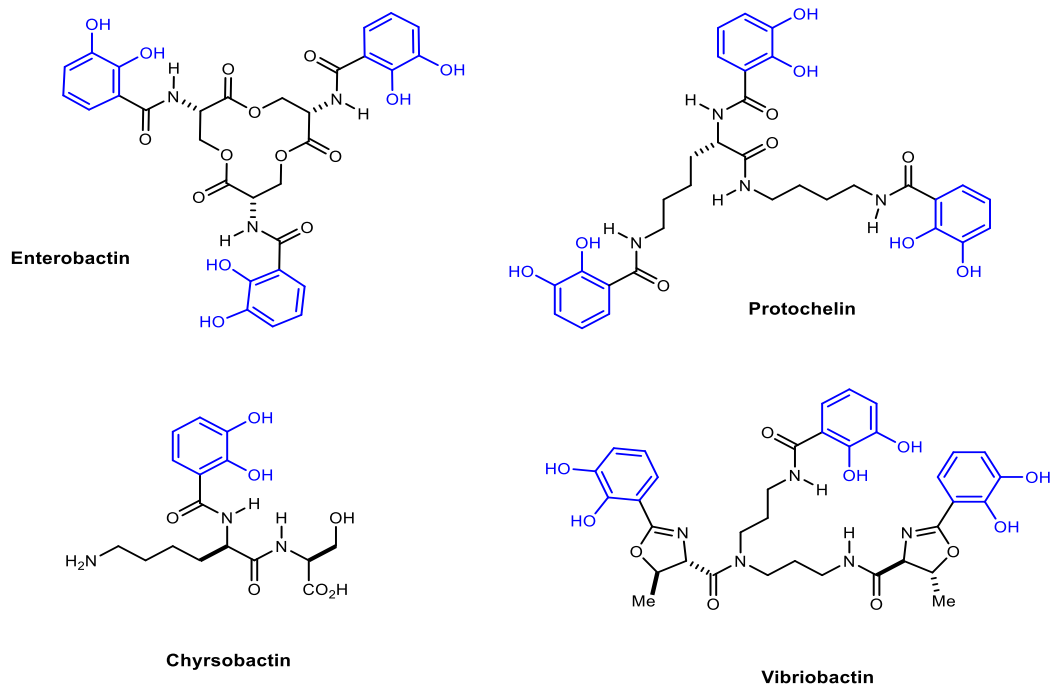

Figure 5. Select examples of catecholate type siderophores.

Several examples of mixed ligand type siderophores have also been reported which possess varying combinations of iron-chelating moieties (Figure 6). *Yersinia pestis* is believed to be responsible for the medieval Black Death and produces the stealth siderophore yersiniabactin which plays a large role in pathogenicity in *Y. pestis* infections.[85] [86] Several mycobacterium, including *M. tuberculosis*, produce the mixed ligand siderophore mycobactin.[87] [88] [89] Another example of the diversity within this class are the pyoverdine which are fluorescent siderophores produced by *Pseudomonas aeruginosa*.[90]

The mixed ligand type siderophores encompass the most structural diversity within any of the classifications given the wide array of cyclization and dehydration features observed in nature.

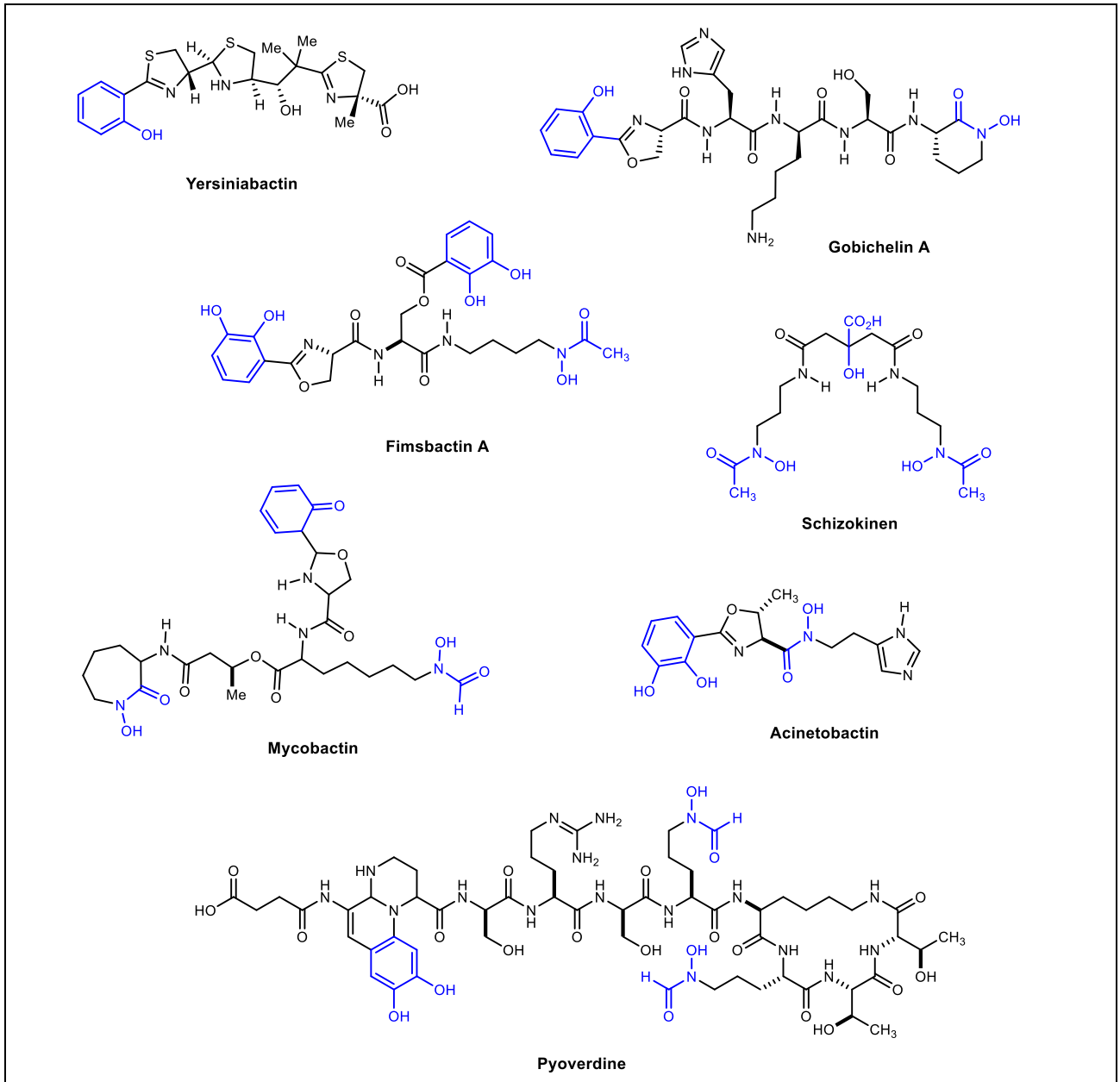

Figure 6. Select examples of mixed ligand type siderophores.

1.2 Select Syntheses of Siderophores

The vast array of structural diversity and utility to probe bacterial metal acquisition pathways have prompted several research groups to pursue synthetic endeavors toward several siderophores.

1.2.1 Amamistatin B

During a screening for tumor cell growth inhibitors, amamistatins A and B were discovered and isolated from *Nocardia asteroides*.[91] Amamistatin A showed antiproliferative effects against breast (MCF-7 IC_{50} 0.48 μM), lung (A549, IC_{50} 0.56 μM), and stomach (MKN45, IC_{50} 0.24 μM) cancer cell lines.[92] Shortly following isolation, the first synthesis of amamistatin A was reported confirming the structure reported upon isolation and providing material for further biological evaluation.

In 2008, Marvin Miller and coworkers reported the total synthesis of amamistatin B and subsequent evaluation of inhibition of tumor cell growth, HDACs, and *Mycobacterium tuberculosis*.[93] The authors reasoned that the amamistatins may inhibit histone deacetylase (HDAC) inhibitors through the *N*-formyl hydroxylamine functionality. In order to further interrogate the biological activities of the amamistatins and structural analogues, Miller and coworkers embarked on a total synthesis of amamistatin B.

Suitably protected lysine (**1.6**) upon treatment with nitroferricyanide, yielded a mixture of the desired hydroxynorleucine (**1.7**) and the dehydration product (**1.8**). The obtained mixture was carried forward through a coupling with *O*-benzyl protected hydroxylamine affording the desired benzyl hydroxamate (**1.9**). A subsequent two-step cyclization procedure yielded a mixture of the desired cyclic hydroxamate (**1.11**) as well as the *O*-cyclized hydroximate. Fragments **1.12** and **1.13** could then be coupled together to give **1.14** *(*Figure 7).

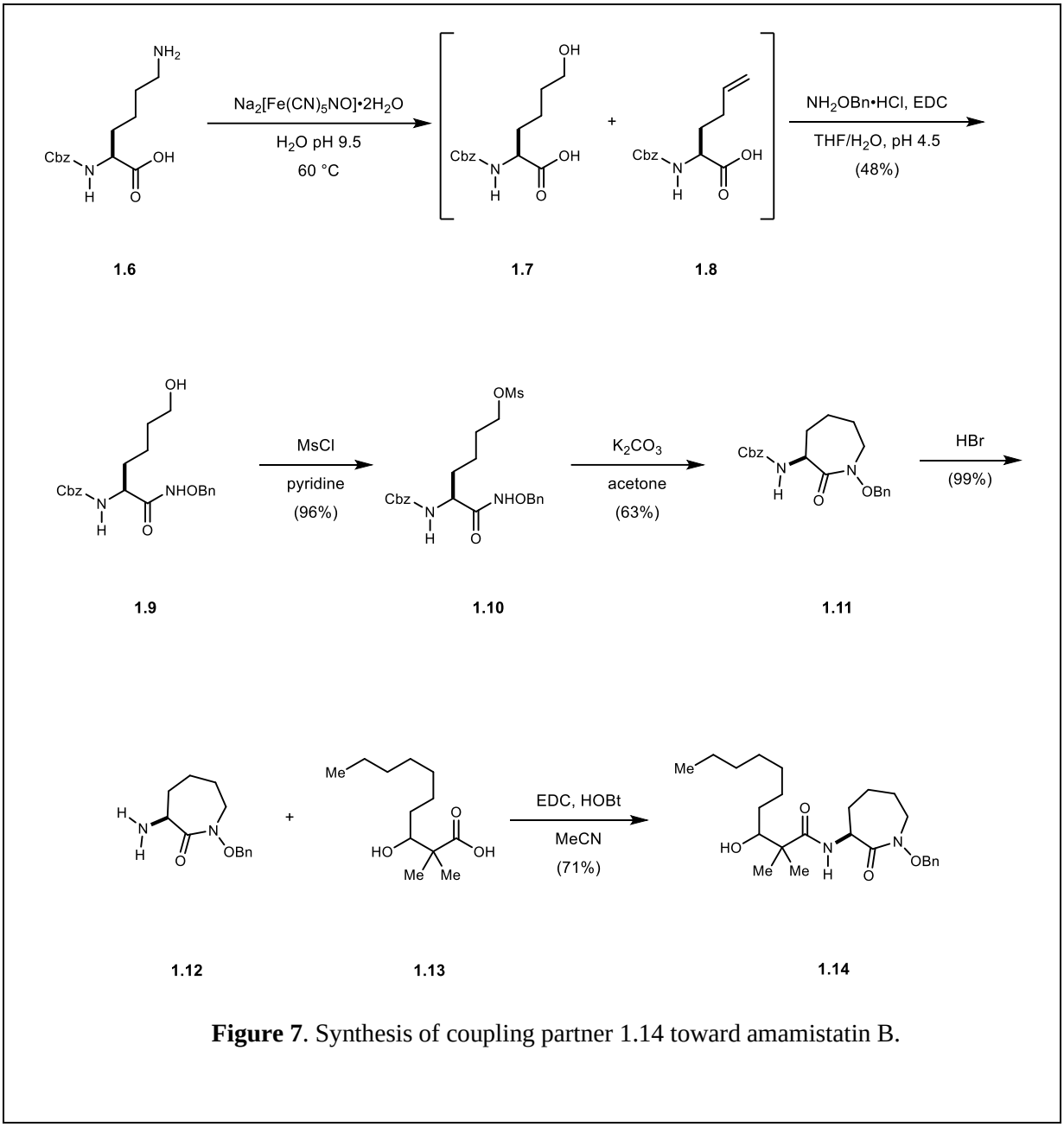

Figure 7. Synthesis of coupling partner 1.14 toward amamistatin B.

Free hydroxyl (**1.14**) could then be subjected to a DCC mediated esterification to yield **1.16** Global hydrogenolysis and coupling with hydroxyphenyl oxazole (**1.18**) afforded amamistatin B (**1.19**) (Figure 8). Miller and coworkers were able to employ this synthetic strategy to access amamistatin B (**1.19**), a diastereomer, and a structural analog.

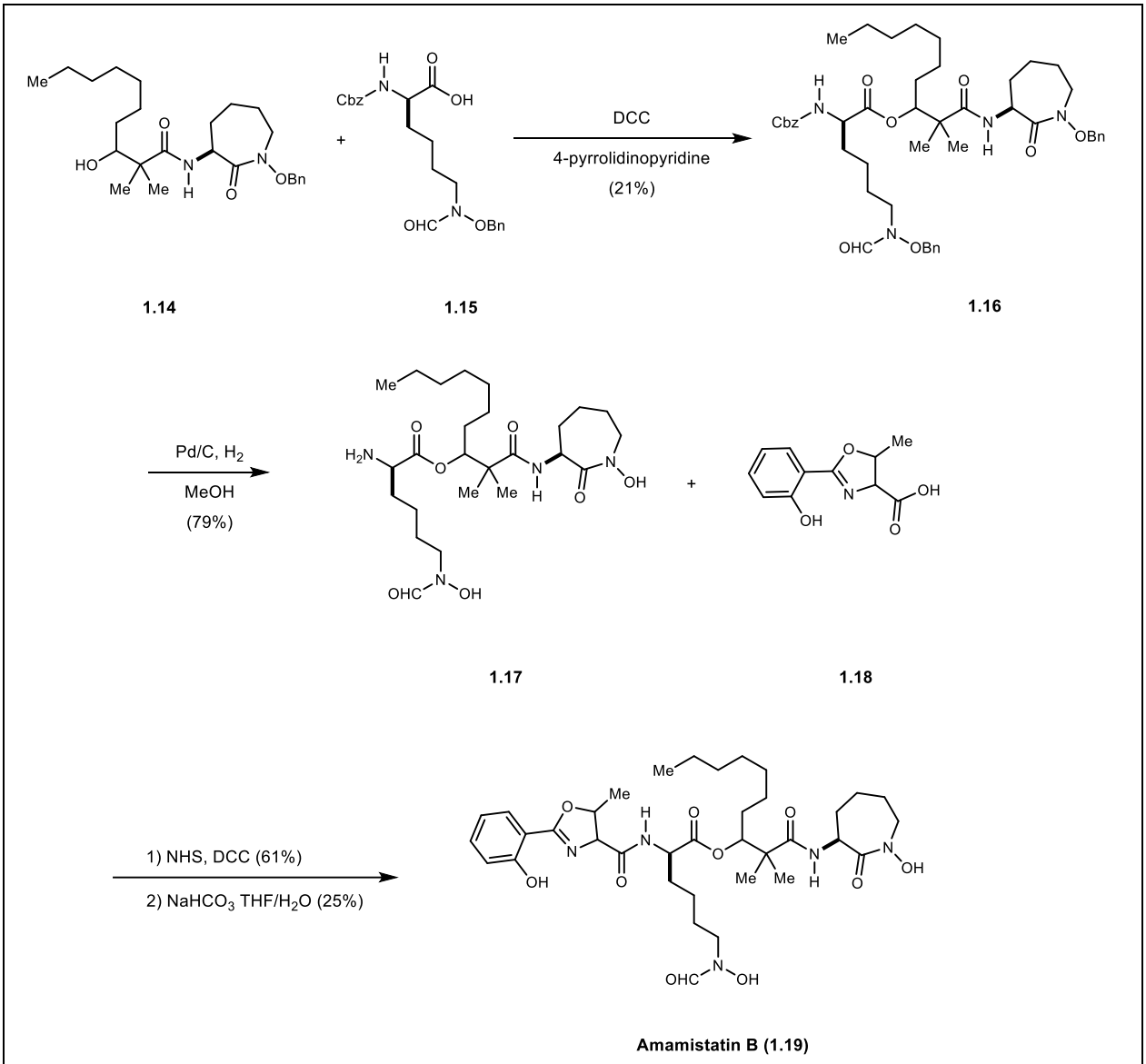

Figure 8. Completion of the total synthesis of amamistatin B.

First, a chrome azurrol S (CAS) assay was used to evaluate the iron chelation ability of amamistatin and analogues. All three compounds promote the growth of several strains of both Gram-positive and Gram-negative bacteria demonstrating synthetic amamistatin could function as a bacterial siderophore. Next, amamistatin B and analogues were evaluated for growth inhibition of bacterial strains and tumor cells, respectively. While demonstrating growth inhibition in MCF-7(IC_{50} 120 nM to 14 µM) and PC-3 (IC_{50} 8-16 µM) tumor cell lines, there was no evidence of HDAC inhibition *in vitro*. Amamistatin B demonstrated modest activity against M. tuberculosis (46 µM).[94] Miller and coworkers report further exploration of the structure-activity relationships of the amamistatins in tumor growth inhibition.[95 96]

1.2.2 Staphyloferrin B

Staphyloferrin A and B were isolated from *Staphylococcus hyicus* grown under iron restriction.[97] [98] [99] Preliminary studies indicate that staphyloferrin B plays a significant role in virulence and severity of the infection. In 2015, Elizabeth Nolan and coworkers reported a total synthesis of staphyloferrin B enabling further biological study.[100] Staphyloferrin B is a carboxylate type siderophore produced by *Staphylococcus aureus* when colonizing a vertebrate host and contributes to virulence. In an effort to further interrogate the role of staphyloferrin B as a virulence factor, a synthetic strategy was devised allowing access to natural product and structural analogues.

Synthesis of staphyloferrin B commenced with the coupling of α-ketoglutaric acid (**1.20**) and *N*-Boc-diamino ethane (**1.21**) followed by deprotection of the Boc protecting group and cyclization to yield hemiaminal **1.22** (Figure 9). Attention was then turned toward the synthesis of the coupling partner with a two-step sequence from Cbz-L-asparagine (**1.23**). First with benzyl protection of **1.24** followed by Hofmann rearrangement to yield free amine **1.25** (Figure 9).

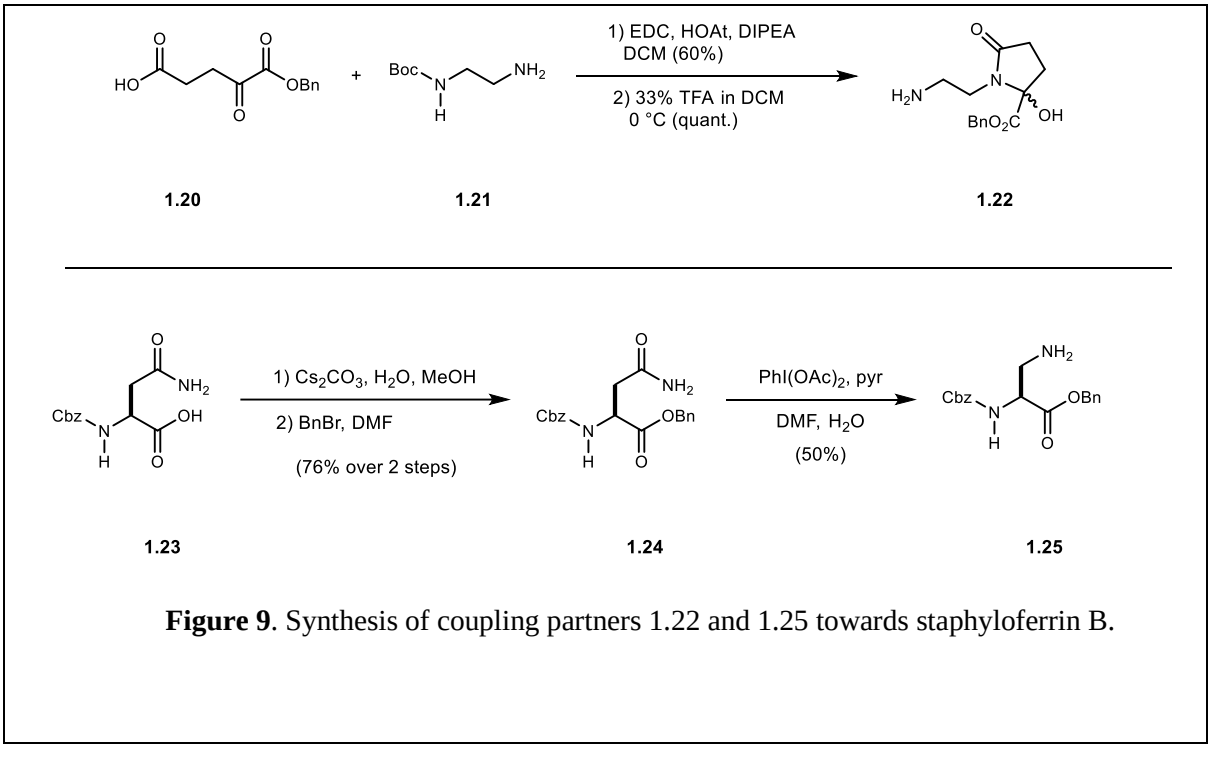

Figure 9. Synthesis of coupling partners 1.22 and 1.25 towards staphyloferrin B.

(*S*)-Malic acid (**1.26**) was then treated with pivaldehyde to give dioxolanone (**1.27**), which following treatment with allyl bromide and lithium hexamethyldisilazide resulted in α-allylation (**1.28**) (Figure 10). Subsequent transesterification afforded benzyl ester (**1.29**) which was coupled with free amine (**1.25**) under HATU-mediated amide coupling to give amide (**1.30**). Oxidative cleavage of amide (**1.30**) gave carboxylic acid (**1.31**) which was coupled with hemiaminal (**1.22**) to give amide (**1.32**) as the synthetic precursor to staphyloferrin B. Exhaustive hydrogenolysis mediated global produced staphyloferrin B in 12 steps as the first reported total synthesis of this siderophore.

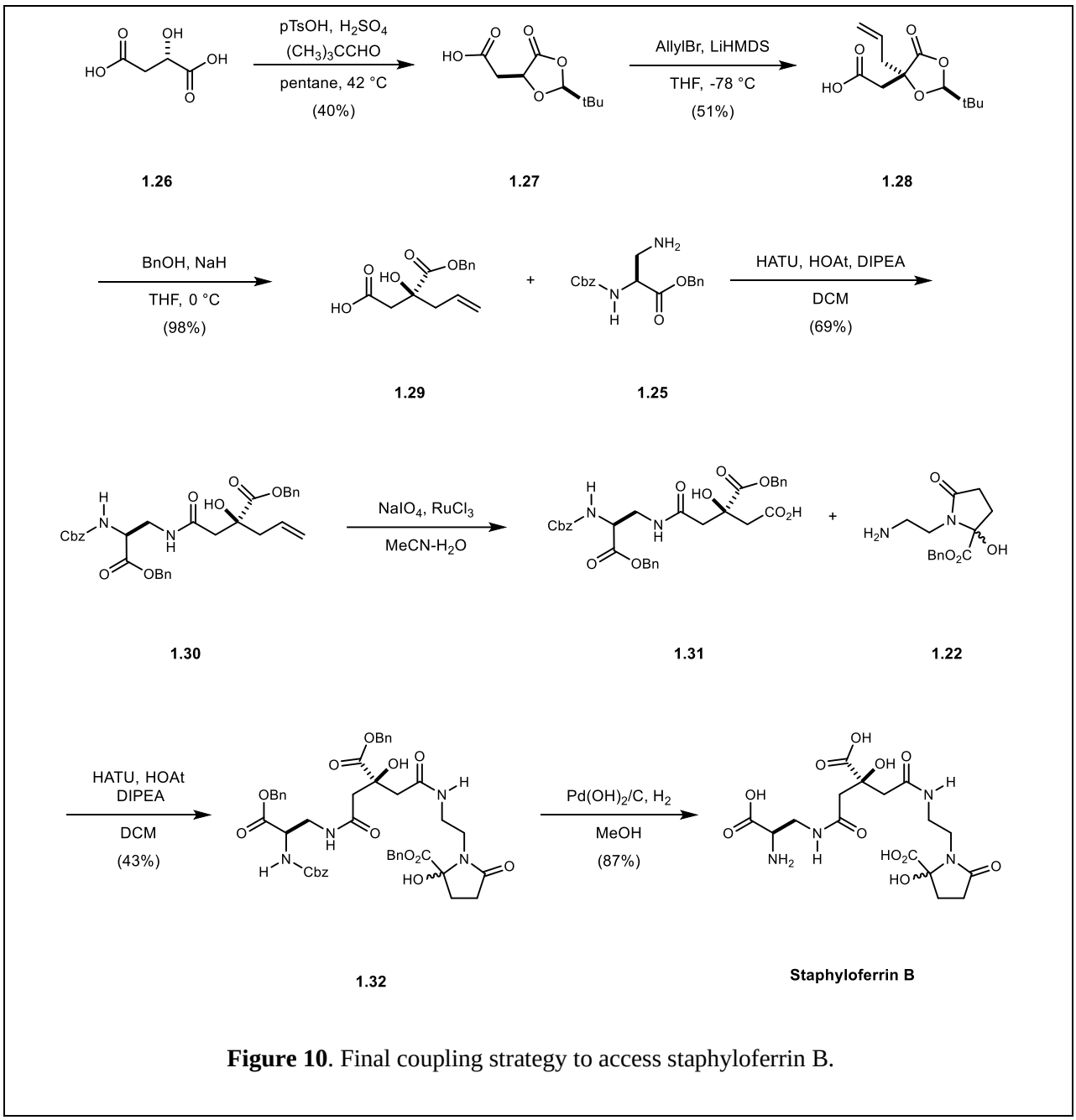

Figure 10. Final coupling strategy to access staphyloferrin B.

This successful synthesis allowed for confirmation of the structure of staphyloferrin B, which remained unresolved since its isolation.

1.2.3 Petrobactin

In 2012, Philip Low and coworkers reported a synthesis of petrobactin, a siderophore produced by *Bacillus anthracis*.[101] Intrigued by the potential utility of petrobactin in the treatment of *Bacillus* infections, the total synthesis of petrobactin commenced with mesylation of amino alcohol **1.33** and was followed by displacement with amine **1.35** to afford *N*-Boc protected amine (**1.36**). Subsequent hydrogenolysis revealed free amine **1.37** (Figure 11).

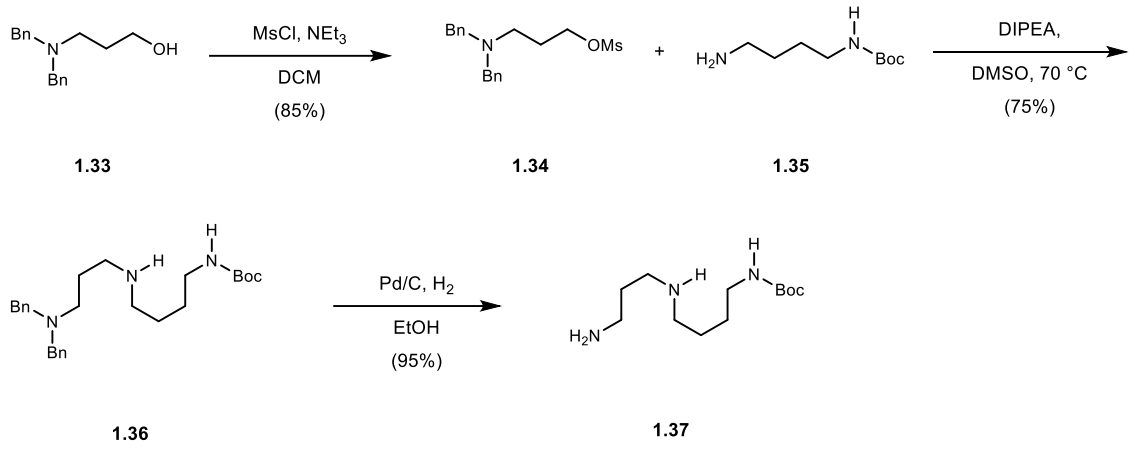

Figure 11. Synthesis of free amine 1.37 toward petrobactin.

With coupling partner **1.37** in hand, synthesis of petrobactin commenced with esterification of 3,4-dihydroxybenzoic acid and suitable protection of the catechol as its benzyl ether **1.39** (Figure 12). Ester **1.39** and amine **1.37** were then coupled together through an $Sb(OEt)_3$-mediated ester-amide exchange to yield the corresponding amide. TFA-mediated deprotection was followed by coupling with **1.41** to afford **1.42**, following global deprotection, petrobactin was provided. This concise synthetic strategy enabled access to petrobactin in 8 steps from commercial starting materials in 22.5% overall yield.

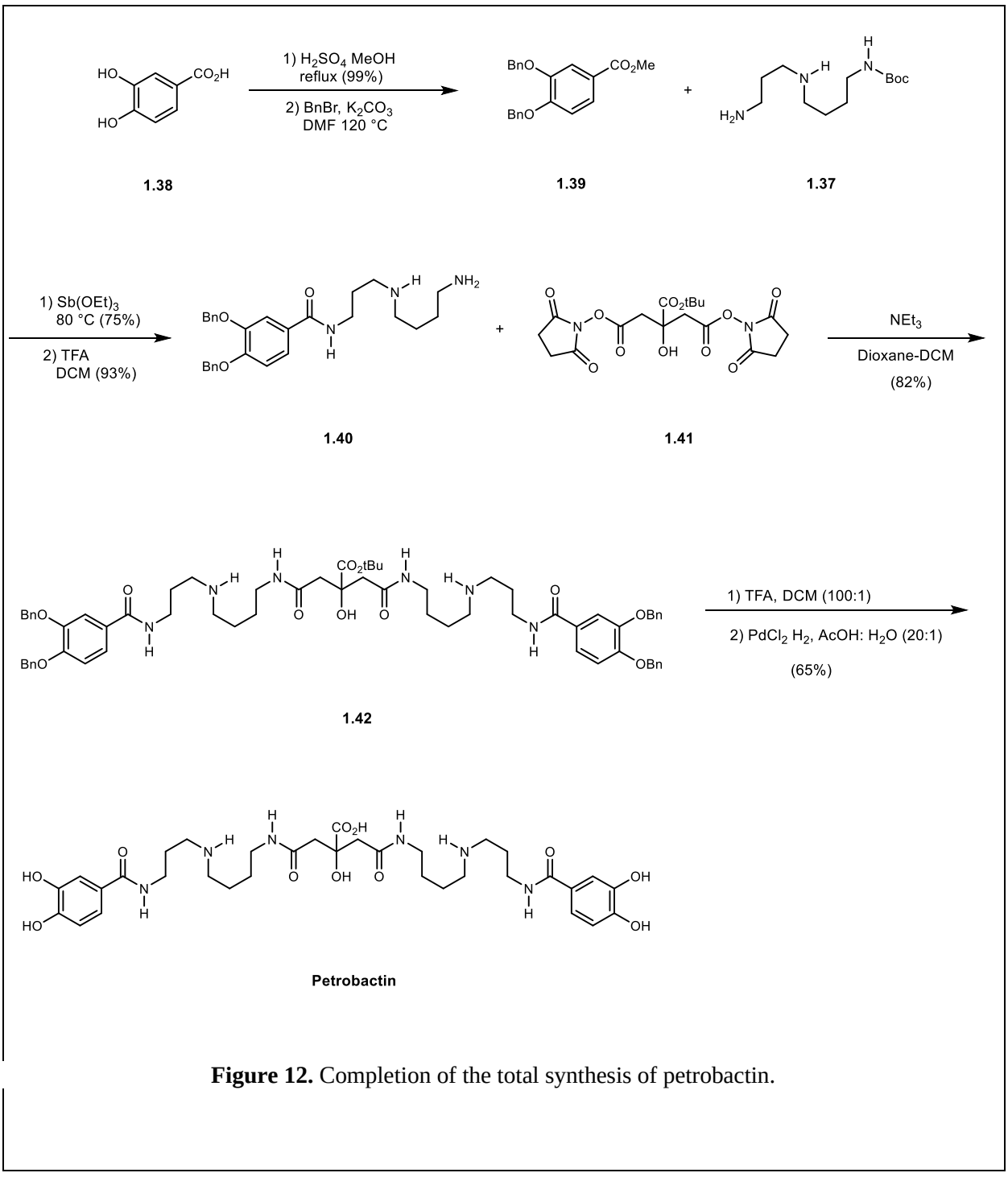

Figure 12. Completion of the total synthesis of petrobactin.

1.2.4 Danoxamine

Streptomyces violaceus secretes a series of siderophore-aminoglycosides termed the salmycins A-D, where danoxamine refers to the siderophore portion of the salmycins.[102] In 2000, Marvin Miller and coworkers reported the total synthesis of the siderophore danoxamine.[103] Miller and coworkers reasoned that an efficient synthesis of danoxamine would provide sufficient material for the preparation of siderophore-drug conjugates. Synthesis of danoxamine commenced with the displacement of 5-chlorovalernitrile with Boc-NH-OBn (**1.43**) to yield nitrile **1.44**. Selective reduction with Raney nickel afforded amine **1.45** (Figure 13).

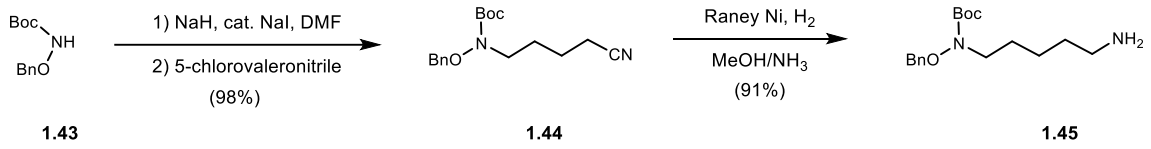

1.43 **1.44** **1.45**

Figure 13. Synthesis of amine 13.3 toward danoxamine.

Monoprotection of 1,5-pentanediol (**1.46**) with benzyl bromide afforded **1.47** which was converted to the corresponding tosylate and displaced with Boc-NHOBn to afford *O*-benzyl hydroxylamine (**1.48**) (Figure 14). Following TFA-mediated deprotection, **1.49** was coupled with succinic anhydride to yield amide **1.50** which was next coupled with amine **1.45** to yield amide **1.51**. Two additional rounds of acylation with succinic anhydride and amide coupling yielded the benzyl-protected precursor to danoxamine. Hydrogenolysis of the remaining benzyl ethers revealed danoxamine, thus demonstrating the success of their synthetic strategy and its amenability toward diversification.

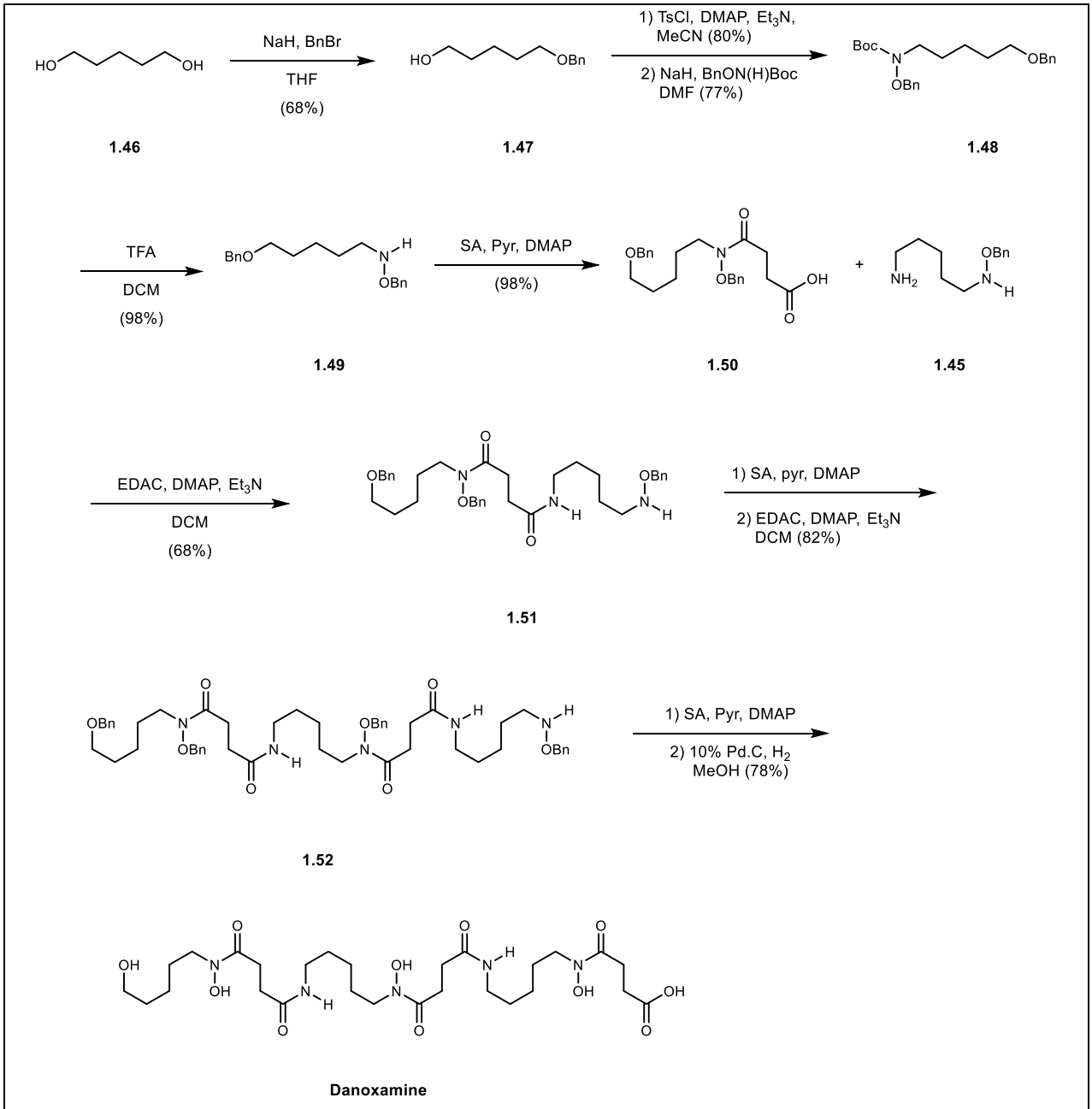

Figure 14. Total synthesis of danoxamine.

1.2.5 Gobichelin

In 2018, Sridhar and coworkers reported the first total synthesis of the siderophore gobichelin B, which is a siderophore produced by *Streptomyces*.[104] Uniquely, the mixed ligand type

siderophore is comprised of a hydroxamate, a salicylate, and two basic amino groups. Sridhar and coworkers reasoned that gobichelin could be divided into two halves, which could be obtained from a series of amide bond-forming reactions.

Synthesis of the first half of gobichelin commenced with the coupling of suitably protected D-lysine (**1.53**) and *O*-benzyl protected serine (**1.54**) to yield carboxylic acid (**1.55**) which was used directly in coupling with an α-amino lactam (**1.56**) to give **1.57** (Figure 15). Acidic deprotection of the *N*-Boc protecting group revealed free amine (**1.58**) primed for coupling with the other half of gobichelin.

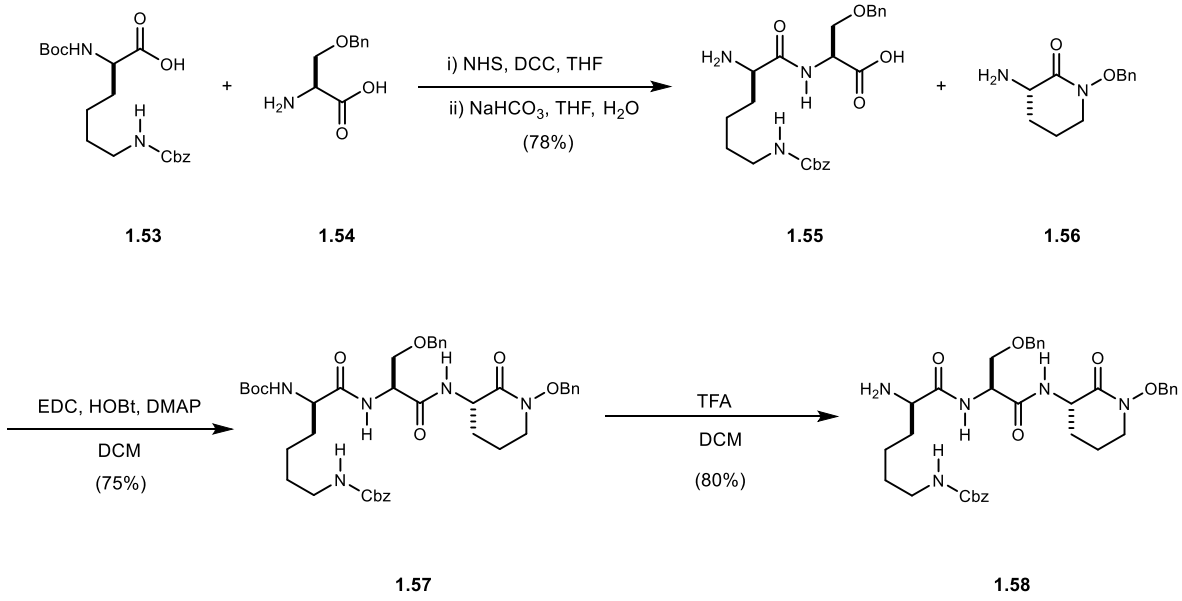

1.53 **1.54** **1.55** **1.56**

1.57 **1.58**

Figure 15. Synthesis of the first half of gobichelin.

Synthesis of the other half of gobichelin began with DCC-mediated coupling of *O*-benzyl protected salicylic acid (**1.59**) and *O*-benzyl protected serine (**1.60**) (Figure 16). The resulting carboxylic acid (**1.61**) was next coupled with protected histidine methyl ester (**1.62**) to yield amide (**1.63**). Subsequent saponification yielded carboxylic acid (**1.64**). Amine (**1.58**) was then coupled with **1.64** to give the synthetic precursor (**1.65**) to gobichelin which upon hydrogenolysis revealed the siderophore gobichelin.

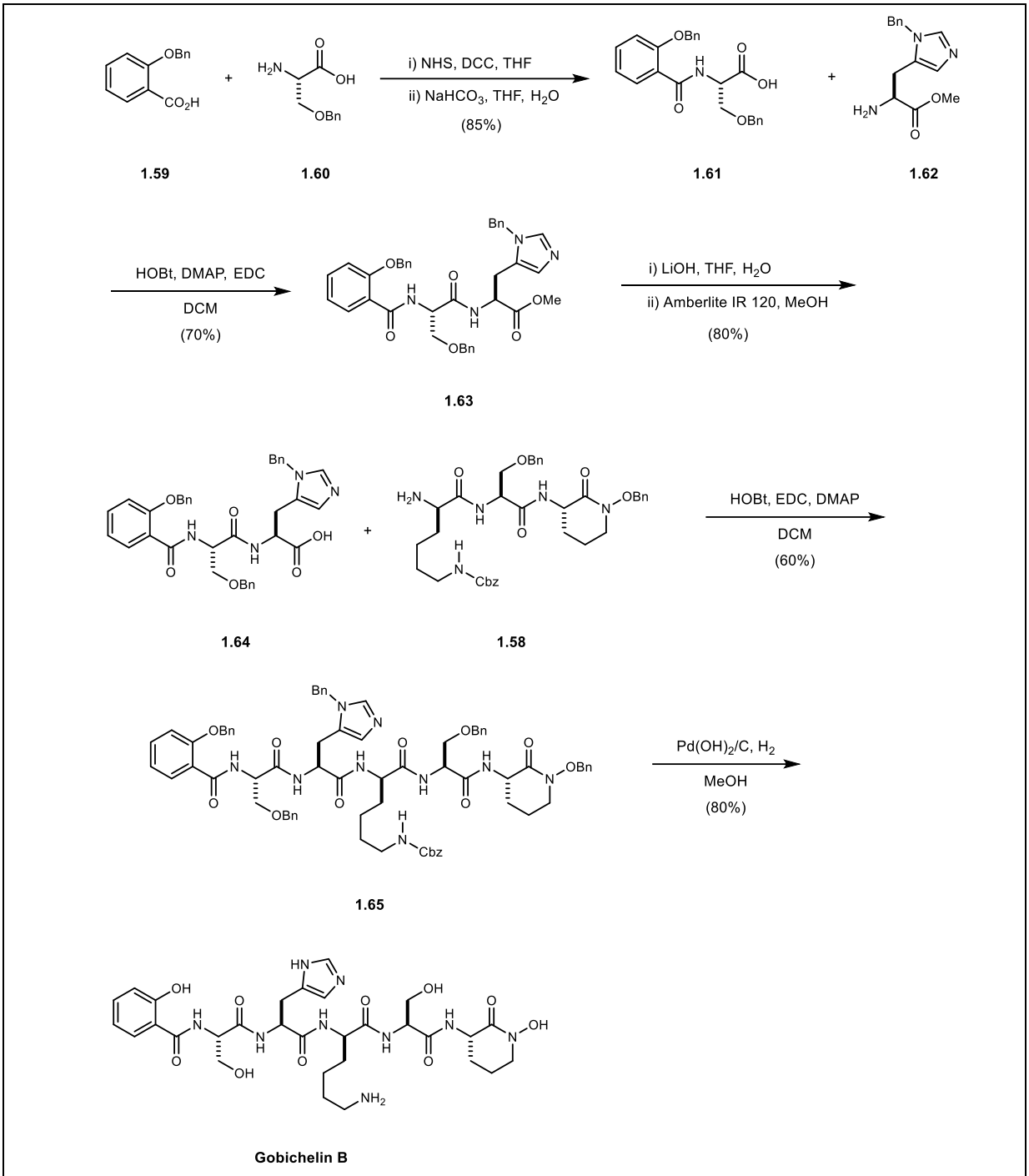

Figure 16. Completion of the synthesis of gobichelin.

1.2.6 Yersiniabactin

In 2001, Akina Ino and Akira Murabayashi reported the total synthesis of yersiniabactin, the mixed ligand type siderophore produced by *Yersinia enterocolitica and Yersinia pestis*.[105] Yersiniabactin was first isolated as a mixture of two diastereomers bearing structural similarities to micacoidin and pyochelin. The authors reasoned that yersiniabactin could be synthesized using a similar approach as outlined in their previous synthesis of micacoidin whereby two functionalized fragments could be brought together to afford yersiniabactin.[106] Notably, they inferred the absolute configuration of yersiniabactin based on their previous work with structurally-related micacoidin.

Synthesis of yersiniabactin commenced with a condensation of a Weinreb amide (**1.66**) and 2-methoxybenzoyl chloride affording ester **1.68** (Figure 17). TFA-mediated deprotection of the carbamate followed by alkaline-mediated acyl migration afforded the desired amide (**1.69**) in quantitative yield. The methyl ether was removed following treatment with BCl_3 and the obtained phenol (**1.70**) was converted to the corresponding thioamide (**1.71**) via an oxazoline intermediate. The obtained thioamide (**1.71**) upon treatment with Burgess' reagent was converted to thiazoline, the free phenol was silyl protected to give **1.72**, and the Weinreb amide was reduced to reveal aldehyde **1.73**. as the first fragment.

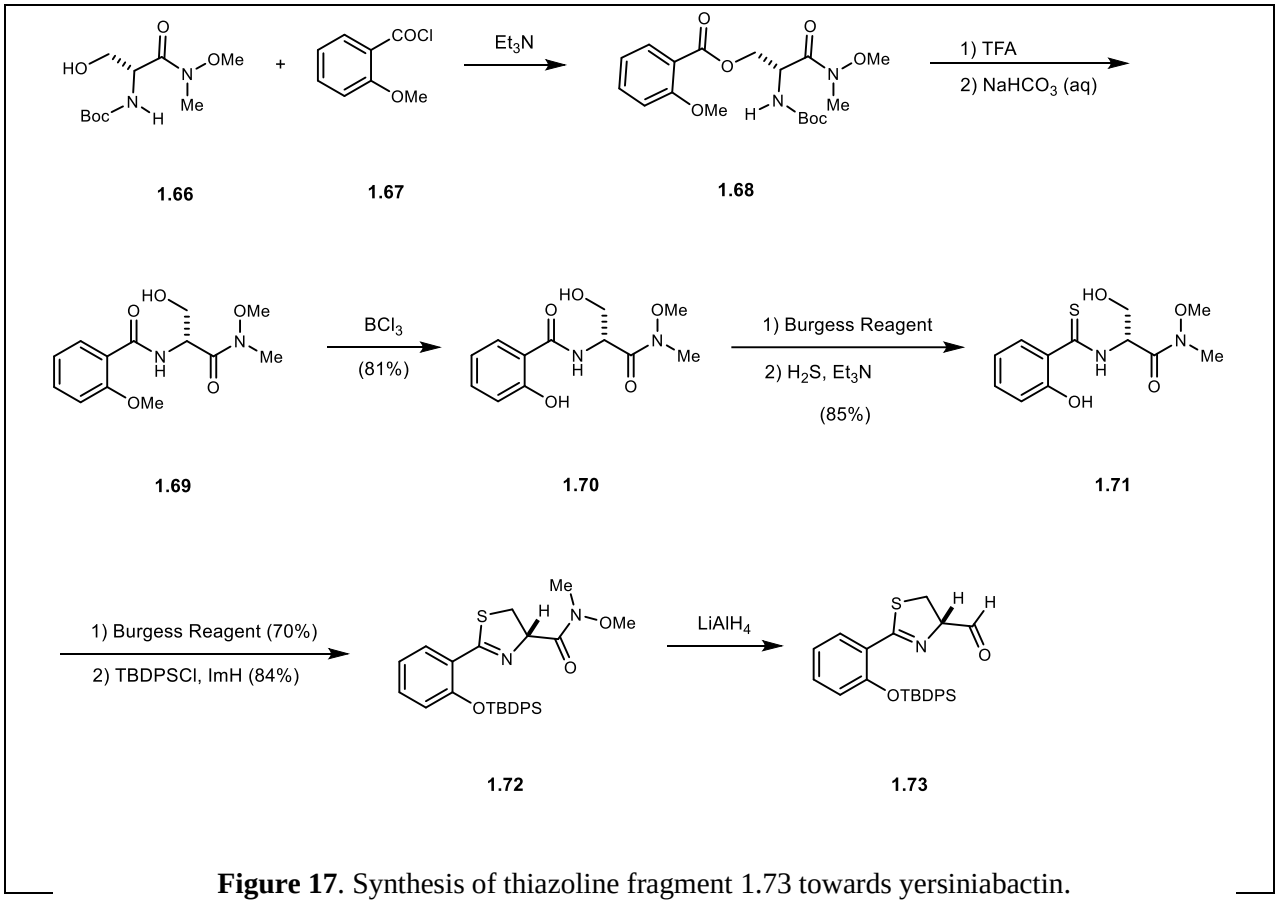

Figure 17. Synthesis of thiazoline fragment 1.73 towards yersiniabactin.

With the first fragment in hand, Ino and Murabayashi utilized a synthesis of thiazoline **1.74** as outlined in the synthesis of micacoidin.[107] Subsequent global deprotection reveals free thiol and amino groups (**1.75**) primed for condensation with the first fragment (**1.73**) (Figure 18). TBAF-mediated deprotection and saponification of the methyl ester afforded yersiniabactin.

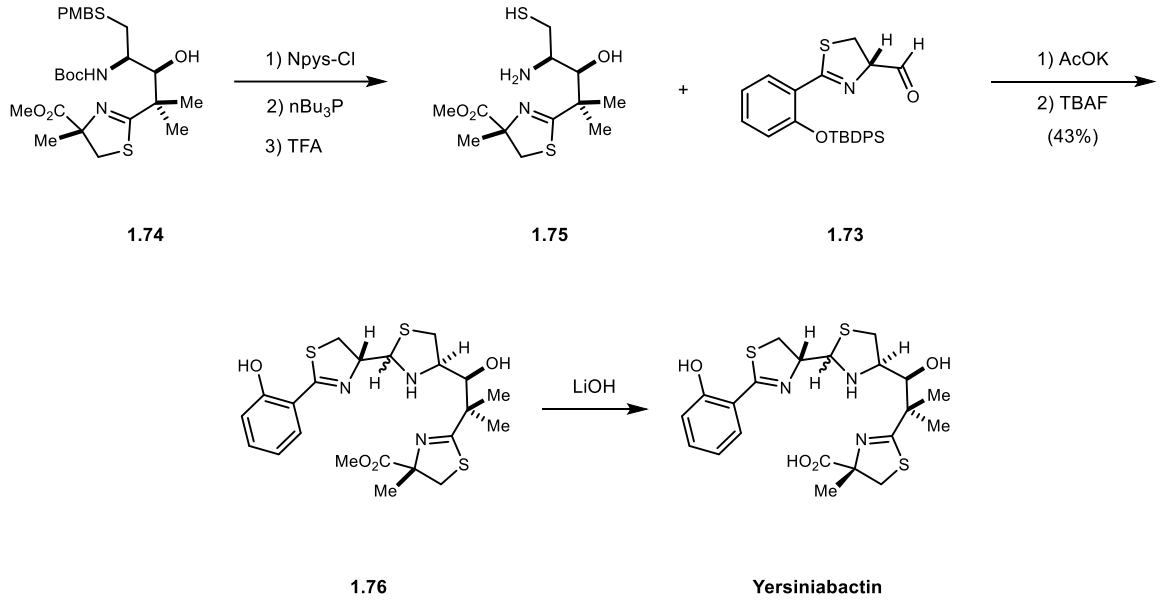

Figure 18. Final coupling and deprotection sequence toward yersiniabactin.

1.2.7 Desferrioxamine

Desferrioxamine is one of the most well-studied siderophores produced by *Streptomyces pilosus* and first characterized in 1960.[108] Desferrioxamine is capable of chelating various metals including aluminum, gallium, and chromium, but exhibits exquisite specificity for ferric iron. There have been several approaches to synthesize desferrioxamine B. [109 110 111]

The first total synthesis of desferrioxamine B was accomplished by Prelog and coworkers beginning with semi reduction of nitro **1.77** with zinc to afford hydroxylamine **1.78** (Figure 19). The obtained hydroxylamine **1.78** was acetylated and the terminal Cbz protecting group was cleaved to yield amine **1.79.**

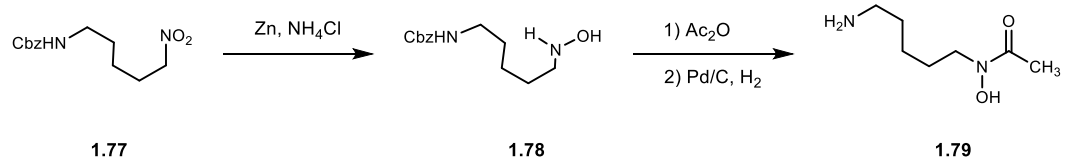

1.77 **1.78** **1.79**

Figure 19. Synthesis of hydroxamic acid 1.79 toward desferrioxamine.

Hydroxylamine **1.81** was also diverted toward the synthesis of **1.82** following treatment with succinic anhydride (Figure 20). This transformation served two purposes as a means of *N*-acylation and concomitant activation of the desired carbonyl toward nucleophilic addition. Subsequent reaction with amine **1.79** and active ester **1.82** yielded dihydroxamate **1.83**. The terminal *N*-Cbz was cleaved and the free amine was coupled with another equivalent of **1.82** to afford trishydroxamate **1.85**. Final hydrogenolytic cleavage revealed desferrioxamine B (**1.86**).

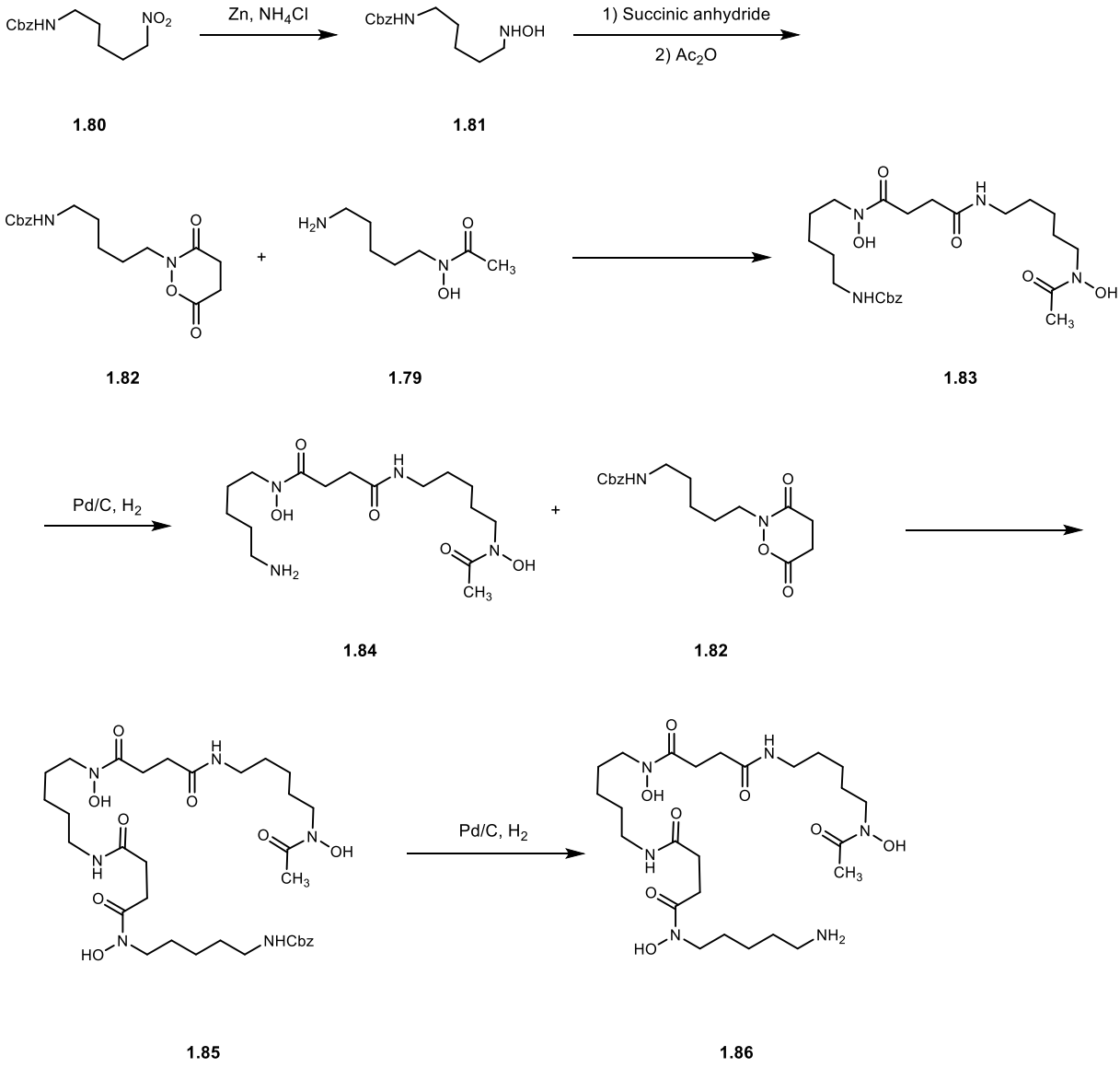

Figure 20. Final coupling and deprotection sequence to afford desferrioxamine.

1.3 Utility of Siderophore Conjugates

Following the successful synthesis of siderophores, many research programs have focused on the development of siderophore-drug conjugates as a method for delivering a payload of interest intracellularly.

Some microorganisms have evolved to produce siderophore-antibiotic conjugates, which are referred to as sideromycins (Figure 21). The salmycins are one such example. These conjugates are comprised of a hydroxamate type siderophore conjugated to an aminoglycoside which has been implicated in protein synthesis inhibition.[112] It's proposed that upon intracellular entry and reduction of iron an intramolecular cyclization cascade results in the release of the aminoglycoside. The albomycins represent one of the most well-studied sideromycins produced by *Streptomyces violaceus*.[113] A peptidase releases the hydroxamate type siderophore from the thionucleoside, which has been characterized as an inhibitor of protein synthesis. *Streptomyces griseoflavus* produces another hydroxamate-type sideromycin referred to as ferrimycin A1.[114]

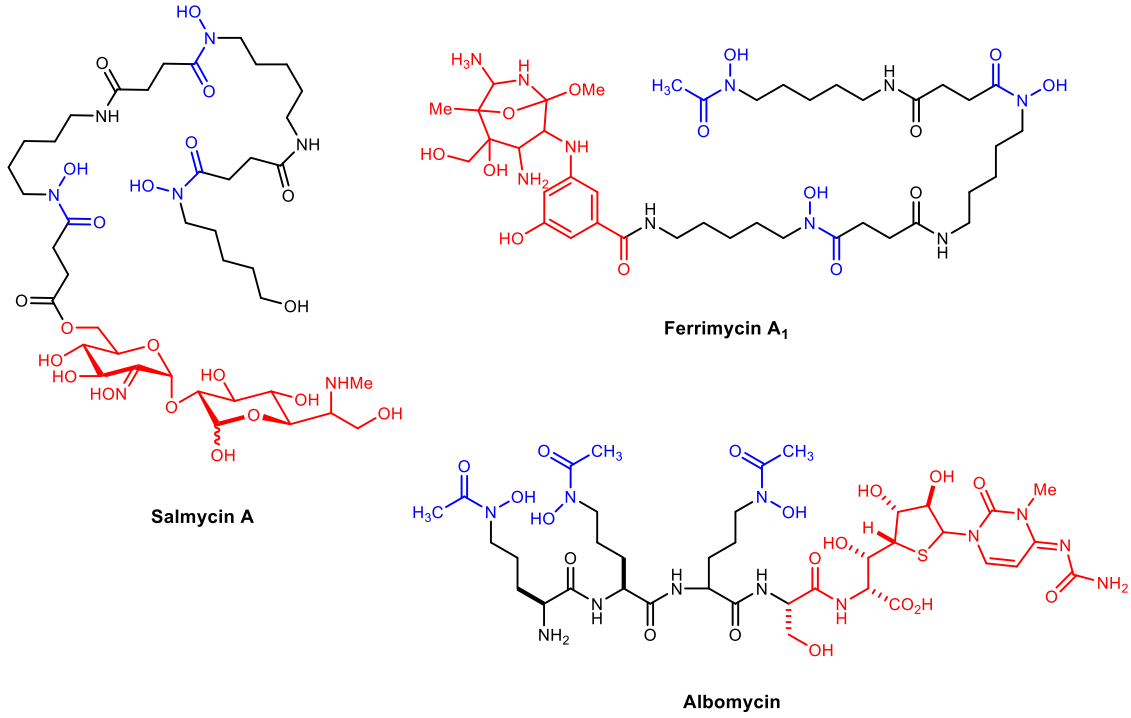

Figure 21. Naturally occurring sideromycins.

Following this strategy outlined in nature, several research groups have synthesized siderophore-antibiotic conjugates.[115] [116] This Trojan Horse strategy would require conjugation of a suitable siderophore to an antibiotic of interest thus allowing for active transport into the bacterial cell.[117] The bacterial siderophore uptake receptors would recognize the siderophore-metal complex and subsequently internalize the siderophore and its antibiotic payload. Once within the cell, the payload could be released and affect cellular function. This strategy allows for improved cell permeability of antibiotics, especially in Gram-negative pathogens where cell permeation remains a challenge.

In the design of siderophore-conjugates, the main requirement is the synthesis of a compound that will effectively chelate iron and be recognized and internalized by iron-uptake systems. Siderophore uptake systems utilize fairly promiscuous receptors, which is a feature research groups have taken advantage of in the design of such conjugates. Reports have indicated that the metal center is the key feature recognized in siderophore reuptake, which suggests the receptor and transport proteins might not require recognition of the full siderophore structure for internalization. This could also serve as justification for the observed siderophore piracy, whereby microbes can utilize siderophores which are produced by other microbes in their environment. A further consideration is the incorporation of a linker between the siderophore and its payload. The nature of this linker could provide for the release of a payload of interest such as an antibiotic or probe. Researchers have synthesized and evaluated various combinations of isolated siderophores with payloads to find compounds with improved antibacterial activity among other applications (Figure 22). [118] [119] [120] [121] [122] [123] [124]

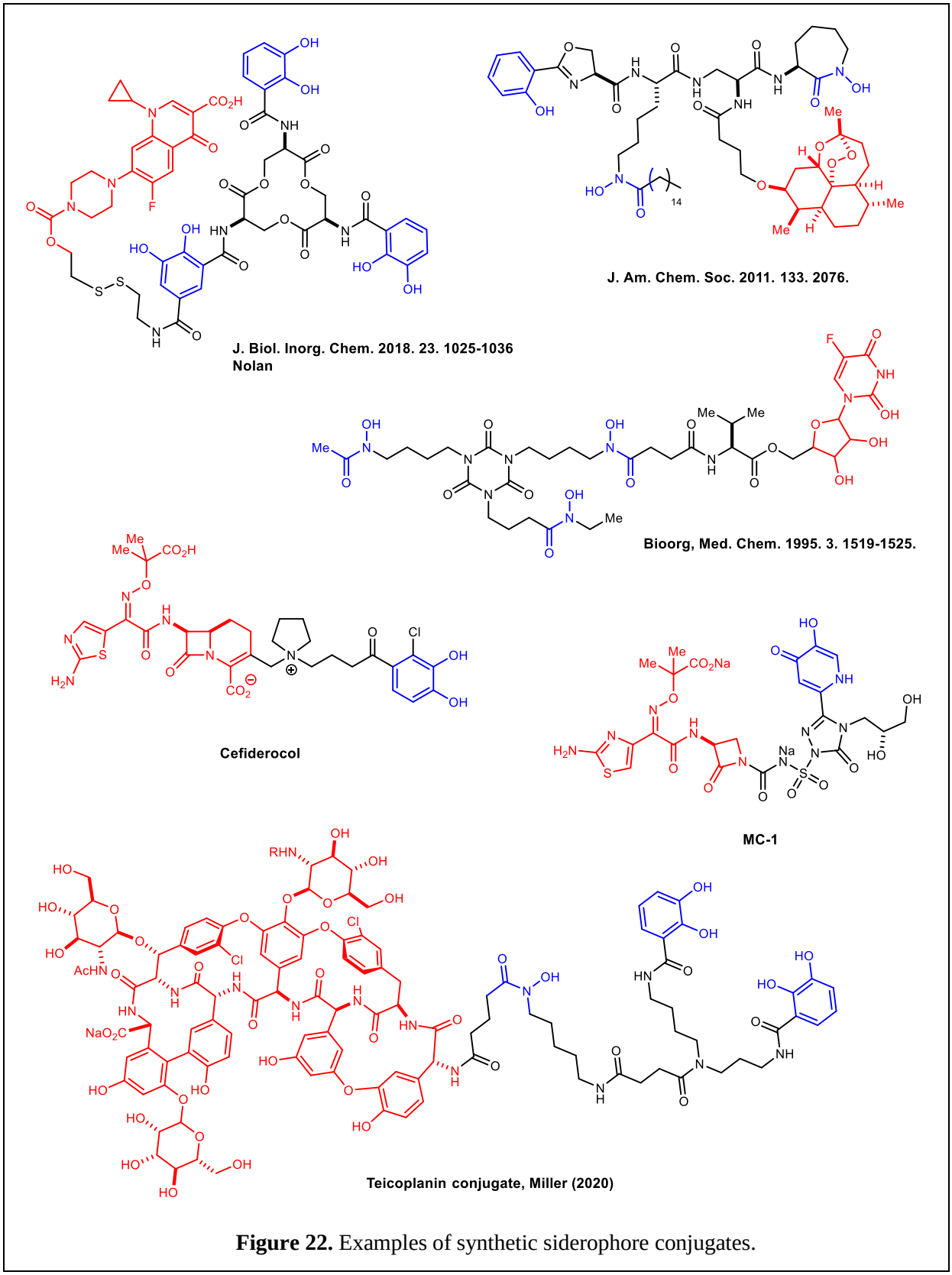

Figure 22. Examples of synthetic siderophore conjugates.

1.4 Discovery, Isolation, and Characterization of Coelichelin

With recent advances in genomic sequencing technology came the challenges associated with complex data analysis and interpretation. Through careful analysis, research groups have identified sequence motifs indicative of various biosynthetic pathways, including non-ribosomal peptide synthetases (NRPS).[125] Specific domains used to catalyze reactions within NRPSs have been characterized and can be used to correlate isolated natural products with genes encoding their sequence.[126] Recent advances have demonstrated that these characteristic genomic signatures could be used alone to predict the structure of natural products prior to isolation. [127] [128]

1.4.1 Discovery of Coelichelin using Genome Mining

In 2000, Challis and coworkers identified a unique siderophore produced by *Streptomyces coelicolor* using genome mining, a powerful technique used to elucidate and characterize biosynthetic gene clusters.[129] [130] [131] Following thorough genomic analysis, they identified a gene cluster (*cch*) that was indicative of a nonribosomal peptide synthetase (NRPS). Further analysis indicated that the CchH synthetase encodes three modules composed of ten NRPS domains: three adenylation (A) domains, three peptidyl carrier protein (PCP) domains, two condensation (C) domains, and two epimerization (E) domains (Figure 23).[132] They noted the absence of a thioesterase (TE) domain which usually catalyzes cleavage of the newly formed product from the NRPS. Challis and coworkers noted that at that time no secondary metabolites had been isolated from *S. coelicolor* and as such, they reasoned that this gene cluster was responsible for the synthesis of a novel natural product. The authors sought to predict the structure of this natural product based solely on genomic analysis.

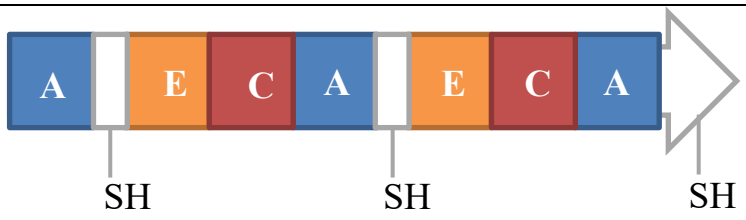

Figure 23. Modules identified in CchH synthetase, where A= adenylation domain, E= epimerization domain, and C= condensation domain.

The colinearity rule dictates that the number of adenylation domains in the NRPS is indicative of the number of amino acids incorporated into the NRPS product.[133] The adenylation domains in this synthetase recognize three amino acids: L-5-hydroxy-5-formylornithine, L-5-hydroxyornithine, and L-threonine.[134] Thus, Challis and coworkers reasoned that this trimodular NRPS would produce a tripeptide (Figure 24). Given the presence of two epimerization domains, the authors proposed the CchH synthetase to generate a D-D-L-tripeptide containing the aforementioned amino acids. The authors proposed two structures for the natural product, deemed coelichelin, produced by the synthetase favoring **1.89** over **1.88** due to the absence of a domain to catalyze cleavage of the NRPS product.[135] The incorporation of hydroxamic acid groups into coelichelin suggested that it may function as a bacterial siderophore.

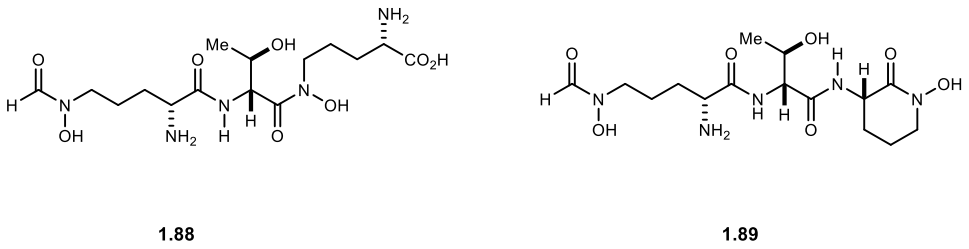

Figure 24. Proposed structures of coelichelin based on genomic sequence.

This represented one of the first examples of the complete structural prediction of a natural product based solely on the analysis of conserved sequences. Given their structural prediction, they next aimed to confirm the proposed structure of the siderophore coelichelin following isolation and characterization.

1.4.2 Isolation of Coelichelin from *Streptomyces coelicolor*

In 2005, Challis reported successful isolation of the siderophore synthesized by the CcH synthetase and assigned the tetrapeptide coelichelin.[136] The hydroxamic acid moieties present in the natural product indicated that it functions as a siderophore produced by *Streptomyces coelicolor* under iron-deficient conditions. The authors reasoned the conditions necessary to isolate coelichelin from *S. coelicolor* would require iron-deficient media.

The authors inactivated *cchH* in *S. coelicolor* generating a mutant (W5) incapable of producing coelichelin. They grew *S. coelicolor* wildtype (WT) and W5 knockout under iron restriction and compared the metabolites produced by both. They identified a product in the WT metabolic profile which was not observed in the W5 knockout. Production of this metabolite was suppressed when the WT strain was grown in the presence of ferric iron suggesting its production was linked to iron-restriction. Following purification of the culture supernatant using semi-preparative HPLC, the ferric iron was removed upon treatment with 8-hydroxyquinoline and the resulting desferri-coelichelin was purified further using semi-preparative HPLC. The authors report desferri-coelichelin as unstable and therefore treated with Ga(III) to prepare a more stable and NMR characterizable Ga-coelichelin complex allowing for purification and characterization. This unique workflow demonstrates the utility of genome mining in the prediction of natural product structures prior to isolation and challenges associated with siderophore isolation.

1.4.3 Structural Characterization of Coelichelin

Following isolation of coelichelin and formation of its corresponding Ga(III) complex, Challis and coworkers used a variety of analytical techniques to characterize the structure of coelichelin.[137] Preliminary HMRS analysis of desferri-coelichelin was indicative of a product with molecular formula $C_{21}H_{39}N_7O_{11}$. Further tandem MS/MS analysis suggested the product contained two hydroxyformylornithine residues, one threonine residue, and one hydroxyornithine residue. The authors report instability of desferri-coelichelin and as such form Gallium (III) complex as reported in the characterization of ornibactin. [138]

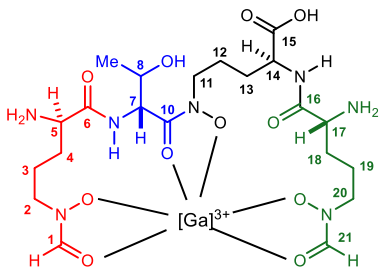

Assignment	^{1}H δ	^{13}C δ
1	8.17,s	153.5
2	3.41, m; 3.51, m	
3	1.42, m; 1.50, m	
4	1.91, m; 1.50, m	
5	3.97, dd (*J* = 3.0, 3.0 Hz)	
6		168.5
7	4.59, dd (*J* = 9.0, 9.0 Hz)	58.0
8	3.82, m	66.0
9	1.14, d (*J* = 5.5 Hz)	21.0
10		162.5
11	3.45, m; 3.93, m	
12	1.83, m; 1.83, m	
13	1.76, m	
14	4.24, dd (*J* = 11.0, 8.5 Hz)	
15		173
16		170
17	4.15, dd (*J* = 11.0, 1.9 Hz)	
18	1.64, m; 2.29 m	
19	1.96, m; 1.76 m	
20	3.76, m	
21	8.22, s	153.5

Figure 25. Structural assignment of coelichelin based on 1D- and 2D-NMR analysis.

The authors further characterized the Ga-coelichelin using 1D- and 2D-NMR spectroscopy: ^{1}H, DQF-COSY, TOCSY, HMBC, and ROESY (Figure 25). Notably, the authors did not acquire a ^{13}C NMR or an HSQC experiment and all carbons in the natural product were not listed nor were they assigned. The aforementioned NMR experiments were utilized to rationalize the connectivity of the natural product. Surprisingly, these results demonstrate the incorporation of four amino acids into a natural product synthesized by a trimodular NRPS. This was without literature precedent and the authors reasoned their model could not have predicted a tetrapeptide product given the knowledge available at the time.

Focus next turned toward detailing the stereochemistry of the α-carbons present in the siderophore. The relative stereochemistry of the four α-carbons was determined by theory-based tools using molecular modeling, analysis of inter-residue distances calculated from the ROESY spectra, and dihedral angles acquired following analysis of ^{1}H NMR spectra. The relative stereochemistry of the α- and β-carbons was reported following derivatization as the *N*-trifluoroacetyl isopropyl ester and subsequent analysis using chiral gas chromatography. The authors also relied on knowledge of NRPS incorporation of L-amino acids, which can be epimerized to the corresponding D-amino acids.[139] Given the presence of two epimerization domains in the CchH synthetase, the authors reasoned that the absolute configuration of coelichelin was D-hydroxyformylornithine, D-allo-threonine, L-hydroxyornithine, and D-hydroxyformylornithine.

1.5 Total Synthesis of Coelichelin

Herein we report the total synthesis of the bacterial siderophore coelichelin and its utility in the design of siderophore conjugates.

1.5.1 Synthetic Strategy

We envisioned the tetrapeptide coelichelin (**1.90**) could be synthesized through sequential amide couplings of three fragments: $^{\delta}$*N*-hydroxy-L-ornithine (**1.92**), D-*allo*-threonine (**1.93**), and $^{\delta}$*N*-formyl-$^{\delta}$*N*-hydroxy-D-ornithine (**1.94**) (Figure 26).[140] [141] Taking advantage of the pseudosymmetry of coelichelin, D-*allo*-threonine (**1.93**) and **1.92** could be coupled together followed by a second amide coupling with two equivalents of **1.94** or **1.95**. Subsequent global

deprotection would reveal coelichelin and its acetyl congener acetyl coelicehlin.

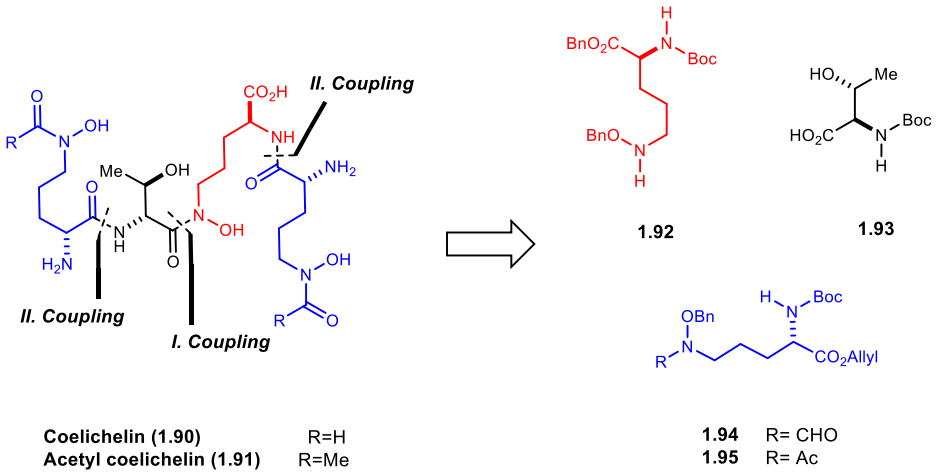

Figure 26. Retrosynthetic analysis of coelichelin.

We reasoned D-*allo*-threonine (**1.93**) could be accessed from D-threonine using a well-precedented strategy.[142, 143] $^{\delta}$*N*-Formyl-$^{\delta}$*N*-hydroxy-D-ornithine (**1.93**) and $^{\delta}$*N*-hydroxy-L-ornithine (**1.92**) could be prepared from D- and L-pyroglutamic acid, respectively, using several reported strategies to access hydroxylamines and hydroxamic acids.[144]

1.5.2 Synthesis of *N*-Boc protected D-*allo*-threonine 1.93

Following literature precedent, D-threonine (**1.96**) was converted to **1.93** in five steps beginning with esterification of D-threonine to **1.97** (Figure 27).[145] The corresponding methyl ester was converted to benzamide **1.98** upon treatment with benzoyl chloride and triethylamine. **1.98** was subsequently treated with thionyl chloride for 5 days at 0 °C yielding the requisite oxazoline with concomitant inversion of the stereocenter at the β-position. Oxazoline **1.99** was hydrolyzed under reflux in 6 N HCl to provide D-*allo*-threonine (**1.100**) in near quantitative yield. Carbamate protection of the free amine afforded **1.93** for use in the first amide coupling.[146]

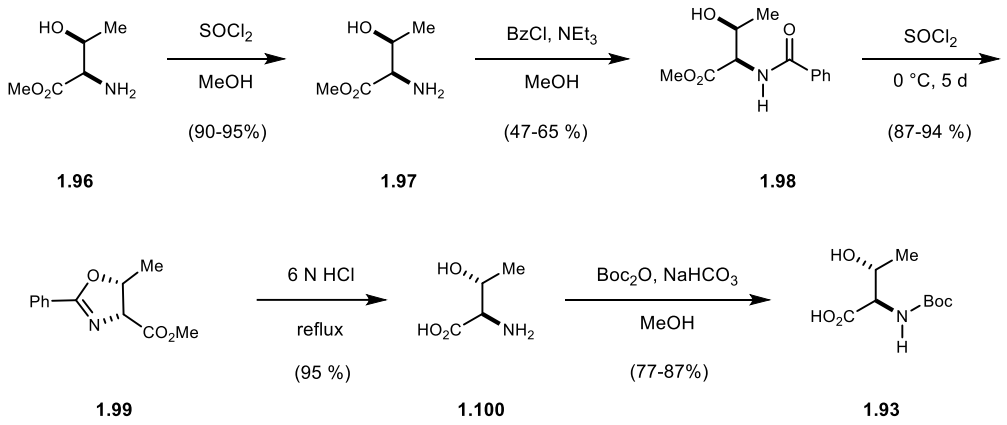

Figure 27. Synthesis of protected threonine 1.93.

1.5.3 Synthesis of $^{\delta}$*N*-hydroxy-L-ornithine 1.92

With protected D-*allo*-threonine **1.93** in hand, we began the synthesis of its coupling partner, $^{\delta}$*N*-hydroxy-L-ornithine **1.92** (Figure 28). The synthesis of **1.92** commenced with esterification of commercially available L-pyroglutamic acid (**1.101**) to afford benzyl ester **1.102**, which we reasoned could be removed concomitantly with benzyl ethers in the late-stage global deprotection.[147] [148] [149] [150] *N*-Boc protection of **1.103** and subsequent reduction and hydrolysis with sodium borohydride yielded linear alcohol **1.104**. Efforts to optimize the oxidation of alcohol **1.104** to the corresponding aldehyde were unsuccessful, resulting in complex mixtures and low yields likely due to the instability of the aldehyde. Ultimately, a one-pot oxidation and

oxime formation strategy proved successful. Parihk-Doering oxidation of **1.104** yielded an intermediate aldehyde which was condensed *in situ* with *O*-benzylhydroxylamine hydrochloride to afford oximes **1.105**. Finally, reduction with sodium cyanoborohydride at low pH afforded the desired $^{\delta}$*N*-benzyloxy-L-ornithine **1.92**.[151]

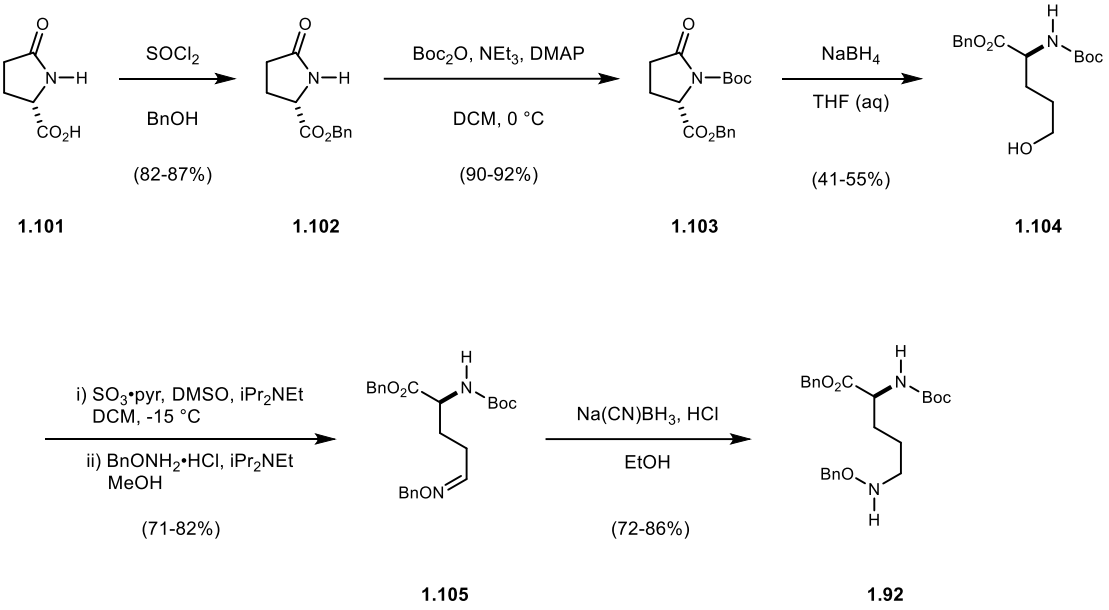

Figure 28. Synthesis of $^{\delta}$*N*-hydroxy-L-ornithine 1.92

1.5.4 Synthesis of $^{\delta}$*N*-formyl-$^{\delta}$*N*-hydroxy-D-ornithine 1.94

We reasoned that the same synthetic strategy used in the preparation of **1.92** could be applied to **1.94** beginning instead with the enantiomer D-pyroglutamic acid (**1.106**) (Figure 29). Esterification of **1.106** with allyl alcohol afforded allyl ester **1.107**, which we reasoned would serve as a useful orthogonal protecting group.[152] **1.107** was *N*-Boc protected and treated with sodium borohydride to yield **1.109**.[153] The previously described one-pot oxidation and oxime formation provided **1.110**, which was subsequently reduced with sodium cyanoborohydride at low pH to yield **1.111.** The obtained hydroxylamine was subjected to *N*-formylation followed by Pd(0)-mediated deprotection of the allyl ester to reveal carboxylic acid **1.114**, which could be used toward the synthesis of coelichelin. Lability of formyl groups was observed under a variety of conditions. Alternatively, we reasoned that hydroxylamine (**1.111**) could be *N*-acetylated and used toward the synthesis of an *N*-acetylated analog of coelichelin.

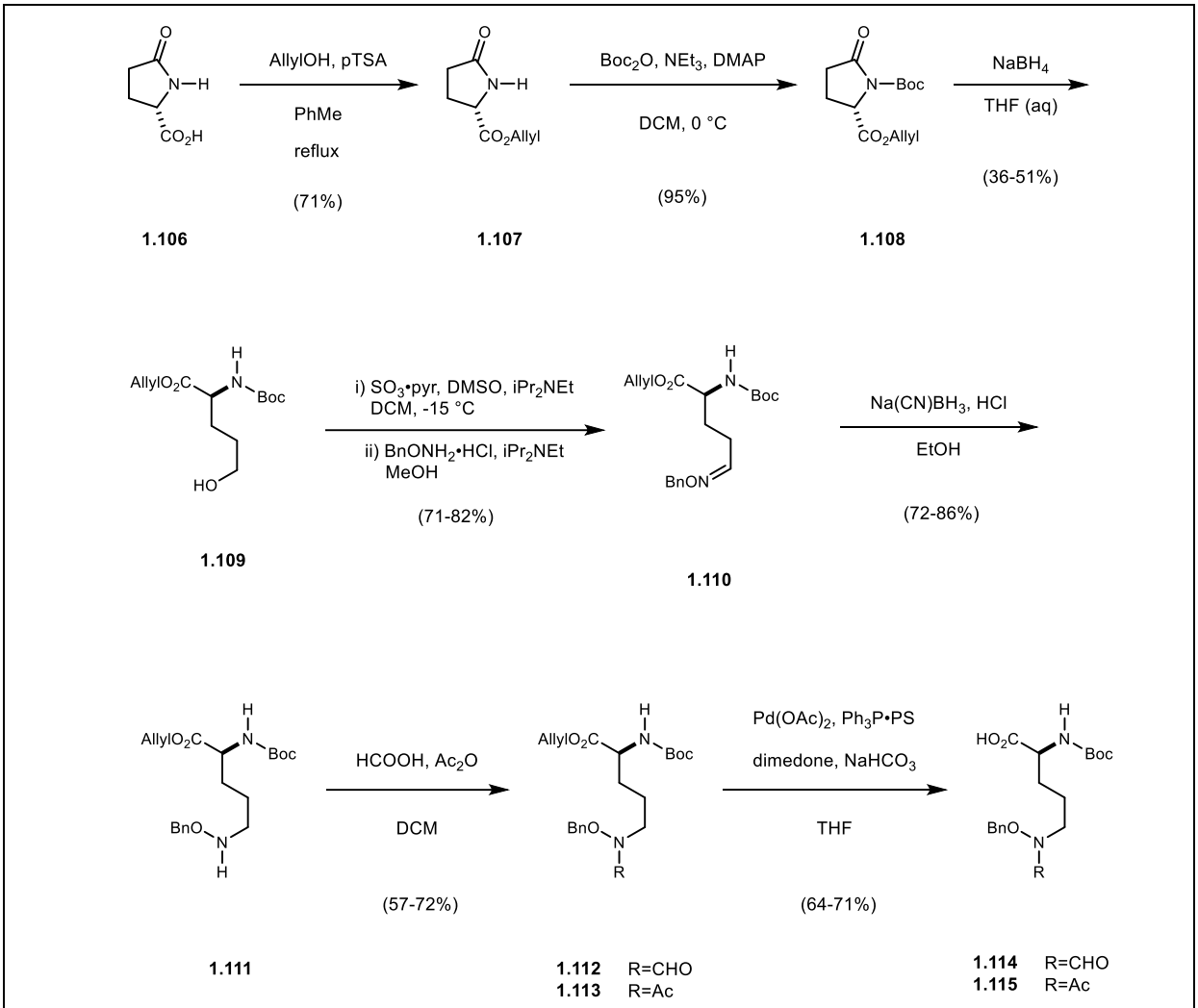

Figure 29. Synthesis of $^{\delta}$*N*-formyl-$^{\delta}$*N*-hydroxy-D-ornithine (1.114) and $^{\delta}$*N*-acetyl-$^{\delta}$*N*-hydroxy-D-ornithine (1.115).

1.5.5 Completion of the synthesis of coelichelin (1.90) and acetyl coelichelin (1.91)

With all three peptide coupling partners in hand, we began screening conditions to couple **1.92** and **1.93** (Figure 30). Preliminary efforts to affect the desired transformation with various coupling reagents, including EDC/HOBt, PyBOP, PyCLU, proved unsuccessful.[154] Successful coupling of **1.92** and **1.93** was achieved under HATU coupling conditions and dipeptide **1.116** was subjected to TFA-mediated deprotection to reveal peripheral amino groups primed for the second peptide coupling. Gratifyingly, **1.117** and two equivalents of **1.114** were coupled under HATU conditions to complete the fully protected tetrapeptide **1.118**. Hydrogenolysis provided **1.120** and subsequent *N*-Boc deprotection afforded coelichelin (**1.90**).

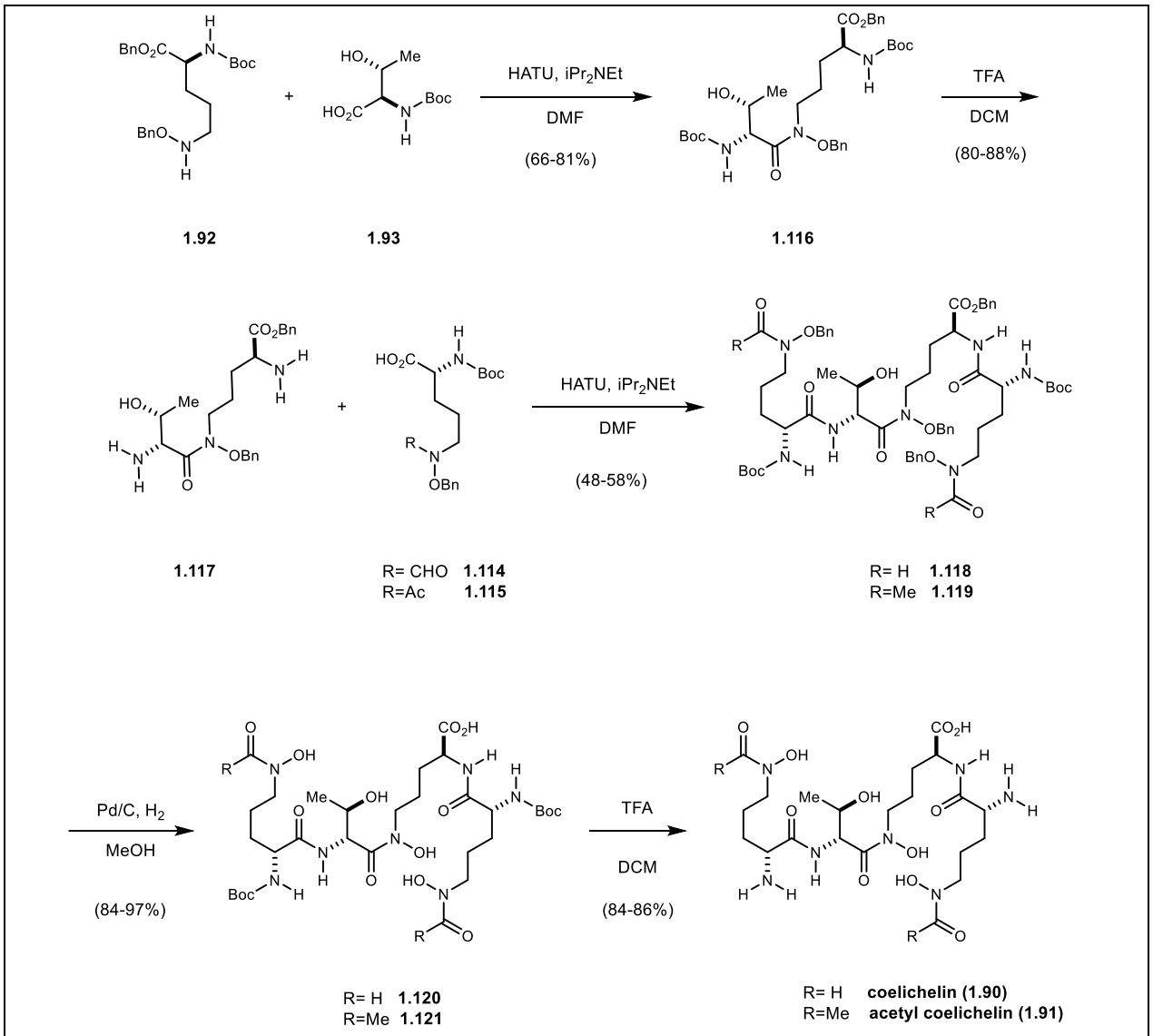

Figure 30. Final coupling and deprotection sequence to afford coelichelin (1.90) and acetyl coelichelin (1.91).

We reasoned that our synthetic strategy could be employed to synthesize an *N*-acetyl analog of coelichelin, which would also be capable of iron chelation. To this end, HATU-mediated coupling of **1.117** with 2 equivalents of **1.115** afforded the *N*-acetylated tetrapeptide **1.119**. Subsequent hydrogenolysis and *N*-Boc deprotection afforded the *N*-acetylated analog, acetyl coelichelin (**1.91**). Thus, completing the first reported total synthesis of the bacterial siderophore coelichelin and its *N*-acetylated congener, acetyl coelichelin.[155]

1.6 Utility of Synthetic Coelichelin by P. aeruginosa

1.6.1 Chrome Azurol S (CAS) Assay for the Detection of Siderophores

In order to confirm the utility of synthetic coelichelin and its congeners, they were evaluated as a viable siderophores to be recognized and used by a microbe as a source of iron in a deficient environment. First, we wanted to confirm that synthetic coelichelin and its congeners were able to chelate ferric iron. A chrome azurol s (CAS) assay, which is a colorimetric assay used to detect the presence of siderophores in media.[156] [157] This assay has been adapted to confirm the chelation ability of synthetic chelators. A color change accompanies the transfer of ferric iron from the Fe-CAS complex to the siderophore, which results in a quantifiable color change from blue to orange.

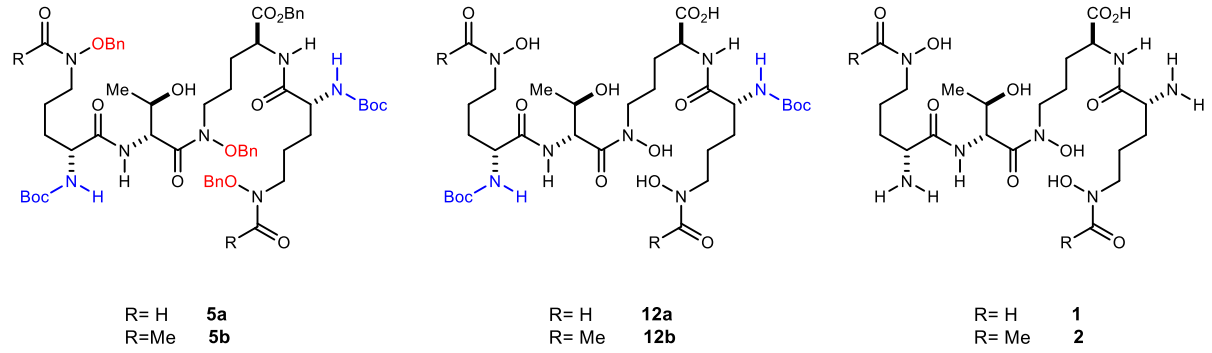

Figure 31. Coelichelin and derivatives evaluated in assays.

We conducted CAS assays on coelichelin (**1**) and acetyl coelichelin (**2**), *N*-Boc protected (**12a**) and (**12b**); and *N*,*O*-protected (**5a**) and (**5b**). Commercially available desferrioxamine (DFO)

served as a positive control and doubly distilled water (ddH_2O) served as a negative control. (Figure 31).

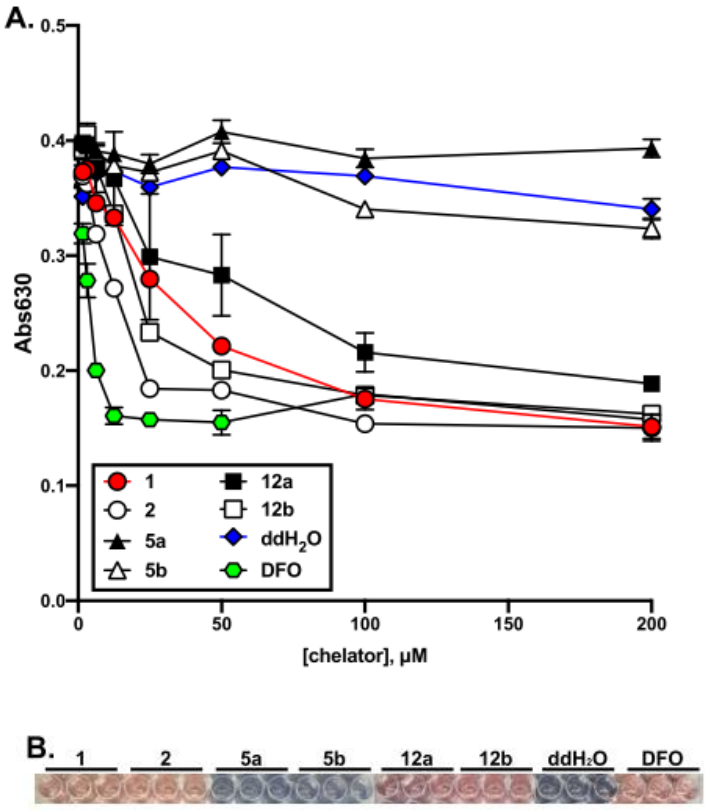

Figure 32. CAS Assay evaluating iron chelation ability of coelichelin and congeners.

The CAS assay demonstrated the ability of coelichelin (**1**) and acetyl coelichelin (**2**) to chelate iron when compared to desferrioxamine (DFO) (Figure 32). Further, *N*,*O*-protected analogues (**5a**) and (**5b**), are ineffective iron chelators due to the protection of the hydroxamic acid moieties involved in chelation. Notably, *N*-Boc protected coelichelin (**12a**) and *N*-Boc protected acetyl coelichelin (**12b**) were also capable of iron chelation. This has positive implication for design of siderophore conjugates as the peripheral amino groups can tolerate additional functionality without perturbing iron chelation ability.

1.6.2 Growth Promotion Assays

Following confirmation of chelation ability, we evaluated coelichelin and its synthetic congeners ability to serve as the sole source of iron in a growth promotion assay. Many bacteria express receptor proteins for pirating xenosiderophores, which are siderophores produced by another microorganism. We conducted these growth promotion assays using a strain of *P. aeruginosa* (IA614) which was devoid of endogenous siderophore production.[158] This mutant strain is non-fluorescent and debilitated for growth under iron restriction. When grown under iron restriction, the growth of this strain becomes wholly dependent on the utilization of supplemental xenosiderophores.

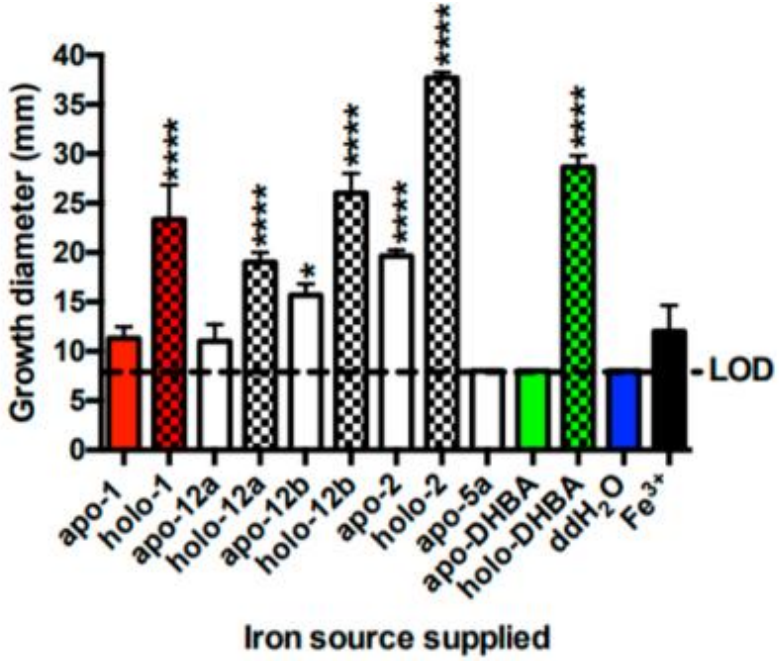

Figure 33. Growth promotion assays.

Following overnight growth under iron-restriction, *P. aeruginosa* (IA614) was treated with apo- and holo- forms of coelichelin and its congeners and evaluated for their ability to promote the growth of the bacteria (Figure 33) .The *apo-* or iron-loaded forms were superior growth promoters when compared to the holo-forms. Coelichelin (**1**) and unnatural congeners (**2**, **12a**, and **12b**) were all capable of growth promotion when compared to controls.

1.6.3 Fluorescence Assay

To corroborate the findings of the previous experiments, a fluorescence assay was conducted

with siderophore-proficient strain of *P. aeruginosa* (PAO1) following iron-restriction. This strain produces two endogenous siderophores, pyochelin and pyoverdine, which are fluorescent. Pseudomonads have been shown to pirate siderophores from other microorganisms and concomitantly decrease production of endogenous siderophores.[159] [160] We reasoned that following treatment with synthetic coelichelin there would be an observable decrease in endogenous siderophore production.

Following treatment with coelichelin (**1**), a dose-dependent decrease in pyochelin and pyoverdine fluorescence was observed (Figure 34). We reasoned that this further supported that synthetic coelichelin was being used as a siderophore for *P. aeruginosa* (PAO1). Further, treatment with *N,O*-protected tetrapeptide (**5a**) resulted in no observable changes in fluorescence. Bacteria grew comparably following treatment with **1** and **5a** indicating that the observed decrease in fluorescence was not attributed to a decrease in bacteria viability. This is in agreement with previous findings as the hydroxamic acid moieties are protected in **5a** and therefore incapable of iron chelation.

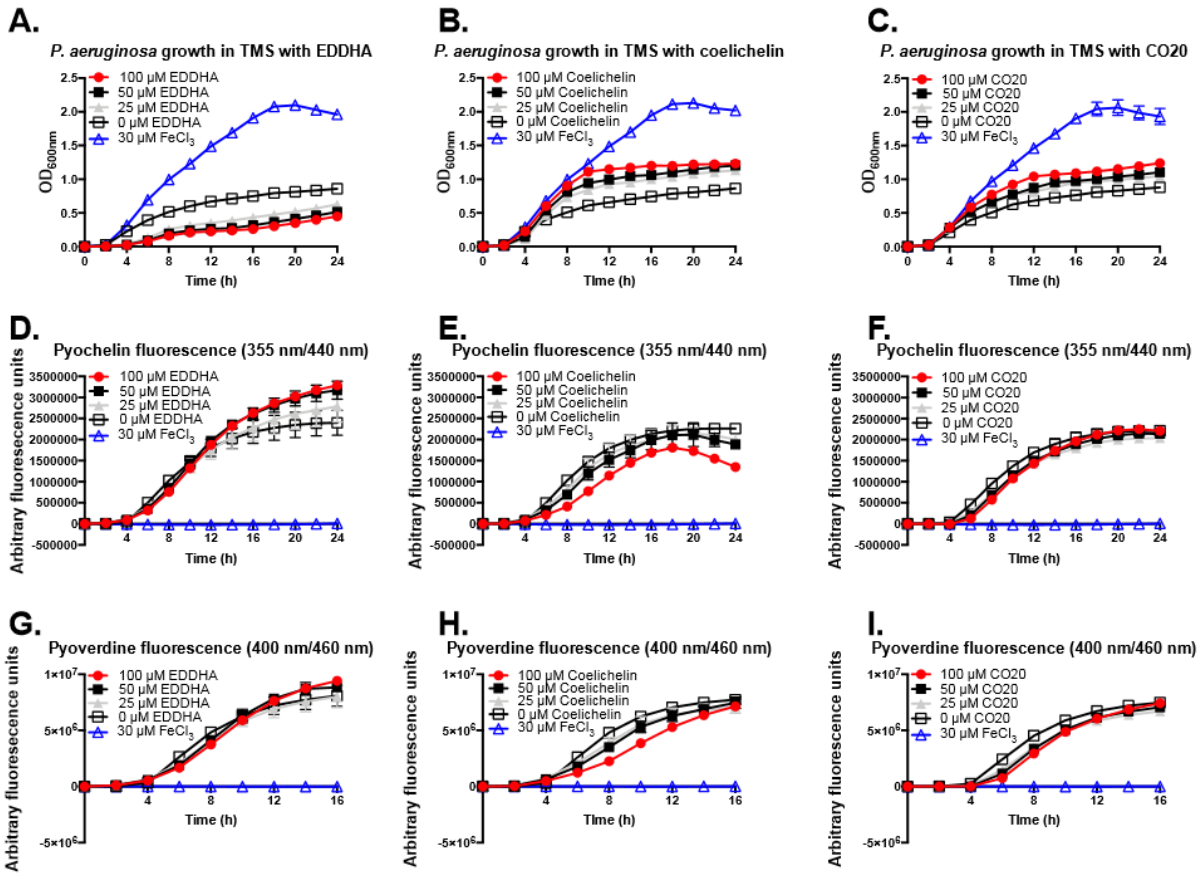

Figure 34. Fluorescence assay measuring endogenous siderophore production following treatment with **coelichelin (1)** and **5a**.

Together these results demonstrate that synthetic coelichelin (**1**) functions as an iron chelator and bacterial siderophore. Further, the unnatural acetyl congener (**2**) also functions comparably to natural coelichelin. Notably, the free amino groups present in **12a** and **12b** can tolerate additional functionality which could serve as a reactive handle for further diversification into siderophore-conjugates.

1.7 Future Directions

To date, we have reported the first total synthesis of the bacterial siderophore coelichelin (**1**) and an unnatural congener acetyl coelichelin (**2**) (Figure 35). Our synthetic strategy allowed for material to begin preliminary evaluation of coelichelin's utility in the study of bacterial metal acquisition. We were able to confirm that coelichelin and its congeners were capable of chelating ferric iron and could be used as siderophores for *P. aeruginosa* in growth promotion assays. Through our preliminary evaluation, we uncovered that the peripheral amino groups can tolerate additional functionality without loss of siderophore activity. We reason these sites could serve as reactive handles allowing for introduction of small- or large- molecule payloads.

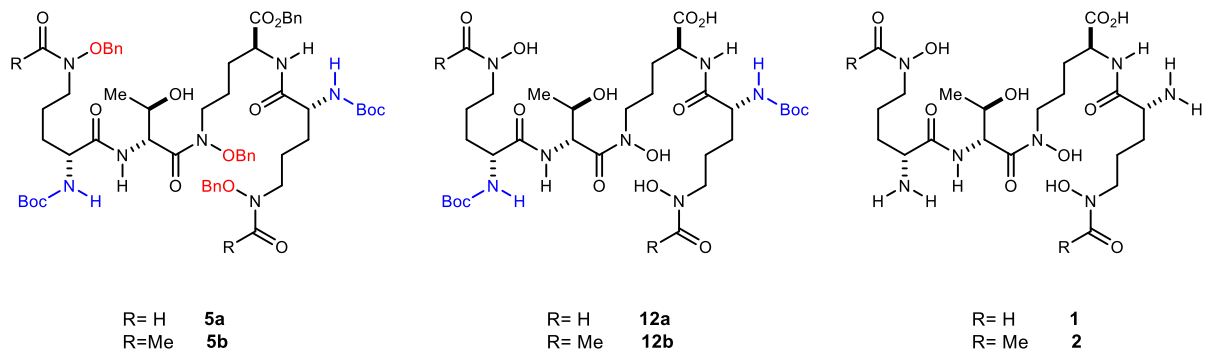

Figure 35. Coelichelin and its synthetic congeners.

1.7.1 Design of Siderophore Conjugates

One area which has gained increasing attention in targeting bacterial metal acquisition is the synthesis of siderophore-conjugates. This strategy has several advantages. It allows for active uptake of the siderophore-conjugate via iron transport systems, improved cell permeability, especially in gram-negative pathogens, and delivery of small molecule antibacterial agents.[161 162 163 164 165 166] This is exemplified by the recent report of Cefiderocol, a cephalosporin siderophore, which has been efficacious in a Phase II Clinical trial for Gram-negative multi-drug resistant urinary tract infections.[167 168]

In consideration of making a more efficient synthesis of coelichelin-conjugates, we hypothesize

that the full length tetrapeptide is not essential for siderophore activity. Using our current synthetic strategy, we can access appreciable quantities of the tripeptide (Figure 36).

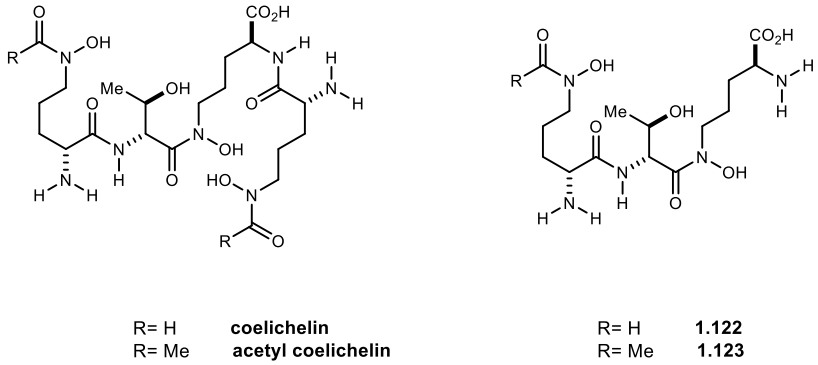

Figure 36. Coelichelin and tripeptide analogues.

To evaluate its utility, we will first evaluate ferric iron chelation ability using the CAS assay for detection of siderophores. Following evaluation of chelation ability, we will probe the tripeptides ability to serve as the sole source of iron for a mutant strain of *P. aeruginosa* devoid of endogenous siderophore production. This should serve as sufficient preliminary data regarding the siderophore activity of the tripeptide and allow for a more efficient synthesis while also introducing an alternative reactive handle for conjugation.

Using our current synthetic strategy, we were able to synthesize an unnatural *N*-acetyl analog of coelichelin (**2**). Our preliminary results indicate that the unnatural *N*-acetyl coelichelin facilitates growth of *P. aeruginosa* to a greater extent than its congeners. While the understanding of why the *N*-acetyl analog promotes growth to a greater extent is unknown, it is something to consider in design of conjugates. We propose evaluation of both the *N*-acetyl and *N*-formyl coelichelin analogues in synthesis of coelichelin conjugates to further probe these differences.

An additional consideration is whether to introduce a linker between the siderophore and its payload. There is precedent for conjugating siderophores directly to antibacterial agents, such as cefiderocol and examples of introducing a chemical linker between the siderophore and its conjugate. Design of a siderophore-conjugate depends on the means by which we propose to use this tool compound. There are three options with regard to introducing a linker between the siderophore and its payload: 1) to conjugate the siderophore directly, 2) use an enzymatically

cleavable linker which would allow release of payload, 3) use a chemical linker such as a polyethylene glycol (PEG) linker.

In consideration of what is conjugated to the siderophore, there are two main areas we can consider: evaluating antibacterial activity or studying metal acquisition pathways. To probe antibacterial activity, we propose conjugation of coelichelin to members of the main classes of antibiotics, including the penicillins and cephalosporins. The second strategy would be to conjugate the siderophore to an affinity or fluorescent probe to further study metal acquisition pathways. Understanding these pathways from a mechanistic standpoint allows for development of improved therapeutic strategies.

1.7.2 Characterize Antibacterial Activity

To interrogate the antibacterial activity of coelichelin-antibiotic conjugates, we propose evaluation of the antibacterial activity (especially for gram-negative pathogens) and cell permeability. Furthermore, it would be beneficial to study how quickly resistance develops when utilizing these conjugates. Finally, reports have indicated that complexing the siderophore to gallium prior to treatment is another way to improve antibacterial activity of this class of compounds. We propose evaluation of several antibiotic resistant strains by treating with the coelichelin-conjugate of the corresponding antibiotic for which resistance has developed. Compound **X.X** will serve as a negative control in all off these assays given its inability to chelate ferric iron and promote bacterial growth. We will also evaluate the antibacterial activity of coelichelin, acetyl coelichelin, tripeptide analogues, and the antibiotic alone for statistical comparison.

1.7.3 Biofilm Formation

Organisms growing in biofilms have been reported as more resistant to clinical antibiotics than their planktonic counterparts.[169] [170] Biofilm formation is problematic in a clinical setting, especially with regard to medical and dental biomaterials. Given the growing need to address antibiotic resistance of biofilms in both dental and medical communities, it would be of benefit to evaluate the coelichelin conjugates.

Recent reports have indicated that siderophores play a role in the development of biofilm through

key processes involved in surface attachment and polysaccharide synthesis.[171 172 173 174] Targeting siderophore synthesis of function provides an alternative approach to combat resistance associated with biofilm formation.

1.7.4 Chelation Ability of Other Biologically Relevant Metals

Understanding the mechanisms by which pathogens acquire metal nutrients can provide novel therapeutic targets for treating infectious disease. Using coelichelin as a probe to study these pathways allows for unique insight as it is directly involved in the metal acquisition process.

It would be beneficial to have a small molecule probe to study bacterial acquisition of other metal nutrient such as zinc, manganese, and copper. There's literature precedence that coelichelin chelates zinc, which we would like to confirm. There are several methods for confirming chelation ability of siderophores to various metals. We propose getting crystal structures of metals complexed with coelichelin. Additionally, we could employ MS experiments to identify metal complexes following literature precedent. It would be beneficial to evaluate the chelation ability of coelichelin, N-acetyl coelichelin, and the tripeptide. This would provide further insight in conjugate design. Finally, there are alternative spectrophotometric assays such as the CAS assay for other metals in addition to iron.

CHAPTER 2

TOTAL SYNTHESIS OF CYCLIC DEPSIPEPTIDE COCHINMICINS

2.1 Introduction

Nature efficiently incorporates structural diversity in natural products to fulfill specific biological roles. Chemists have long sought to construct these unique scaffolds to further the field of organic chemistry, develop new reactions, and evaluate the biological activity of prepared products. Each reported strategy and synthesis highlights unique approaches and unanticipated challenges, which needed to be addressed. We, as chemists, share a strong desired to develop chemistry which rivals nature in both complexity and efficiency. The work disclosed herein describes one such example, which undoubtedly demonstrates that if we are to rival nature, we still have much to learn in the construction of complex natural products.

2.1.1 Cyclic depsipeptides represent a diverse class of natural products with unique biological activity.

Isolation chemists often discover complex natural products isolated from diverse sources.[175] Peptide natural products have long served as a source of clinically-relevant small-molecules.[176] Cyclic depsipeptides refer to one such class of peptidic natural products containing at least one ester linkage in place of an amide bond within the macrocycle (Figure 37).[177] These cyclic peptides often feature non-proteinogenic amino acids, complex cross-linking of amino acid side chains, and D-amino acids. The unique structural features observed in these macrocyclic products are often accompanied by equally interesting biological activity.

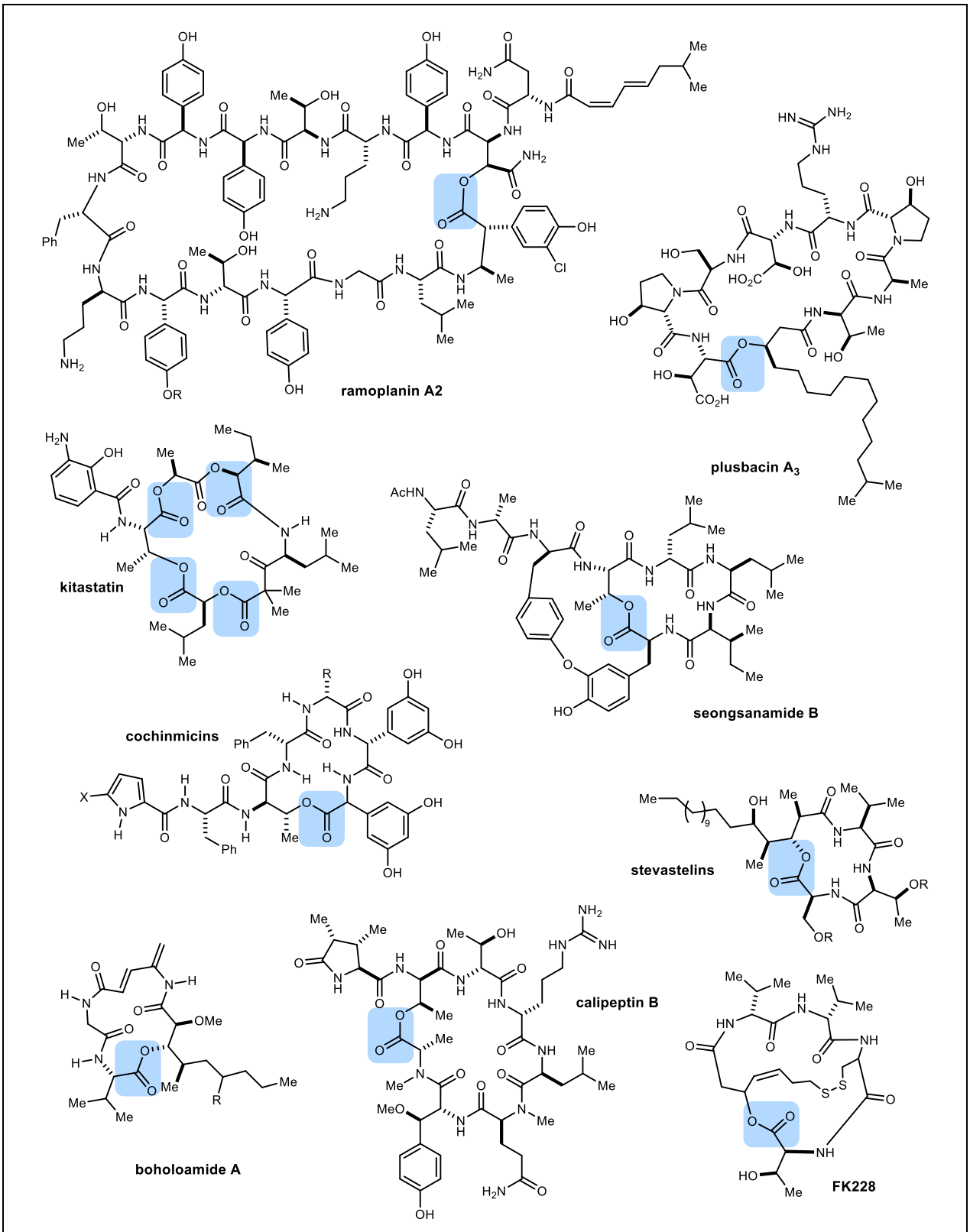

Figure 37. Cyclic depsipeptides are structurally diverse natural products possessing an ester linkage.

2.1.2 Challenges in the total synthesis of cyclic depsipeptides

The intriguing structural complexity and accompanying biological activity prompts chemists to pursue total syntheses. Notably, the most challenging synthetic step is often the macrocyclization. To this end, chemists either employ a macrolactonization or macrolactamization approach to access the desired cyclic system. This requires novel approaches to access these privileged structures enabling evaluation of the unique biological activity.

These seemingly benign cyclic depsipeptides have a propensity to undergo side reactions. Diolide formation resulting from dimerization of the *seco*-acid is a major competitive pathway in macrocyclization efforts. Further complications arise from epimerization of the C-terminus, especially with non-canonical amino acids, rendering the construction of these larger macrocycles even more challenging. *O*→*N*-Acyl transfer and other undesired decomposition pathways make the construction of macrocyclic depsipeptides even more challenging. These challenges have driven the development of mild reaction conditions to mitigate undesired reaction pathways.

2.2 Macrolactamization approaches to access privileged cyclic depsipeptides

Considerable examples demonstrate the challenges inherent to the depsipeptidic linkage, especially via macrolactonization. As a result, many successful approaches to access cyclic depsipeptides feature a macrolactamization. This strategy takes advantage of the relative difference in nucleophilicity of amines when compared to hydroxyls, which enables construction of the desired macrocycle. Numerous syntheses have been accomplished following successful macrolactamization.

2.2.1 Boholamide A

Tumor hypoxia remains a major challenge in the design of novel chemotherapeutics. It has been implicated in malignancy, resistance to treatment, and poor disease prognosis.[178] Boholamide A represents a cytotoxic cyclic depsipeptide possessing a 15-membered macrocycle and a unique amino-2,4-pentadienolate (APD) moiety.[179] Further evaluation revealed boholamide A possessed hypoxia-selective cytotoxicity. The unique structural features and the potent hypoxia-selective cytotoxicity (IC_{50}= 100-400 nM) prompted Zhang and coworkers to pursue a total synthesis.[180] Following precedence in the synthesis of related ADP-containing natural products, the authors employed a macrolactamization strategy to construct the 15-membered macrocycle. Concomitant deprotection of the *N*-Boc and *tert*-butyl ester upon treatment with trifluoroacetic acid revealed the *seco*-acid, which was directly cyclized under HATU-mediated coupling conditions. A subsequent deprotection and elimination sequence furnished boholamide A (Figure 39). Gram-scale preparation of the macrocycle enabled further evaluation of the hypoxia-selective cytotoxicity. Thus, demonstrating the value of an efficient and robust synthesis of a cyclic depsipeptide enabling biological study.

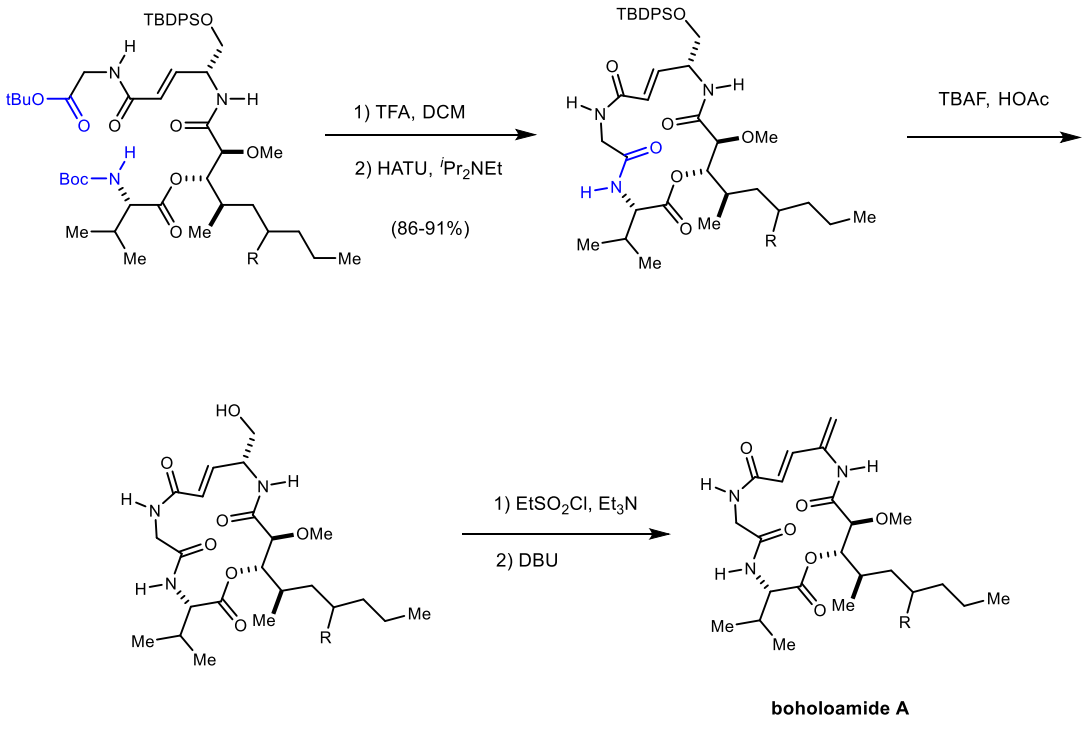

Figure 38. Macrolactamization approach to access cytotoxic depsipeptides boholoamide A.

2.2.2 Seongsanamide B

The incidence of allergenic diseases, such as asthma and allergic rhinitis, continues to rise prompting researchers to identify and develop novel anti-allergenic compounds.[181] [182] Seongsanamides A-D are bicyclic depsipeptides isolated from *Bacillus safensis*, which possess unique antiallergenic properties.[183] The seongsanamides feature a single depsipeptidic linkage and a biaryl ester linkage. Intrigued by this interesting biological activity and the synthetic challenge of installing the tyrosine cross-link, Hutton and coworkers were encouraged to pursue synthesis of the seongsanamides.[184] Preliminary efforts to construct the depsipeptide via macrolactonization were unsuccessful. A transannular esterification was next considered, which could be facilitated by the constraint of the reactive hydroxyl and carboxylic acid within the larger macrocycle. However, no further macrolactonization attempts yielded the desired bicyclic depsipeptide (Figure 40).

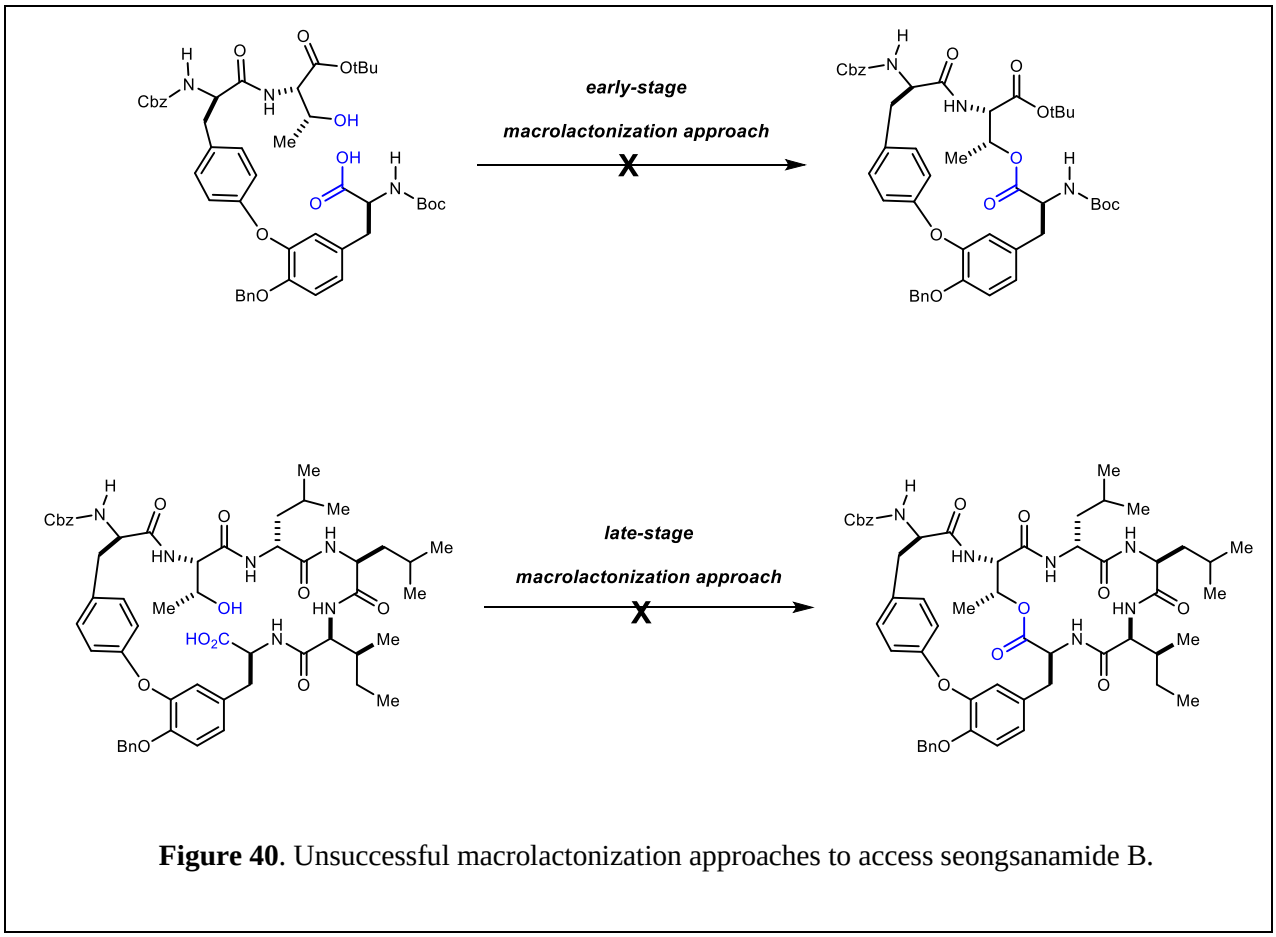

Figure 40. Unsuccessful macrolactonization approaches to access seongsanamide B.

Following unsuccessful macrolactonization attempts, a macrolactamization strategy was next evaluated. The depsipeptidic linkage was first incorporated via intermolecular esterification and the resulting *seco*-acid was subjected to HATU-mediated macrolactamization to construct the eastern macrocycle. Further elaboration and construction of the biaryl ether linkage yielded bicyclic seongsanamide B (Figure 41). Completion of this synthesis enabled the ongoing evaluation of the anti-allergenic properties of the seongsanamides. This work demonstrates the flexibility in design of synthetic strategies, whereby synthetic precursors can be assembled in a distinct order to affect a macrocyclization.

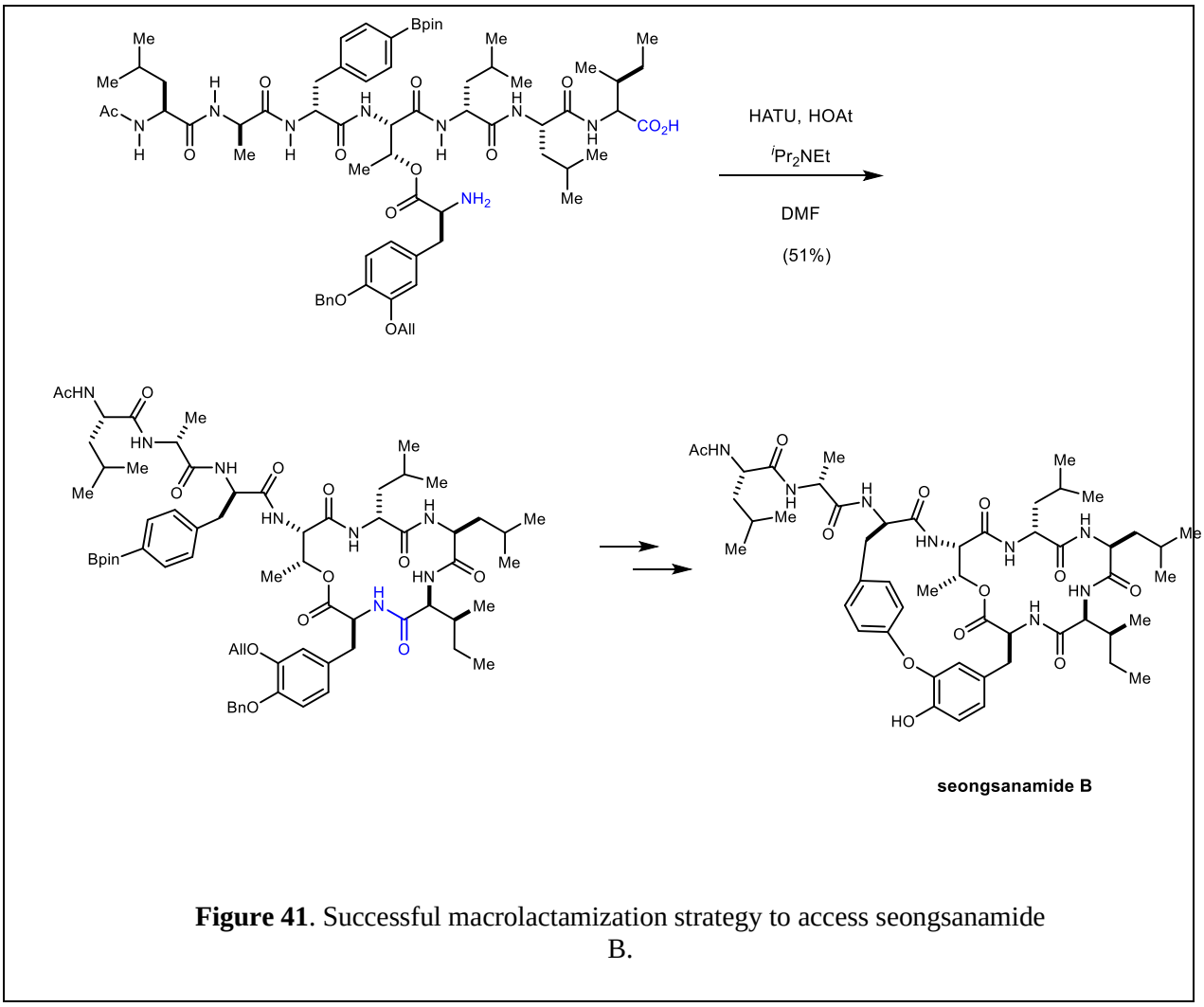

Figure 41. Successful macrolactamization strategy to access seongsanamide B.

2.2.3 Plusbacin A_3

In pursuit of novel antibacterial agents, Ichikawa and coworkers embarked on a synthesis of plusbacin A_3, which is a cyclic depsipeptide isolated from *Pseudomonas sp* PB-6250.[185] Preliminary evaluation of plusbacin A_3 indicated its activity against antibiotic-resistant strains, including methicillin-resistant *Staphylococcus aureus* (MRSA) and vancomycin-resistant *Enterococci* (VRE).[186 187] The mechanism of action is not well-understood and the development of a concise approach to access plusbacin A_3 enables further evaluation of this antibacterial activity. The authors first envisaged construction of the 28-membered macrocycle via macrolactonization (Figure 42). Efforts to activate the carboxylic acid as the corresponding acyl fluoride and affect the macrolactonization resulted in complex mixtures of unidentifiable products or recovered *seco*-acid. Further evaluation of a truncated model system was unsuccessful with various activation methods resulting in no conversion to the lactone, decomposition, or formation of an elimination product.

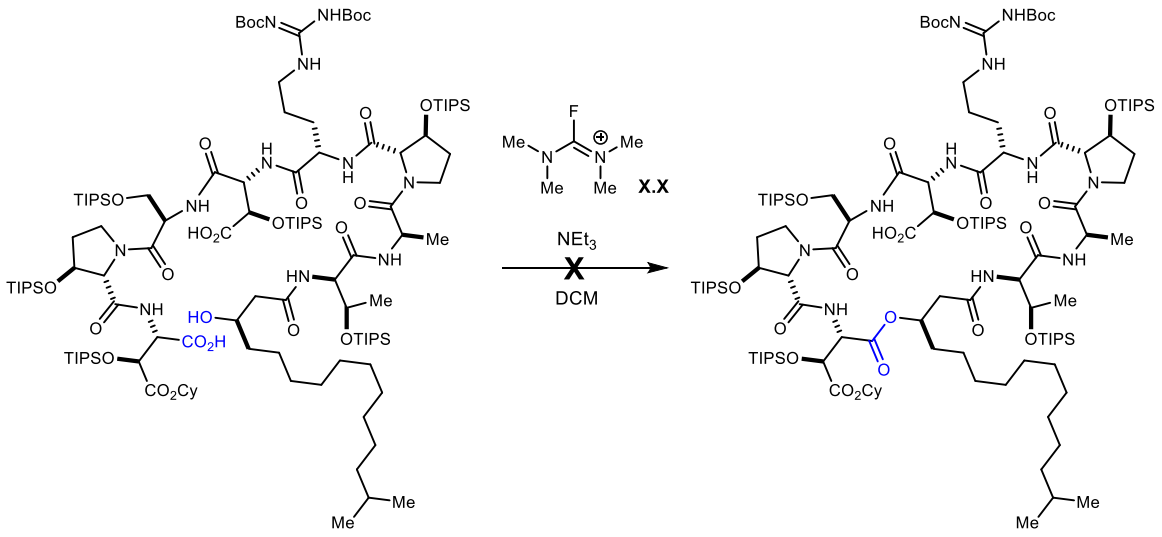

Figure 42. Unsuccessful macrolactonization approach via acyl fluoride toward plusbacin A3.

Following challenges in the macrolactonization approach, the authors revisited their strategy and opted instead for a macrolactamization approach. Pd(0) mediated allyl ester deprotection revealed the requisite carboxylic acid followed by *N*-Boc deprotection to yield the macrolactamization precursor, which upon treatment with EDCI in the presence of racemization-suppressing agent HOAt yielded the desired 28-membered macrocycle (Figure 43). A subsequent

global deprotection yielded plusbacin A_3. This synthetic strategy has enabled the ongoing evaluation of structure-activity relationships and the mechanism of action for the observed antibacterial activity.

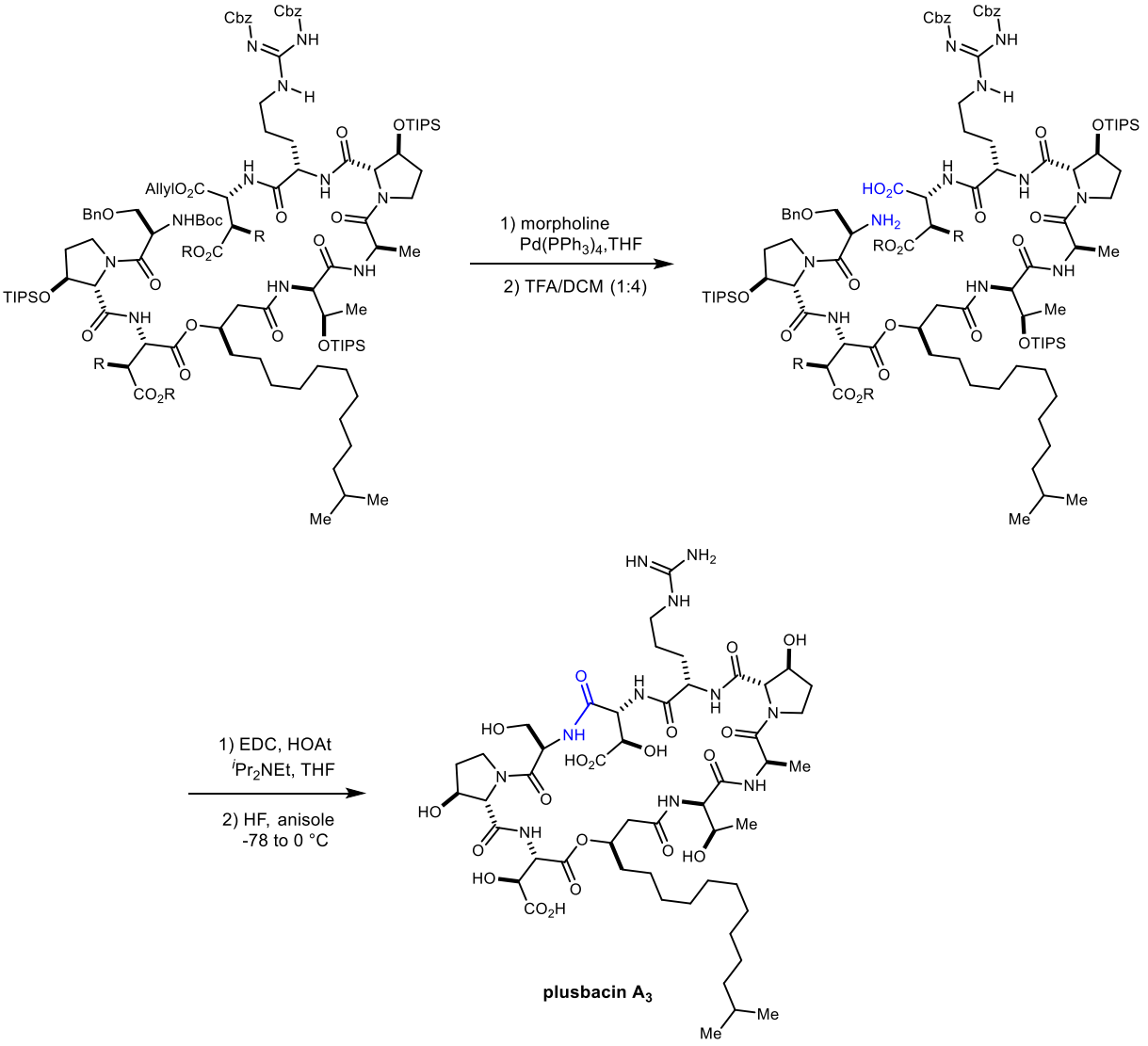

Figure 43. Revised macrolactamization strategy to complete the synthesis of plusbacin A_3.

2.2.4 FK228

Histone acyltransferases (HATs) and histone deacyltransferases (HDACs) are crucial components regulating gene expression and repression.[188] Numerous drug discovery efforts have centered on the development of small molecules capable of modulating these regulatory enzymes, referred to as HDAC inhibitors. In tandem, researchers have also sought HDAC inhibitors from natural sources as a method to incorporate novel structural diversity into drug discovery campaigns. FK228 is a bicyclic depsipeptide possessing unique selectivity for HDACs which are dysregulated in numerous cancers.[189]

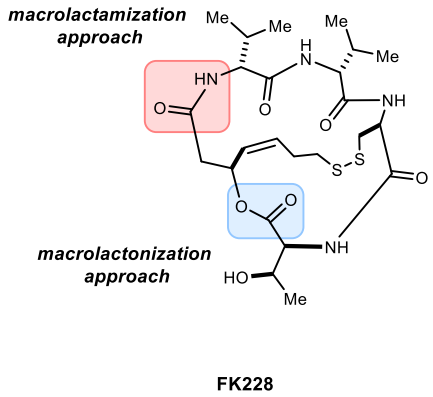

Figure 44. Approaches to access FK228.

Due to its intriguing structural features and accompanying biological activity, numerous total syntheses of FK228 have been reported to date. A macrolactonization was central to many of the previously reported approaches to access FK228 and related analogues (Figure 44).[190] [191] [192] However, Ganesan and coworkers found the macrolactonization approach to be low-yielding and irreproducible. They reasoned that steric encumbrance around the carboxylic acid rendered macrolactonization via carboxylic acid activation ultimately unsuccessful. Treatment of the *seco*-acid under Mitsunobu esterification conditions afforded the desired macrolactone, albeit in low yields (10-20%). Furthermore, removal of excess reagents was especially cumbersome and deemed prohibitive for scale-up. Thus, Ganesan and coworkers elected to revamp their synthetic strategy employing a macrolactamization strategy to access the bicyclic depsipeptide.[193]

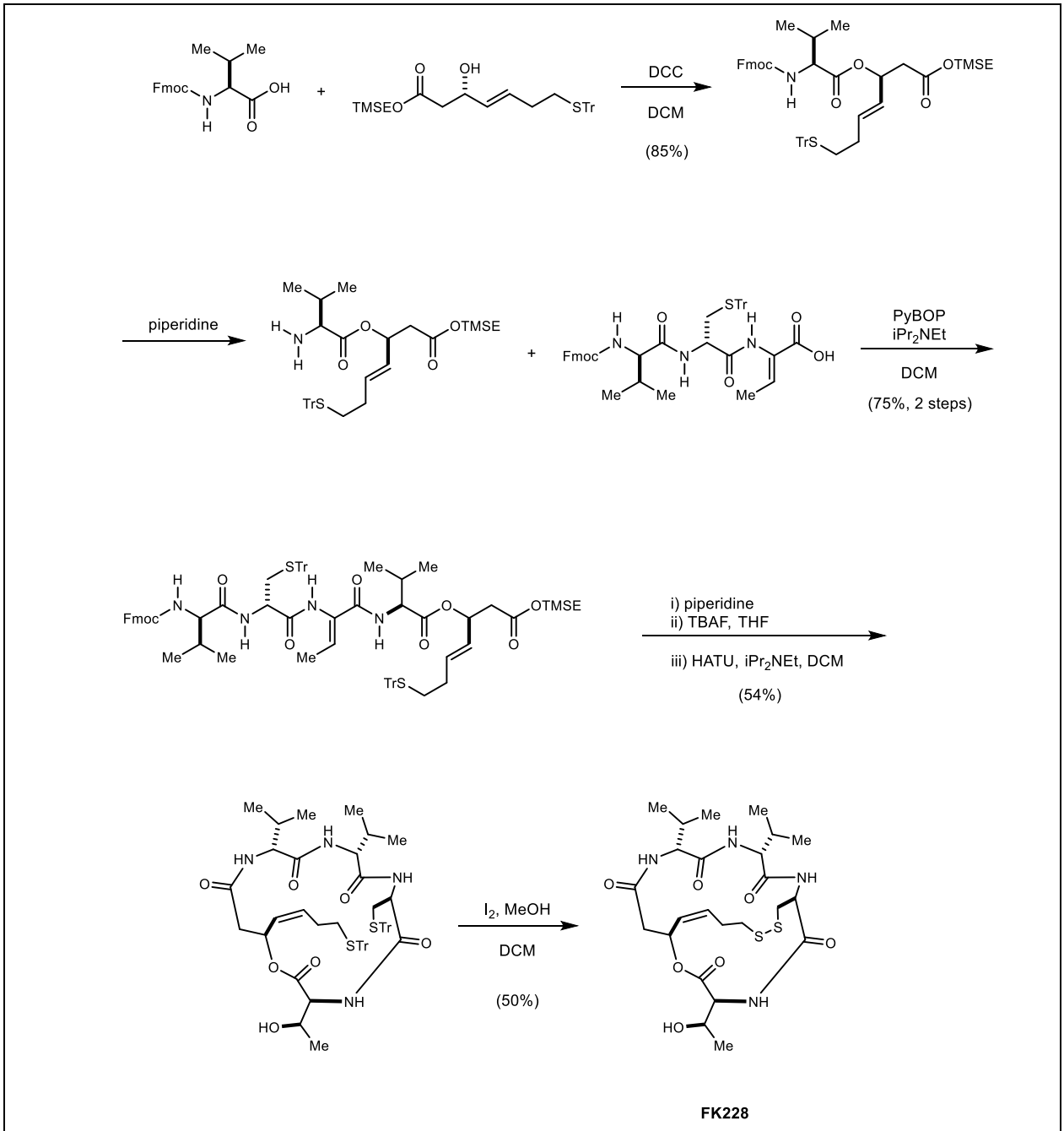

Figure 45. Successful macrolactamization approach to FK228.

However, efforts to incorporate the ester linkage in fragments earlier in the synthetic sequence were found to be equally challenging. Success was found only when the intermolecular esterification was conducted as the first step in the route to access FK228 (Figure 45). With ester in hand, the authors were able to elaborate to the requisite macrolactamization precursor. This macrolactamization approach was readily scaled to provide grams of FK228 for evaluation, thus demonstrating the advantage macrolactamization offered over macrolactonization efforts.

2.2.5 Kitastatin

In 2007, two novel cyclic depsipeptides, kitastatin and respirantin, were isolated and demonstrated especially potent cytotoxic activity, specifically against pancreatic tumor cells (BXPC-3, GI_{50}= 6.6 ng/mL).[194] While the biological activity was intriguing, further evaluation was restricted by the quantity of material accessed via fermentation (2.6 mg of kitastatin per 380 L of fermentation broth). To address this, Batey and coworkers envisioned a convergent approach to access kitastatin and respirantin.[195] Uniquely, these ester-rich depsipeptides contain a single amide linkage within the 18-membered macrocycle, which was constructed via macrolactamization. The requisite macrocyclization precursor was prepared following a series of intermolecular esterification reactions followed by concomitant deprotection of the terminal *N*-Boc and *tert*-butyl ester. Macrolactamization was accomplished with HATU and further elaboration afforded kitastatin (Figure 46).

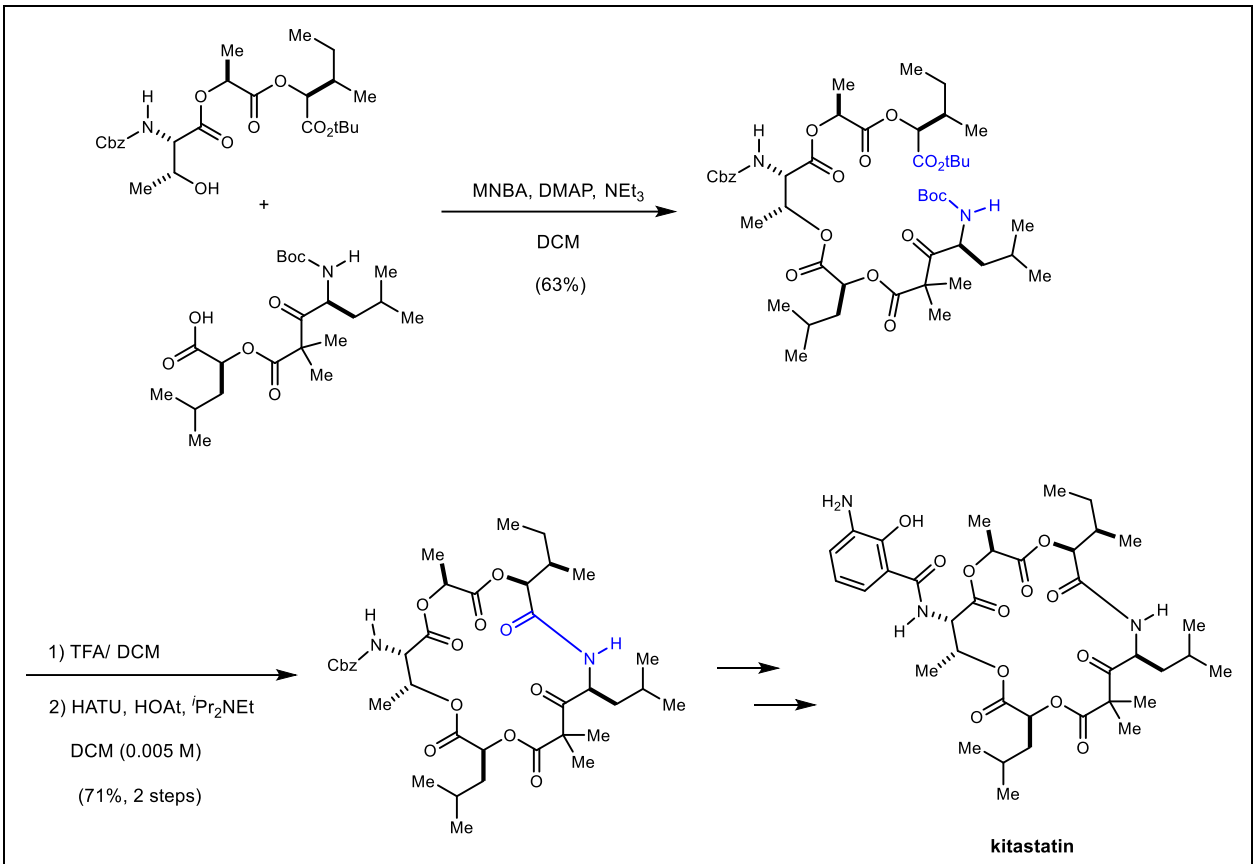

Figure 46. Macrolactamization approach to access kitastatin.

However, a macrolactamization approach might not be a viable synthetic strategy given functionality present on the *seco*-acid, observed epimerization in the macrocyclization step, or premature cleavage of the endo-ester linkage. In these cases, a macrolactonization approach serves as a suitable alternative.

2.3 Macrolactonization approaches to access privileged cyclic depsipeptides

Macrolactonization approaches are considerably more challenging and often low-yielding or failing to produce the desired macrocycle. To this end, numerous protocols have been developed to address these challenges including Corey-Nicolaou, Yamaguchi, Boden-Keck, Mitsunobu, Shiina, and other macrolactonization conditions. [ref]

2.3.1 Calipeptins B and M

Callipeptins B and M are depsipeptidic natural products isolated from marine sponges and characterized by potent cytotoxicity.[196] [197] [198] Previous syntheses of callipeptin natural products were constructed via elaboration of the C-terminus and completed with a macrolactamization.[199] However, these approaches were limited in their ability to prepare callipeptin analogues. Konno and coworkers envisioned a macrolactonization approach to access the macrocycle and analogues for biological evaluation.[200] To this end, the authors constructed the *seco*-acid using Fmoc solid-phase peptide synthesis (SPPS) (Figure 47). Evaluation of a series of macrolactonization activation methods revealed conversion to the desired macrocycle albeit with low to modest conversion (13-44% yield). Notably, construction of the macrocycle occurred at the hindered hydroxyl of a threonine residue, which might account for the low yield.

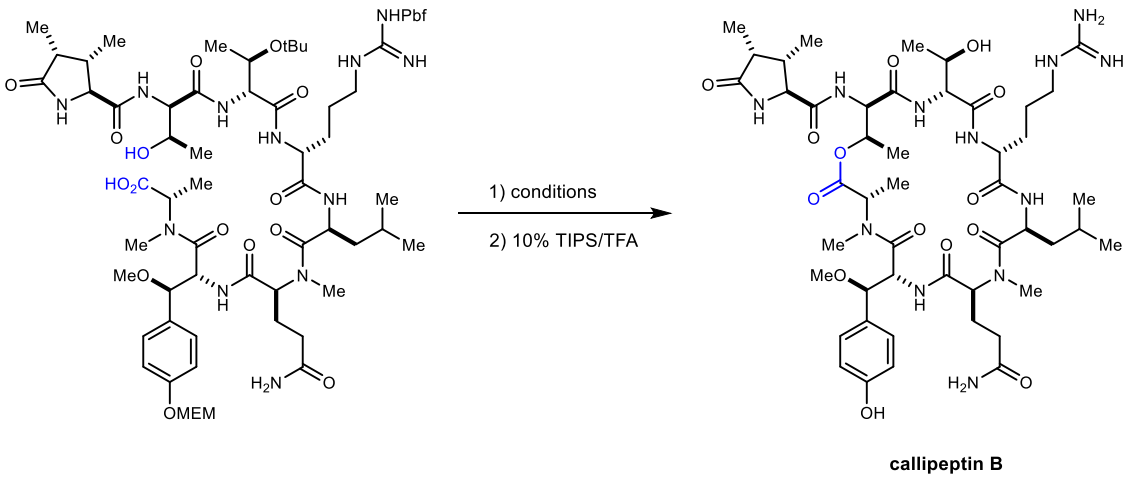

Figure 47. Macrolactonization approach to access callipeptin B.

2.3.2 Acyl Depsipeptide A54556

To address considerable challenges attributed to poor reactivity, research groups have devised creative activation methods. For example, synthesis of acyl depsipeptide A54556 was enabled by a lanthanide (III) triflate-mediated macrolactonization approach.[201] Batey and coworkers attempted several existing macrolactonization protocols none of which provided synthetically useful quantities of the desired macrocycle. It was discovered that Shiina's reagent offered the greatest conversion to the desired macrocycle (15% yield) and a reasonable starting point for optimization studies (Figure 48). Following considerable precedence using transition metal Lewis acid catalysis to promote macrolactonization, the authors investigated the use of Lewis acid additives to improve conversion.[202] [203] [204] [205]

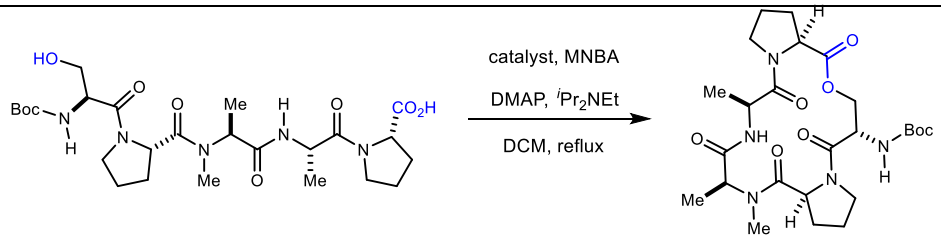

Figure 48. Lewis acid catalyzed macrolactonization to access acyldepsipeptides.

2.3.3 LI-F04a

The Fusaricidin class of cyclic depsipeptides, represented by LI-F04a, exhibit antifungal and antibacterial activity.[206] [207] However, further evaluation of this biological activity has been limited to access via biosynthetic means. Jolliffe and coworkers elected to employ a macrolactonization approach due to the readily available *seco*-acids prepared with Fmoc-SPPS.[208] Preliminary evaluation of Corey-Nicolaou, Boden-Keck, and Yamaguchi macrolactonization conditions resulted in considerable epimerization of the C-terminus during macrocyclization (Figure 49). Optimized reaction conditions utilizing modified Yonemitsu conditions improved conversion but resulted in 5-12% formation of the undesired epimer.[209] Completion of the synthesis of LI-F04a and analogues enabled further evaluation of the antifungal activity.

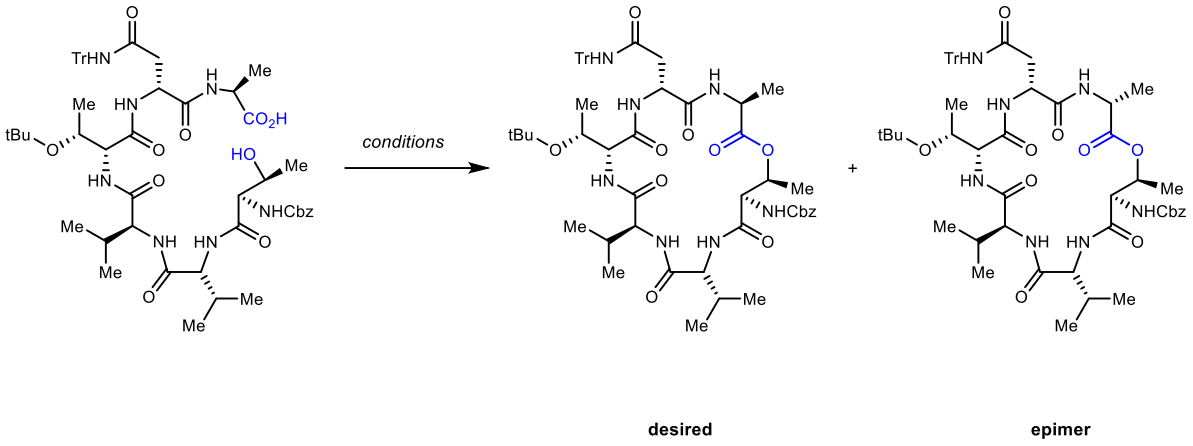

Figure 49. Macrolactonization afforded LI-F04a and its undesired epimer

2.3.4 Stevastelin B3

The stevastelins represent a family of depsipeptides that exhibit immunosuppressive activity via inhibition of dual-specificity phosphatase VHR. [210] [211] [212] Due to this clinically-relevant biological activity, Chakraborty and coworkers began a synthesis of stevastelin B3 featuring a macrolactonization to construct the 13-membered ring[213] (Figure 50). Notably, the authors report no conversion to the 15-membered ring characteristic of other stevastelins, which would result from cyclization of the C-14 hydroxyl rather than the C-16 hydroxyl. On-going efforts center on the selective construction of the 15-membered macrocycle to enable further evaluation of all the stevastelins and analogues of interest.

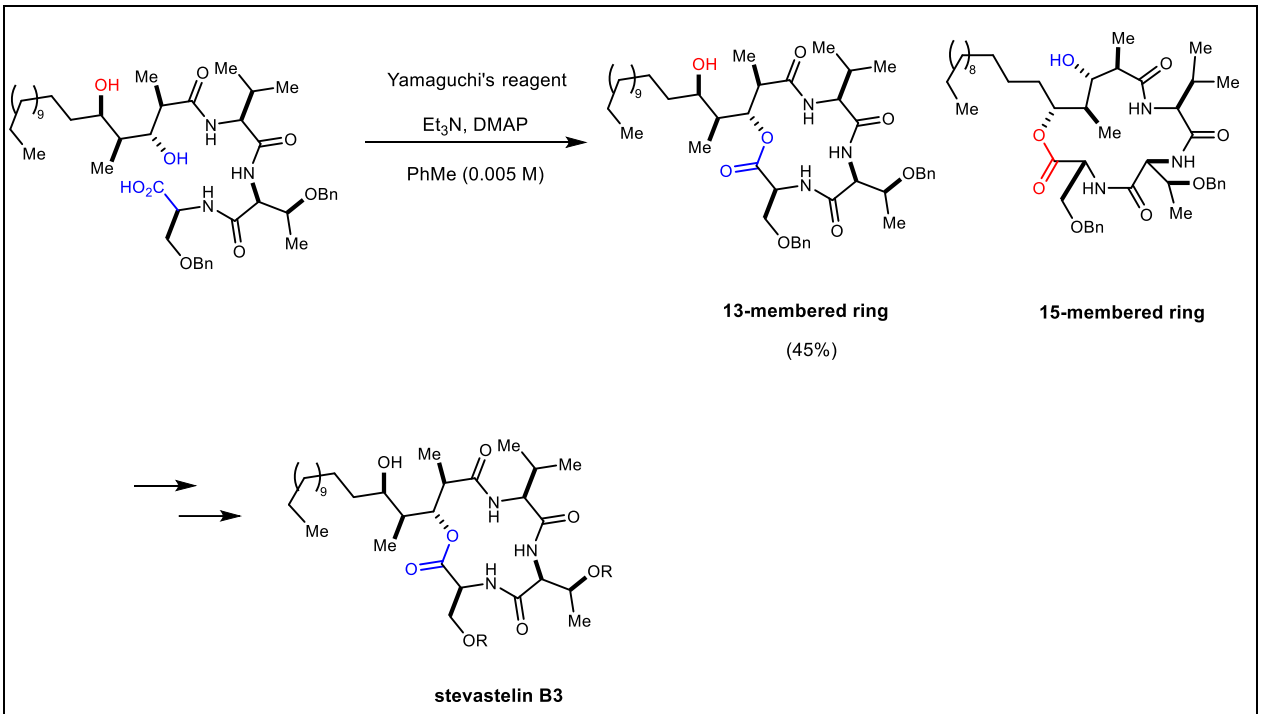

Figure 50. Yamaguchi macrolactonization to access the stevastelins.

Although numerous groups have developed creative approaches to access cyclic depsipeptides, macrolactonization and macrolactamization efforts often are inefficient and require optimization dependent on the substrate.

2.4 Alternative macrocyclization methods to access cyclic depsipeptides

Given the challenges associated with the synthesis of cyclic depsipeptides, researchers have identified novel approaches that deviate from conventional carboxylic acid activation methods. These strategies have enabled successful preparation of numerous depsipeptides and undoubtedly encourage the development of additional methods to access these privileged scaffolds.

2.4.1 Chondramide C

F-Actin is a filamentous polymer, which is involved in several cellular processes and essential for cell division.[214] [215] Several natural products, such as chondramide C, have been reported to stabilize F-actin, resulting in modulation of cytoskeleton maintenance. Synthetic efforts to access chondramide C and related natural products have been pursued to further explore this activity. Previous efforts to access other family members featured a macrolactonization to furnish the 18-membered macrocycle.[216] In contrast, Waldmann and coworkers sought to construct the macrocycle via ring-closing metathesis (Figure 51).[217] The authors reasoned that this approach would provide inherent flexibility allowing for the incorporation of various building blocks to access chondramide derivatives as well as assign the configuration of all stereocenters.

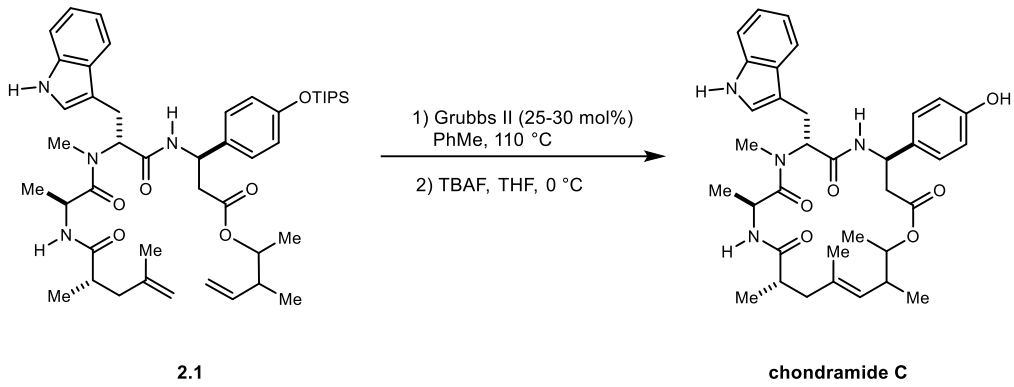

Figure 51. Ring closing metathesis approach to access chondramide C.

The macrocyclization precursor **2.1** was prepared using solid-phase peptide synthesis (Figure 51). Treatment of **2.1** with Grubb's second-generation catalyst under refluxing conditions afforded a mixture of isomers which, following global deprotection, revealed chondramide C and three unnatural isomers. This RCM approach allowed for the assignment of the configuration of all stereocenters of the natural product and established that the configuration at C7 is significant for actin stabilization.[217] This C-C bond forming approach enabled the successful synthesis of chondramide c and derivatives for further study.

2.4.2 Nannocystin A

The nannocystins constitute a class of 21-membered cyclic depsipeptides isolated from myxobactiera *Nannocystis* sp. MB1016, which possesses anti-cancer activity across 14 cancer cell lines, including drug-resistant cell lines.[218 219] uniquely, nannocystin A features an α,β-epoxy amide, consecutive *E*-alkenes, and nine stereocenters within the macrocycle. Its potent anti-proliferative activity and synthetic challenge prompted numerous research groups to pursue synthetic endeavors.

Ye and coworkers reported the first total synthesis of nannocystin A employing an intramolecular Suzuki cross-coupling (10 steps LLS, 32.5% overall yield). (Figure 52)[220] The authors reasoned that this convergent approach would allow for rapid construction of the macrocyclization precursor and preparation of analogues for SAR. Three unique fragments were coupled together via amide-bond forming reactions to afford the linear macrocyclization precursor. A subsequent intramolecular Suzuki coupling smoothly afforded nannocystin A in high yields (88%) providing ample material to reproduce the anti-proliferative activity in several colon cancer cell lines (IC_{50}= 4.4-12.2 nM) as well as liver cancer cell lines (IC_{50}=0.5-1.2 nM).

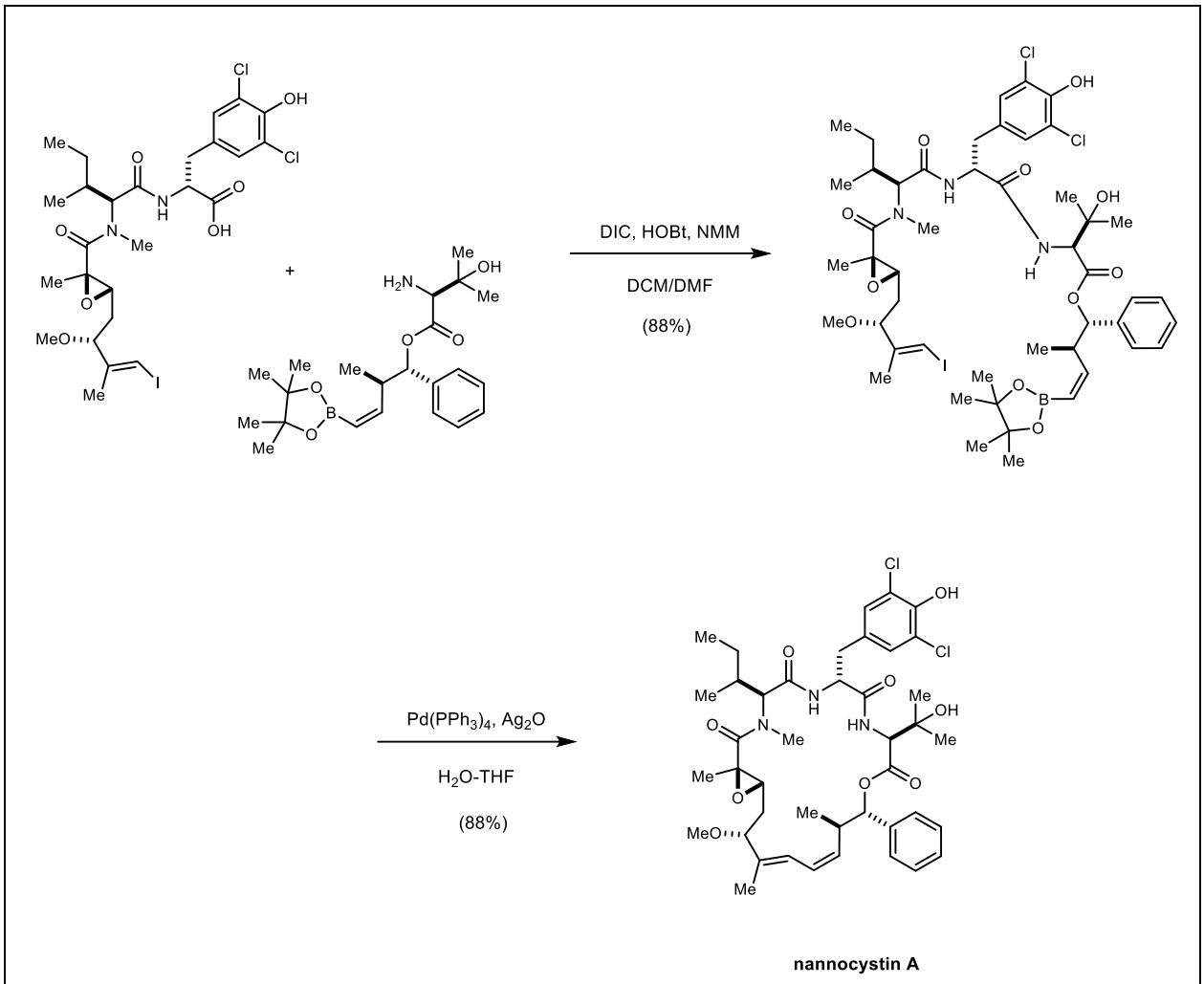

Figure 52. Ye's intramolecular Suzuki reaction provided nannocystin A.

Shortly thereafter, Chen and coworkers envisioned a Heck cross-coupling strategy to access the 21-membered macrocycle.[221] Chen's approach constitutes the same macrocyclization disconnection as Ye's reported approach. In contrast, the macrocyclization precursor instead contained terminal olefin and vinyl iodide coupling partners (Figure 53). To this end, they employed a series of amide bond-forming reactions to construct the linear precursor, which was subjected to a $Pd(OAc)_2$-mediated, intramolecular Heck coupling to yield nannocystin A (10 steps LLS, and 4.1% overall yield). Current efforts center on the preparation of analogues via incorporation of diverse building blocks. The authors sought to identify the minimal pharmacophore, which is responsible for the potent anti-proliferative activity. Notably, each of the approaches toward nannocystin A employed a C-C bond-forming reaction rather than a macrolactonization or macrolactamization approach.

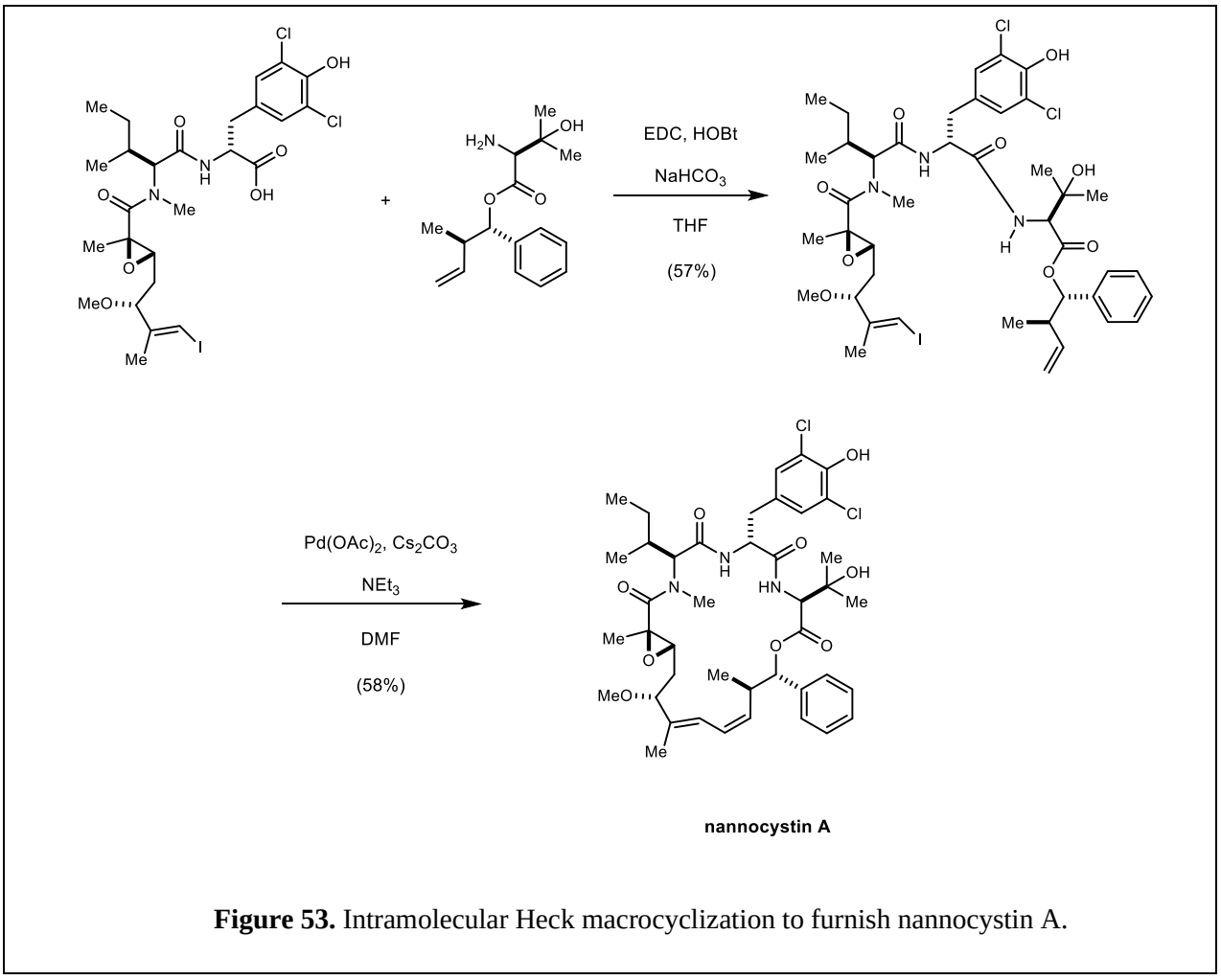

Figure 53. Intramolecular Heck macrocyclization to furnish nannocystin A.

2.4.3 Seongsanamide E

Hutton and coworkers recently demonstrated the preparation of cyclic peptides via late-stage silver(I)-promoted macrolactamization of thioamides.[222 223] This macrocyclization approach is facilitated by the propensity for thioamides to generate isoimides that undergo facile intramolecular acylation reactions to generate cyclic peptides. They have since extended this methodology to prepare cyclic depsipeptides via silver(I)-promoted macrolactonization.

This approach enabled the efficient preparation of both seongsanamide E and kahalalide E (Figure 54).[224] This unique approach circumvents many of the challenges associated with macrolactamization and macrolactonization approaches to access cyclic depsipeptides. Further, it demonstrates the creativity with which chemists develop methodology to access challenging targets.

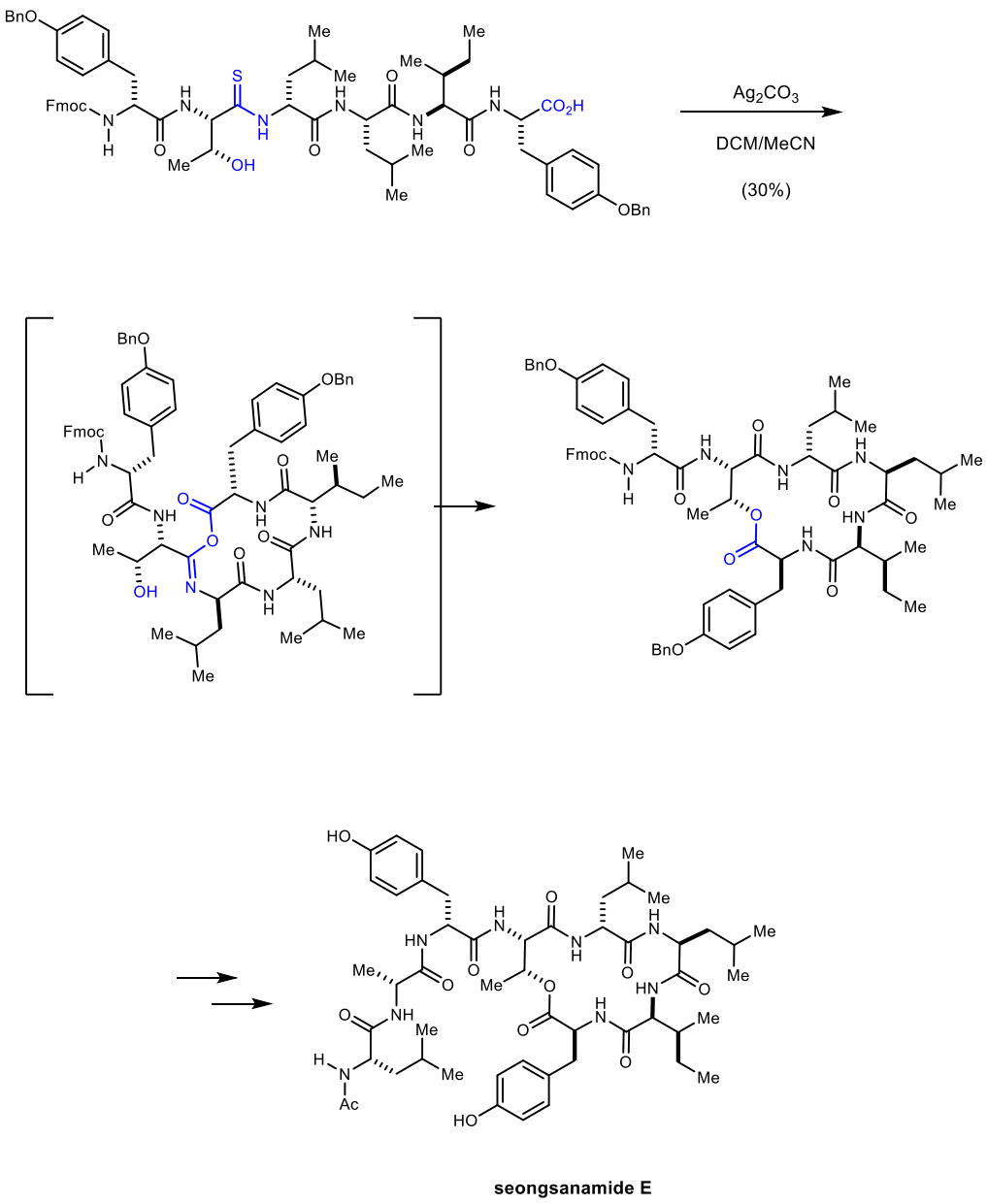

Figure 54. Silver(I)-promoted macrolactonization approach to access seongsanamide E.

2.4.4 Macrocyclooligomerization approach to verticilide and bassianolide

The construction of larger macrocycles is reportedly more challenging and as such chemists have sought alternative approaches to rapidly gain access to these clinically-relevant scaffolds. To this end, Johnston and coworkers reported an alternative macrocyclooligomerization (MCO) approach to access cyclic depsipeptides, such as verticilide and bassianolide (Figure 55).[225]

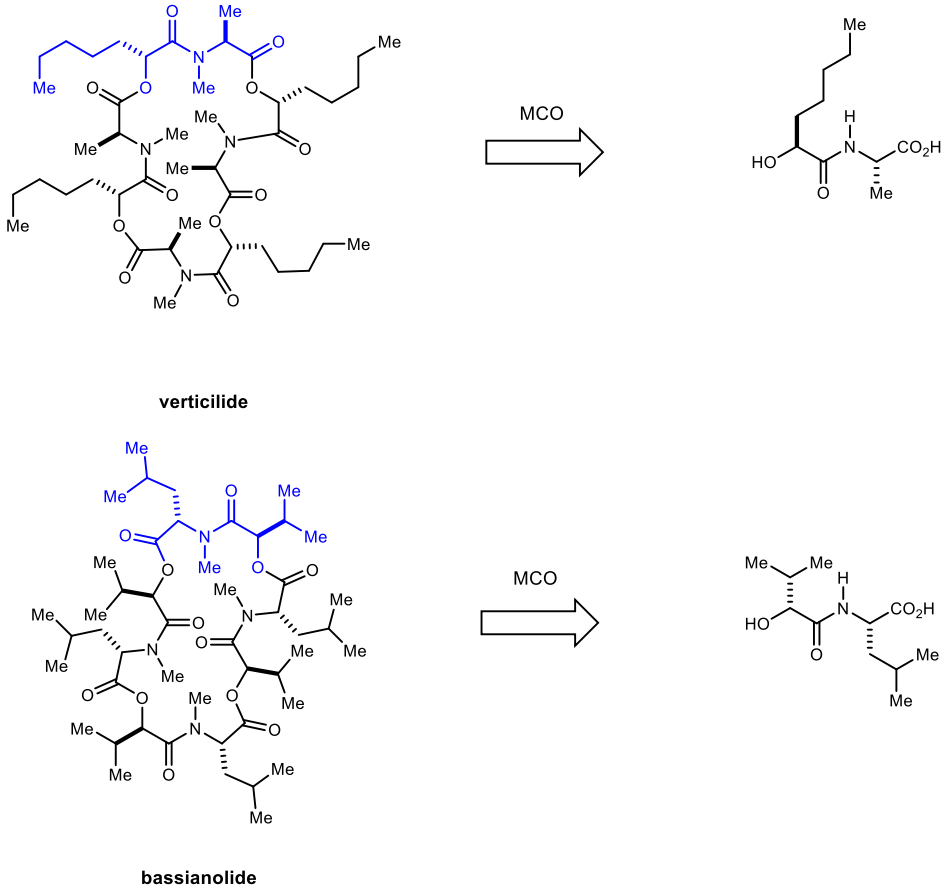

Figure 55. Macrocyclooligomerization approach to access verticilide and bassianolide.

A repeating dipeptide unit was identified and utilized in optimized MCO conditions to give desired macrocycles. A subsequent permethylation yielded verticilide in six steps (Figure 56). This approach represents an improvement in efficiency over the previously reported 14-step synthesis.[226]

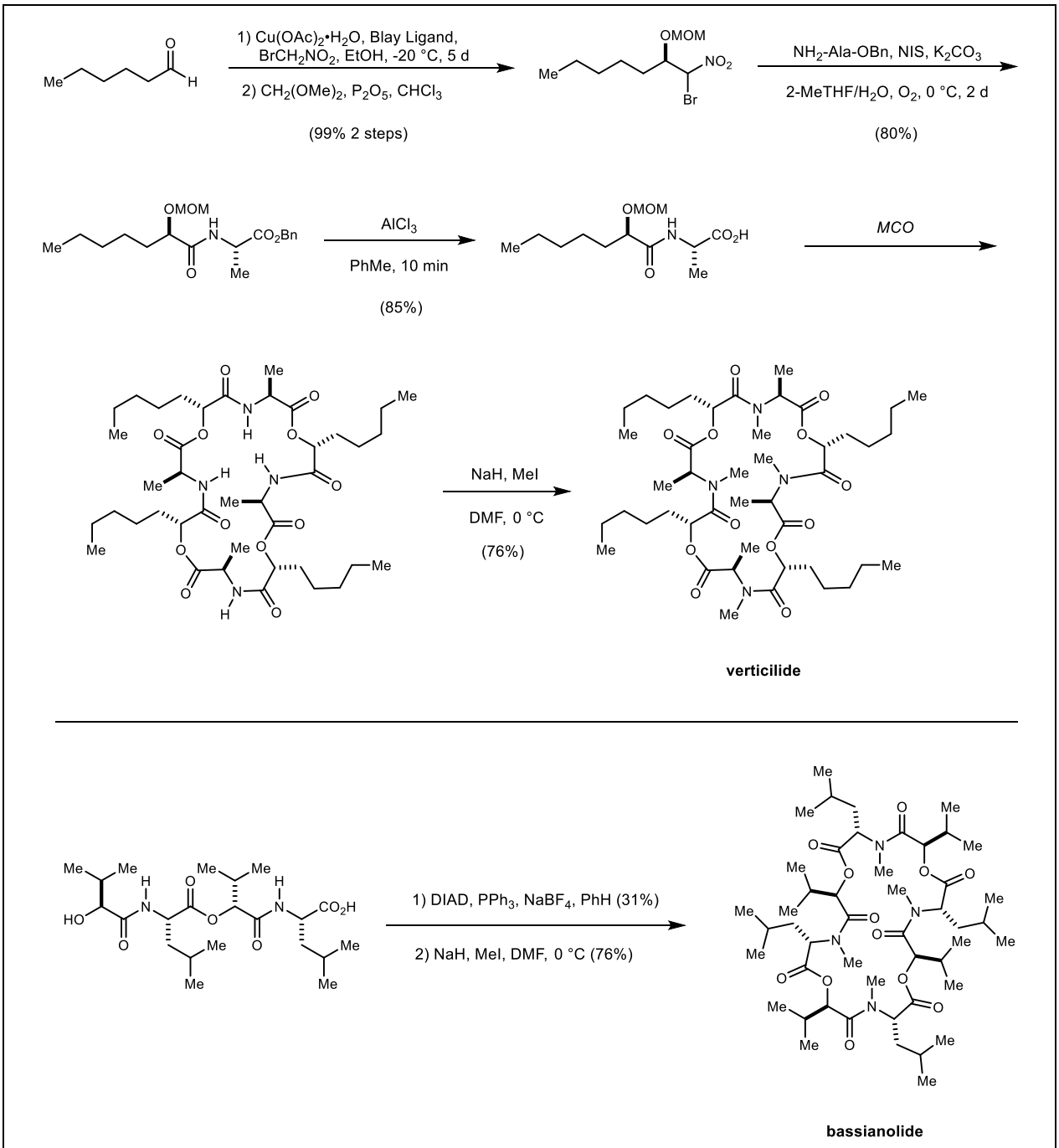

Figure 56. MCO approach to access verticilide and bassianolide.

Furthermore, this MCO approach provided rapid access to several unnatural analogues, including various large ring sizes, which are more challenging to construct via linear synthetic strategies. By varying the dipeptide building block incorporated in the macrocyclization, Johnston and coworkers were able to access a large, diverse library of verticilide analogues enabling further biological study. On-going efforts center on the development of verticilide analogues with improved potency and cell-permeability. Undoubtedly, the preparation of such analogues is enabled by this robust and efficient macrocyclooligomerization approach.

2.4.5 Ring expansion reactions

Similarly, Unsworth and coworkers reported their own efforts to develop an iterative approach to access macrocyclic natural products possessing lactones.[227] Large macrocycles are notably challenging to make due to the energetic requirement to affect an end-to-end cyclization event from a linear precursor. Successful macrocyclizations are largely substrate-dependent and conformational constraints can impede progression down the desired reaction pathway over competitive oligomerization or epimerization pathways. This substrate dependence has rendered the identification of a generalizable method more challenging and often requires the evaluation of numerous macrocyclization conditions to identify a successful condition.

Unsworth and coworkers report the preparation of macrolactones employing a Successive Ring Expansion approach (SuRE). First, they evaluated α-hydroxy acids that result in 8- to 13-membered cyclic imides that smoothly undergo ring expansion to yield the desired macrocycles in good yields (83-97%). (Figure 57) This was also successful with β-hydroxy acids ranging from 6- to 13-membered cyclic imides that were converted effectively to the desired macrocycles. Uniquely, prepared macrocyclic lactones could be further elaborated to include numerous depsipeptidic linkages. While this work only features a few examples of substituted depsipeptides, it represents a unique starting point for rapid preparation of diverse libraries.

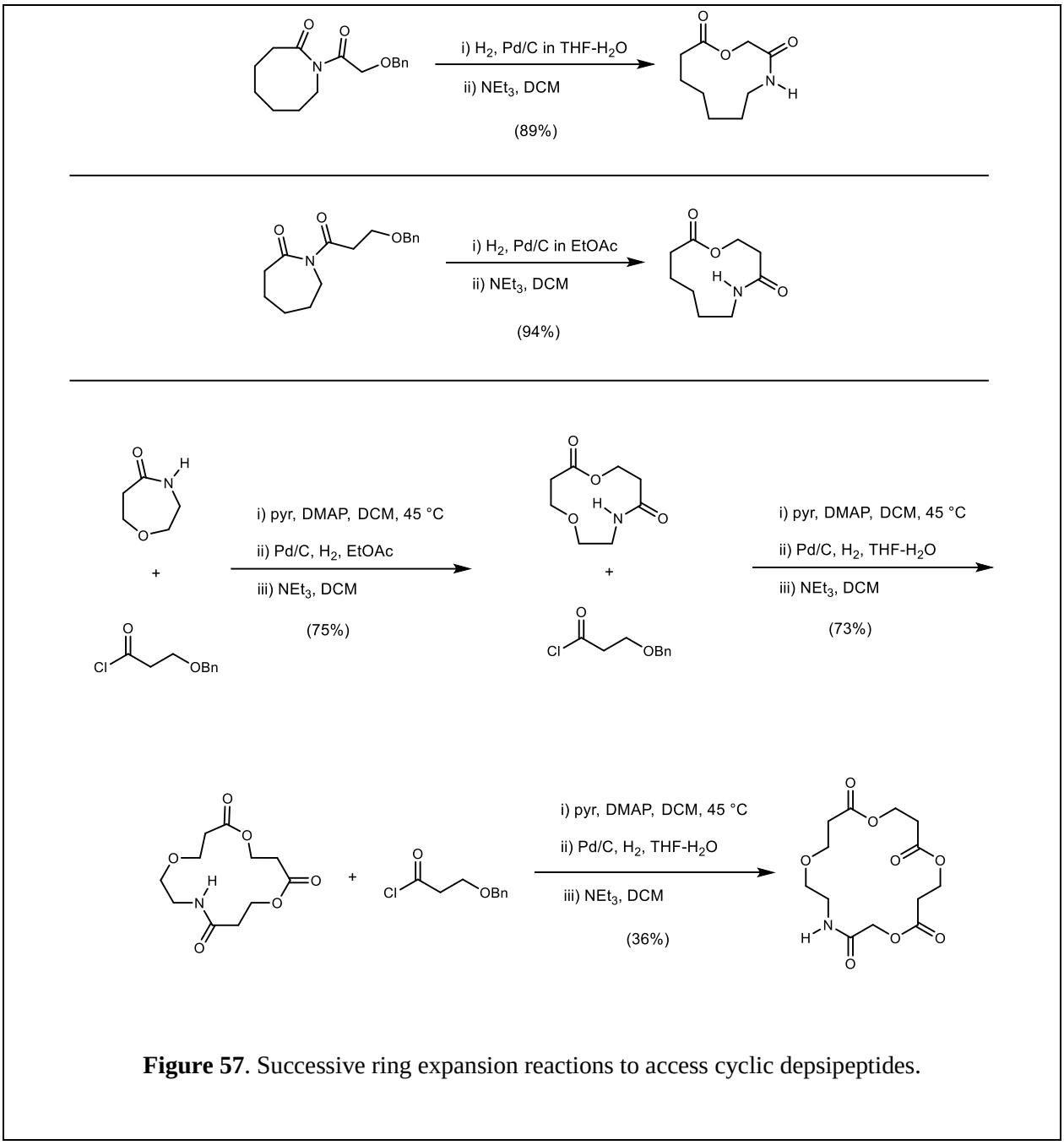

Figure 57. Successive ring expansion reactions to access cyclic depsipeptides.

2.4.6 *In vitro* ribosomal synthesis

The preparation of cyclic depsipeptides via chemical synthesis remains a challenge, which has prompted Suga and coworkers to consider a biosynthetic approach to construct macrocyclic depsipeptides of various ring sizes.[228] A self-acylating motif (Ser-Pro-Cys-Gly) was identified which was capable of *in vitro* trans-thioesterification and undergoes a selective *S*-to-*O* acylation resulting in macrocyclization(Figure 58). This approach allows for the high-throughput construction of a large library of cyclic depsipeptides possessing 7 to 17 residues. Further evaluation revealed that there is also flexibility in the acylation motif allowing for greater diversity in the sequences of the constructed macrocycles.

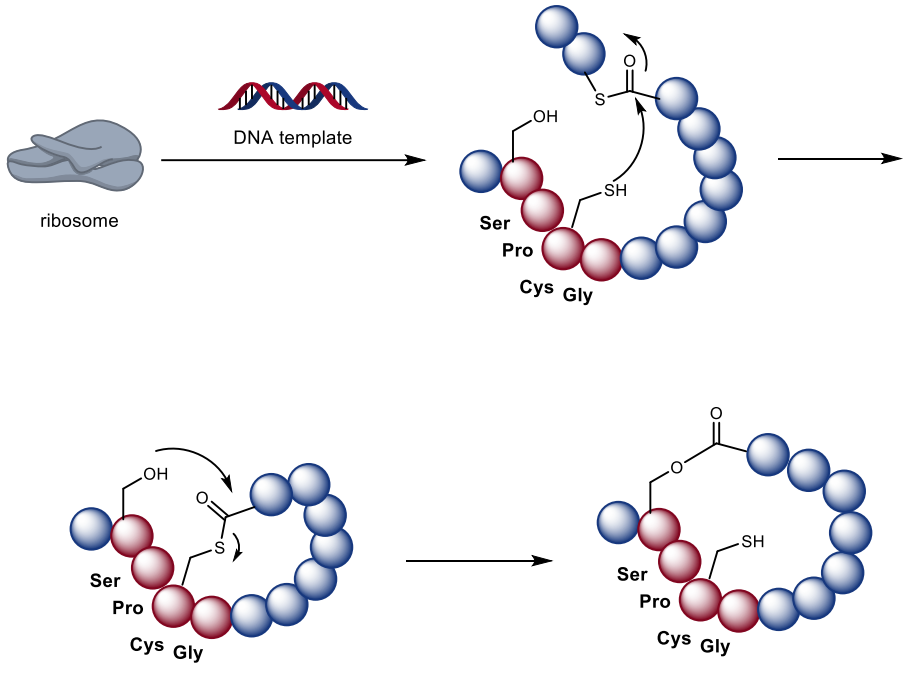

Figure 58. In vitro ribosomal preparation of cyclic depsipeptides.

Together these studies represent alternative approaches to conventional macrolactonization or macrolactamization strategies, which offer advantages in efficiency, robustness, and generation of analogues.

2.5 Synthesis of aryl glycine containing natural products

2.5.1 Feglymycin

In 1999, the novel peptide feglymycin was isolated from *Streptomyces* sp. DSM11171, which was found to exhibit both anti-viral and anti-bacterial activity (Figure 59).[229] Notably, nine of the thirteen amino acids in feglymycin are arylglycine residues, which are prone to racemization during chemical synthesis. This challenging structural feature required careful consideration in the design of a synthetic strategy and identification of suitable reaction conditions.

Due to its ability to inhibit the formation of HIV syncytia and challenging structural features,

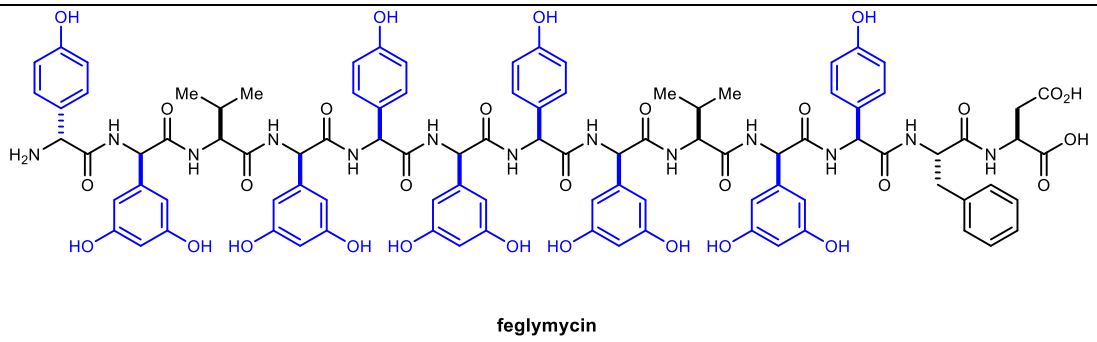

Figure 59. Aryl glycine-rich peptide feglymycin.

Süssmuth and coworkers embarked on a total synthesis of feglymycin and its enantiomer.[230] The synthetic endeavors also provided fragments, which provided preliminary structure-activity relationship (SAR) studies and enabled the identification of relevant motifs for anti-HIV activity. The foremost challenge in this synthetic endeavor was attributed to the propensity of arylglycine residues to epimerize during chemical synthesis. The prevalence of these residues required special considerations for coupling the sensitive arylglycine building blocks and the design of a protecting group strategy to mitigate the epimerization of the *C*-terminus. Furthermore, late-stage separation of diastereomeric mixtures of advanced fragments was not feasible. To this end, Süssmuth and coworkers sought conditions that would avoid mixed anhydride formation at the *C*-terminus of DPG residues (Figure 60). The authors reasoned a convergent approach would allow for efficient coupling with minimized activation of the DPG residues. To this end, larger

fragments would be constructed and then coupled together as opposed to an iterative approach where the *C*-terminus is elongated one residue followed by another.

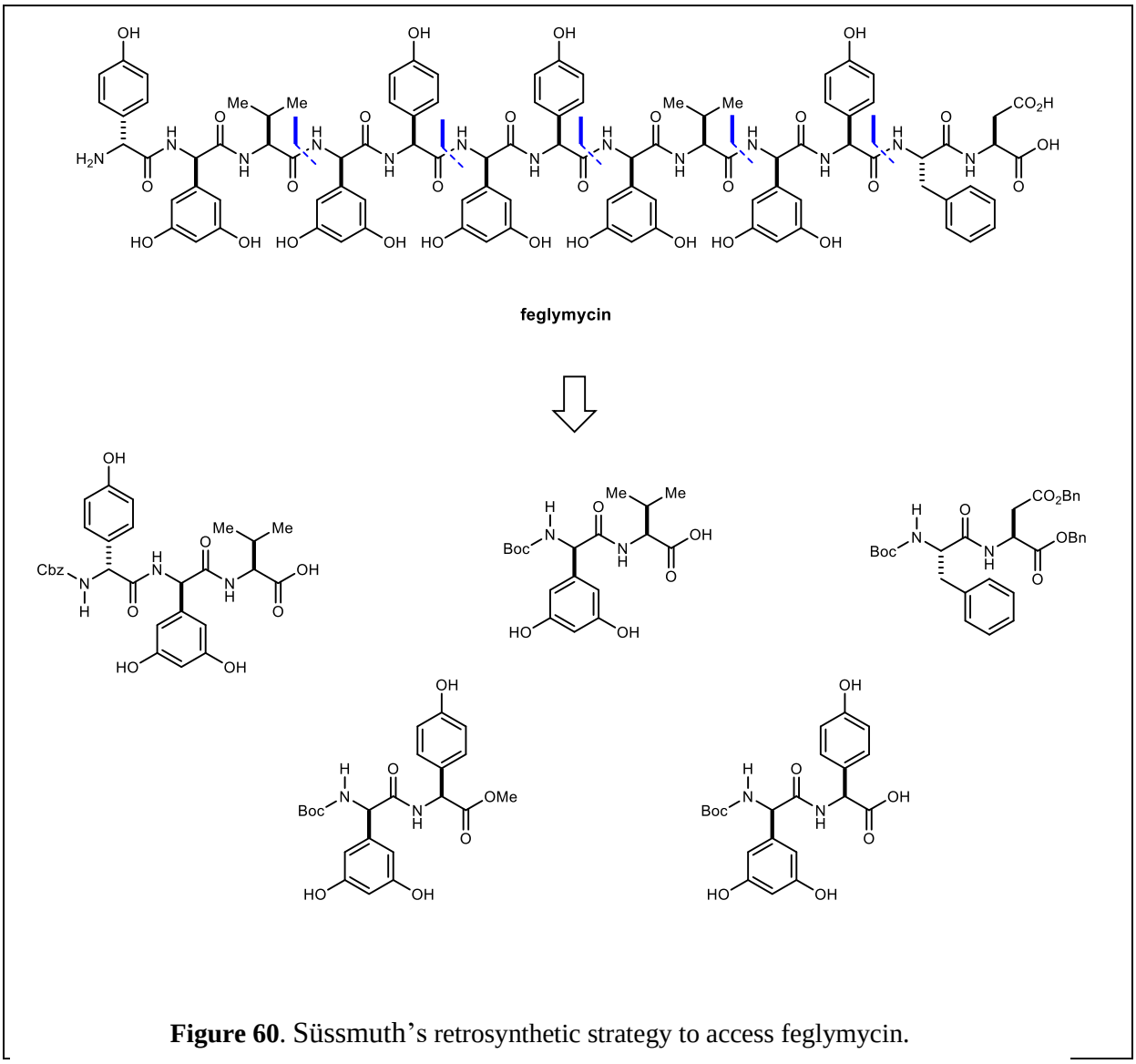

Figure 60. Süssmuth's retrosynthetic strategy to access feglymycin.

Synthesis began with preparation of the requisite aryl glycine building blocks. Following precedence in the synthesis of other arylglycinamides, the aryl glycine residues were prepared via Sharpless asymmetric aminohydroxylation followed by oxidation to the desired carboxylic acid (Figure 61).

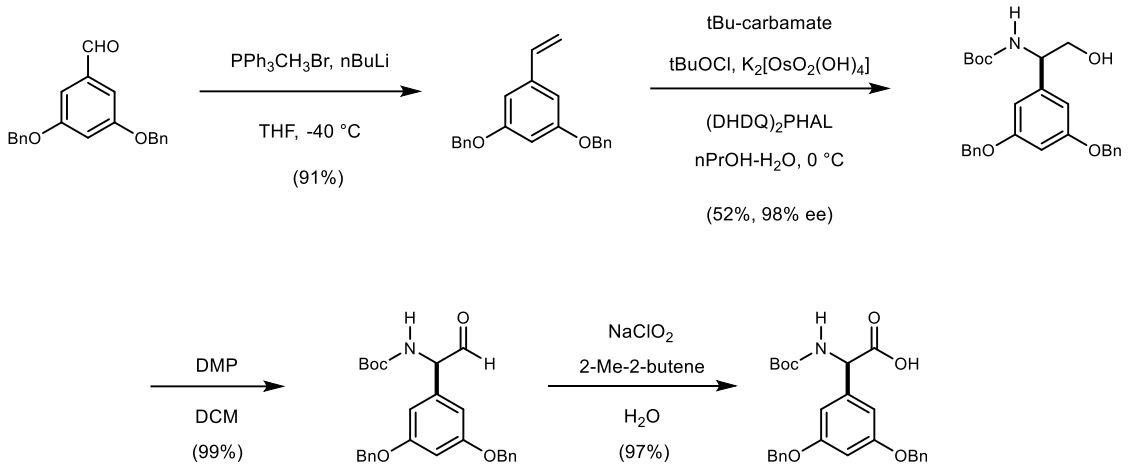

Figure 61. Preparation of DPG amino acids for feglymycin using Sharpless asymmetric aminohydroxylation.

DPG-building block **X.X** could then be coupled with suitably protected residues to provide access to the larger fragments necessary for synthesis of feglymycin (Figure 62). The peptide coupling reactions were conducted with DEPBT and $NaHCO_3$. The authors note any deviation from these conditions resulted in racemization of the arylgylcine residues or diminished conversion. Further, an especially challenging solubility profile for larger fragments was highlighted, specifically when side chains were fully protected. This ultimately complicated synthetic efforts and required deprotection of sidechains to enable completion of the synthesis.

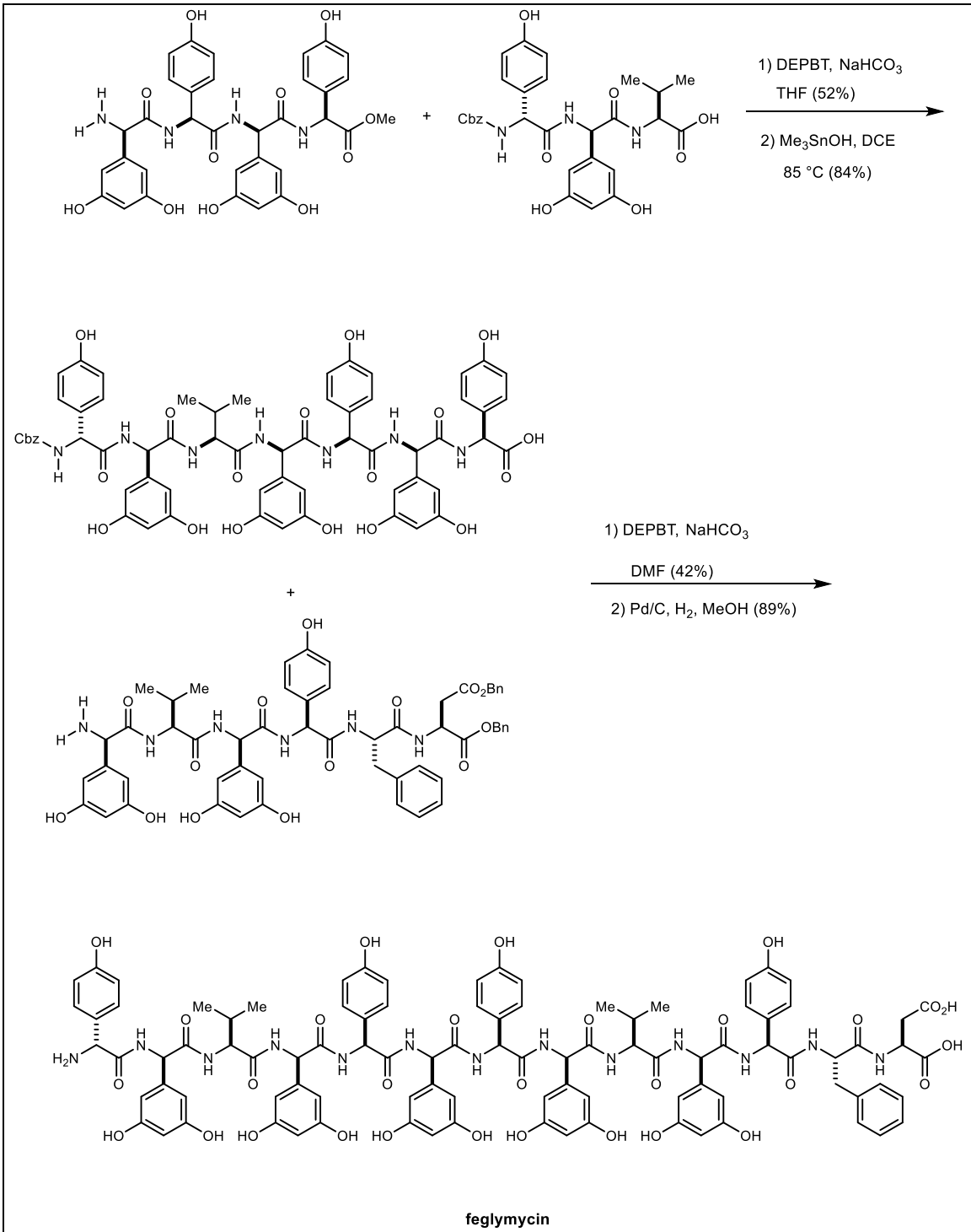

Figure 62. Coupling of fragments to and global deprotection to access feglymycin.

Uniquely, Süssmuth demonstrated the utility of the methyl ester protecting group in this synthesis. Deprotection of the methyl ester was accomplished with trimethyltin hydroxide without epimerization.[231] This represents the first reported synthesis of the antiviral peptide feglymycin, which enabled further evaluation of its anti-HIV and antibacterial activity.[232]

Due to challenges with solubility, racemization, and purification, Süssmuth and coworkers employed a convergent approach to access feglymycin. To address some of these challenges, Fuse and coworkers reported a distinct approach to feglymycin employing a micro-flow technology.[233] Their goal was to prepare arylglycine-rich feglymycin in a linear fashion, which contrasted Süssmuth and coworkers convergent synthetic strategy. Fuse and coworkers demonstrated that the micro-flow approach suppressed undesired epimerization during synthesis and allow for precise control of reaction time and temperature. This approach boasts rapid coupling times (≤5.3 s), amenability to reaction scale-up, and ease of analog preparation. Further, this micro-flow approach enabled elongation of the *C*-terminus of racemization-prone arylglycine residues.

2.5.2 Ramoplanin A2

Ramoplanin represents a glycodepsipeptide isolated from Actinoplanes sp ATCC 33076. [234]. [235] Further characterization revealed potent antibacterial activity (MIC= 0.5 μg/mL) of methicillin-resistant *enterococci* and methicillin-resistant *S. aureus* (MRSA). In addition to its unique antibacterial activity, ramoplanin also possesses a 49-membered macrocycle that contains 17 residues (12 non-canonical and 7 D-amino acids) and one ester linkage.[236] [237] Notably, the macrolactone is formed between the *C*-terminus of the 3-chloro-4-hydroxyphenylglycine (Chp) residue and the hydroxyl of the β-hydroxy-asparagine (HAsn).

Boger and coworkers embarked on the synthesis of ramoplanin and analogues to enable rapid evaluation of key structural features which are responsible for antibacterial activity.[238] The authors envisioned a convergent approach would divide the 49-membered macrocycle into three unique fragments: heptapeptide, pentadepsipeptide, and pentapeptide (**Figure 63**). The strategic coupling sites were selected to minimize epimerization, minimize protecting group manipulations, and facilitate macrocyclization. The authors note that several of the Hpg residues were especially sensitive in amide couplings. If DEPBT was not used for these coupling, the authors report decreased yields and substantial epimerization.

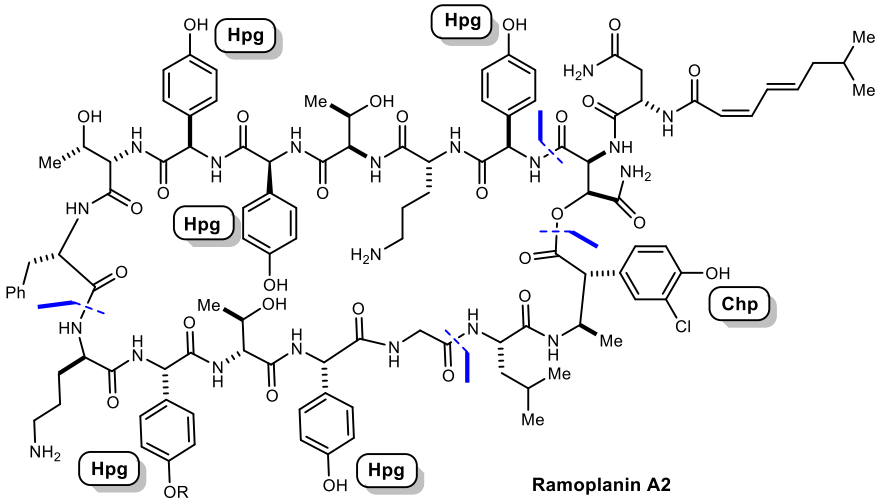

Figure 63. Synthetic strategy to access ramoplanin A2.

Synthesis of the depsipeptide fragment proved especially challenging. Specifically, the intermolecular esterification with the C-terminus of the racemization-prone Chp residue. In order to achieve the desired transformation without epimerization, extremely specific reaction conditions were required. Optimized conditions required activation of the Chp residue with EDCI in the presence of catalytic DMAP for one hour at 0 °C (Figure 64**Error! Reference source not found.**). Any slight deviations from these conditions, such as increasing reaction time, reaction temperature, or equivalents of DMAP, would compromise both conversion and diastereoselectivity.

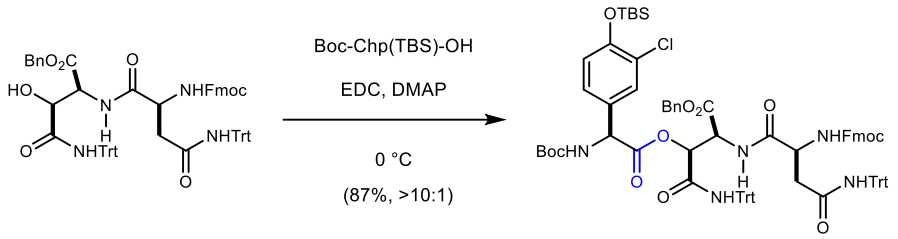

Figure 64. Intermolecular esterification of Chp residue toward the synthesis of ramoplanin.

Upon successful preparation of the requisite fragments, Boger and coworkers began assembly of the macrolactamization precursor. Notably, the depsipeptidic bond proved to be particularly labile. The use of strong tertiary amine bases led to competitive hydrolysis or β-elimination. Further, exposure of the product to methanol resulted in hydrolysis/methanolysis of the depsipeptidic bond. This rendered late-stage modifications and even transfer of isolated products more challenging. Nonetheless, Boger and coworkers persevered and eventually reported the first total synthesis of ramoplanin and its aglycone (Figure 65**Error! Reference source not found.**). These initial synthetic studies enabled future preparation of analogues, which were utilized to explore ramoplanin's unique mechanism of action.[239]

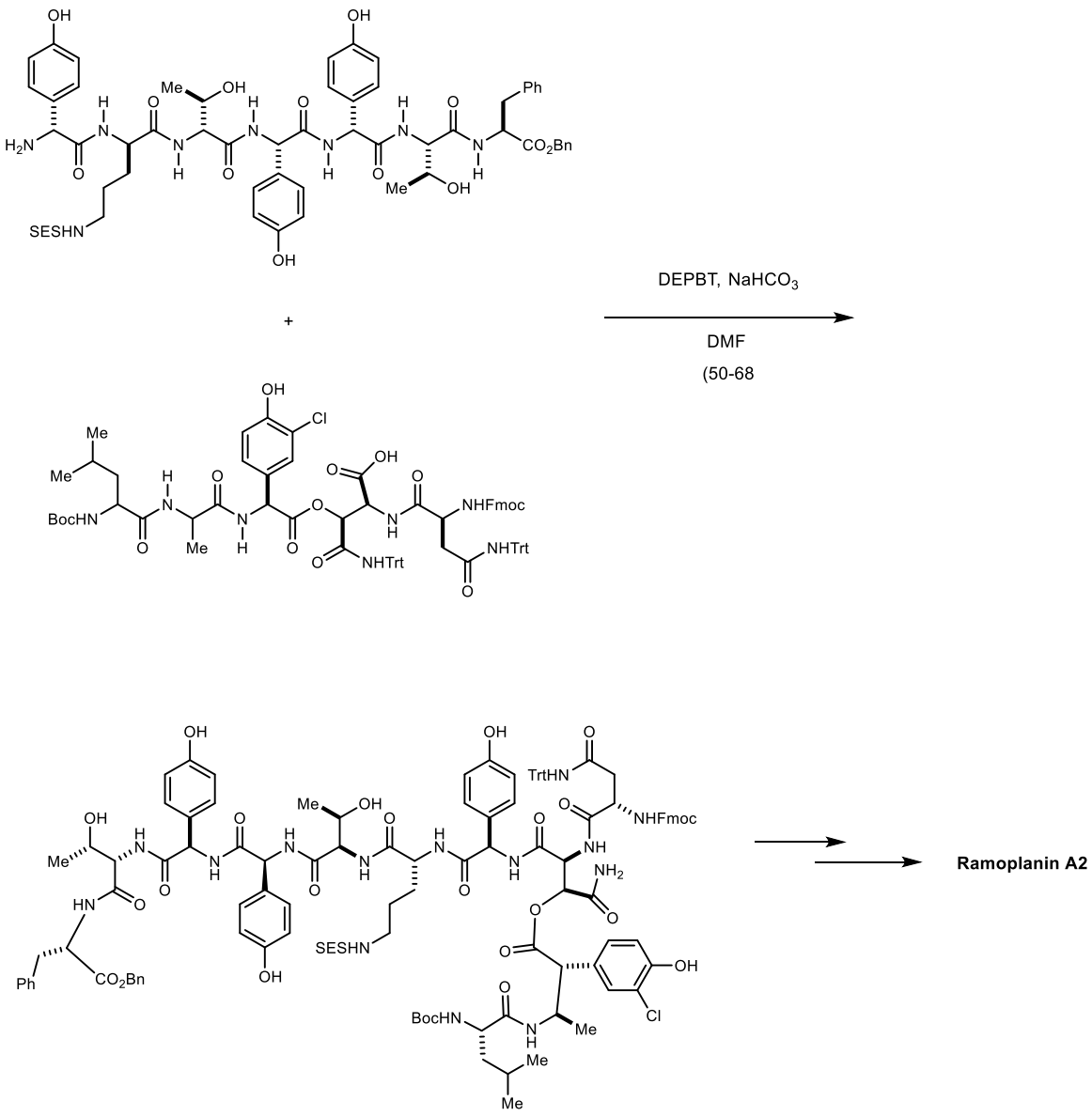

Figure 65. Assembly of fragments to complete the synthesis of ramoplanin A2.

In particular, this work highlights several unanticipated challenges associated with preparation of cyclic depsipeptides. Furthermore, it uniquely addresses the fine tuning that is required in order to balance selectivity and conversion in construction of the depsipeptidic linkage, especially when adjacent to a racemization-prone residue.

2.6 Umpolung Amide Synthesis

Numerous methods have been developed to access amide bonds in an efficient and selective manner. One such approach refers to Umpolung Amide Synthesis (UmAS), which refers to a novel amide bond forming reaction that is mechanistically distinct from other amide couplings.[240] Shen and coworkers hypothesized that an α-halo nitroalkane could be coupled with an amine in an aza-Nef reaction to give amide products.[241] Following extensive experimentation, Johnston and coworkers described the formation of amide bonds via formation of an *N*-haloamine. In this transformation, an enantioenriched α-halo nitroalkane is coupled with an activated amine. This unique activation mode was termed Umpolung Amide Synthesis (UmAS), whereby a traditionally electron-rich amine is converted to an electron-deficient *N*-haloamine or otherwise electrophilic amine. Under mildly basic conditions, the α-halo nitroalkane is converted to halonitronate, which can undergo electrophilic amination with *N*-haloamine to afford a putative tetrahedral intermediate. This key intermediate can then be converted to the amide product (Figure 66).

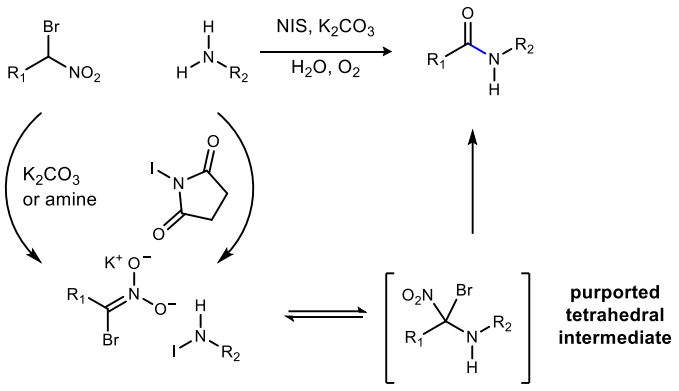

Figure 66. Amide bond formation between α-halo nitroalkane and N-haloamine

In order to further elucidate the mechanism by which UmAS furnishes amides from α-halo nitroalkanes and amines. Shackleford and coworkers considered an ^{18}O labeling strategy to identify the method by which the purported tetrahedral intermediate was converted to the isolated amides.[242] Preliminary mechanistic hypotheses centered on the introduction of the amide carbonyl oxygen from water via hydrolysis. However, incorporation of ^{18}O-labeled-H_2O in the reaction mixture revealed the oxygen was not incorporated via hydrolysis.[243] This unique observation indicated the carbonyl oxygen must come from an alternative source. Further evaluation uncovered two possible pathways by which the carbonyl oxygen could be introduced aerobically or anaerobically (**Figure 67**).

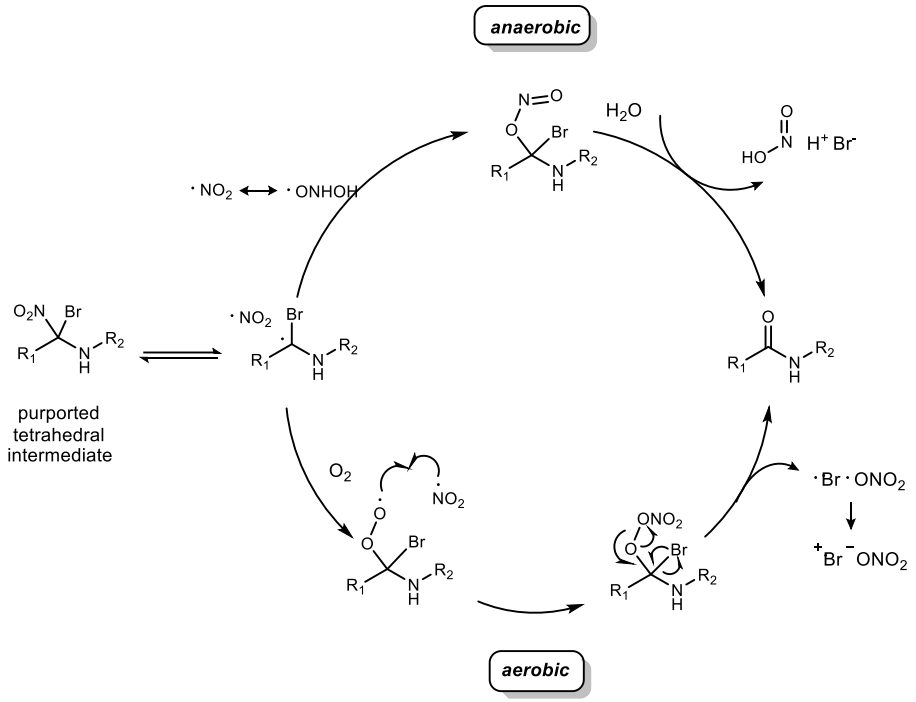

Figure 67. Possible anaerobic or aerobic pathways to convert purported tetrahedral intermediate to amide product.

Notably, the inherent polarity of the coupling partners is reversed in UmAS. This contrasts conventional condensative coupling reactions where the amine serves as the nucleophile and the carboxylic acid partner is activated (**Figure 68**). In conventional condensative approaches, the carboxylic acid is converted to an active ester intermediate upon treatment with coupling reagent. The resulting activated species can then be converted to the desired amide following treatment with amine of interest. In some cases, the α-proton of the active ester can be sufficiently acidic where epimerization is competitive with amide bond formation.

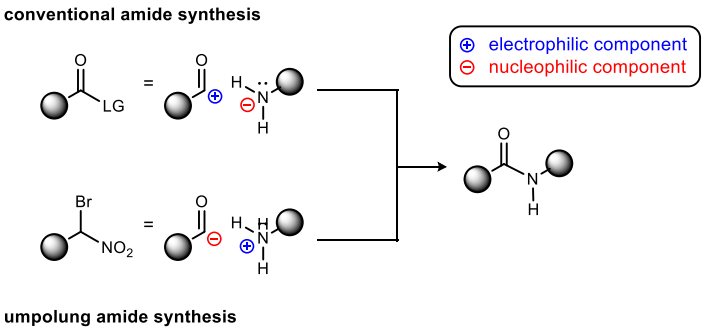

Figure 68. Comparison of UmAS to conventional amide bond forming reactions.

To date, UmAS has been applied in the preparation and on-going synthesis of numerous peptide natural products. Johnston and coworkers also began working on an alternative racemization-free approach to access the antiviral peptide feglymycin. Encouraged by early studies demonstrating the use of UmAS to access arylgycinamides, Makley and coworkers devised a first-generation synthetic strategy to access aryl glycine-rich feglymycin (**Figure 69**).

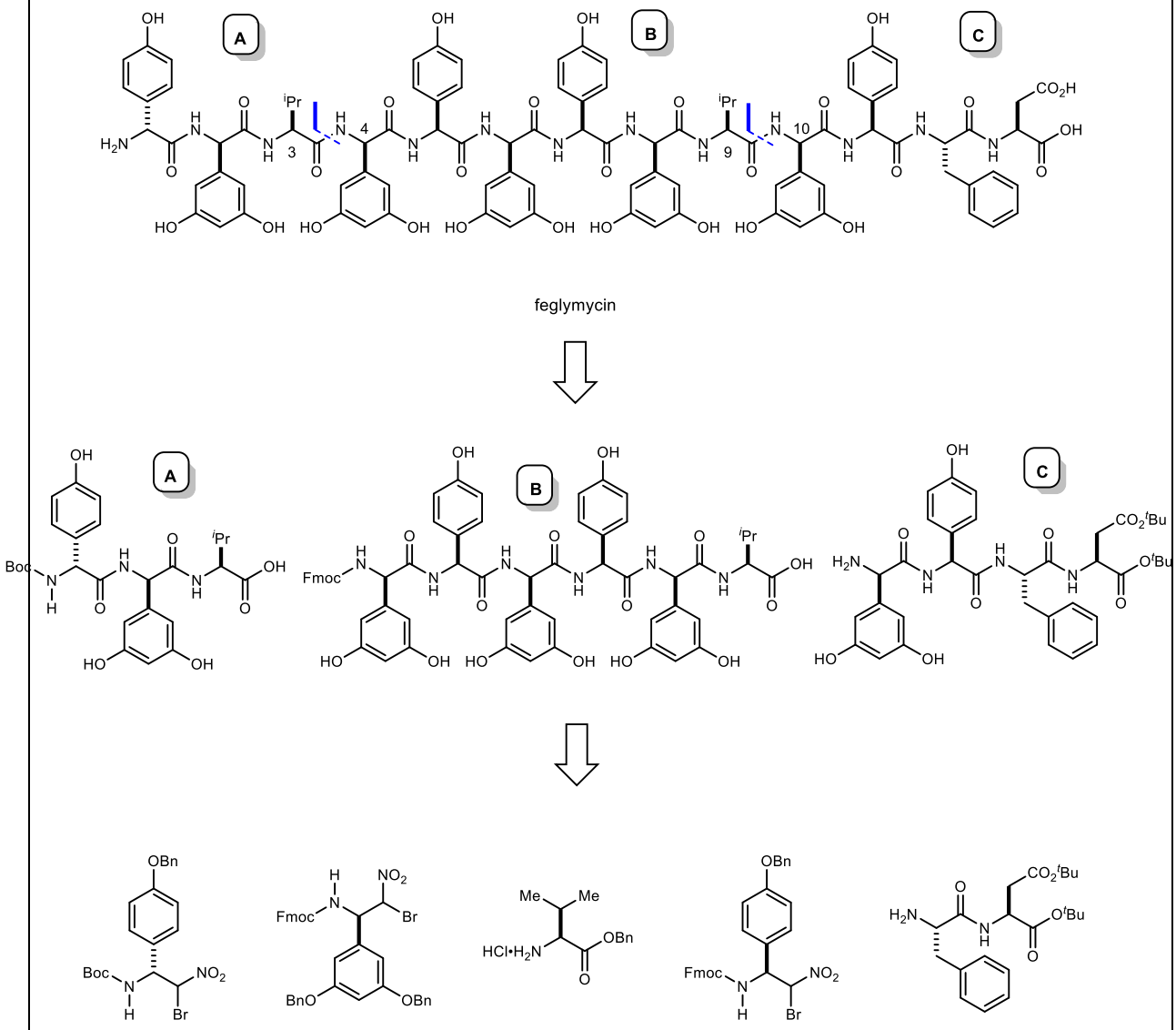

Figure 69. Early synthetic proposal to access feglymycin using UmAS.

Considerable and creative efforts were undertaken by numerous talented chemists toward incarnation of this synthetic route. However, several unanticipated challenges arose during the course of these synthetic efforts. Notably, the solubility of key intermediates and challenging purifications limited this approach. This did not deter the next generation of chemistry graduate students from developing this synthetic strategy further.

Employing this same synthetic strategy, Schweiter and coworkers were able to access a fluorinated feglymycin analog termed Ffeglymycin (**Figure 70**).[244] The authors incorporated 2,4-difluorophenylglycine residues due to their commercial availability and ease of access. To this end, the authors adapted their synthetic strategy to incorporate these difluoro residues in place of the DPG residues. This successful approach demonstrated the utility of UmAS in the preparation of an aryl glycine-rich peptide and set the foundation for future approaches to access feglymycin itself. The authors also attempted preparation of a 3,5-difluorophenylglycine analog and a 3,5-dibromophenylglycine analog. However, these approaches were abandoned due to incredibly challenging solubility profiles accompanied by challenging purifications . The authors attribute these challenges to the 3,5-substitution pattern.

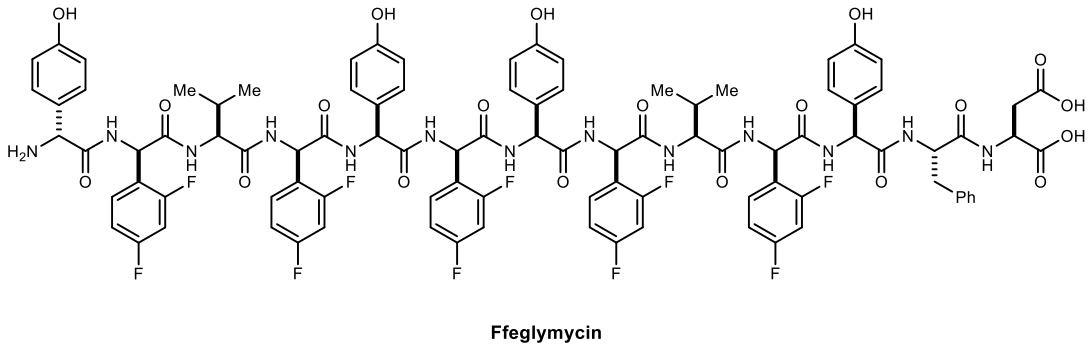

Figure 70. Structure of Ffeglymycin, a fluorinated analog of feglymycin.

Encouraged by these results, Johnston and coworkers persisted in their synthetic efforts toward feglymycin. Dr. Jade Bing and Dr. Rashanique Quarels spearheaded a third generation approach.[245] Together, their creativity and persistence culminated in the most advanced synthesis from the group to date. This significant achievement has enabled the preparation of other arylglycine natural products in the Johnston lab.

To date UmAS has also been used to access numerous biologically relevant cyclic depsipeptides. Batiste and coworkers developed synthetic strategies to access valinomycin, bassianolide, verticilide, and others.[246] Together, this body of work demonstrates the creativity with which talented chemists have utilized unique approaches and UmAS to access structurally diverse and challenging natural products.

2.7 Discovery, Isolation, and Characterization of the Cochinmicins

2.7.1 Discovery and Isolation

Endothelin-1 (ET-1) is a peptidic vasoconstrictor, which is secreted by endothelial cells in response to external stimuli and stressors. ET-1 activates two main G protein-coupled receptors referred to as ETA and ETB.[247] Overexpression of ET-1 results in downstream activation of several pathways which contribute to bronchoconstriction, angiogenesis, and neuropathic pain.[248] Further, ET-1 has been implicated in the inflammatory response, including the activation of the NF-κB pathway and overexpression of other proinflammatory cytokines.[249] This overexpression results in the stimulation and aggregation of adhesion molecules which accumulate in the arteries and result in structural modifications to the vasculature.[250] Increased expression of endothelin-1 has been observed in both experimental model systems and clinical patient populations.[251] Upregulation of endothelin-1 has been extensively documented in patients with increased disease severity.[252] Given the correlation between endothelin-1upregulation and poor disease prognosis ET-1 antagonism is considered a viable treatment option for these patient populations.

The prevalence of pulmonary arterial hypertension and related ET-1 disease pathologies has prompted significant research efforts to identify and develop endothelin-1 inhibitors. While screening for endothelin antagonists, Garrity and coworkers discovered a novel class of cyclic depsipeptides produced by gram-positive *Microbispora* sp. ATCC 55140.[253] The producing organism was isolated from a soil sample collected in Cochin, India. Culture fractionation was guided by inhibition of ET-1 binding to bovine aortic membranes. The active layers were collected and purified by column chromatography. Fractions were re-evaluated for ET-1 inhibition, the active fractions were pooled, and further purification using semi-preparative HPLC afforded three compounds referred to as 1, 2, and 3. Efforts to scale up the fermentation and subsequent isolation yielded two structurally-related natural products referred to as 4 and 5.

2.7.2 Characterization

Preliminary analysis of UV, FT-IR, and ^{1}H NMR data revealed the first three isolates contained three distinct products which possessed structural similarities.[254] The authors began efforts to elucidate the structures of the first three isolates. Isolates 2 and 3 were proposed to be isomeric based on the available NMR, HRFAB-MS data (isolate 2: m/z=924.3005, isolate 3: m/z=924.2949), and optical rotation data (isolate 2: +20.0, isolate 3: -10.0). Additionally, the respective ion clusters of isolates 2 and 3 were indicative of a chlorine present in each natural product. Similarly, the molecular formula of isolate 1 was deduced ($C_{46}H_{47}N_7O_{12}$, $[M+H]^+$ m/z: 890.3380) and unlike isolates 2 and 3, isolate 1 was found to be lacking a chlorine.

Structural analysis was predominantly conducted on isolate 2 due to its abundance relative to the other isolates. Further analysis of isolate 2 revealed a cyclic structure containing 7 residues: dihydroxyphenyl glycine (2), phenylalanine (2), *allo*-threonine (1), alanine (1), and 5-chloropyrrole-2-carboxylic acid (1). Upon treatment with methanolic HCl, isolate 2 was converted to a methyl ester indicative of a lactone in the natural product. The available ^{1}H NMR and HMBC correlations were consistent with a cyclic depsipeptide, where the lactone is formed between the hydroxyl of the *allo*-threonine and dihydroxyphenyl glycine residues. After deducing the connectivity of the residues, the authors shifted their attention to determining the absolute stereochemistry of the isolates using both α-methylbenzyl isothiocyanate and the Marfey method. Uniquely, this peptide is characterized by the incorporation of D-amino acids, especially within the macrocycle. The authors noted consistencies in the ^{1}H NMR spectra of

isolates 1 and 3. Given the low abundance of isolate 1, it was presumed that the structures of 1 and 3 were equivalent except for the pyrrole-2-carboxylic acid residue.

2.8 Total Synthesis of Cochinmicins

Given the unique structural features and the potential to evaluate unique biological activity, we embarked on a synthesis of the cochinmicins.

2.8.1 Key Synthetic Features

The cochinmicins (I-V) are cyclic depsipeptides containing a single ester linkage to a hindered secondary alcohol within the 16-membered macrocycle (**Figure 71**). Further, the cochinmicins possess the rare amino acids 3,5-dihydroxyphenylglycine (DPG) and pyrrole-2-carboxylic acid and are especially rich in D-amino acids. Notably, the two contiguous DPG residues are incorporated into the macrocycle via an ester linkage, rendering synthesis of the depsipeptide significantly more challenging. Considerable precedence demonstrates DPG residues are especially prone to epimerization in condensative couplings.[255]

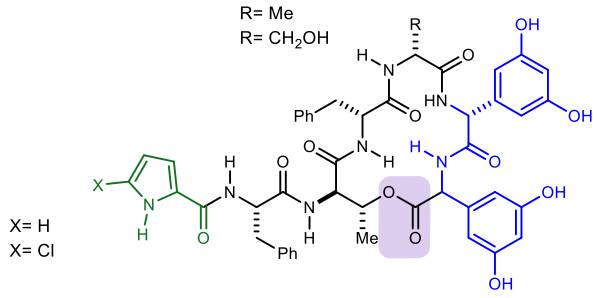

Figure 71. Key synthetic features of the aryl glycine-rich cochinmicins

2.8.2 Unified Synthetic Strategy to Access the Cochinmicins

Given the structural similarities in the five cochinmicins, we reasoned a convergent and modular approach would provide efficient access to all five of the isolated cochinmicins, as well as allow for the preparation of unnatural analogues.

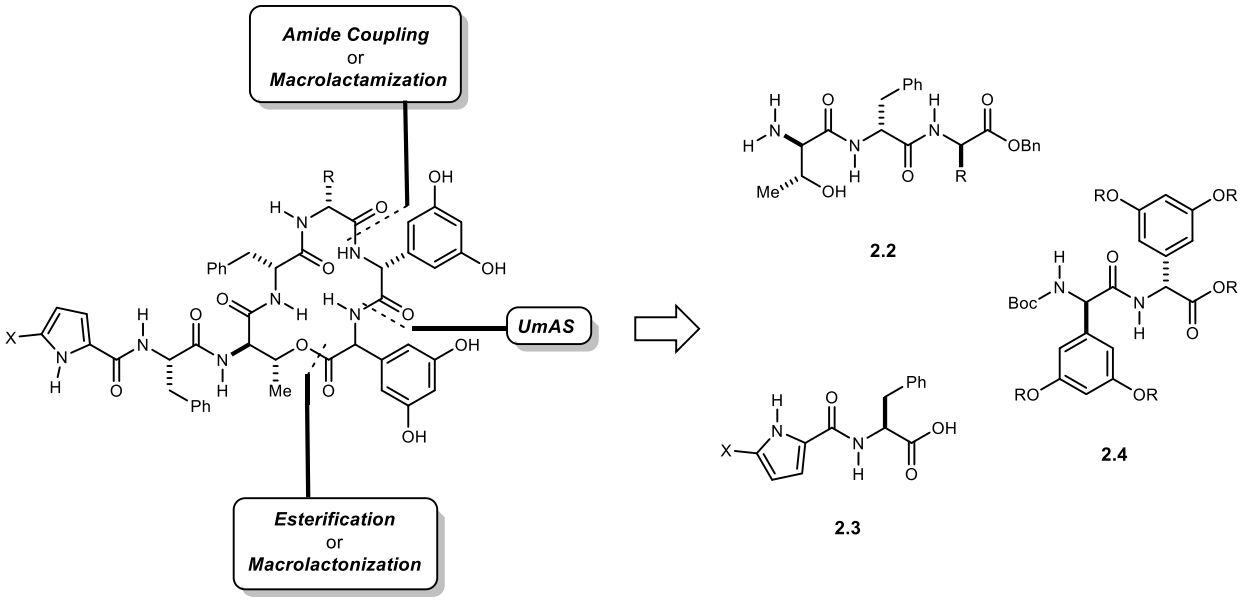

Figure 72. Retrosynthetic analysis to access the cochinmicins.

We envisioned three disconnections would give rise to three fragments **2.2**, **2.3**, and **2.4**, which could readily be exchanged to incorporate diversity toward the five cochinmicins (**Figure 72**). The epimerization-prone DPG dipeptide fragment (**2.4)** could be accessed using Umpolung Amide Synthesis (UmAS). In the design of a flexible approach, the macrocycle of the cyclic depsipeptide could be accessed via either a macrolactonization or macrolactamization approach. The requisite macrocyclization precursor could readily be accessed following assembly of the three fragments either via intermolecular esterification or amine coupling.

2.8.3 A convergent synthesis of A-B fragment (2.16)

Preparation of fragment A (**2.5**) began with Tollen's oxidation of pyrrole-2-carbaldehyde (**2.6**) to afford carboxylic acid **2.7**, which was coupled with suitably protected L-phenylalanine to give **2.8**. Finally, hydrogenolysis revealed carboxylic acid **2.5** (**Figure 73**).

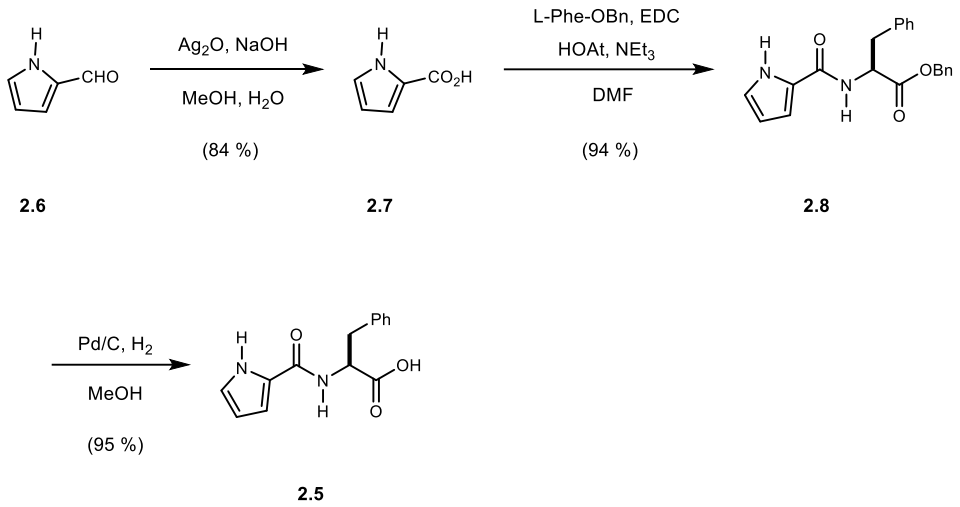

Figure 73. Synthesis of fragment A (2.5) from pyrrole-2-carbaldehyde (2.6)

Synthesis of fragment B (**2.15**) began with esterification of D-alanine to give **2.10** (**Figure 74**). Benzyl ester **2.10** was then subjected to acidic *N*-Boc deprotection and the resulting amine **2.11** was coupled with D-phenylalanine to give dipeptide **2.12**. Subsequent TFA-mediated deprotection revealed amine **2.13** which was coupled with D-*allo*-threonine. The resulting tripeptide **2.14** was subjected to *N*-Boc deprotection to afford amine **2.15** as fragment B.

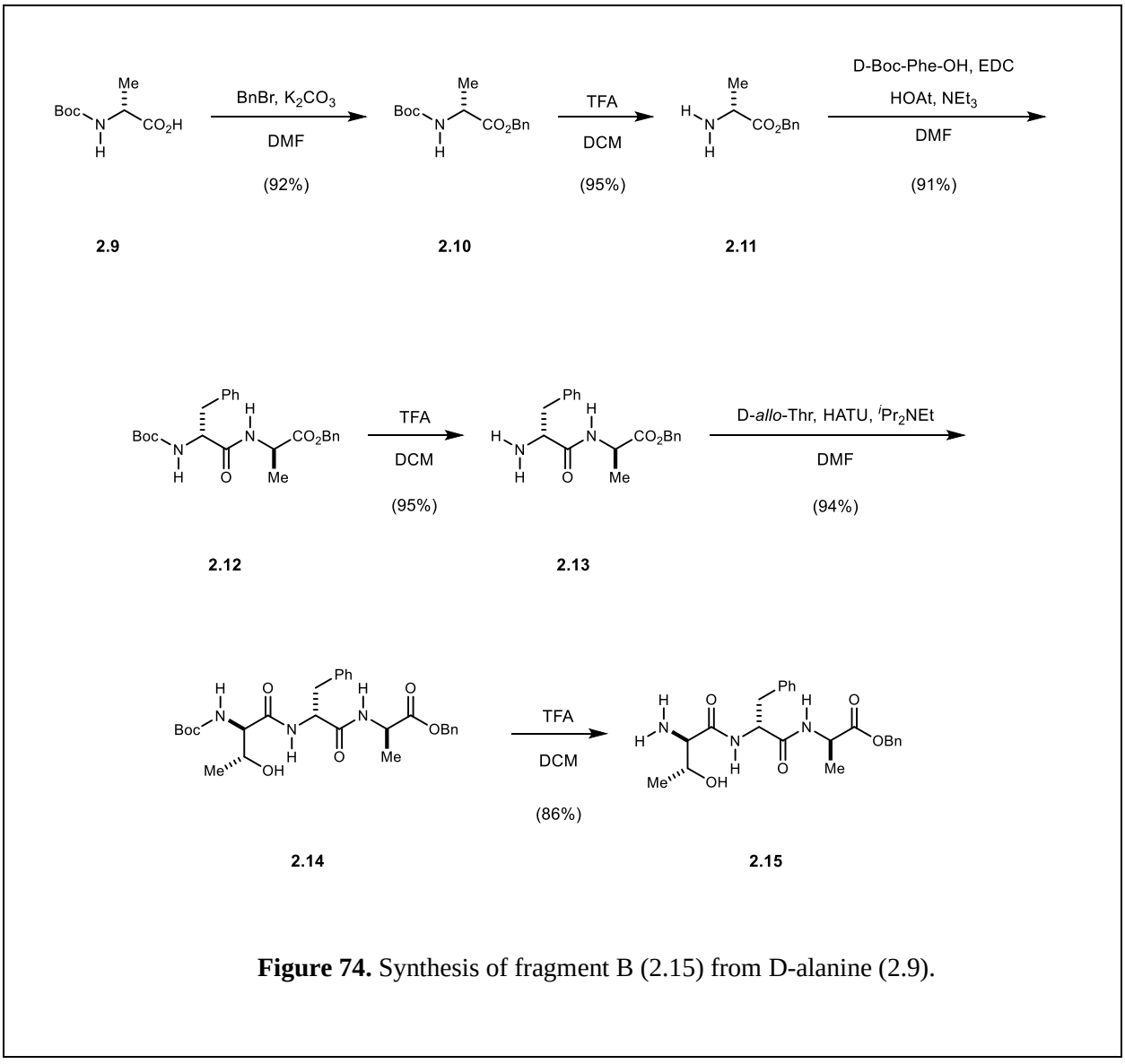

Figure 74. Synthesis of fragment B (2.15) from D-alanine (2.9).

Fragments A (**2.5**) and B (**2.15**) were successfully coupled together to give pentapeptide **2.16**, which represents completion of the western half of the macrocycle (**Figure 75**). Following successful preparation of pentapeptide **2.16**, we next turned our attention to preparation of the DPG-rich fragment.

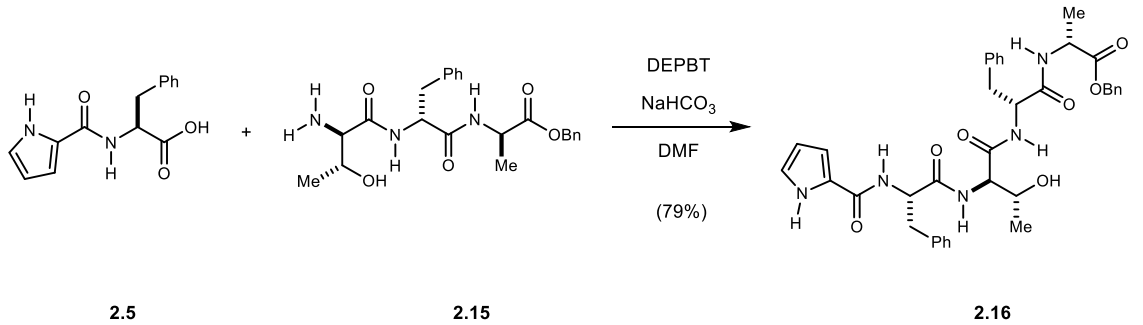

Figure 75. Amide coupling to give the A-B fragment 2.16.

2.8.4 Synthesis of fragment C

Synthesis of the DPG-rich fragment C required strategic consideration given the propensity for racemization of DPG residues during synthesis. We reasoned that employing a traditional condensative approach to access the DPG-rich fragment would result in epimerization and as such an alternative strategy was considered (**Figure 76**). To this end, we hypothesized Umpolung Amide Synthesis (UmAS) would present an alternative approach to the requisite DPG-rich fragment.[256] [257] [258] Uniquely, this reaction mechanistically avoids an active ester intermediate and as such provides for an epimerization-free approach to access these especially racemization-prone substrates. Previous efforts in the synthesis of feglymycin and analogues demonstrated that UmAS offers a reliable method to access aryl glycinamides without racemization. [259]

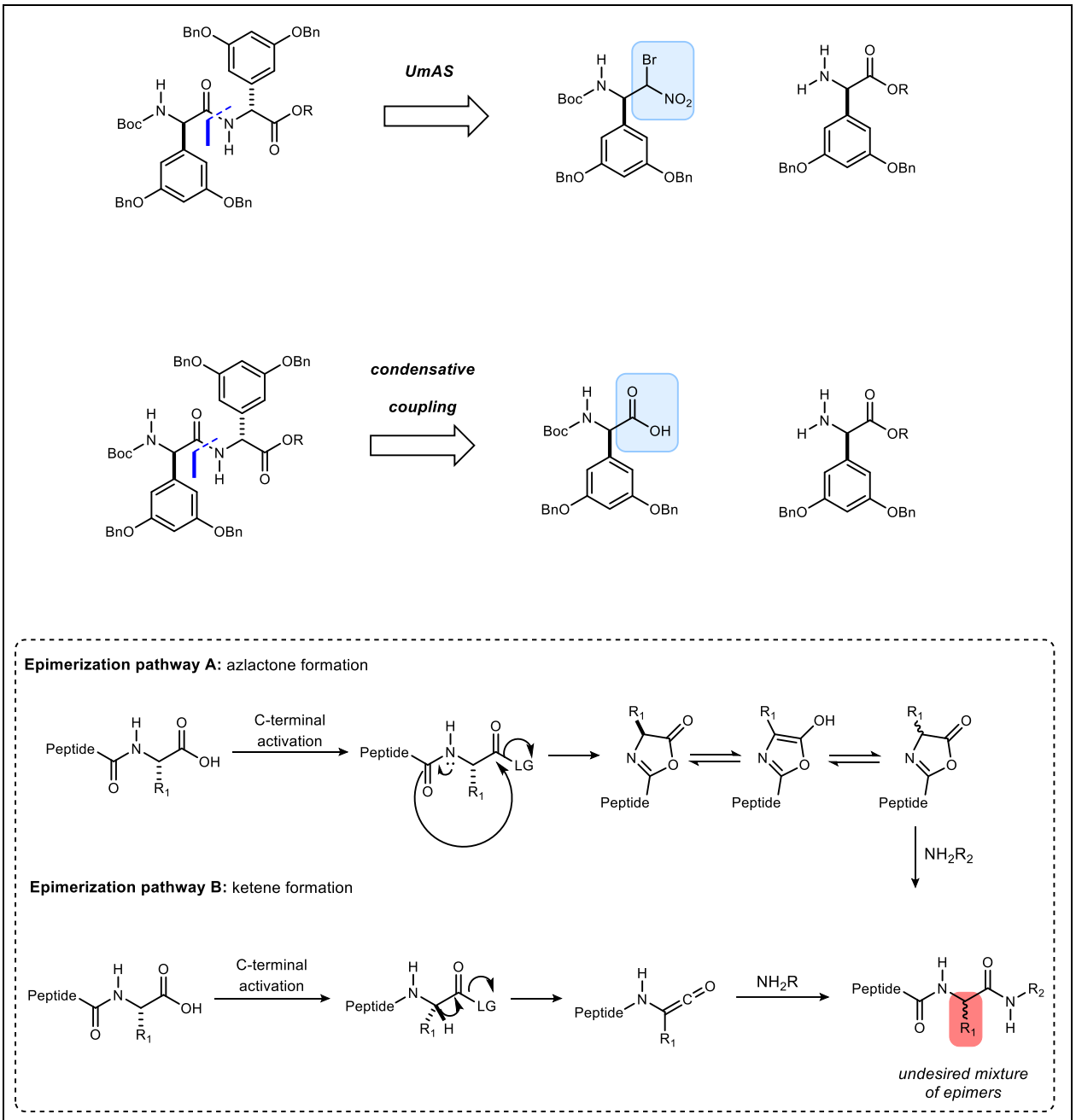

Figure 76. Comparison of the racemization-prone condensative approaches to amide bond couplings and UmAS.

2.8.4.1 An enantioselective aza-Henry approach to access bromonitroalkanes for UmAS

To synthesize the DPG-rich dipeptide using UmAS, we required a reliable method to prepare the UmAS coupling partners: amine and bromonitroalkane. Based on prior experience, an enantioselective aza-Henry reaction was expected to provide an efficient approach to access enantioenriched bromonitroalkanes. [260]

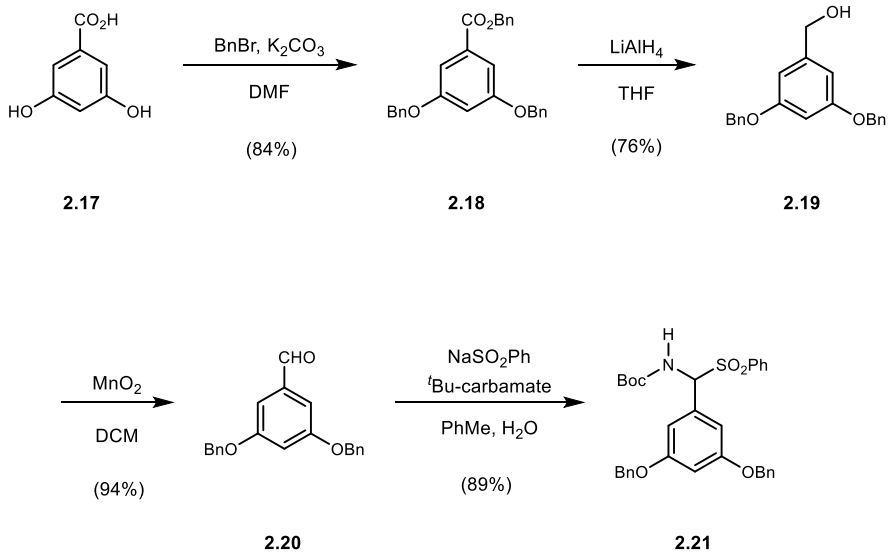

Figure 77. Synthesis of α-amido sulfone precursor to DPG bromonitroalkanes.

Synthesis of the requisite α-amido sulfones began with a perbenzylation of **2.17** and subsequent reduction of the resulting ester **2.18** (Figure 77). The obtained primary alcohol (**2.19**) was readily oxidized and converted to the desired α-amido sulfone (**2.21**).[259]

With the sulfone (**2.21**) in hand, we next turned our attention toward the preparation of the enantioenriched bromonitroalkanes. This two-step sequence begins first with an elimination to access an intermediate imine **2.22**, which is used immediately due to its propensity for hydrolysis (**Figure 78**). Crude imine **2.22** is then carried forward to an enantioselective aza-Henry reaction using chiral (bis)-amidine catalysis (PBAM catalyst). Utilizing the (*R,R*)-PBAM catalyst provides access to (*R*)-bromonitroalkane **2.23**, which can be converted to a D-amino acid, whereas the (*S,S*)-PBAM provides access to (*S*)-bromonitroalkane **2.24** and the corresponding L-amino acid.

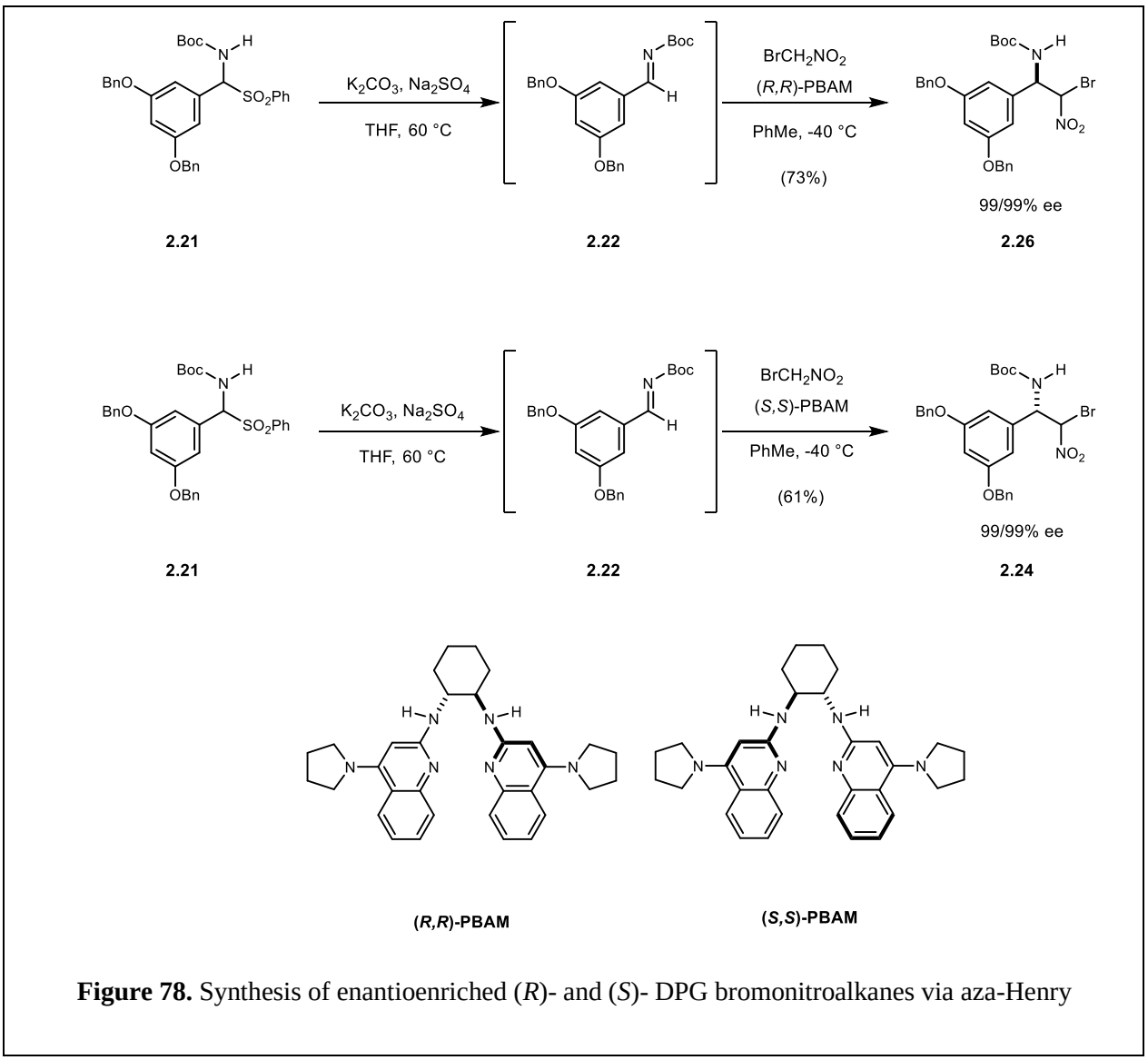

Figure 78. Synthesis of enantioenriched (*R*)- and (*S*)- DPG bromonitroalkanes via aza-Henry

We reasoned that this efficient and scalable approach would provide access to both the D- and L-DPG residues observed in the cochinmicins. This two-step procedure provided for the gram-scale synthesis of bromonitroalkanes, which can be used directly or serve as functional handles for further elaboration.

2.8.4.2 *N*-Me Amide Approach

With a concise and scalable method to access enantioenriched bromonitroalkanes, we next turned our attention to the elaboration of these bromonitroalkanes to DPG building blocks useful in the synthesis of the cochinmicins. Our first approach centered on the preparation of an *N*-Me amide DPG dipeptide (**Figure 79**).

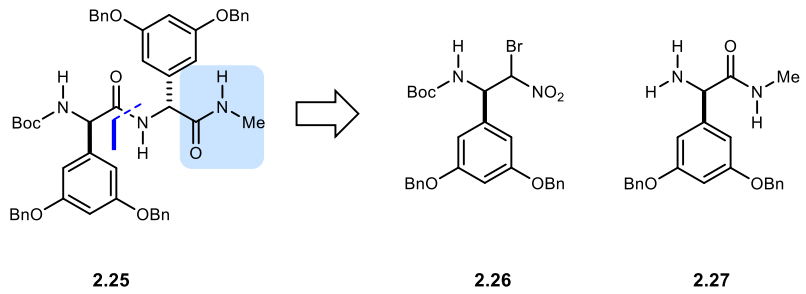

Figure 79. Synthetic strategy to access N-Me amide DPG-rich dipeptide

N-Me amides have previously been incorporated in syntheses as a carboxylic acid protecting group, which could be selectively nitrosated and hydrolyzed to afford the desired carboxylic acid without epimerization.[261 262 263] Given the propensity of the DPG residues for racemization, we reasoned the *N*-Me amide could serve as a masked carboxylic acid and later be revealed to form the macrolactone of the cochinmicins. Previous efforts toward the synthesis of feglymycin demonstrated the utility of the *N*-Me amide in the synthesis of DPG-rich peptides (**Figure 80**).[264]

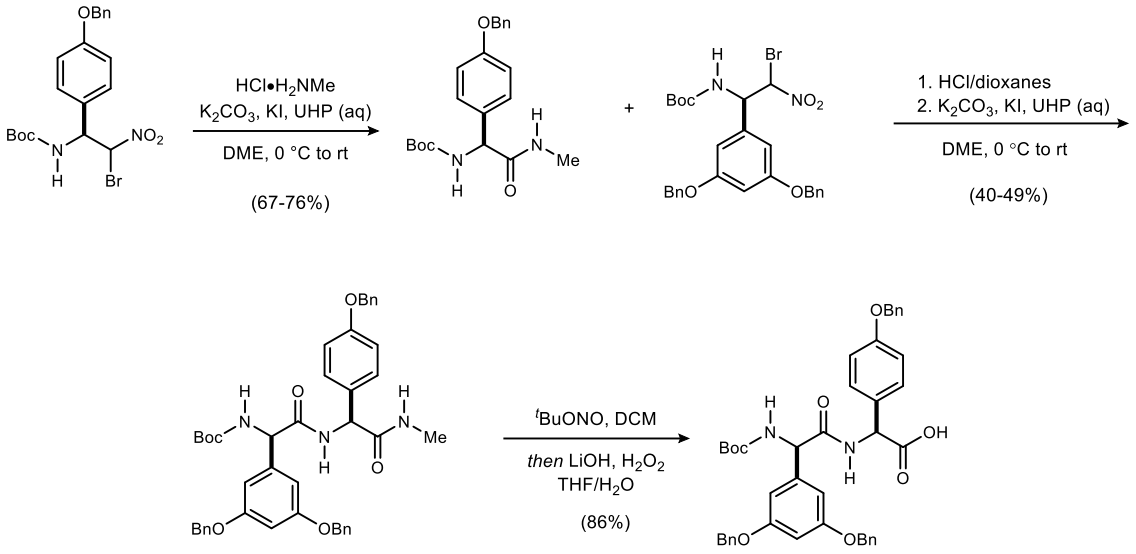

Figure 80. N-Me amide approach used in feglymycin fragment synthesis

Following this precedence, the enantioenriched DPG bromonitroalkanes were converted to an *N*-Me amide using UmAS. We first attempted the standard conditions used in the feglymycin fragment synthesis. Treatment of bromonitroalkane **2.26** with methylamine under UmAS conditions yielded the *N*-Me amide **2.28**, albeit in low yields (Table 1, entry 1).

Table 1. Synthesis of *N*-Me amide 2.27.[a]

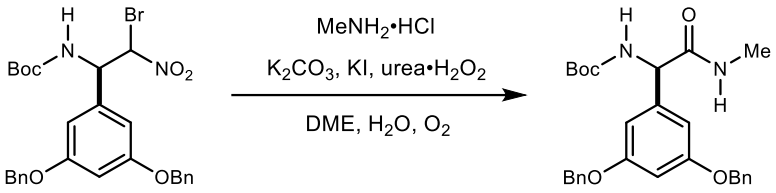

2.26 **2.28**

entry	temperature	UHP addition time	time	yield (%) (isolated)
1	0 °C	2 h	20 h	20
2	0 °C	2 h	4 d	20
3	0 °C 2 h, then 25 °C	2 h	40 h	27
4	0 °C 2 h, then 25 °C	2 h	30 h	40
5	0 °C 2 h, then 25 °C	3 min	30 h	35

[a] Bromonitroalkane (1 equiv), amine (1 equiv), and KI (2 equiv) in DME (0.1 M) at 0 °C. K_2CO_3 (6 equiv) added after 30 min followed by UHP (solution in water) and placed under O_2 atmosphere.

Surprisingly, the good yields (67-76%) observed with the HPG substrate were not replicated in the DPG system (20%).[264] We reasoned that efforts to optimize this early step in the synthesis of the cochinmicins would be beneficial. Extending the reaction time at 0 °C did not offer any improvement in isolated yield (Table 1, entry 2). Drawing from precedence toward the synthesis of feglymycin, we first increased the reaction temperature from 0 °C to ambient temperature, which did confer slight improvements to yield. Unfortunately, efforts to further improve these yields by varying reaction parameters were largely unsuccessful.

Despite the low-yielding preparation of *N*-Me amide **2.28**, we began our efforts to construct the DPG-rich fragment C. Acidic deprotection of carbamate **2.28** yielded amine **2.27**, which was then subjected to UmAS with an equivalent of bromonitroalkane **2.26**. (**Figure 81**).

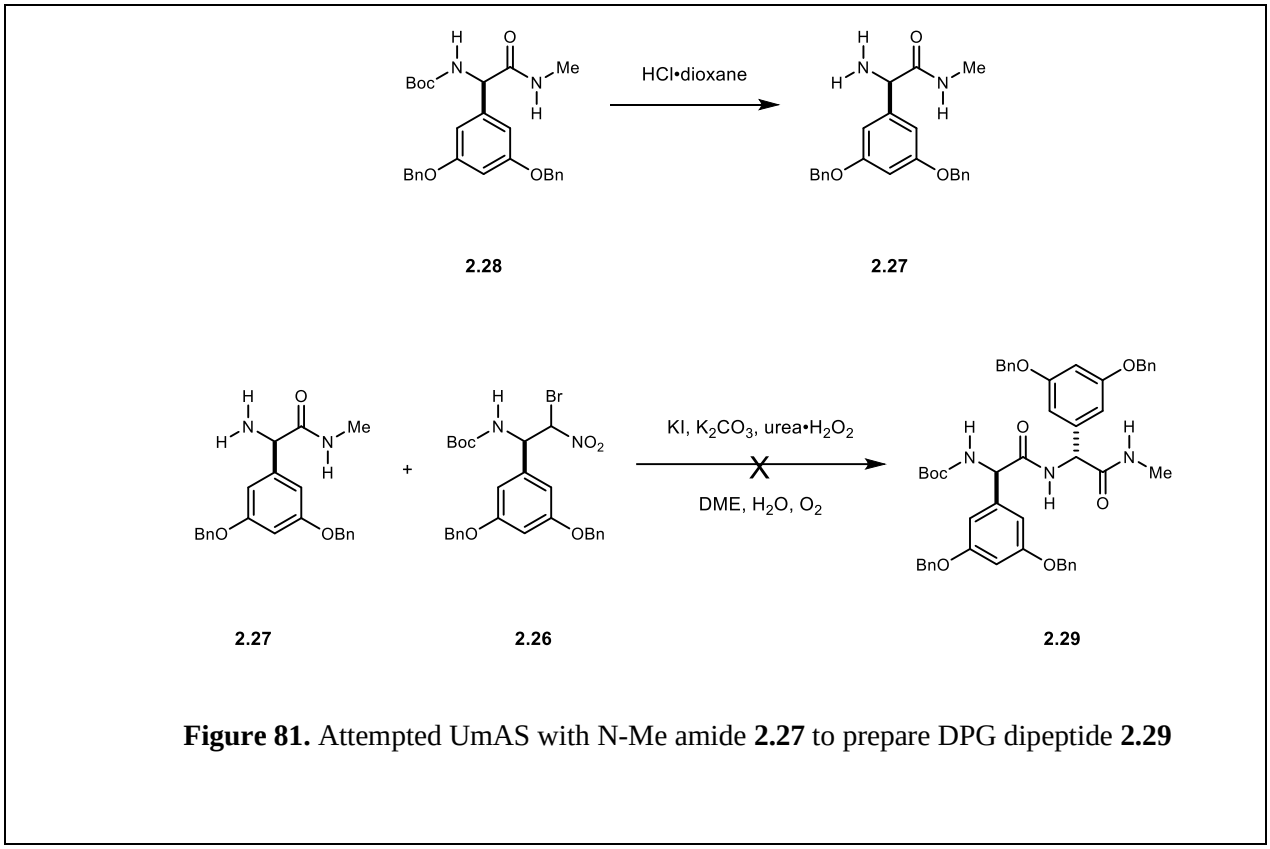

Figure 81. Attempted UmAS with N-Me amide **2.27** to prepare DPG dipeptide **2.29**

However, efforts to affect this amide bond formation were plagued by insolubility. The major product isolated was a white solid, which was surprisingly insoluble. Efforts to dissolve the obtained material in DMSO-d_6 with heating were remarkably unsuccessful and confirmation that the desired coupling occurred was not be obtained. Nonetheless, to employ this approach, efforts to address this challenging solubility profile were required. This was not unsurprising given the reports, by both Sussmuth and Johnston, stressing the solubility challenges associated with protected DPG side chains.

At this juncture, we reasoned that the number of benzyl ethers and the *N*-Me were contributing significantly to the challenging solubility profile of anticipated dipeptide **2.29**. To confirm that the desired coupling took place and improve the solubility profile of the expected dipeptide **2.29**, we subjected the obtained material to hydrogenolysis (**Figure 82**). To improve solubility during the reaction and access anticipated product **2.30**, the material was first heated in dilute DMF (0.001 M) prior to hydrogenolysis. Unfortunately, these attempts resulted in an apparent partial deprotection, and confirmation of the DPG dipeptide **2.29** remained inconclusive.

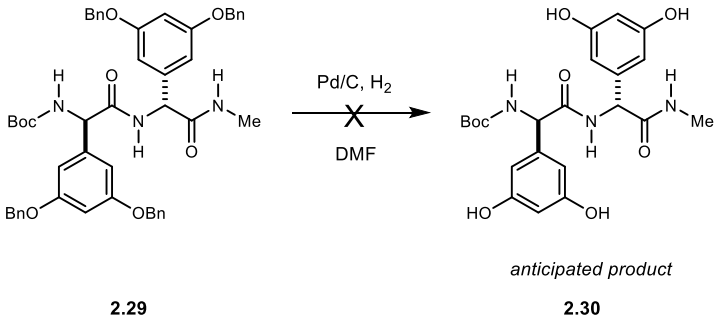

Figure 82. Hydrogenolysis of anticipated DPG dipeptide **2.30**.

Nonetheless, we were encouraged by the improved solubility profile. We hypothesized that debenzylation of the *N*-Me amide prior to amide-bond formation would help to alleviate some of the challenges associated with solubility. The obtained *N*-Me amide **2.28** was first subjected to hydrogenolysis to give **2.31** and then *N*-Boc deprotection revealed amine coupling partner (**2.32**) for UmAS. (**Figure 83**)

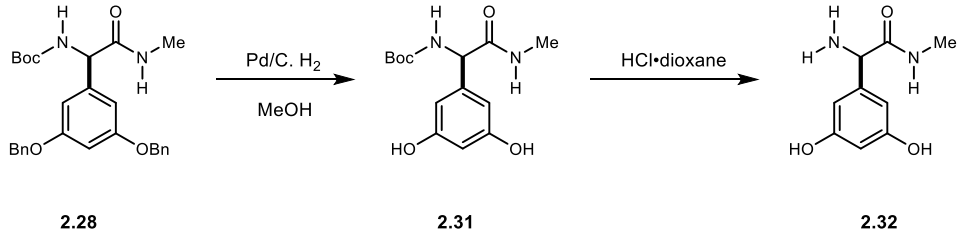

Figure 83. Benzyl ether deprotection of N-Me amide 2.28.

To prepare a DPG dipeptide with an improved solubility profile, fully deprotected *N*-Me amide **2.32** and its DPG bromonitroalkane coupling partner (**2.26**) were subjected to UmAS (**Figure 84**). The results of this reaction were also inconclusive. Although peptidic material was recovered there was no clear evidence the desired amide (**2.33**) was formed.

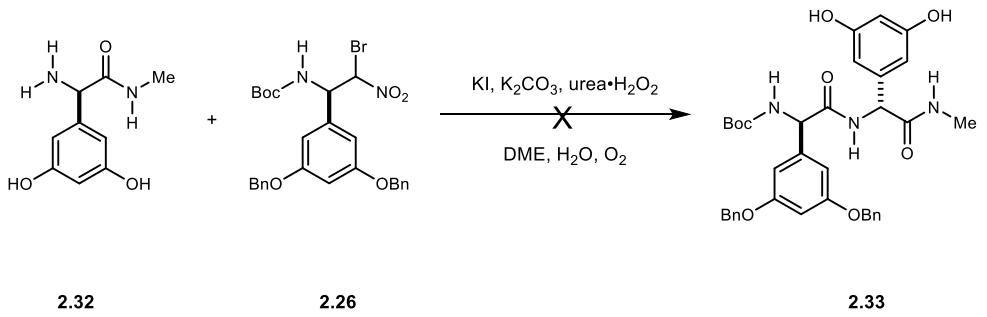

Figure 84. UmAS with DPG bromonitroalkane and fully deprotected N-Me amide.

Together, the low-yielding reactions and the challenging solubility profile rendered the *N*-Me amide approach unsuitable for scalable and efficient synthesis of the cochinmicins. We reasoned an alternative strategy to access the DPG-rich fragment C would offer advantages over this approach.

2.8.4.3 Mioskowski- Nef Approach

Our new aim centered on the preparation of DPG building blocks with improved solubility profiles that would enable the synthesis of DPG-rich fragment C. It was found in the preparation of feglymycin building blocks that a terminal ester improved the solubility profile of key intermediates as well as reaction yields. [265] To access the requisite ester building blocks, a modified Mioskowski-Nef reaction was employed to convert enantioenriched nitroalkanes to carboxylic acids which could be readily protected as a variety of esters (**Figure 85**).

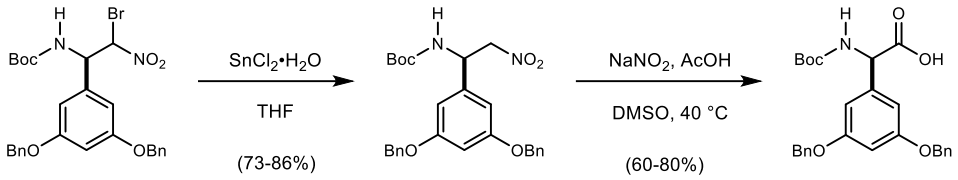

Figure 85. Debromination and Mioskowski-Nef sequence to access DPG amino acids toward the synthesis of feglymycin.

Encouraged by these improvements toward the synthesis of feglymycin, we hypothesized that converting the bromonitroalkanes to their corresponding DPG amino acids would offer an improved solubility profile providing access to the DPG-rich fragment C (**Figure 86**).

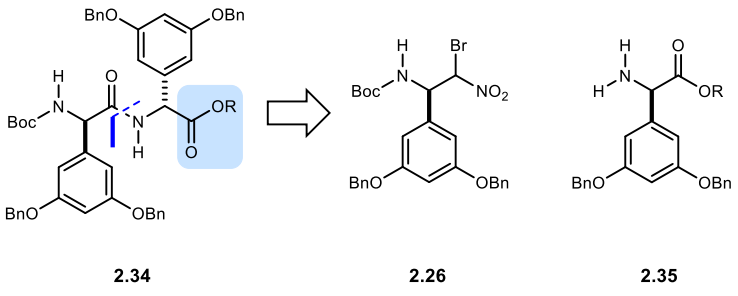

Figure 86. Revised Fragment C retrosynthetic analysis.

To this end, bromonitroalkane **2.26** was subjected to tin-mediated debromination to give nitroalkane **2.36** which yielded the *N*-Boc protected DPG amino acid **2.37** following Mioskowski-Nef reaction. (**Figure 87**) The DPG amino acid **2.37** was then converted to the desired methyl ester via acidic esterification, which resulted in concomitant cleavage of the *N*-Boc protecting group yielding the requisite amine coupling partner **2.38** in a single step.

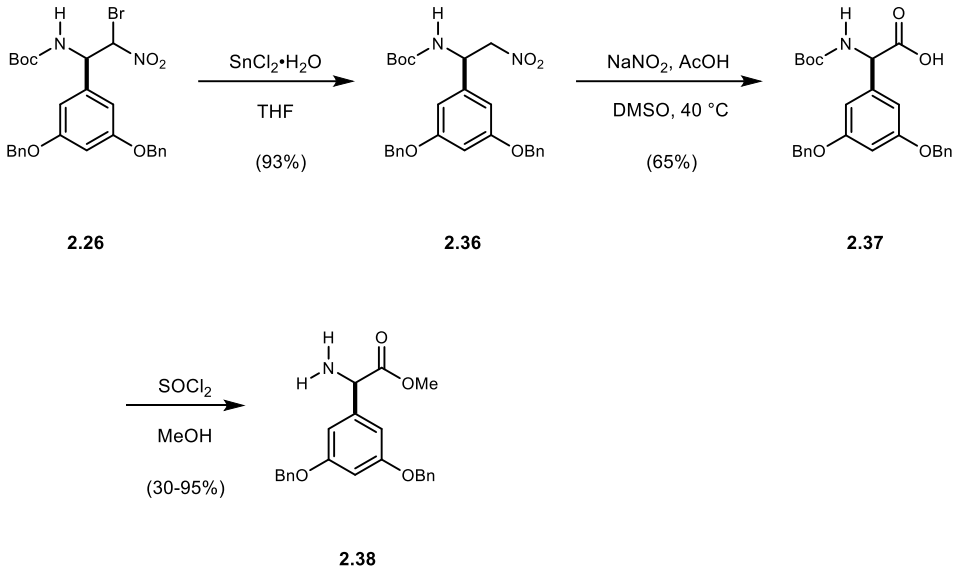

Figure 87. Preparation of DPG amino acids from DPG nitroalkanes.

With a straightforward method to prepare the amine (**2.38**) coupling partner, we began evaluating conditions to construct fragment C using UmAS. The use of the crude methyl ester (**2.38)** in UmAS resulted in no observed conversion to the desired DPG dipeptide (Table 2, entries1-2). The unpurified amine as the HCl salt was especially reluctant to go into solution, and this was considered detrimental to conversion. Notably, when the amine was purified via HPLC before use and isolated as the TFA salt, the DPG dipeptide (**87.8)** was readily accessed, albeit in modest yields (Table 2, entries 6-7). This was a notable finding as efforts to prepare the desired DPG dipeptide using conventional methods (DEPBT) afforded a 1:1 mixture of diastereomers. This demonstrated the value of UmAS as a synthetic strategy to access these racemization-prone substrates. Unfortunately, efforts to improve reaction yields by varying temperature, rate of reagent addition, and equivalency were unsuccessful. Another unisolable peptidic product accounts for the modest yields.

Table 2. Evaluation of UmAS conditions to access the DPG dipeptide methyl ester **2.39**.[a]

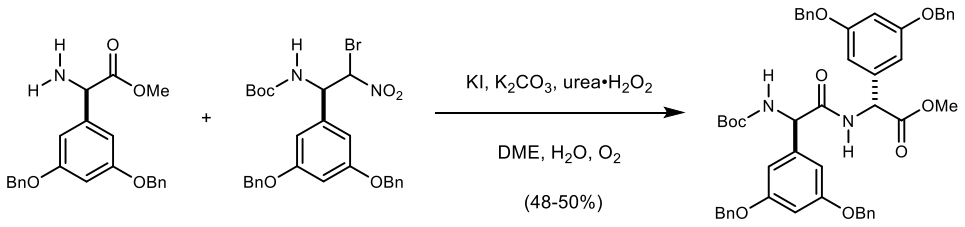

2.38 **2.26** **2.39**

entry	amine	temp	UHP addition time	time	yield (%) (isolated)
1	crude	0 °C 2 h, then 25 °C	2 h	20 h	n.r.
2	crude	0 °C 2 h, then 25 °C	3 min	16 h	n.r.
3	purified (hplc)	0 °C	3 min	40 min	n.r.
4	purified (hplc)	0 °C	3 min	2 h	n.r.
5	purified (hplc)	0 °C	3 min	6 h	n.r.
6	purified (hplc)	0 °C	3 min	16 h	50
7	purified (hplc)	0 °C 2 h, then 25 °C	3 min	17 h	48

[a] Bromonitroalkane (1 equiv), amine (1 equiv), and KI (2 equiv) in DME (0.1 M) at 0 °C. K_2CO_3 (6 equiv) added after 30 min followed by UHP (solution in water) and placed under O_2 atmosphere.

2.8.4.4 Comparison of UmAS to DEPBT Coupling Experiment

DEPBT is a coupling reagent frequently utilized in the synthesis of racemization-prone targets.[266] DEPBT has been used to access other aryl glycine-rich natural products, such as feglymycin and ramoplanin.[267] [268] Süssmuth and coworkers report high yields and no evidence of epimerization even in cases where the active ester is formed at the *C*-terminus of the arylglycine residue (**Figure 88**).

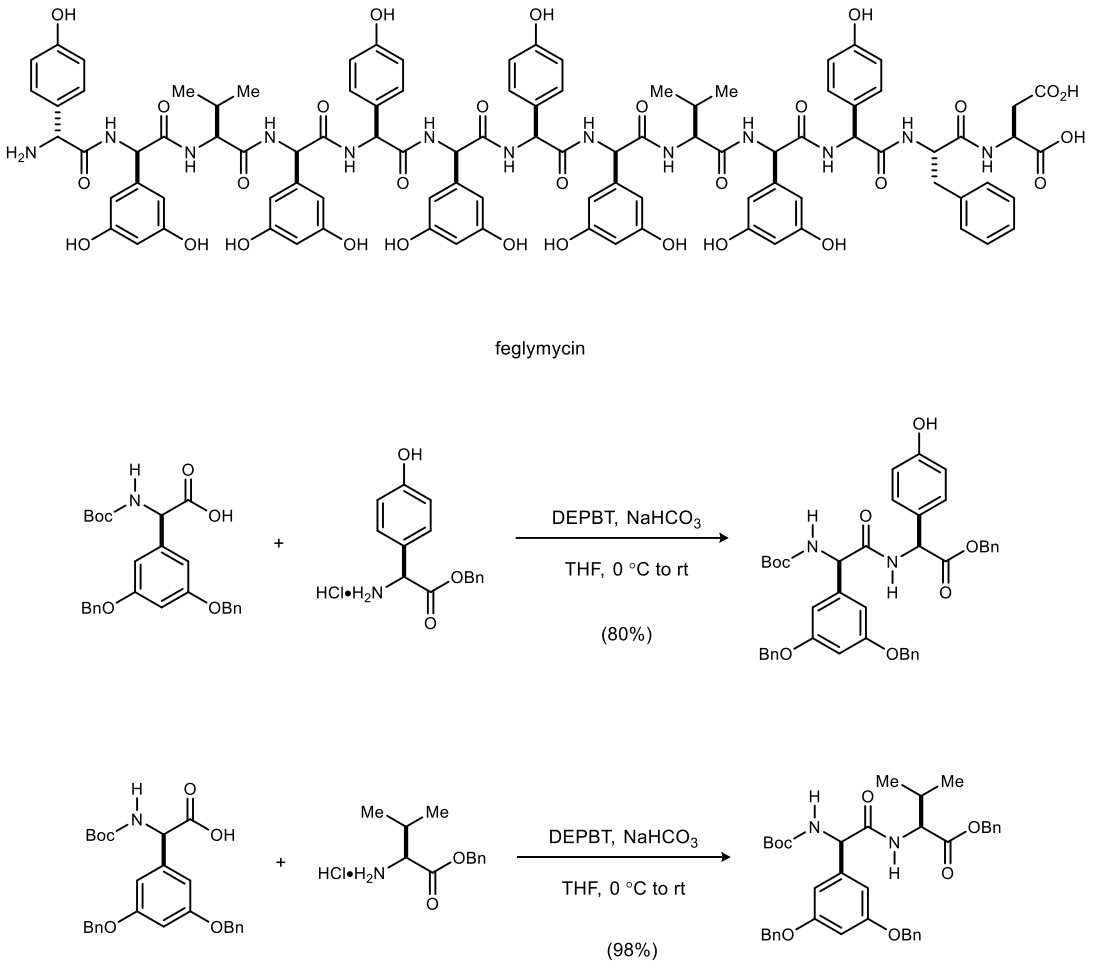

Figure 88. DEPBT couplings used to construct fragments in the synthesis of feglymycin (Süssmuth).

The opportunity to compare DEPBT couplings to Umpolung Amide Synthesis (UmAS) in preparation of the DPG-rich dipeptide was intriguing given the unique mechanisms of the two approaches, the propensity for DPG residues to racemize during synthesis, and the precedence using DEPBT to construct other aryl glycinamides (**Figure 89**).

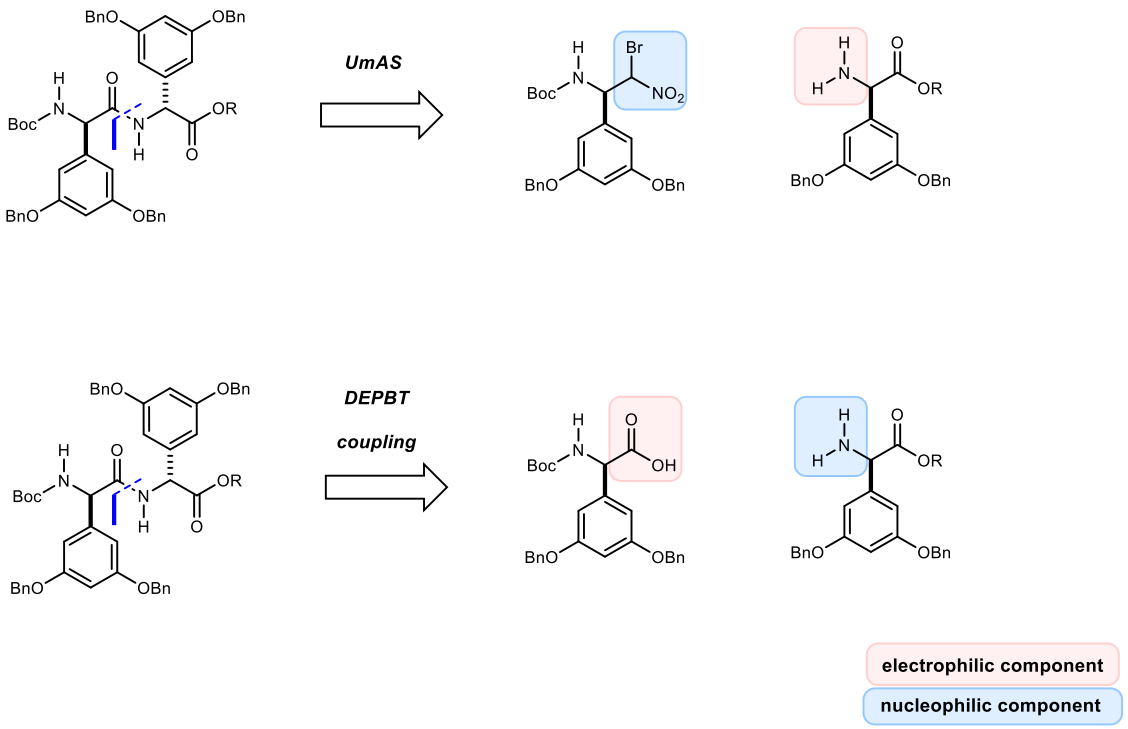

Figure 89. Comparison synthetic strategies in DEPBT coupling and UmAS to access DPG-rich dipeptide.

Upon pre-activation of the carboxylic acid **2.37** with DEPBT and treatment with amine **2.38**, the DPG dipeptide was furnished as a mixture of epimers **2.40** in modest yields (**Figure 90**). Following Süssmuth's approach, the reaction was maintained at low temperature and under mildly basic conditions to mitigate epimerization of the α-stereocenter. However, we were unsuccessful in preparing the DPG dipeptide **2.40** as a single diastereomer.

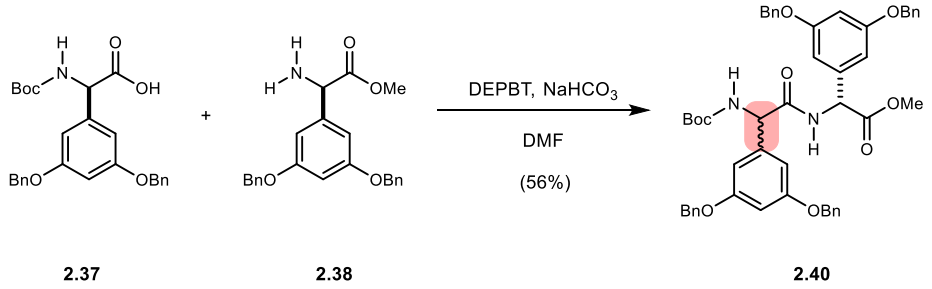

Figure 90. DEPBT coupling to access DPG dipeptide and its epimer (2.40).

By comparison, we have demonstrated that UmAS can be used to access the DPG dipeptide as a single diastereomer. Amine **2.38**. and bromonitroalkane **2.26** were subjected to standard UmAS conditions to yield dipeptide **2.39** with no observed epimerization (**Figure 91**).

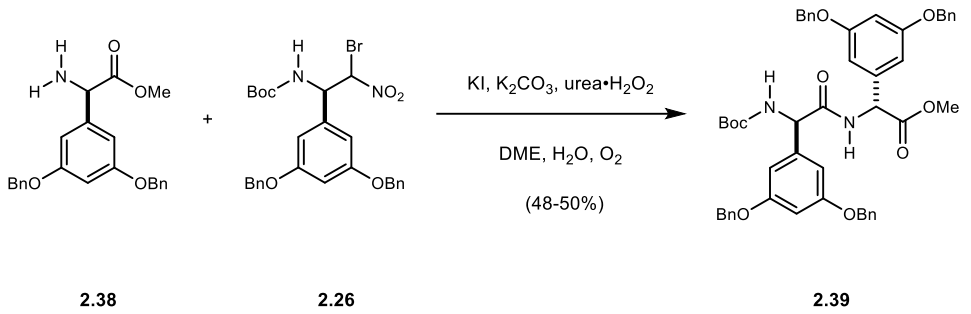

Figure 91. Preparation of DPG-dipeptide (2.39) using UmAS

The observed epimerization during synthesis of the DPG dipeptide with a traditional, condensative approach (DEPBT) demonstrated the utility of UmAS in preparation of aryl glycinamides, such as the cochinmicins. We reasoned that this is undoubtedly attributed to the lack of an active ester intermediate in UmAS and the overall mild reaction conditions.

2.8.4.5 Apparent Epimerization

To our surprise, in one of our attempts to access the DPG dipeptide using UmAS, we noted evidence of epimerization of an α-stereocenter (Figure 92). This was unexpected as the conditions employed in UmAS are mild and tailored to racemization-prone substrates. We wanted to further probe this apparent epimerization to better understand how this undesired reaction pathway is occurring in an otherwise epimerization-free transformation.

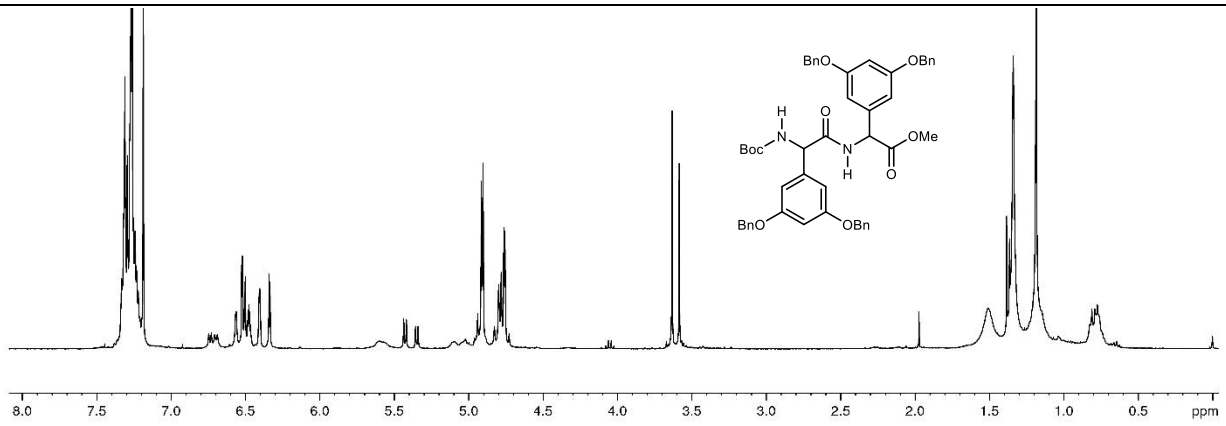

Figure 92. First evidence of epimerization in UmAS preparation of DPG dipeptide.

We noticed upon reaction set-up that the amine was sparingly soluble in the reaction solvent and reluctant to go into solution for several hours at 0 °C. This prompted us to consider that the reluctance of the amine to go into solution might contribute to the apparent epimerization. We hypothesized that the insolubility limited the access of the amine coupling partner to the reaction and that allowed for the otherwise slow reaction pathways to be detected. Under our initial attempts at this transformation, the amine was used directly in crude form and as the HCl-salt. This prompted us to consider that the HCl-salt was responsible for some insolubility, which limited the availability of the requisite amine to the reagents necessary for amide bond formation. To evaluate this further, we evaluated several conditions to determine what effect the HCl salt had on epimerization. To this end, we prepared the TFA salt of the amine as a comparison to the HCl-salt, used a purified amine, and the free-base of the amine. In each of the cases, no epimerization was observed when the amine went immediately into solution (Figure 93).

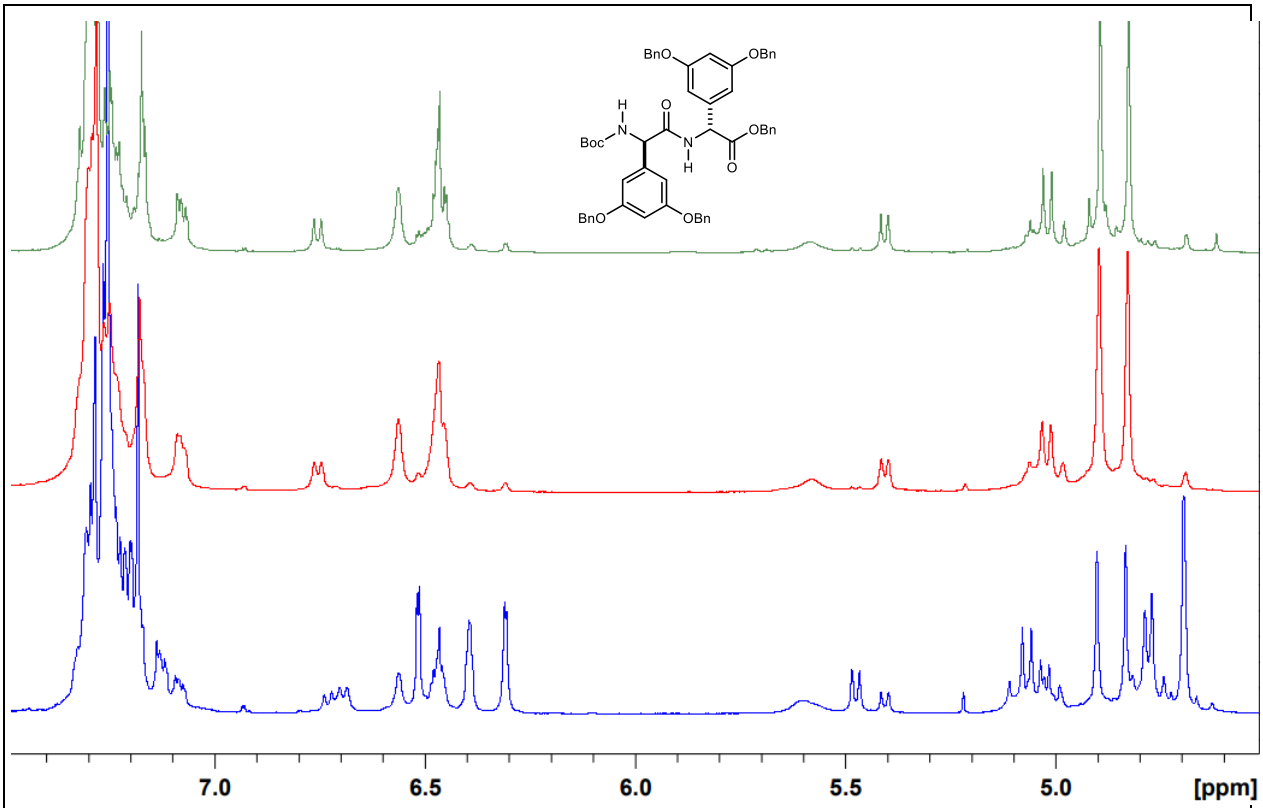

Figure 93. (A) Amine used as TFA salt in UmAS, (B) amine used as free base in UmAS, and (C) amine used as HCl salt in UmAS.

Intrigued by this result, we considered that the stirring efficiency might also play a role in the undesired epimerization pathway. The heterogeneous mixture with the HCl salt was suspected to have inefficient stirring when compared to the reaction mixture when the amine goes immediately into solution. Notably, when the stirring is slow and ineffective (100-200 rpm), there was observable epimerization. However, when the stirring is efficient (700-800 rpm), there was no detectable epimerization (

Figure **94**). These results again confirm the propensity of these residues to epimerize as well as the ability to mitigate epimerization by careful attention to reaction setup.

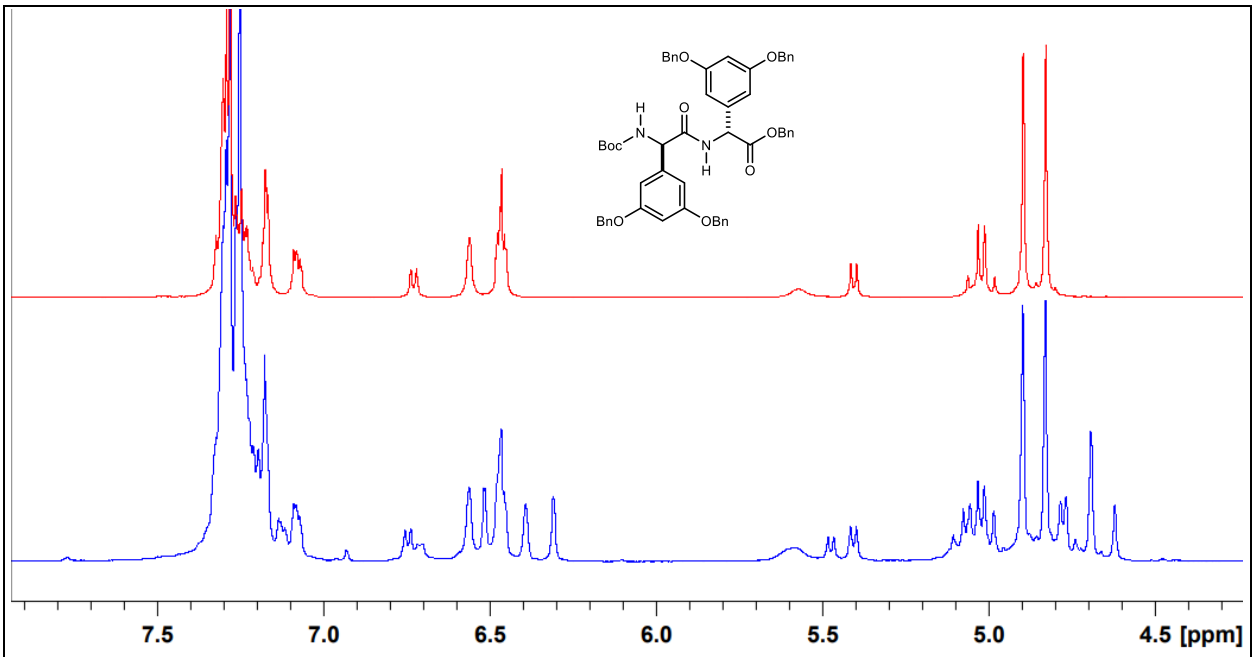

Figure 94. Efficient stirring yields a single diastereomer whereas inefficient stirring yields a mixture of epimers.

With a reliable method to prepare the methyl ester dipeptide **2.39**, we next began evaluating conditions to deprotect the methyl ester and reveal the requisite carboxylic acid (Figure 95). Following precedence from Sössmuth and coworkers, we reasoned a trimethyltin hydroxide (TMTH)-mediated deprotection would provide an epimerization-free method to access the desired carboxylic acid **2.41** [269] [270] This approach resulted in the formation of carboxylic acid **2.41** but unfortunately, tin-byproducts were not easily removed. These challenges in purification raised concerns regarding the scale-up of the synthesis of this fragment.

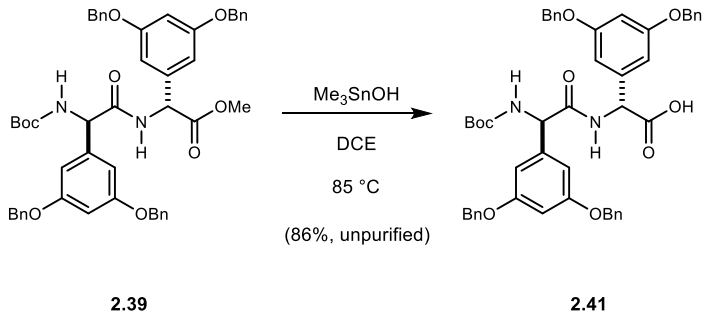

Figure 95. Trimethyltin hydroxide-mediated deprotection of methyl ester 2.41.

Unsurprisingly, traditional saponification conditions resulted in epimerization of the α-center (Table 3, entries 1-3). We next reasoned that a less basic hydrolysis using a combination of lithium hydroxide and hydrogen peroxide would help to mitigate the undesired epimerization (Table 3, entries 4-6). Unfortunately, epimerization was still competitive with hydrolysis under these conditions. Thus demonstrating again the propensity of these DPG residues for racemization in synthesis. Due to these challenges in the preparation of the desired carboxylic acid (**2.41**), we reasoned this is not a viable protecting group strategy for completing the synthesis of the cochinmicins.

Table 3. Attempted saponification of DPG dipeptide **2.39** resulted in the formation of undesired epimers.

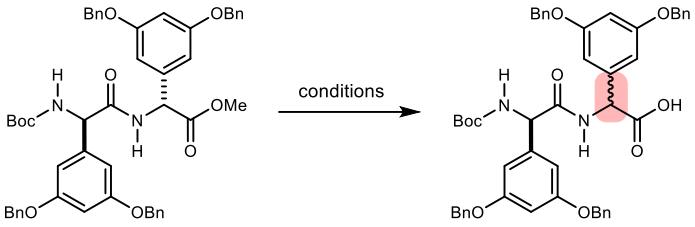

2.39 **2.42**

entry	reagents	temp	time	outcome
1	1 M LiOH (1.5 eq), 1:1 THF-H_2O	25 °C	1 h	1:1 mixture of epimers (73%)
2	1 M LiOH (1.5 eq), 1:1 THF-H_2O	0 °C	25 min	<10% conversion
3	1 M LiOH (1.5 eq), 1:1 THF-H_2O	0 °C	1.5 h	1:1 mixture of epimers
4	1 M LiOH (1.5 eq), 30% H_2O_2 (8 eq), 1:1 THF-H_2O	0 °C	2 h	<10% conversion
5	1 M LiOH (1.5 eq), 30% H_2O_2 (8 eq), 3:1 THF-H_2O	0 °C	1.5 h	<10% conversion
6	1 M LiOH (1.5 eq), 30% H_2O_2 (8 eq), 3:1 THF-H_2O	0 °C 30 min, then 25 °C	1.5 h	<10% conversion

2.8.4.6 Benzyl Ester DPG Dipeptide

Faced with the competitive epimerization in the methyl ester deprotection, we considered an alternative protecting group strategy that would allow for successful deprotection of the DPG dipeptide without epimerization. We reasoned that utilizing a benzyl ester would allow for concomitant deprotection of the benzyl ethers, improve the efficiency of the route, and provide an epimerization-free deprotection method.

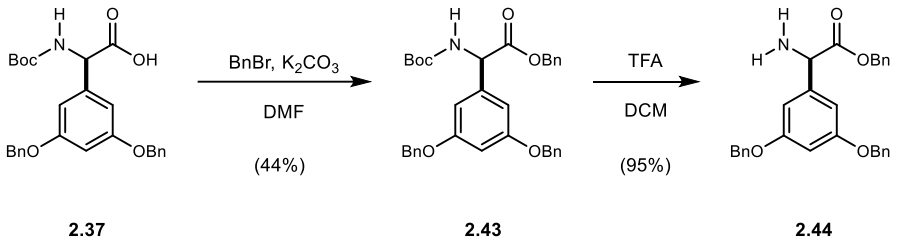

2.37 **2.43** **2.44**

Figure 96. Preparation of benzyl ester 2.44 for UmAS.

Carboxylic acid **2.37** was treated with benzyl bromide under mildly basic conditions to give benzyl ester **2.43**. Subsequent deprotection under acidic conditions revealed amine coupling partner **2.44** (Figure 96). Amine **2.44** and bromonitroalkane **2.26** subjected to UmAS successfully furnished the DPG dipeptide (**2.45**) as a single diastereomer (Table 4, entries 1-4).

Table 4. UmAS to access DPG dipeptide benzyl ester **2.45**.[a]

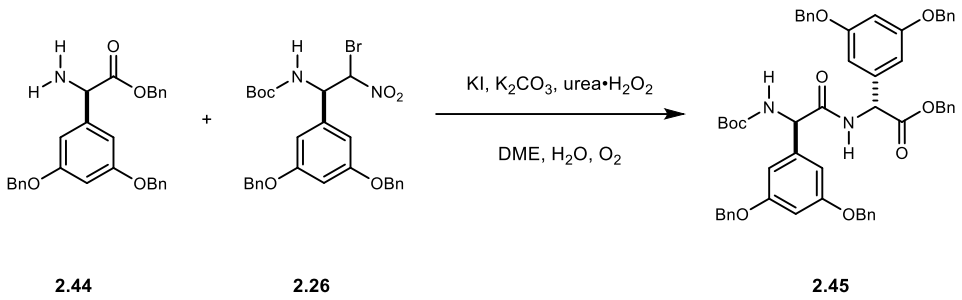

2.44 **2.26** **2.45**

Entry	Amine	UHP addition	temp	time	yield (%) (isolated)
1	TFA salt	direct inj (3.0 M)	0 °C	19 h	52
2	free base	direct inj (3.0 M)	0 °C	18 h	48
3	TFA salt	direct inj (3.0 M)	0 °C	16 h	44
4	TFA salt	direct inj (3.0 M)	0 °C	18 h	50
5	TFA salt	30 min (3.0 M)	0 °C 2 h, then 25 °C	18 h	38
6	TFA salt	30 min (1.0 M)	0 °C 2 h, then 25 °C	16 h	46
7	TFA salt	2 h (3.0 M)	0 °C 2 h, then 25 °C	23 h	50

[a] Bromonitroalkane (1 equiv), amine (1 equiv), and KI (2 equiv) in DME (0.1 M) at 0 C. K_2CO_3 (6 equiv) added after 30 min followed by UHP (solution in water) and placed under O_2 atmosphere.

Efforts to improve the yields of the dipeptide (**2.45**) stemmed from previous work conducted toward the preparation of late-stage feglymycin intermediates. We first attempted to increase the reaction temperature to encourage formation of the desired amide (**2.45**). (Table 4, entry 5). Furthermore, varying the addition of the urea·H_2O_2 solution did not offer significant advantages and isolated yields remained modest.

Following the preparation of benzyl ester **2.45**, hydrogenolysis revealed the desired free carboxylic acid **2.46** (Figure 97). Unsurprisingly, there was no observed epimerization upon deprotection. However, the cleavage of the benzyl ethers and benzyl ester drastically changed the solubility profile of dipeptide. This impacted the utility of this substrate in subsequent reactions.

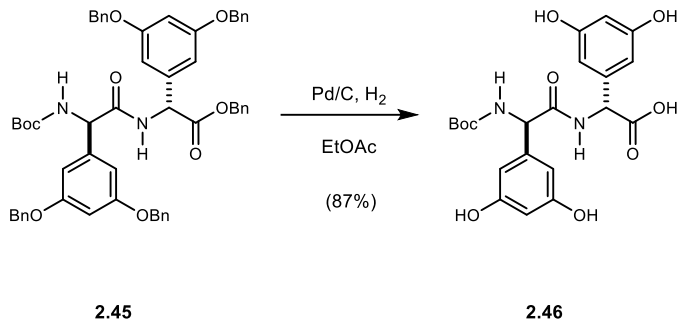

2.45 **2.46**

Figure 97. Hydrogenolysis of benzyl ester dipeptide 2.46.

2.8.4.7 Allyl Ester DPG Dipeptide

We reasoned that an orthogonal protecting group strategy could help improve some of the undesirable properties of the benzyl ester substrate, which arose following global deprotection. We reasoned an allyl ester would offer an advantage allowing for selective deprotection of the ester without perturbation of the benzyl ethers.

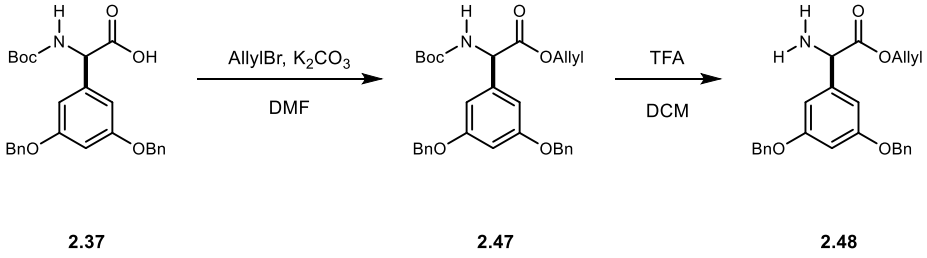

2.37 **2.47** **2.48**

Figure 98. Preparation of allyl ester coupling partner for UmAS.

To this end, we have prepared the allyl ester **2.47** from carboxylic acid **2.37**. Subsequent treatment with TFA yielded amine **2.48** for use in UmAS (Figure 98). To our delight, amine **2.48** was successfully coupled with bromonitroalkane **2.26**. to furnish the desired DPG dipeptide **2.49** in modest yields (Table 5).

Table 5. UmAS to access DPG dipeptide allyl ester **2.49**.[a]

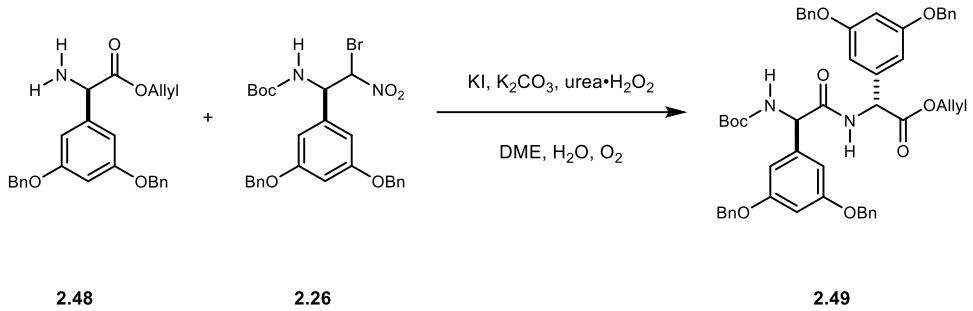

entry	UHP addition	temp	time	yield (%) (isolated)
1	direct inj (3.0 M)	0 °C	12 h	30
4	direct inj (3.0 M)	0 °C	22 h	40
2	30 min (3.0 M)	0 °C 2 h, then 25 °C	19 h	60
3	30 min (3.0 M)	0 °C 2 h, then 25 °C	22 h	63

[a] Bromonitroalkane (1 equiv), amine (1 equiv), and KI (2 equiv) in DME (0.1 M) at 0 C. K_2CO_3 (6 equiv) added after 30 min followed by UHP (solution in water) and placed under O_2 atmosphere.

At this juncture, we turned our attention to optimizing the preparation of the allyl ester dipeptide (**100.5**). Preliminary efforts resulted in modest yield (30%), which significantly limited the overall robustness of our synthetic approach (Table 5, entry 1). Drawing again from previous optimization efforts, we first evaluated reaction time and found that longer reaction time at 0 °C did not confer significant increase in yield. Initial attempts to change reaction temperature conferred modest improvements in yield (Table 5, entry 3-4). Next, the rate of addition of the urea·H_2O_2 was varied, which also conferred modest improvements in yield. However, modification to any other reaction parameters did not confer improvements and these optimized reaction conditions were employed to prepare the macrocyclization precursor.

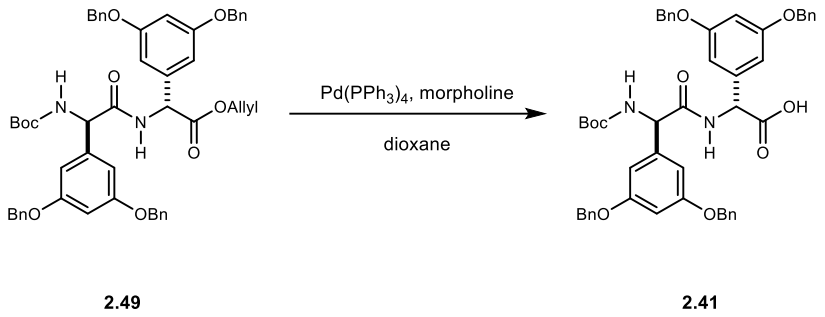

2.49 **2.41**

Figure 99. Pd(0) mediated deprotection of allyl ester 2.49.

We next turned our attention toward selective deprotection of the allyl ester upon treatment with a Pd(0) source and a π-allyl scavenger. Allyl ester **2.49** was treated with $Pd(PPh_3)_4$ and morpholine to give the desired carboxylic acid **2.41** in excellent yields with no observed epimerization (Figure 99).

Notably, this orthogonal protecting group strategy helped to improve the solubility profile of the carboxylic acid coupling partner as anticipated. We hypothesized that the improved profile of this substrate would improve its utility in completing the synthesis of the cochinmicins.

2.8.4.8 Preparation of Natural and Unnatural DPG Dipeptides

In the design of our synthetic approach, we envisioned a flexible route that was amenable toward diversification to access all five of the isolated cochinmicins as well as unnatural analogues. To this end, we employed both (*R*,*R*) and (*S*,*S*)-PBAM to access the corresponding (*R)*- and (*S)*-bromonitroalkanes, respectively. (*S)*-Bromonitroalkane **2.24** was subjected to debromination to yield nitroalkane **2.50**, which following a Mioskowksi-Nef reaction afforded carboxylic acid **2.51**. Esterification of **2.51** with benzyl bromide yielded benzyl ester **2.52**, which upon *N*-Boc deprotection afforded amine **2.53** (Figure 100).

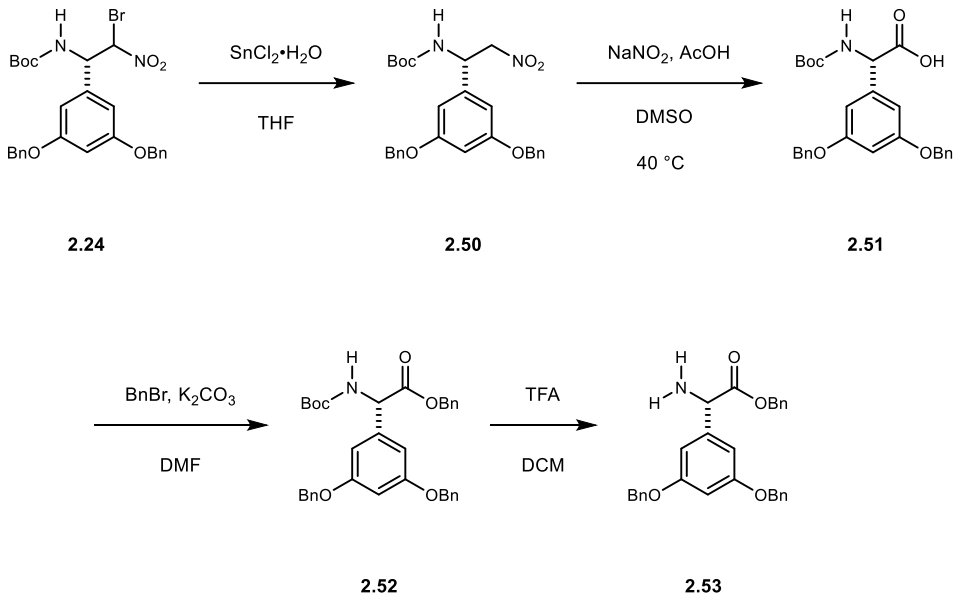

Figure 100. Conversion of *S*-bromonitroalkanes to DPG amino acid building blocks.

This strategy readily provided access to sufficient quantities of the *R* amine **2.44** and *R* bromonitroalkane **2.26** as well as the *S* amine **2.53** and the *S* bromonitroalkane **2.24 (**Figure 101). With all four coupling partners for UmAS prepared, we turned our attention to assembling all four diastereomers of the DPG dipeptide.

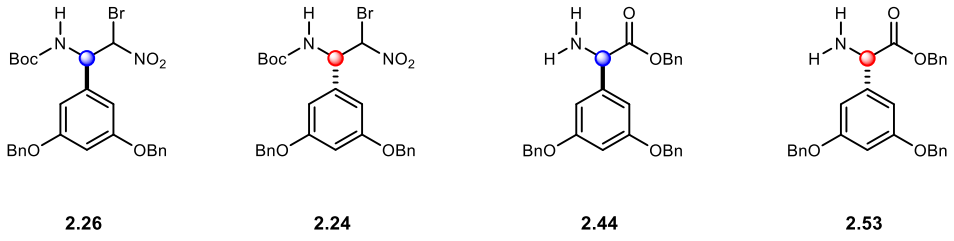

Figure 101. Representative R- and S-DPG building blocks for Umpolung Amide Synthesis (UmAS).

Beginning first with the preparation of the D-DPG-D-DPG dipeptide observed in cochinmicin 1 and 3, the *R* bromonitroalkane **2.26** and *R* amine **2.44** were successfully coupled together using UmAS to provide the D-DPG-D-DPG dipeptide (**2.45**) as a single diastereomer.

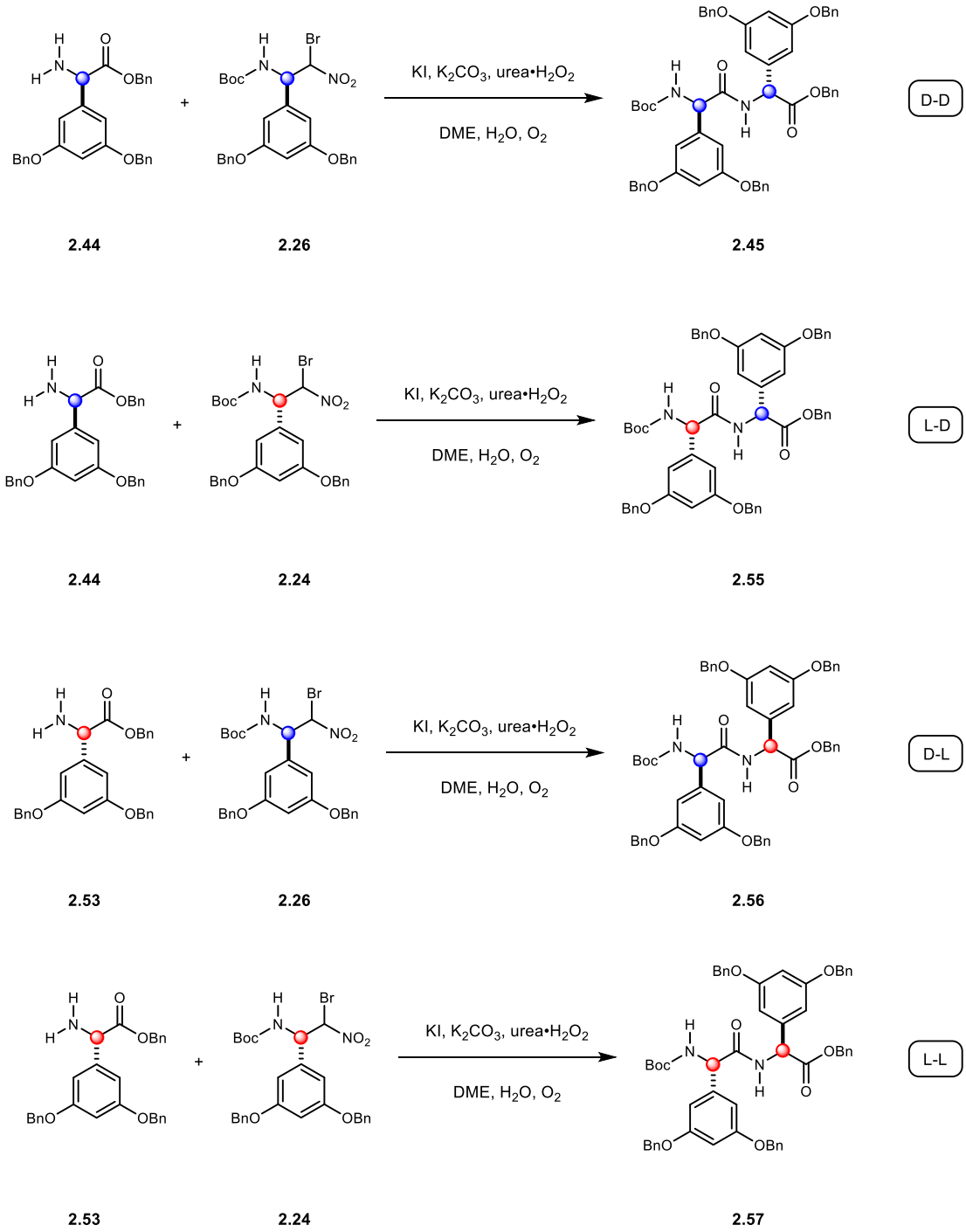

Figure 102. Preparation of all possible diastereomeric DPG dipeptides.

This same approach was used to access the D,L (**2.56**), L,D (**2.55**), and L,L (**2.57**) stereoisomers by employing the different enantioenriched DPG building blocks in UmAS. (Figure 102)

2.8.5 Assembling the Macrocyclization Precursor

With all three fragments in hand, we next turned our attention toward the assembly of the macrocyclization precursor, considering both macrolactonization and macrolactamization approaches.

2.8.5.1 Macrolactonization approach

Our first approach centered on the closure of the 16-membered macrocycle via macrolactonization. To this end, the requisite *seco*-acid would be constructed via amide bond formation from precursor carboxylic acid **2.59** and DPG dipeptide amine **2.60**. (Figure 103).

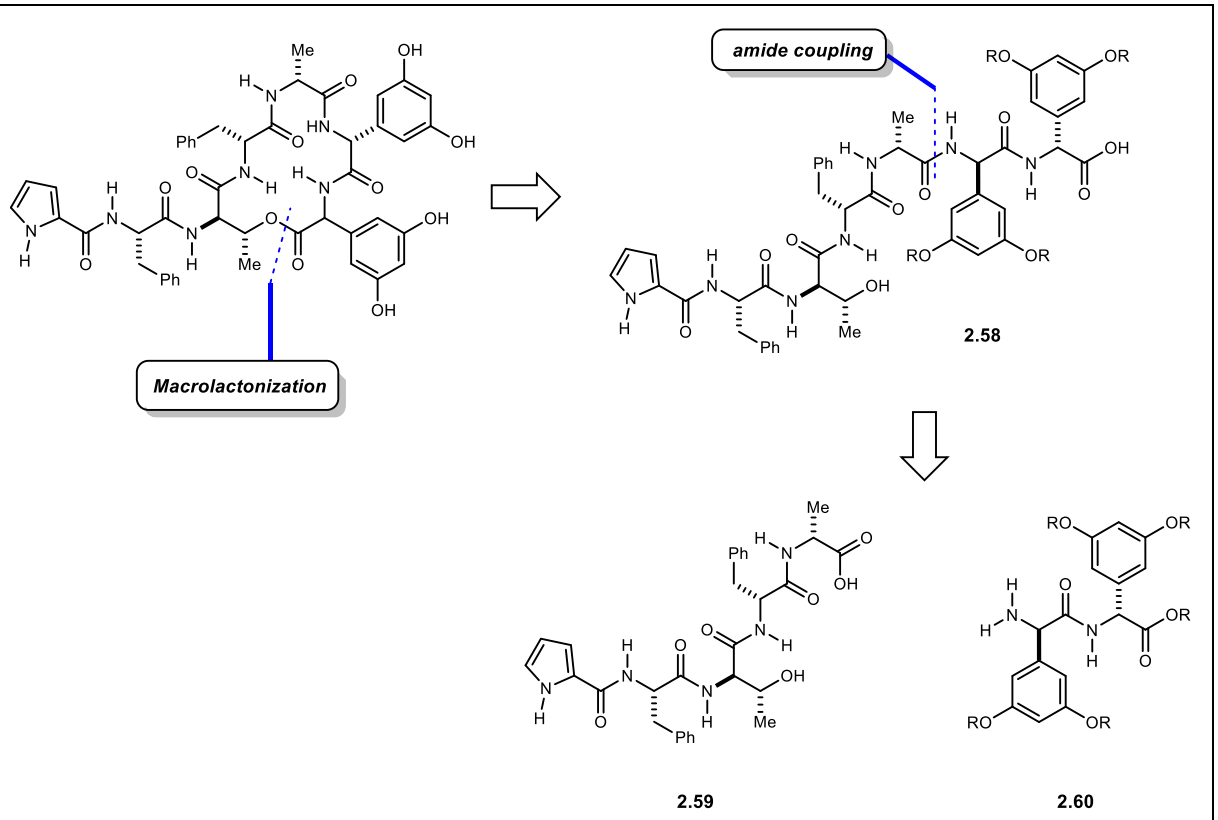

Figure 103. Proposed macrolactonization strategy to access the cochinmicins.

2.8.5.2 Preparation of Benzyl Ester Heptapeptide

Given the availability of different DPG-dipeptides accessed with UmAS, we reasoned this would provide alternative protecting group strategies for the evaluation of macrolactonization conditions. We first evaluated a benzyl ester substrate (**106.1**) which would allow for global deprotection to yield the cochinmicin *seco*-acid (Figure 104).

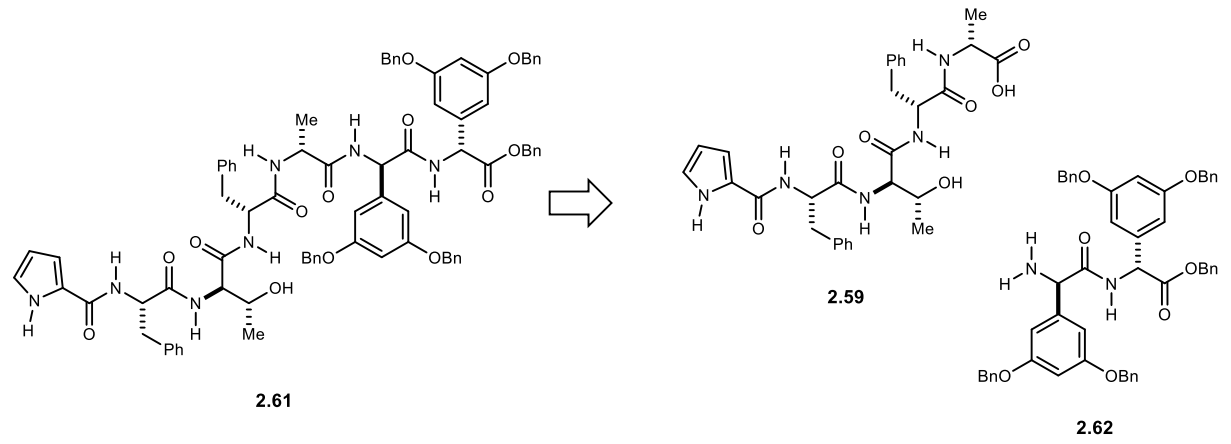

Figure 104. Synthetic strategy to access benzyl ester heptapeptide 2.61.

Preparation of the linear heptapeptide began with hydrogenolysis of pentapeptide **2.16** to reveal carboxylic acid **2.59**. DPG dipeptide **2.45** was then treated with TFA to reveal amine coupling partner **2.62**. (Figure 105)

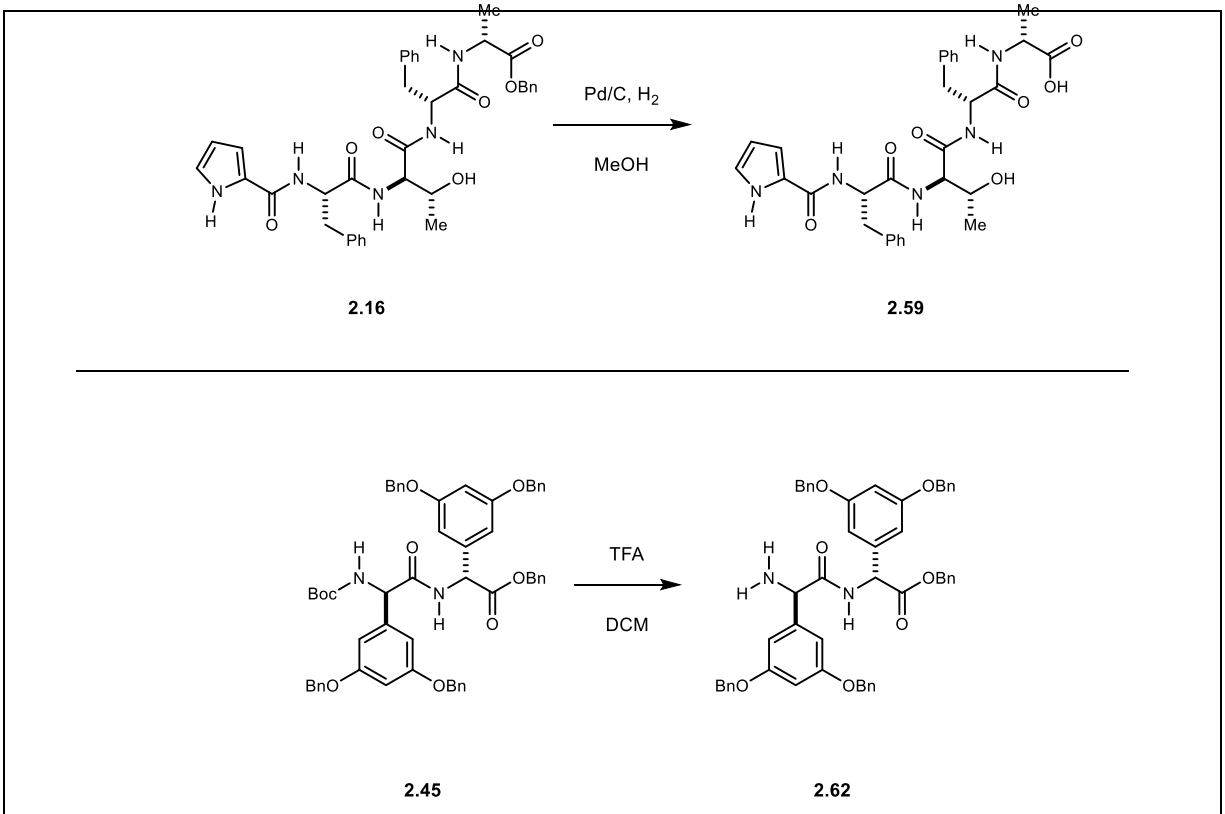

Figure 105. Preparation of carboxylic acid 2.59 and amine 2.62 coupling partners for synthesis of the linear heptapeptide.

Successful coupling of pentapeptide **2.59** and DPG dipeptide **2.62** was accomplished with DEPBT to give heptapeptide **2.61** with no detectable racemization. The solubility of this material rendered purification and subsequent steps particularly challenging. During the work-up, the desired heptapeptide would partially precipitate from the organic ethyl acetate extract. To address this challenge, the organic extract would be directly concentrated and simple trituration of the crude material with acetonitrile resulted in 80% pure heptapeptide. Further reverse-phase purification (90% MeCN-H_2O) yielded pure benzyl ester heptapeptide **2.61**.

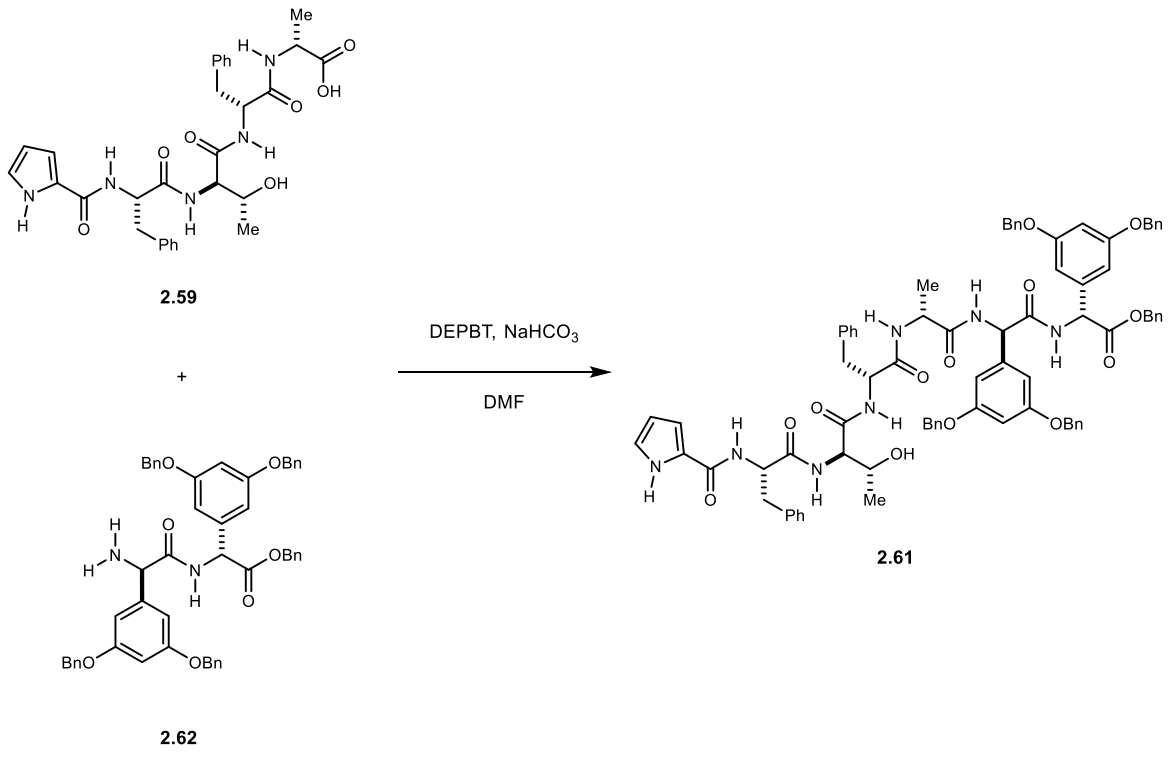

Figure 106. DEPBT-mediated amide coupling to access benzyl ester heptapeptide 2.61.

Due to the challenging solubility profile of the benzyl ester heptapeptide, consideration was given to an immediate global deprotection. Successful hydrogenolysis was accomplished under very dilute conditions (0.001 M) to cleave the benzyl ethers and benzyl ester (Figure 107).

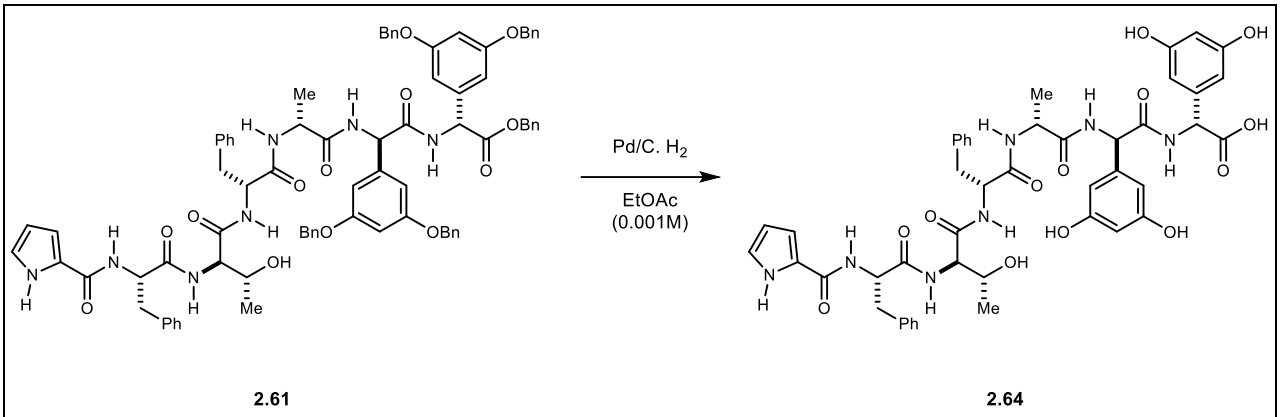

Figure 107. Global benzyl deprotection to afford cochinmicin 1 seco-acid.

Unfortunately, global deprotection to give *seco*-acid **2.64** did not vastly improve the solubility profile of the heptapeptide. This rendered subsequent macrolactonization attempts more challenging.

2.8.5.3 Macrolactonization attempts with cochinmicin 1 *seco*-acid

Preliminary efforts to access cochinmicin 1 began with evaluating macrolactonization conditions of *seco*-acid **2.64**, which we reasoned would mirror the biosynthesis of these natural products.

Table 6. Attempted macrolactonization to access cochinmicin 1.

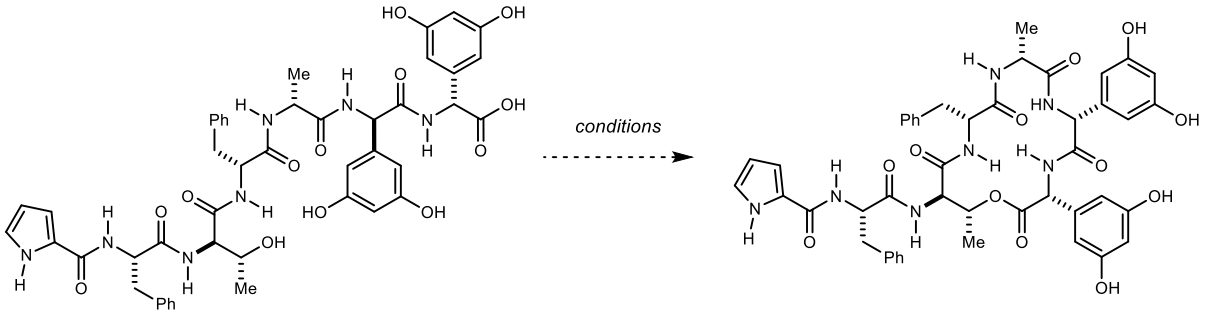

2.64 **2.65**

entry	reagents	temp	*seco*-acid addition	time
1	TCBCl (1.2 eq), DMAP (1.0 eq), NEt_3 (3.0 eq), PhMe/THF (0.001 M)	25 °C	9 h	40 h
2	TCBCl (1.2 eq), DMAP (1.0 eq), NEt_3 (3.0 eq), DMF (0.001 M)	25 °C	direct injection	21 h
3	TCBCl (5.2 eq), DMAP (5.2 eq), NEt_3 (5.2 eq), THF (0.001 M)	25 °C	direct injection	4.5 h
4	EDC (1.5 eq), DMAP(1.5 eq), DCE/DMF (0.001M)	0 °C then 25 °C	direct injection	22 h
5	EDC (2 eq), DMAP (2 eq), DMF (0.001 M)	25 °C then 50 °C	direct injection	23 h
6	TCB-DMAP (1.3 eq), iPr_2NEt (1.3 eq), THF-d_8 (0.001 M)	25 °C	J. Young NMR tube	24 h

Yamaguchi macrolactonization conditions have been employed in the synthesis of numerous cyclic depsipeptides. Following considerable precedence, *seco*-acid **2.64** was slowly added to a dilute mixture of 2,4,6-trichlorobenzoyl chloride (TCBCl), DMAP, and trimethylamine in THF/PhMe (Table 6, entry 1). While peptidic material was recovered, notably the ^{1}H NMR spectrum lacked the characteristic protons of the DPG residues. These conditions resulted in the apparent decomposition of the *seco*-acid. We hypothesized the challenging solubility profile was

contributing to this undesired outcome and as such, we attempted the transformation again but in dilute DMF (0.001 M, Table 6, entry 2). However, peptidic material was again isolated lacking characteristic DPG residues, even with the improved solubility of the *seco*-acid in DMF. We next reasoned the reagents could be reacting with other unprotected functionality and elected to increase the equivalents available for the desired acylation to occur (Table 6, entry 3). Challenges with Yamaguchi macrolactonization conditions were largely attributed to the reactivity of the acyl chloride and the insolubility of *seco*-acid **2.64**.

We next considered carbodiimide-based modes of activation. Treatment of *seco*-acid **2.64** with EDC and DMAP in DMF/DME resulted in a complex mixture of peptidic products with no indication of macrocyclization (Table 6, entry 4). We reasoned the solvent mixture could be hindering reactivity given the apparent insolubility of the *seco*-acid. However, treatment of *seco*-acid **2.64** with EDC and DMAP in DMF at 50 °C furnished a peptidic product, but not consistent with macrocyclization. (Table 6, entry 5).

In order to further evaluate what was occurring over the course of the reaction mixture, we considered monitoring the reaction in real-time by ^{1}H NMR. Encouraged by the opportunity to identify possible undesired reaction pathways, we employed a J. Young NMR tube (Table 6, entry 6). However, consumption of starting *seco*-acid occurred very rapidly and there was no clear evidence of formation of the corresponding mixed anhydride or subsequent cyclization.

To date, none of the macrolactonization attempts on this substrate were successful, which we attributed to the challenging solubility profile of the *seco*-acid (**2.64**).

2.8.5.4 Preparation of Allyl Ester Heptapeptide

To address the challenging solubility profile observed with the fully deprotected *seco*-acid **2.64**, we reasoned that an orthogonal protecting group strategy would offer advantages. Preparation of the allyl ester heptapeptide **2.66** commenced with acidic *N*-Boc deprotection to give amine **2.68** (Figure 108).

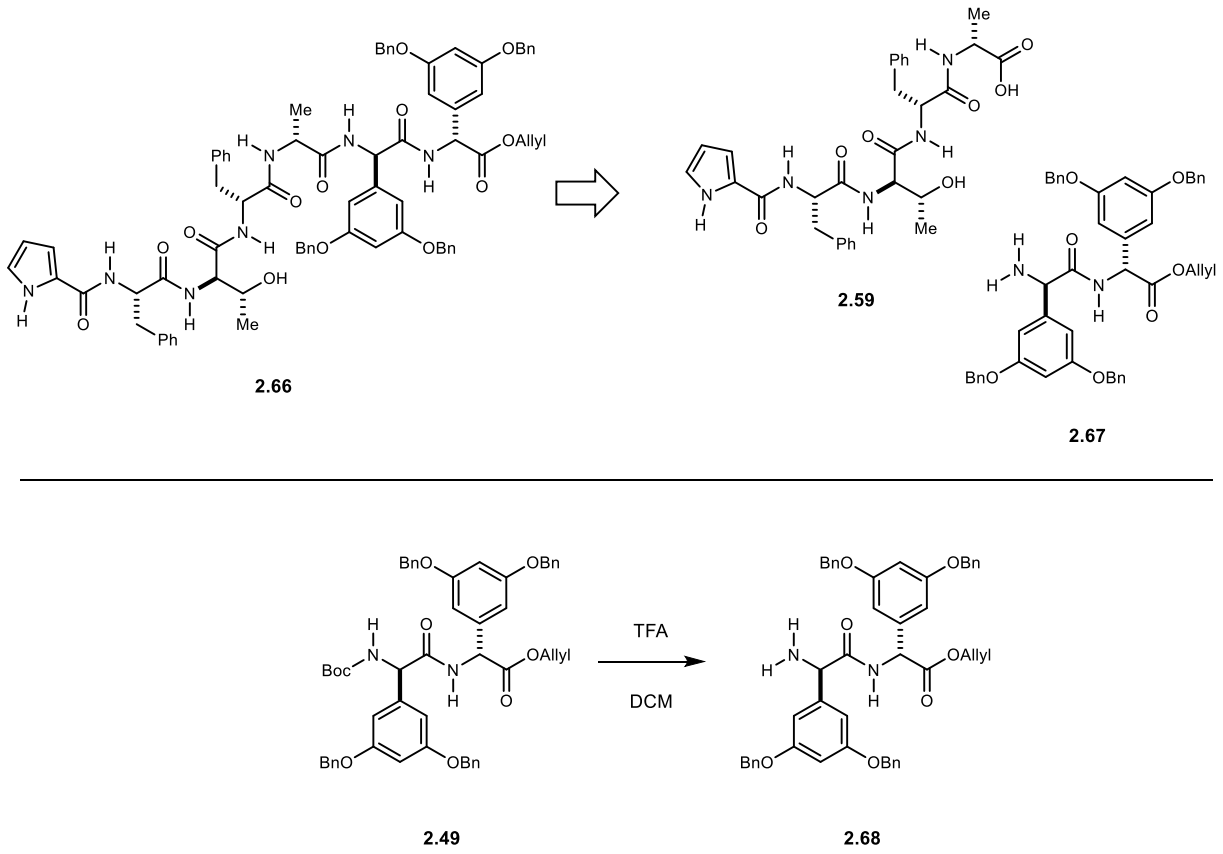

Figure 108. Synthetic strategy to access allyl ester heptapeptide.

Carboxylic acid **2.59** was then coupled with amine **2.68** to afford heptapeptide **2.66** (Figure 108). As was observed with the benzyl ester heptapeptide, the product began precipitating out of the organic extract during the work-up. The resulting crude material was triturated with acetonitrile to give material that was approximately 85% pure, which could be further purified via reverse-phase purification (90% MeCN-H_2O) to provide clean heptapeptide. While allyl ester **2.66** had an improved solubility profile when compared to the benzyl ester heptapeptide, it was still sparingly soluble in numerous solvents.

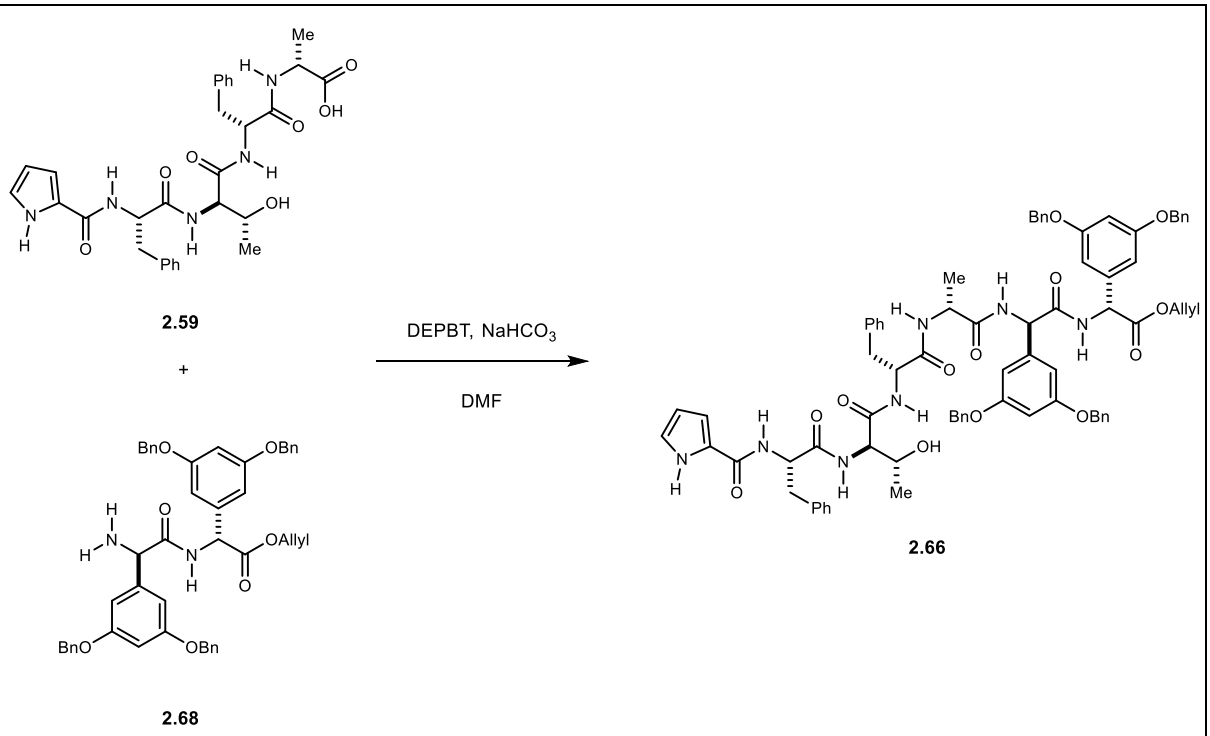

Figure 109. DEPBT-mediated coupling of carboxylic acid 2.59 and DPG dipeptide 2.68 to afford allyl ester heptapeptide 2.66.

With an approach to access heptapeptide **2.66** we next turned our attention to deprotection of the allyl ester to furnish *seco*-acid **2.69**. Treatment of **2.66** with $Pd(PPh_3)_4$ and morpholine revealed *seco*-acid **2.69** which could be used directly or further purified via reverse-phase purification (Figure 110). Notably, the solubility profile of this *seco*-acid **2.69** is greatly improved over the fully-deprotected *seco*-acid **2.64**. We hypothesized this improvement in solubility would provide for a more extensive evaluation of macrolactonization conditions.

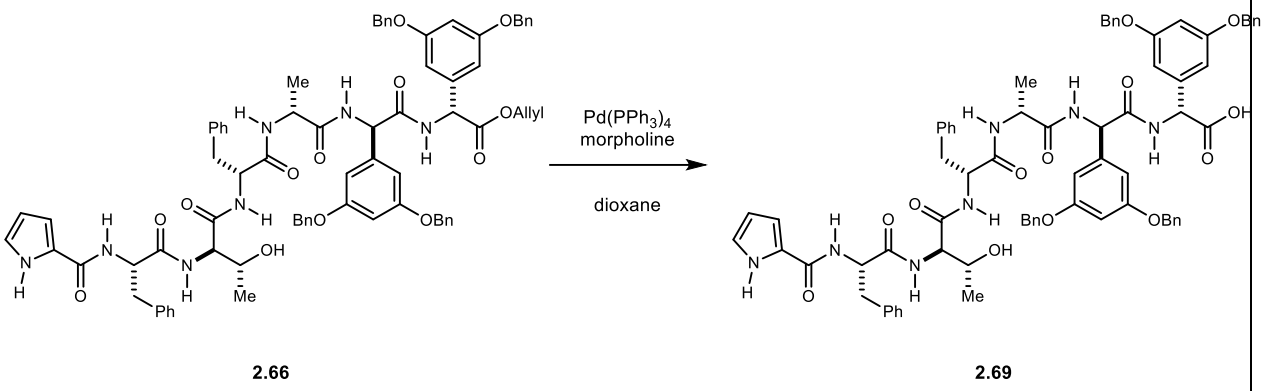

Figure 110. Pd(0)-mediated allyl ester deprotection to give seco-acid 2.69.

We next evaluated a series of reported macrolactonization conditions to furnish macrocycle **2.70** from *seco*-acid **2.69** (Table 7). Preliminary evaluation of carbodiimide activation methods resulted in the recovery of starting material with no evidence of macrocyclization (Table 7, entry1-2). Although Yamaguchi macrolactonization conditions are frequently reported to prepare cyclic depsipeptides, we were unable to construct the desired macrocycle under these conditions (Table 7, entries 3-6). In each case, starting material was recovered or a complex mixture of peptidic products was produced with no indication of macrolactonization. Numerous reports indicate Shiina macrolactonization conditions offer an advantage in the preparation of challenging macrocycles. However, treatment of *seco*-acid **2.69** with MNBA was also unsuccessful in producing the desired macrocycle (Table 7, entries 7-11). While *seco*-acid **2.69** had an improved solubility profile, we were unable to affect the desired macrolactonization under any of the attempted conditions.

Table 7. Attempted macrolactonization on benzyl ether protected heptapeptide 2.69 to access 2.70.

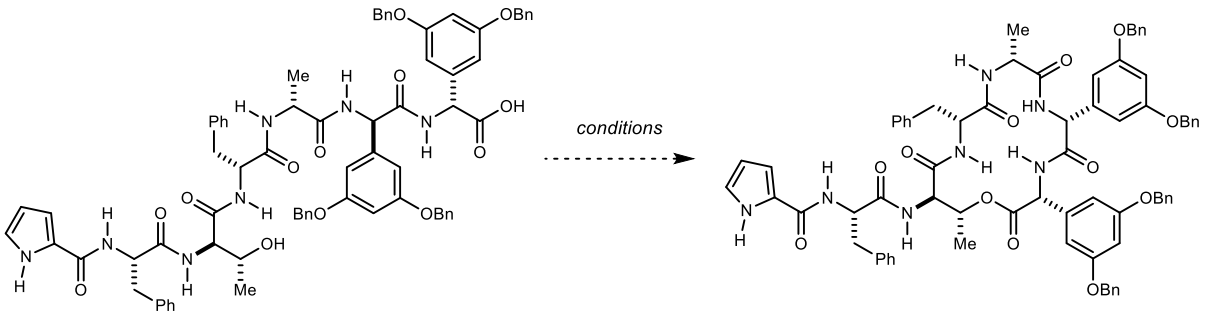

2.69 **2.70**

entry	reagents	temp	time
1	EDC (1.5 eq), DMAP (1.5 eq), DMF (0.001 M)	0 °C then 25 °C	24 h
2	DCC (10 eq), pyridine (20 eq), PPTS (10 eq), DCE (0.001M)	25 °C	4 h
3	TCBCl (1.25 eq), DMAP (1.5 eq), NEt_3 (1.5 eq), 2-Me-THF (0.001M)	25 °C	23 h
4	TCBCl (1.25 eq), DMAP (2.0 eq), NEt_3 (1.5 eq), THF (0.001M)	50 °C	3 h
5	TCBCl (1 eq), NEt_3 (1 eq), THF (0.07 M)		2 h
6	TCBCl (1.05 eq), DMAP (2 eq), NEt_3 (1.5 eq), THF (0.0035 M)	70 °C	
7	MNBA (1.5 eq), DMAP (3 eq), PhMe/THF (0.001 M)		
8	MNBA (1.5 eq), DMAP (3 eq), NEt_3 (2 eq), THF (0.001 M)	70 °C	3 h
9	MNBA (1.5 eq), DMAP (3 eq), NEt_3 (2 eq), PhMe (0.001 M)	25 °C	
10	MNBA (1.5 eq), DMAP (3 eq), NEt_3 (2 eq), THF (0.001 M)	65 °C	1 h
11	MNBA (3 eq), DMAP (6 eq), iPr_2NEt (3 eq), $La(OTf)_3$ (0.3 eq), THF (0.002 M)	65 °C	20 h

We reasoned that the challenges associated with the solubility of the respective *seco*-acids and the apparent lack of reactivity rendered the macrolactonization strategy ineffective. Given the modular nature of our synthetic strategy, we reasoned intermolecular esterification followed by macrolactamization would be more successful.

2.8.5.5 Macrolactamization Approach

We next turned our attention toward the construction of the 16-membered macrocycle via macrolactamization, which requires the construction of the *endo*-ester bond and then late-stage amide bond formation to affect the ring closure. (Figure 111)

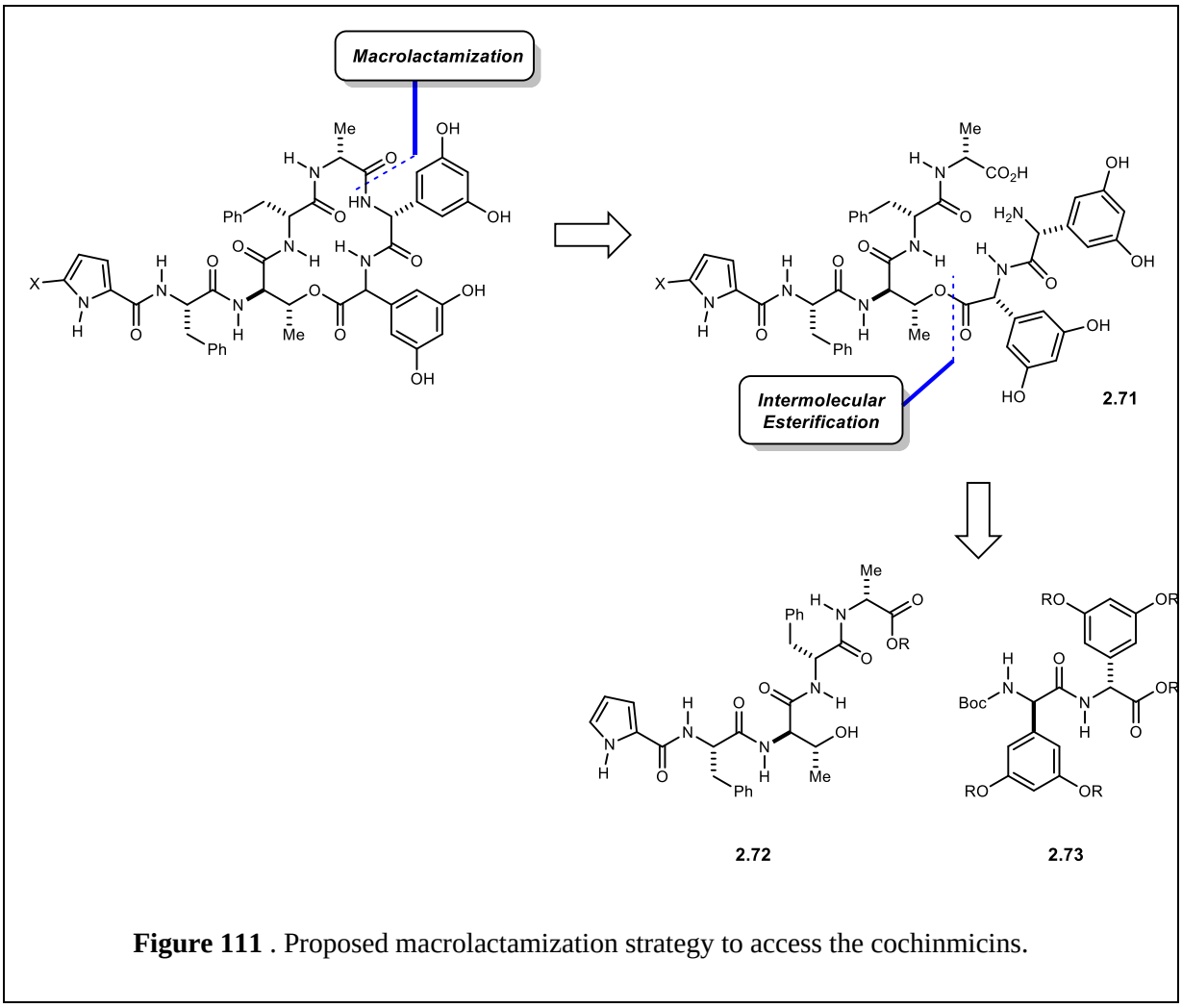

Figure 111 . Proposed macrolactamization strategy to access the cochinmicins.

2.8.5.6 Intermolecular Esterification

Our first challenge was to identify suitable conditions to access the desired ester. To this end, we evaluated a model system using the DPG dipeptide **2.46** and protected threonine **2.75** (Table 8). Treatment of carboxylic acid **2.46** with EDC and DMAP in the presence of protected D-threonine **2.75** provided no evidence of acylation (Table 8, entry 1). Only reagents and unreacted D-threonine **2.75** were recovered from the reaction. Notably, there was no evidence of any DPG-derived products from this attempted transformation. We reasoned an alternative activation mode might address this apparent decomposition. To this end, a Mitsunobu esterification was attempted (Table 8, entry 2). While these conditions did not result in the decomposition of carboxylic acid **2.46**, they did not produce the desired ester **2.76** and starting materials were recovered.

Table 8. DPG dipeptide intermolecular esterification model system.

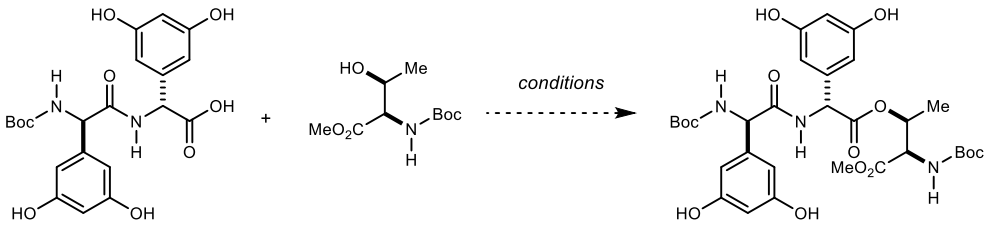

2.46 **2.75** **2.76**

entry	reagents	carboxylic acid (equiv)	alcohol (equiv)	time	outcome
1	EDC (1.5 eq), DMAP (1.5 eq), DMF (0.001 M)	1.0	1.5	20 h	decomposition
2	PPh3 (2 eq), DIAD (2 eq), THF (0.05 M)	1.0	1.0	20 h	n.r

We reasoned the challenging solubility profile of the carboxylic acid and the apparent decomposition rendered this substrate less suitable for the desired esterification. Further attempts to convert the carboxylic acid **2.46** to the corresponding Yamaguchi mixed anhydride **2.77** resulted in complex mixtures of products (Figure 112). Based on these results, we reasoned a two-step approach to preparing the desired ester from the isolated mixed anhydride would be unsuccessful and considered other activation modes.

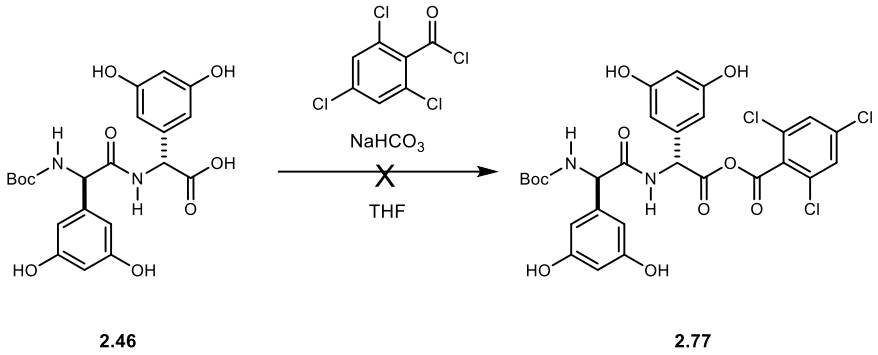

2.46 **2.77**

Figure 112. Attempted preparation of the Yamaguchi mixed anhydride from dipeptide **2.46.**

Further efforts to convert carboxylic acid **2.46** to the corresponding acyl halide were largely unsuccessful (Figure 113). The resulting complex mixture was likely attributed to the acid-labile functionality on the substrate, which resulted in the undesired decomposition of carboxylic acid **2.46**.

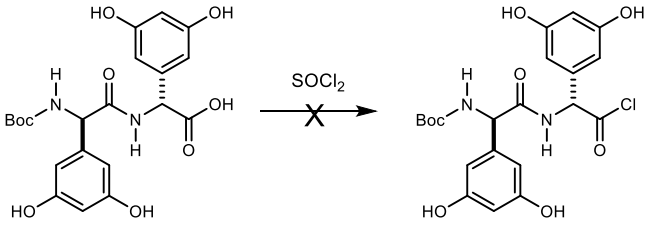

2.46 **2.78**

Figure 113. Attempted conversion of carboxylic acid **2.46** to acyl chloride **2.78**.

Given the observed challenges with the deprotected carboxylic acid **2.46**, we reasoned the analogous benzyl ether protected **2.41** would confer improvements in solubility and reactivity allowing opportunities to form the desired ester linkage. However, efforts to transform carboxylic acid **2.41** to the desired ester **2.79** resulted in the recovery of starting material (Figure 114).

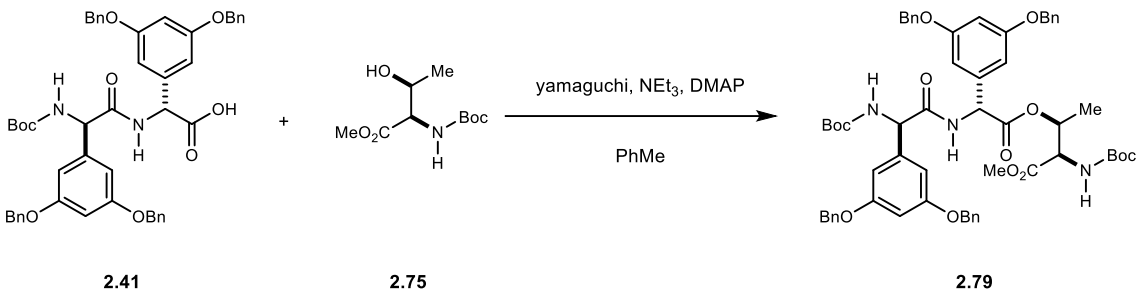

Figure 114. Attempted esterification of carboxylic acid 2.41 and protected threonine 2.75.

Given the challenges associated with the DPG-dipeptide substrate, we considered an even simpler model system using protected D-DPG **2.37** and D-threonine residues **2.75** to identify suitable acylation conditions.

Table 9. Intermolecular esterification with D-DPG 2.37 and protected D-threonine 2.75.[a]

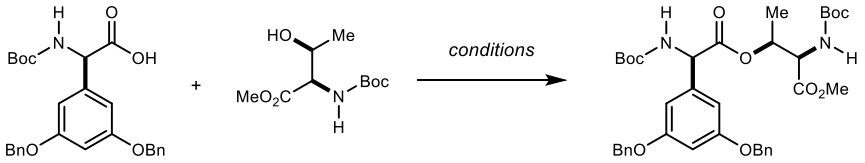

entry	reagents	carboxylic acid (equiv)	alcohol (equiv)	time	outcome
1	PPh_3 (2 eq), DIAD (2 eq), THF (0.05 M)	1.0	1.0	22 h	n.r.
2	EDC (3 eq), DMAP (0.3 eq), DCM (0.1 M)	2.0	1.0	24 h	<10%
3	EDC (1.5 eq), DMAP (1.5 eq), DMF (0.001 M)	1.0	1.5	7 h	not isolated
4	TCBCl (1.25 eq), NEt_3 (3 eq), DMAP (2 eq), PhMe (0.1 M)	1.0	1.05	6 h	35%
5	TCBCl (1.25 eq), NEt_3 (1.5 eq), DMAP (0.1 eq), DMF (0.1 M)	1.0	1.05	38 h	<10%
6	DEPBT (1.5 eq), iPr_2NEt (1.5 eq), DMF (0.1 M)	1.0	1.05	51 h	<10%
7	EDC (1.2 eq), HOAt (1.2 eq), iPr_2NEt (1.2 eq), DMF (0.1 M)	1.0	1.5	48 h	<10%

There was no observed reaction between carboxylic acid **2.37** and threonine **2.75** under Mitsunobu esterification conditions (Table 9, entry 1). Carbodiimide activation with catalytic DMAP resulted in less than 10% conversion to the desired ester **2.80**. (Table 9, entry 2). However, when DMAP was added in excess, the desired ester was observed for the first time (Table 9, entry 3). However, preactivation of carboxylic acid **2.37** with the Yamaguchi reagent then addition to a solution of DMAP and protected threonine **2.75** resulted in the formation of the desired ester (**2.80**), albeit as a 1:1 mixture of epimers (Table 9, entry 4). Efforts to mitigate epimerization at a lower temperature under Yamaguchi esterification conditions were detrimental to conversion (Table 9, entry 5). Further efforts to address the undesired racemization under other activation modes were also detrimental to conversion (Table 9, entries 6-7).

Following successful acylation of the protected threonine model system, we saw a further opportunity to evaluate the viability of the unprotected DPG residue in the esterification conditions. To this end, carboxylic acid **2.81** was activated with Yamaguchi's reagent in the presence of protected threonine **2.75** (Figure 115). However, there was no observed conversion to the desired ester **2.82**.

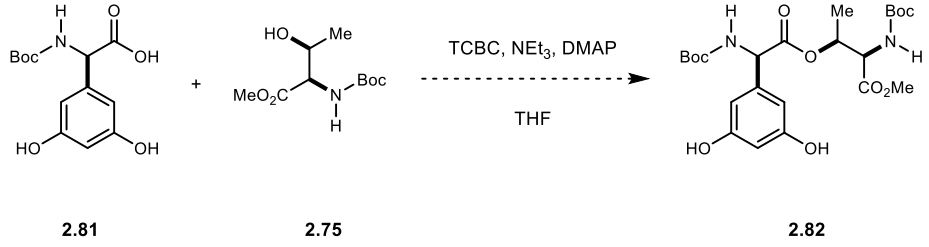

2.81 **2.75** **2.82**

Figure 115. Attempted esterification with unprotected DPG residue 2.81

Encouraged by the results of the model system, we sought to extend these results to acylation of the pentapeptide **2.16** (Table 10). Application of the successful Yamaguchi esterification protocol afforded the desired ester linkage, albeit in low yield and as a 1.1:1 mixture of epimers (Table 10, entry 1). Unfortunately, these conditions also resulted in the undesired acylation of pentapeptide **2.16** with the Yamaguchi's reagent (Figure 116). Notably, we were recovering >50% of the starting pentapeptide from these attempts, which accounted for the low yields of ester **2.84**. We sought to improve the yields of this reaction, mitigate the undesired acylation of the pentapeptide, and favor the formation of the desired epimer.

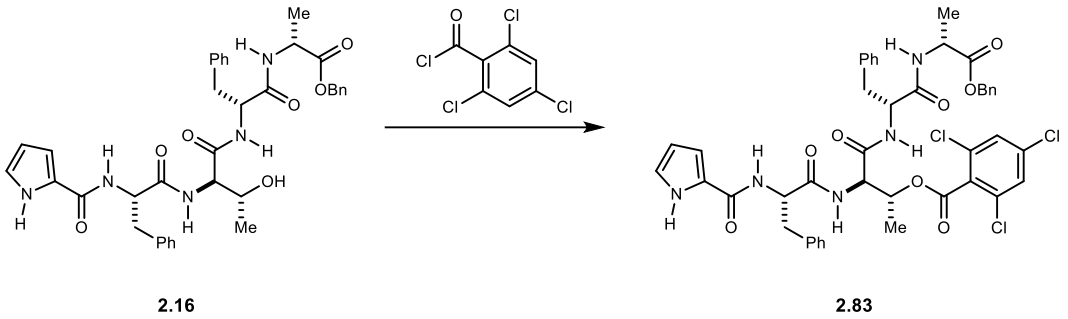

Figure 116. Formation of undesired yamaguchi ester 2.83.

Efforts to run the reaction at lower temperature and with a different base offered minimal improvements in the ratio of epimers and was also detrimental to conversion (Table 10, entry 2-3). We considered that the solubility of the reactants in the THF-PhMe mixtures played an unfavorable role in conversion. While employing 2-Me-THF resulted in a two-fold improvement in yield it did not offer improvements in the undesired acylation and racemization (Table 10, entry 5). We hypothesized that excess Yamaguchi reagent was responsible for the undesired acylation. Treatment of carboxylic acid **2.37** with Yamaguchi reagent (1 equiv) reduced the undesired acylation but did not eliminate it (**Table 10**, entries 6-7). We reasoned increasing the available carboxylic acid would sequester the acyl chloride during the preactivation step, effectively reducing the available acid chloride which could undergo undesired acylation of the pentapeptide. To our delight, this approach resulted in the formation of the desired ester with no observed acylation of the pentapeptide with the Yamaguchi reagent (Table 10, entry 9-10).

Table 10. Intermolecular esterification with pentapeptide 2.16 and D-DPG 2.37

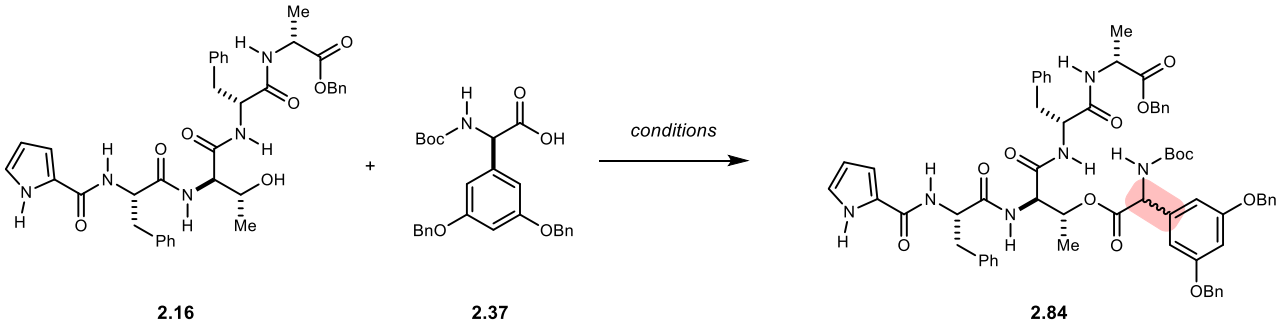

2.16 **2.37** **2.84**

entry	reagents	carboxylic acid (equiv)	alcohol (equiv)	preactivation time	temp	time	dr	yield (%) (isolated)
1	TCBCl (1.25 eq), NEt_3 (1.5 eq), DMAP (1 eq), THF-PhMe	1.0	1.05	30 min	25 °C	1 h	1.1:1	25
2	TCBCl (1.25 eq), NEt_3 (1.5 eq), DMAP (1 eq), THF-PhMe	1.0	1.05	45 min	0 °C	1.5 h	1.2:1	14
3	TCBCl (1.25 eq), $NaHCO_3$ (1.5 eq), DMAP (1 eq), THF-PhMe	1.0	1.05	2.5 h	0 °C	3 h	1.4:1	15
4	TCBCl (1.25 eq), NEt_3 (1.5 eq), DMAP (1 eq), THF-PhMe	1.0	1.05	30 min		2 h	1:1.1	18
5	TCBCl (1.25 eq), NEt_3 (1.5 eq), DMAP (1 eq), 2MeTHF	1.0	1.0	1.5 h		24 h	1:1.2	47
6	TCBCl (1.0 eq), NEt_3 (1.5 eq), DMAP (1 eq), 2MeTHF	1.2	1.0	1.5 h	25 °C	23 h	1:1	39
7	TCBCl (1.0 eq), NEt_3 (1.5 eq), DMAP (1 eq), 2MeTHF	1.0	1.0	1.5 h	25 °C	23 h	1:1	40
8	TCBCl (1.0 eq), NEt_3 (1.5 eq), DMAP (1 eq), 2MeTHF	2.0	1.0	1.5 h	25 °C	23 h	1:1.1	27
9	TCBCl (2.0 eq), NEt_3 (2.1 eq), DMAP (1 eq), 2MeTHF, PhH	3.0	1.0	2 h	25 °C	11.5 h	1:1	48

Encouraged by the model system results, we sought to extend these improved conditions to the desired esterification of DPG-dipeptide (**2.85** or **2.86**) and pentapeptide **2.16** to prepare the requisite macrolactamization precursor. Preliminary efforts with the deprotected dipeptide **2.85** were unsuccessful (Table 11, entries 1-2). From these attempts, we recovered unreacted pentapeptide, undesired acylated product, and quenched reagents. We reasoned that the challenging solubility profile of the deprotected dipeptide **2.85** was detrimental to conversion.

We next evaluated the benzyl ether-protected equivalent (**2.86**). In all cases, pentapeptide **2.16** was recovered and there was no discernible ester formation. To date, there were no indications of the formation of the desired ester with either of these substrates.

Table 11. Attempted extension of model system to DPG-dipeptide esterification to yield 2.87.[a]

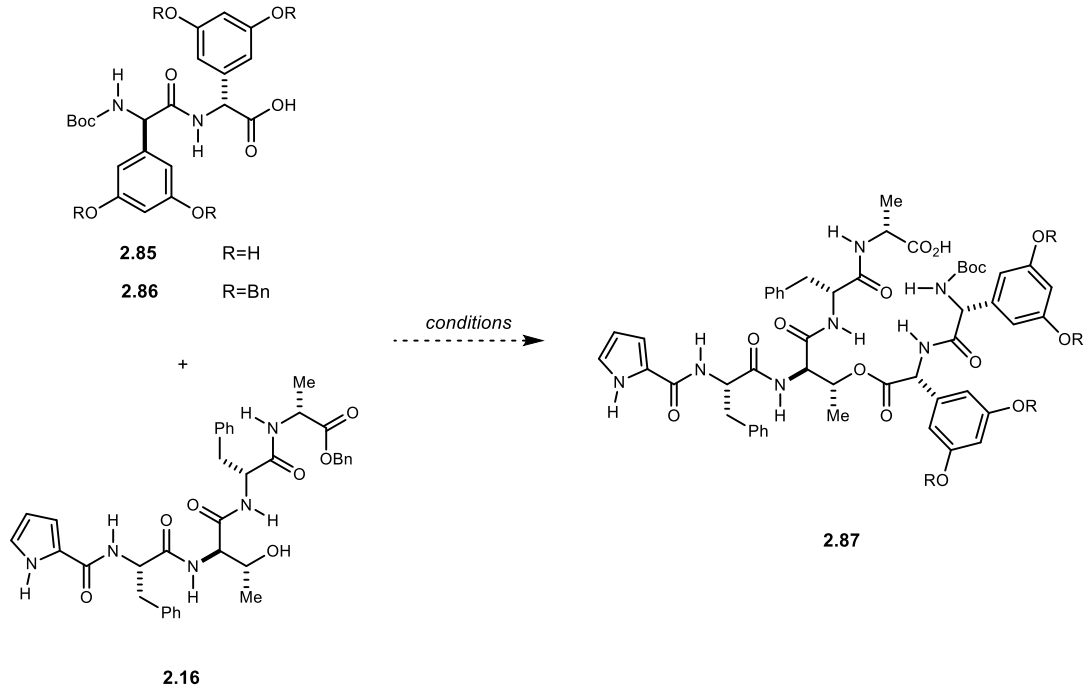

entry	R	reagents	carboxylic acid (equiv)	alcohol (equiv)	preactivation time	temp	time
1	H	TCBCl (1.25 eq), NEt3 (3 eq), DMAP (2 eq), PhMe	1.0	1.05	-	25 °C	20 h
2	H	EDC (1.2 eq), HOAt (1.2 eq), iPr_2NEt (1.2 eq), DMF	1.0	1.5	-	0 °C	17 h
3	Bn	TCBCl (1.25 eq), DMAP (1.5 eq), NEt_3 (1.5 eq), PhMe-THF	1.0	1.05	45 min	0 °C	2 h
4	H	EDC (1.5 eq), DMAP (0.1 eq), DMF (0.05 M)	1.0	1.2	-	0 °C 3 h then 25 °C	6 h
5	Bn	MNBA (1.5 eq), DMAP (3 eq), NEt_3 (2 eq), THF (0.01 M)	1.0	1.05	30 min		3 h

We next turned our attention to improving conversion to the desired ester (**2.84**) and reducing the recovery of starting pentapeptide **2.16**. We uncovered that purifications with MeOH in DCM resulted in degradation of ester **2.84** to pentapeptide **2.16**. Purifications with more hindered ^{i}PrOH in DCM offered moderate improvements in isolation. However, employing polar aprotic MeCN in DCM offered the best isolation conditions.

Due to the challenges with Yamaguchi's reagent and undesired acylation, we reasoned that the acyl chloride was too reactive. Previous reports demonstrate the utility of TCB-DMAP in the preparation of esters where the acyl chloride is problematic. [271] TCB-DMAP was prepared according to Yamamoto's procedure.[272] Treatment of carboxylic acid **2.37** with TCB-DMAP in the presence of Hünig's base and pentapeptide **2.16** resulted in clean conversion to the desired ester (**2.84**) in modest yield (Table 12, entry 1). Notably, we observed no formation of the undesired acylation product. However, this approach did not rectify the epimerization of the DPG residue in this esterification.

Efforts to strike a balance between conversion and competitive racemization were challenging. We hypothesized that cooling the reaction would confer improvement in selectivity. Although epimer ratios were improved, it was at the expense of conversion to the desired ester and greater than 50% of the pentapeptide starting material was recovered (Table 12, entry 2). Further, replacing Hünig's base with $NaHCO_3$ also offered improvement in selectivity at the expense of conversion (Table 12, entry 3).

Table 12. Evaluation of TCB-DMAP reagent in intermolecular esterification of DPG 2.37 and pentapeptide 2.16.

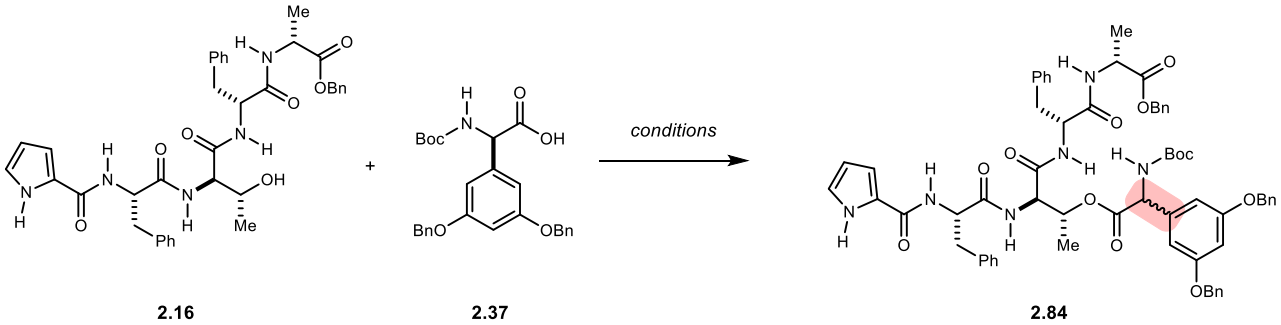

2.16 **2.37** **2.84**

entry	reagents	carboxylic acid (equiv)	alcohol (equiv)	temp	time	dr	yield
1	TCB-DMAP (1.3 eq), iPr_2NEt (1.3 eq), 1:1 THF-PhMe	1.0	1.0	25 °C	18 h	1:1	55
2	TCB-DMAP (1.3 eq), iPr_2NEt (1.3 eq), 1:1 THF-PhMe	1.0	1.0	0 °C	18 h	10:1	6
3	TCB-DMAP (1.3 eq), $NaHCO_3$ (1.3 eq), 1:1 THF-PhMe	1.0	1.0	25 °C	18 h	4:1	5
4	TCB-DMAP (1.3 eq), iPr_2NEt (1.3 eq), 1:1 THF-PhMe	1.0	1.0	0 °C 2 h, then 25 °C	19 h	3:1	51
5	TCB-DMAP (1.3 eq), iPr_2NEt (1.0 eq), 1:1 THF-PhMe	1.0	1.0	25 °C	12 h	5:1	43
6	TCB-DMAP (1.3 eq), iPr_2NEt (1.0 eq), 1:1 THF-PhMe	1.0	1.0	0 °C	8 h	4:1	54
76	TCB-DMAP (1.3 eq), iPr_2NEt (1.3 eq), THF	1.0	1.0	0 °C 2 h, then 25 °C	12 h	1:1	61
8	TCB-DMAP (1.3 eq), iPr_2NEt (1.3 eq), THF	1.0	1.0	0 °C 2 h, then 25 °C	12 h	1:1.1	60
9	TCB-DMAP (1.3 eq), pyridine (1.3 eq), THF	1.0	1.0	0 °C 2 h, then 25 °C	23 h	1.1:1	39
10	TCB-DMAP (1.4 eq), iPr_2NEt (1.0 eq), THF	1.1	1.0	0 °C	18 h	3:1	79
11	TCB-DMAP (1.3 eq), iPr_2NEt (1.0 eq), THF	1.0	1.0	0 °C	17 h	3:1	53

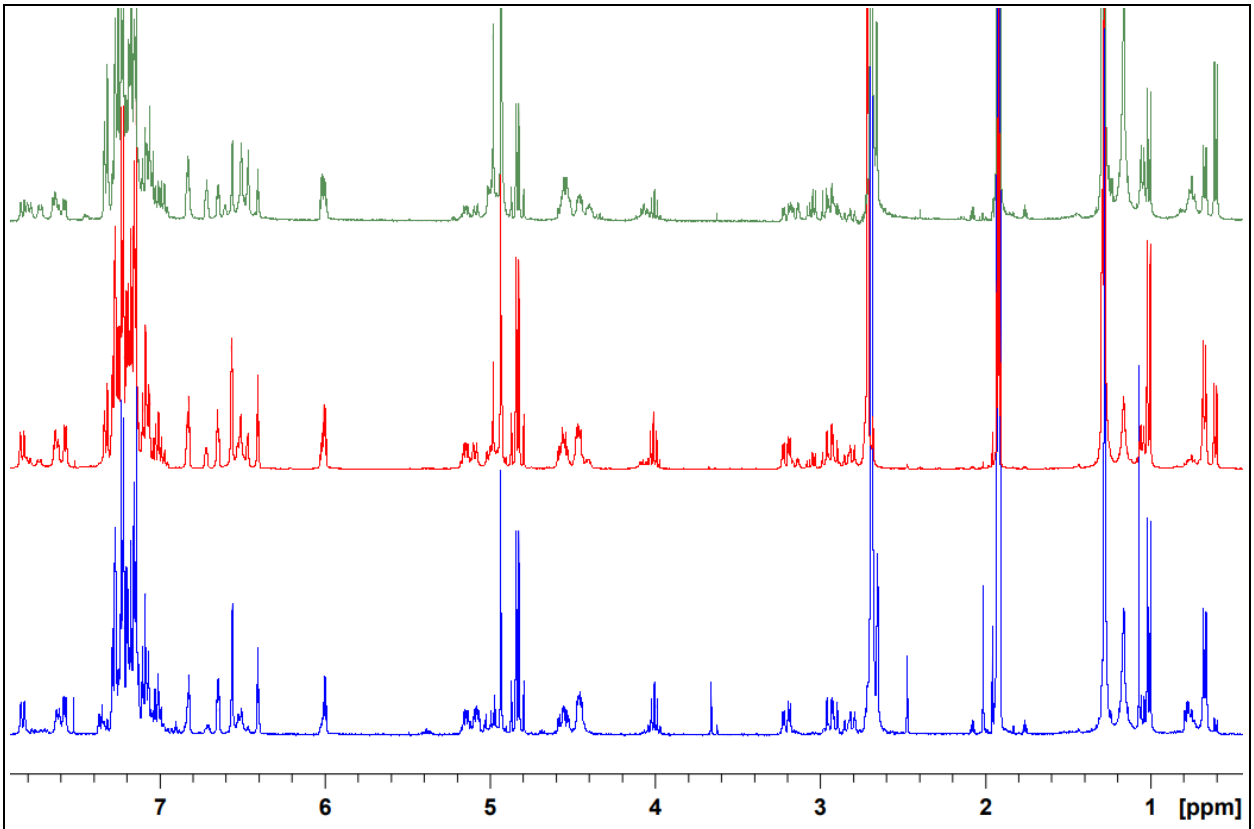

Figure 117. First evidence that epimers 2.84 were separable via column chromatography.

While decreasing the equivalents of the base did not offer great improvement in selectivity, this was the first indication that the epimers could be separable using chromatography (Table 12, entry 5). Fractions collected from the beginning, middle, and end all had varying levels of enrichment (14:1, 1:1, 1:2, respectively), which indicated further optimization of this separation could yield each epimer exclusively (Figure 117). Encourage by these results, we further explored the viability of separating the epimers via chromatographic methods. To this end, we identified method by which epimers were separable by HPLC (Figure 118).

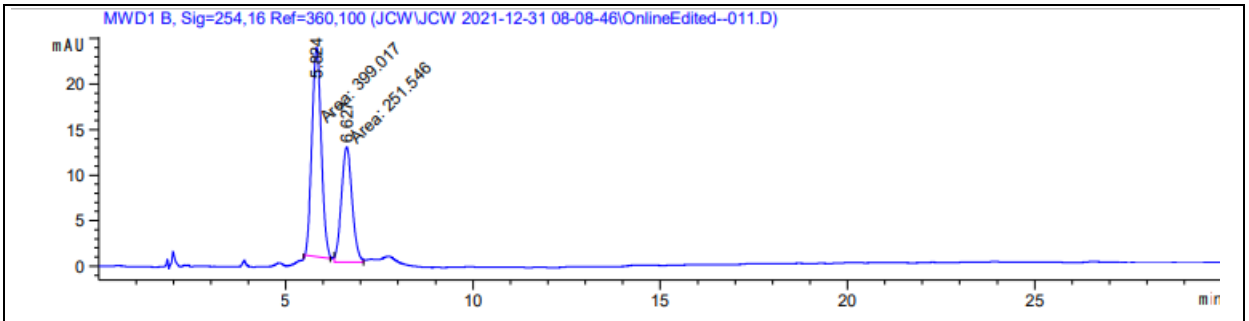

Figure 118. Evaluation of separation of epimers 2.84 via HPLC. Depicted is a 1.5:1 ratio of epimers which is slightly favoring the major epimer.

Serendipitously, we uncovered the minor epimer to be crystalline enabling separation of the major and minor epimers (Figure 119). Further efforts to grow a single crystal for further analysis are on-going. We will report the findings of this structural analysis in due course and expect this will provide insight into the mechanism by which the undesired epimerization is occurring.

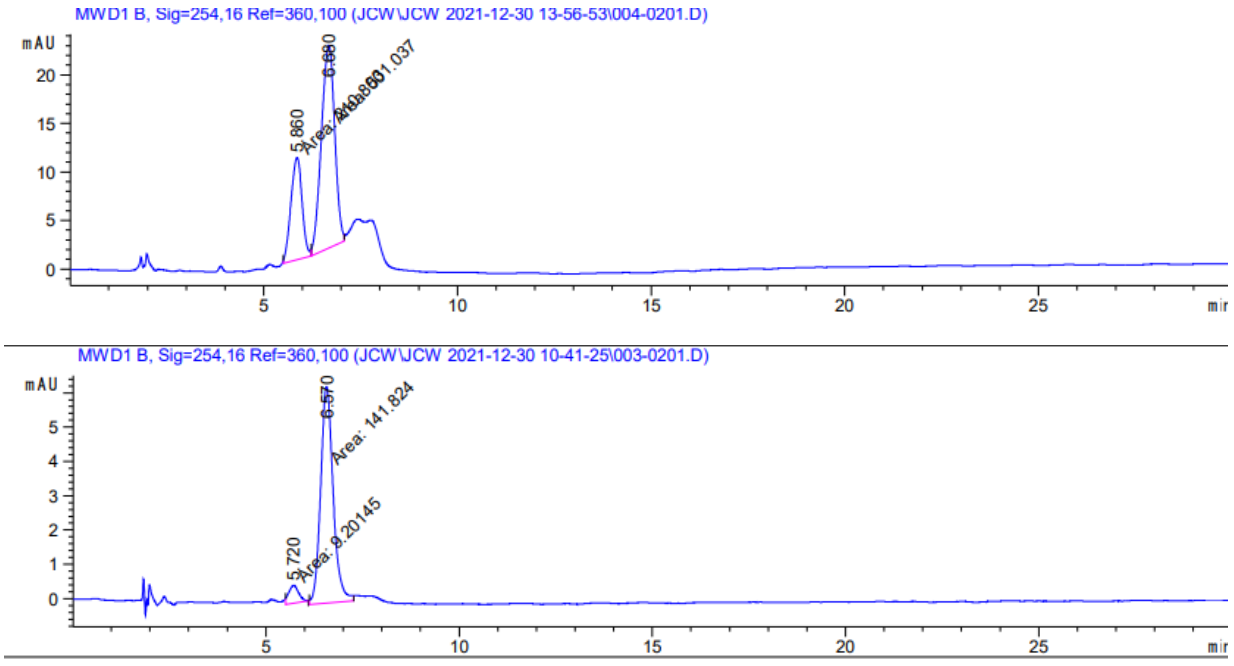

Figure 119. Enrichment of the minor epimer (retention time = 6.6 min) following diffusion chamber crystallization (Et_2O/Acetone). Began with ester 2.84 with a ratio of epimers slightly favoring the minor (1:3) and crystallization provided a 6:94 ratio of epimers significantly favoring the minor epimer.

Decreasing the equivalents of base and cooling the reaction favored the formation of the desired epimer (4:1 d.r.) and provided compromise for conversion (Table 12, entry 6). Notably, pre-activation of carboxylic acid **2.37** with TCB-DMAP for 1 h prior to addition of pentapeptide **2.16** resulted in the best conversion and selectivity to date (**Table 12**, entry 11). This pre-activation method provides an opportunity for improved conversion without compromising selectivity.

To our knowledge, this represents the first example of TCB-DMAP reagent being utilized in the preparation of a cyclic depsipeptide. Efforts to evaluate post-reaction epimerization and further optimize this transformation are on-going.

2.8.5.7 Completion of the Synthesis

Alternatively, we considered the extension of ester **2.84** to the desired macrolactamization precursor via installation of the second DPG residue. Given our previous success in the preparation of the DPG dipeptide, we reasoned UmAS would provide an efficient strategy to install the remaining DPG residue without epimerization. To this end, ester **2.84** upon treatment with TFA furnished amine **2.89**. (Figure 120).

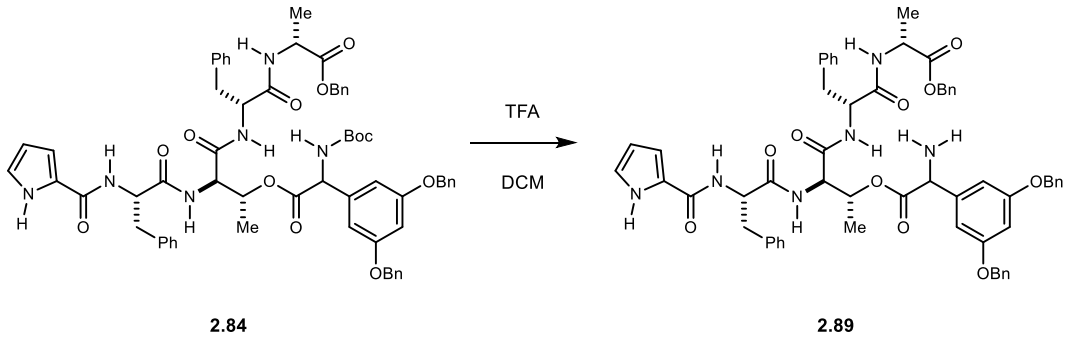

Figure 120. Preparation of amine **2.89** for UmAS.

To our delight, amine **2.89** was coupled with one equivalent of *R*-bromonitroalkane to afford amide **2.90**. However, low to modest yields restricted the efficiency of this approach. Efforts to improve conversion were plagued by competitive hydrolysis of the ester to give pentapeptide **2.16**. Unsurprisingly, due to the presence of mildly basic aqueous conditions in this approach. While the pentapeptide could be recycled, this competitive reaction pathway limited this

approach, and efforts to improve this were largely unsuccessful. Alternative, UmAS conditions are currently being evaluated to mitigate undesired hydrolysis and improve yields.

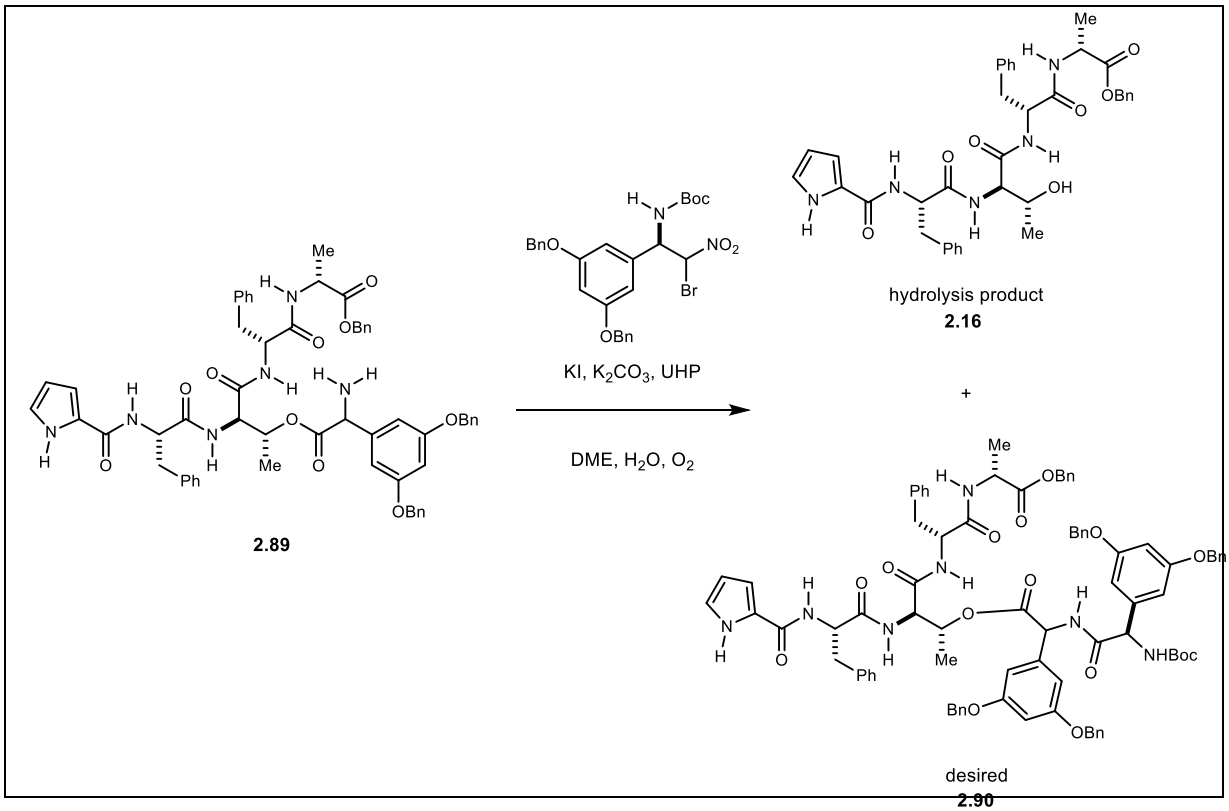

Table 13. UmAS to access **2.90**.[a]

entry	UHP addition	temp	time	hydrolysis product (%) (isolated)	yield (%) (isolated)
1	direct inj (3.0 M)	0 °C	30 h	40	60
2	direct inj (3.0 M)	0 °C 2 h, then 25 °C	17 h	not recovered	32
3	direct inj (3.0 M)	0 °C 12 h, then 25 °C	17 h	not recovered	31
4	direct inj (3.0 M)	0 °C 2 h, then 25 °C	22 h	40	25
5	direct inj (3.0 M)	0 °C 2 h, then 25 °C	25 h	not recovered	65
6	direct inj (3.0 M)	0 °C	17 h	54	15
7	direct inj (3.0 M)	0 °C	29 h	79	19
8	direct inj (3.0 M)	0 °C 22 h, then 25 °C	32 h	43	36
9	direct inj (3.0 M)	0 °C 2 h, then 25 °C	12 h	not recovered	17
10	direct inj (3.0 M)	0 °C 2 h, then 25 °C	38 h	not recovered	49

[a] Bromonitroalkane (1 equiv), amine (1 equiv), and KI (2 equiv) in DME (0.1 M) at 0 C. K_2CO_3 (6 equiv) added after 30 min followed by UHP (solution in water) and placed under O_2 atmosphere.

UmAS product **2.90** was then subjected to hydrogenolysis to reveal carboxylic acid **2.91**, which following treatment with TFA yielded macrolactamization precursor **2.92** (Figure 121).

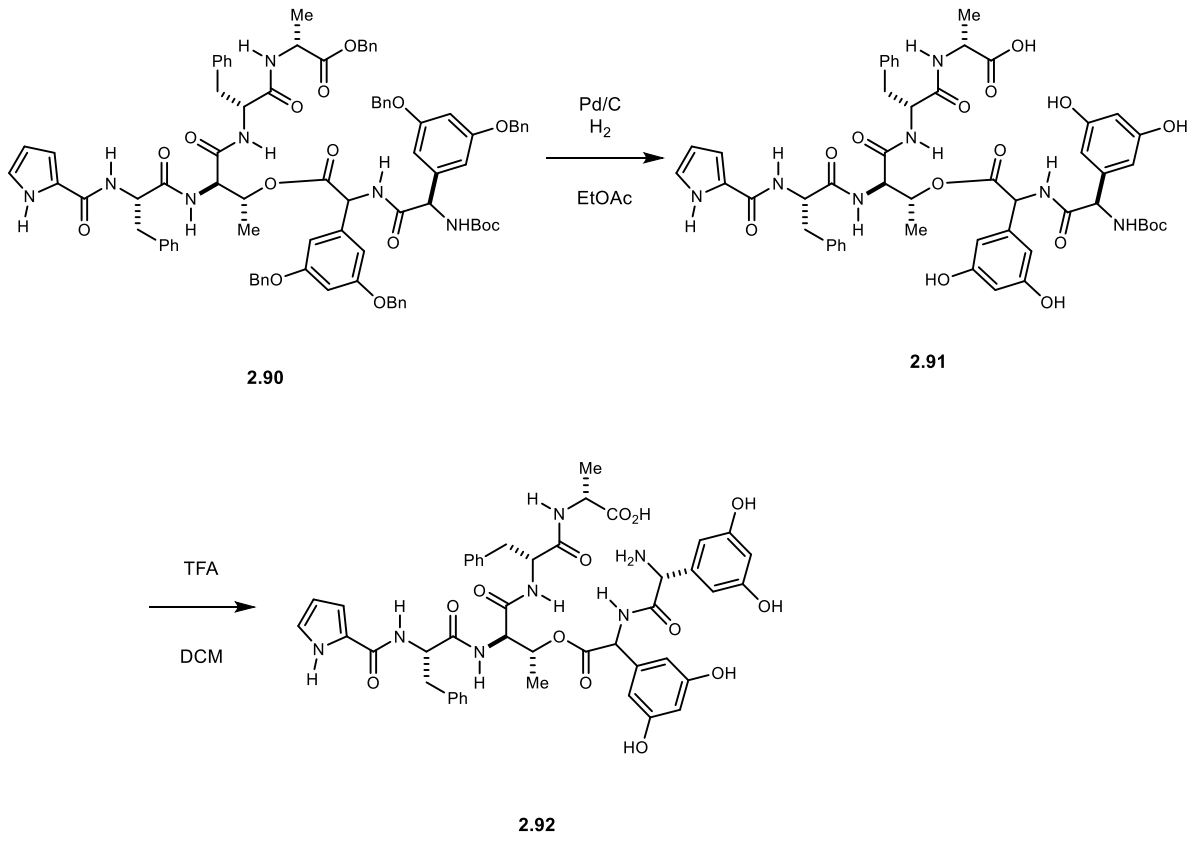

Figure 121. Deprotection sequence to furnish macrolactamization precursor 2.92.

Seco-acid **2.92** was then subjected to macrolactamization conditions to furnish the cochinmicins. Preliminary evaluation of conditions was challenging due to lack of knowledge regarding the solubility and lability of the product. To our delight, treatment of *seco*-acid **2.92** with DEPBT resulted in macrolactamization to give a mixture of cochinmicin 1 and 5 (**2.93**), albeit in low yields (Table 14). Although a mixture, isolation of this small amount of the natural product demonstrated the viability of our synthetic strategy. While there is much room for improvement in this approach, that optimization is enabled by this demonstration. We hope to report the fruits of these efforts in due course.

Table 14. Macrolactamization to access cochinmicin 1 and 5 (2.93).[a]

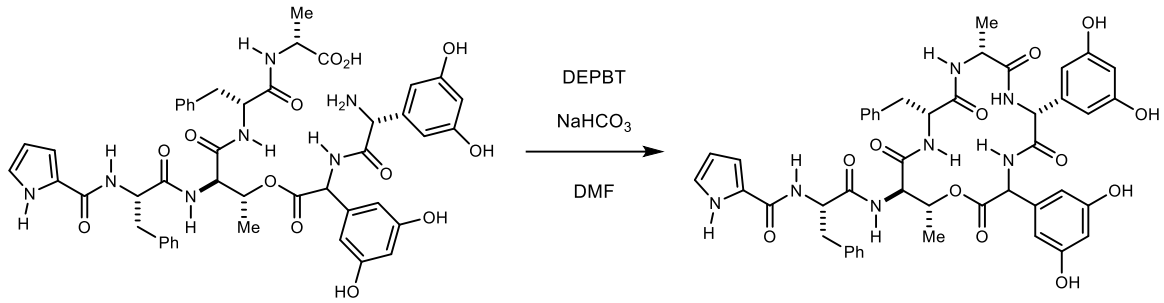

2.92 **cochinmicin 1 + cochinmicin 5 (2.93)**

entry	reagents	temp	time	outcome
2	DEPBT (2 eq), NaHCO3 (3 eq), DMF (0.01 M)	0 °C 2 h then 25 °C	24 h	not isolated
3	DEPBT (1 eq), NaHCO3 (3 eq), DMF (0.01 M)	0 °C 2 h then 25 °C	22 h	9%
4	DEPBT (2 eq), NaHCO3 (3 eq), DMF (0.01 M)	0 °C 2 h then 25 °C	48 h	on-going

2.9 Future Directions

To date, we describe the first reported total synthesis of cochinmicins 1 and 5. While this approach demonstrates the viability of this strategy to access the desired macrocycles, there are several areas which could stand to be improved in our synthesis. First, the intermolecular esterification reaction was modest in yield and resulted in a mixture of epimers. Efforts to improve the selectivity of this reaction will enable exclusive preparation of each of the cochinmicins and eliminate the need for a late-stage separation of mixtures of macrocycles. Second, competitive hydrolysis of the depsipeptidic linkage during UmAS could be eliminated, The result would be concomitant improvement of yield. Lastly, optimization of the macrolactamization step is certainly possible. Following optimization of this synthetic route, extension of our modular approach to access the remaining cochinmicins is clear (Figure 122).

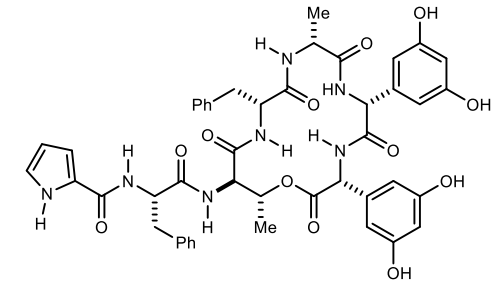

cochinmicin 1

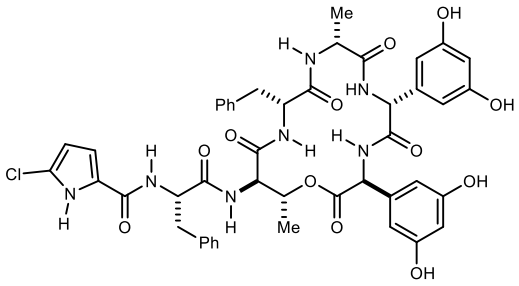

cochinmicin 2

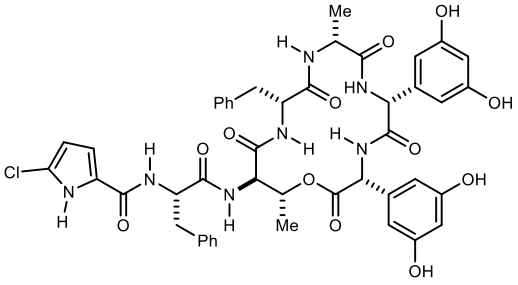

cochinmicin 3

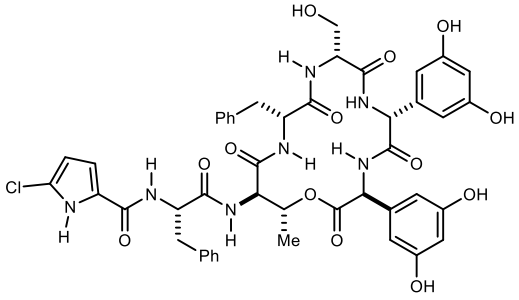

cochinmicin 4

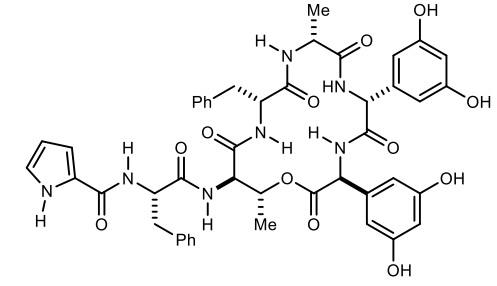

cochinmicin 5

Figure 122. Cochinmicins 1-5.

Following improved synthesis of the cochinmicins, we propose evaluation of biological activity of the cochinmicins and synthetic precursors, including the macrolactamization and macrolactonization precursors. The cochinmicins were previously reported as endothelin-1 antagonists.[273] Completion of this synthesis and subsequent optimization will enable further evaluation of the key functionality that confers biological activity.

3 Appendix

3.1 General Procedure

All non-aqueous reactions were performed in flame-dried round-bottomed flasks under an atmosphere of argon. Stainless steel syringes were used to transfer air- and moisture-sensitive liquids. Reactions temperatures were controlled using a thermocouple thermometer and analog hotplate stirrer. Reactions were conducted at room temperature (rt, *ca.* 23 °C) unless otherwise noted. Flash column chromatography was conducted using silica gel 230-400 mesh. Analytical thin layer chromatography (TLC) was performed on E. Merck silica gel 60 F254 places and visualized using UV, and potassium permanganate and ninhydrin stains. Yields were reported as isolated, spectroscopically pure compounds.

3.2 Materials

Solvents and chemicals were purchased from Sigma-Aldrich except D-pyroglutamic acid and O-benzylhydroxylamine hydrochloride (Combi-Blocks) and di-tert-butyldicarbonate, (Oakwood Chemicals). Dry dichloromethane (CH_2Cl_2) was collected from an MBraun MB-SPS solvent system. Triethylamine, *N*,*N*-dimethylformamide (DMF) and dimethyl sulfoxide (DMSO) were used as received in a bottle with a Sure/Seal. *N*,*N*-diisopropylethylamine was distilled from calcium hydride and stored over KOH. Deuterated solvents were purchased from Cambridge Isotope Laboratories. All commercial reagents were used as received.

3.3 Instrumentation

Preparative reverse phase HPLC (Gilson) was performed using a Phenomenex Luna column (5 micron, 100 Å, 50 x 21.20 mm, flow rate 30 mL/min) with UV/Vis detection. Infrared spectra were obtained as thin films on NaCl plates using a Thermo Electron IR100 series instrument and are reported in terms of frequency of absorbance (cm^{-1}). ^1H NMR spectra were recorded on Bruker 400 or 600 MHz spectrometers and are reported relative to internal

chloroform (^{1}H, δ=7.26), methanol (^{1}H, δ=3.31), and DMSO (^{1}H, δ=2.50). Data for ^{1}H NMR spectra are reported as follows: chemical shift (δ ppm), multiplicity (s=single, d=doublet, t=triplet, q=quartet, m=multiplet, br=broad), coupling constants (Hz), and integration. ^{13}C NMR were recorded on Bruker 100 or 150 MHz spectrometers and are reported relative to internal chloroform (^{13}C, δ= 77.1), methanol (^{13}C, δ=49.2), and DMSO (^{13}C, δ=40.3). Low-resolution mass spectra were acquired on an Agilent Technologies Series 1200 single quad ChemStation autosampler system using electrospray ionization (ESI) in positive mode. High-resolution mass spectra (HRMS) were obtained from the Department of Chemistry and Biochemistry, University of Notre Dame Mass Spectrometry Center or the Mass Spectrometry Research Center at Vanderbilt University.

3.4 Compound Preparation Relevant to Chapter 1

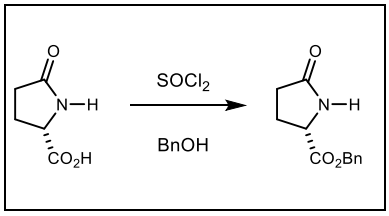

Benzyl (*S*)-5-oxopyrrolidine-2-carboxylate (1.102) To a solution of L-pyroglutamic acid (2.50 g, 19.4 mmol) in benzyl alcohol (17.7 mL, 171 mmol) at 0 °C was added thionyl chloride (2.81 mL, 38.8 mmol) dropwise. The reaction mixture was allowed to warm to room temperature and stirred for 16 h. The reaction was quenched by the slow addition of saturated aq. $NaHCO_3$ and extracted with EtOAc. The combined organic extracts were washed with brine, dried, and concentrated. Benzyl alcohol was removed by vacuum distillation and the resulting residue purified by column chromatography (gradient: 80:20 hexanes:EtOAc to EtOAc) affording the product (3.6 g, 85%) as a colorless oil. Compound characterization data was consistent with previous reports.[274]

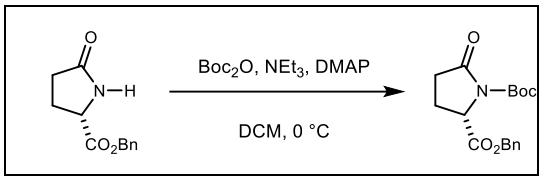

2-benzyl 1-(*tert*-butyl) (*S*)-5-oxopyrrolidine-1,2-dicarboxylate (1.103) To a solution of **1.102** (3.60 g, 16.4 mmol) in CH_2Cl_2 (82 mL, 0.20 M) at 0 °C was added 4-dimethylaminopyridine (200 mg, 1.64 mmol), triethylamine (2.3 mL, 16 mmol), and di-*tert*-butyl dicarbonate (4.30 g, 19.7 mmol). The reaction mixture was maintained at 0 °C for 1 h and then brought to room temperature and stirred for 16 h. The reaction was diluted with CH_2Cl_2, washed with saturated aq. NH_4Cl and brine, then dried and concentrated to afford the carbamate (4.73 g, 90%) as a yellow solid. Compound characterization data was consistent with previous reports. [275]

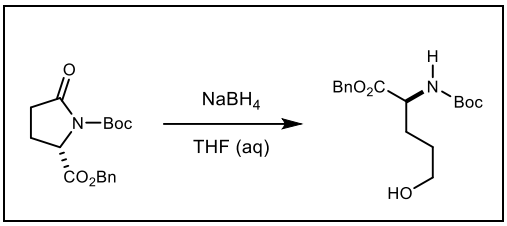

Benzyl (*S*)-2-((*tert*-butoxycarbonyl)amino)-5-hydroxypentanoate (1.104) To a solution of **1.103** (1.3 g, 4.1 mmol), THF (16 mL, 0.25 M), and dH_2O (2.97 mL) at 0 °C was added sodium borohydride (307 mg, 8.14 mmol). The reaction mixture was maintained at 0 °C for 1 h then allowed to warm to room temperature and stirred for 1 h. The reaction mixture was concentrated *in vacuo* and the resulting residue suspended in EtOAc and washed with water. The aqueous layer was extracted with EtOAc and the combined organic extracts washed with water, brine, dried, and concentrated. Column chromatography (40-60% ethyl acetate in hexanes) yielded alcohol (641 mg, 49%) as a colorless oil. Compound characterization data was consistent with previous reports. [276]

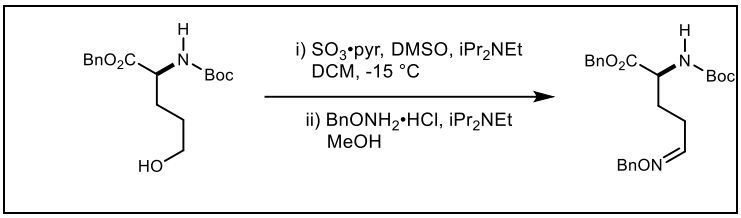

Benzyl (*S*)-5-((benzyloxy)imino)-2-((*tert*-butoxycarbonyl)amino)pentanoate (1.105) To a solution of **1.104** (520 mg, 1.61 mmol) in CH_2Cl_2 (4.6 mL, 0.35 M) was added *N*,*N*-diisopropylethylamine (0.64 mL, 3.70 mmol) and DMSO (2.5 mL). The resulting solution was cooled to -15 °C and SO_3·pyr complex (591 mg, 3.70 mmol) dissolved in DMSO (2.5 mL) was added dropwise. The reaction was stirred in the cooling bath until the temperature rose to -5 °C at which point the reaction mixture was allowed to warm to room temperature and maintained until judged complete by TLC (ca. 30 min). To the reaction was then EtOH (1.99 mL) was added. The reaction was stirred for 5 min before *N*, *N*-diisopropylethylamine (0.32 mL, 1.82 mmol) was added, followed by *O*-benzylhydroxylamine hydrochloride (290 mg, 1.82 mmol). The reaction mixture was stirred at room temperature for an additional 2 h. The reaction was diluted with Et_2O and water. The layers were separated and the organic extract washed with 1 N HCl followed by saturated aq. $NaHCO_3$ and brine. The organics were dried and concentrated to afford oximes as an inseparable mixture of geometric isomers as a colorless oil (633 mg). The mixture was carried forward crude without further purification.

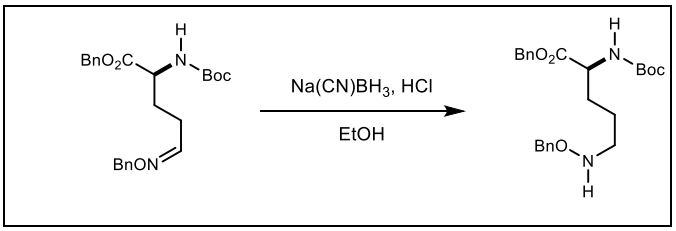

Benzyl (*S*)-5-((benzyloxy)amino)-2-((*tert*-butoxycarbonyl)amino)pentanoate (1.92) To a solution of oxime **1.105** (647 mg, 1.52 mmol), EtOH (15 mL, 0.10 M), and concentrated hydrochloric acid (0.15 mL) was added sodium cyanoborohydride (59 mg, 1.0 mmol). The reaction mixture was monitored by TLC until judged complete (ca. 1.5 h). The reaction mixture diluted with EtOAc and water. The organic extract was washed with brine, dried, and concentrated. Column chromatography (20-40% ethyl acetate in hexanes) afforded **1.105** (470 mg, 72% from **1.105**) as a colorless oil: R_f 0.23 (4:1 hexanes: EtOAc) ; $[\alpha]_D^{23}$ -12.3; IR (neat) 3354, 3030, 2968, 1713, 1507, 1454 cm^{-1} ; ^1H NMR (400 MHz, $CDCl_3$) δ 7.37-7.27 (m, 10H),

5.28 (s, 2H), 5.23-5.10 (app q, 3H), 4.67 (s, 2H), 4.39-4.31 (br, 1H), 2.90 (t, *J* = 6.8 Hz, 2H), 1.92- 1.79 (m, 1H), 1.75-1.63 (m, 1H), 1.61-1.49 (m, 2H), 1.44 (s, 9H); ^{13}C NMR (150 MHz, $CDCl_3$) δ 172.5, 155.3, 137.8, 135.4, 128.5, 128.4, 128.3, 128.2, 127.8, 79.8, 76.2, 66.9, 53.3, 51.3, 30.2, 28.3, 23.2; HRMS (ESI-TOF MS) calculated for $C_{24}H_{32}N_2O_5$ $(M+H)^+$ m/z: 429.2384, measured 429.2360.

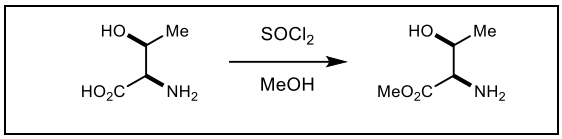

Methyl D-threoninate hydrochloride (1.97) To MeOH (10 mL, 0.40 M) at 0 °C was added thionyl chloride (0.23 mL, 3.1 mmol) dropwise, followed by D-threonine (500 mg, 4.20 mmol). The reaction was then heated to reflux, maintained for 1 h, allowed to cool to room temperature, and concentrated to afford methyl ester (530 mg, 94%) as a white solid. Compound characterization data was consistent with previous reports. [277]

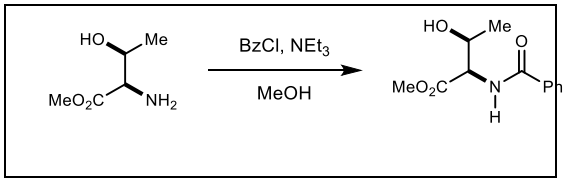

Methyl benzoyl-D-threoninate (1.98) To a solution of **1.97** (250 mg, 1.87 mmol) in MeOH (2.5 mL, 1.2 M) was added triethylamine (0.72 mL, 5.1 mmol). The reaction mixture was stirred at room temperature for 15 min, cooled to 0 °C, and benzoyl chloride (0.24 mL, 2.1 mmol) was added dropwise over 10 min. The reaction mixture was maintained at 0 °C for 2 h. The reaction was concentrated to remove excess MeOH, the residue dissolved in water, and the resulting suspension extracted with EtOAc. The combined organic extracts were washed with water, brine, dried, and concentrated. The resulting residue was recrystallized from Et_2O to give benzamide (291 mg, 65%) as a white solid. Compound characterization data was consistent with previous reports. [278]

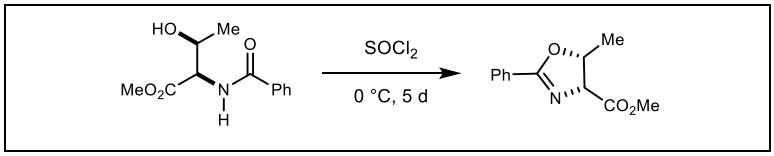

Methyl (4*R*,5*R*)-5-methyl-2-phenyl-4,5-dihydrooxazole-4-carboxylate (1.99) To thionyl chloride (0.88 mL, 1.3 M) at 0 °C, benzamide (270 mg, 1.14 mmol) was added in three portions.

The reaction mixture was maintained at 0 °C for 5 d. Excess thionyl chloride was removed *in vacuo* and the resulting residue was suspended in $CHCl_3$. The resulting solution was then poured slowly into saturated aq. Na_2CO_3. The aqueous layer was extracted with CH_2Cl_3. The combined organic extracts were washed with water, brine, dried, and concentrated to afford oxazoline (213 mg, 86%) as a yellow oil. Compound characterization data was consistent with previous reports.[279]

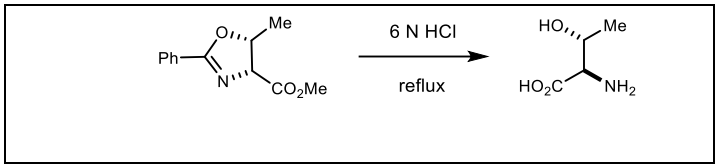

D-*allo*-threonine (1.100) Oxazoline **1.99** (168 mg, 0.760 mmol) was dissolved in 6N HCl (1.9 mL, 0.40 M) and refluxed for 5 h. The reaction mixture was then allowed to cool to room temperature and washed with Et_2O. The aqueous layer was concentrated to afford 98 mg (crude) of D-*allo*-threonine as a white foam. Compound characterization data was consistent with previous reports.[280]

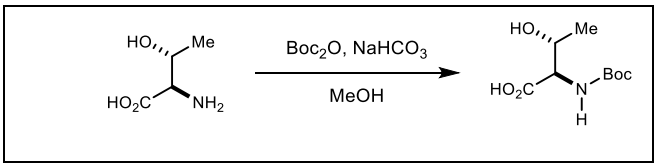

(*tert*-butoxycarbonyl)-D-*allo*-threonine (1.93) To a solution of amine (130 mg, 1.09 mmol) in MeOH (2.2 mL, 0.50 M) was added $NaHCO_3$ (140 mg, 1.68 mmol) followed by di-*tert*-butyl dicarbonate (347 mg, 1.59 mmol). The reaction mixture was concentrated *in vacuo* after 14 h and the resulting residue was suspended in Et_2O, acidified with 2 N HCl, and extracted with EtOAc. The combined organic extracts were washed with brine, dried, and concentrated to afford carbamate (203 mg, 86%) as a pale-yellow oil. Compound characterization data was consistent with previous reports.[281]

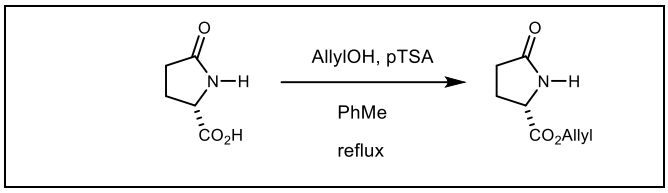

Allyl (*R*)-5-oxopyrrolidine-2-carboxylate (1.107) To a suspension of D-pyroglutamic acid (6.00 g, 46.5 mmol) in toluene (185 mL, 0.25 M) was added allyl alcohol (12.6 mL, 185 mmol) and *p*-toluenesulfonic acid hydrate (441 mg, 2.31 mmol). The reaction mixture was brought to reflux, maintained until judged complete by TLC (ca. 3 h), allowed to cool to room temperature, and quenched with saturated aq. $NaHCO_3$. The resulting solution was concentrated then extracted with DCM, washed with brine, dried, and concentrated to give allyl ester (5.6 g, 71 %) as a white solid. Compound characterization data was consistent with previous reports.[282]

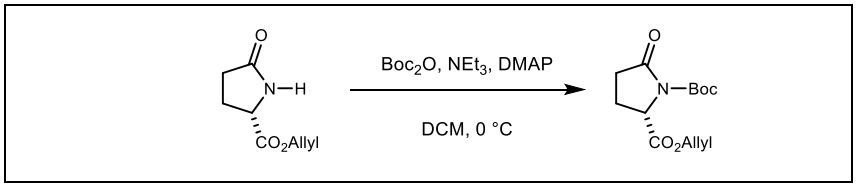

2-allyl 1-(*tert*-butyl) (*R*)-5-oxopyrrolidine-1,2-dicarboxylate (1.108) To a solution of lactam (5.56 g, 32.9 mmol) in CH_2Cl_2 (140 mL, 0.24 M) was added 4-dimethylaminopyridine (401 mg, 3.29 mmol), and triethylamine (5.05 mL, 36.2 mmol). The solution was allowed to cool to 0 °C and di-*tert*-butyl dicarbonate (7.83 g, 36.2 mmol) was added. The reaction was allowed to warm to room temperature until judged complete by TLC (ca. 16 h). The reaction mixture was diluted with CH_2Cl_2, the organic layer washed with saturated aq. NH_4Cl, brine, dried, and concentrated to afford carbamate (8.83 g, 95 %) as a yellow solid: R_f 0.44 (2:1 hexanes: EtOAc); $[\alpha]_D^{23}$ +35.3; IR (neat) 3550, 2981, 1790, 1751, 1458 cm^{-1} ; ^1H NMR (400 MHz, $CDCl_3$) δ 5.94-5.81 (m, 1H), 5.38-5.12 (m, 2H), 4.69-4.56 (m, 3H), 2.66-2.53 (m, 1H), 2.52-2.41 (m, 1H), 2.38-2.23 (m, 1H), 2.07-1.96 (m, 1H), 1.45 (s, 9H); ^{13}C NMR (100 MHz, $CDCl_3$) δ 173.1, 170.2, 149.1, 130.9, 119.5, 83.7, 66.0, 59.2, 30.7, 27.7, 21.1; HRMS (ESI-TOF MS) calculated for $C_{13}H_{19}NO_5$ $(M+Na)^+$ m/z: 292.1155, measured 292.1171.

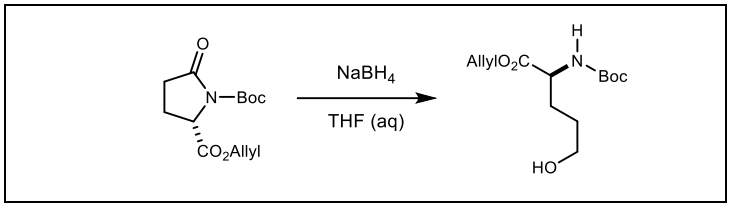

Allyl (*R*)-2-((*tert*-butoxycarbonyl)amino)-5-hydroxypentanoate (1.109) To a solution of **1.108** (1.00 g, 3.71 mmol), THF (6.1 mL, 0.6 M), and water (1.2 mL) at 0 °C was added sodium borohydride (210 mg, 5.57 mmol). The reaction mixture was maintained at 0 °C for 1 h, allowed to warm to room temperature and maintained for 1 h. The reaction was concentrated *in vacuo* and the resulting residue dissolved in EtOAc and washed with water. The aqueous layer was back extracted with EtOAc. The combined organic extracts were washed with water, brine, dried, and concentrated. The residue was purified by column chromatography (gradient: 40-60% ethyl acetate in hexanes) to afford alcohol (395 mg, 40%) as a colorless oil: R_f 0.32 (1:1 hexanes: EtOAc); $[\alpha]_D^{23}$ -3.59; IR (neat) 3370, 2969, 2358, 1706, 1519, 1451, 1369 cm^{-1} ; ^1H NMR (400 MHz, $CDCl_3$) δ 5.95-5.813 (m, 1H), 5.35-5.18 (m, 3H), 4.66-4.55 (m, 2H), 4.39-4.25 (br, 1H), 3.637 (t, *J* = 6.1 Hz, 2H), 2.18 (s, 1H), 1.96-1.82 (m, 1H), 1.791-1.667 (m, 1H), 1.66-1.54 (m, 2H), 1.41 (s, 9H); ^{13}C NMR (100 MHz, $CDCl_3$) δ 172.6, 155.6, 131.7, 118.9, 79.8, 65.9, 62.0, 53.3, 29.5, 28.4; HRMS (ESI-TOF MS) calculated for $C_{13}H_{23}NO_5$ $(M+H)^+$ m/z: 274.1649, measured 274.1666.

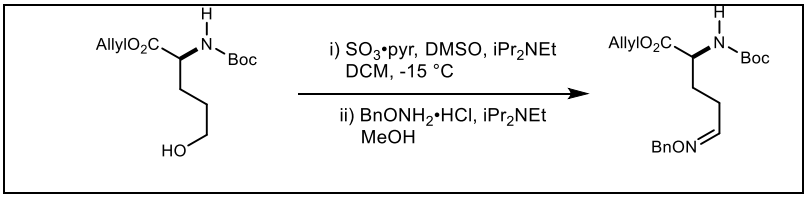

Allyl (*R*)-2-((*tert*-butoxycarbonyl)amino)-5-(hydroxyimino)pentanoate (1.110) To a solution of alcohol **1.109** (750 mg, 2.74 mmol) in CH_2Cl_2 (11.9 mL, 0.23 M) was added *N*,*N*-diisopropylethylamine (1.43 mL, 8.22 mmol) and DMSO (5.95 mL) under inert atmosphere. The resulting solution was cooled to -15 °C and SO_3·pyr complex (1.31 g, 8.22 mmol) dissolved in DMSO (5.95 mL) was added dropwise. The reaction was stirred in the cooling bath until the temperature rose to -5 °C at which point the reaction mixture was allowed to warm to room temperature and maintained until judged complete by TLC (ca. 30 min). To the reaction was then added EtOH (5.95 mL) was added and after 5 min *N, N*-diisopropylethylamine (0.72 mL, 4.11

mmol) was added, followed by *O*-benzylhydroxylamine hydrochloride (655 mg, 4.11 mmol). The reaction mixture was maintained for an additional 2 h, diluted with Et_2O, washed with water, 1 N HCl followed by saturated aq. $NaHCO_3$, brine, dried, and concentrated to afford oxime (890 mg, crude). The mixture was carried forward crude without further purification.

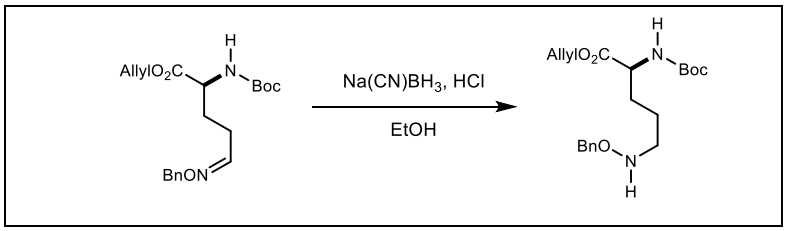

Allyl (*R*)-5-((benzyloxy)amino)-2-((*tert*-butoxycarbonyl)amino)pentanoate (1.111) To a stirred solution of oximes (**1.110**) (890 mg, 2.36 mmol) in MeOH (78.6 mL, 0.030 M) was added concentrated hydrochloric acid (0.79 mL) followed by sodium cyanoborohydride (222 mg, 3.54 mmol). The reaction was stirred at room temperature for 2 h then concentrated to half volume and diluted with EtOAc and water. The organic layer was washed with brine, dried, and concentrated to afford **1.111** (755 mg, 84%) as a colorless oil: R_f 0.37 (2:1 hexanes:EtOAc); $[\alpha]_D^{23}$ -4.0; IR (neat) 3355, 2932, 1713, 1508, 1452, 1366 cm^{-1} ; ^1H NMR (400 MHz, $CDCl_3$) δ 7.38-7.27 (m, 5H), 5.97-5.83 (m, 1H), 5.37-5.09 (m, 3H), 4.72-4.58 (m, 4H), 4.36-4.27 (br, 1H), 2.93 (t, *J* = 6.7 Hz, 2H), 1.94-1.79 (br, 1H), 1.76-1.64 (m, 1H), 1.63- 1.52 (m, 2H), 1.44 (s, 9H); ^{13}C NMR (100 MHz, $CDCl_3$) δ 172.3, 155.3, 137.7, 131.5, 128.3, 128.3, 127.7, 118.6, 79.7, 76.2, 65.7, 53.2, 51.3, 30.2, 28.2, 23.2; HRMS (ESI-TOF MS) calculated for $C_{20}H_{30}N_2O_5$ $(M+H)^+$ m/z: 379.2227, measured 379.2228.

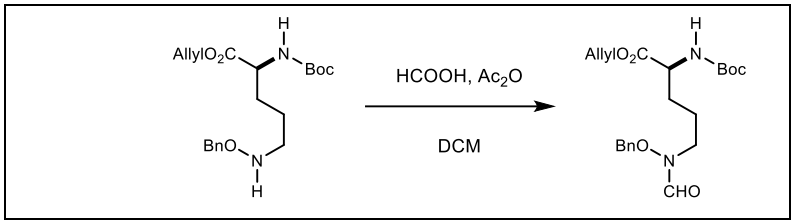

Allyl (*R*)-5-(*N*-(benzyloxy)formamido)-2-((*tert*-butoxycarbonyl)amino)pentanoate (1.112) To a solution of **1.111** (200 mg, 0.528 mmol) in CH_2Cl_2 (2.6 mL, 0.20 M) was added formic acetic anhydride (0.35 mL) dropwise. Consumption of starting materials was monitored by TLC (ca. 40 min) and upon completion the reaction was diluted with CH_2Cl_2, washed with saturated aq. $NaHCO_3$, brine, dried, and concentrated. The resulting residue was purified by column

chromatography (30% ethyl acetate in hexanes) to afford **1.112** (151 mg, 73 %) as a colorless oil: R_f 0.39 (2:1 hexanes:EtOAc); $[\alpha]_D^{23}$ -10.93; IR (neat) 2974, 2357, 1705, 1512 cm-1 ; ^{1}H NMR(400 MHz, $CDCl_3$) δ 8.20 (s, 1H), 7.38 (s, 5H), 5.935.83 (m, 1H), 5.33-5.22 (m, 2H), 5.04 (br, 1H), 4.82 (br, 1H), 4.60 (d, *J* = 4.8 Hz, 2H), 4.32 (br, 1H), 3.59 (br, 1H), 1.84-1.67 (m, 4H), 1.57 (s, 2H), 1.43 (s, 9H); ^{13}C NMR (100 MHz, $CDCl_3$) δ 172.0, 163.1, 155.3, 131.4, 129.4, 129.1, 128.7, 118.8, 79.9, 77.7, 65.9, 53.0, 43.6, 29.8, 29.6, 28.2, 22.9; HRMS (ESI-TOF MS) calculated for $C_{21}H_{31}N_2O_6^+$ $(M+H)^+$ m/z: 407.2177, measured 407.2165.

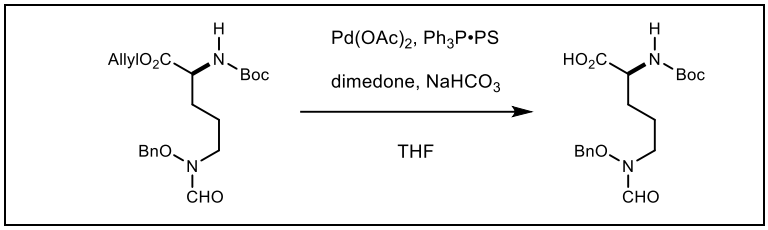

(*R*)-5-(*N*-(benzyloxy)formamido)-2-((*tert*-butoxycarbonyl)amino) pentanoic acid (1.114) To a stirred solution of $NaHCO_3$ (21.6 mg, 0.258 mmol), dimedone (36.2 mg, 0.258 mmol), THF (2 mL, 0.13 M), and water (2 mL) was added polymer supported PPh_3 (43.2 mg, 0.090 mmol) and $Pd(OAc)_2$ (2.89 mg, 0.012 mmol) under inert atmosphere. After 3 min, allyl ester (105 mg, 0.258 mmol) was added to the reaction mixture. When the reaction mixture was judged complete by TLC (ca. 1 h), the reaction mixture was diluted with water and washed with CH_2Cl_2. The aqueous was filtered and concentrated to afford carboxylic acid (78 mg, 82%) as a colorless oil: R_f 0.5 (9:1 DCM:MeOH); $[\alpha]_D^{23}$ -10.93; IR (neat) 2974, 2357, 1705, 1512 cm^{-1}; ^{1}H NMR (400 MHz, MeOD) δ 8.08 (s, 1H), 7.52-7.32 (m, 5H), 4.96 (br, 2H) 4.02 (br, 1H), 3.64 (br, 1H), 3.50 (br, 1H), 1.88-1.61 (m, 4H), 1.44 (s, 9H) **;** ^{13}C NMR (100 MHz, MeOD) δ 163.4, 159.0, 156.6, 129.4, 129.3, 129.0, 128.6, 128.3, 128.0, 79.05, 76.9, 52.9, 42.8, 28.5, 27.3, 22.8; HRMS (ESI-TOF MS) calculated for $C_{18}H_{26}N_2O_6$ $(M+H)^+$ m/z: 367.1864, measured 367.1854

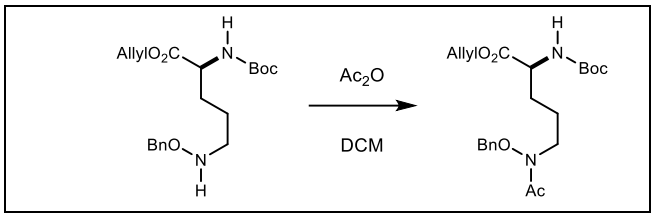

Allyl (*R*)-5-(*N*-(benzyloxy)acetamido)-2-((*tert*-butoxycarbonyl)amino)pentanoate (1.113) To **1.111** (97 mg, 0.23 mmol) was added acetic anhydride (0.4 mL) and pyridine (0.4 mL). The reaction was maintained until judged complete by TLC (ca. 1 h) and concentrated *in vacuo*. The residue was suspended in $CHCl_3$, washed with 1N HCl, saturated aq. $NaHCO_3$, brine, dried, and concentrated to give **1.113** (83 mg, 77%) as a colorless oil: R_f 0.25 (2:1 hexanes:EtOAc); $[\alpha]_D^{23}$ -2.4 ; IR (neat) 3324, 2927, 1712, 1659, 1515, 1451, 1371 cm^{-1}; ^1H NMR (400 MHz, $CDCl_3$) δ 7.41-7.30 (m, 5 H), 5.92-5.80 (m, 1H), 5.34-5.17 (m, 2H), 5.12-5.04 (br, d, *J* = 7.7 Hz 1H), 4.79 (s, 1H), 4.63-4.53 (br, d, *J* = 4.6 Hz, 2H), 4..31 (br, 1H), 3.65 (t, *J* = 6.2 Hz, 2H), 2.07 (s, 3H), 1.80-1.60 (m, 4H), 1.42 (s, 9H) ; ^{13}C NMR (100 MHz, $CDCl_3$) δ172.1, 155.3, 134.3, 131.5, 129.1, 128.9, 128.6, 118.7, 79.8, 76.3, 65.8, 53.1, 29.8, 28.2, 22.9, 20.4; HRMS (ESI-TOF MS) calculated for $C_{22}H_{33}N_2O_6^+$ $(M+H)^+$ m/z: 421.2333, measured 421.2318. For further discussion of line broadening [283]

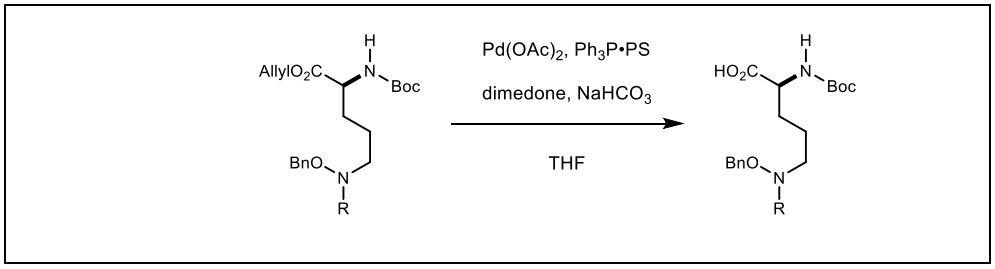

(*R*)-5-(*N*-(benzyloxy)acetamido)-2-((*tert*-butoxycarbonyl)amino) pentanoic acid (1.115) To a solution of $NaHCO_3$ (13.7 mg, 0.164 mmol), dimedone (13.3 mg, 0.095 mmol) in THF (1.26 mL, 0.13 M), and water (1.26 mL) was added polymer supported PPh_3 (27 mg, 0.057 mmol) and $Pd(OAc)_2$ (1.8 mg, 0.0082 mmol). After 3 min, allyl ester (69 mg, 0.164 mmol) was added to the reaction. When the reaction was judged complete by TLC (ca. 1 h), the reaction mixture was diluted with water and washed with CH_2Cl_2. The aqueous was filtered and concentrated to afford the carboxylic acid (47.2 mg, 75%) as a colorless oil. Compound characterization data was consistent with previous reports.

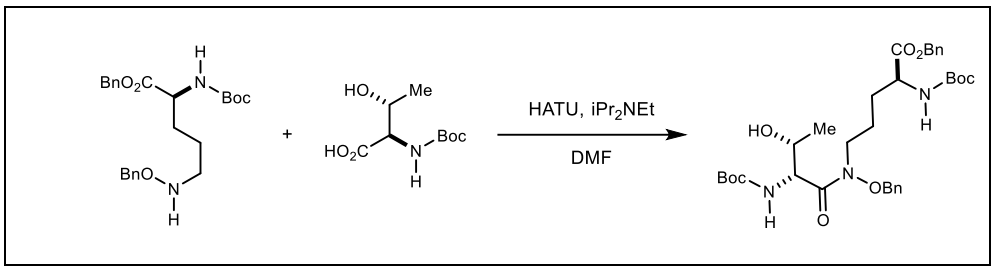

Benzyl (*S*)-5-((2*R*,3*R*)-*N*-(benzyloxy)-2-((*tert*-butoxycarbonyl)amino)-3-hydroxybutanamido)-2-((*tert*-butoxycarbonyl)amino)pentanoate (1.116) To solution of carboxylic acid (105 mg, 0.482mmol) in DMF (1 mL, 0.5 M) at 0 °C was added HATU (275 mg, 0.723 mmol). After 30 min, a solution of **1.92** (217 mg, 0.507 mmol) and *N*,*N*-diisopropylethylamine (0.11 mL, 0.64 mmol) in DMF (0.6 mL) was added dropwise at 0 °C. The reaction mixture was allowed to warm to room temperature, maintained at that temperature for 2.5 h, and upon completion diluted with EtOAc. The organic was then washed with water, brine, dried, and concentrated. The residue was purified by column chromatography (gradient:30-50% ethyl acetate in hexanes) to afford amide (244 mg, 80%) as a white foam: R_f 0.27 (2:1 hexanes: EtOAc); $[\alpha]_D^{23}$ -9.23; IR (neat) 3348, 2974, 1707, 1648, 1505, 1452 cm^{-1} ; ^1H NMR (600 MHz, $CDCl_3$) δ 7.47- 7.17 (m, 10H), 5.53 (d, *J* = 6.0 Hz, 1H), 5.17-5.04 (m, 3H), 4.97 (d, *J* = 9.6 Hz, 1H), 4.91-4.79 (m, 2H), 4.41-4.30 (br, 1H), 4.02-3.88 (br, 2H), 3.40-3.28 (br, 1H), 3.09-2.94 (br, 1H), 1.88-1.77 (br, 1H), 1.75-1.58 (m, 4H), 1.43 (d, *J* = 19.8 Hz, 18H), 1.10 (d, *J* = 5.7 Hz, 3H); ^{13}C NMR (150 MHz, $CDCl_3$) δ 172.6, 171.8, 155.8, 155.3, 135.5, 134.1, 129.8, 129.4, 129.0, 128.9, 128.7, 128.6, 80.3, 80.2, 76.3, 69.5, 67.4, 55.0, 53.2, 44.8, 30.1, 28.6, 28.5, 22.9, 19.6; HRMS (ESI-TOF MS) calculated for $C_{33}H_{48}N_3O_9^+$ m/z: 630.3385, measured 630.3359.

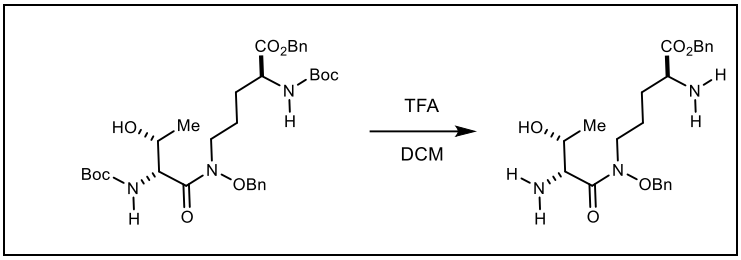

Benzyl (*S*)-2-amino-5-((2*R*,3*R*)-2-amino-*N*-(benzyloxy)-3-hydroxybutanamido)pentanoate (1.117) To a stirred solution of **1.116**, (50 mg, 0.079 mmol) in CH_2Cl_2 (4 mL, 0.02 M) was added trifluoroacetic acid (0.2 mL) dropwise. The reaction was judged complete by TLC (ca. 2 h), concentrated *in vacuo*, and the residue was purified by reverse phase HPLC (10-45% MeCN-

H_2O with 0.1% TFA) to yield amine (36 mg, 88%) as a TFA salt: : R_f 0.33 (9:1 DCM:MeOH); IR(neat) 3411, 2937, 2120, 1664, 1392 cm^{-1}; ^{1}H-NMR (400 MHz, MeOD) δ 7.47 - 7.41 (m, 5H), 7.38 – 7.31 (m, 5H), 5.26 (d, *J* = 12.0 Hz, 1H), 5.22 (d, *J* = 12.0 Hz, 1H), 5.02 (d, *J* = 10.2 Hz, 1H), 4.91 (d, *J* = 10.2 Hz, 1H), 4.38 – 4.33 (m, 2H), 4.12 (t, *J* = 6.2 Hz, 1H), 4.07 – 4.00 (m, 1H), 3.59 – 3.52 (m, 1H), 2.00 – 1.79 (m, 3H), 1.03 (d, *J* = 7.3 Hz, 3H); ^{13}C-NMR (150 MHz, MeOD) δ 170.2, 168.3, 136.3, 135.2, 130.7, 130.5, 130.0, 129.9, 129.8, 77.89, 69.2, 64.7, 58.2, 53.6, 45.4, 28.8, 23.4, 17.6; HRMS (ESI-TOF MS) calculated for $C_{23}H_{31}N_3O_5$ $(M+Na)^+$ m/z: 452.2156, measured 452.2187.

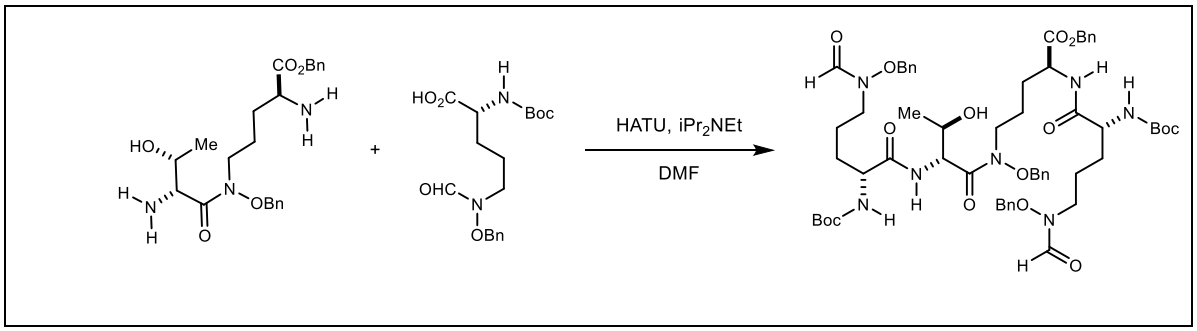

Benzyl (7*R*,10*R*,16*S*)-12-(benzyloxy)-16-((*R*)-5-(*N*-(benzyloxy)formamido)-2-((*tert*-butoxycarbonyl) amino)pentanamido)-7-((*tert*-butoxycarbonyl)amino)-3-formyl-10-((*R*)-1-hydroxyethyl)-8,11-dioxo-1-phenyl-2-oxa-3,9,12-triazaheptadecan-17-oate (1.118) To a stirred solution of carboxylic acid (19.7 mg, 0.053 mmol) in DMF (0.5 mL, 0.11 M) at 0 °C was added HATU (29.2 mg, 0.076 mmol). After 30 min, a solution of amine (16 mg, 0.025 mmol) and *N*,*N*-diisopropylethylamine (20 µL, 0.12 mmol) in DMF (0.5 mL) was added dropwise at 0 °C. The reaction mixture was warmed to room temperature and maintained until the reaction was judged complete by LC-MS (ca. 4 h). Upon completion the reaction mixture was diluted with EtOAc, organic layer was then washed with water, brine, dried, and concentrated. The residue was purified by reverse phase HPLC (Gilson) (gradient: 25-70% MeCN-H_2O with 0.1% TFA) to afford tetrapeptide (16.7 mg, 58%) as a white foam: R_f 0.41 (95:5 DCM:MeOH); $[\alpha]_D^{20}$ +0.86; IR (neat) 3313, 2927, 1669, 1510 cm^{-1}, ^{1}H (600 MHz, DMSO) δ 8.16-8.11 (m, 2H), 7.88-7.79 (m, 2H), 7.43-7.25 (m, 20H), 6.88-6.85 (d, *J* = 7.0 Hz, 1H), 6.73 (d, *J* = 7.4 Hz, 1H), 5.00-4.96 (m, 3H), 4.89-4.87 (m, 1H), 4.80-4.77 (m, 4H), 4.22 (br, 1H), 3.97 (br, 1H), 3.80 (br, 1H). 3.69 (br, 1H), 3.42-3.30 (br, 8H), 1.67 (br, 1H), 1.60-1.37 (m, 10H), 1.28 (d, *J* = 4.4 Hz, 18H), 0.98 (br, 3H); ^{13}C (150 MHz, DMSO) δ 172.5, 172.1, 171.5, 163.1, 158.6, 155.8, 155.7, 136.3, 135.7, 135.2, 134.9, 130.1, 129.9, 129.6, 129.2, 128.9, 128.8, 128.4, 128.1, 78.6, 78.5, 77.1, 76.2, 75.5,

67.2, 66.3, 55.4, 54.3, 54.0, 52.1, 47.5, 43.9, 43.3, 30.1, 29.7, 29.5, 28.6, 24.1, 23.4, 20.2; HRMS (ESI-TOF MS) calculated for $C_{59}H_{80}N_7O_{15}^+$ $(M+H)^+$: 1126.5707, measured 1126.5655.

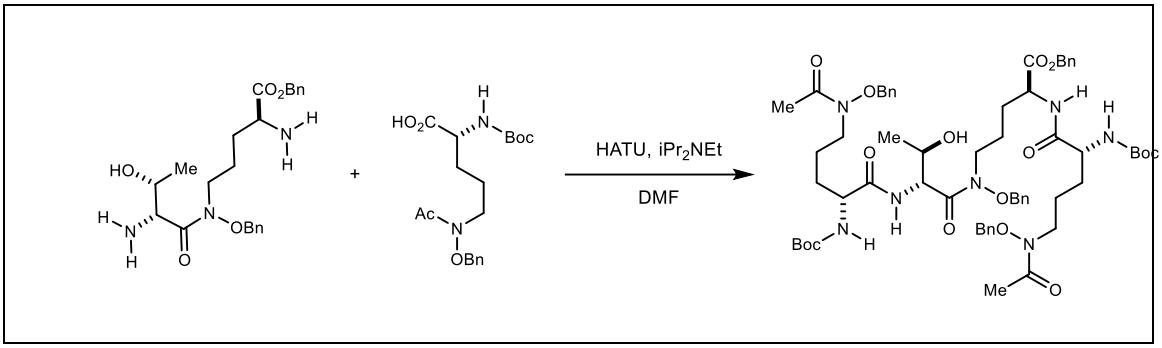

Benzyl (7*R*,10*R*,16S)-3-acetyl-12-(benzyloxy)-16-((*R*)-5-(*N*-(benzyloxy)acetamido)-2-((*tert*-butoxycarbonyl)amino)pentanamido)-7-((*tert*-butoxycarbonyl)amino)-10-((*R*)-1-hydroxyethyl)-8,11-dioxo-1-phenyl-2-oxa-3,9,12-triazaheptadecan-17-oate (1.119) A stirred solution of carboxylic acid (48 mg, 0.13 mmol) in DMF (0.5 mL, 0.25 M) at 0 °C was added HATU (68 mg, 0.18 mmol). After 30 min, a solution of amine (26 mg, 0.060 mmol) and *N*,*N*-diisopropylethylamine (47 µL, 0.27 mmol) in DMF (0.5 mL) was added dropwise at 0 °C. The reaction mixture was warmed to room temperature and maintained until the reaction was judged complete by LC-MS (ca. 4 h). Upon completion the reaction mixture was diluted with EtOAc, organic layer was washed with water, brine, dried, and concentrated. The residue was purified by reverse phase HPLC (Gilson) (gradient: 25-70% MeCN-H_2O with 0.1% TFA) to afford tetrapeptide (27.5 mg, 57%) as a white foam: R_f 0.33 (95:5 DCM:MeOH); $[\alpha]_D^{23}$ +3.2; IR (neat) 3307, 2928, 2357, 1656, 1509, 1451 cm^{-1}; ^1H (400 MHz, DMSO) ; 8.23 (d, *J* = 7.2 Hz, 1H), 7.86 (d, *J* = 8.5 Hz, 1H), 7.53 (m, 2H), 7.48-7.31 (m, 20H), 6.94 (d, *J* = 8.1 Hz, 1H), 6.82 (d, *J* = 8.2 Hz 1H), 5.15-5.02 (m, 3H), 4.97 (d, *J* = 7.4 Hz, 1H), 4.87 (d, *J* = 6.6 Hz, 4H) 4.31 (br, 1H), 4.04 (br, 2H), 3.87 (t, *J* = 6.7 Hz, 1H), 3.80 (m, 1H), 3.59 (m, 4H), 3.41 (m, 1H), 2.01 (d, *J* = 4.1 Hz, 6H), 1.80-1.45 (m, 12H), 1.41-1.36 (d, *J* = 5.4 Hz, 18H), 1.07(d, *J* = 5.7 Hz, 3H); ^{13}C (150 MHz) δ 172.6, 172.1, 171.6, 155.8, 155.7, 136.3, 135.3, 134.9, 129.9, 129.8, 129.1, 128.9, 128.8, 128.4, 128.1, 78.6, 78.5, 76.2, 75.8, 67.2, 66.3, 55.4, 54.3, 54.1, 53.9, 52.0, 44.4, 43.9, 30.1, 29.7, 28.6, 23.7, 23.6, 23.4, 20.7, 20.2; HRMS (ESI-TOF MS) calculated for $C_{61}H_{84}N_7O_{15}^+$ $(M+H)^+$: 1154.6020, measured: 1154.6051

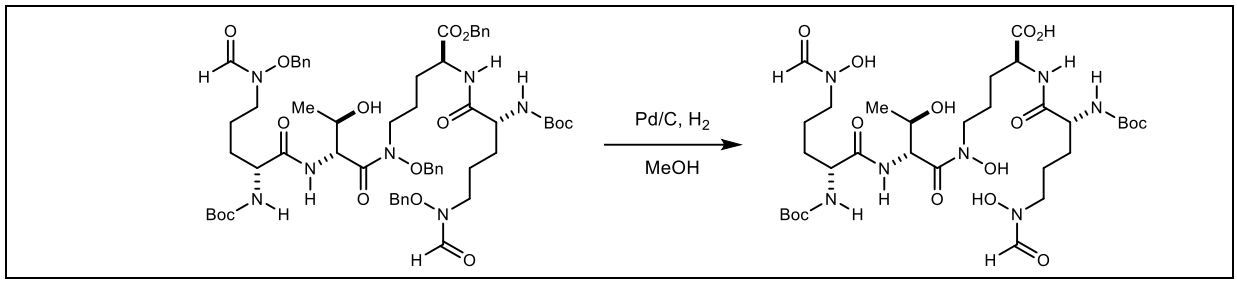

(6*R*,9*R*,15*S*)-15-((*R*)-2-((*tert*-butoxycarbonyl)amino)-5-(*N*-hydroxyformamido)pentanamido)-11-hydroxy-9-((*R*)-1-hydroxyethyl)-6-(3-(*N*-hydroxyformamido)propyl)-2,2-dimethyl -4,7,10-trioxo-3-oxa-5,8,11-triazahexadecan-16-oic acid (1.120) After a solution of tetrapeptide (13.1 mg, 0.012 mmol) in MeOH (2 mL) was purged with argon for 15 min 10% Pd/C (ca. 5 mg) was added, and the mixture was purged with argon for an additional 5 min and stirred under H_2 (1atm) for 1.5 h. The reaction was purged with argon for 5 min before being filtered through a plug of Celite and rinsed well with MeOH (8 mL). The filtrate was concentrated under reduced pressure to afford carboxylic acid (8.3 mg, 93%) as an orange foam: R_f 0.14 (9:1 DCM:MeOH); $[\alpha]_D^{20}$ +7.6; IR (neat) 3393, 2955, 2841, 2122, 1649, 1401 cm^{-1}; ^1H NMR (600 MHz, DMSO) 9.89-9.77 (br, 1H), 8.16 (s, 1H), 7.91 (br, 1H), 7.82 (s, 1H), 7.50 (br, 1H),6.89 (d, *J* = 6.7 Hz, 1H), 6.71 (br, 1H), 4. 97 (t, *J* = 6.4 Hz, 1H), 4.69 (br, 1H), 4.09 (br, 1H), 3.94-3.83 (br, 3H), 3.56 (br, 1H), 3.39- 3.19 (br, 10H), 2.44 (s, 3H), 1.64-1.35 (br, 12H), 1.31 (s, 18H), 0.93 (d, *J* = 4.8 Hz, 3H) ; ^{13}C NMR (150 MHz, DMSO) δ 173.8, 172.5, 172.4, 172.3, 170.1, 162.1, 161.4, 157.5, 155.6, 78.6, 78.5, 66.8, 54.6, 54.5, 51.9, 49.2, 47. 3, 45.9, 45.8, 37.2, 29.8, 29.4, 29.0, 28.8, 28.6, 28.4, 23.8, 23.8, 23.2, 23.0, 19.1; HRMS (ESI-TOF) calculated for $C_{31}H_{56}N_7O_{15}^+$ $(M+H)^+$ m/z: 766.3829, measured 766.3807.

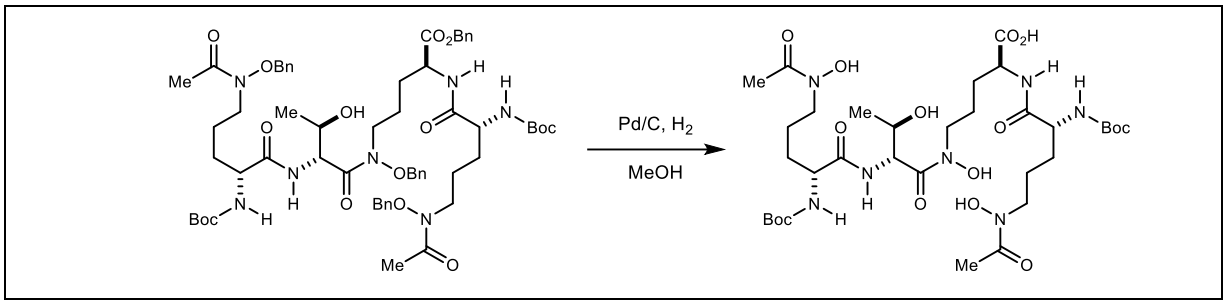

(6*R*,9*R*,15*S*)-15-((*R*)-2-((*tert*-butoxycarbonyl)amino)-5-(*N*-hydroxyacetamido)pentanamido)-11-hydroxy-6-(3-(*N*-hydroxyacetamido)propyl)-9-((*R*)-1-hydroxyethyl)-2,2-dimethyl-4,7,10-trioxo-3-oxa-5,8,11-triazahexadecan-16-oic acid (1.121) After a solution of tetrapeptide (10 mg, 0.013 mmol) in MeOH (1 mL) was purged with argon 15 min, 10% Pd/C (ca. 3 mg) was added, the mixture was purged with argon for an additional 5 min, and stirred under H_2 (1atm) for 1.5 h. The reaction mixture purged with argon for 5 min before being filtered through a plug of Celite, and rinsed well with MeOH (7 mL). The filtrate were concentrated to afford carboxylic acid (5.6 mg, 81%) as a pale orange oil: $[\alpha]_D^{20}$ +42.4 ; IR (neat) 3285, 2926, 1640, 1524, 1440 cm^{-1}; ^1H NMR (600 MHz, DMSO) 9.95 (br, 1H), 9.70 (br, 1H), 7.83 (br, 1H),7.52 (d, *J* = 8.0 Hz, 1H), 6.92 (d, *J* = 7.2 Hz, 1H), 6.80 (d, *J* = 6.7 Hz, 1H), 5.03 (app q, 1H), 4.13 (br, 1H), 4.05-3.89 (m, 3H), 3.62 (m, 1H), 3.58-3.29 (m, 5H), 1.97(d, *J* = 3.9 Hz, 6H), 1.72-1.41 (m, 12H), 1.38 (s, 18H), 1.00 (d, *J* = 5.8 Hz, 3H); ^{13}C NMR (150 MHz, DMSO) 172.8, 171.0, 170.1, 156.0, 155.9, 78.5, 54.6, 41.0, 29.6, 29.4, 28.6, 23.4, 20.8, 20.7, 19.2 ; HRMS (ESI-TOF MS) calculated for $C_{33}H_{60}N_7O_{15}^+$ $(M+H)^+$ m/z: 794.4142, measured 794.4161

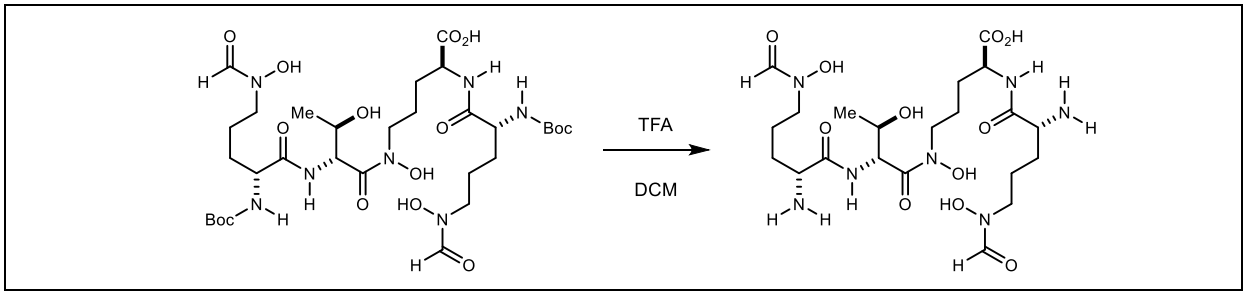

Coelichelin (1.90) To a stirred solution of carboxylic acid (9 mg, 0.012 mmol) in CH_2Cl_2 (0.4 mL, 0.02 M) was added TFA (0.4 mL) dropwise. The reaction mixture was stirred vigorously for 1 h and judged complete by LC-MS analysis. The reaction mixture was concentrated *in vacuo* affording 5.4 mg of **coelichelin (1.90)** as an orange oil: $[\alpha]_D^{20}$ +0.86; IR (neat) 3402, 2950, 2844, 2125, 1654, 1408 cm^{-1}; ^1H NMR (600 MHz, DMSO) 8.76 (d, *J* = 7.7 Hz, 1H),8.71 (d, *J* = 7.7 Hz, 1H) 8.43- 8.31 (dd, *J* = Hz, 1H), 8.25 (s, 2H), 8.20-8.07 (m, 8H), 7.90 (s, 1H), 5.46 (br, 1H), 5.10 (br, 1H), 4.27 (br, 1H), 4.04 (t, *J* = 5.2 Hz, 1H), 3.92 (br, 1H), 3.83 (br, 1H), 3.71 (br, 1H), 3.48-3.37 (m, 4H), 3.30 (br, 1H), 3.06 (m, 1H), 2.49 (s, 4H), 1.76-1.50 (m, 16H), 1.27 (br, 1H), 1.04(d, *J* = 5.1 Hz, 3H); ^{13}C NMR (150 MHz, DMSO); 173.4, 169.6, 168.8, 162.3, 158.6, 158.3, 70.3, 65.9, 55.4, 52.3, 52.2, 52.1, 49.1, 45.8, 40.8, 35.8, 31.9, 29.5, 29.3, 29.1, 28.6, 25.5, 23.0, 22.7, 22.5, 22.2, 22.0, 18.8, 14.4; HRMS (ESI-TOF MS) calculated for $C_{21}H_{40}N_7O_{11}^+$ $(M+H)^+$ m/z: 566.2780, measured 566.2758.

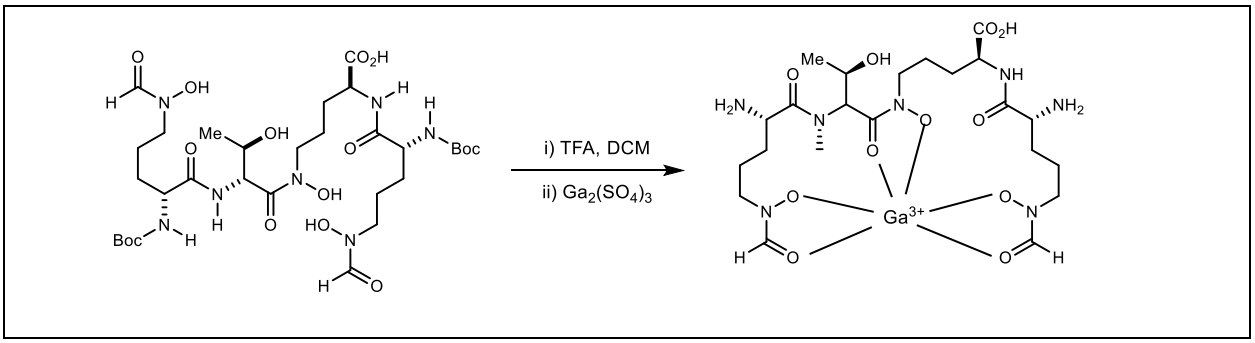

Ga-Coelichelin. To a stirred solution of carboxylic acid (9.0 mg, 0.012 mmol) in CH_2Cl_2 (0.4 mL, 0.02 M) was added TFA (0.4 mL) dropwise. The reaction mixture was stirred vigorously for 1 h and the reaction was judged complete by LC-MS analysis. The reaction mixture was concentrated *in vacuo* and **coelichelin (1.90)** complexed to gallium(III) sulfate crude using a literature procedure affording 5.5 mg (83 %) as a white solid. Compound characterization data was consistent with previous reports: HRMS (ESI-TOF MS) calculated for $C_{21}H_{40}GaN_7O_{11}^+$ $(M+H)^+$ m/z: 632.1801 and 634.1798, measured 632.1794 and 634.1784. [284] [285] [286]

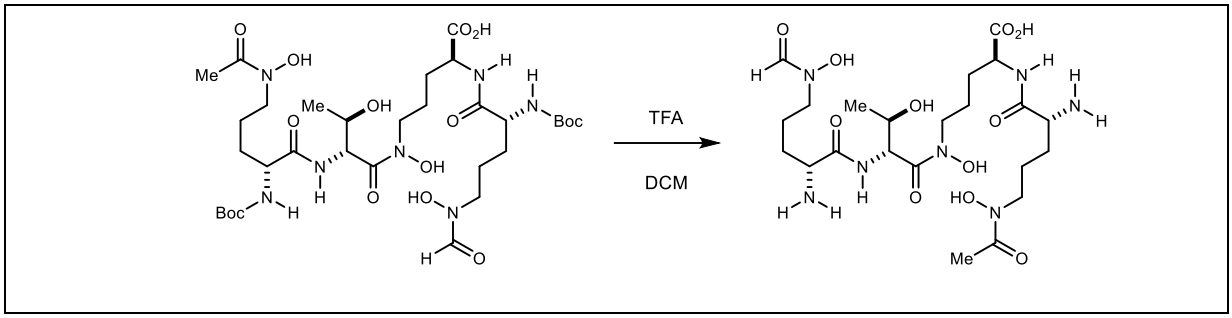

Acetyl Coelichelin (1.91) To a stirred solution of carboxylic acid **1.121** (6.0 mg, 0.008 mmol) in CH_2Cl_2 (0.3 mL, 0.03 M) was added TFA (0.3 mL) dropwise. The reaction mixture was stirred vigorously for 1 h at which point the reaction was judged complete by LC-MS. The reaction mixture was concentrated *in vacuo* affording 4.3 mg of the **acetyl coelichelin (1.91)** as an orange oil: $[\alpha]_D^{20}$ +7.7 ; IR (neat) 2930, 1679, 1434 cm^{-1}; ^1H NMR (600 MHz, DMSO) 8.77-8.65 (br, m, 2H), 8.29 (d, *J* = 8.3 Hz, 1H), 8.17-8.06 (m, 10H), 7.95 (br, 1H), 4.45 (br, 1H), 5.11 (app q, 1H), 4.27 (d, br, *J* = 5.1 Hz, 1H), 4.04 (t, *J* = 5.8 Hz, 1H), 3.92 (br, 1H), 3.83 (d, br, *J* = 4.5 Hz, 2H), 3.74-3.69 (m, 1H), 3.58-3.40 (m, 6H), 3.30 (m, 1H), 2.49 (s, 3H), 1.98 (d, *J* = 4.7 Hz, 6H), 1.80- 1.49 (m, 14H), 1.27 (d, *J* = 6.1 Hz, 1H), 1.04 (d, *J* = 6.2 Hz, 3 H); ^{13}C NMR (150 MHz, DMSO) 173.3, 171.0, 169.6, 169.1, 168.9, 158.6, 70.2, 65.8, 55.4, 52.4, 52.3, 52.0, 47.1, 47.0, 46.8, 40.9, 29.4, 29.1, 28.6, 23.0, 22.5, 22.4, 22.3, 20.8, 20.7, 18.8, 14.4; HRMS (ESI-TOF MS) calculated for $C_{23}H_{44}N_7O_{11}^+$ $(M+H)^+$ m/z: 594.3093, measured 594.3111.

Evaluation of Siderophore Activity

Bacterial strains and growth conditions

Experiments were performed with *Pseudomonas aeruginosa* PAO1 or its isogenic siderophore-deficient mutant *P. aeruginosa* IA614, as indicated.[287] The strain was generated through N-methyl-N'-nitro-N-nitrosoguanidine mutagenesis of PAO1 and the mutations are mapped to the loci encoding pyoverdine (Pvd-) and pyochelin (Pch-) biosynthesis. The mutant is non-fluorescent, and severely debilitated for growth under iron restriction and for the uptake of free ferric iron.

All media and reagents were prepared in polypropylene vessels or glassware washed with 0.1 M HCl to reduce contaminating iron. Bacteria were recovered from freezer stocks on Lysogeny Broth agar (BD) and were routinely cultivated at 37°C with shaking at 180 rpm in Tris Minimal Succinate (TMS) media.[288] TMS agar was prepared by adding 1% w/v Bacto Agar (BD) to TMS media prior to autoclaving. When required for the iron-restricted growth of wild-type *P. aeruginosa* PAO1, TMS was treated with 5 g of Chelex-100 resin (Sigma-Aldrich) per 100 mL media overnight at 4°C with stirring. Chelex was removed from the media by filtration prior to use.

Siderophore plate bioassays

P. aeruginosa IA614 was grown overnight in iron-restricted TMS media. Overnight cultures were sub-cultured 1:100 in fresh TMS and incubated with shaking at 37°C until the optical density at 600 nm (OD_{600}) reached approximately 1.0 (~8 h). Bacterial cells were pelleted by centrifugation at 3,200 x g for 10 min and washed three times with sterile phosphate buffered saline (PBS). After washing, cells were resuspended in PBS and diluted to an OD_{600} of 0.1 (1.5 x 10^8 colony forming units (CFU)/mL). Molten TMS agar was decanted to 50 mL conical tubes and cooled to 50°C. The synthetic chelator ethylenediamine-N,N'-bis(2-hydroxyphenylacetic acid) (EDDHA; LGC Standards) was added to the agar at concentrations of 20, 10 or 5 μM, as indicated. To each 50 mL conical of agar, 14 μL of prepared bacteria were added and mixed with

the agar by inversion. Exactly 25 mL of agar was decanted per petri dish (1.0×10^6 CFU of bacteria per plate). Agar was allowed to solidify before plates were inverted and incubated in the dark for 12 h at room temperature.

To determine what substrates can support the iron-dependent growth of *P. aeruginosa* IA614, 8 mm sterile paper discs were impregnated with 10 µL of 10 mM stocks of coelichelin or its derivatives. Holo-siderophores were prepared by loading the siderophores with 1/3rd the saturating concentration of iron. Sterile ddH_2O and 2,5-dihydroxybenzoic acid (DHBA; Sigma) were provided as negative and positive controls, respectively. Discs were applied to the plates, and the plates were incubated at 37ºC for up to 24 h. Growth promotion of *P. aeruginosa* IA614 was assessed by measuring the growth diameter about the paper disc. The limit of detection (LOD) was set at the diameter of the disc (8 mm). Data are representative of three independent experiments, each with three biological replicates. Statistical significance was calculated using a one-way analysis of variance (ANOVA) where $*p \leq 0.05$ and $****p < 0.0001$.

Chrome azurol S (CAS) assays for detection of iron mobilization

Modified CAS reagent was prepared using the method described below and derived from the original protocols described by Schwyn and Neilands and Alexander and Zuberer. [289] [290] In brief, a 2 mM CAS solution was prepared by dissolving 0.121 g of CAS (Sigma-Aldrich) in 100 mL ddH_2O. A stock solution of 10 mM iron(III) chloride was prepared by dissolving 0.01622 g of anhydrous $FeCl_3$ in 10 mL of 100 mM HCl. The stock solution of 10 mM $FeCl_3$ was subsequently diluted to 1 mM $FeCl_3$ in 10 mM HCl. The dye was iron-loaded by slowly mixing 1.5 mL of 1 mM $FeCl_3$ and 7.5 mL of CAS solution. To stabilize the CAS-iron complex, hexadecyltrimethylammonium bromide (CTAB; USP Reference Standards) was added by dissolving 21.9 mg of CTAB in 25 mL of ddH_2O over low heat (30-40°C), and then subsequently adding the dye complex to this solution (CAS-iron-CTAB). The solution was buffered with 2-(N-morpholino)ethanesulfonic acid (MES; Sigma-Aldrich) by first dissolving 9.76 g of MES in 50 mL of ddH_2O, pH adjusted to 5.6 with KOH, and then mixing the 1 M MES solution with the CAS-iron-CTAB solution. The CAS reagent was transferred to a volumetric flask and topped up to 100 mL with ddH_2O. Immediately prior to use, CAS shuttle solution was prepared by adding 0.2 M 5-sulfosalicyclic acid to a final concentration of 4 mM.

To determine the CAS activity of coelichelin and its derivatives, 100 µL of CAS shuttle solution was mixed with an equal volume of substrate at various concentrations (2-fold dilutions from 200 µM to 1.5626 µM) in a 96-well plate. Equal volumes of ddH_2O were run as negative controls, and equivalent concentrations of desferrioxamine (DFO; Sigma-Aldrich) were run as positive controls. The plate was incubated in the dark for 1 hour, prior to measurement. Siderophore activity was detected by colorimetric change from blue to pink/orange and by assessing the absorbance at 630 nm. A reduction in A_{630nm} is indicative of iron mobilization from CAS to another chelator. Data are representative of three independent experiments, with three technical replicates per experiment.

Pyoverdine and pyochelin fluorescence assays

Under iron-restriction, wild-type *P. aeruginosa* PAO1 will secrete two fluorescent siderophores, pyoverdine (excitation 400 nm, emission 460 nm) and pyochelin (excitation 355 nm, emission 440 nm). Iron-starvation of *P. aeruginosa* can be assessed by quantifying the fluorescence of these siderophores.[291] *P. aeruginosa* PAO1 was grown at 37°C in TMS overnight with shaking at 180 rpm. The bacteria were subcultured 1:100 in fresh chelexed TMS (cTMS) and grown until OD_{600} was approximately 1.0. Bacterial cells were pelleted by centrifugation at 3,200 x g for 10 min and washed three times with sterile PBS. Cells were normalized to an OD_{600} of 0.1 in cTMS. In a 96-well plate, 2-fold dilution series using substrate concentrations of 100 µM to 3.125 µM were prepared for coelichelin, CO20 (**5a**), and EDDHA in cTMS. Free $FeCl_3$ was added at a concentration of 30 µM to show that excess iron represses fluorescence to cells. Each well was inoculated with prepared bacterial cells to a calculated OD_{600nm} of 0.005. The plate was incubated at 37°C with continuous medium amplitude linear shaking in a Cytation 5 Cell Imaging Multi-Mode Reader (BioTek) for 24 h. OD_{600} and fluorescence were measured every 30 minutes for up to 24 h. Detection of pyoverdine fluorescence was truncated at 16 h, as the values exceeded the limit of detection beyond this timepoint. Data are representative of two independent experiments, each with three biological replicates.

To confirm the bioactivity of coelichelin and its congeners, a fluorescence assay was employed to assess iron-restriction of siderophore-proficient *P. aeruginosa* PA01 through detection of its

fluorescent siderophores, pyochelin and pyoverdine. As previously discussed, pseudomonads are known to decrease production of their endogenous siderophores when xenosiderophores are available. Coelichelin and congeners were provided in a two-fold serial dilution, and the fluorescence of pyochelin (excitation 355 nm, emission 440 nm) and pyoverdine (excitiation 400 nm, emission 460 nm) were assessed as a measure of iron availability to the bacterium. In the presence of coelichelin, a dose-dependent decrease in pyochelin and pyoverdine fluorescence is observed, indicating that this siderophore is being utilized by *P. aeruginosa* as an iron source. In contrast, no dose-dependent changes to fluorescence were observed when *P. aeruginosa* was provided with the fully protected tetrapeptide, indicating that is not utilized as an iron source by the bacterium. Bacteria grew comparably when provided with either coelichelin or CO20 (5a), suggesting that differences in fluorescence are not due to difference in growth of the bacteria. These results are consistent with the inability of CO20 (5a) to bind iron, as determined by CAS assay, and its lack of growth promotion of siderophore-deficient *P. aeruginosa* in the bioassay.

3.5 Compound Preparation Relevant to Chapter 2

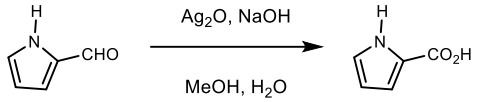

1H-Pyrrole-2-carboxylic acid (2.7). To a solution of 1H-pyrrole-2-carbaldehyde (150 mg, 1.57 mmol) in MeOH (0.8 mL) was added water (8 mL), Ag_2O (727 mg, 3.14 mmol), and NaOH (125 mg, 3.14 mmol). After 2 h, the reaction mixture was filtered to remove precipitate. The filtrate was washed with Et_2O. The aqueous layer was acidified with 6 N aq HCl and extracted with Et_2O. The combined organic extracts were dried and concentrated to afford the product (147 mg, 84%) as a pale brown solid. Analytical data (^{1}H, ^{13}C NMR) was consistent with previous reports.[292]

Benzyl (1H-pyrrole-2-carbonyl)-L-phenylalaninate (2.8). To a solution of EDC (1.04 g, 5.40 mmol) and HOAt (734 mg, 5.40 mmol) in DMF (20 mL) at 0 °C was added 1H-pyrrole-2-carboxylic acid (500 mg, 4.50 mmol) in DMF (10 mL). After 15 min, triethylamine (1.25 mL, 9.00 mmol) was added dropwise at 0 °C, followed by dropwise addition of a solution of benzyl L-phenylalaninate (1.44 g, 4.95 mmol) in DMF (10 mL). The reaction was maintained at 0 °C for 1 h then brought to room temperature and stirred until judged complete by TLC (ca. 16 h). The reaction was quenched with water and extracted with EtOAc. The combined organic extracts were washed with water, 1 N aq HCl, and brine, and then dried and concentrated. Column chromatography (20% ethyl acetate in hexanes) of the residue yielded the product (1.48 g, 94%) as a white foam. R_f 0.37 (2:1 hexanes:EtOAc); $[\alpha]_D^{23}$+27.2 (*c* 0.6 $CHCl_3$); IR (neat) 3263, 3033, 2928, 1734, 1634, 1557, 1513, 1444, 1411 cm^{-1}; ^{1}H NMR (400 MHz, $CDCl_3$) δ 9.99 (br s, 1H), 7.28-7.20 (m, 5H), 7.13-7.10 (m, 3H), 6.97-6.95 (m, 2H), 6.82 (m , 1H), 6.46 (s, 1H), 6.39 (d, *J* = 7.6 Hz, 1H), 6.11 (m, 1H), 5.09 (ABq, *J* = 12.1 Hz, 2H),5.02 (m, 1H), 3.15 (dd, *J* = Hz, 1H), 3.11 (dd, 1H); ^{13}C NMR (100 MHz, $CDCl_3$) δ 171.5, 160.6, 135.6, 135.0, 129.3, 128.6, 128.5, 128.4, 127.0, 125.2, 122.1, 109.8, 109.7, 67.3, 53.0, 38.1; HRMS (ESI): Exact mass calcd for $C_{21}H_{21}N_2O_3$ $[M+H]^+$ 349.1547, found 349.1543.

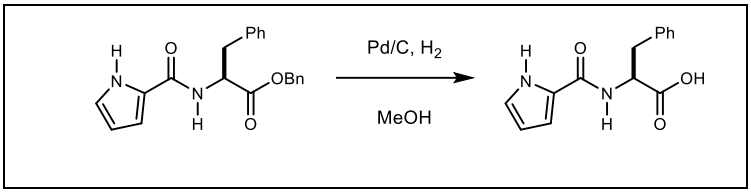

(1*H*-Pyrrole-2-carbonyl)-L-phenylalanine (2.5). After a solution of benzyl (1H-pyrrole-2-carbonyl)-L-phenylalaninate (150 mg, 0.431 mmol) in MeOH (4. 3 mL) was purged with argon for 15 min, 10% Pd/C (ca. 5 mg) was added, and the mixture was purged with argon for an additional 10 min, and then stirred under H_2 (1 atm) for 2 h. The reaction was purged with argon for 5 min before its filtration through a plug of Celite (rinsed well with MeOH). The filtrate was concentrated to afford the product (95 mg, 86%) as a white foam. R_f 0.2 (9:1 DCM:MeOH); $[\alpha]_D^{23}$ -24 (*c* 0.48, MeOH); IR (neat) 3288, 2930, 2487, 1718, 1626, 1555, 1437, 1346, 1202, 1125, 744, 700 cm^{-1}; ^1H NMR (400 MHz, MeOD) δ 7.14-7.05 (m, 5H), 6.78 (s, 1H), 6.68 (m, 1H), 6.03 (m, 1H), 4.71 (ddd, *J* = 11.3, 6.3, 6.3 Hz, 1H), 3.18 (dd, *J* = 13.8, 5.3 Hz, 1H), 2.99 (dd, *J* = 13.8, 9.0 Hz, 1H); ^{13}C NMR (100 MHz, MeOD) δ 173.7, 161.9, 137.2, 128.8, 127.9, 126.3, 124.9, 121.8, 110.9, 108.8, 53.5, 36.9; HRMS (ESI): Exact mass calculated for $C_{14}H_{14}N_2O_3$ $[M+H]^+$ 259.1077, found 259.1076.

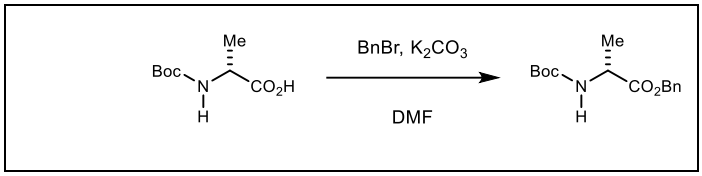

Benzyl (*tert*-butoxycarbonyl)-D-alaninate (2.10). To a solution of (*tert*-butoxycarbonyl)-D-alanine (500 mg, 2.64 mmol) in DMF (5.3 mL, 0.5 M) was added K_2CO_3 (1.09 g, 7.92 mmol) followed by dropwise addition of benzyl bromide (410 μL, 3.44 mmol). After 16 h, the reaction was quenched by slow addition of 1 N aq HCl and the resulting solution was diluted with EtOAc. The aqueous layer was extracted with EtOAc and the combined organic extracts were washed with satd aq $NaHCO_3$, water, brine, dried, and concentrated. Column chromatography (20% ethyl acetate in hexanes) furnished the product (663 mg, 90%) as a colorless oil. Compound characterization data was consistent with previous reports.[293]

Benzyl D-alaninate (2.11). Benzyl (*tert*-butoxycarbonyl)-D-alaninate (200 mg, 716 µmol) was dissolved in 4 M HCl-dioxane (7.16 mL) and stirred until judged complete by TLC (ca. 2 h). The reaction mixture was concentrated and co-evaporated thrice with diethyl ether to afford the product (128 mg) as a white foam. Compound characterization data was consistent with previous reports.[294]

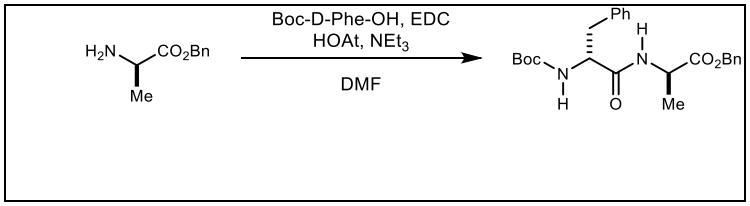

Benzyl (*tert*-butoxycarbonyl)-D-phenylalanyl-D-alaninate (2.12). To a solution of EDC (502 mg, 2.62 mmol) and HOAt (354 mg, 2.62 mmol) in DMF (12 mL) at 0 °C was added (*tert*-butoxycarbonyl)-D-phenylalanine (578 mg, 2.18 mmol) in DMF (6 mL), triethylamine (610 µL, 4.36 mmol), and benzyl D-alaninate (430 mg, 2.40 mmol) in DMF (6 mL). The reaction was maintained at 0 °C for 1 h, brought to room temperature, and maintained until judged complete by TLC (ca. 16 h). The reaction was quenched with water and the aqueous layer was extracted with EtOAc. The combined organic extracts were washed with water, 1 N aq HCl, and brine, and then dried and concentrated. Column chromatography (30% ethyl acetate in hexanes) afforded the product (926 mg, 95%) as a white foam. R_f 0.34 (2:1 hexanes:EtOAc); $[\alpha]_D^{23}$ +2.86 (*c* 1.08, $CHCl_3$); IR (neat) 3298, 3064, 2975, 2929, 1742, 1665, 1535, 1453 cm^{-1}; ^1H NMR (400 MHz, $CDCl_3$) δ 7.31-7.08 (m, 10H), 6.57 (br s, 1H), 5.05 (s, 2H), 4.48 (t, *J* = 7.1 Hz, 1H), 4.32 (br s, 1H), 2.96 (d, *J* = 5.5 Hz, 2H), 1.31 (s, 9H), 1.26 (d, *J* = 7.1 Hz, 3H); ^{13}C NMR (100 MHz, $CDCl_3$) δ 172.3, 171.0, 155.4, 136.6, 135.3, 129.3, 128.5, 128.4, 128.3, 128.1, 126.7, 79.9, 66.9, 55.5, 48.1, 38.4, 28.2, 18.1; HRMS (ESI) calcd for $C_{24}H_{31}N_2O_5$ $[M+H]^+$ m/z: 427.2227, obsd 427.2226.

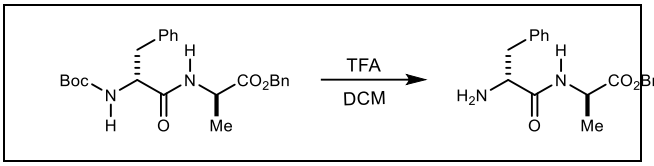

Benzyl D-phenylalanyl-D-alaninate (2.13). To a solution of the dipeptide (1.40 g, 3.84 mmol) in DCM (38.4 mL, 0.10M) was added TFA (3.8 mL) dropwise. The reaction was stirred under inert atmosphere until judged complete by TLC (*ca*. 3 h). The reaction mixture was concentrated and co-evaporated with Et_2O to give the product (1.26 g) as a white foam, which was used directly without further purification. R_f 0.53 (9:1 DCM/MeOH); $[\alpha]_D^{23}$ +12.0 (*c* 0.99, MeOH) ; IR (neat) 3052, 2926, 1739, 1675, 1557, 1500, 1455 cm^{-1}; ^1H NMR (400 MHz, MeOD) δ 7.29-7.17 (m, 10H), 5.07 (q, *J* = 12.3 Hz, 2H), 4.43 (q, *J* = 7.3 Hz, 1H), 4.03 (dd, *J* = 8.6, 5.5 Hz, 1H), 3.13 (dd, *J* = 14.4, 5.5 Hz, 1H), 2.85 (dd, *J* = 14.4, 8.6 Hz, 1H), 1.33 (d, *J* = 7.3 Hz, 3H); ^{13}C NMR (100 MHz, MeOD) δ 171.8, 168.2, 135.7, 135.0, 129.2, 129.1, 128.6, 128.2, 127.9, 127.9, 127.4, 66.6, 54.1, 37.1, 15.9; HRMS (ESI): Exact mass calcd for $C_{19}H_{23}N_2O_3$ $[M+H]^+$ 327.1703, found 327.1700.

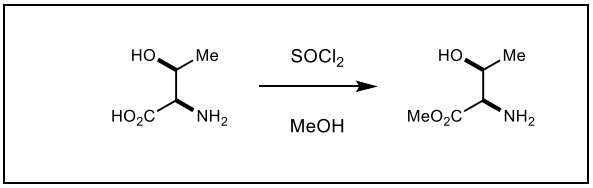

Methyl D-threoninate (2.94). To MeOH (10 mL) at 0 °C was added thionyl chloride (0.23 mL, 3.1 mmol) and D-threonine (500 mg, 4.2 mmol). The reaction mixture was warmed to room temperature and then to reflux for 1 h. The mixture was allowed to cool to room temperature, and concentrated under reduced pressure to yield the product (640 mg) as a white foam, which was used directly without further purification. Analytical data (^1H, ^{13}C NMR) was consistent with previous reports.[295]

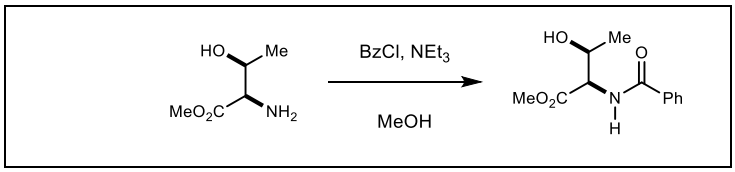

Methyl benzoyl-D-threoninate (2.95) To a solution of methyl D-threoninate (640 mg, 3.77 mmol) in MeOH (3.0 mL, 1.2 M) was added triethylamine (1.42 mL, 10.2 mmol). After 15 min, benzoyl chloride (410 µL, 4.15 mmol) was added dropwise over 10 min at 0 °C. The reaction mixture was concentrated under reduced pressure when judged complete by TLC (ca. 4 h). The resulting residue was resuspended in water and extracted with EtOAc. The combined organic extracts were washed with water and brine, and then dried and concentrated to yield a crude yellow solid. Recrystallization from Et_2O afforded the amide as a white solid (564 mg, 64%). Analytical data (^1H, ^{13}C NMR) was consistent with previous reports.[295]

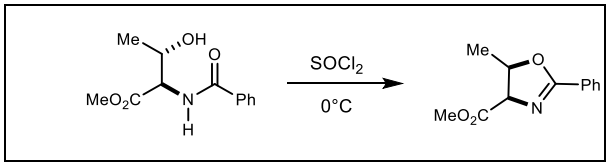

Methyl (4*R*,5*R*)-5-methyl-2-phenyl-4,5-dihydrooxazole-4-carboxylate (2.96). To thionyl chloride (650 µL, 1.3 M) at 0 °C was added methyl benzoyl-D-threoninate (200 mg, 842 µmol) in three portions. After 5 d at 0 °C, excess thionyl chloride was removed *in vacuo* and the resulting residue was dissolved in $CHCl_3$. The solution was poured slowly into satd aq $NaHCO_3$ at 0 °C. The aqueous layer was extracted with $CHCl_3$. The combined organic extracts were washed with water and brine, and then dried and concentrated to give the oxazoline (160 mg, 87%) as a yellow oil. The material was used directly without further purification. Analytical data (^1H, ^{13}C NMR) was consistent with previous reports. [295]

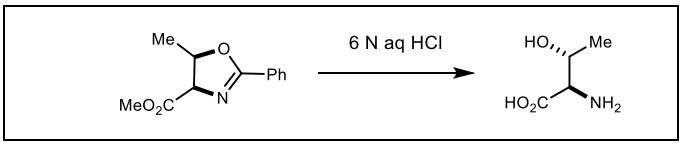

D-*allo*-Threonine (2.97). Methyl (4*R*,5*R*)-5-methyl-2-phenyl-4,5-dihydrooxazole-4-carboxylate (160 mg, 0.73 mmol) was dissolved in 6 N aq HCl (1.82 mL, 0.40 M), and heated refluxed for 5 h. The reaction mixture was cooled to room temperature and washed with Et_2O. The aqueous layer was concentrated to give the product (96 mg) as a white foam, which was used directly without further purification. Analytical data (^1H, ^{13}C NMR) was consistent with previous reports. [295]

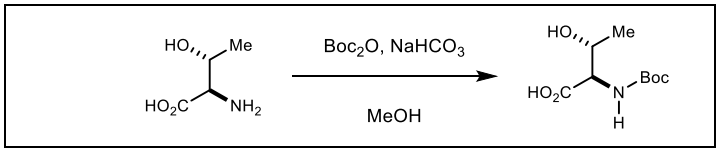

(*tert*-Butoxycarbonyl)-D-*allo*-threonine (2.98). To a solution of D-*allo*-threonine (200 mg, 1.18 mmol) in MeOH (2.3 mL, 0.50 M) was added triethylamine (180 µL, 1.29 mmol), followed by Boc anhydride (257 mg, 1.18 mmol). The reaction mixture was concentrated when judged complete by TLC (ca. 20 h). The resulting white solid was resuspended in Et_2O and acidified with 1 N HCl. The aqueous layer was extracted with EtOAc and the combined organic extracts were washed with brine, dried, and concentrated *in vacuo* to give the product (207 mg, 75%) which was used directly without further purification. Analytical data (^1H, ^{13}C NMR) was consistent with previous reports.[296]

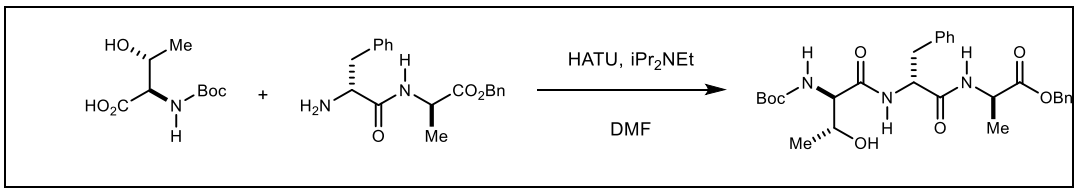

Benzyl (*tert*-butoxycarbonyl)-D-allothreonyl-D-phenylalanyl-D-alaninate (2.14). To a solution of carboxylic acid (160 mg, 0.73 mmol) in DMF (1.5 mL) at 0 °C was added HATU (414 mg, 1.09 mmol). After 30 min at 0 °C, the amine (250 mg, 0.76 mmol) and *N*,*N*-diisopropylethylamine (0.32 mL, 1.8 mmol) were added. The reaction mixture was maintained at 0 °C for 1 h, brought to room temperature, and stirred at room temperature until judged complete by TLC (ca. 16 h). The reaction mixture was poured over ice water and extracted with EtOAc. The combined extracts were washed with brine, dried, and concentrated. Column chromatography (3% MeOH in dichloromethane) yielded the tripeptide as a white foam (320 mg, 83%). R_f 0.25 (95:5 DCM:MeOH); $[\alpha]_D^{23}$ +46 (*c* 0.42, $CHCl_3$); IR (neat) 3303, 3062, 2979, 2932, 1963, 1888, 1746, 1695, 1650, 1633, 1538, 1517, 1504, 1454, 1393, 1337, 1019, 952, 843, 746, 700cm^{-1}; ^{1}H NMR (400 MHz, MeOD) δ 8.26 (d, *J* = 5.9 Hz, 1H), 8.01 (d, *J* = 7.7 Hz, 1H), 7.28-7.04 (m, 10H), 5.04 (ABq, *J* = 12.5 Hz, 2H), 4.59 (br m, 1H), 4.34 (dq, *J* = 7.4, 7.4 Hz, 1H), 3.84 (br m, 1H), 3.72 (dq, *J* = 6.4, 6.1 Hz, 1H), 3.09 (dd, *J* = 14.4, 4.6 Hz, 1H), 2.76 (dd, *J* = 13.9, 9.4 Hz, 1H), 1.31 (s, 9H), 1.27 (d, *J* = 7.3 Hz, 3H), 1.00 (d, *J* = 6.1 Hz, 3H); ^{13}C NMR (100 MHz, MeOD) δ 172.1, 171.9, 171.8, 156.3, 136.9, 135.8, 128.9, 128.1, 127.9, 127.8, 127.7, 126.2, 79.3, 67.6, 66.4, 60.1, 54.2, 48.4, 36.9, 27.2, 18.5, 15.6; HRMS (ESI): Exact mass calcd for $C_{28}H_{37}N_3O_7$ $[M]^+$ 527.2632, found 527.2587.

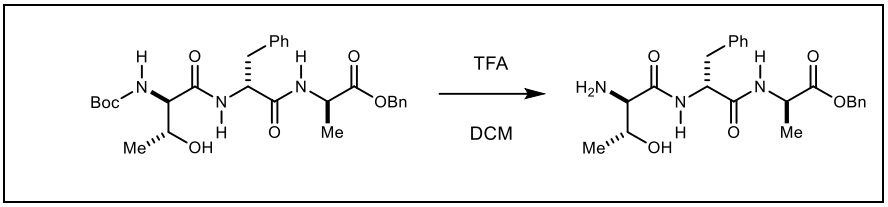

Benzyl D-allothreonyl-D-phenylalanyl-D-alaninate (2.15). To a solution of the tripeptide (43 mg, 82 μmol) in DCM (0.8 mL, 0.1M) was added trifluoroacetic acid (80 μL, 0.0011 mmol). The reaction was stirred at room temperature until judged complete by TLC (ca. 3.5 h), and then concentrated to give a white foam (34 mg), which was used directly without further purification. R_f 0.12 (90:10 DCM:MeOH); $[\alpha]_D^{23}$ +3.5 (*c* 1.16, MeOH); IR (neat) 3261, 3063, 2922, 1715, 1672, 1556, 1455, 1338, 1201, 1136, 1019, 951, 800, 747, 701 cm^{-1}; ^1H NMR (400 MHz, MeOD) δ 7.29-7.10 (m, 10H), 5.06 (ABq, *J* = 12.3 Hz, 2H), 4.65 (q, *J* = 4.8 Hz, 1H), 4.37 (m, 1H), 4.12 (dq, *J* = 6.5, 6.4 Hz, 1H), 3.73 (d, *J* = 5.1 Hz, 1H), 3.07 (dd, *J* = 14.4, 4.7 Hz, 1H), 2.75 (dd, *J* = 14.4, 9.7 Hz, 1H), 1.30 (d, *J* = 7.2 Hz, 3H), 1.08 (d, *J* = 6.6 Hz, 3H) ;^{13}C NMR (150 MHz, MeOD) 172.5, 170.8, 161.3, 137.4, 136.4, 129.6, 128.9, 128.8, 128.6, 128.3, 127.3, 69.0, 66.5, 61.1, 59.4, 48.4, 38.5, 19.6, 17.2 ppm; HRMS (ESI): Exact mass calcd for $C_{23}H_{30}N_3O_5$ $[M+H]^+$ 428.2185, found 428.2180.

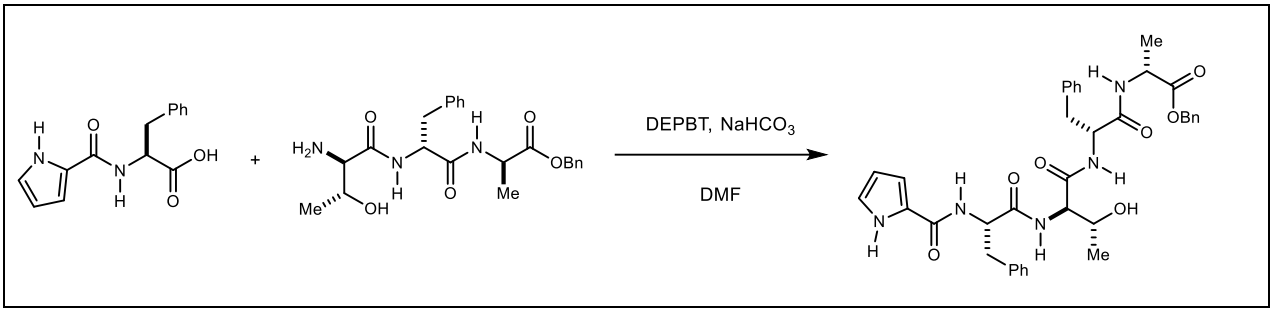

Benzyl (1*H*-pyrrole-2-carbonyl)-L-phenylalanyl-D-allothreonyl-D-phenylalanyl-D-alaninate (2.16). To a solution of (1*H*-pyrrole-2-carbonyl)-L-phenylalanine (49 mg, 0.19 mmol) in DMF (1.9 mL) at 0 °C was added DEPBT (113 mg, 0.378 mmol) and $NaHCO_3$ (15.8 mg, 0.189 mmol). After 2 h at 0 °C, benzyl D-allothreonyl-D-phenylalanyl-D-alaninate (85 mg, 0.20 mmol) in DMF (1.9 mL) was added, followed by $NaHCO_3$ (31.8 mg, 0.378 mmol). The reaction mixture was maintained at 0 °C for 2 h, brought to room temperature, and maintained until judged complete by TLC (ca. 18 h). The reaction was poured over ice-water and extracted with EtOAc. The combined organic extracts were washed with satd aq $NaHCO_3$, 1 N aq HCl, and brine, and then dried and concentrated. Reversed phase HPLC (gradient: 10-50% MeCN-H_2O with 0.1% TFA) yielded the pentapeptide (100 mg, 79 %) as a pale yellow foam. R_f 0.23 (5:95 MeOH:DCM); $[\alpha]_D^{23}$ +28.8 (*c* 0.42, $CHCl_3$); IR (neat) 3280, 3064, 3031, 2957, 2924, 2653, 2411, 1736 cm^{-1}; ^1H NMR (400 MHz, acetone-d_6) δ 10.59 (br s, 1H), 7.83 (d, *J* = 9.1 Hz, 1H), 7.78 (d, *J* = 6.4 Hz, 1H), 7.69 (d, *J* = 6.9 Hz, 1H), 7.44 (d, *J* = 6.9 Hz, 1H), 7.26-7.02 (m, 15H), 6.82 (m, 1H), 6.72 (m, 1H), 6.01 (m, 1H), 4.99 (s, 2H), 4.55 (m, 2H), 4.09 (dq, *J* = 14.4, 7.3 Hz, 1H), 4.00 (t, *J* = 6.72 Hz, 1H), 3.66 (dq, *J* = 13.1, 6.5 Hz, 1H), 3.17 (dd, *J* = 13.8, 3.7 Hz, 1H), 3.03 (dd, *J* = 14.0, 7.0 Hz, 1H), 2.97-2.88 (m, 2H), 1.09 (d, *J* = 7.3 Hz, 3H), 0.64 (d, *J* = 6.4 Hz, 3H); ^{13}C NMR (100 MHz, acetone-d_6) δ 173.2, 172.1, 170.9, 170.4, 161.9, 138.4, 137.6, 136.4, 129.3, 128.4, 128.1, 127.8, 127.7, 126.5, 126.2, 125.5, 122.1, 110.9, 109.1, 67.0, 66.1, 65.9, 59.4, 56.1, 54.3, 54.2, 48.3, 36.9, 36.8, 18.5, 16.4; HRMS (ESI) calcd for $C_{37}H_{41}N_5O_7$ $[M]^+$ m/z: 667.3006, obsd 667.2962.

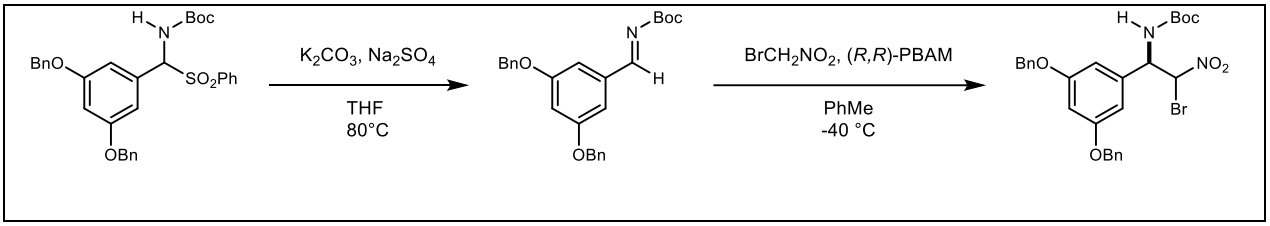

***tert*-Butyl ((1*R*)-1-(3,5-bis(benzyloxy)phenyl)-2-bromo-2-nitroethyl)carbamate (2.26).** A stirred solution of sulfone (20.0 g, 35.7 mmol), K_2CO_3 (24.6 g, 178 mmol), and Na_2SO_4 (25.4 g, 178 mmol) in THF was heated to reflux for 7 h. Upon consumption of sulfone as indicated by ^{1}H NMR, the reaction mixture was allowed to cool to room temperature and filtered through a coarse glass frit. The filtrate was concentrated to give the desired imine as a pale yellow solid (15 g), which was used immediately without further purification.

To a solution of the crude imine (15 g, 35.7 mmol) in PhMe (357 mL, 0.1 M) at -40 °C was added (*R*,*R*)-PBAM (361 mg, 714 µmol). After 10 min, bromonitromethane (3.0 mL, 42 mmol) was added dropwise at -40 °C. The reaction mixture was brought to -20 °C where it was maintained for 44 h. The reaction mixture was diluted with EtOAc, filtered through a large silica plug, and then concentrated. The resulting crude solid was recrystallized from EtOAc/hexanes to give the desired bromonitroalkane as a white solid (14 g, 73%, 99%/99% ee).[297]

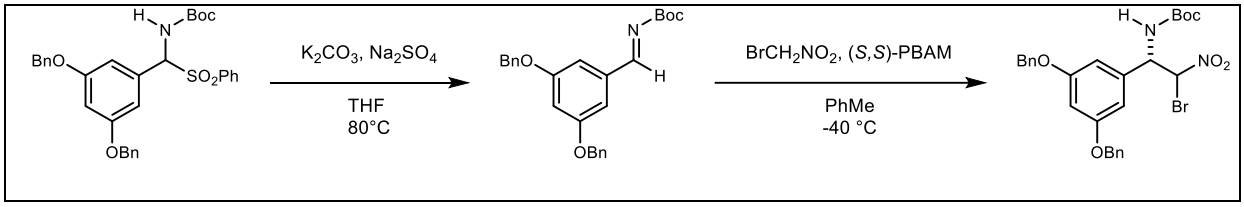

***tert*-Butyl ((1*S*)-1-(3,5-bis(benzyloxy)phenyl)-2-bromo-2-nitroethyl)carbamate (2.24).** A stirred solution of sulfone (2.0 g, 3.6 mmol), K_2CO_3 (2.48, 17.9 mmol), and Na_2SO_4 (2.54 g, 17.9 mmol) in THF (17.9 mL, 0.20 M) was heated at reflux for 7 h. Upon consumption of sulfone as indicated by ^{1}H NMR, the reaction mixture was allowed to cool to room temperature and filtered through a coarse glass frit. The filtrate was concentrated to give the desired imine as a pale yellow solid (1.5 g), which was used immediately without further purification.

To a solution of the crude imine (1.49 g, 3.57 mmol) in PhMe (35.7 mL, 0.1 M) at -40 °C was added (*S*,*S*)-PBAM (36 mg, 71 µmol). After 10 min, bromonitromethane (0.29 mL, 4.3 mmol)

was added dropwise at -40 °C. The reaction mixture was brought to -20 °C where it was maintained for 40 h. The reaction mixture was diluted with EtOAc, filtered through a large plug of silica gel, and then concentrated. The resulting crude solid was recrystallized from EtOAc/hexanes to give the desired bromonitroalkane as a white solid (1.2 g, 60%, 99%/99% ee). R_f 0.55 (3:1 hexanes:EtOAc); IR (neat) 3370, 2981, 1685, 1597 cm^{-1}; ^1H NMR (400 MHz, $CDCl_3$) δ 7.35-7.24 (m, 10H), 6.51 (s, 1H), 6.46 (s, 2H), 6.16 (br s, 1H), 5.53 (br m, 1H), 5.23 (d, *J* = 9.5 Hz, 1H), 4.94 (s, 4H), 1.36 (s, 9H); ^{13}C NMR (100 MHz, $CDCl_3$) δ 160.3, 154.5, 137.6, 136.3, 128.6, 128.1, 127.5, 106.3, 102.1, 85.1, 81.2, 70.2, 57.8, 28.1; HRMS (ESI): Exact mass calcd for $C_{27}H_{33}BrN_3O_6$ $[M+NH_4]^+$ 574.1547, found 574.1539.

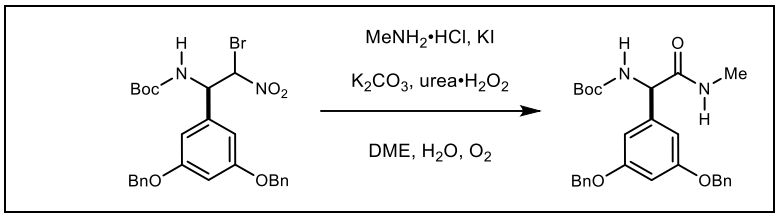

***tert*-Butyl (*R*)-(1-(3,5-bis(benzyloxy)phenyl)-2-(methylamino)-2-oxoethyl)carbamate (2.28).** To a solution of bromonitroalkane (200 mg, 0.358 mmol) and methylamine hydrochloride (29 mg, 0.43 mmol) in DME (3.6 mL, 0.1 M) was added KI (119 mg, 0.717 mmol) at 0 °C. After 20 min at 0 °C, K_2CO_3 (297 mg, 2.15 mmol) was added, followed by immediate addition of urea·H_2O_2 (101 mg, 1.08 mmol, 3.0 M solution in water). The reaction was maintained at 0 °C for 2 h and then brought to room temperature where it was maintained until judged complete by TLC (ca. 22 h). The reaction was quenched at 0 °C with satd sodium thiosulfate and extracted with EtOAc. The combined extracts were washed with 1 N aq HCl and brine, and then dried and concentrated to give a yellow foam. Column chromatography (0 to 30% ethyl acetate in hexanes) afforded the methyl amide (51 mg, 30%). R_f 0.35 (1:1 hexanes:EtOAc); $[\alpha]_D^{23}$ -81 (*c* 0.22, $CHCl_3$); IR (neat) 3356, 3288, 3093, 3064, 3034, 2930, 1680, 1605, 1524, 1450 cm^{-1}; ^1H NMR (400 MHz, $CDCl_3$) δ 7.32-7.22 (m, 10H), 6.57 (s, 2H), 6.45 (s, 1H), 6.02 (br s, 1H), 5.93 (br s, 1H), 5.08 (br s, 1H), 4.82 (m, 4H), 2.66 (d, *J* = 4.8 Hz, 3H), 1.35 (s, 9H); ^{13}C NMR (100 MHz, $CDCl_3$) δ170.4, 160.2, 155.4, 141.1, 136.6, 128.6, 128.5, 127.9, 127.5, 105.9, 101.8, 80.0, 69.9, 58.2, 28.3, 26.4; HRMS (ESI): Exact mass calcd for $C_{28}H_{32}N_2O_5Na$ $[M+Na]^+$ 499.2203, found 499.2202.

(*R*)-2-amino-2-(3,5-bis(benzyloxy)phenyl)-*N*-methylacetamide (2.27). A solution of *N*-Me amide (95 mg, 0.199 mmol) in 4 M HCl-dioxanes (2 mL) was stirred at room temperature until judged complete by TLC (ca. 1.5 h). The reaction mixture was concentrated and co-evaporated thrice with diethyl ether to afford a pale yellow solid (80 mg), which was used immediately without further purification. R_f 0.19 (5:95 MeOH:DCM); $[\alpha]_D^{23}$ -1.5 (*c* 0.52, $CHCl_3$); IR (neat) 3315, 3032, 2923, 2852, 1660, 1595, 1536, 1497, 1453 cm^{-1}; ^1H NMR (400 MHz,DMSO-d_6) δ 7.96, (1H), 7.46-7.33 (m, 10H), 6.68 (s, 1H), 6.67 (s, 1H), 6.56 (t, *J* = 2.1 Hz, 1H), 5.06 (s, 4H), 4.25 (br s, 1H), 2.59 (d, *J* = 4.5 Hz, 3H); ^{13}C NMR (100 MHz, DMSO-d_6) δ 173.6, 159.6, 145.7, 137.4, 128.8, 128.2, 128.1, 106.4, 100.5, 69.7, 59.5, 25.9; HRMS (ESI) calcd for $C_{23}H_{25}N_2O_3$ $[M+H]^+$ m/z: 377.1860, obsd 377.1862.

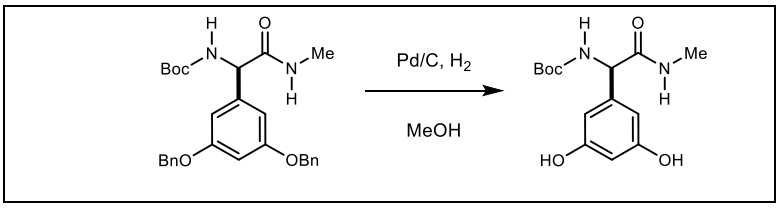

***tert*-butyl (*R*)-(1-(3,5-dihydroxyphenyl)-2-(methylamino)-2-oxoethyl)carbamate (2.31).** A solution of N-Me amide (20 mg, 42 µmol) in MeOH (4 mL) was purged with argon, Pd/C (10% w/w, ca. 2 mg), and the reaction purged again with argon. The reaction mixture was placed under H_2 atmosphere until judged complete (ca. 17 h). The reaction was purged with argon, filtered through a pad of celite, and concentrated to give the product (17 mg), which was used directly without further purification. R_f 0.07 (95:5 DCM:MeOH); $[\alpha]_D^{23}$ -73.2 (*c* 0.92, MeOH); ^1H NMR (400 MHz, acetone-d_6) δ 7.18 (br s, 1H), 6.31 (s, 2H), 6.16 (s, 1H), 6.10 (br s, 1H), 4.89 (br d, *J* = 7.0 Hz, 1H), 2.58 (d, *J* = 4.8 Hz, 3H), 1.26 (s, 9H); ^{13}C NMR (100 MHz, acetone-d_6) δ 170.5, 158.5, 154.8, 141.5, 105.6, 101.9, 78.4, 57.9, 27.6, 25.4; HRMS (ESI): Exact mass calcd for $C_{14}H_{20}N_2NaO_5$ $(M+Na)^+$ 319.2164, found 319.1265.

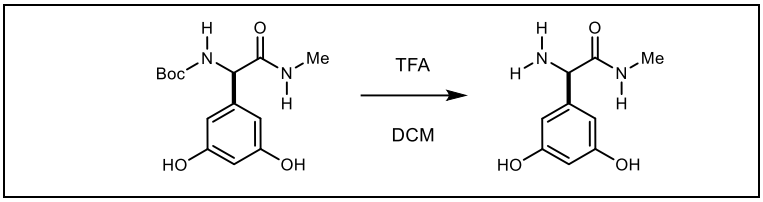

(*R*)-2-amino-2-(3,5-dihydroxyphenyl)-*N*-methylacetamide (2.32) To a solution of the *N*-Me amide (19.2 mg, 64.8 μmol) in DCM (0.65 mL, 0.10 M) was added trifluoroacetic acid (100 μL). The reaction was stirred at room temperature until judged complete by TLC (ca. 2 h), and then concentrated to give a orange foam (13 mg), which was used directly without further purification. R_f 0.1 (90:10 DCM:MeOH); ^{1}H NMR (400 MHz, acetone-d_6) δ 6.44 (br s, 2H), 6.34 (br s, 1H), 5.81 (br s, 1H), 2.66 (br d, J = 6.8 Hz, 3H); HRMS (ESI): Exact mass calcd for $C_9H_{13}N_2O_3$ $[M+H]^+$ 197.0921, found 197.0921.

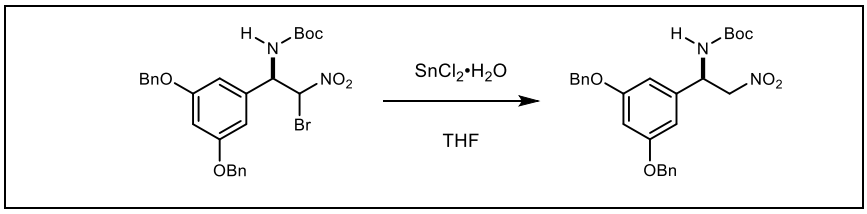

***tert*-butyl (*R*)-(1-(3,5-bis(benzyloxy)phenyl)-2-nitroethyl)carbamate (2.36).** To a stirred solution of the bromonitroalkane (1.00 g, 1.79 mmol) in THF (17.9 mL, 0.1 M) was added $SnCl_2 \cdot H_2O$ (807 mg, 3.58 mmol). When judged complete by TLC (ca. 2 h), the reaction mixture was diluted with water and extracted with Et_2O. The combined organic extracts were filtered through a plug of Celite and the filtrate was dried and concentrated. Column chromatography (15% ethyl acetate in hexanes) yielded the product (845 mg, >95%) as a white powder. Compound characterization data was consistent with previous reports.[298]

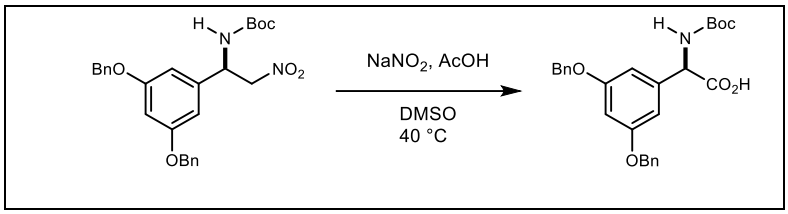

(*R*)-2-(3,5-bis(benzyloxy)phenyl)-2-((*tert*-butoxycarbonyl)amino)acetic acid (2.37). To a stirred solution of the nitroalkane (100 mg, 209 µmol) and sodium nitrite (43.3 mg, 627 µmol) in DMSO (1.6 mL, 0.13 M) was added AcOH (0.18 mL, 3.1 mmol) dropwise. The reaction mixture was heated to 40 °C for 18 h, allowed to cool to room temperature, and diluted with 1 N HCl. The aqueous layer was extracted with DCM, and the combined organic extracts were washed with ice water, dried, and concentrated to give the product (93 mg) as a crude yellow oil, which was carried forward without further purification.[299]

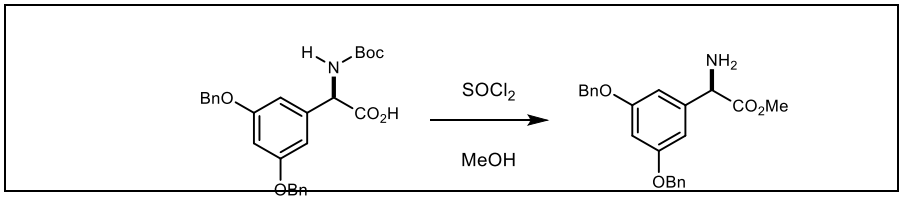

Methyl (*R*)-2-amino-2-(3,5-bis(benzyloxy)phenyl)acetate (2.38). To a solution of the carboxylic acid (100 mg, 215 µmol) in MeOH (0.93 mL) at 0 °C was added thionyl chloride (31 µL, 430 µmol) dropwise. The reaction mixture was maintained at 0 °C for 2 h, and then brought to room temperature where it was maintained until judged complete by TLC (*ca*. 2 h). The reaction mixture was concentrated under reduced pressure and co-evaporated with Et_2O to afford the desired methyl ester as a white solid (86 mg), which was used directly without further purification.[300]

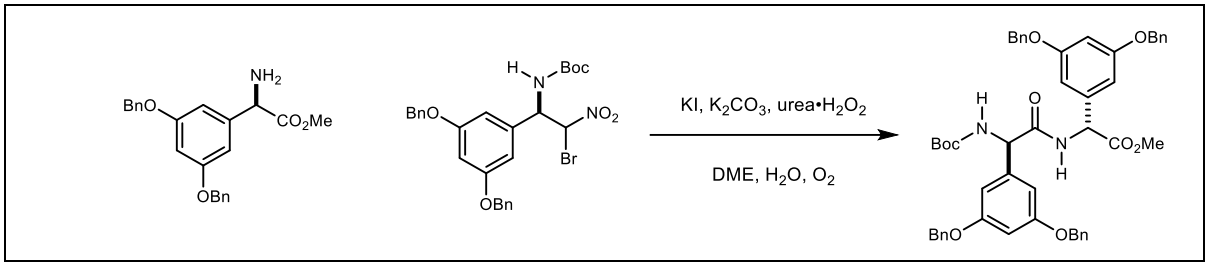

Methyl (*R*)-2-(3,5-bis(benzyloxy)phenyl)-2-((*R*)-2-(3,5-bis(benzyloxy)phenyl)-2-((*tert*-butoxycarbonyl)amino)acetamido)acetate (2.39). To a stirred solution of the amine (25 mg, 66 µmol) and the bromonitroalkane (36.9 mg, 66 µmol) in DME (0.7 mL, 0.1 M) at 0 °C, was added KI (21.9 mg, 132 µmol). After 30 min at 0 °C, K_2CO_3 (54.8 mg, 397 µmol) was added followed by immediate dropwise addition of a solution of urea-H_2O_2 (18.6 mg, 199 µmol, 3.0 M solution in water) and the reaction mixture was placed under O_2 atmosphere. Upon consumption of starting material as indicated by TLC (ca. 16 h), the reaction mixture was quenched at 0 °C with satd aq sodium thiosulfate, and then diluted with EtOAc. The aqueous layer was extracted with EtOAc and the combined organic extracts were washed with satd aq sodium thiosulfate, satd aq $NaHCO_3$, 1 N aq HCl, and brine, and then dried and concentrated. Column chromatography (20% ethyl acetate in hexanes) yielded the product (25.9 mg, 48%) as a yellow wax. R_f 0.22 (3:1 hexanes:EtOAc); $[\alpha]_D^{23}$ -59.9 (*c* 1.18, $CHCl_3$); IR (neat) 3350, 2921, 1734, 1653, 1607, 1518, 1448 cm^{-1}; ^1H NMR (600 MHz, $CDCl_3$) δ 7.37-7.21 (m, 20H), 6.75 (d, *J* = 6.8 Hz, 1H), 6.56 (s, 2H), 6.50-6.46 (m, 4H), 5.57 (br, 1H), 5.35 (d, *J* = 6.8 Hz, 2H), 5.04 (br, 1H), 4.90 (s, 4H), 4.89 (s, 4H), 3.58 (s, 3H), 1.34 (s, 9H); ^{13}C NMR (150 MHz, $CDCl_3$) δ 170.4, 169.2, 160.4, 160.3, 140.1, 138.3, 136.6, 136.5, 128.6, 128.5, 128.4, 128.1, 128.0, 127.6, 127.5, 106.4, 106.3, 102.2, 102.1, 80.2, 77.4, 70.2, 58.7, 56.7, 52.9, 28.3; HRMS (ESI): Exact mass calcd for $C_{50}H_{51}N_2O_9$ $(M+H)^+$ 823.3589, found 823.3591.

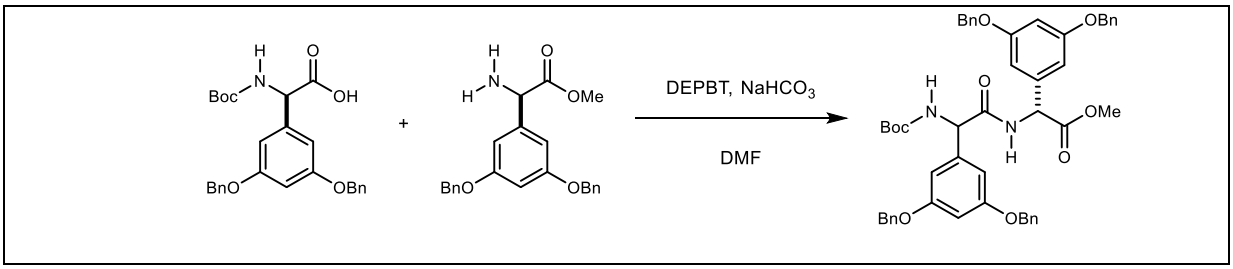

Methyl (*R*)-2-(3,5-bis(benzyloxy)phenyl)-2-((*R*)-2-(3,5-bis(benzyloxy)phenyl)-2-((*tert*-butoxycarbonyl)amino)acetamido)acetate (2.40). To a solution of carboxylic acid (20 mg, 43 µmol) in DMF (0.5mL) at 0 °C was added DEPBT (38.5 mg, 129 µmol) and $NaHCO_3$ (3.6 mg, 43 µmol). After 2 h at 0 °C, amine (19.5 mg, 51.7 µmol) in DMF (0.3 mL) was added to the reaction followed by $NaHCO_3$ (10.8 mg, 129 µmol). The reaction was stirred at 0 °C until judged complete by TLC (ca. 18 h). The reaction was poured over ice water and extracted with EtOAc. The combined extracts were washed with 1 N HCl, water, NaHCO3, and brine then dried and concentrated. Column chromatography (20% to 40% ethyl acetate in hexanes) of the residue afforded the dipeptide as a mixture of epimers (19.9 mg, 56%).

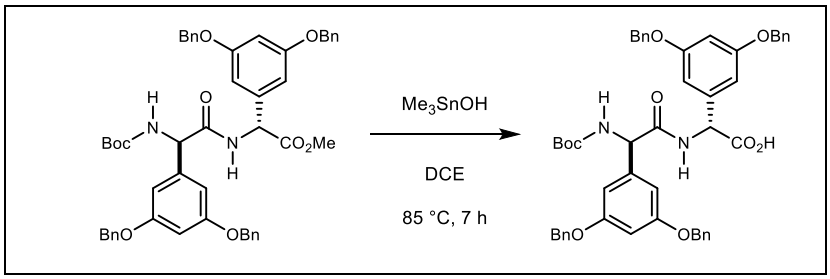

***R*)-2-(3,5-bis(benzyloxy)phenyl)-2-((*R*)-2-(3,5-bis(benzyloxy)phenyl)-2-((*tert*-butoxycarbonyl)amino)acetamido)acetic acid (2.41).** To a solution of methyl ester (18 mg, 22 µmol) in DCE (0.32 mL, 0.10 M) was added trimethyltin hydroxide (11.4 mg, 43.7 µmol) and the reaction heated to 85 °C for 7 h.[301302] The reaction mixture was allowed to cool to ambient temperature and concentrated. The obtained residue was resuspended in a 10% citric acid solution, sonicated, and extracted with EtOAc. The combined organic extracts were washed with 10% citric acid and brine then dried and concentrated. The resulting white solid was resuspended in DCM and washed with satd aq $NaHCO_3$. The aqueous layer was acidified with 1 N HCl and extracted with EtOAc. The combined organic extracts were dried and concentrated to give the desired carboxylic acid (15 mg, 85% unpurified). Compound characterization was consistent

with our other preparations of 2.41.

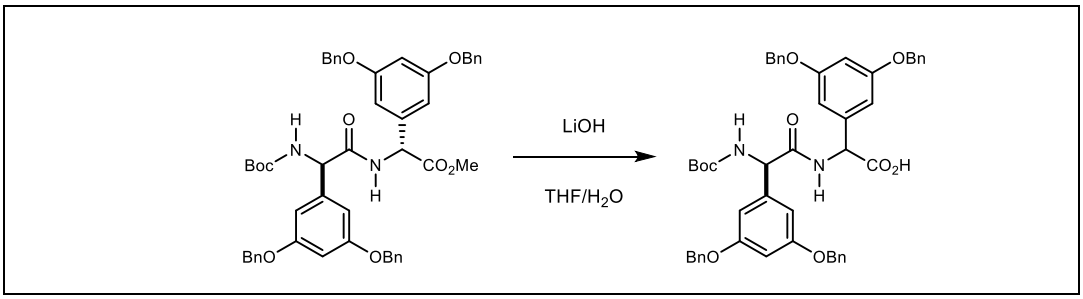

(*R*)-2-(3,5-bis(benzyloxy)phenyl)-2-((*R*)-2-(3,5-bis(benzyloxy)phenyl)-2-((*tert*-butoxycarbonyl)amino)acetamido)acetic acid (2.42). To a solution of methyl ester (14.4 mg, 17.4 µmol) in THF/water (1:1) (0.32 mL, 0.05M) was added a 1M aq. LiOH (26 µL) dropwise. Upon consumption of methyl ester as monitored by TLC (ca. 1 h), the reaction was concentrated to remove excess THF and the resulting residue acidified with 1 N HCl. The aqueous was extracted with EtOAc and the combined extracts dried and concentrated. Column chromatography (5% MeOH in DCM) yielded the carboxylic acid (4.5 mg) and undesired epimer (4.3 mg). Compound characterization data was consistent with our other preparations of 2.41.

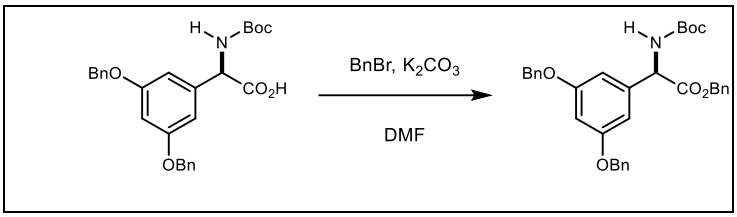

Benzyl (*R*)-2-(3,5-bis(benzyloxy)phenyl)-2-((*tert*-butoxycarbonyl)amino)acetate (2.43). To a stirred solution of (*R*)-2-(3,5-bis(benzyloxy)phenyl)-2-((*tert*-butoxycarbonyl)amino)acetic acid (80 mg, 170 µmol) in DMF (0.34 mL, 0.50 M) was added K_2CO_3 (36 mg, 260 µmol) followed by benzyl bromide (21 µL, 180 µmol). The reaction mixture was quenched at 0 °C with 1 N HCl when judged complete by TLC (ca. 20 h), and the resulting solution was diluted with EtOAc. The aqueous layers were extracted with EtOAc. The combined organic extracts were washed with satd aq $NaHCO_3$, water, and brine, and then dried and concentrated. Column chromatography (10% ethyl acetate in hexanes) of the residue yielded the ester (42 mg, 44%) as a colorless oil. R_f 0.5 (3:1 hexanes:EtOAc); $[\alpha]_D^{23}$ -35.9 (*c* 1.03, $CHCl_3$); IR (neat) 3369, 3032, 2976, 2930, 1742, 1713, 1596, 1497, 1454 cm^{-1}; ^1H NMR (400 MHz, $CDCl_3$) δ 7.29-7.11 (m, 15H), 6.50 (s, 2H), 6.46 (s, 1H), 5.45 (d, *J* = 7.0 Hz, 1H), 5.22 (d, J = 7.3 Hz, 1H), 5.04 (s, 2 H),

4.85 (s, 4H), 1.35 (s, 9H); ^{13}C NMR (100 MHz, $CDCl_3$) δ 170.7, 160.2, 154.8, 138.9, 136.6, 135.2, 128.5, 128.4, 128.3, 128.0, 127.5, 106.2, 102.1, 80.1, 70.1, 67.3, 57.6, 28.3; HRMS (ESI): Exact mass calcd for $C_{34}H_{36}NO_6$ $(M+H)^+$ 554.2537, measured 554.2530.

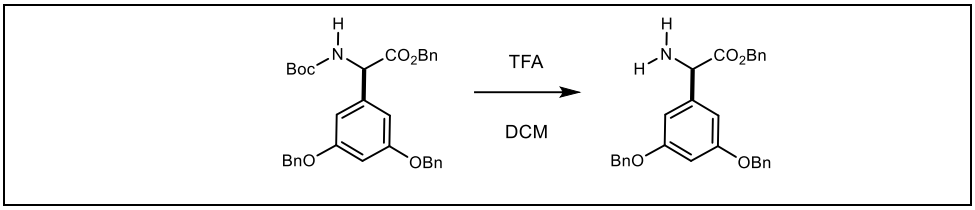

Benzyl (*R*)-2-amino-2-(3,5-bis(benzyloxy)phenyl)acetate (2.44). To a solution of the ester (17 mg, 31 μmol) in DCM (0.31 mL, 0.1 M) was added trifluoroacetic acid (31 μL, 0.41 μmol) dropwise. Upon completion as judged by TLC (ca. 3 h), the reaction mixture was concentrated to give a crude white foam (14 mg), which was used directly without further purification. R_f 0.28 (95:5 DCM:MeOH); $[\alpha]_D^{23}$ -8.5 (*c* 0.82, $CHCl_3$); IR (neat) 3033, 2924, 1746, 1680, 1598, 1453 cm^{-1}; ^{1}H NMR (400 MHz, acetone-d_6) δ 7.38-7.17 (m, 15H), 6.80-6.74 (m, 2H), 6.67 (m, 1H), 5.41 (s, 1H), 5.16 (ABq, *J* = 12.1 Hz, 2H), 4.97 (ABq, *J* = 11.9 Hz, 4H); ^{13}C NMR (100 MHz, acetone-d_6) δ 168.0, 160.4, 136.9, 135.2, 134.3, 128.3, 128.2, 128.1, 127.8, 127.6, 107.3, 103.1, 69.8, 67.5, 56.3; HRMS (ESI): Exact mass calcd for $C_{29}H_{28}NO_4$ $[M+H]^+$ 454.2013, found 454.2016.

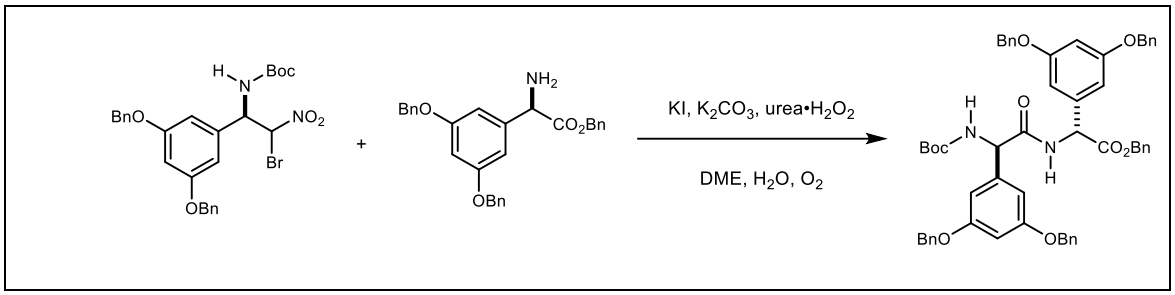

Benzyl (*R*)-2-(3,5-bis(benzyloxy)phenyl)-2-((*R*)-2-(3,5-bis(benzyloxy)phenyl)-2-((*tert*-butoxycarbonyl)amino)acetamido)acetate (2.45). To a stirred solution of the amine (14.7 mg, 32.4 μmol) and bromonitroalkane (18.0 mg, 32.4 μmol) in DME (0.34 mL, 0.1 M) at 0 °C was added KI (10.7 mg, 64.8 μmol). After 30 min at 0 °C, K_2CO_3 (26.8 mg, 0.194 mmol) was added followed by immediate dropwise addition of a solution of urea-H_2O_2 (9.1 mg, 97.2 μmol, 3.0 M in water). The reaction mixture was placed under O_2 atmosphere, maintained at 0 °C for 2 h, then brought to room temperature until judged complete by TLC (ca. 18 h). The reaction was quenched at 0 °C with satd aq sodium thiosulfate. The aqueous layer was extracted with EtOAc. The combined organic extracts were washed with satd aq sodium thiosulfate, satd aq $NaHCO_3$, 1 N aq HCl, and brine. The organic layer was dried and concentrated, and the residue was purified by flash column chromatography (20% ethyl acetate in hexanes) to afford the product (14.2 mg, 49%) as a yellow foam. R_f 0.23 (3:1 hexanes:EtOAc); $[\alpha]_D^{23}$ -33.3 (*c* 1.12, $CHCl_3$); IR (neat) 3350, 3064, 3033, 2924, 2853, 1726, 2683, 1653, 1607, 1597, 1556, 1518, 1498, 1447 cm^{-1}, ^1H NMR (600 MHz, $CDCl_3$) δ 7.34-7.22 (m, 25H), 7.09 (m, 2H), 6.73 (d, *J* = 7.2 Hz, 2H), 6.56 (s, 2H), 6.47 (m, 4H), 5.41 (d, *J* = 7.2 Hz, 1H), 5.03 (q, *J* = 11.7 Hz, 2H), 4.90 (s, 4H), 4.83 (s, 4H), 1.34 (s, 9H); ^{13}C NMR (150 MHz, $CDCl_3$) δ 169.7, 169.2, 160.4, 160.3, 160.2, 155.1, 140.1, 138.2, 136.6, 136.5, 134.9, 128.7, 128.6, 128.5, 128.5, 128.4, 128.3, 128.1, 128.0, 127.6, 127.6, 106.3, 102.3, 80.2, 70.2, 70.1, 67.5, 58.7, 56.8, 28.3; HRMS (ESI) calcd for $C_{56}H_{55}N_2O_9$ $[M+H]^+$ 899.3902, found 899.3890.

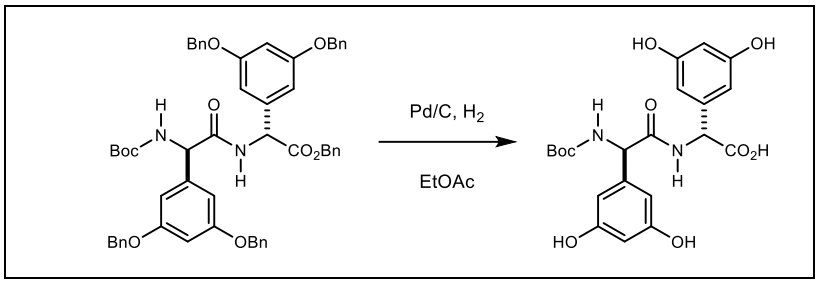

(*R*)-2-((*R*)-2-((*tert*-butoxycarbonyl)amino)-2-(3,5-dihydroxyphenyl)acetamido)-2-(3,5-dihydroxyphenyl)acetic acid (2.46).[303] A solution of dipeptide (27 mg, 30 µmol) in MeOH (0.3 mL) was purged with argon, Pd/C (10% w/w, ca. 0.5 mg), and the reaction purged again with argon. The reaction mixture was placed under H_2 atmosphere until judged complete (ca. 2 h). The reaction was purged with argon, filtered through a pad of celite, and concentrated to give the product (12 mg), which was used directly without further purification. ^{1}H NMR (400 MHz, acetone-d_6) δ 7.76 (br d, *J* = 6.8 Hz, 1H), 6.37 (br s, 2 H), 6.33 (br s, 2H), 6.15 (br m, 2H), 5.19 (d, *J* = 7.1 Hz, 1H), 5.13 (d *J* = 7.2 Hz, 1H), 1.25 (s, 9H); HRMS (ESI): Exact mass calcd for $C_{21}H_{25}N_2O_9$ $(M+H)^+$ 449.1555, found 449.1547.

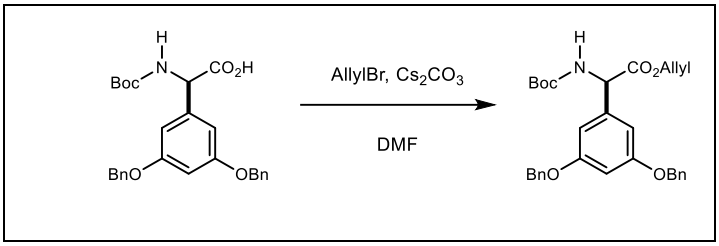

Allyl (*R*)-2-(3,5-bis(benzyloxy)phenyl)-2-((*tert*-butoxycarbonyl)amino)acetate (2.47). To a solution of the carboxylic acid (80 mg, 0.17 mmol) in DMF (0.34 mL, 0.50 M) was added cesium carbonate (91 mg, 0.26 mmol) and allyl bromide (16 µL, 0.19 mmol). The reaction mixture was quenched at 0 °C with 1 N HCl when judged complete by TLC (ca. 21 h), and the resulting solution was diluted with EtOAc. The aqeuous layers were extracted with EtOAc. The combined organic extracts were washed with satd aq $NaHCO_3$, water, and brine, and then dried and concentrated. Column chromatography (10% ethyl acetate in hexanes) of the residue yielded the ester (50 mg, 58%) as a colorless oil. R_f 0.7 (2:1 hexanes:EtOAc); $[\alpha]_D^{23}$ -54.8 (*c* 0.94, $CHCl_3$); IR (neat) 3377, 3064, 3032, 2977, 2931, 2873, 1742, 1713, 1648 cm^{-1}; ^{1}H NMR (400 MHz, $CDCl_3$) δ 7.35-7.23 (m, 10H), 6.55 (m, 2H), 6.48 (m, 1H), 5.74 (m, 1H), 5.45 (d, *J* = 6.6 Hz, 1H), 5.20 (d, *J* = 7.9 Hz, 1H), 5.15-5.09 (m , 2H), 4.93 (s, 4H), 4.52 (dddd, 2H), 1.36 (s, 9H); ^{13}C NMR (100 MHz, $CDCl_3$) ppm 170.5, 160.2, 154.7, 138.9, 136.6, 131.3, 128.5, 127.9, 127.5,

118.5, 106.3, 102.0, 80.1, 70.1, 66.1, 57.6, 28.3; HRMS (ESI): Exact mass calcd for $C_{30}H_{33}NNaO_6$ $[M+Na]^+$ 526.2200, measured 526.2200.

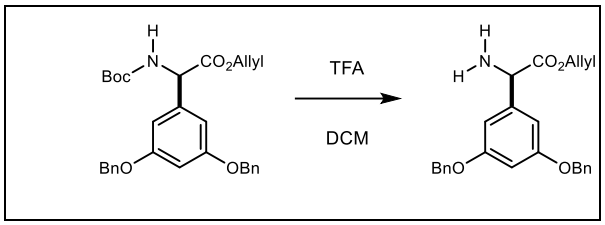

Allyl (*R*)-2-amino-2-(3,5-bis(benzyloxy)phenyl)acetate (2.48). To a solution of the carbamate (50 mg, 99.2 μmol) in DCM (0.9 mL, 0.1 M) was added trifluoroacetic acid (90 μL) dropwise. Upon consumption of starting material as judged complete by TLC (ca. 1.5 h), the reaction was concentrated to afford a crude white foam (40 mg), which was used directly without further purification. R_f 0.20 (95:5 DCM:MeOH); $[\alpha]_D^{23}$ -39.2 (*c* 1.00, $CHCl_3$); IR (neat) 3033, 2923, 1746, 1680, 1599, 1520, 1498, 1453 cm^{-1}; ^1H NMR (400 MHz, acetone-d_6) δ 7.35-7.19 (m, 10H), 6.83 (m, 2H), 6.59 (s, 1H), 5.71 (m, 1H), 5.22-5.02 (br m, 3H), 4.97 (s, 4H), 4.53 (dddd, 2H); ^{13}C NMR (100 MHz, acetone-d_6) δ 167.8, 160.4, 136.9, 134.3, 131.7, 128.3, 127.8, 127.6, 117.9, 107.3, 103.1, 69.8, 66.4, 56.3; HRMS (ESI): Exact mass calcd for $C_{25}H_{26}NO_4$ $[M+H]^+$ 404.1856, found 404.1859.

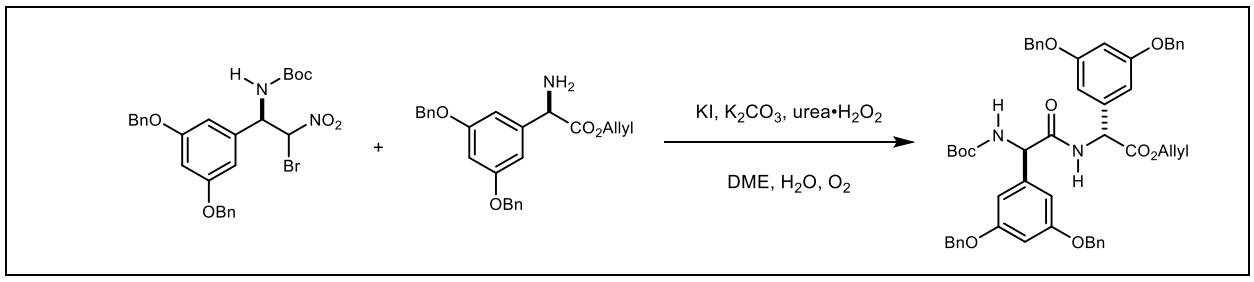

Allyl (*R*)-2-(3,5-bis(benzyloxy)phenyl)-2-((*R*)-2-(3,5-bis(benzyloxy)phenyl)-2-((*tert*-butoxycarbonyl)amino)acetamido)acetate (2.49). To a stirred solution of the amine (40 mg, 99 μmol) and the bromonitroalkane (55.3 mg, 99.2 μmol) in DME (1 mL, 0.1 M) at 0 °C, was added KI (32 mg, 0.19 mmol). After 30 min at 0 °C, K_2CO_3 (82.2 mg, 0.595 mmol) was added followed by dropwise addition of a solution of urea-H_2O_2 (27.9 mg, 0.297 mmol, 3.0 M solution in water) over 30 min and the reaction mixture was placed under O_2 atmosphere. Upon consumption of starting material as indicated by TLC (ca. 16 h), the reaction mixture was

quenched at 0 °C with satd aq sodium thiosulfate, and then diluted with EtOAc. The aqueous layer was extracted with EtOAc and the combined organic extracts were washed with satd aq sodium thiosulfate, satd aq $NaHCO_3$, 1 N aq HCl, and brine, and then dried and concentrated. Column chromatography (20% ethyl acetate in hexanes) yielded the product (50 mg, 60%) as a yellow wax. R_f 0.55 (2:1 hexanes:EtOAc); $[\alpha]_D^{23}$ -41 (*c* 0.92, $CHCl_3$); IR (neat) 3353, 3064, 3033, 2922, 2853, 2366, 2344, 1793, 1773, 1654, 1597, 1543, 1518, 1498, 1449 cm^{-1}; ^1H NMR (600 MHz, $CDCl_3$) δ 7.36-7.22 (m, 20H), 6.80 (d, *J* = 6.6 Hz, 1H), 6.57 (s, 2H), 6.52 (m, 2H), 6.46 (m, 2H), 5.68 (m, 1H), 5.38 (d, *J* = 6.6 Hz, 1H), 5.10-5.04 (m, 2H), 4.89 (s, 4H), 4.88 (s, 4H), 4.47 (dddd, 2H) 1.33 (s, 9H); ^{13}C NMR (150 MHz, $CDCl_3$) δ 169.6, 169.3, 160.7, 160.4, 160.3, 160.2, 155.2, 140.1, 138.3, 136.7, 136.5, 131.2, 128.6, 128.5, 128.1, 128.0, 127.6, 127.6, 118.8, 106.4, 106.3, 102.2, 80.2, 70.1, 66.4, 58.6, 56.8, 28.3; HRMS (ESI): Exact mass calcd for $C_{52}H_{52}N_2O_9Na(M+Na)^+$ 871.3565, found 871.3566.

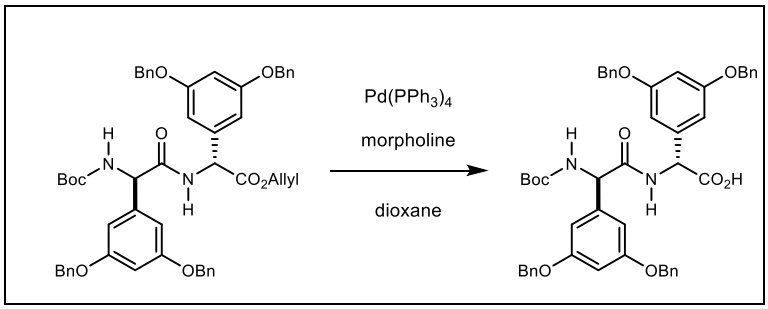

(*R*)-2-(3,5-bis(benzyloxy)phenyl)-2-((*R*)-2-(3,5-bis(benzyloxy)phenyl)-2-((*tert*-butoxycarbonyl)amino)acetamido)acetic acid (2.41). To a solution of allyl ester (56.0 mg, 65.9 μmol) in dioxane (0.70 mL) was added $Pd(PPh_3)_4$ (7.6 mg, 6.59 μmol) followed by morpholine (56 μL, 659 μmol). Upon consumption of starting material as indicated by ^1H NMR, the reaction mixture was acidified with 1 N HCl then extracted with EtOAc. The combined organic extracts were washed with brine, dried, and concentrated. Column chromatography (5% MeOH in DCM) afforded the desired carboxylic acid (27 mg, 51%). $[\alpha]_D^{23}$ -33 (*c* 0.33, $CHCl_3$); IR (neat) 3355, 3032, 2924, 2854, 1714, 1696, 1683, 1652, 1597, 1556, 1539, 1518, 1506, 1497 cm^{-1}; ^1H NMR (600 MHz, DMSO-d_6) δ 8.69 (br s, 1H), 7.42-7.31 (m, 20H), 6.78 (br s, 2 H), 6.73 (br s, 1H) 6.59 (br s, 1H), 6.56 (br s, 1H), 5.29 (br d, J = Hz, 1H), 5.19 (br s, 1H), 5.07 (br m, 8 H), 1.39 (s, 9H); ^{13}C NMR (150 MHz, DMSO-d_6) δ 169.8, 159.9, 159.8, 141.4, 137.4, 137.3,

128.9, 128.3, 128.2, 107.0, 106.9, 101.3, 78.9, 69.8, 69.8, 28.6; HRMS (ESI): Exact mass calcd for $C_{49}H_{49}N_2O_9Na(M+NH)^+$ 809.3431, found 809.3433.

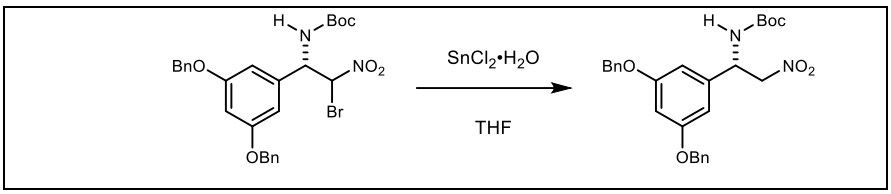

***tert*-Butyl (*S*)-(1-(3,5-bis(benzyloxy)phenyl)-2-nitroethyl)carbamate (2.50**). To a stirred solution of the bromonitroalkane (400 mg, 0.719 mmol) in THF (7.2 mL, 0.1 M) was added $SnCl_2 \cdot H_2O$ (323 mg, 1.44 mmol). When judged complete by TLC (ca. 1.5 h), the reaction mixture was diluted with water and extracted with Et_2O. The combined organic extracts were filtered through a plug of Celite, and the filtrate was dried and concentrated. Column chromatography (15% ethyl acetate in hexanes) yielded the product (243 mg, 68%) as a white powder. R_f 0.42 (3:1 hexanes:EtOAc); $[\alpha]_D^{23}$ +23.4 (*c* 1.09, $CHCl_3$); IR (neat) 3032, 2977, 2929, 1698, 1596 cm^{-1}; ^1H NMR (400 MHz, $CDCl_3$) δ 7.36-7.25 (m, 10H), 6.49 (m, 1H), 6.46 (m, 2H), 5.23 (br m, 1H), 5.14 (br m, 1H), 4.94 (s, 4H), 4.76 (br m, 1H), 4.58 (dd, *J* = 12.5, 5.4 Hz, 1H), 1.37 (s, 9H); ^{13}C NMR (100 MHz, $CDCl_3$) δ 160.4, 154.8, 139.4, 136.4, 128.6, 128.1, 127.6, 105.7, 101.7, 80.6, 78.7, 70.2, 52.8, 28.2; HRMS (ESI): Exact mass calcd for $C_{27}H_{31}N_2O_6$ $[M+H]^+$ 479.2177, found 479.2167.

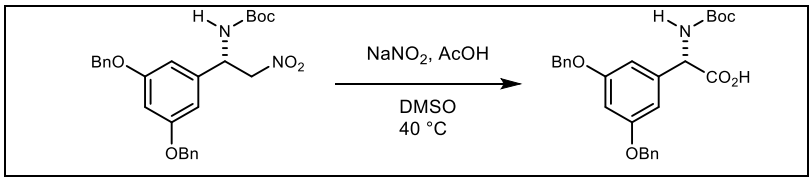

(*S*)-2-(3,5-bis(benzyloxy)phenyl)-2-((*tert*-butoxycarbonyl)amino)acetic acid (2.51). To a stirred solution of the nitroalkane (100 mg, 209 µmol) and sodium nitrite (43 mg, 627 µmol) in DMSO (1.6 mL, 0.13 M) was added AcOH (180 µL, 3.13 mmol) dropwise. The reaction mixture was heated to 40 °C for 18 h, allowed to cool to room temperature, and diluted with 1 N HCl. The aqueous layer was extracted with DCM, and the combined organic extracts were washed with ice water, dried, and concentrated to give a crude yellow oil. Column chromatography (3% MeOH in DCM to 20% MeOH in DCM) afforded the carboxylic acid (63 mg, 66%) as a white foam. R_f 0.34 (90:10 DCM:MeOH); $[\alpha]_D^{23}$ +47 (*c* 0.78, MeOH); IR (neat) 3066, 3033, 2926,

2854, 1718, 1707, 1686, 1686, 1662, 1655, 1638, 1597, 1458 cm^{-1}; ^1H NMR (400 MHz, MeOD) δ 7.28-7.14 (m, 10H), 6.61 (s, 2H), 6.41 (s, 1H), 4.98 (br s, 1H), 4.86 (s, 4H), 1.32 (s, 9H); ^{13}C NMR (100 MHz, MeOD) δ174.1, 159.9, 155.9, 140.6, 137.1, 128.0, 127.4, 127.2, 106.3, 101.1, 79.3, 69.3, 58.7, 38.9, 27.3; HRMS (ESI): Exact mass calcd for $C_{27}H_{30}NO_6$ $[M+H]^+$ 464.2068, found 464.2060.

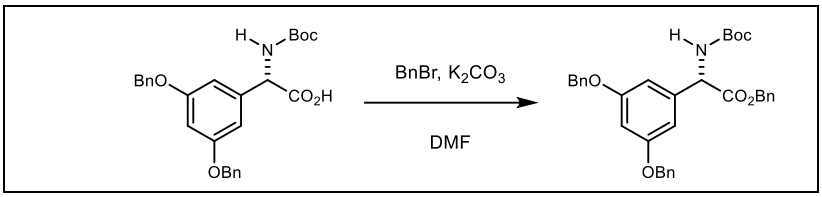

Benzyl (*S*)-2-(3,5-bis(benzyloxy)phenyl)-2-((*tert*-butoxycarbonyl)amino)acetate (2.52). To a stirred solution of carboxylic acid (50 mg, 110 µmol) in DMF (0.22 mL, 0.50 M) was added K_2CO_3 (22.4 mg, 162 µmol) followed by benzyl bromide (13 µL, 110 µmol). The reaction mixture was quenched at 0 °C with 1 N HCl when judged complete by TLC (ca. 20 h), and the resulting solution was diluted with EtOAc. The aqueous layers were extracted with EtOAc. The combined organic extracts were washed with satd aq $NaHCO_3$, water, and brine, and then dried and concentrated. Column chromatography (10% ethyl acetate in hexanes) of the residue yielded the ester (35 mg, 59%) as a colorless oil. R_f 0.47 (3:1 hexanes:EtOAc); $[\alpha]_D^{23}$ +41.3 (*c*= 0.40, $CHCl_3$); IR (neat) 3032, 2926, 1741, 1713, 1596, 1454 cm^{-1}; ^1H NMR (400 MHz, $CDCl_3$) δ 7.31-7.13 (m, 15H), 6.51 (s, 2H), 6.48 (s 1H), 5.45 (br d, *J* = 7.2 Hz, 1H), 5.23 (br d, *J* = 7.6 Hz, 1H), 5.07 (s, 2H), 4.87 (s, 4H), 1.35 (s, 9H); ^{13}C NMR (100 MHz, $CDCl_3$) δ 170.7, 160.2, 154.7, 138.9, 136.6, 135.2, 128.5, 128.4, 128.3, 127.9, 127.5, 106.2, 102.1, 80.1, 70.0, 67.2, 57.6, 28.3; HRMS (ESI): Exact mass calcd for $C_{34}H_{35}NO_6Na$ [M+Na]+576.2357, obsd 576.2356.

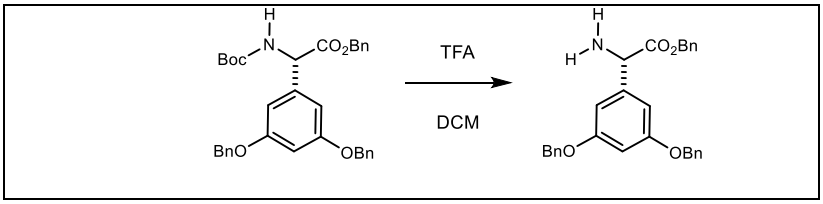

Benzyl (*S*)-2-amino-2-(3,5-bis(benzyloxy)phenyl)acetate (2.53). To a solution of ester **2.52** (26.4 mg, 47.7 µmol) in DCM (0.5 mL, 0.1 M) was added trifluoroacetic acid (47 µL) dropwise. Upon completion as judged by TLC (ca. 2 h), the reaction mixture was concentrated to give a crude white foam (20 mg), which was used directly without further purification. R_f 0.48 (95:5

DCM:MeOH); $[\alpha]_D^{23}$ +30.5 (*c*=0.84, $CHCl_3$); IR (neat) 3033, 2922, 1746, 1680, 1598, 1540, 1498 cm^{-1}; ^1H NMR (400 MHz, acetone-d_6) δ 7.46-7.32 (m, 16H), 6.96 (s, 1H), 6.92 (s, 1H), 6.75 (s, 1H), 5.46 (br s, 1H), 5.26 (ABq, *J* = 12.6 Hz, 2H), 5.09 (m, 4H); ^{13}C NMR (100 MHz, acetone-d_6) δ 167.9, 160.4, 136.9, 135.2, 134.1, 128.4, 128.2, 128.1, 127.8, 127.6, 107.3, 103.7, 69.8, 67.6, 56.4; HRMS (ESI): Exact mass calcd for $C_{29}H_{28}NO_4$ $[M+H]^+$ 454.2013, found 454.2014.

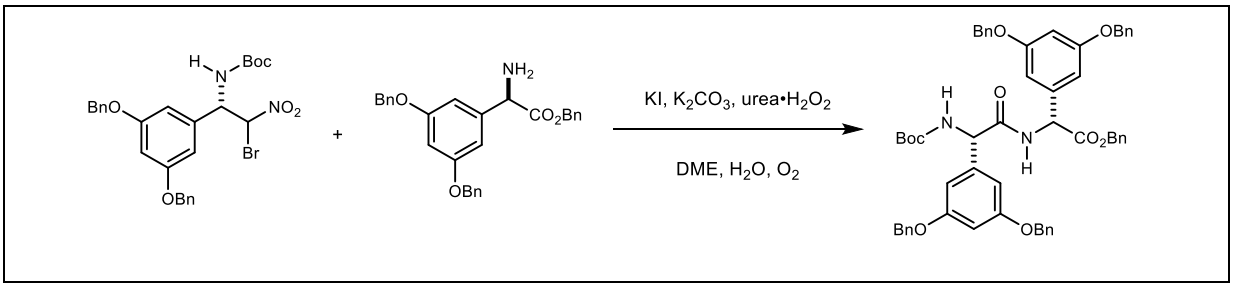

Benzyl (*R*)-2-(3,5-bis(benzyloxy)phenyl)-2-((*S*)-2-(3,5-bis(benzyloxy)phenyl)-2-((*tert*-butoxycarbonyl)amino)acetamido)acetate (2.55). To a stirred solution of the amine (31 mg, 68 µmol) and the bromonitroalkane (38 mg, 68 µmol) in DME (0.70 mL, 0.10 M) at 0 °C, was added KI (23 mg, 0.14 mmol). After 30 min at 0 °C, K_2CO_3 (57 mg, 0.41 mmol) was added followed by immediate dropwise addition of a solution of urea-H_2O_2 (19.3 mg, 205 µmol, 3.0 M in water) and the reaction mixture was placed under O_2 atmosphere. Upon consumption of starting material as indicated by TLC (ca. 16 h), the reaction mixture was quenched at 0 °C with satd aq sodium thiosulfate, and then diluted with EtOAc. The aqueous layer was extracted with EtOAc and the combined organic extracts were washed with satd aq sodium thiosulfate, satd aq $NaHCO_3$, 1 N aq HCl, and brine, and then dried and concentrated. Column chromatography (20% ethyl acetate in hexanes) yielded the product (28 mg, 46%) as a yellow wax. R_f 0.48 (2:1 hexanes:EtOAc); $[\alpha]_D^{23}$ + 12.0 (*c* 0.22, $CHCl_3$); IR (neat) 3033, 2922, 2851, 1744, 1671, 1597, 1497, 1453 cm^{-1}; ^1H NMR (600 MHz, $CDCl_3$) δ 7.28-7.19 (m, 23 H), 7.12 (m, 2H), 6.71 (br m, 1H), 6.52 (m, 2H), 6.39 (m, 2H), 6.31 (m, 2H), 5.62 (br s, 1H), 5.48 (d, *J* = 7.2 Hz, 1H), 5.11 (br, s, 1H), 5.07 (q, *J* = 12.4 Hz, 2H), 4.78 (q, *J* = 11.5 Hz, 4H), 4.69 (ABq, *J* = 4.7 Hz, 4H), 1.34 (s, 9H); ^{13}C NMR (150 MHz, $CDCl_3$) δ 169.9, 169.0, 160.5, 160.3, 160.2, 155.1, 140.2, 137.9, 136.5, 134.9, 128.6, 128.5, 128.4, 128.1, 128.0, 128.0, 127.7, 127.6, 106.2, 105.7, 102.4, 102.3, 80.2, 70.1, 69.9, 67.7, 58.6, 56.5, 28.3; HRMS (ESI): Exact mass calcd for $C_{58}H_{57}N_2O_{11}$ $(M+OAc)^+$ 957.3968, obsd 957.3950.

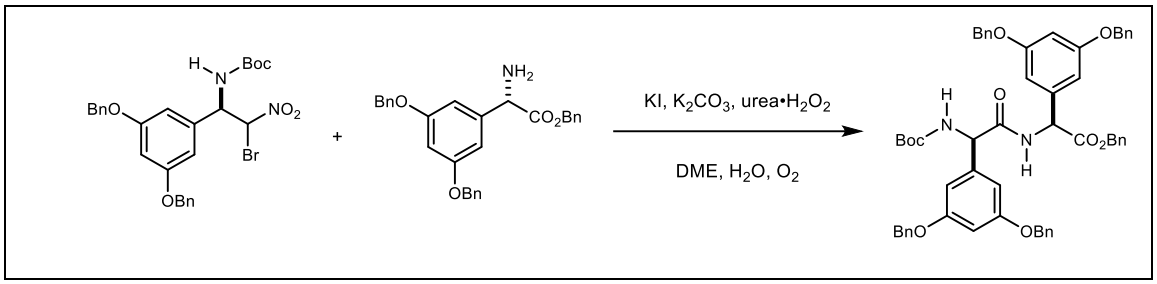

Benzyl (*S*)-2-(3,5-bis(benzyloxy)phenyl)-2-((*R*)-2-(3,5-bis(benzyloxy)phenyl)-2-((*tert*-butoxycarbonyl)amino)acetamido)acetate (2.56). To a stirred solution of the amine (20 mg, 44 μmol) and the bromonitroalkane (25 mg, 44 μmol) in DME (0.44 mL, 0.10 M) at 0 °C, was added KI (15 mg, 88 μmol). After 30 min at 0 °C, K_2CO_3 (36 mg, 0.26 mmol) was added followed by immediate dropwise addition of a solution of urea-H_2O_2 (12.4 mg, 132 μmol, 3.0 M solution in water) and the reaction mixture was placed under O_2 atmosphere. Upon consumption of starting material as indicated by TLC (ca. 16 h), the reaction mixture was quenched at 0 °C with satd aq sodium thiosulfate, and then diluted with EtOAc. The aqueous layer was extracted with EtOAc and the combined organic extracts were washed with satd aq sodium thiosulfate, satd aq $NaHCO_3$, 1 N aq HCl, and brine, and then dried and concentrated. Column chromatography (20% ethyl acetate in hexanes) yielded the product (21 mg, 54%) as a yellow wax. ^{1}H NMR (600 MHz, $CDCl_3$) δ 7.29-7.19 (m, 23H), 7.13 (m, 2H), 6.72 (br d, *J* = 6.5 Hz, 1H), 6.52 (m, 2H), 6.39 (m, 2H), 6.31 (m, 2H), 5.63 (br s, 1H), 5.48 (d, *J* = 7.0 Hz, 1H), 5.11 (br s, 1H), 5.06 (q, *J* = 12.5 Hz, 2H), 4.78 (q, *J* = 11.3 Hz, 4H), 4.69 (ABq, *J* = 11.2 Hz, 4H), 1.33 (s, 9H); ^{13}C NMR (150 MHz, $CDCl_3$) δ 169.9, 169.0, 160.5, 160.2, 155.1, 140.2, 147.9, 136.5, 134.9, 128.6, 128.5, 128.4, 128.1, 128.0, 128.0, 127.7, 127.6, 106.2, 105.8, 102.4, 102.3, 802, 70.1, 69.9, 67.7, 58.6, 56.5, 28.3; HRMS (ESI): Exact mass calcd for $C_{58}H_{57}N_2O_{11}$ $(M+OAc)^+$ 957.3968, obsd 957.3950.

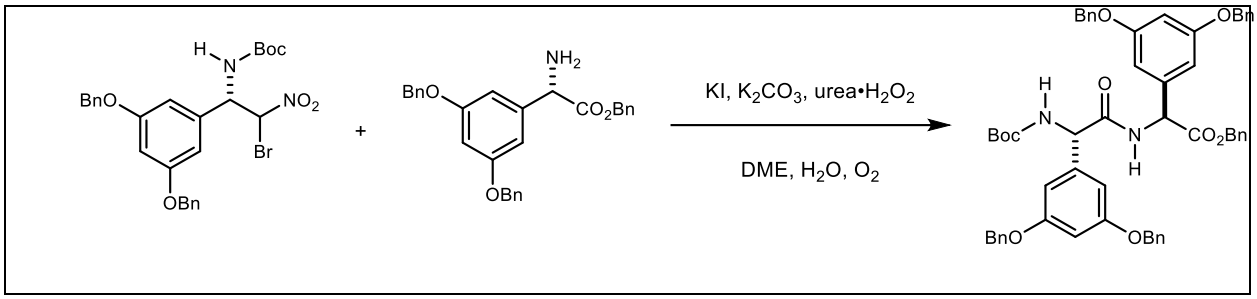

Benzyl (*S*)-2-(3,5-bis(benzyloxy)phenyl)-2-((*S*)-2-(3,5-bis(benzyloxy)phenyl)-2-((*tert*-butoxycarbonyl)amino)acetamido)acetate (2.57). To a stirred solution of the amine (20 mg, 44 µmol) and the bromonitroalkane (24.5 mg, 44 µmol) in DME (0.44 mL, 0.10 M) at 0 °C, was added KI (14.6 mg, 87.9 µmol). After 30 min at 0 °C, K_2CO_3 (36 mg, 264 µmol) was added followed by immediate dropwise addition of a solution of urea-H_2O_2 (12.4 mg, 132 µmol, 3.0 M in water) and the reaction mixture was placed under O_2 atmosphere. Upon consumption of starting material as indicated by TLC (ca. 16 h), the reaction mixture was quenched at 0 °C with satd aq sodium thiosulfate, and then diluted with EtOAc. The aqueous layer was extracted with EtOAc and the combined organic extracts were washed with satd aq sodium thiosulfate, satd aq $NaHCO_3$, 1 N aq HCl, and brine, and then dried and concentrated. Column chromatography (20% ethyl acetate in hexanes) yielded the product (16 mg, 42%) as a yellow wax. R_f 0.47 (2:1 hexanes:EtOAc); $[\alpha]_D^{23}$ +49.9 (*c* 1.10, $CHCl_3$); IR (neat) 3350, 2922, 2851, 1726, 1683, 1653 cm^{-1}; ^1H NMR (600 MHz, $CDCl_3$) δ 7.32-7.08 (m, 25H), 6.76 (d, *J* = 6.8 Hz, 1H), 6.57 (s, 2H), 6.47 (m, 4H), 5.59 (br s, 1H), 5.41 (d, *J* = 6.9 Hz, 1H), 5.02 (m, 3H), 4.89 (s, 4H), 4.83 (s, 4H), 1.34 (s, 9H); ^{13}C NMR (150 MHz, $CDCl_3$) δ 169.8, 169.3, 160.4, 160.3, 155.1, 140.1, 138.1, 136.6, 136.5, 134.9, 128.7, 128.63, 128.58, 128.52, 128.4, 128.3, 128.07, 128.04, 128.03, 127.7, 127.6, 106.3, 102.3, 80.3, 70.2, 70.1, 67.5, 58.7, 56.8, 28.3; HRMS (ESI): Exact mass calcd for $C_{58}H_{57}N_2O_{11}$ $[M+OAc]^+$ 957.3968, found 957.3961.

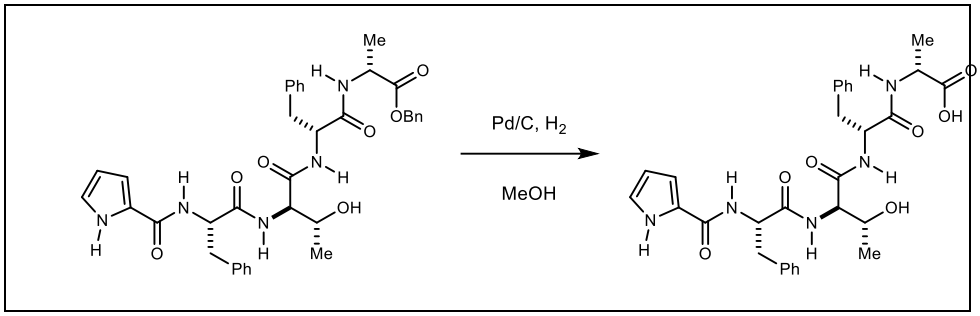

(1*H*-Pyrrole-2-carbonyl)-L-phenylalanyl-D-allothreonyl-D-phenylalanyl-D-alanine (2.59). After a solution of benzyl ester (91 mg, 0.14 mmol) in MeOH (1.4 mL) was purged with argon for 15 min, 10% Pd/C (ca. 5 mg) was added and the mixture was purged with argon for an additional 10 min, and then stirred under H_2 (1 atm) for 2 h. The reaction mixture was purged with argon for 5 min before its filtration through a plug of Celite (rinsed well with MeOH). The filtrate was concentrated to afford the product (73 mg, 92%) as a white foam. R_f 0.12 (9:1 DCM:MeOH); $[\alpha]_D^{23}$ +20.2 (*c* 0.25, MeOH); IR (neat) 3280, 2923, 2853, 1714, 1651, 1556, 1455 cm^{-1}; ^1H NMR (600 MHz, DMSO-d_6) δ 11.34 (br s, 1H), 8.19-8.07 (m, 4H), 7.36-7.08 (m, 13H), 6.85 (m, 2H), 6.08 (s, 1H), 4.77 (ddd, *J* = 13.4, 9.7, 4.5 Hz, 1H), 4.52 (m, 1H), 4.23 (t, *J* = 7.3 Hz, 1H), 4.12 (dq, *J* = 14.2, 7.2 Hz, 1H), 3.76 (dq, *J* = 12.9, 6.5 Hz, 1H), 3.16 (dd, *J* = 14.3, 3.7 Hz, 1H), 3.05 (dd, *J* = 13.9, 4.5 Hz, 1H), 2.88 (m, 2H), 1.25 (d, *J* = 7.3 Hz, 3H), 0.93 (d, *J* = 6.1 Hz, 3H); ^{13}C NMR (150 MHz, DMSO-d_6) δ 174.2, 172.3, 171.2, 170.5, 160.9, 138.6, 138.4, 129.6, 129.5, 128.43, 128.37, 126.5, 126.1, 121.9 111.2, 108.9, 67.8, 58.8, 54.5, 54.2, 48.1, 37.7, 37.1, 19.8, 17.3; HRMS (ESI): Exact mass calculated for $C_{30}H_{35}N_5NaO_7$ $[M+Na]^+$ 600.2429, found 600.2431.

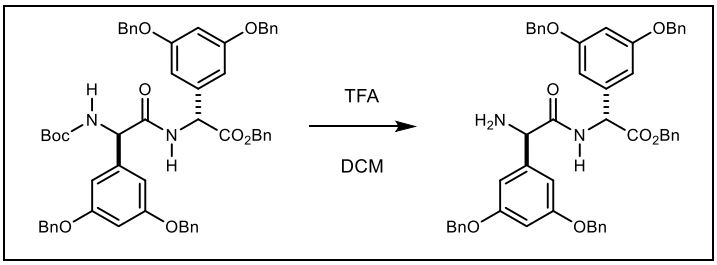

Benzyl (*R*)-2-((*R*)-2-amino-2-(3,5-bis(benzyloxy)phenyl)acetamido)-2-(3,5-bis(benzyloxy)phenyl)acetate (2.62) To a solution of the dipeptide (43 mg, 82 μmol) in DCM (0.8 mL, 0.1M) was added trifluoroacetic acid (80 μL, 0.0011 mmol). The reaction was stirred at room temperature until judged complete by TLC (ca. 3.5 h), and then concentrated to give a

white foam (34 mg), which was used directly without further purification. R_f 0.24 (95:5 DCM:MeOH); $[\alpha]_D^{23}$ -5.2 (*c* 0.65, $CHCl_3$); IR (neat) 3356, 3089, 3063, 3032, 2922, 2872, 1741, 1681, 1596, 1497, 1453, 1416 cm^{-1}; ^1H NMR (400 MHz, acetone-d_6) δ 8.47 (d, *J* = 7.3 Hz, 1H) 7.287-7.16 (m, 25 H), 6.53 (br d, *J* = 2.4 Hz, 2H), 6.51 (br d, *J* = 2.4 Hz, 2 H), 6.42 (t, *J* = 2.4 Hz, 1H), 6.36 (t, *J* = 2.4 Hz, 1H), 5.43 (d, *J* = 7.4 Hz, 1H), 5.08 (m, 2H), 4.80 (m 8H); HRMS (ESI): Exact mass calcd for $C_{44}H_{47}N_2O_7$ $[M+H]^+$ 799.3378, found 799.3378.

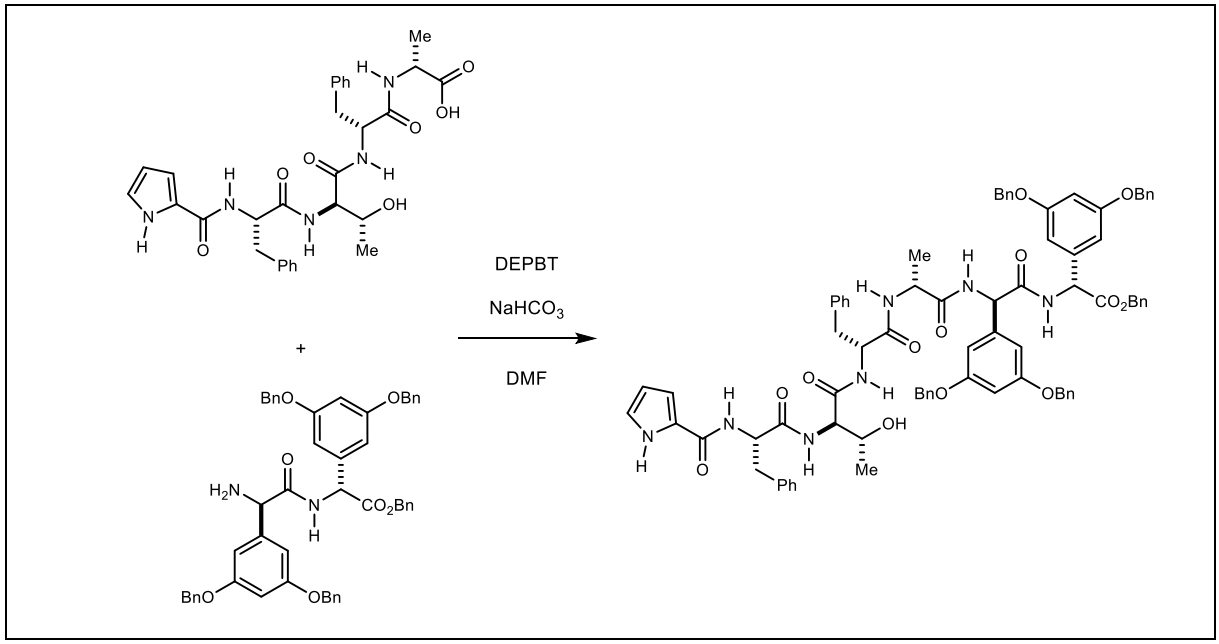

Benzyl (*3S,6R,9R,12R,15R,18R*)-3,9-dibenzyl-15,18-bis(3,5-bis(benzyloxy)phenyl)-6-((*R*)-1-hydroxyethyl)-12-methyl-1,4,7,10,13,16-hexaoxo-1-(1*H*-pyrrol-2-yl)-2,5,8,11,14,17-hexaazanonadecan-19-oate (2.61).[304] To a solution of carboxylic acid (35.3 mg, 61.1 μmol) in DMF (0.6 mL) at 0 °C was added DEPBT (36.6 mg, 122 μmol) and $NaHCO_3$ (5.1 mg, 61.1 μmol). After 2 h at 0 °C, amine (57.1 mg, 71.4 μmol) in DMF (0.6 mL) was added, followed by $NaHCO_3$ (10.3 mg, 122 μmol). The reaction mixture was maintained at 0 °C for 2 h, brought to room temperature, and maintained for 20 h. The reaction was poured over ice-water and extracted with EtOAc. The combined organic extracts were washed with satd aq $NaHCO_3$, 1 N aq HCl, and brine, and then dried and concentrated. Reversed phase HPLC (gradient: 90% MeCN-H_2O with 0.1% TFA) yielded the heptapeptide (19.8 mg) as a foam.; ^1H NMR (600 MHz, DMSO-d_6) δ 11.31 (br s, 1H), 9.14 (d, *J* = 6.9 Hz, 1H), 8.40 (d. *J* = 8.3 Hz, 1H) 8.13-8.02 (m, 4H), 7.39-7.09 (m, 35H), 6.82 (m, 4 H), 6.68 (m, 2H), 6.65 (m, 1H), 6.58 (m, 1H), 6.04 (m, 1H), 5.62 (d, *J* = 8.2 Hz, 1H), 5.44 (d, *J* = 7.0 Hz, 1H), 5.10-4.96 (m, 13H), 4.73 (m, 1H) 4.47 (m, 1H), 4.38 (t,

J = 7.0 Hz, 1H), 4.19 (t, *J* = 7.6 Hz, 1H), 3.7 (m, 1H), 3.06 (dd, *J* = 13.9, 3.7 Hz, 1H), 2.99 (dd, *J* = 14.7, 4.9 Hz, 1H), 2.86 (dd, *J*= 13.6, 10.3 Hz, 1H), 2.79 (dd, *J* = 14.3, 10.0 Hz, 1H), 1.18 (d, *J* = 7.1 Hz, 3H), 0.88 (d, *J* = 6.2 Hz, 3H) ; ^{13}C NMR (150 MHz, DMSO-d_6) δ 172.3, 172.2, 171.2, 170.7, 160.9, 160.1, 159.9, 140.9, 138.7, 138.4, 138.2, 137.4, 137.2, 136.1, 129.7, 129.5, 128.9, 128.9, 128.7, 128.5, 128.4, 128.4, 128.3, 128.2, 128.2, 127.9, 126.6, 126.6, 126.2, 122.0, 111.2, 109.0, 107.6, 106.7, 101.9, 101.3, 69.9, 66.7, 58.8, 56.9, 55.8, 54.5, 54.5, 48.7, 37.9, 37.1, 20,0, 18.3; HRMS (ESI) calcd for $C_{81}H_{79}N_7O_{13}Na$ $[M+Na]^+$ m/z:1380.5628, obsd 1380.5627.

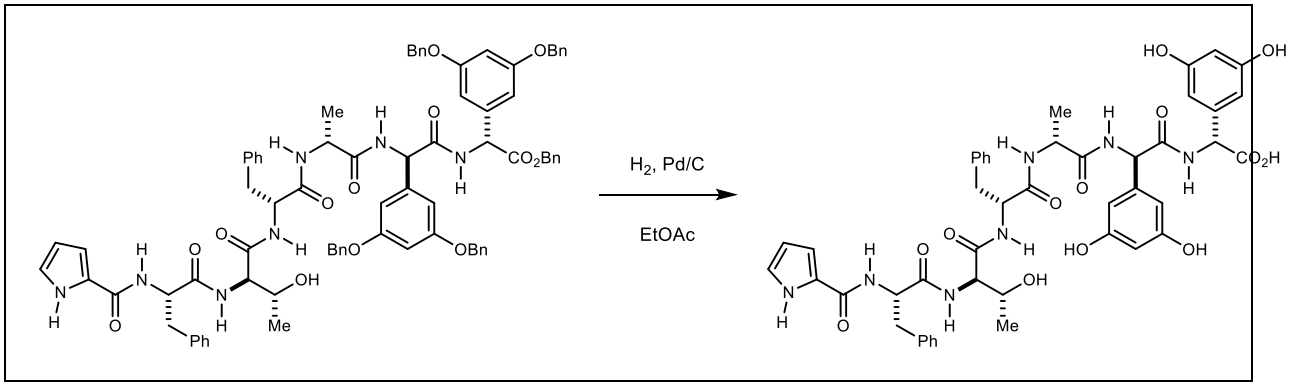

(*3S,6R,9R,12R,15R,18R*)-3,9-dibenzyl-15,18-bis(3,5-dihydroxyphenyl)-6-((*R*)-1-hydroxyethyl)-12-methyl-1,4,7,10,13,16-hexaoxo-1-(1*H*-pyrrol-2-yl)-2,5,8,11,14,17-hexaazanonadecan-19-oic acid (2.64) [305] A solution of heptapeptide (14.8 mg, 10.9 µmol) in EtOAc (10.9 mL) was purged with argon, Pd/C (10% w/w, ca. 0.5 mg), and the reaction purged again with argon. The reaction mixture was placed under H_2 atmosphere until judged complete (ca. 3 h). The reaction was purged with argon, filtered through a pad of celite, and concentrated to give the product (9.0 mg), which was used directly without further purification. ^{1}H NMR (400 MHz, DMSO-d_6) δ 11.35 (br s, 1H), 9.31 (br s, 2H), 9.20 (br s, 2H), 8.22-8.05 (m, 5H), 7.37-7.06 (m, 12H), 6.82 (m, 2H), 6.32 (m, 2H), 6.26 (m, 2H), 6.14 (m, 2H), 6.07 (m, 1H), 5.41 (d, J = 7.9 Hz, 1H) 5.05 (m, 2H), 4.75 (dq, 1H), 4.49 (dq, 1H), 4.37 (t, *J* = 7.2 Hz, 1H) 4.23 (t, *J* = 7.9 Hz, 1H), 3.74 (br m, 1H), 3.08 (dd, *J* = 14.4, 3.8 Hz, 1H), 3.04 (dd, *J* = 13.7, 4.4 Hz, 1H), 2.88 (dd, *J* = 13.3, 10.9 Hz, 1H), 2.82 (dd, *J* = 14.4, 10.3 Hz, 1H), 1.18 (d, *J* = 6.9 Hz, 3H), 0.92 (d, *J* = 6.4 Hz, 3H); ^{13}C NMR (150 MHz, DMSO-d_6) δ 172.2, 171.7, 171.1, 170.8, 169.7, 160.9, 158.8, 158.6, 140.7, 138.7, 138.4, 129.7, 129.6, 128.5, 128.4, 126.6, 126.2, 121.9, 111.2, 109.0, 106.2, 106.2, 102.2, 67.9, 58.6, 54.5, 49.1, 48.5, 37.9, 37.1, 20.0, 18.5; HRMS (ESI): Exact mass calcd for $C_{46}H_{48}N_7O_{13}$ $(M-H)^-$ 906.3316, found 906.3290.

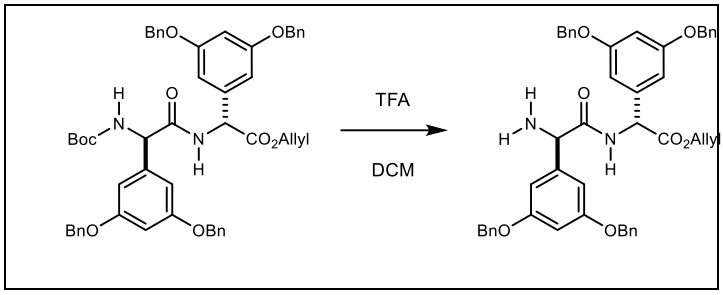

Allyl (*R*)-2-((*R*)-2-amino-2-(3,5-bis(benzyloxy)phenyl)acetamido)-2-(3,5-bis(benzyloxy)phenyl)acetate (2.68) To a solution of the dipeptide (36 mg, 42 μmol) in DCM (0.42 mL, 0.10 M) was added trifluoroacetic acid (42 μL). The reaction was stirred at room temperature until judged complete by TLC (ca. 2.5 h), and then concentrated to give a white foam (39 mg), which was used directly without further purification. R_f 0.4 (95:5 DCM:MeOH); $[\alpha]_D^{23}$ -15.2 (*c* 0.26, $CHCl_3$); IR (neat) 3031, 2919, 2850, 1740, 1683, 1595, 1557, 1540, 1497, 1455cm^{-1}; ^{1}H NMR (600 MHz, acetone-d_6) δ 8.46 (d, *J* = 7.4 Hz, 1H), 7.29-7.16 (m, 20H), 6.53 (br s, 4H), 6.44 (m, 1H), 6.36 (m, 1H), 5.77 (m, 1H), 5.39 (d, *J* = 7.6 Hz, 1H), 5.15 (m, 1H), 5.05 (m, 1H), 4.85-4.81 (m, 8H), 4.79 (br s, 1H), 4.52 (m, 2H); ^{13}C NMR (150 MHz, acetone-d_6) δ 170.3, 169.8, 160.2, 159.8, 141.9, 139.4, 137.2, 137.1, 131.9, 128.3, 128.3, 127.6, 127.5, 117.3, 106.5, 106.0, 101.6, 100.7, 69.6, 69.5, 67.6, 65.5, 55.8, 55.7; HRMS (ESI): Exact mass calcd for $C_{44}H_{45}N_2O_7$ $[M+H]^+$ 749.3221 found 749.3224.

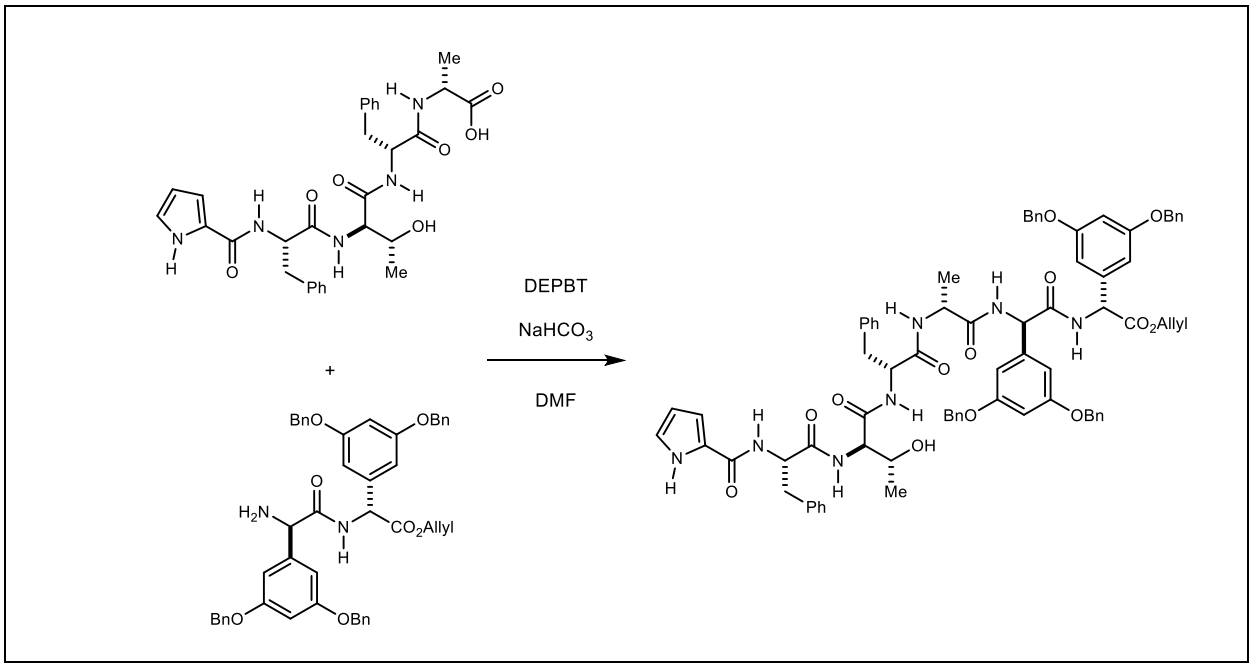

Allyl (*3S,6R,9R,12R,15R,18R*)-3,9-dibenzyl-15,18-bis(3,5-bis(benzyloxy)phenyl)-6-((*R*)-1-hydroxyethyl)-12-methyl-1,4,7,10,13,16-hexaoxo-1-(1*H*-pyrrol-2-yl)-2,5,8,11,14,17-hexaazanonadecan-19-oate (2.66). To a solution of carboxylic acid (20.2 mg, 26.9 µmol) in DMF (0.27 mL) at 0 °C was added DEPBT (16.1 mg, 53.9 µmol) and $NaHCO_3$ (2.3 mg, 26.9 µmol). After 2 h at 0 °C, amine (15.5 mg, 26.9 µmol) in DMF (0.27 mL) was added, followed by $NaHCO_3$ (4.5 mg, 53.9 µmol). The reaction mixture was maintained at 0 °C for 2 h, brought to room temperature, and maintained for 20 h. The reaction was poured over ice-water and extracted with EtOAc. The combined organic extracts were washed with satd aq $NaHCO_3$, 1 N aq HCl, and brine, and then dried and concentrated. Reversed phase HPLC (gradient: 90% MeCN-H_2O with 0.1% TFA) yielded the heptapeptide (20.7 mg) as a foam.; ^{1}H NMR (600 MHz, DMSO-d_6) δ 11.31 (br s, 1H), 9.12 (d, *J* = 7.0 Hz, 1H), 8.39 (d, *J* = 8.1 Hz, 1H), 8.13-8.02 (m, 4H), 7.41-7.29 (m, 30 H), 6.80 (m, 5H), 6.71 (m, 2H), 6.67 (m, 1H), 6.57 (m, 1H), 6.04 (m, 1H), 5.71 (m, 1H), 5.62 (d, *J* = 8.3 Hz, 1H), 5.39 (d, *J* = 7.0 Hz, 1H), 5.10-5.03 (m, 13H), 4.73 (m, 1H), 4.52-4.36 (m, 5H), 4.19 (t, *J* = 8.0 Hz, 1H), 3.72 (m, 1H), 3.07 (dd, *J* = 14.2, 3.6 Hz, 1H), 3.01 (dd, *J* = 14.5, 3.5Hz, 1H), 2.86 (dd, *J* = 13.5, 10.6 Hz, 1H), 2.79 (dd, *J* = 14.2, 10.2 Hz, 1H), 1.18 (d, *J* = 7.2 Hz, 3H), 0.89 (d, *J* = 6.0 Hz, 3H) ; ^{13}C NMR (150 MHz, DMSO-d_6) δ 172.4, 172.1, 171.1, 170.7, 169.9, 169.7, 160.8, 159.9, 159.8, 140.8, 138.6, 138.4, 138.2, 137.3, 137.1, 135.4, 132.4, 129.6, 129.5, 128.8, 128.4, 128.3, 128.3, 128.2, 128.2, 128.1, 128.1, 128.0, 126.5, 126.5, 126.1, 125.1, 121.9, 117.9, 111.4, 108.9, 107.5, 106.6, 101.9, 101.2, 69.8, 69.8, 67.7, 65.6, 65.3, 58.9, 56.8, 55.8, 54.8, 54.6, 48.7, 37.6, 36.9, 19.9, 18.2; HRMS (ESI) calcd for $C_{77}H_{77}N_7O_{13}Na$ $[M+Na]^+$ m/z:1330.5472, obsd 1330.5458.

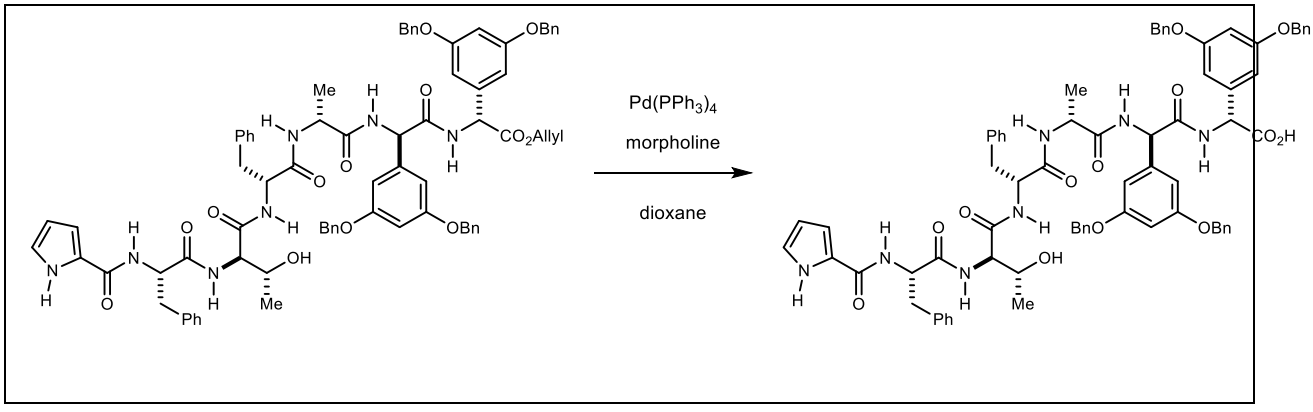

(*3S,6R,9R,12R,15R,18R*)-3,9-dibenzyl-15,18-bis(3,5-bis(benzyloxy)phenyl)-6-((*R*)-1-hydroxyethyl)-12-methyl-1,4,7,10,13,16-hexaoxo-1-(1*H*-pyrrol-2-yl)-2,5,8,11,14,17-hexaazanonadecan-19-oic acid (2.69). To a solution of allyl ester (56.0 mg, 65.9 μmol) in dioxane (0.70 mL) was added $Pd(PPh_3)_4$ (7.6 mg, 6.59 μmol) followed by morpholine (56 μL, 659 μmol). Upon consumption of starting material as indicated by ^1H NMR, the reaction mixture was acidified with 1 N HCl then extracted with EtOAc. The combined organic extracts were washed with brine, dried, and concentrated. Column chromatography (5% MeOH in DCM) afforded the desired carboxylic acid (27 mg, 51%), which was used directly. HRMS (ESI): Exact mass calcd for $C_{74}H_{74}N_7O_{13}(M+H)^+$ 1268,5339, found 1268.5355.

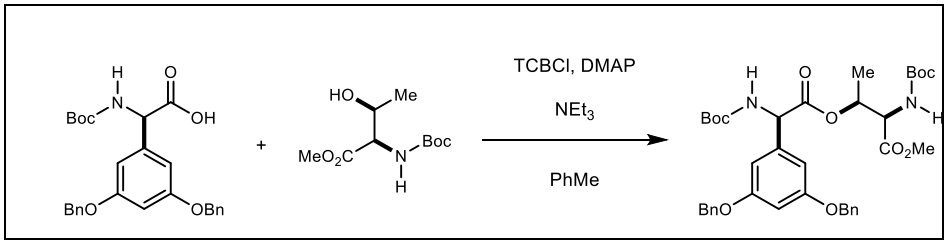

Methyl O-((*R*)-2-(3,5-bis(benzyloxy)phenyl)-2-((*tert*-butoxycarbonyl)amino)acetyl)-*N*-(*tert*-butoxycarbonyl)-D-threoninate (2.80). To a solution of carboxylic acid (20 mg, 43.1 μmol) in PhMe (0.21 mL) was added NEt_3 (18 μL, 0.13 mmol) and 2,4,6-trichlorobenzoyl chloride (8 μL, 54 μmol). Protected threonine (10.5 mg, 45.3 μmol) in PhMe (0.21 mL) was added followed by DMAP (10.5 mg, 86.2 μmol). The reaction was maintained at room temperature until judged complete by TLC (ca. 6 h). The reaction was quenched at 0 °C with satd aq $NaHCO_3$ and extracted with EtOAc. The combined organic extracts were dried and concentrated. HPLC purification yielded the desired ester (10.2 mg, 35%, 1:1 mixture of epimers).

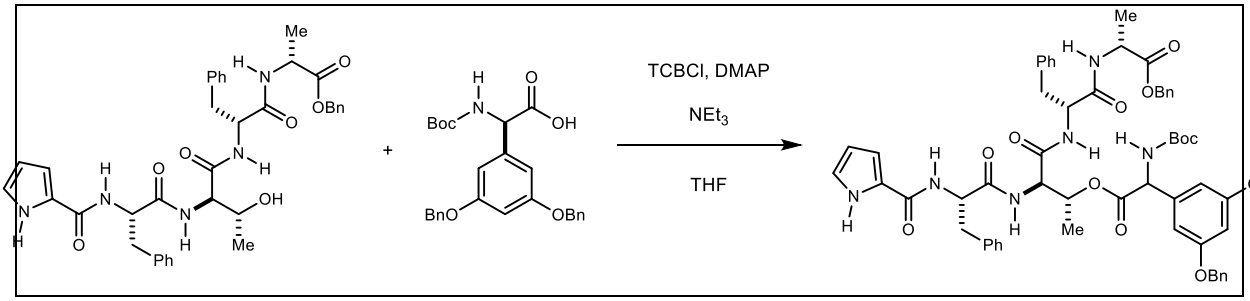

Benzyl *N*-((1*H*-pyrrole-2-carbonyl)-L-phenylalanyl)-O-(2-(3,5-bis(benzyloxy)phenyl)-2-

((*tert*-butoxycarbonyl)amino)acetyl)-D-allothreonyl-D-phenylalanyl-D-alaninate (2.84). To a solution of carboxylic acid (41.6 mg, 89.7 μmol) in THF (0.5 mL) was added 2,4,6-trichlorobenzoyl chloride (9.4 μL, 59.8 μmol) followed by NEt_3 (8.8 μL, 62.9 μmol). After 2 h, the resulting slurry was transferred via syringe filter to a stirred solution of pentapeptide (20 mg, 29.9 μmol) and DMAP (9.7 mg, 79.3 μmol) in THF (0.2 mL). After 8 h, the reaction was quenched with satd aq $NaHCO_3$ and extracted with EtOAc. The combined organic extracts were dried and concentrated. Column chromatography (3% MeOH in DCM) yielded desired ester (16 mg, 48%, 1:1 mixture of epimers) and recovered pentapeptide (10 mg).

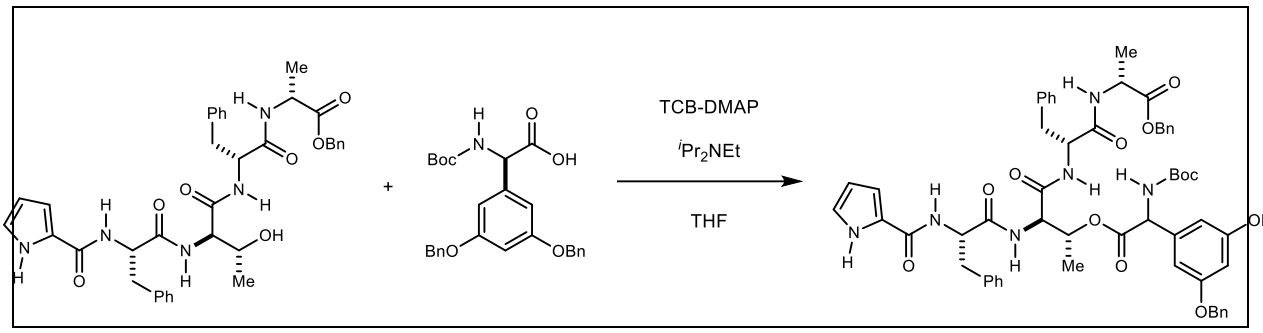

Benzyl *N*-((1*H*-pyrrole-2-carbonyl)-L-phenylalanyl)-O-(2-(3,5-bis(benzyloxy)phenyl)-2-((*tert*-butoxycarbonyl)amino)acetyl)-D-allothreonyl-D-phenylalanyl-D-alaninate (2.84). To a solution of carboxylic acid (40.9 mg, 88.4 µmol) in THF (0.88 mL, 0.10 M) at 0 °C was added TCB-DMAP[306] (42.1 mg, 115 µmol) followed by iPr_2NEt (20 µL, 115 µmol) and pentapeptide (59 mg, 88.4 µmol). The reaction was maintained at 0 °C for 2 h then brought to RT where it was maintained. After 10 h, the reaction was diluted with EtOAc and washed with 1 N HCl. The organic extract washed with water then dried and concentrated. Column chromatography (20% MeCN in DCM) afforded ester (59.2 mg, 60%, 1:1 mixture of epimers).

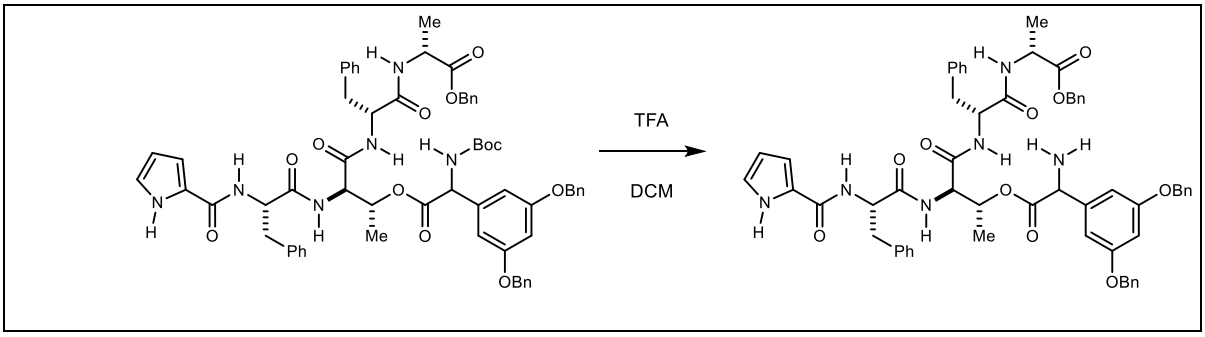

Benzyl *N*-((*1H*-pyrrole-2-carbonyl)-L-phenylalanyl)-*O*-(2-amino-2-(3,5-bis(benzyloxy)phenyl)acetyl)-D-allothreonyl-D-phenylalanyl-D-alaninate (2.89). To a solution of ester (17 mg, 15.3 µmol) in DCM (153 µL) was added TFA (15 µL). Upon consumption of starting material as judged by TLC (ca. 5 h), the reaction was concentrated then co-evaporated with diethyl ether to give amine (15 mg) as a white film. The crude amine was used directly without further purification.

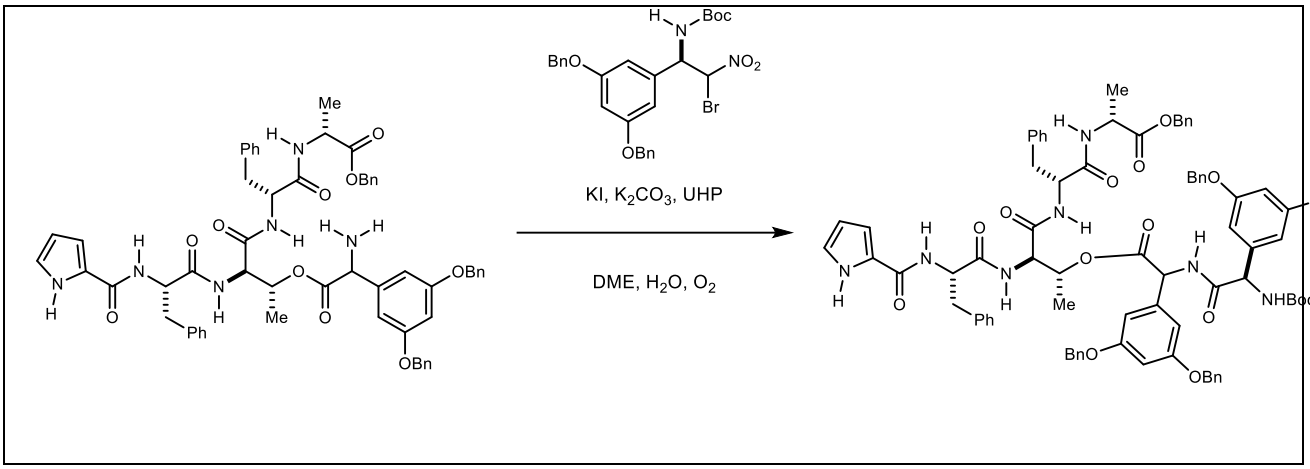

Benzyl *N*-((1*H*-pyrrole-2-carbonyl)-L-phenylalanyl)-O-(2-(3,5-bis(benzyloxy)phenyl)-2-((*R*)-2-(3,5-bis(benzyloxy)phenyl)-2-((*tert*-butoxycarbonyl)amino)acetamido)acetyl)-D-allothreonyl-D-phenylalanyl-D-alaninate (2.90). To a stirred solution of the amine (22 mg, 22 µmol) and the bromonitroalkane (12.5 mg, 44 µmol) in DME (0.44 mL, 0.10 M) at 0 °C, was added KI (14.6 mg, 87.9 µmol). After 30 min at 0 °C, K_2CO_3 (36 mg, 264 µmol) was added followed by immediate dropwise addition of a solution of urea-H_2O_2 (12.4 mg, 132 µmol, 3.0 M in water) and the reaction mixture was placed under O_2 atmosphere. Upon consumption of starting material as indicated by TLC (ca. 16 h), the reaction mixture was quenched at 0 °C with satd aq sodium thiosulfate, and then diluted with EtOAc. The aqueous layer was extracted with EtOAc and the combined organic extracts were washed with satd aq sodium thiosulfate, satd aq $NaHCO_3$, 1 N aq HCl, and brine, and then dried and concentrated. Column chromatography (20% ethyl acetate in hexanes) yielded the product (16 mg, 42%, 1:1 mixture of epimers) as a yellow wax.

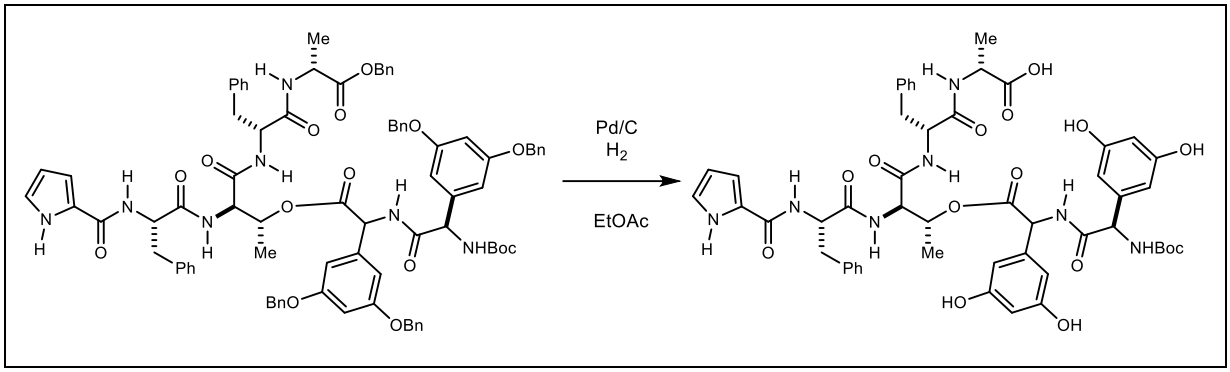

***N*-((1*H*-pyrrole-2-carbonyl)-L-phenylalanyl)-O-(2-((*R*)-2-((*tert*-butoxycarbonyl)amino)-2-(3,5-dihydroxyphenyl)acetamido)-2-(3,5-dihydroxyphenyl)acetyl)-D-allothreonyl-D-phenylalanyl-D-alanine (2.91).** After a solution of benzyl ester (9.1 mg, 6.24 μmol) in EtOAc (3.1 mL) was purged with argon for 15 min, 10% Pd/C (ca. 1 mg) was added and the mixture was purged with argon for an additional 10 min, and then stirred under H_2 (1 atm) for 10 h. The reaction mixture was purged with argon for 5 min before its filtration through a plug of Celite (rinsed well with MeOH). The filtrate was concentrated to afford the product (4.1 mg, 66%, 1:1 mixture of epimers) as a white film.

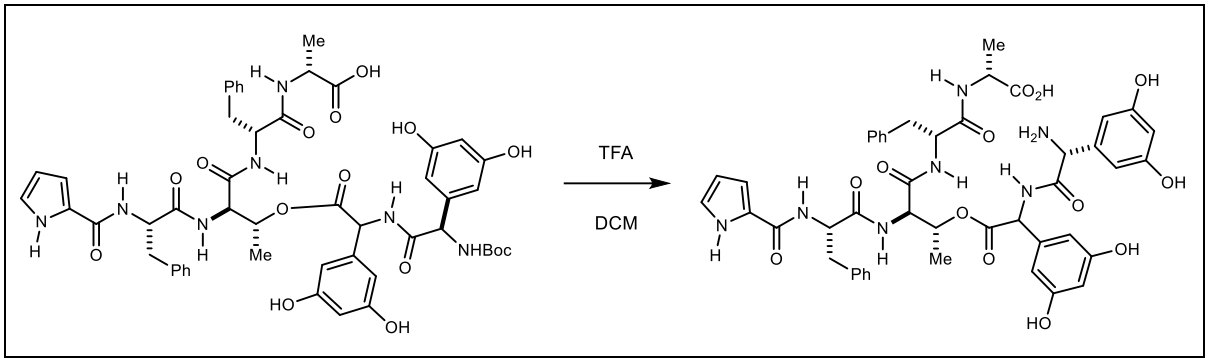

***N*-((1*H*-pyrrole-2-carbonyl)-L-phenylalanyl)-O-(2-((*R*)-2-amino-2-(3,5-dihydroxyphenyl)acetamido)-2-(3,5-dihydroxyphenyl)acetyl)-D-allothreonyl-D-phenylalanyl-D-alanine (2.92)** To a solution of the carbamate (3.7 mg, 3.7 μmol) in DCM (0.1 mL) was added trifluoroacetic acid (10 μL). The reaction was stirred at room temperature until judged complete by TLC (ca. 3 h), and then concentrated to give a white foam (3.2 mg, mixture of epimers), which was used directly without further purification.

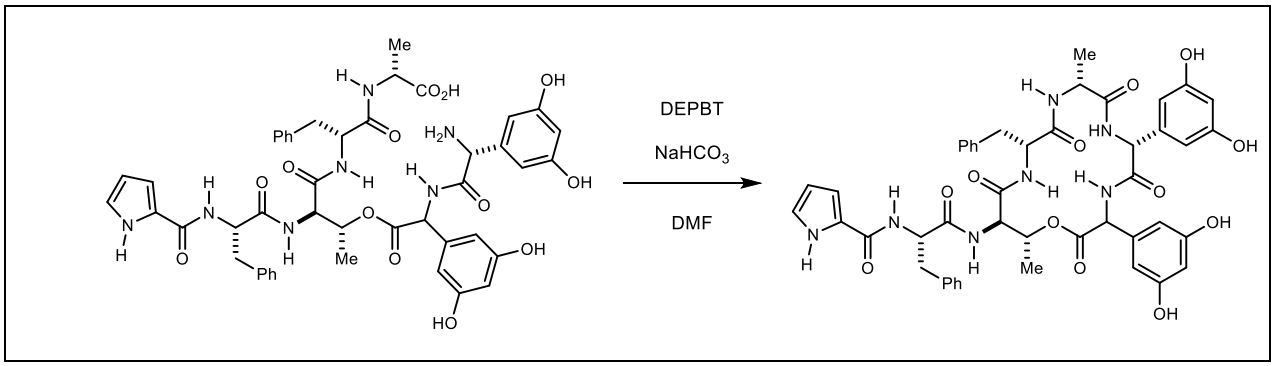

cochinmicin 1 and cochinmicin 5 (2.93): To a solution of *seco*-acid (8.7 mg, 9.6 μmol) in DMF (0.96 mL, 0.01 M) at 0 °C was added DEPBT (2.86 mg, 9.59 μmol) and $NaHCO_3$ (2.4 mg, 28.8 μmol). The reaction was maintained at 0 °C for 2 h then brought to room temperature where it was maintained. After 22 h, the reaction was concentrated and directly purified via pTLC (10% MeOH in DCM) to furnish a mixture of cochinmicins 1 and 5 (0.8 mg, 9%). ^{1}H NMR was consistent with published reports.[307] HRMS (ESI): Exact mass calcd for $C_{46}H_{48}N_7O_{12}(M+H)^+$ 890.3355, found 890.3356.

3.6 NMR Spectra

Figure 123. ^{1}H NMR (400 MHz, $CDCl_3$) spectrum of **1.102**.

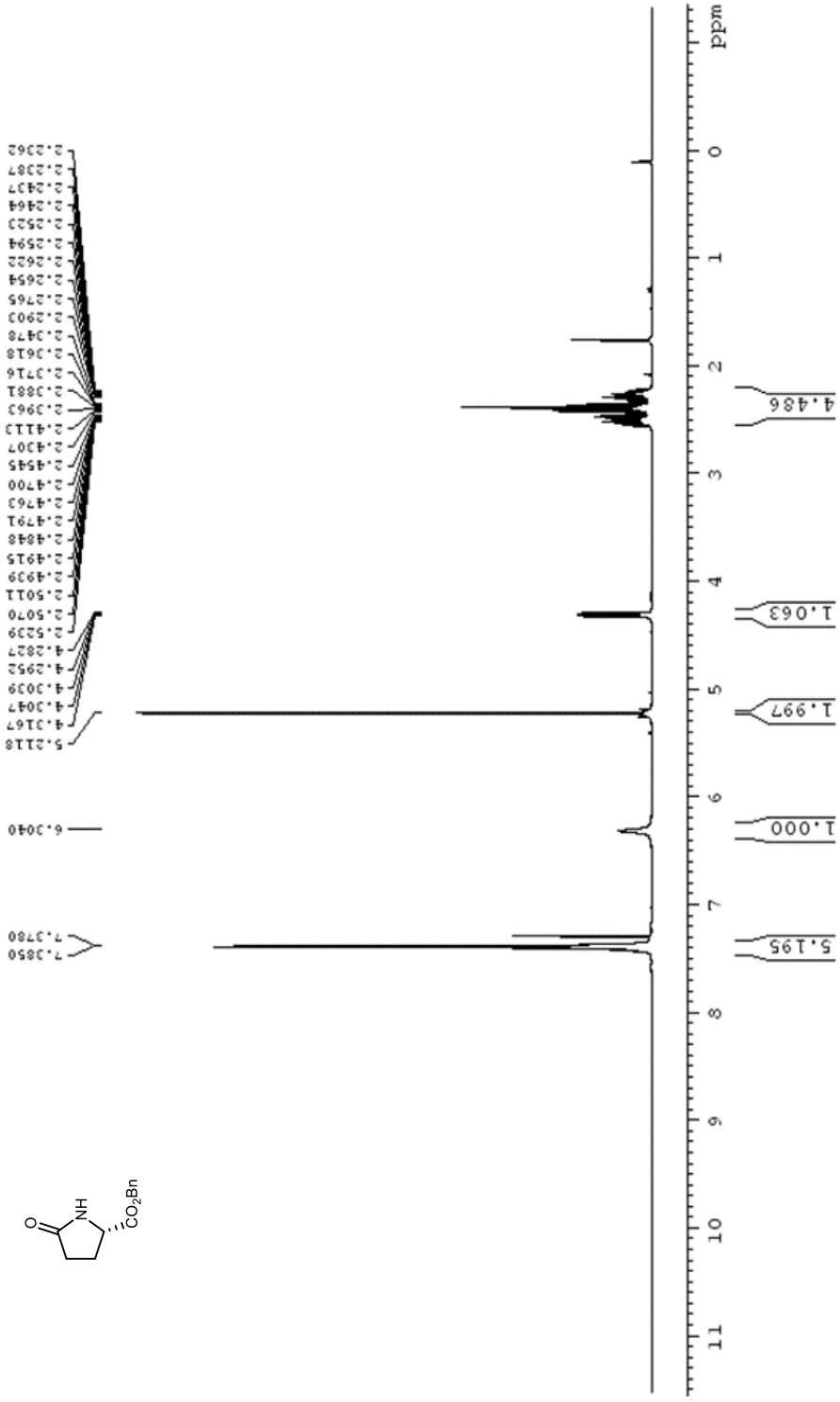

Figure 124. ^{13}C NMR (100 MHz, $CDCl_3$) spectra of **1.102**.

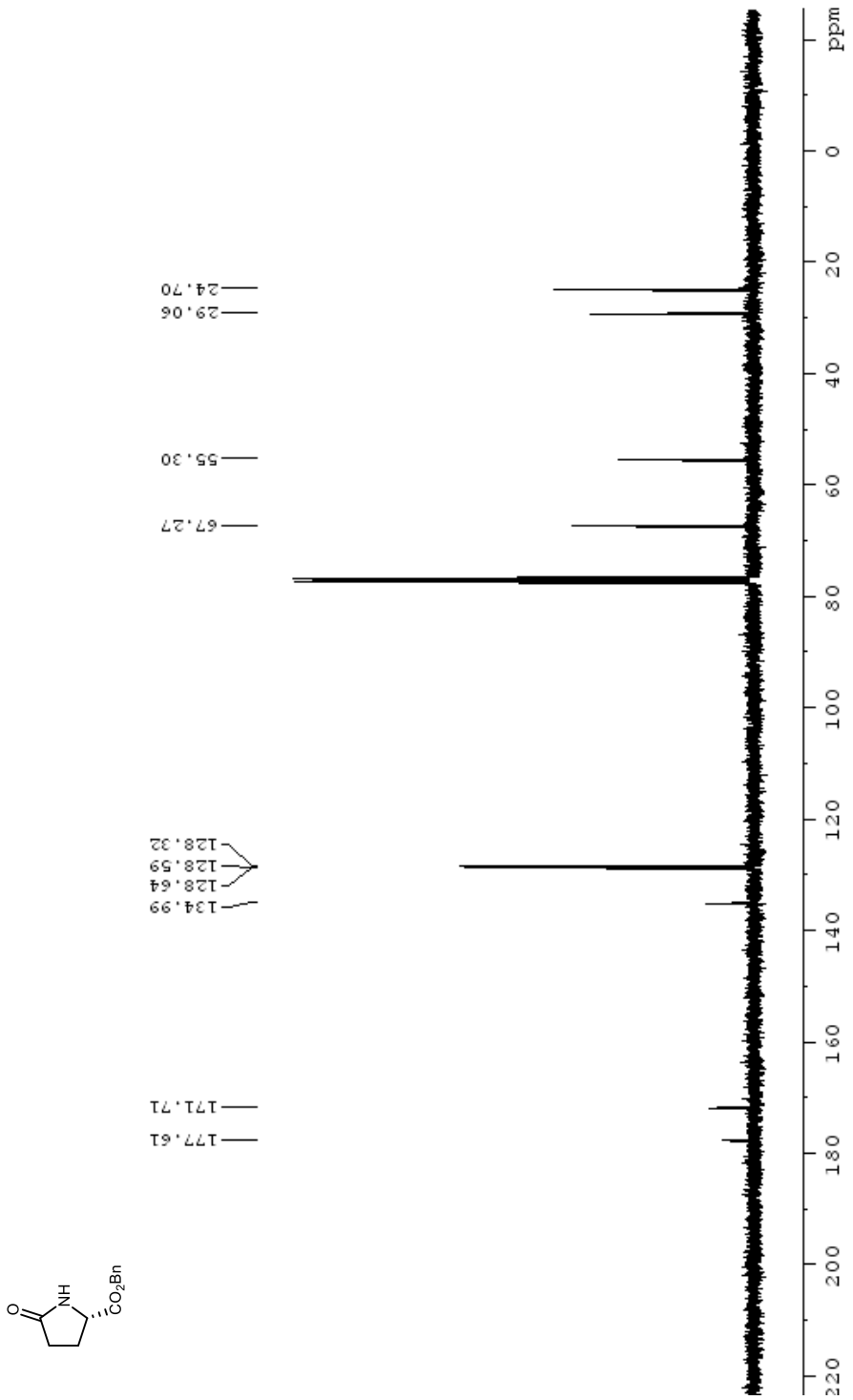

Figure 125. DEPT-135 NMR (100 MHz, $CDCl_3$) spectra of **1.102**.

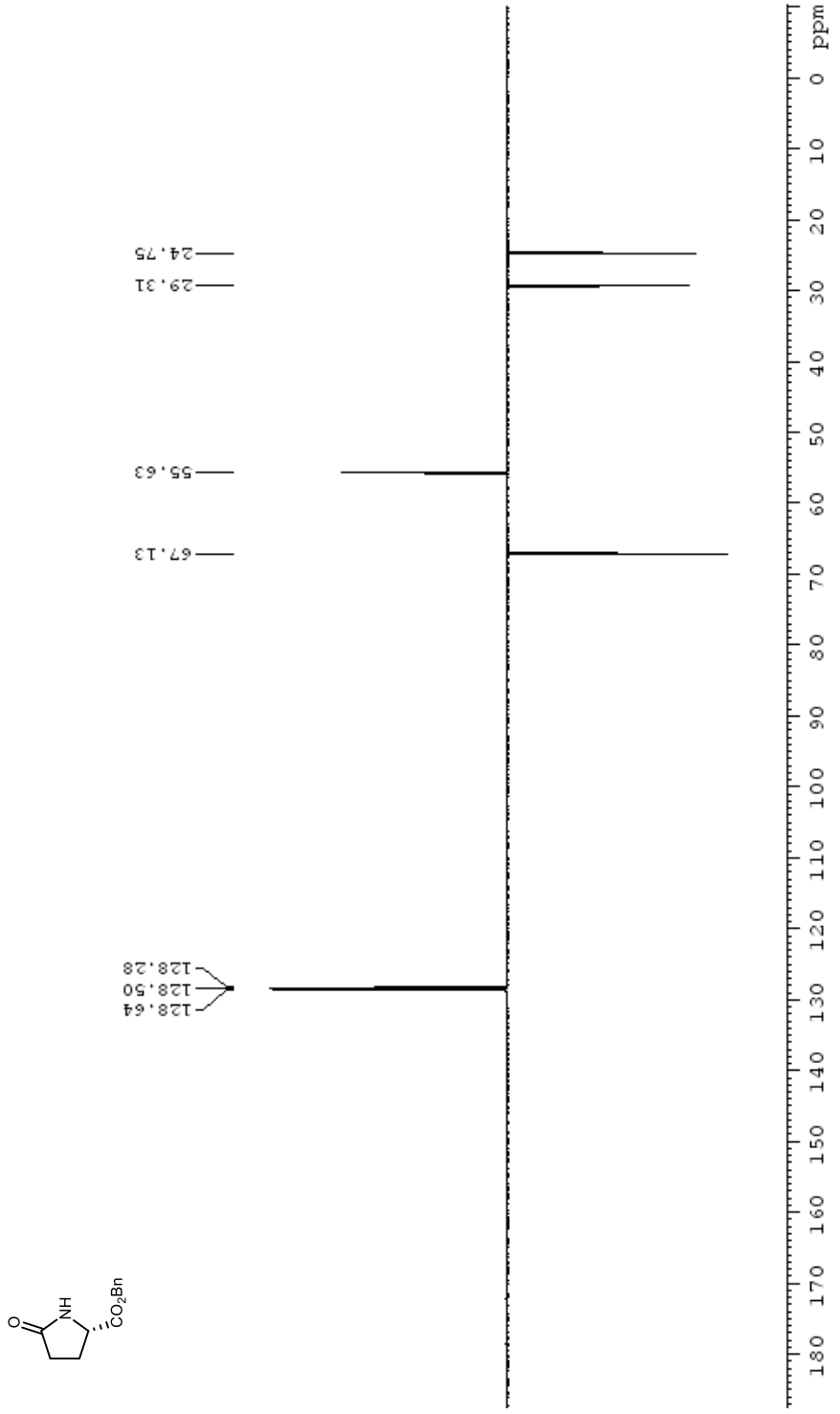

Figure 126. ^{1}H NMR (400 MHz, $CDCl_3$) spectrum of **1.103**.

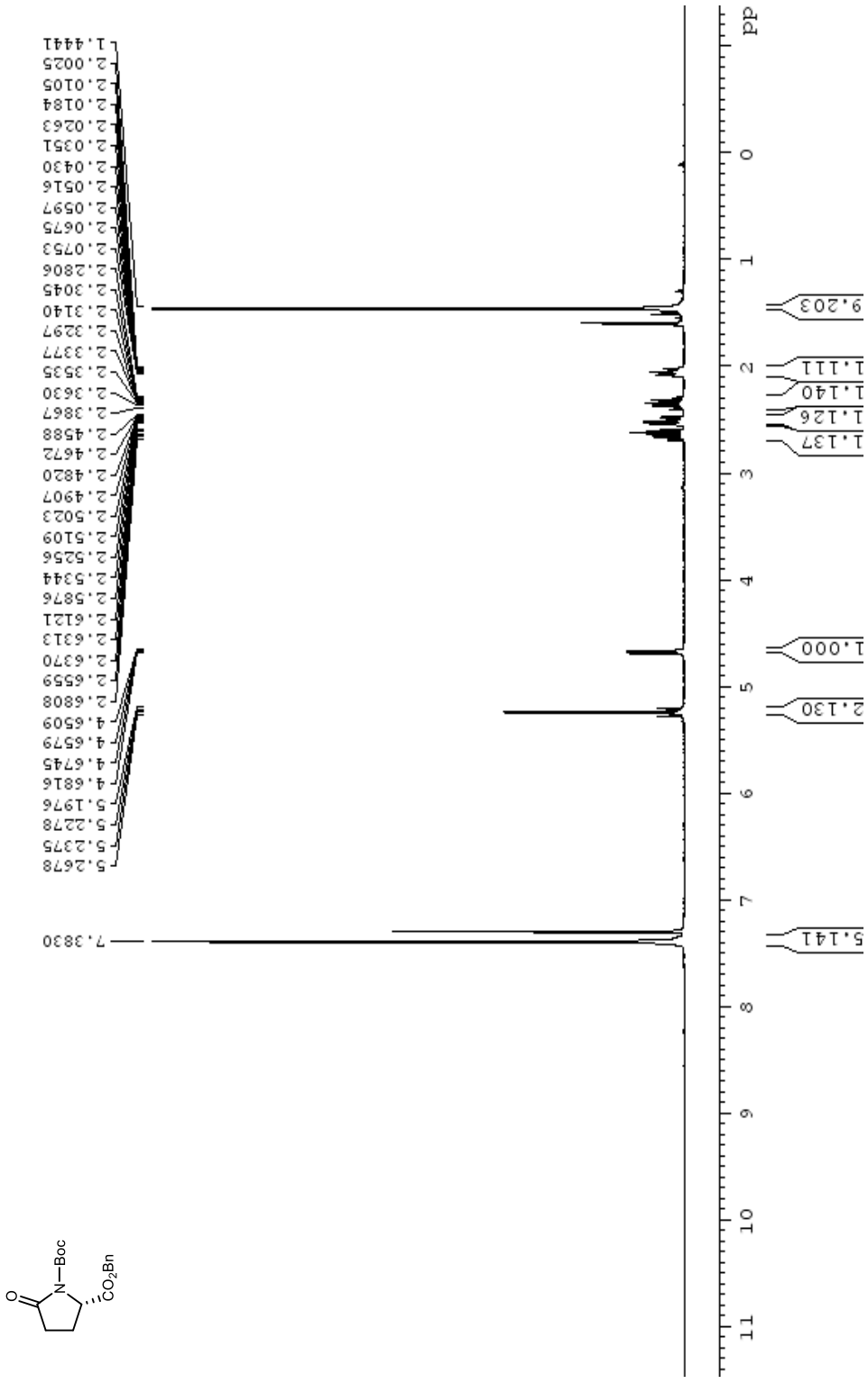

Figure 127. ^{13}C NMR (100 MHz, $CDCl_3$) spectra of **1.103**.

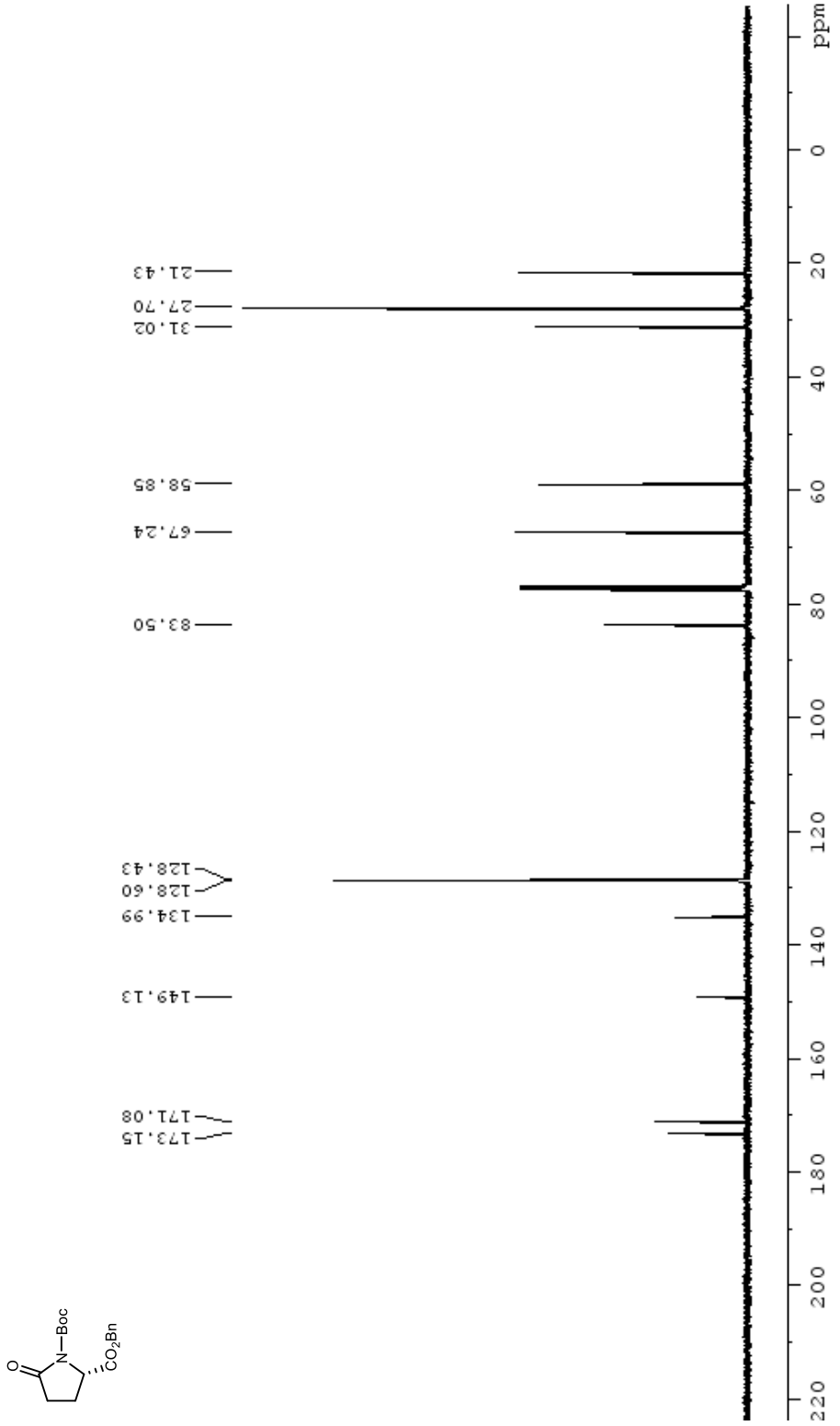

Figure 128. DEPT-135 NMR (100 MHz, $CDCl_3$) spectra of **1.103**.

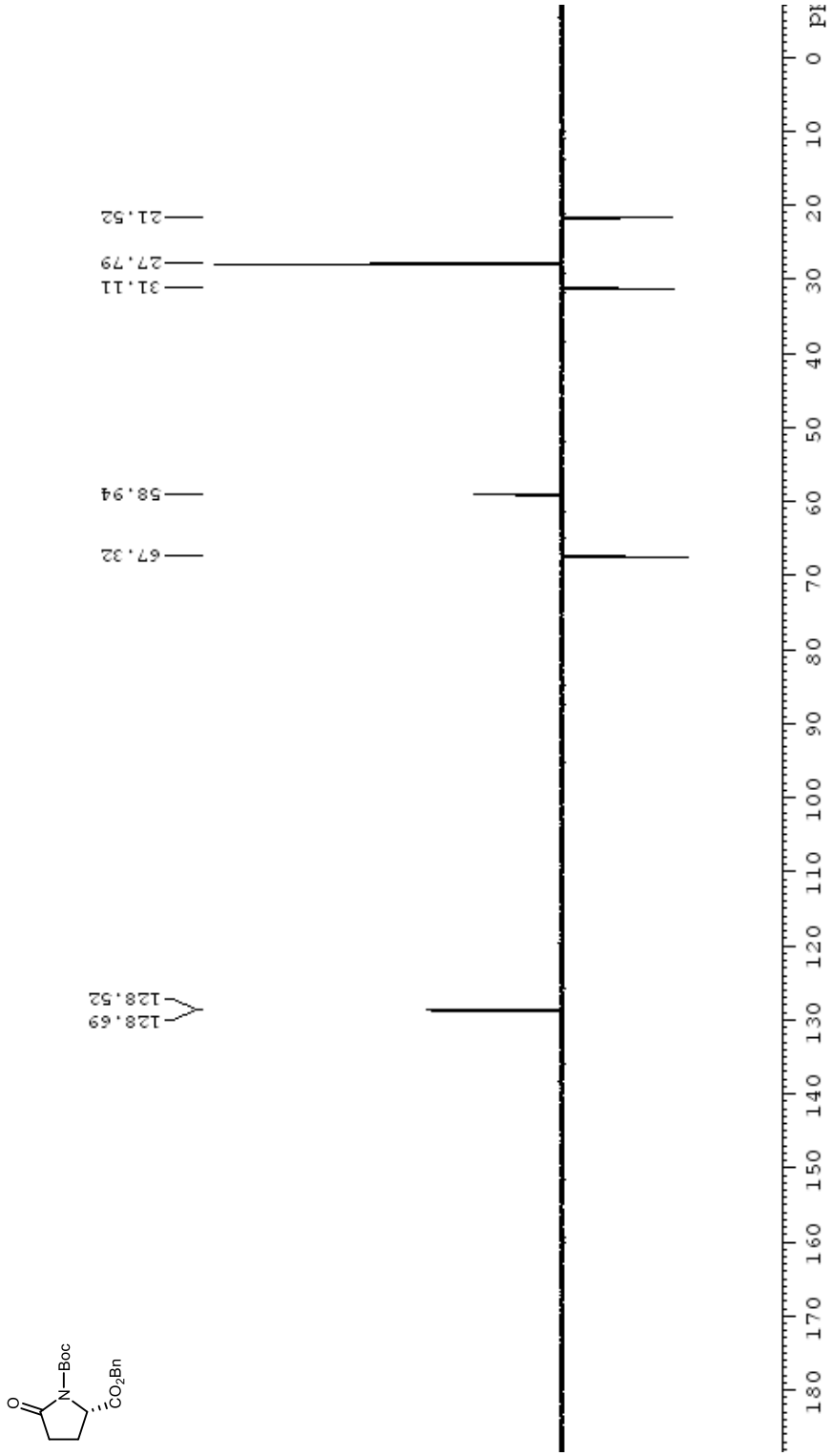

Figure 129. ^{1}H NMR (400 MHz, $CDCl_3$) spectrum of **1.104.**

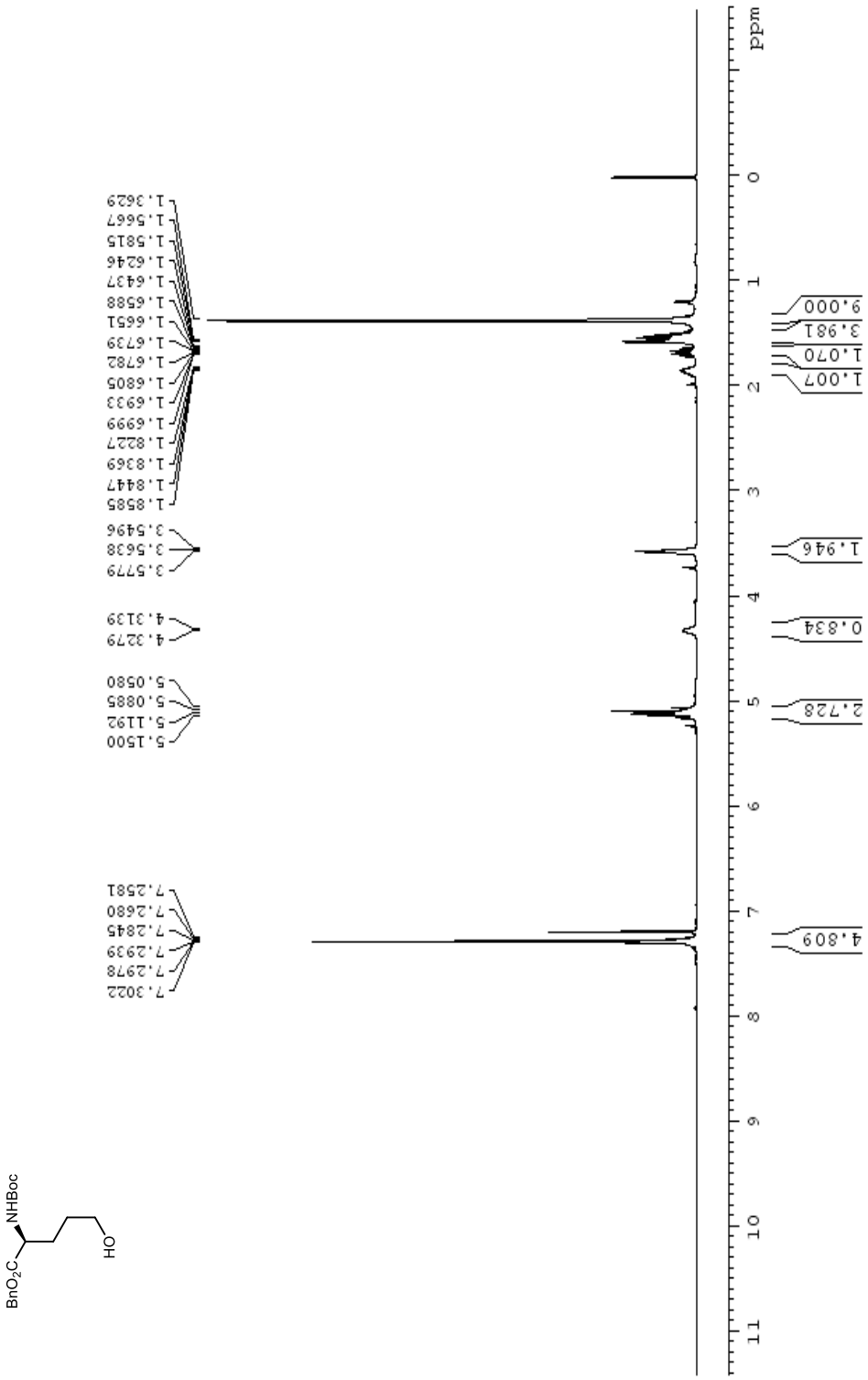

Figure 130. ^{13}C NMR (100 MHz, $CDCl_3$) spectra of **1.104**.

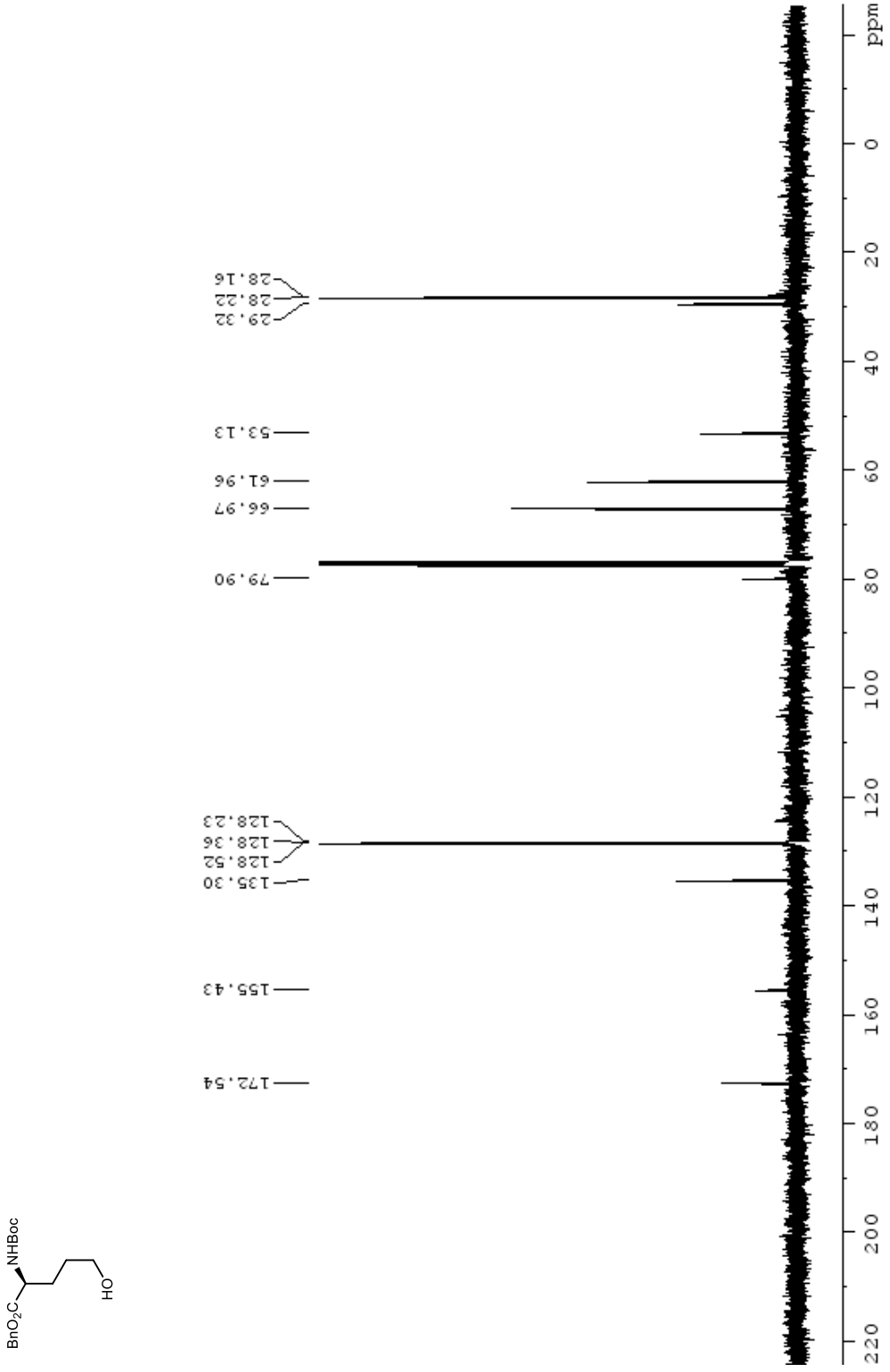

Figure 131. DEPT-135 NMR (100 MHz, $CDCl_3$) spectra of **1.104**.

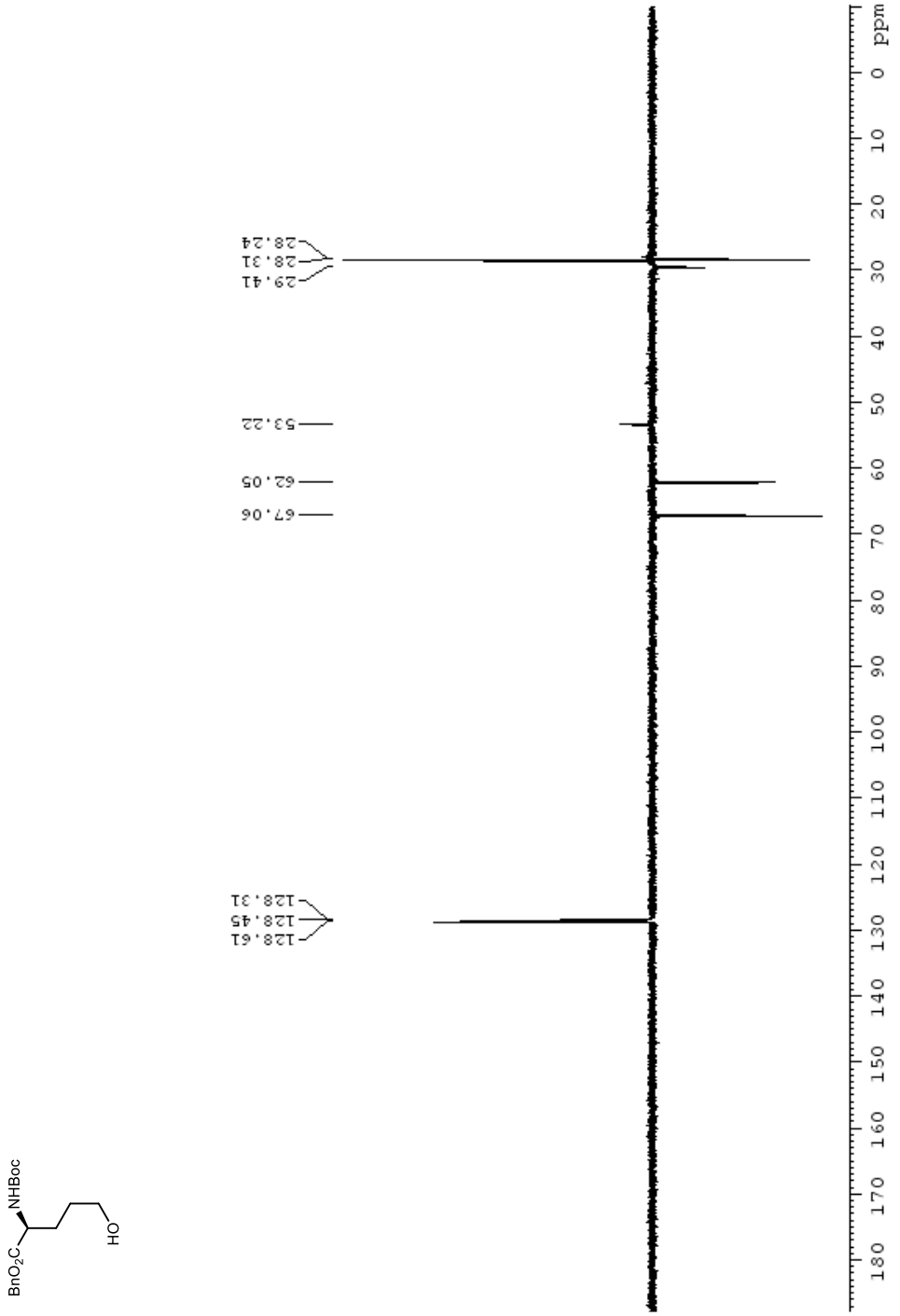

Figure 132. ^{1}H NMR (400 MHz, $CDCl_3$) spectrum of **1.92**.

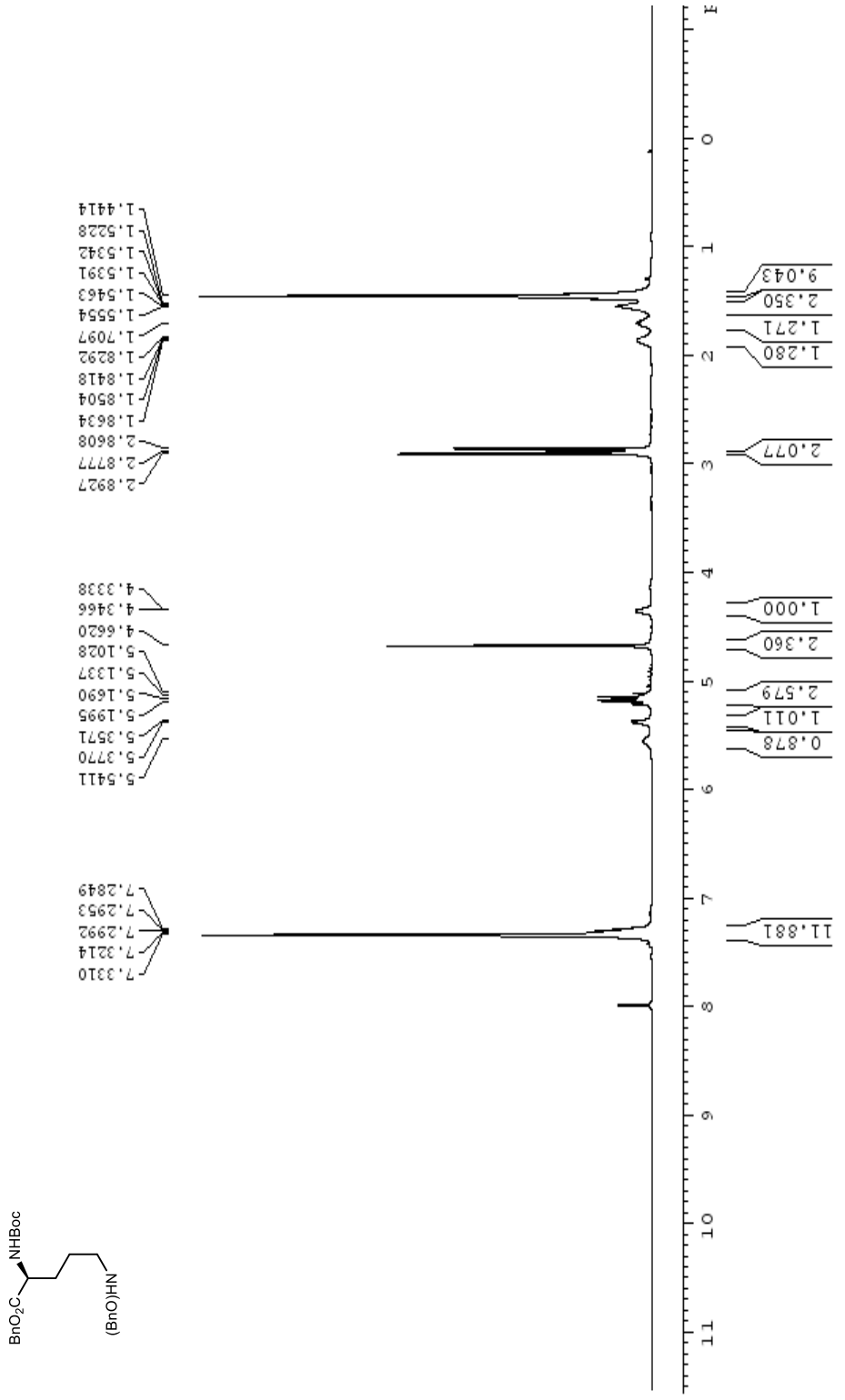

Figure 133. ^{13}C NMR (100 MHz, $CDCl_3$) spectra of **1.92**.

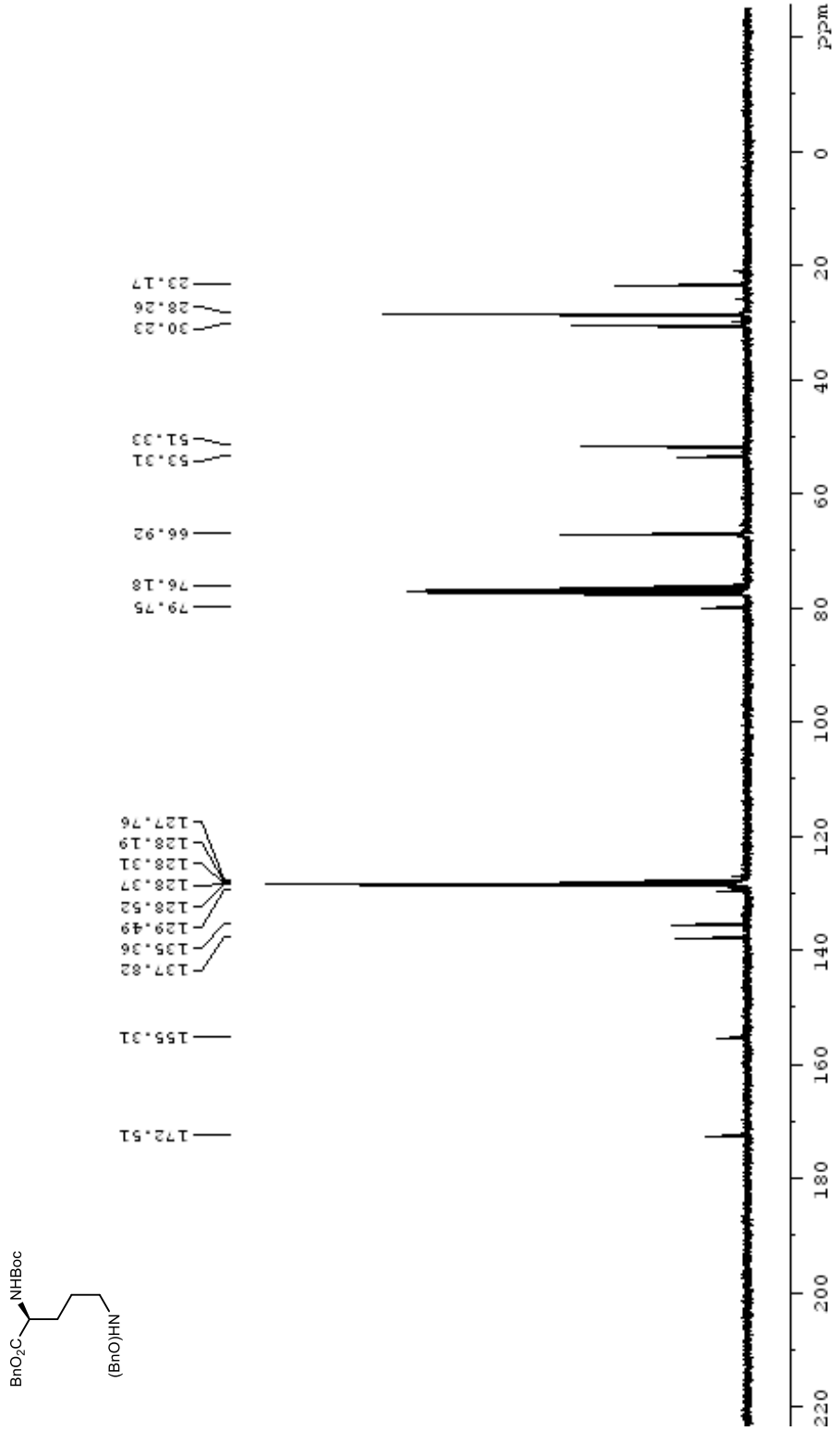

Figure 134. DEPT-135 NMR (100 MHz, $CDCl_3$) spectra of **1.92**.

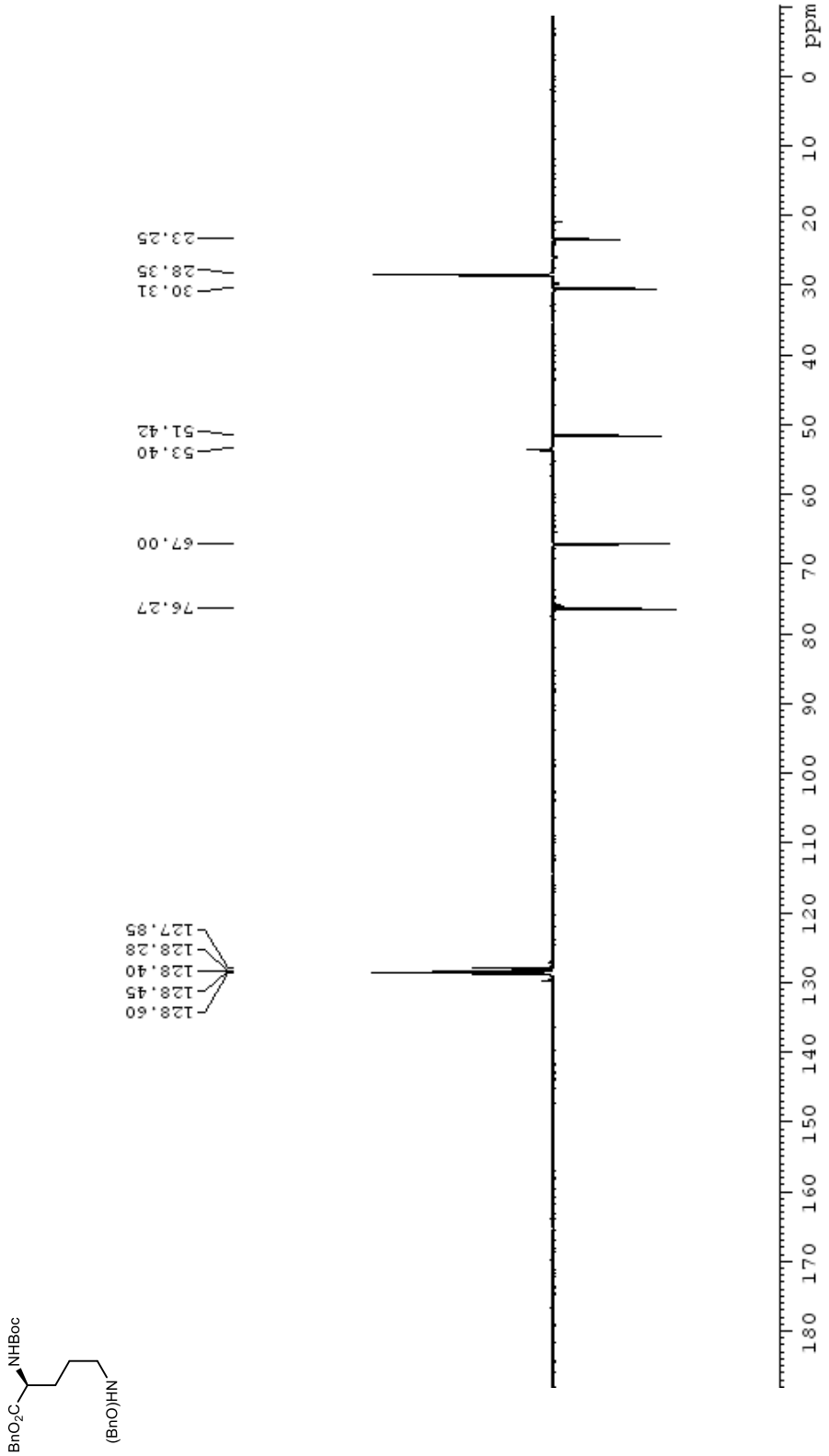

Figure 135. ^{1}H NMR (400 MHz, MeOD) spectrum of **1.97**.

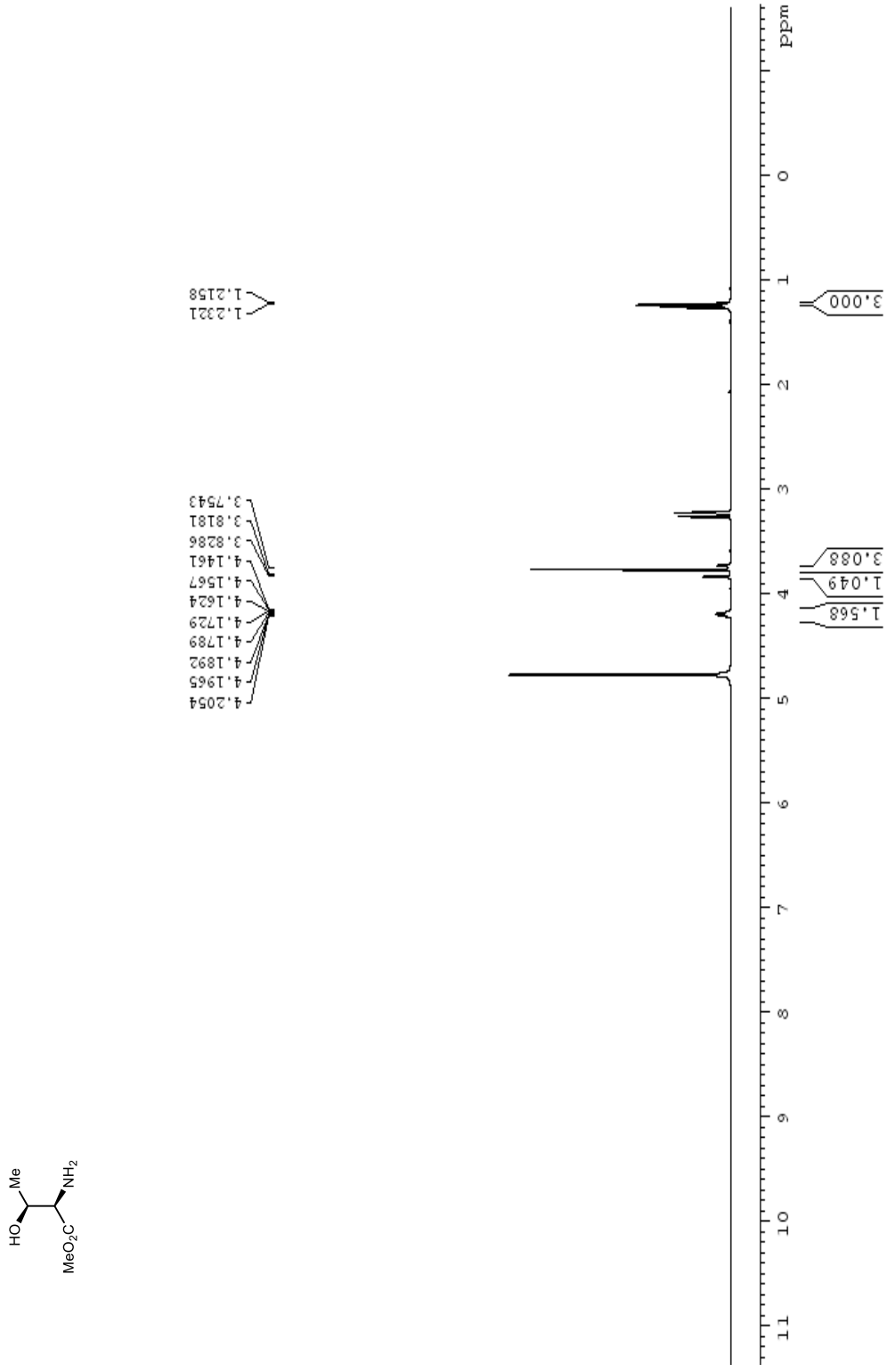

Figure 136. ^{13}C NMR (100 MHz, MeOD) spectrum of **1.97**.

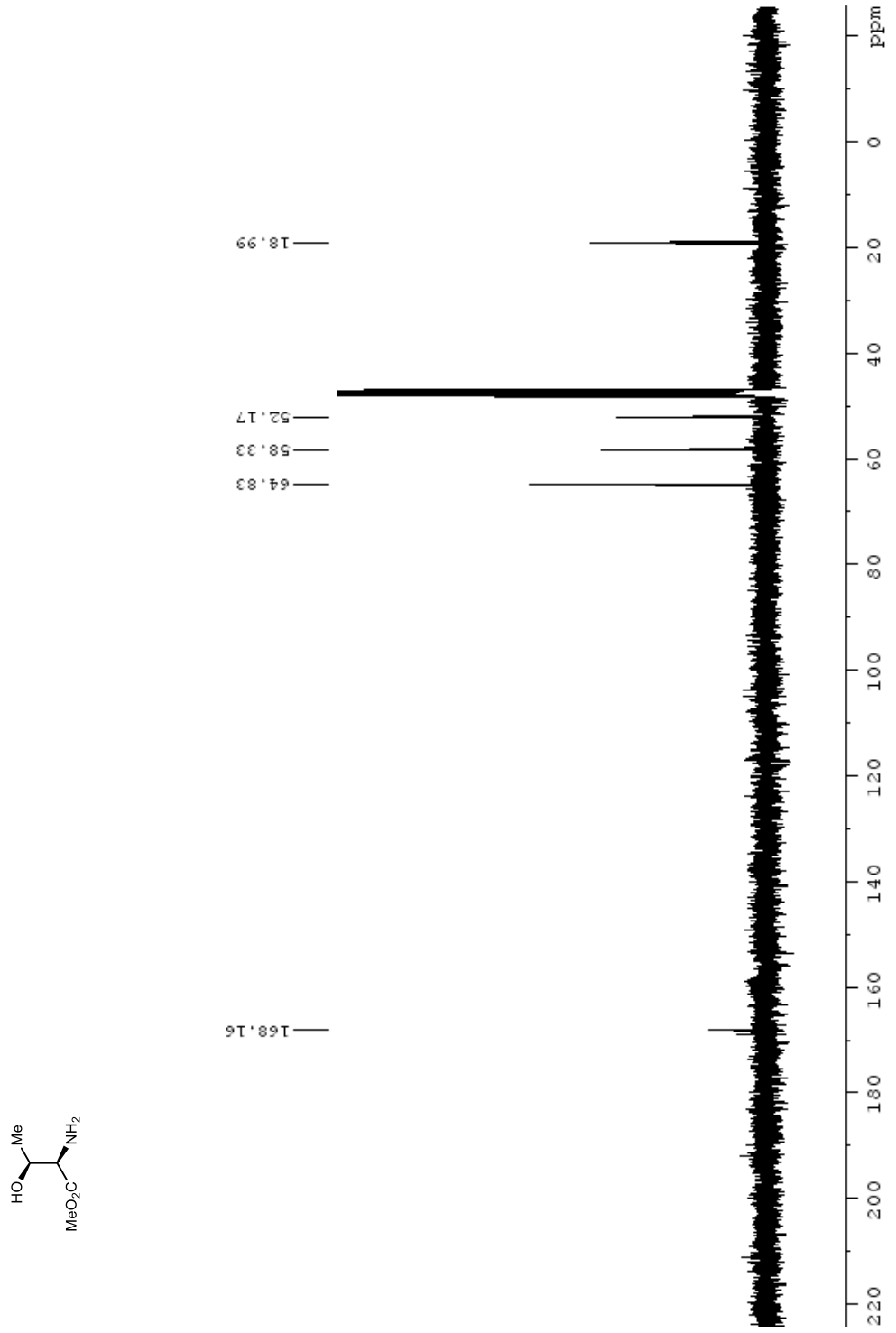

Figure 137. DEPT-135 NMR (100 MHz, MeOD) spectrum of **1.97**.

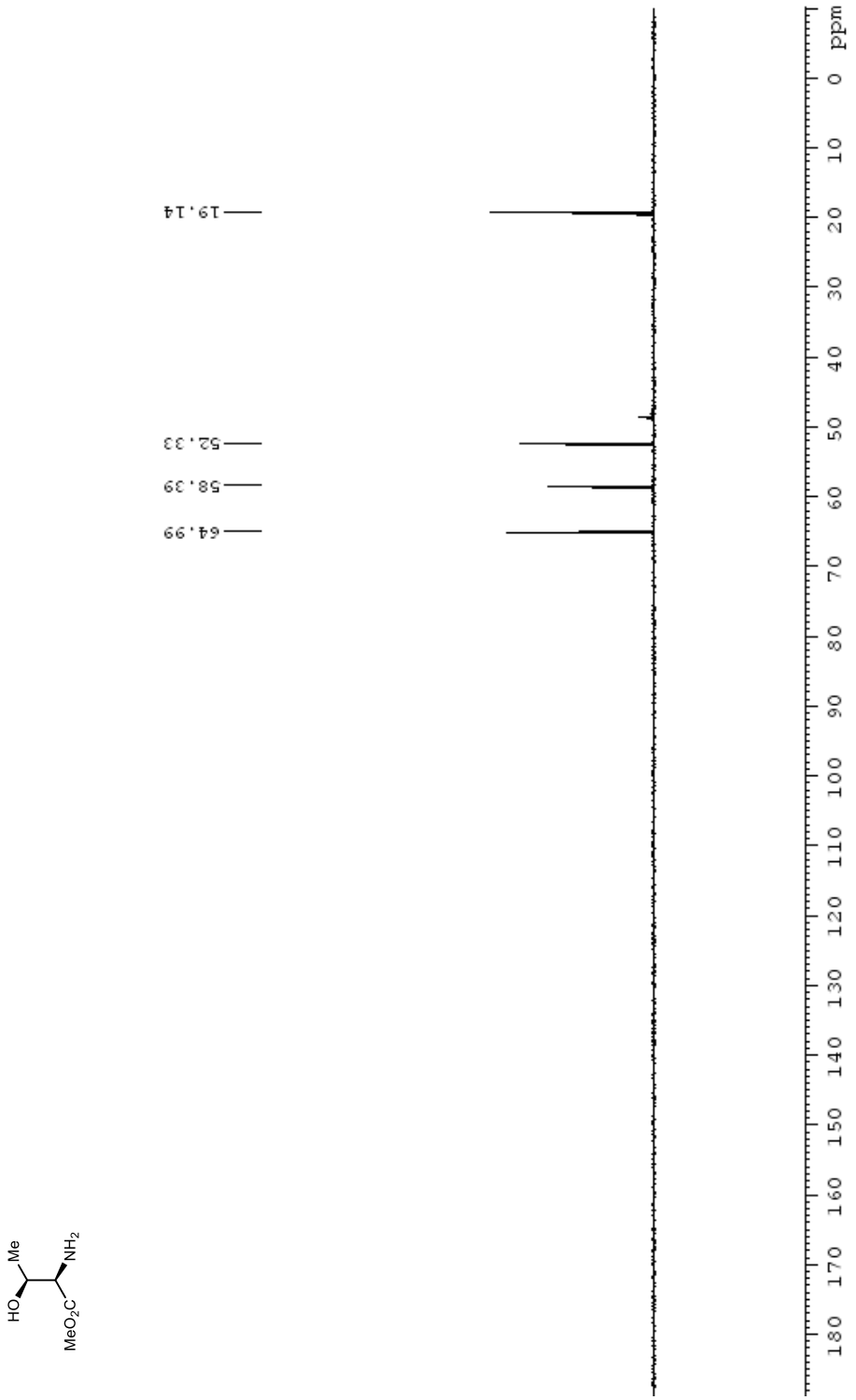

Figure 138. ^{1}H NMR (400 MHz, $CDCl_3$) spectrum of **1.98**.

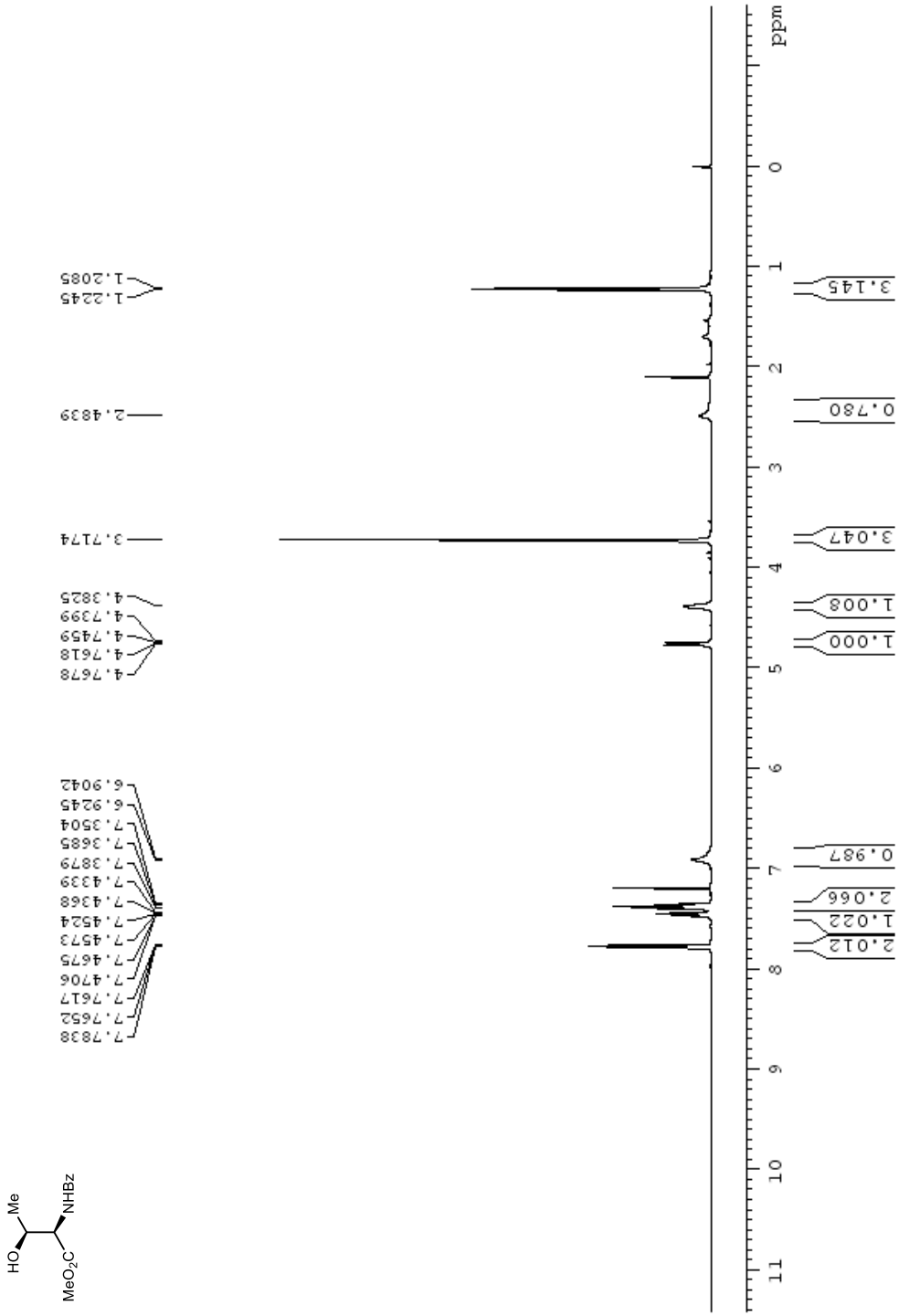

Figure 139. ^{13}C NMR (100 MHz, $CDCl_3$) spectra of **1.98**.

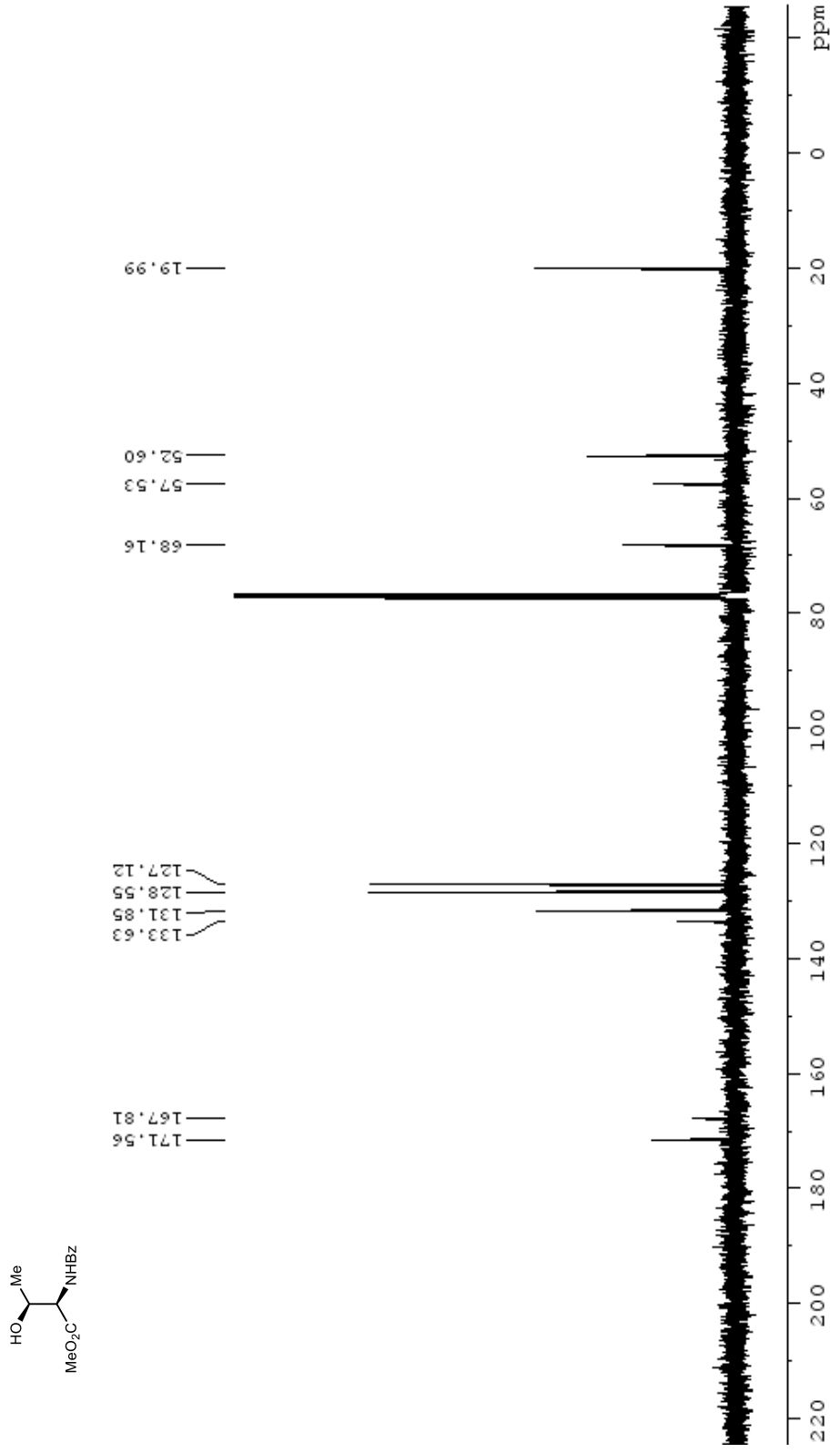

Figure 140. DEPT-135 NMR (100 MHz, $CDCl_3$) spectra of **1.98**.

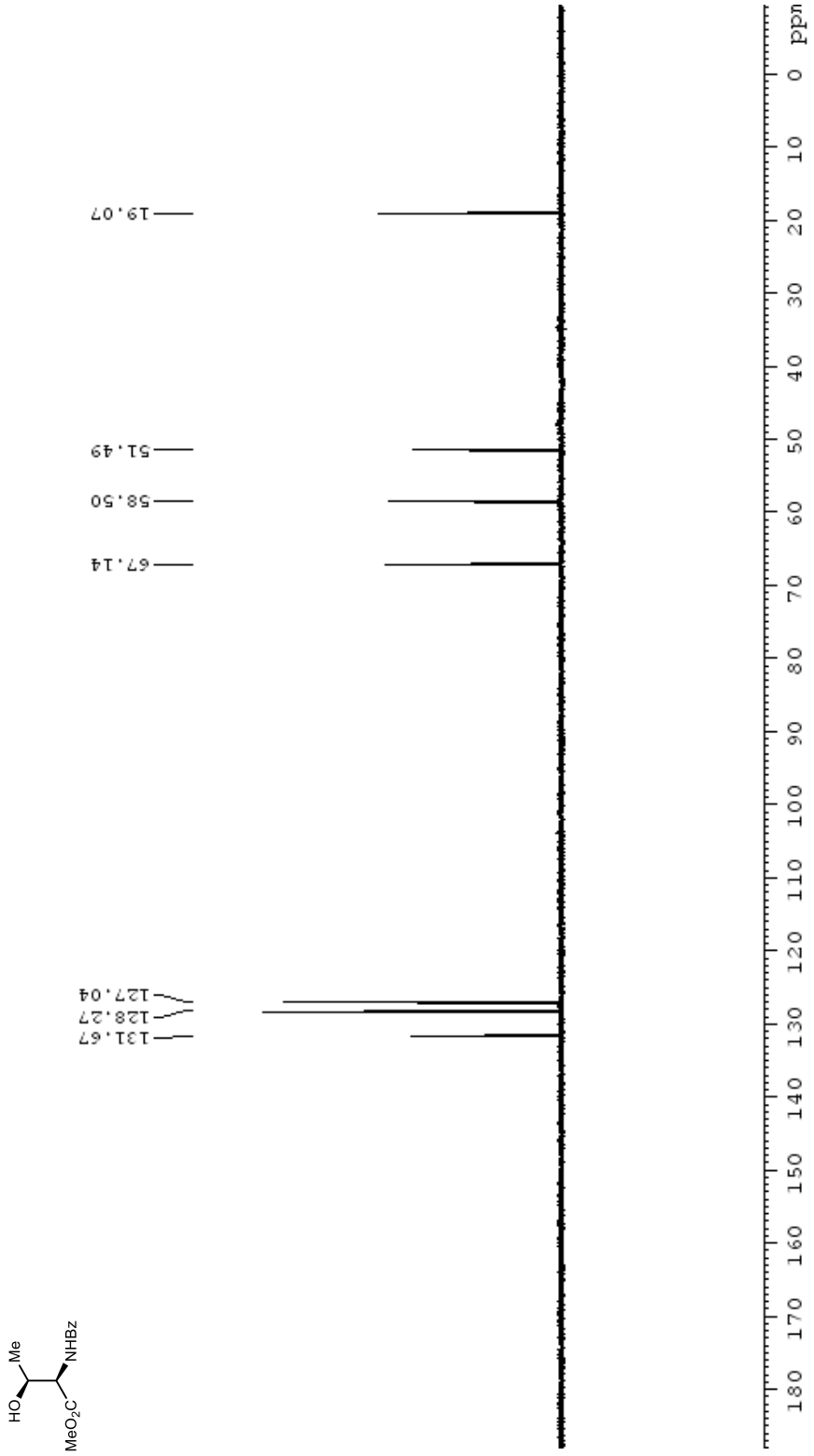

Figure 141. ^{1}H NMR (400 MHz, $CDCl_3$) spectrum of **1.99**.

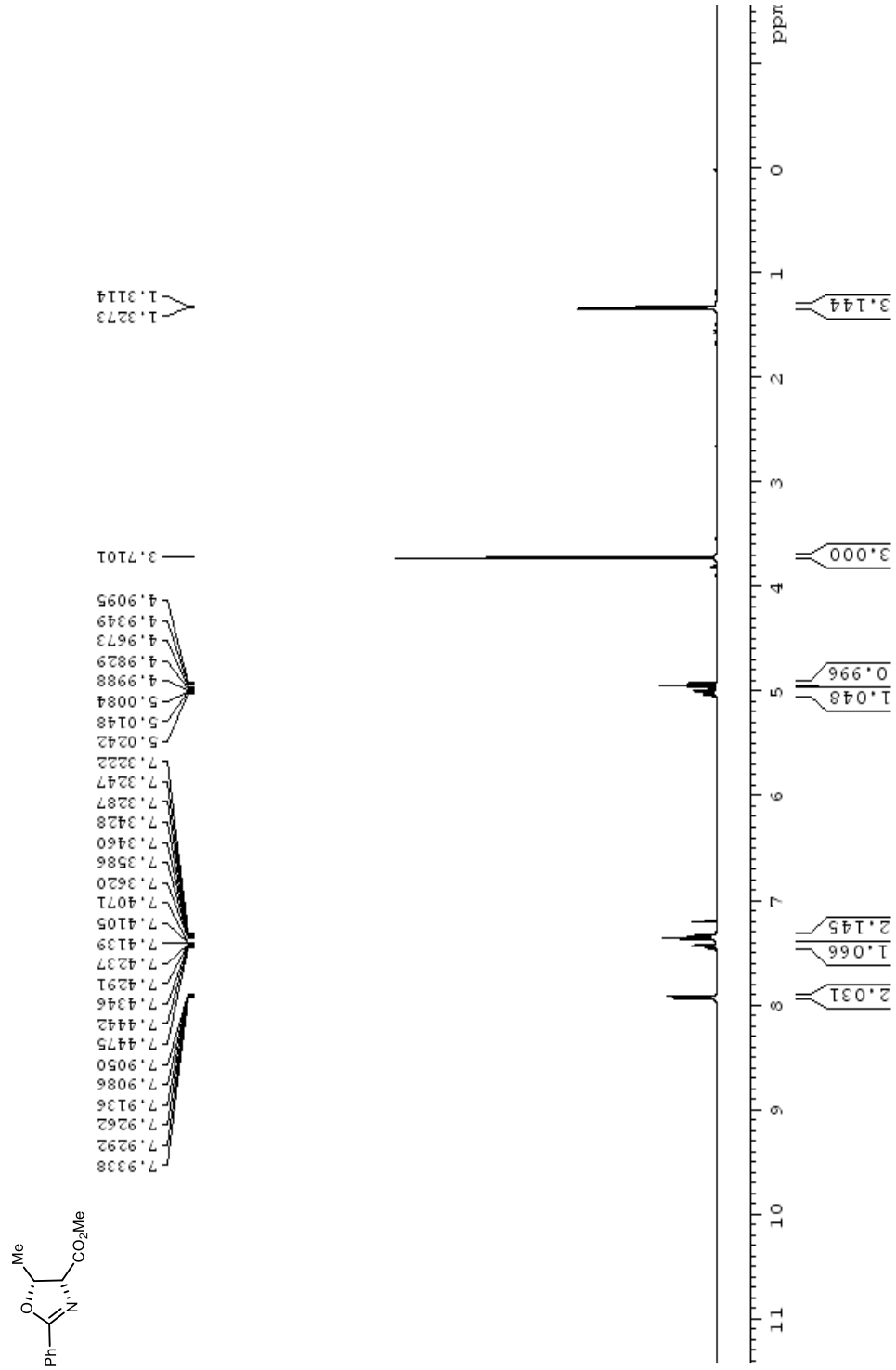

Figure 142. ^{13}C NMR (100 MHz, $CDCl_3$) spectra of **1.99**.

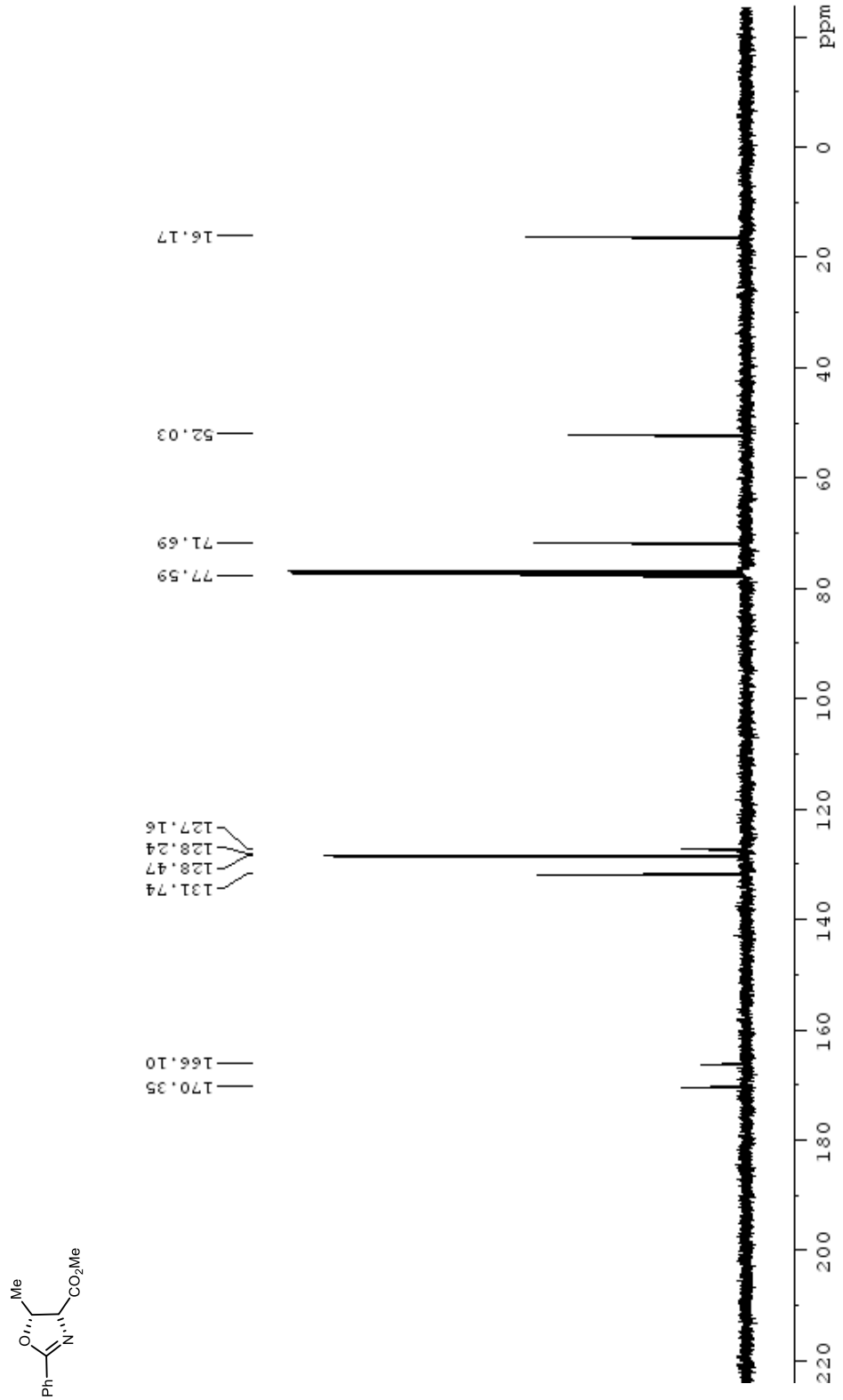

Figure 143. DEPT-135 NMR (100 MHz, $CDCl_3$) spectra of **1.99**.

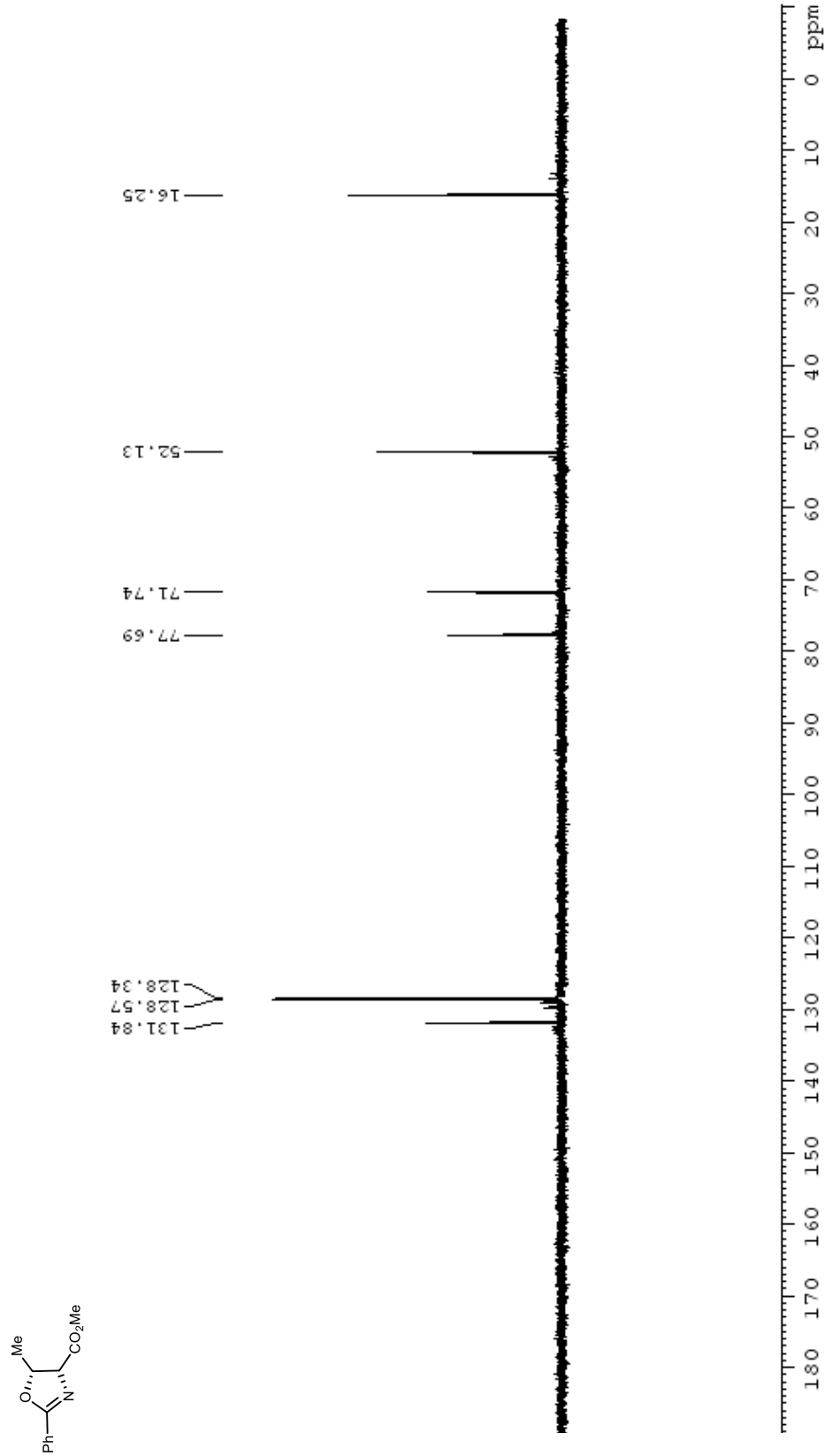

Figure 144. ^{1}H NMR (400 MHz, MeOD) spectrum of **1.100**.

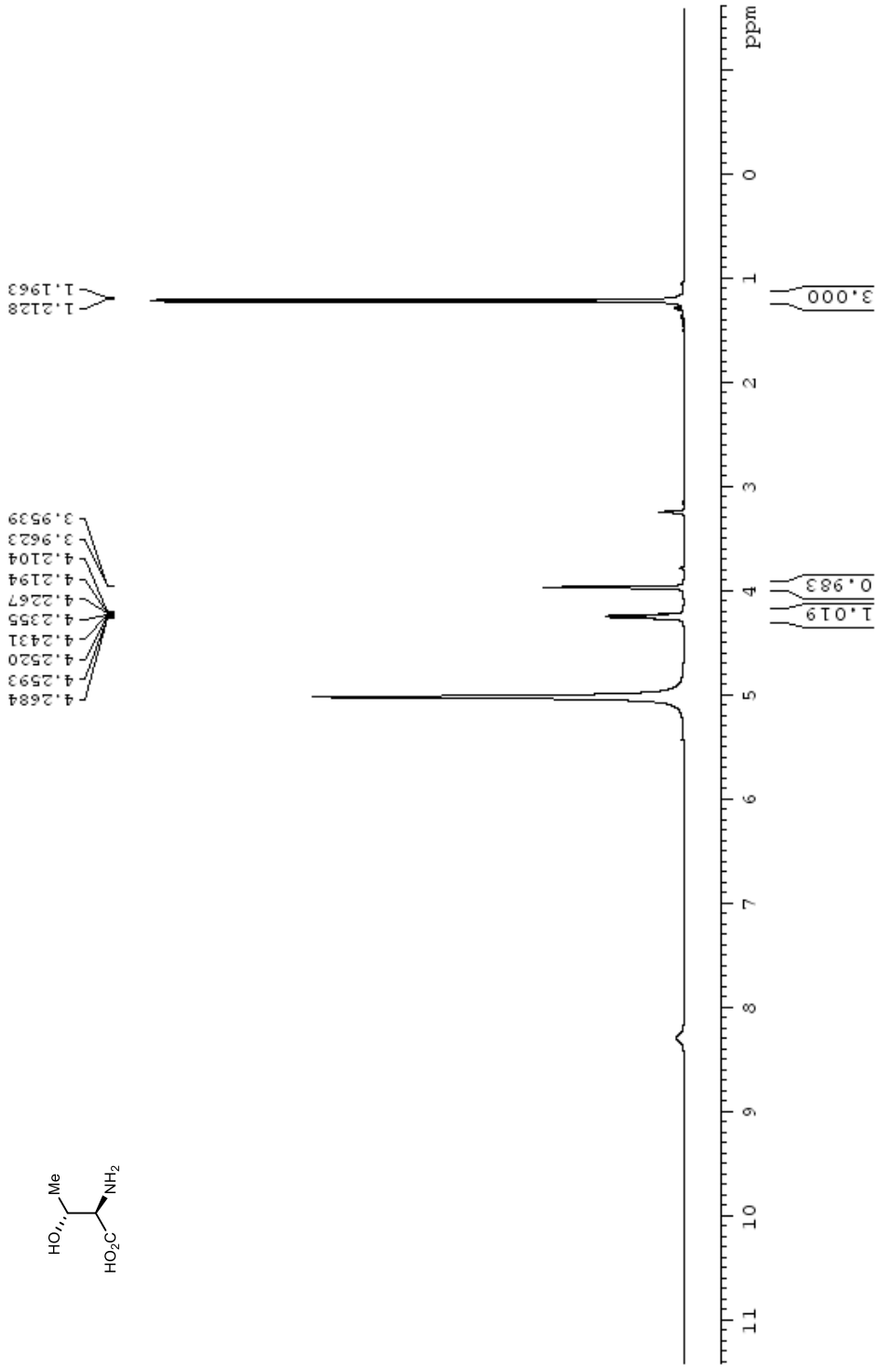

Figure 145. ^{13}C NMR (100 MHz, MeOD) spectrum of **1.100**.

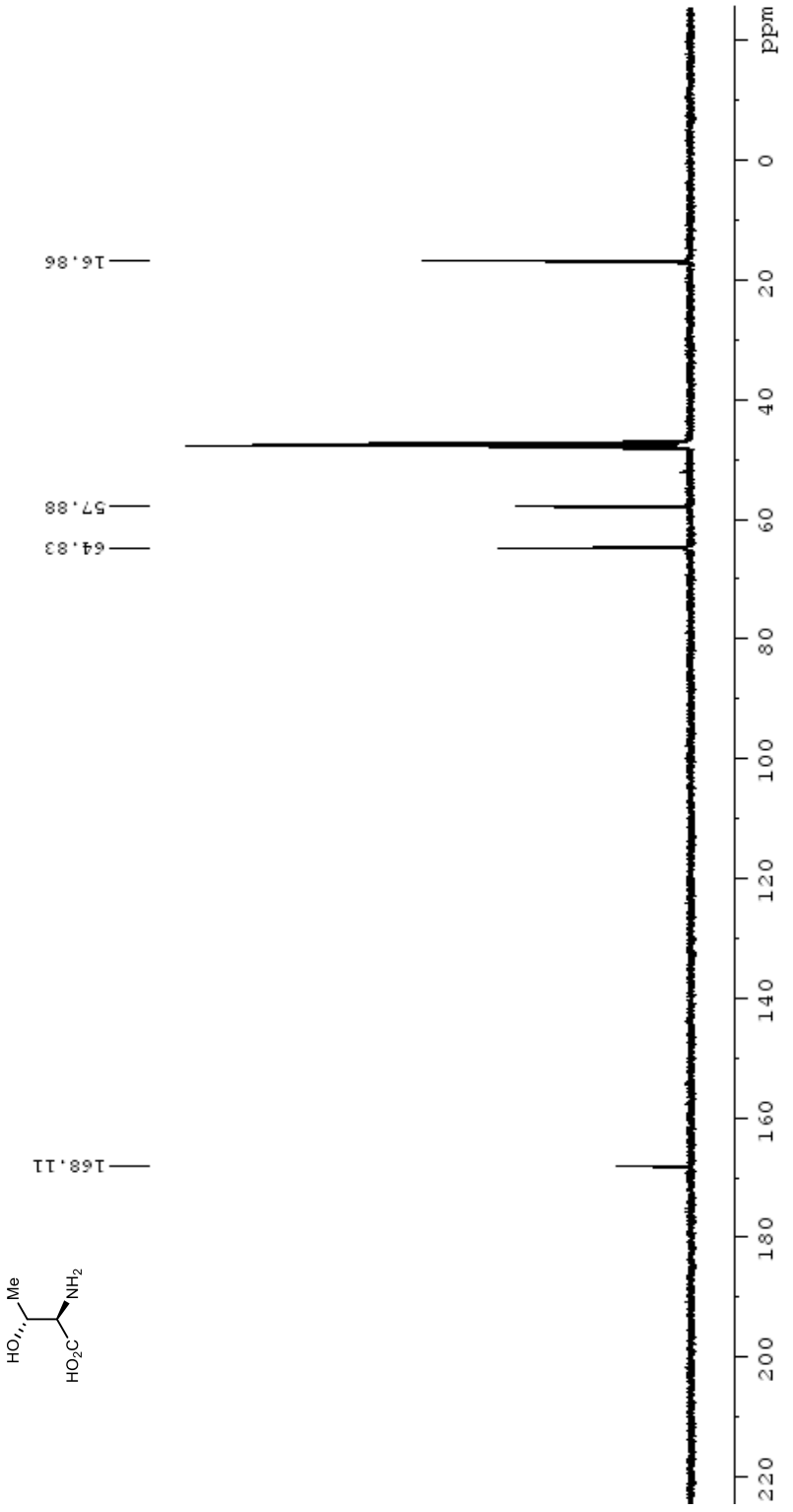

Figure 146. DEPT-135 NMR (100 MHz, MeOD) spectrum of **1.100**.

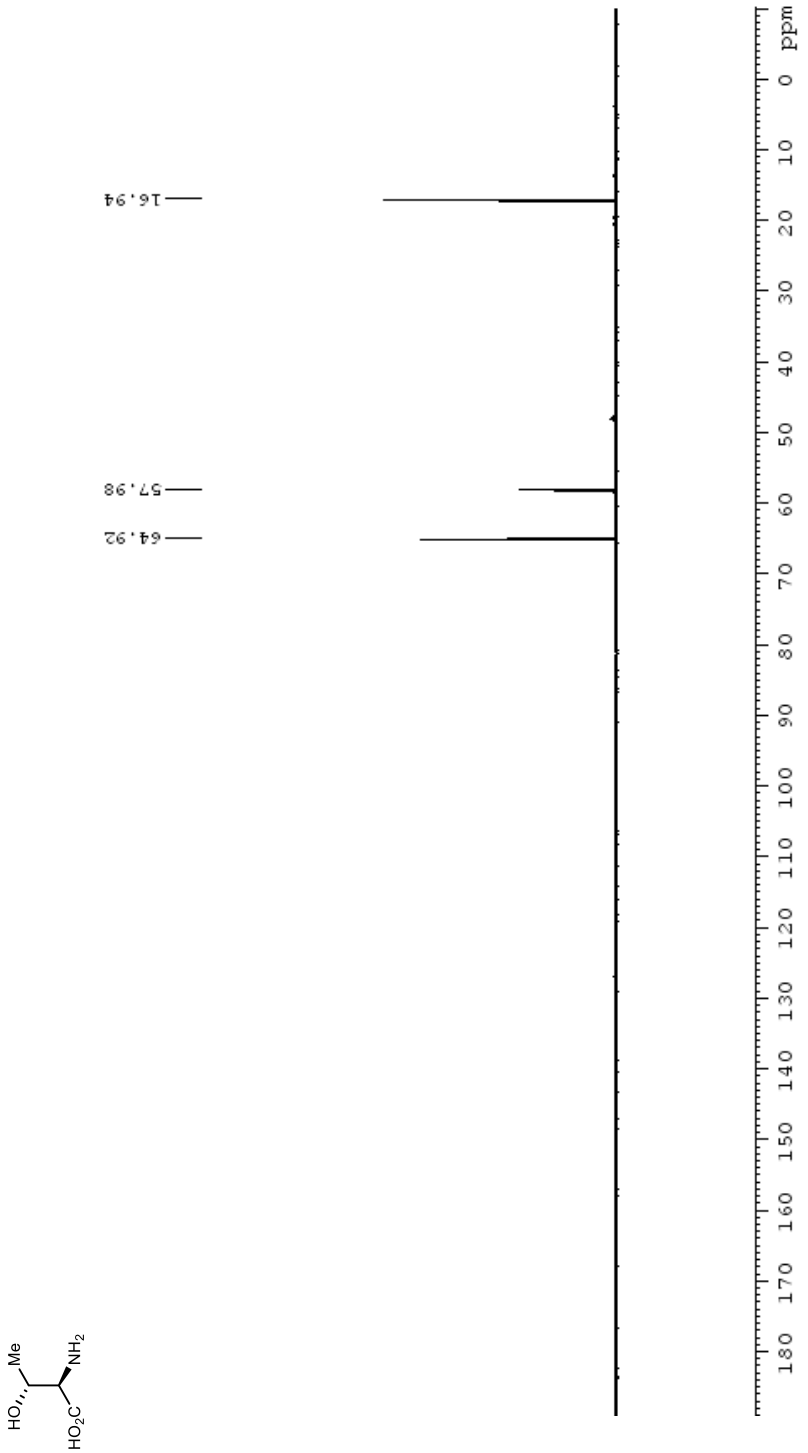

Figure 147. [1]H NMR (400 MHz, MeOD) spectrum of **1.93**.

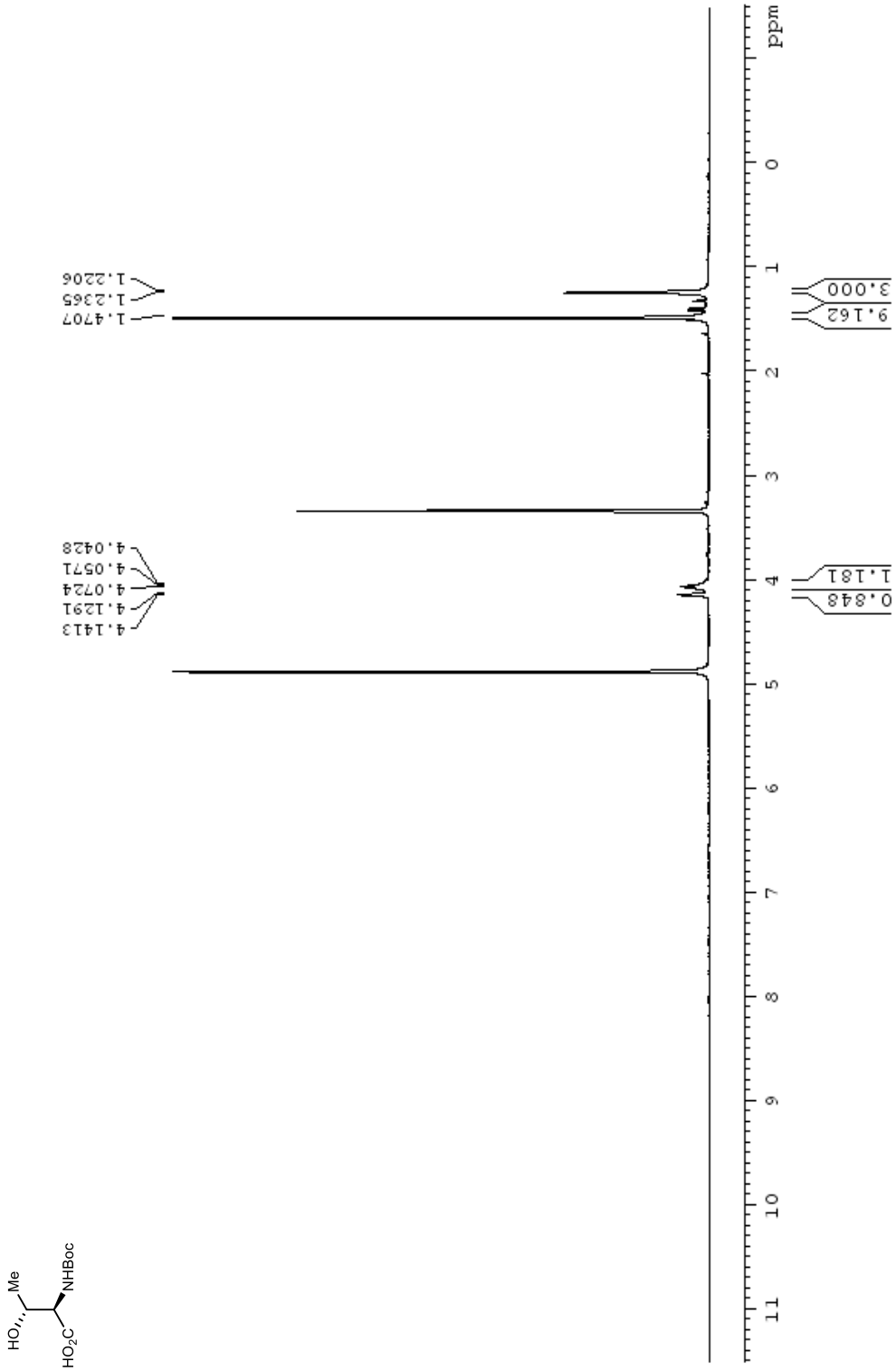

Figure 148. ^{13}C NMR (100 MHz, MeOD) spectrum of **1.93**.

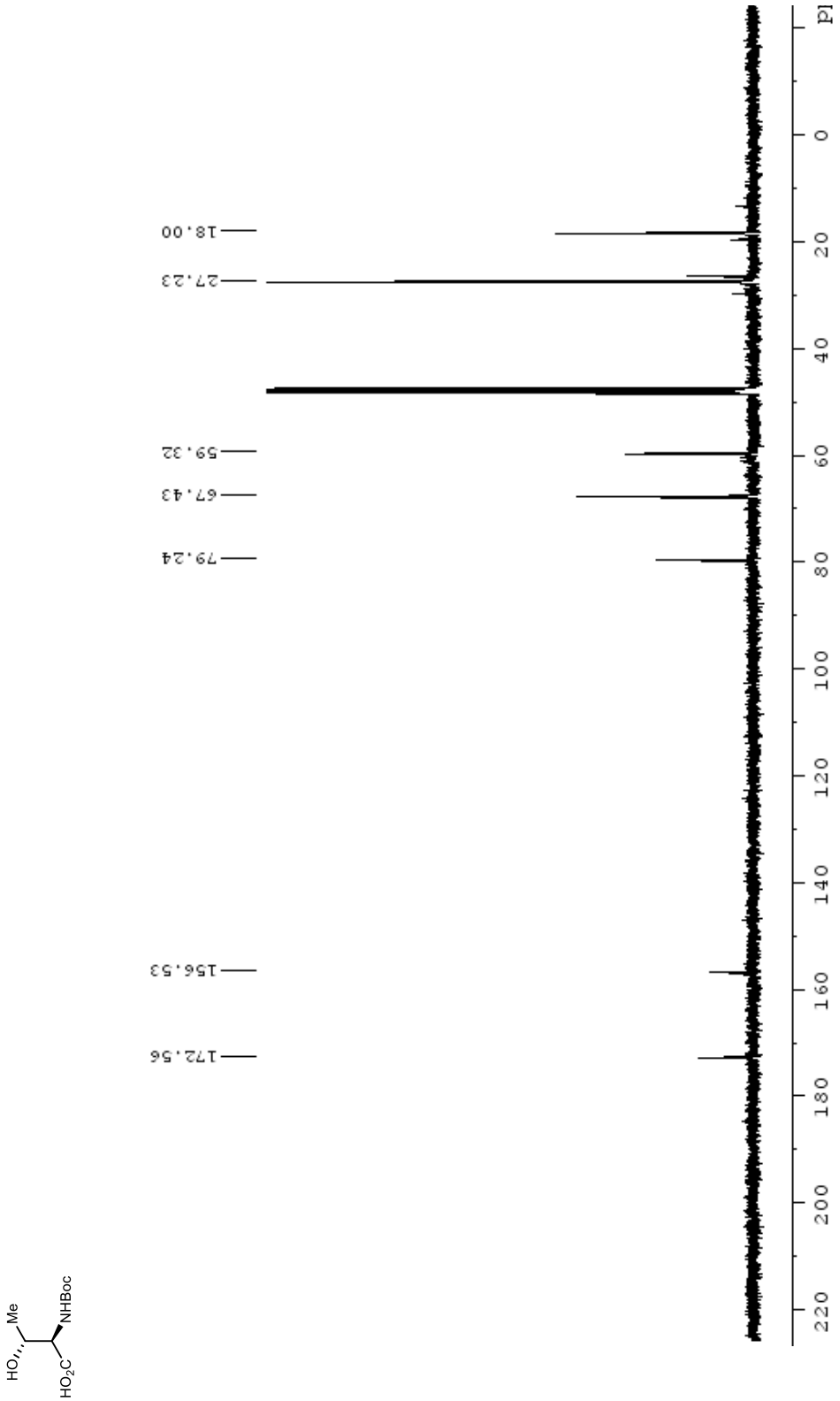

Figure 149. DEPT-135 NMR (100 MHz, MeOD) spectrum of **1.93**.

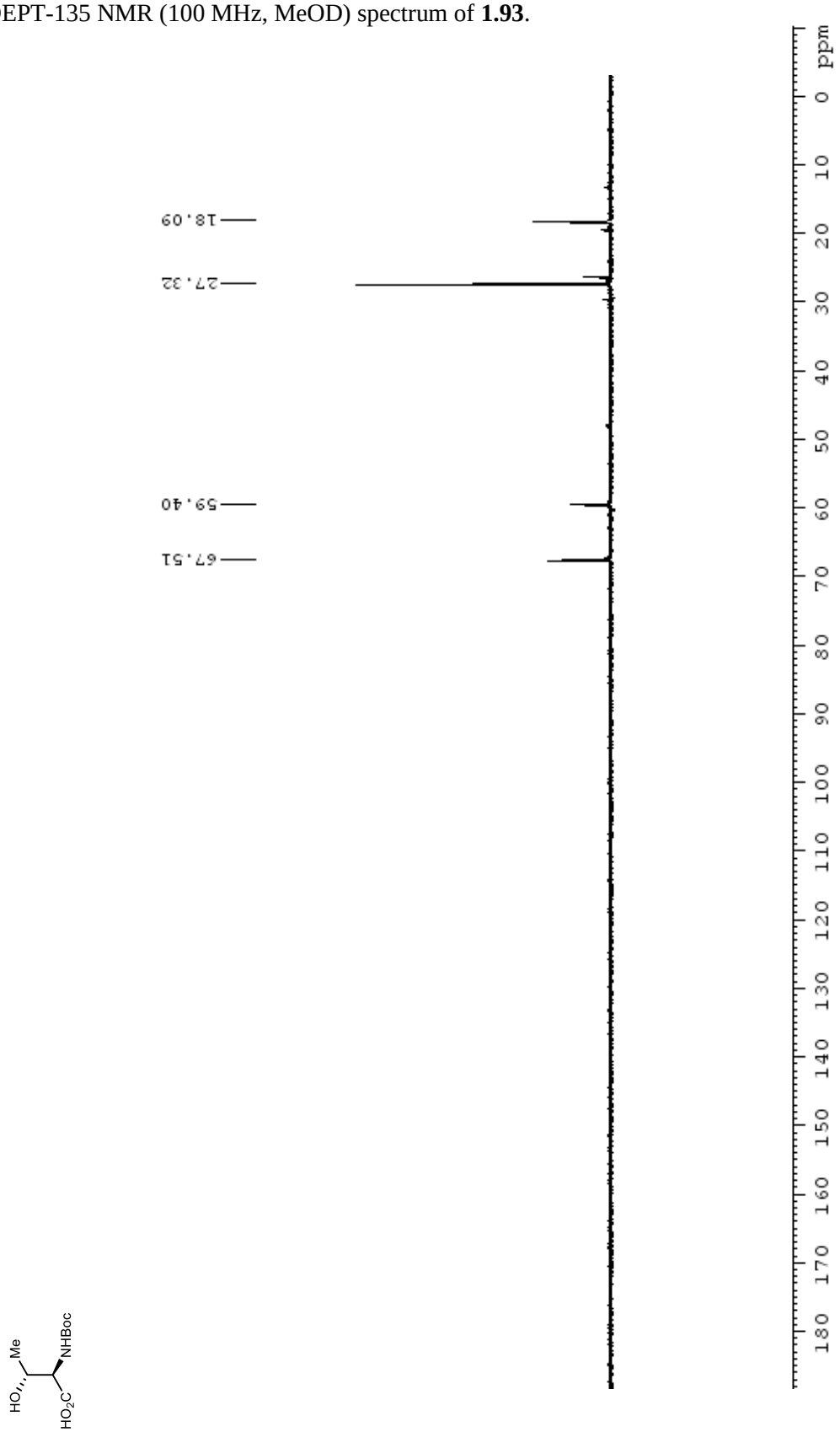

Figure 150. ^{1}H NMR (400 MHz, $CDCl_3$) spectrum of **1.107**.

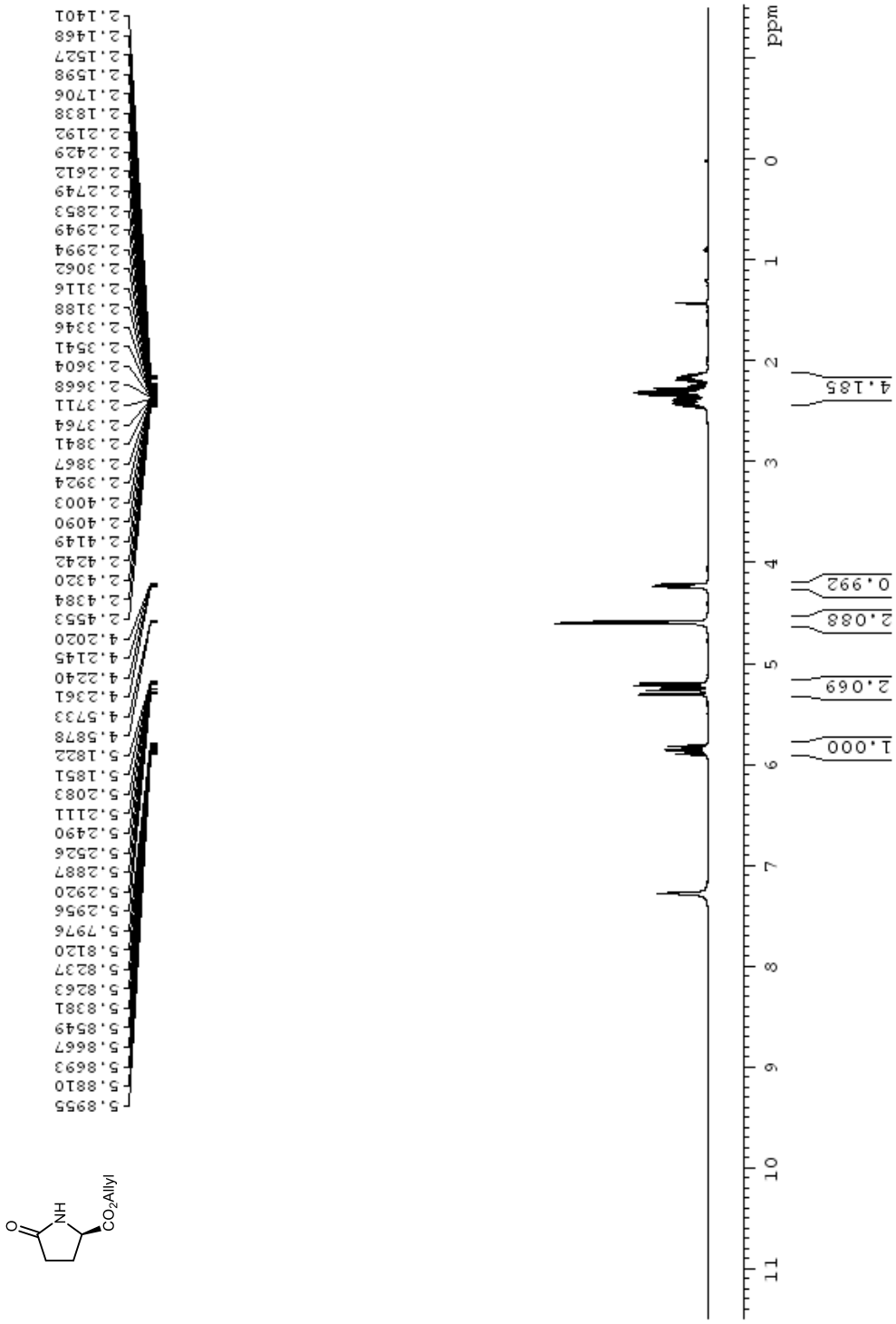

Figure 151. ^{13}C NMR (100 MHz, $CDCl_3$) spectra of **1.107**.

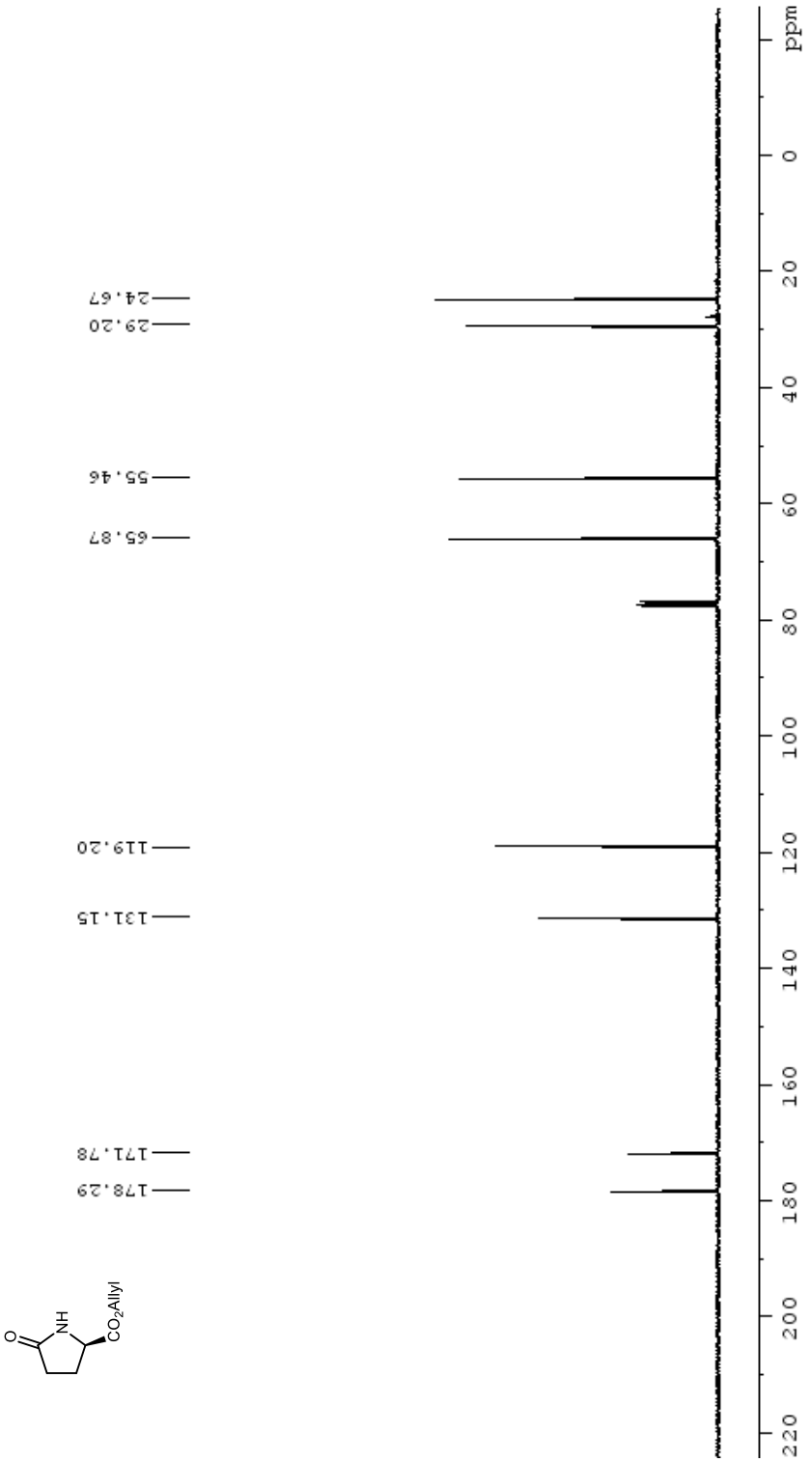

Figure 152. DEPT-135 NMR (100 MHz, $CDCl_3$) spectra of **1.107**.

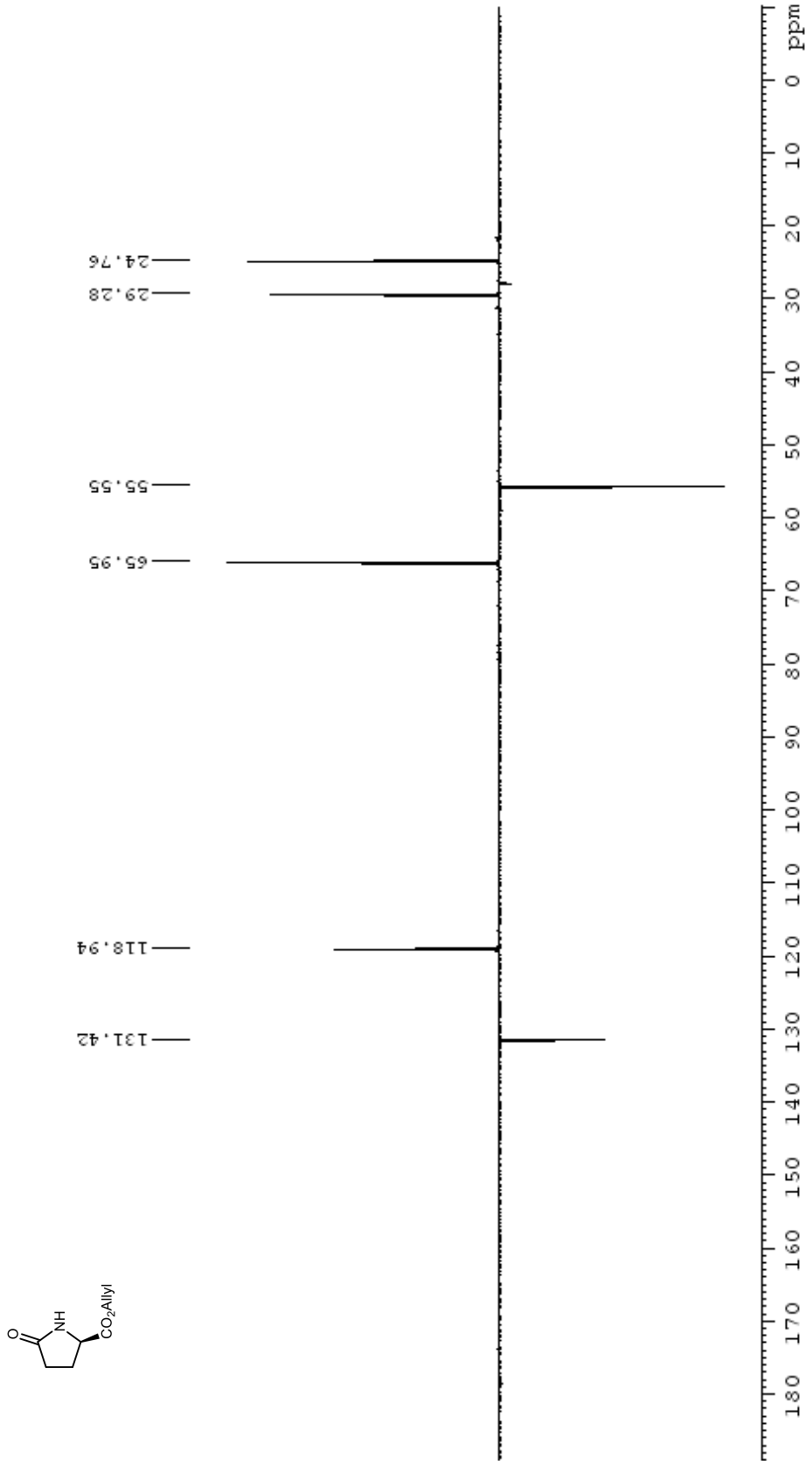

Figure 153. ^{1}H NMR (400 MHz, $CDCl_3$) spectrum of **1.108**.

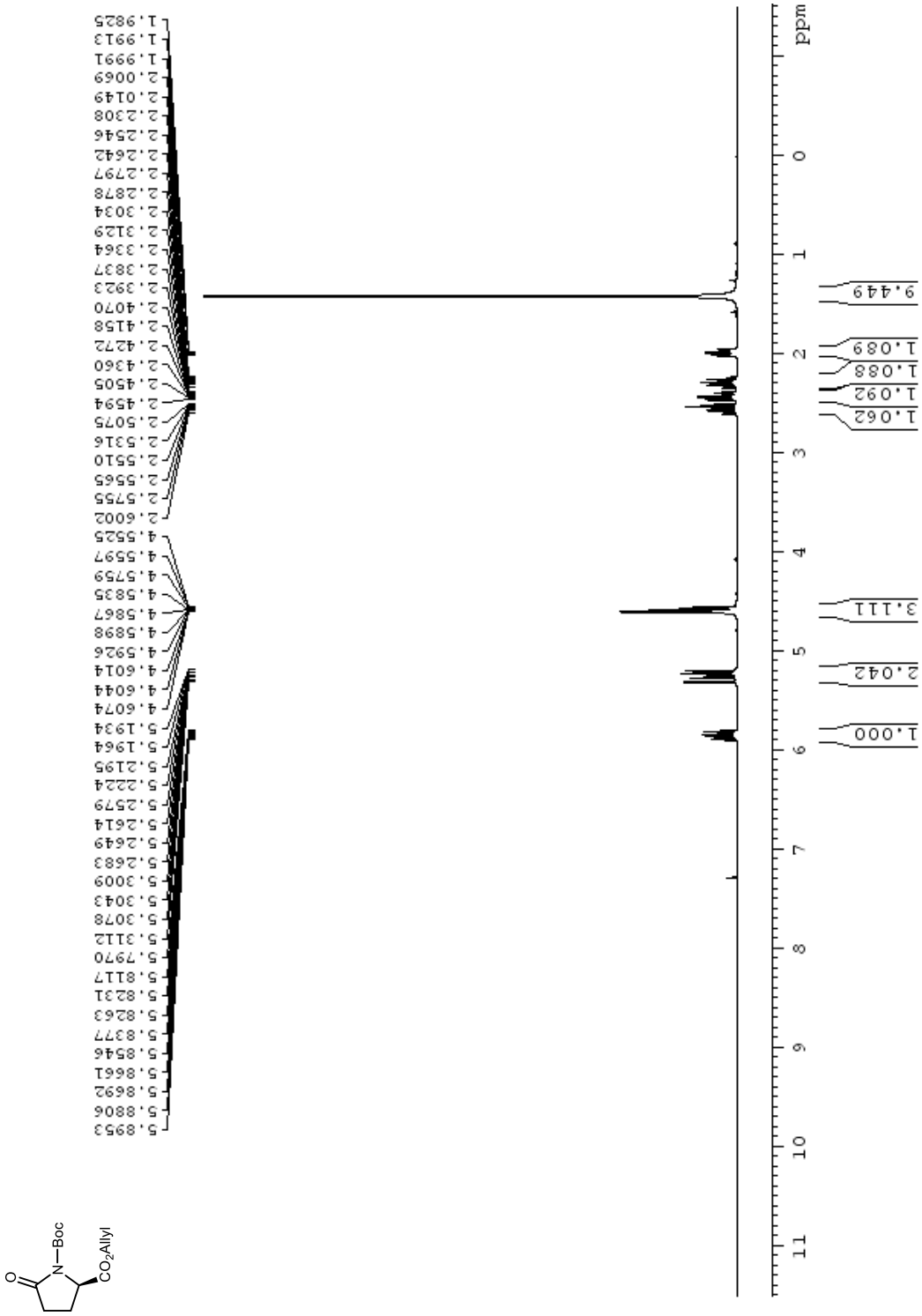

Figure 154. ^{13}C NMR (100 MHz, $CDCl_3$) spectra of **1.108**.

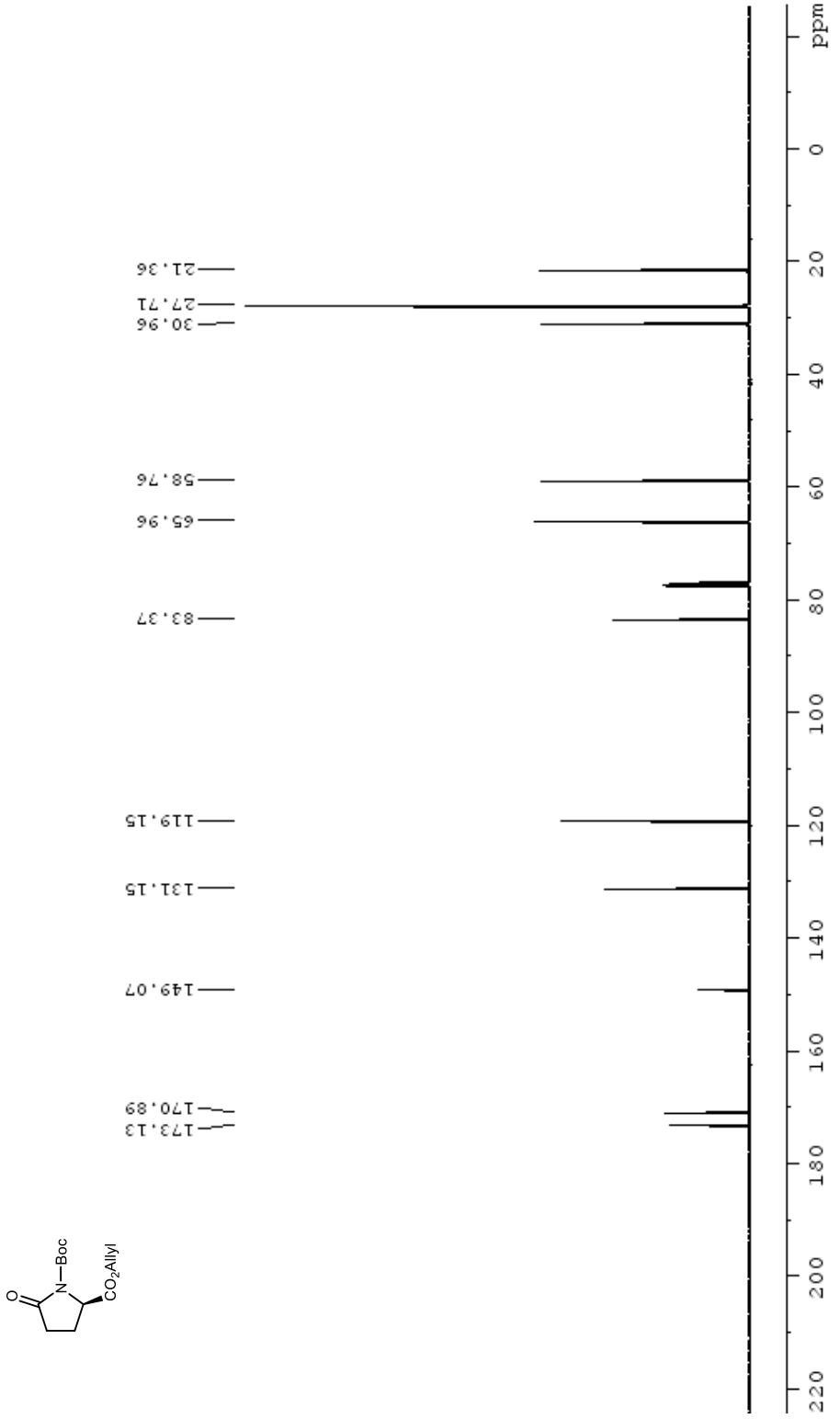

Figure 155. DEPT-135 NMR (100 MHz, $CDCl_3$) spectra of **1.108**.

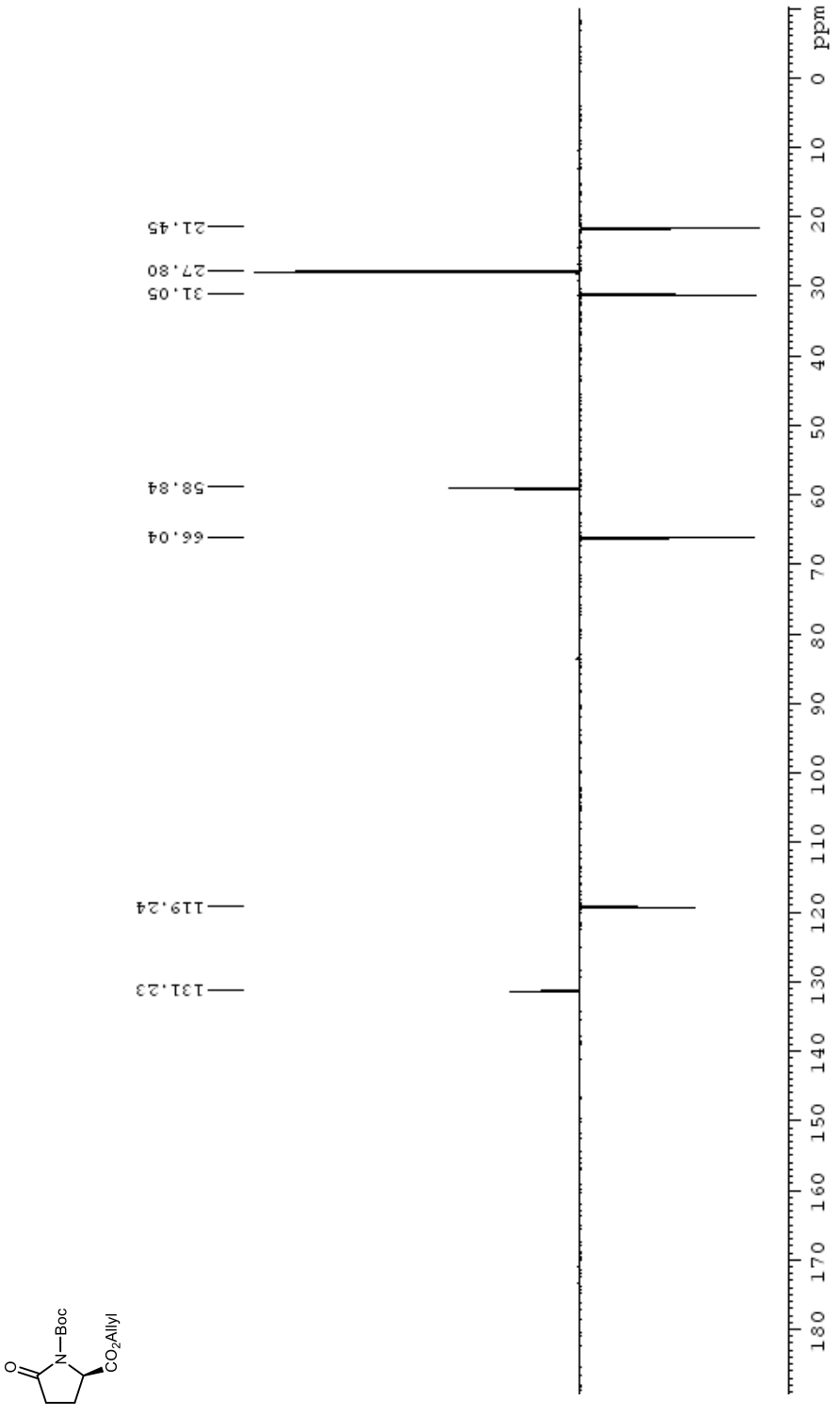

Figure 156. ^{1}H NMR (400 MHz, $CDCl_3$) spectrum of **1.109**.

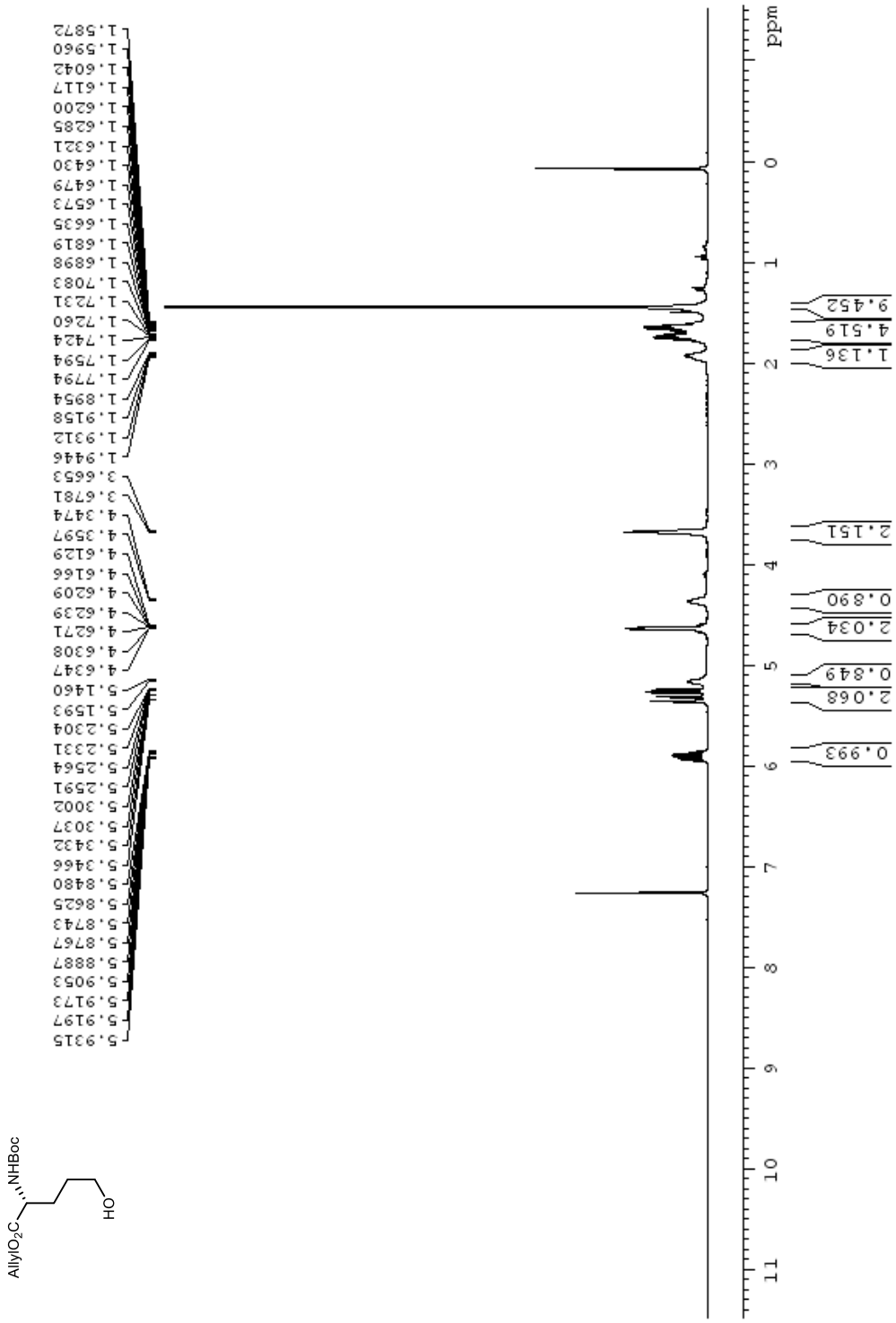

Figure 157. ^{13}C NMR (100 MHz, $CDCl_3$) spectra of **1.109**

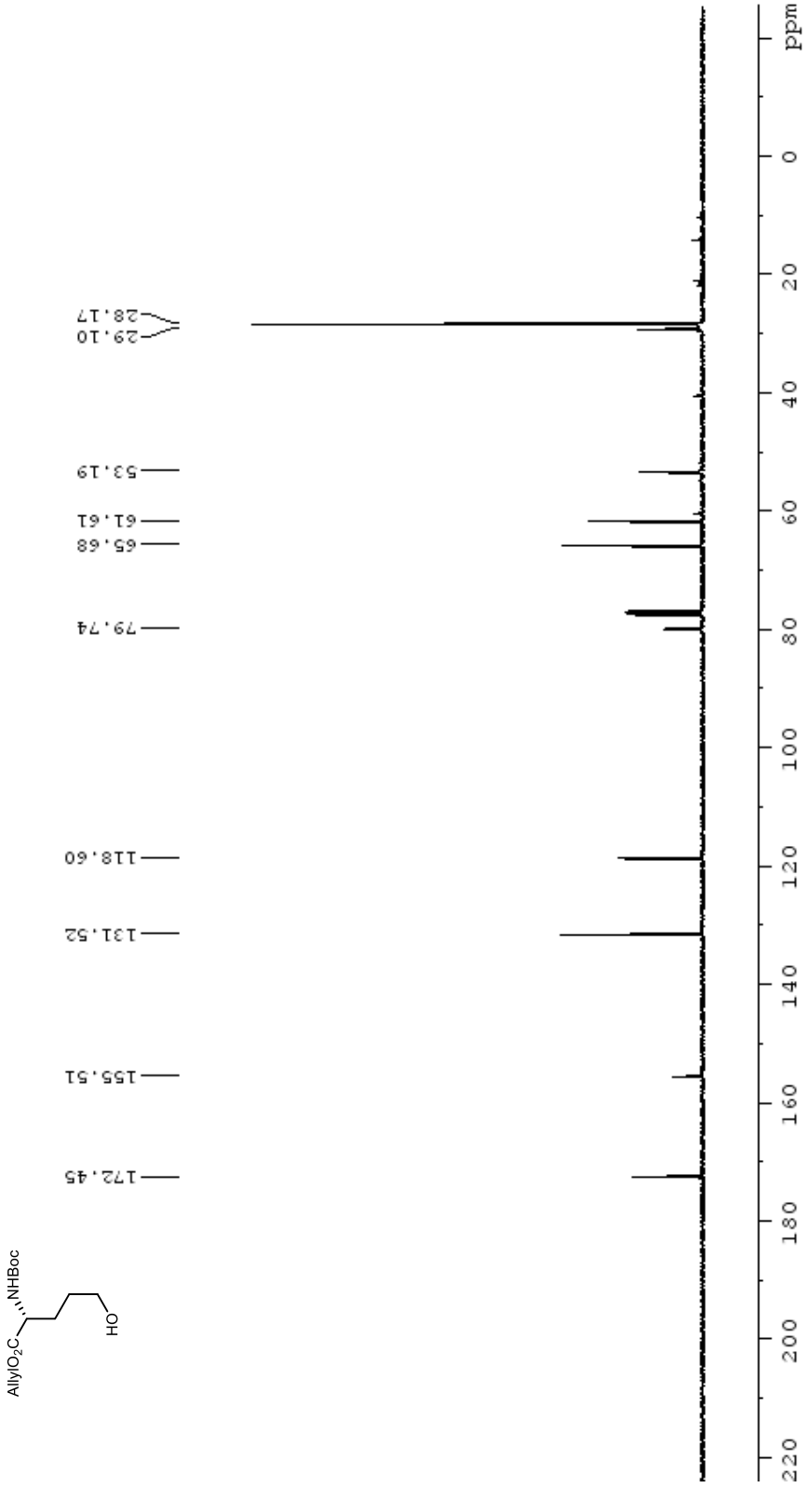

Figure 158. DEPT-135 NMR (100 MHz, $CDCl_3$) spectra of **1.109**.

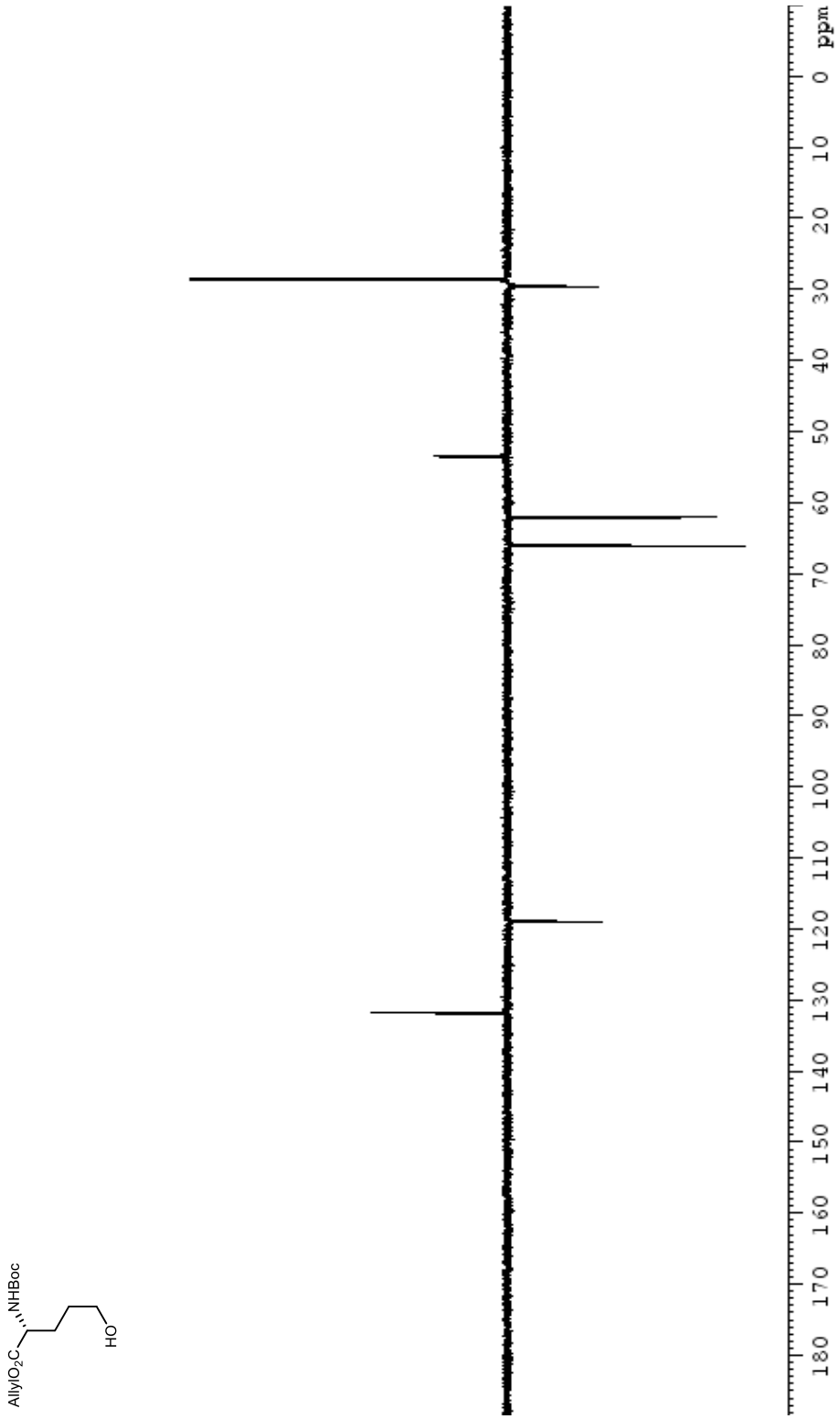

Figure 159. ^{1}H NMR (400 MHz, $CDCl_3$) spectrum of **1.111**.

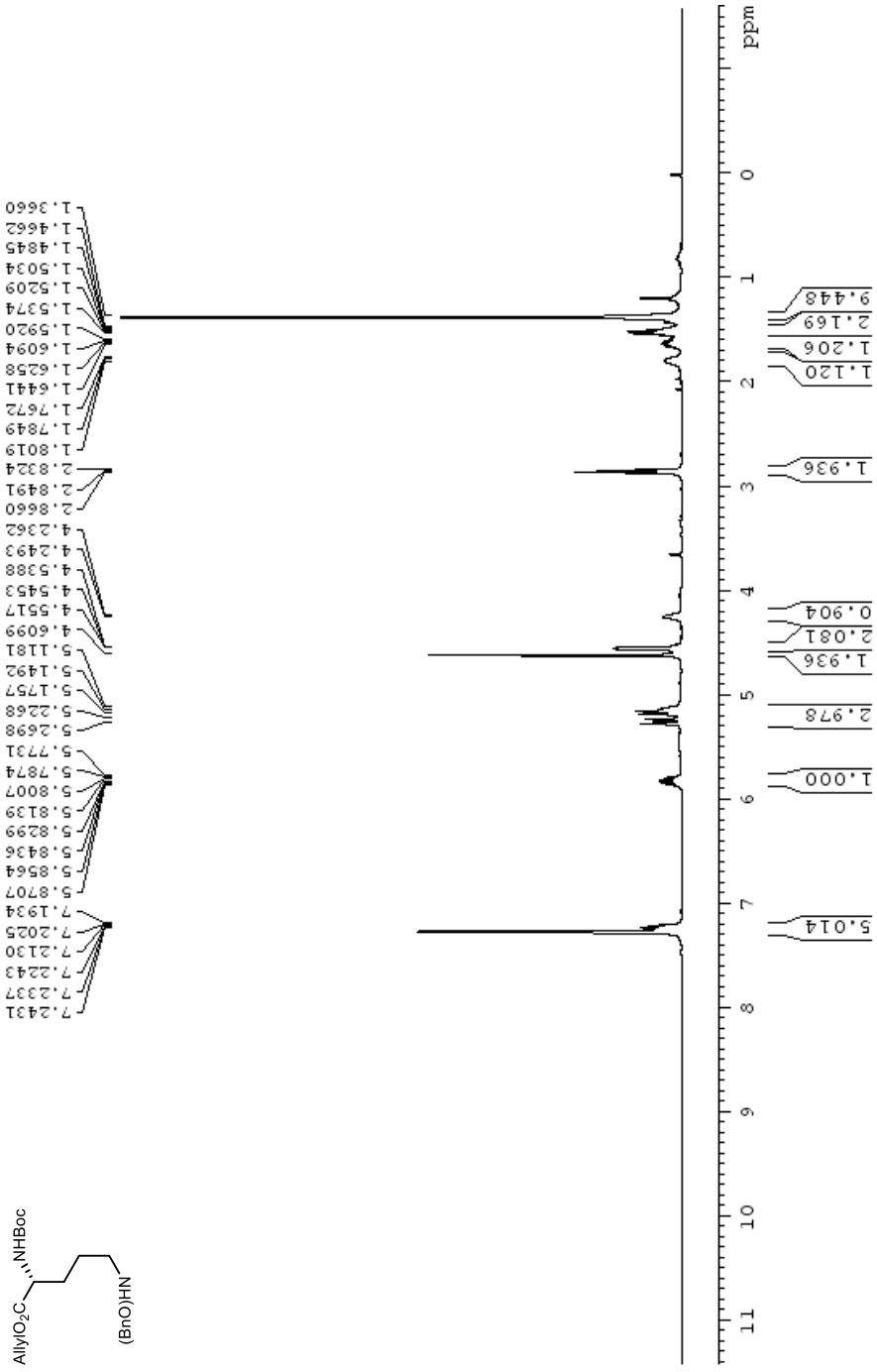

Figure 160. ^{13}C NMR (100 MHz, $CDCl_3$) spectra of **1.111**.

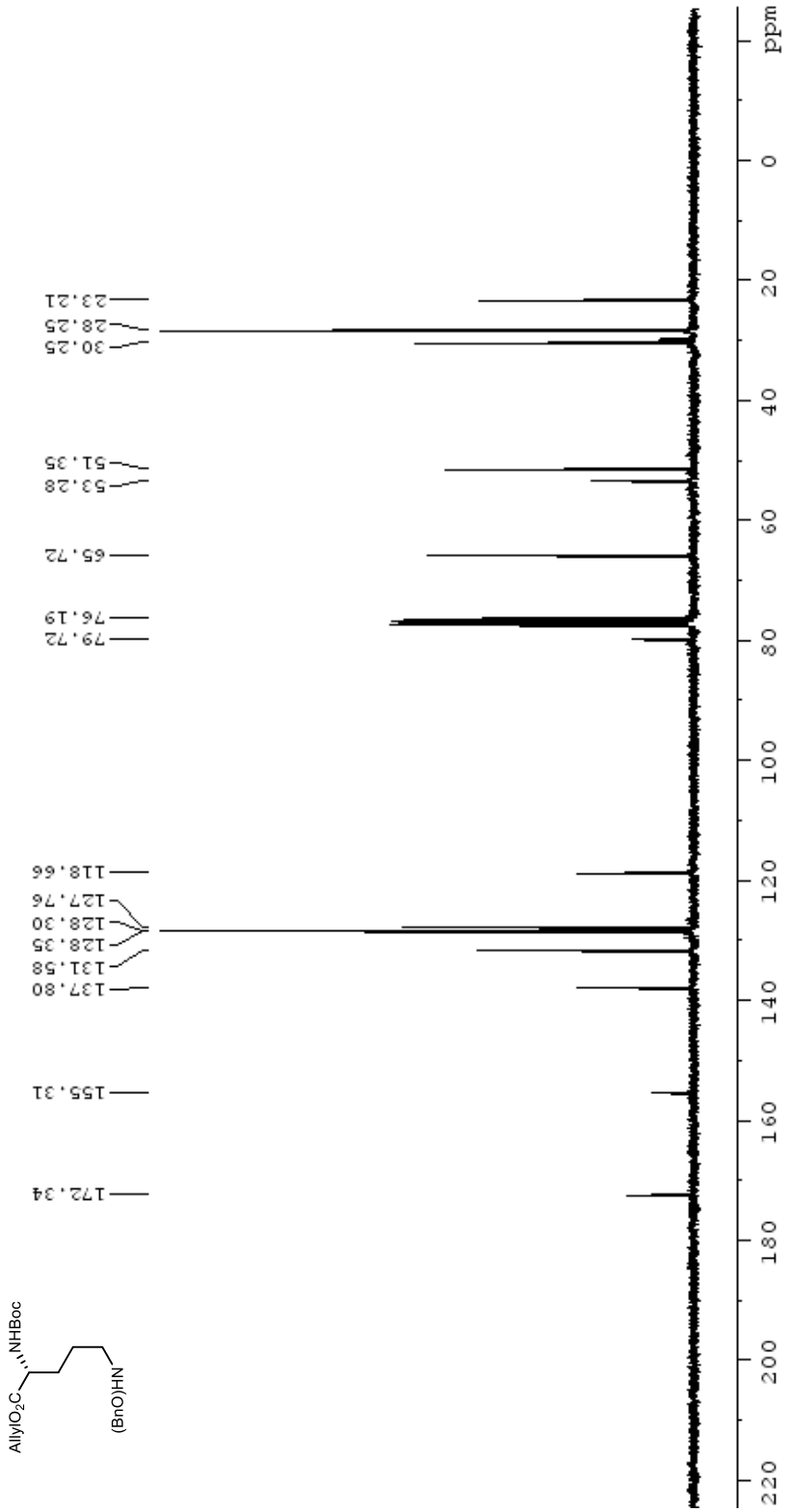

Figure 161. DEPT-135 NMR (100 MHz, $CDCl_3$) spectra of **1.111**.

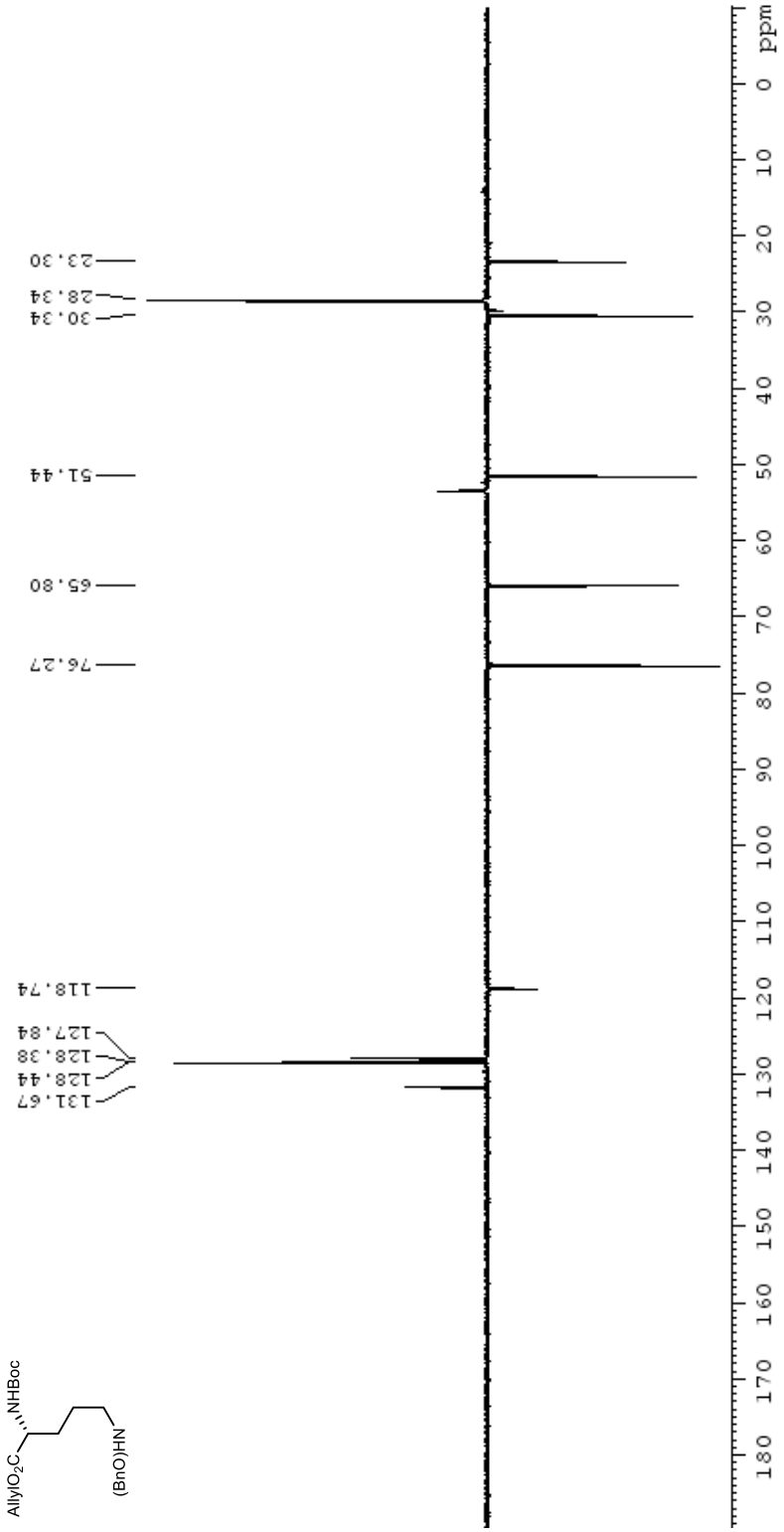

Figure 162. ^{1}H NMR (400 MHz, $CDCl_3$) spectrum of **1.112**.

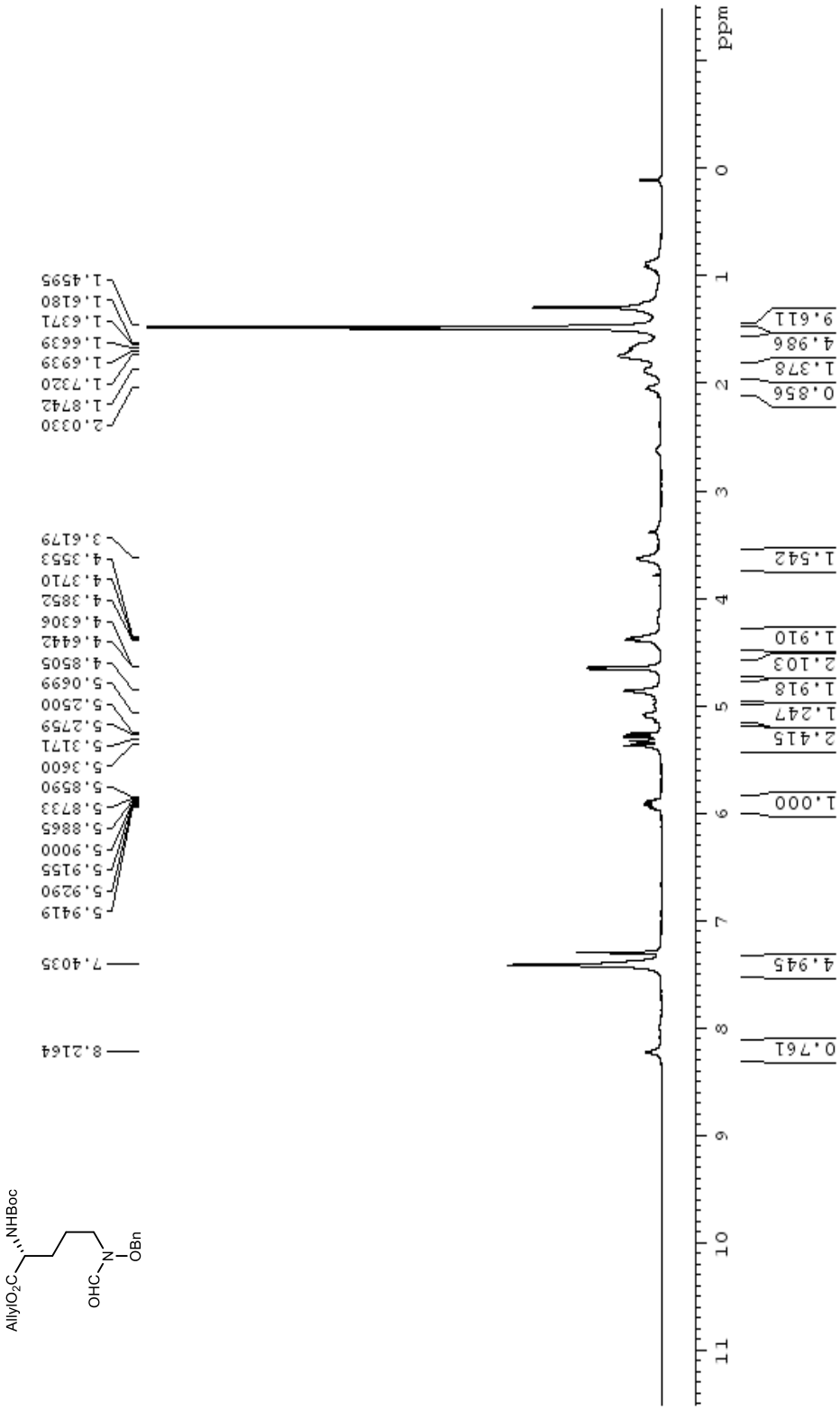

Figure 163. ^{13}C NMR (100 MHz, $CDCl_3$) spectra of **1.112**.

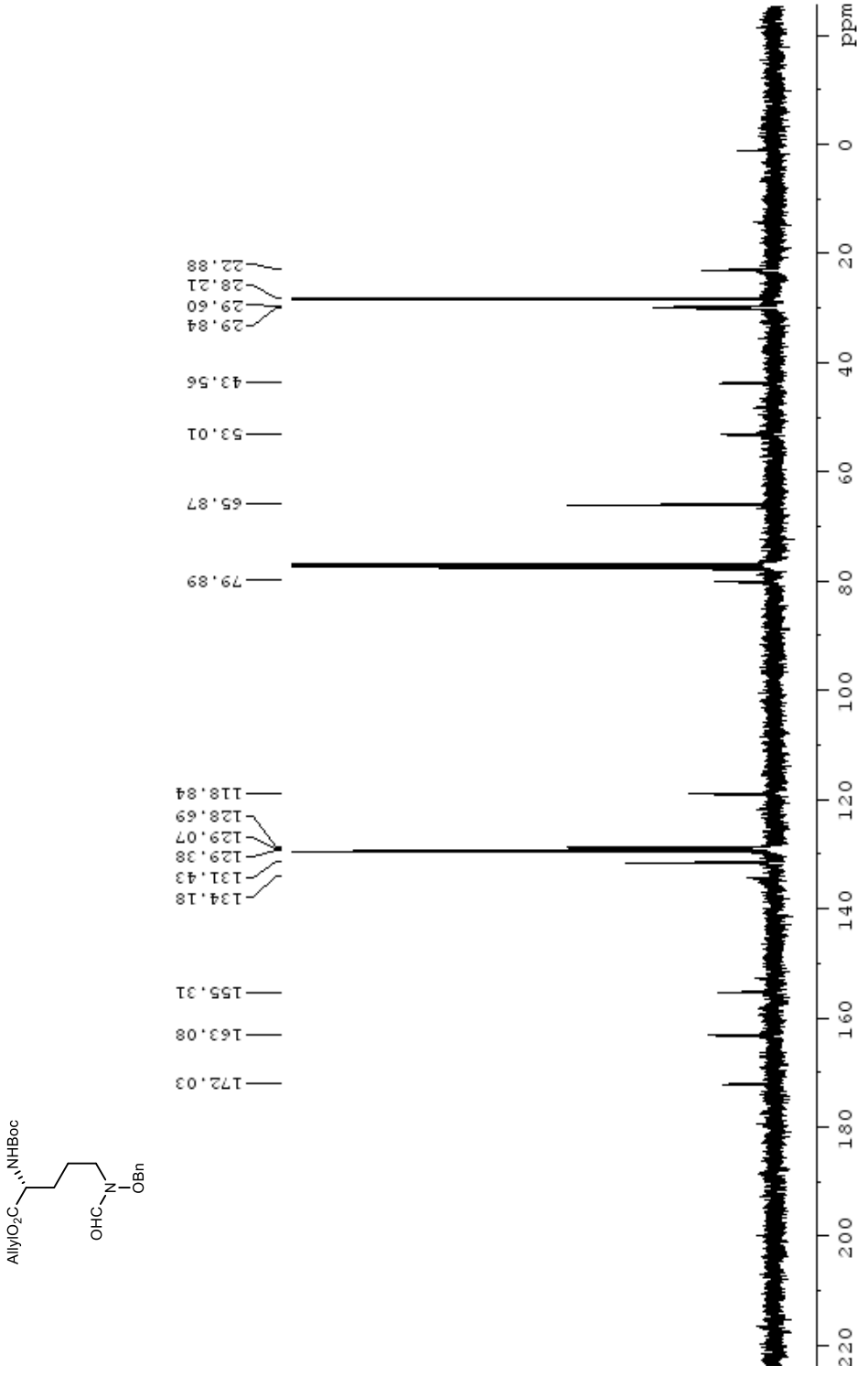

Figure 164. DEPT-135 NMR (100 MHz, $CDCl_3$) spectra of **1.112**.

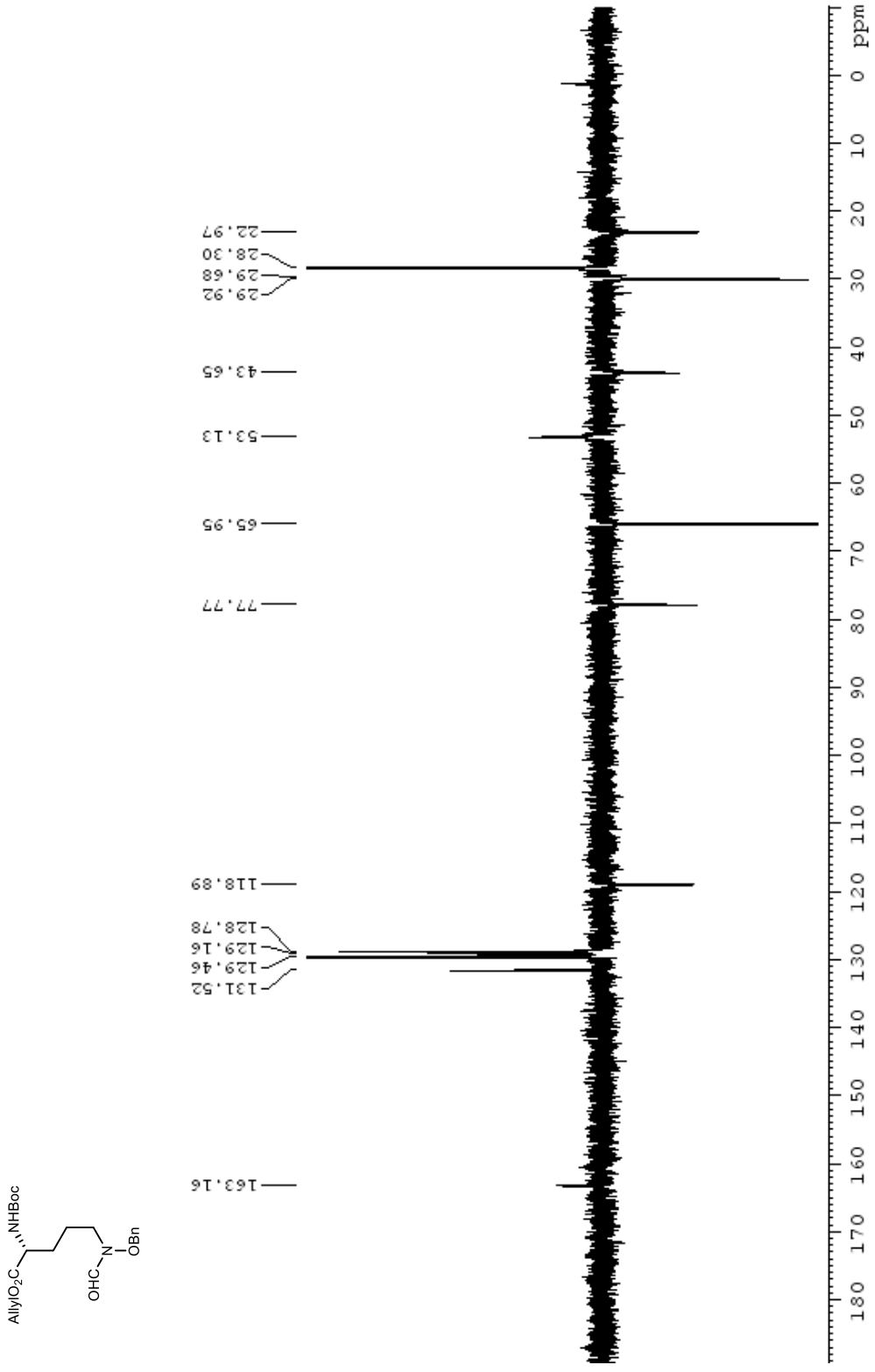

Figure 165. ^{1}H NMR (600 MHz, MeOD) spectrum of **1.114**.

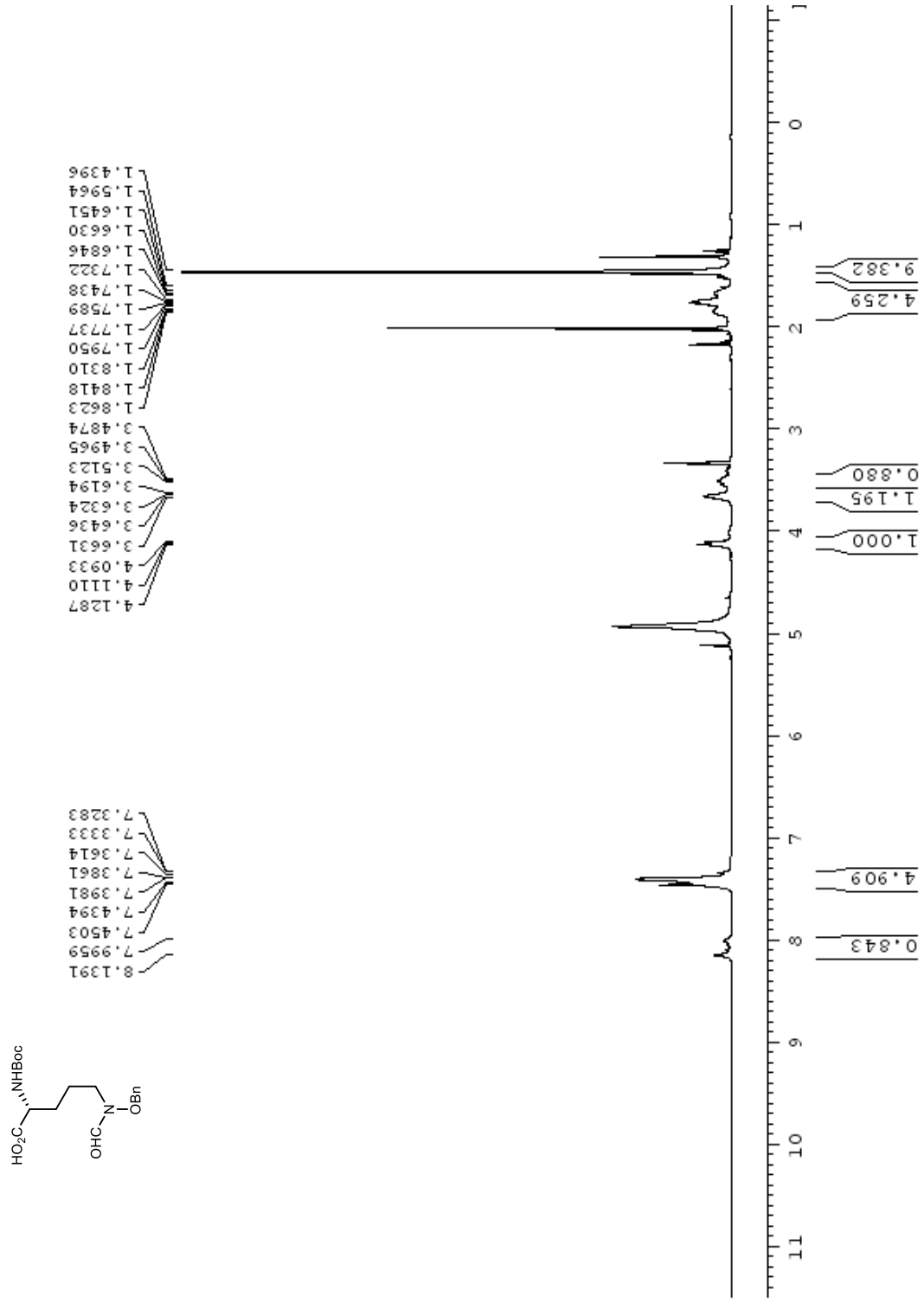

Figure 166. ^{13}C NMR (150 MHz, MeOD) spectrum of **X.X**.

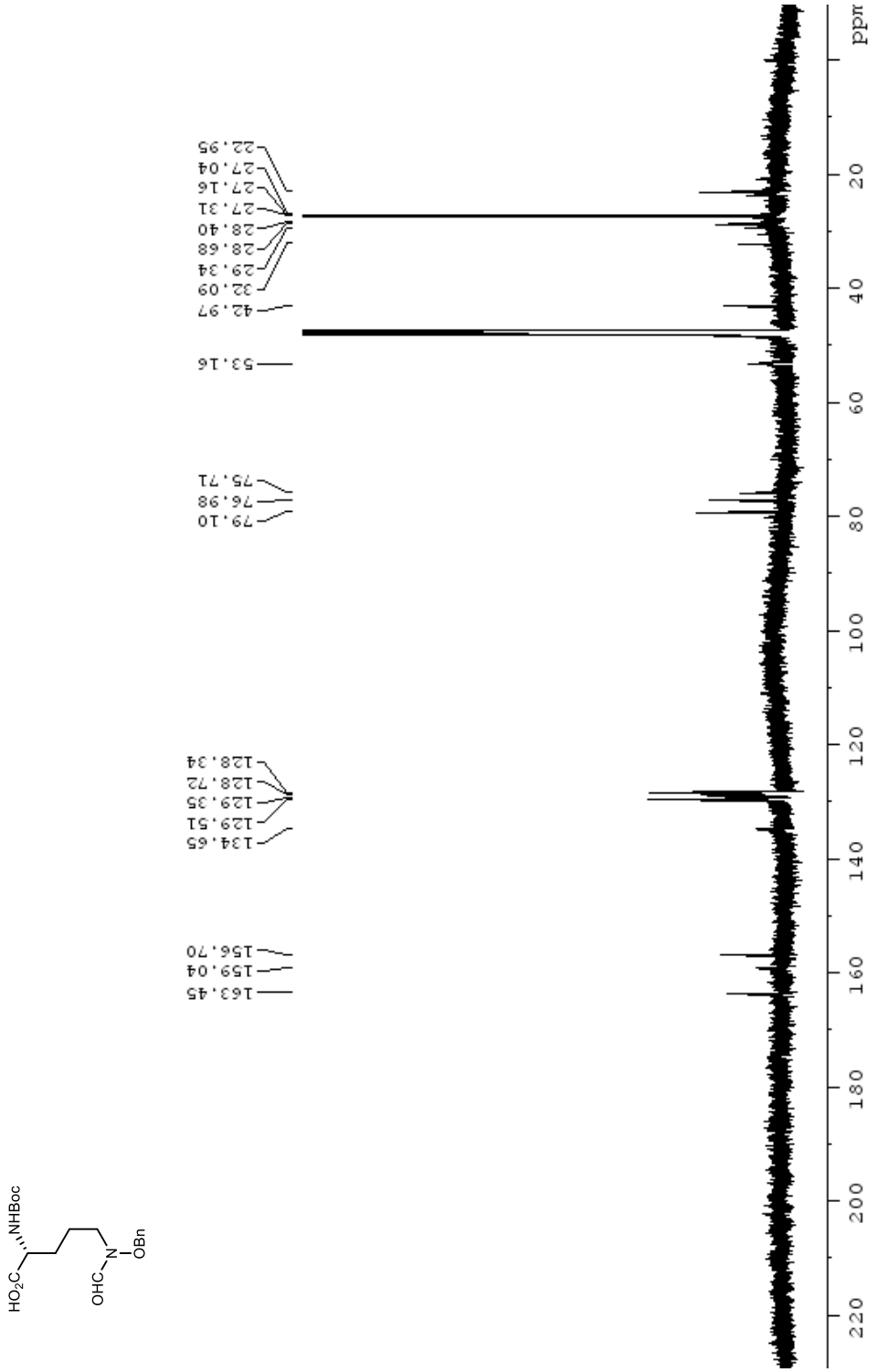

Figure 167. DEPT-135 NMR (150 MHz, MeOD) spectrum of **1.114**.

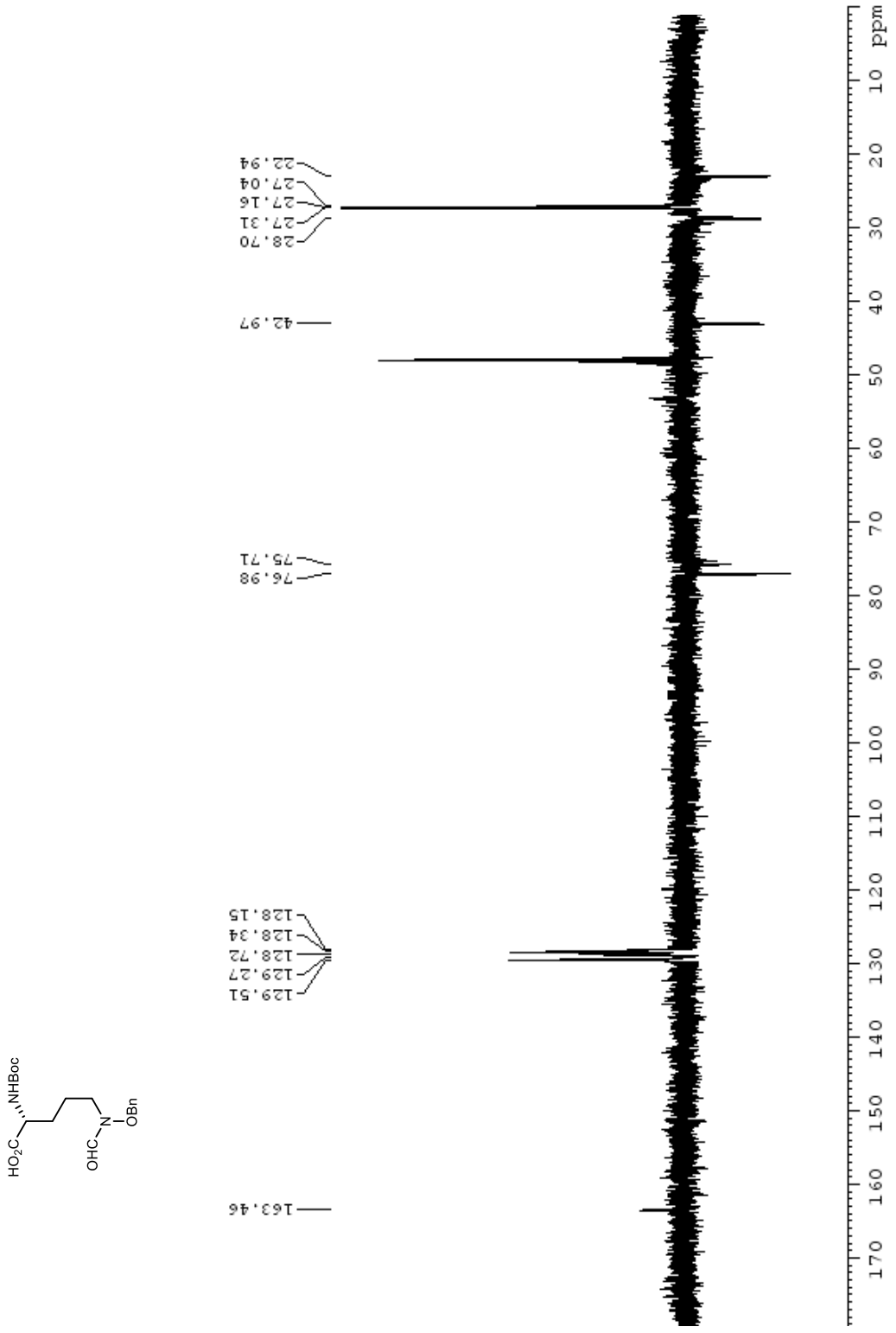

Figure 168. ^{1}H NMR (400 MHz, $CDCl_3$) spectrum of **1.113**.

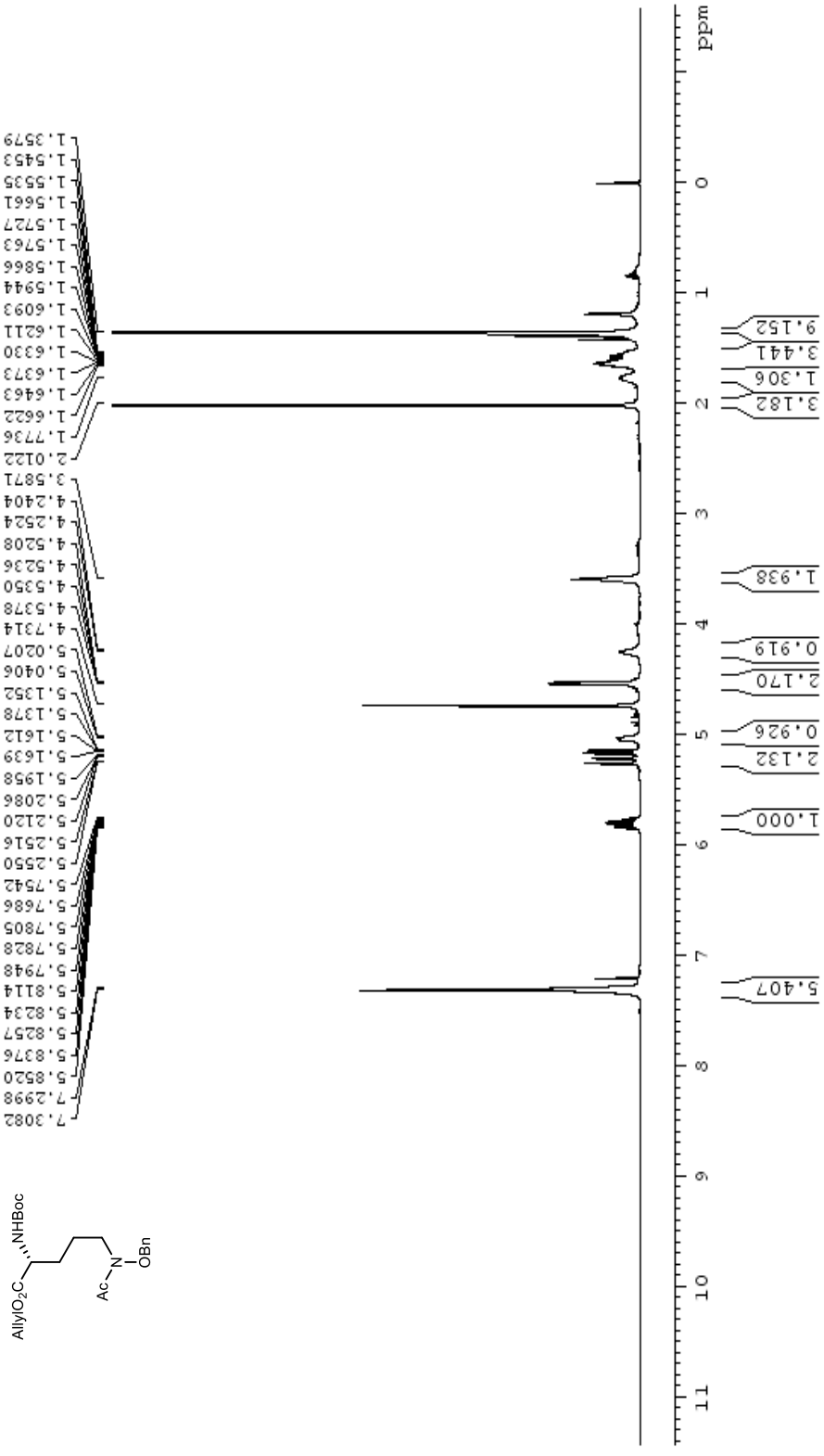

Figure 169. ^{13}C NMR (100 MHz, $CDCl_3$) spectra of **1.113**.

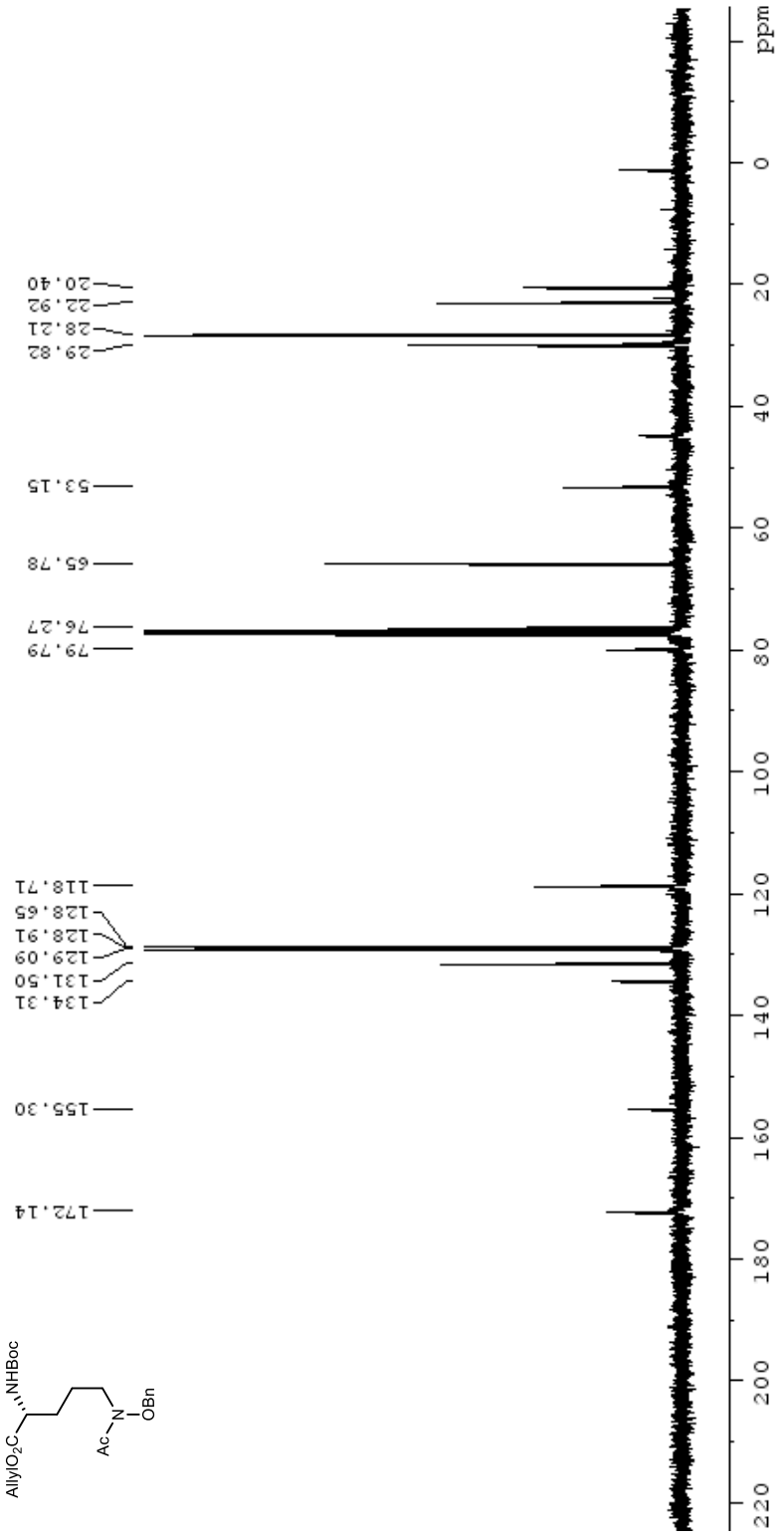

Figure 170. DEPT-135 NMR (100 MHz, $CDCl_3$) spectra of **1.113**.

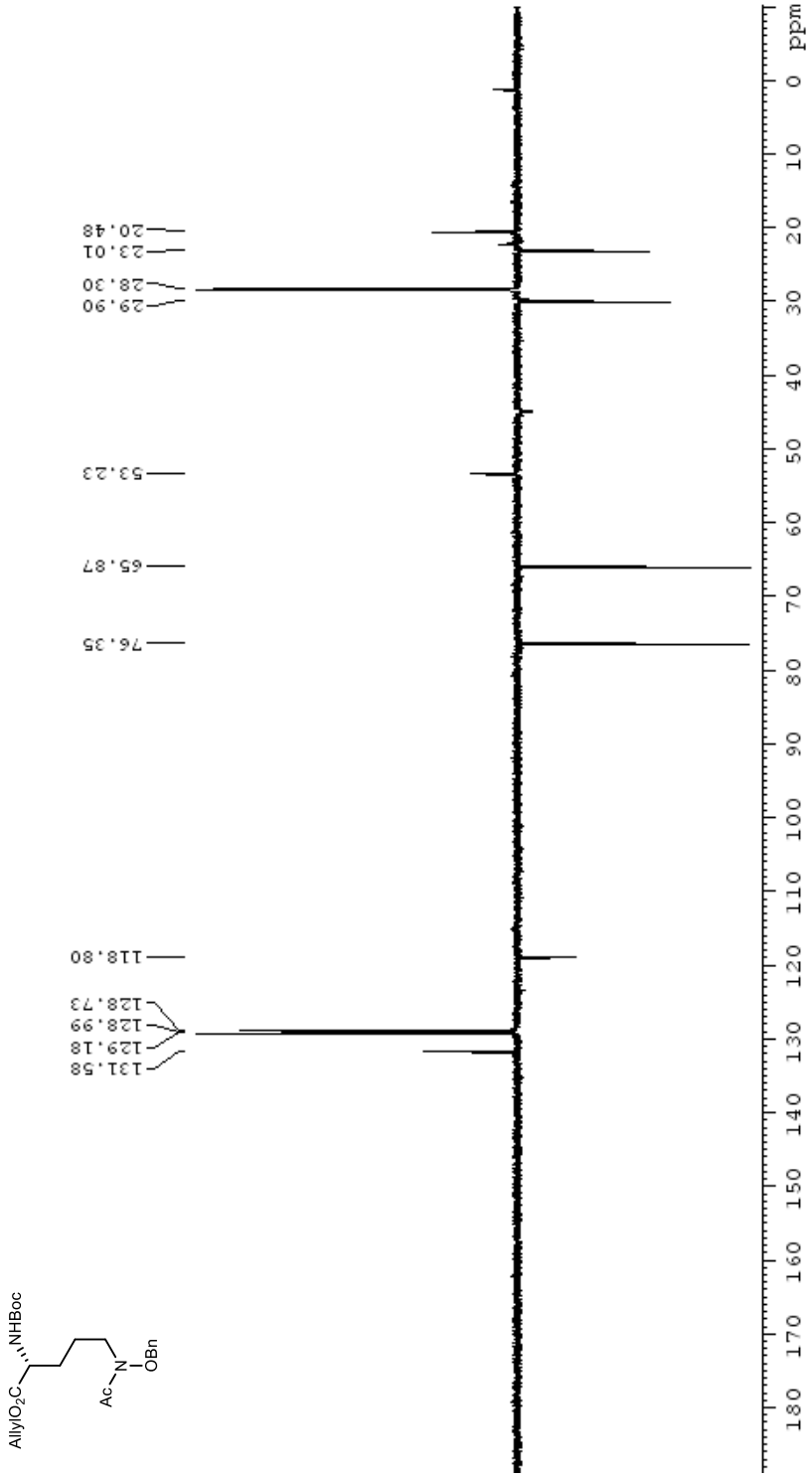

Figure 171. ^{1}H NMR (400 MHz, MeOD) spectrum of **1.115**.

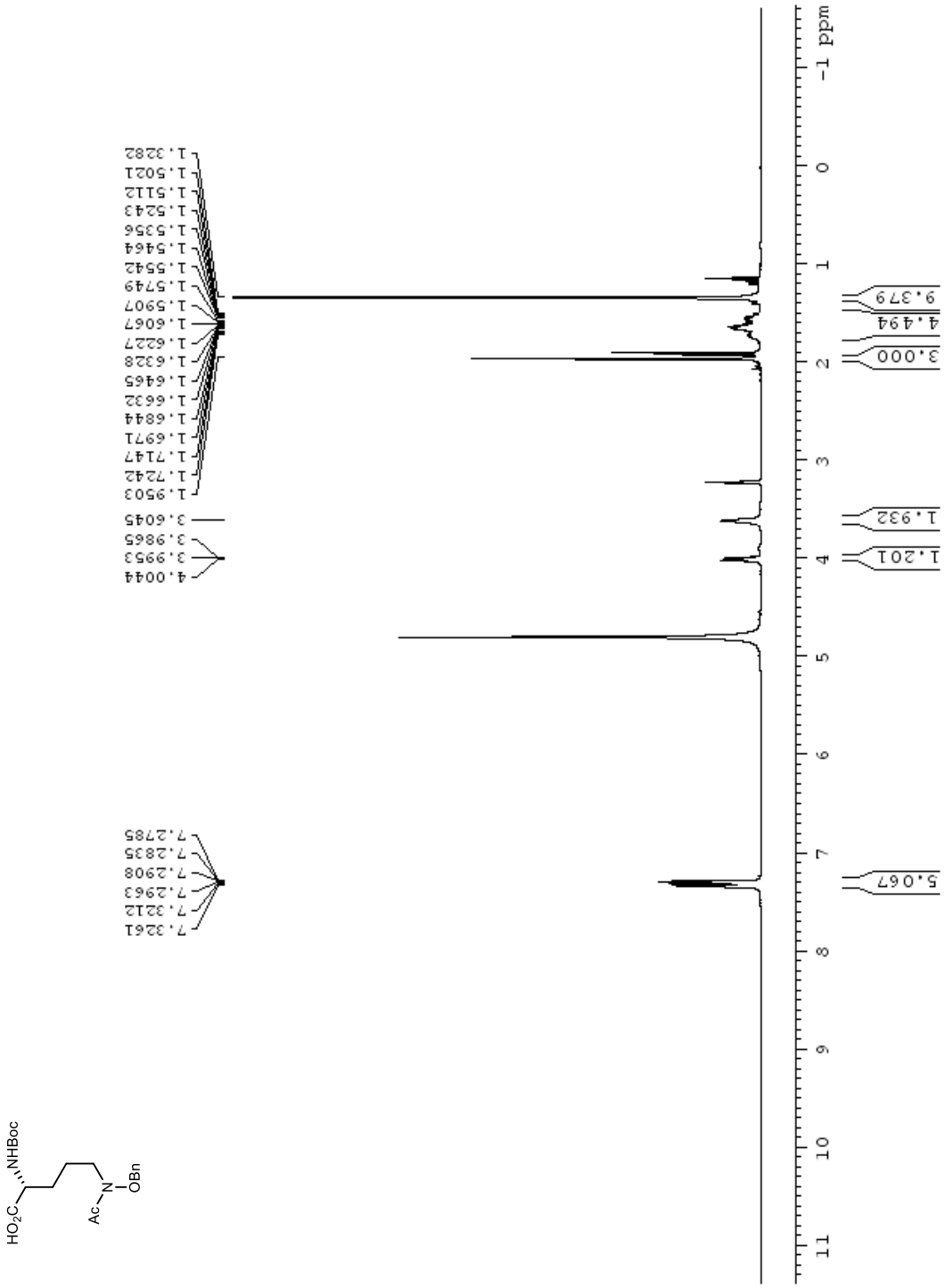

Figure 172. ^{13}C NMR (100 MHz, MeOD) spectrum of **1.115**.

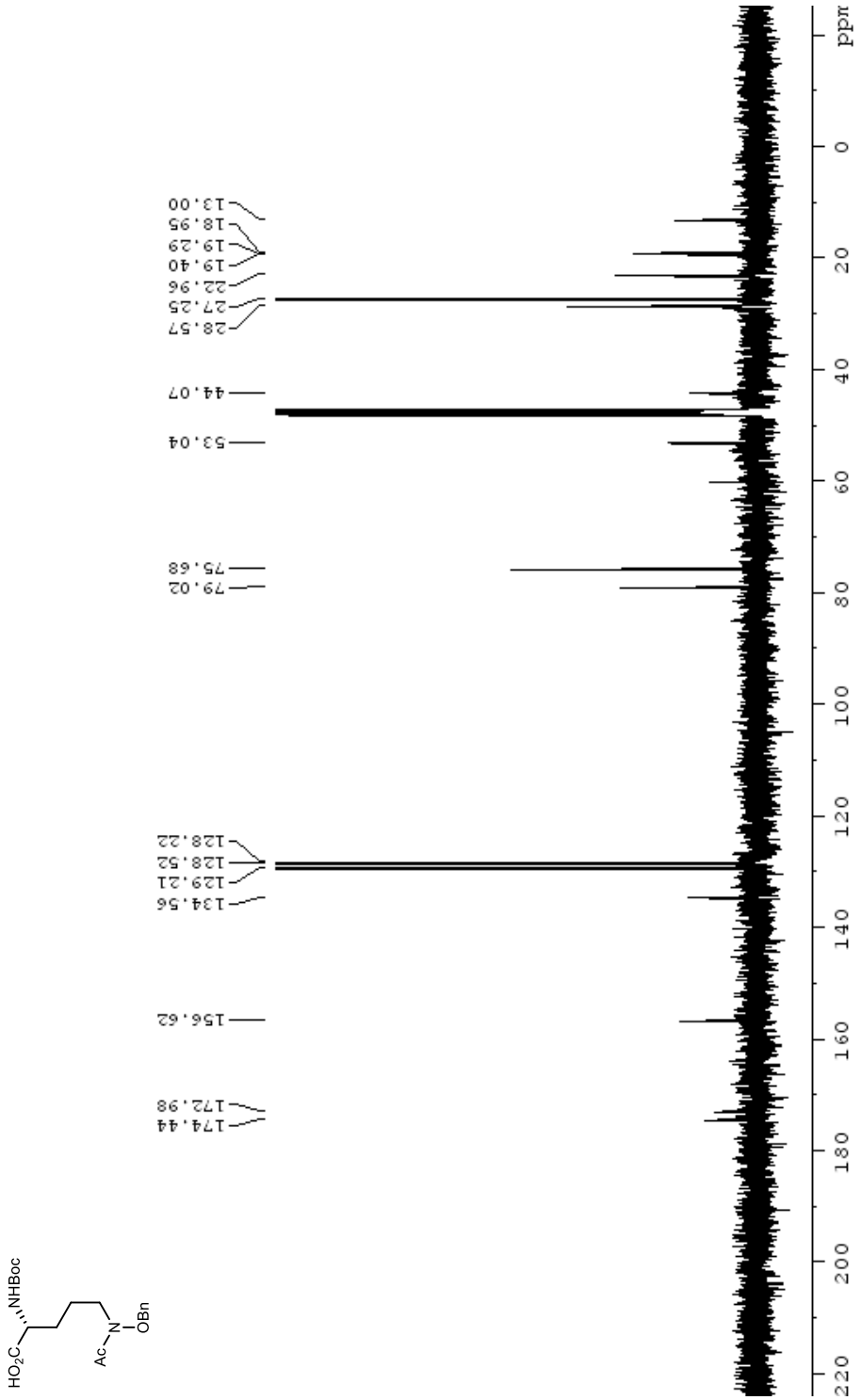

Figure 173. ^{1}H NMR (400 MHz, $CDCl_3$) spectrum of **1.116**.

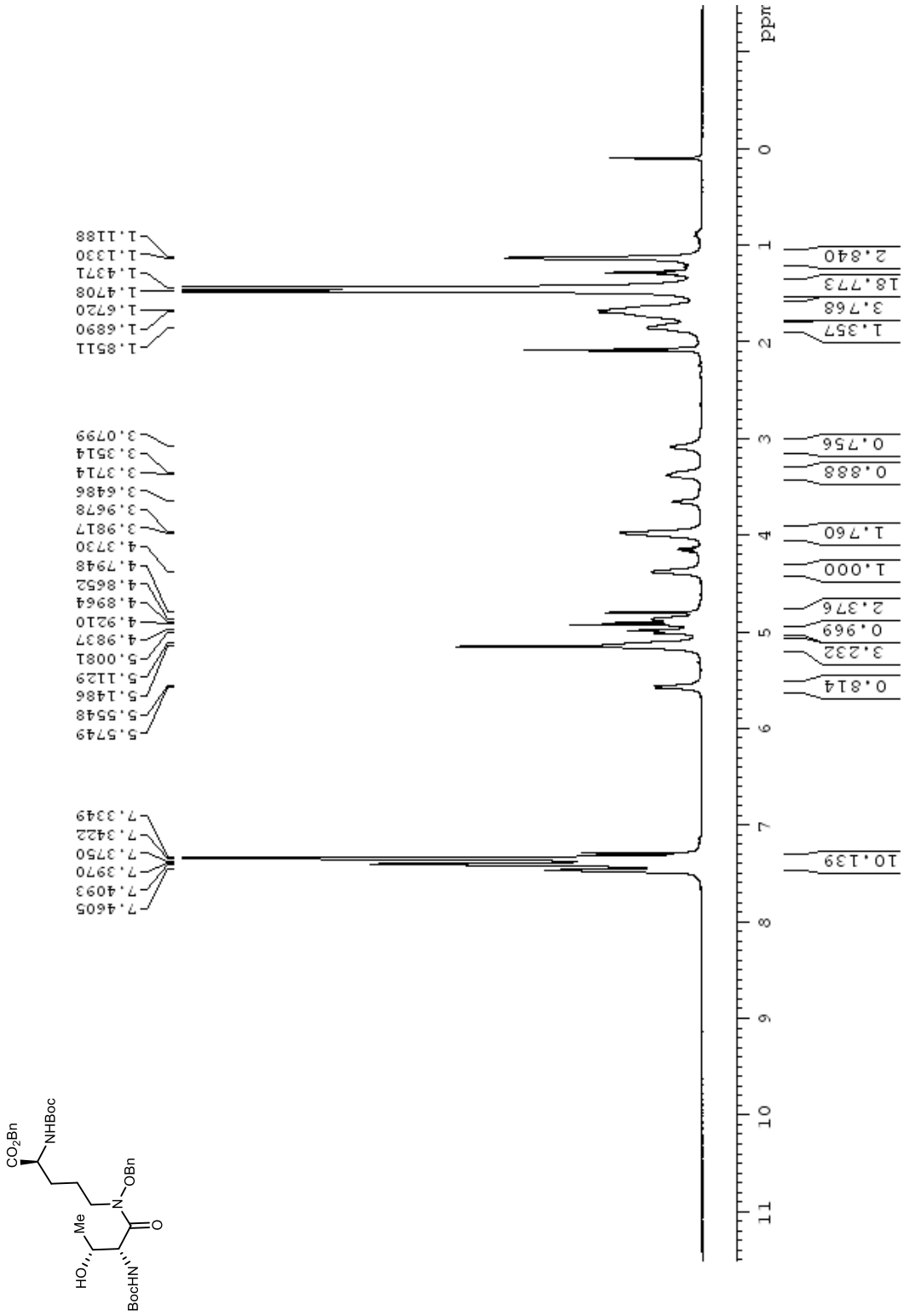

Figure 174. ^{13}C NMR (100 MHz, $CDCl_3$) spectra of **1.116**.

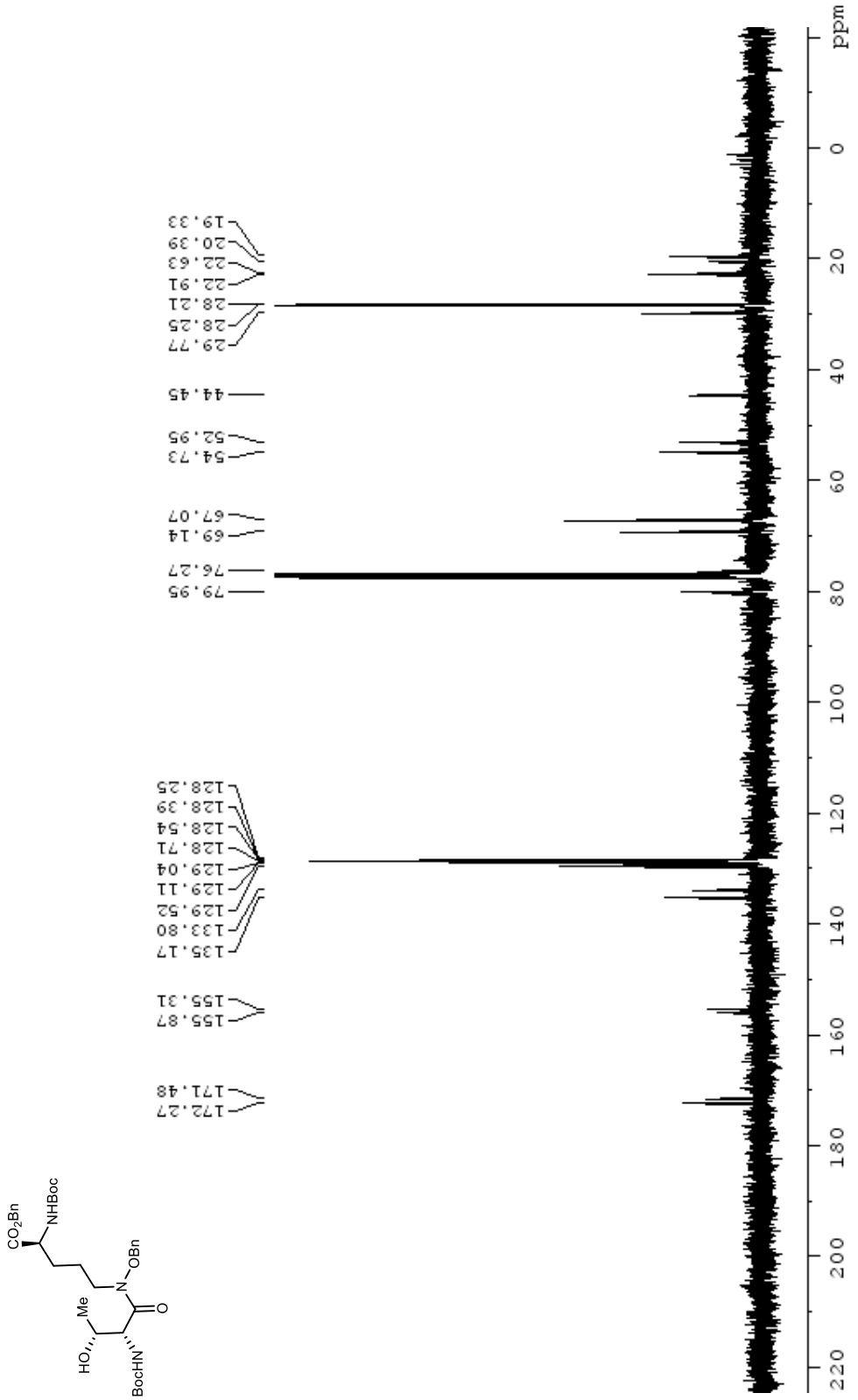

Figure 175. DEPT-135 NMR (100 MHz, $CDCl_3$) spectra of **1.116**.

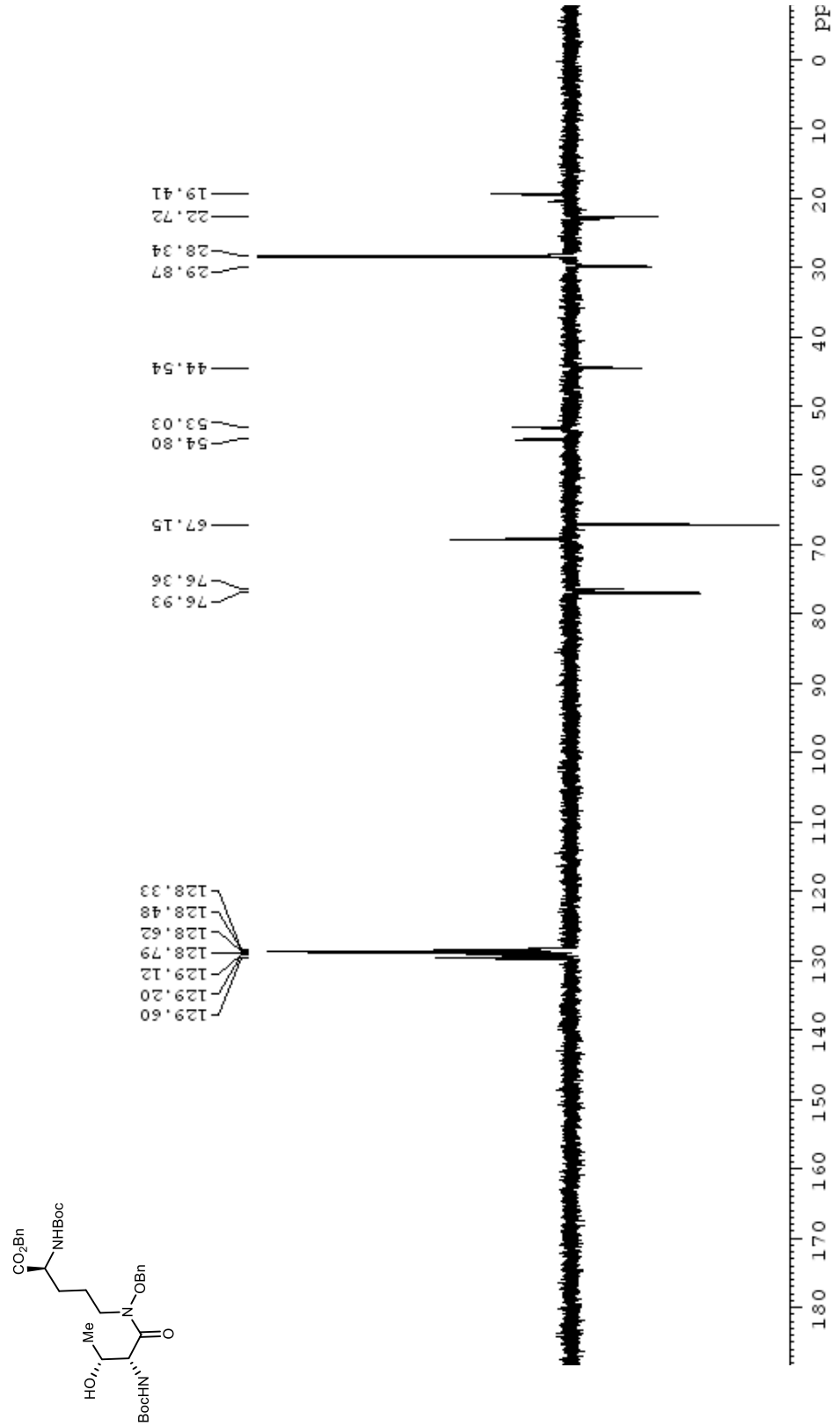

Figure 176. [1]H NMR (400 MHz, MeOD) spectrum of **1.117**.

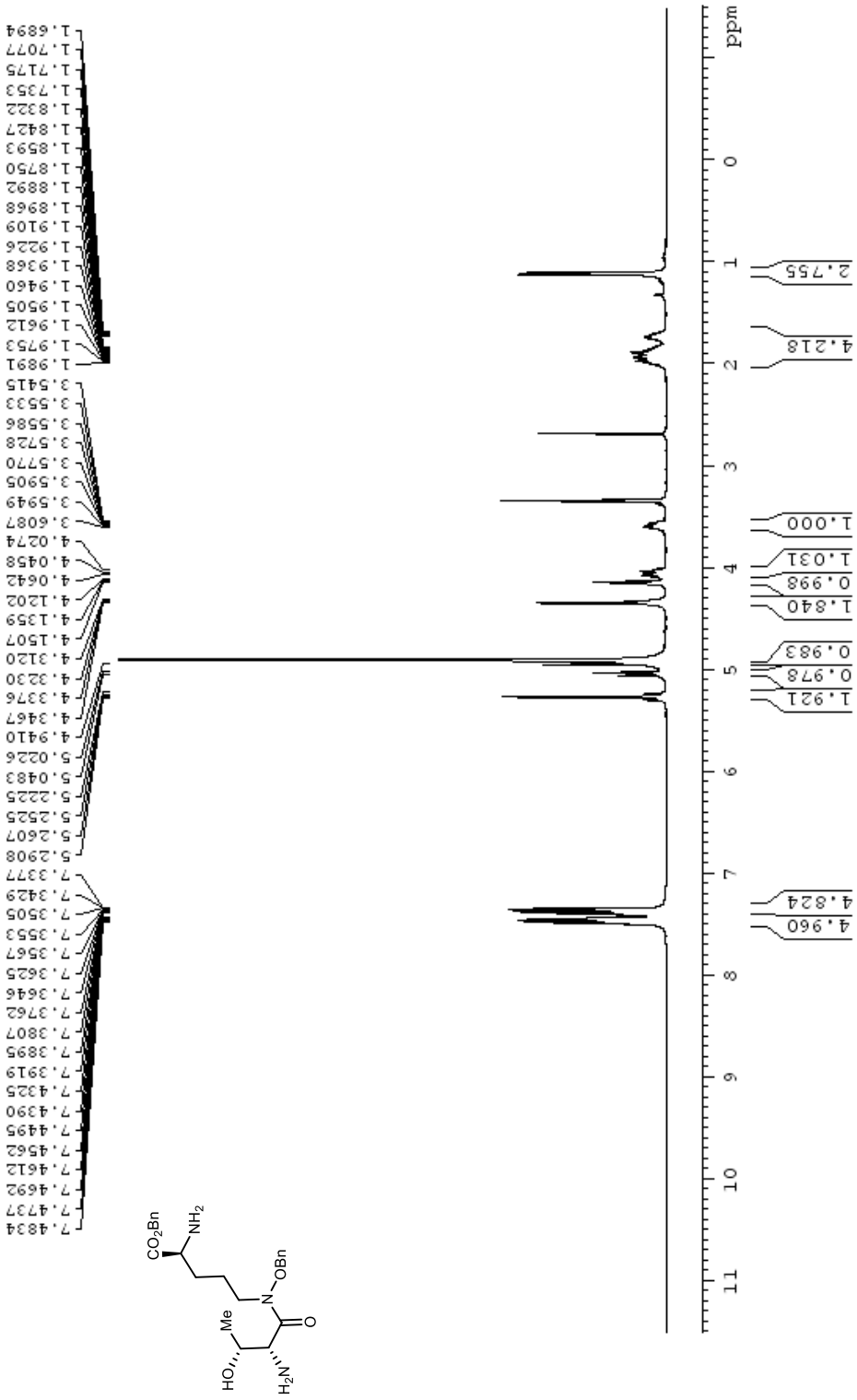

Figure 177. ^{13}C NMR (100 MHz, MeOD) spectrum of **1.117**.

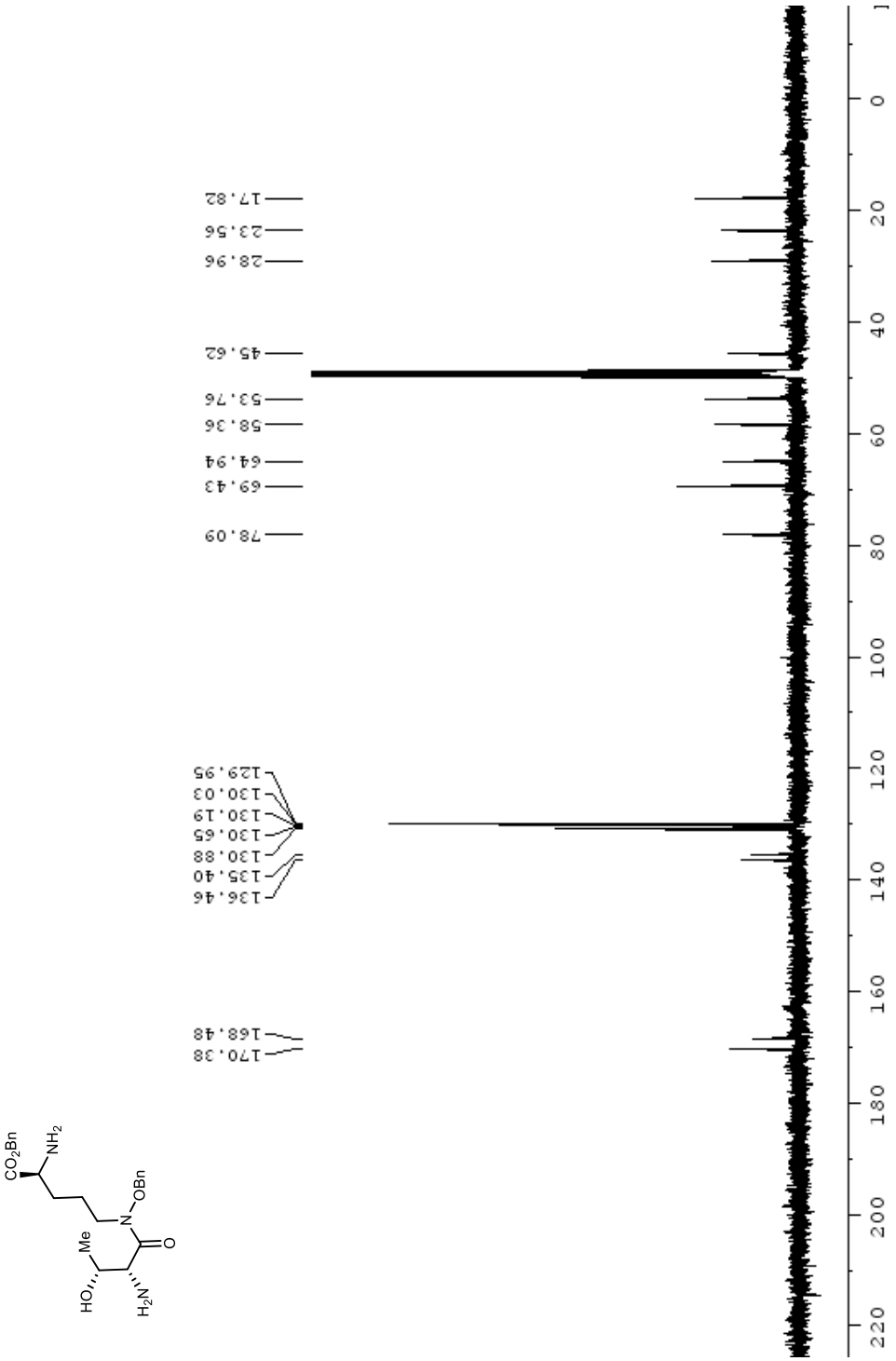

Figure 178. DEPT-135 NMR (100 MHz, MeOD) spectrum of **1.117**.

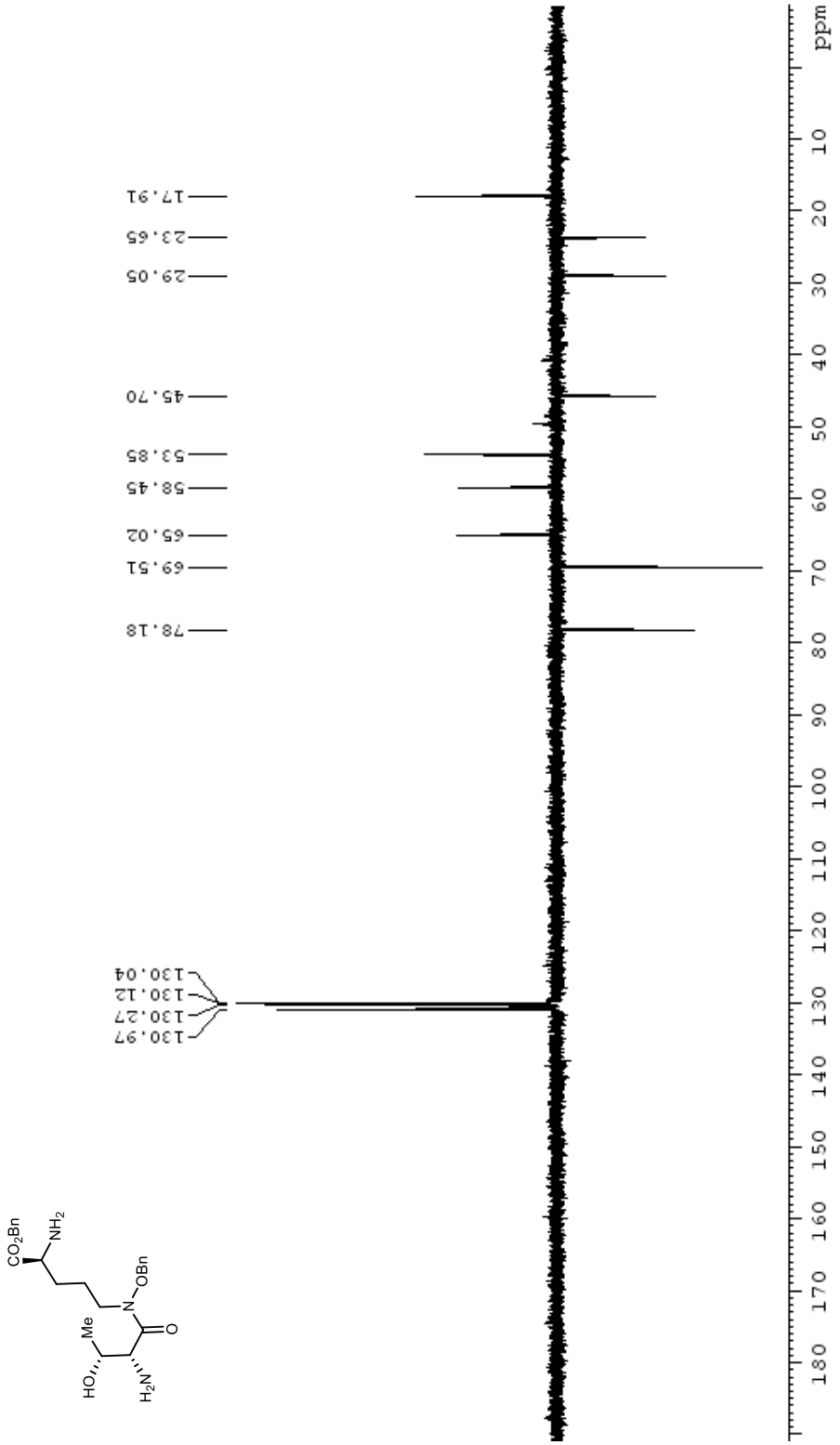

Figure 179. ^{1}H NMR (600 MHz, DMSO-d_6) spectrum of **1.118**.

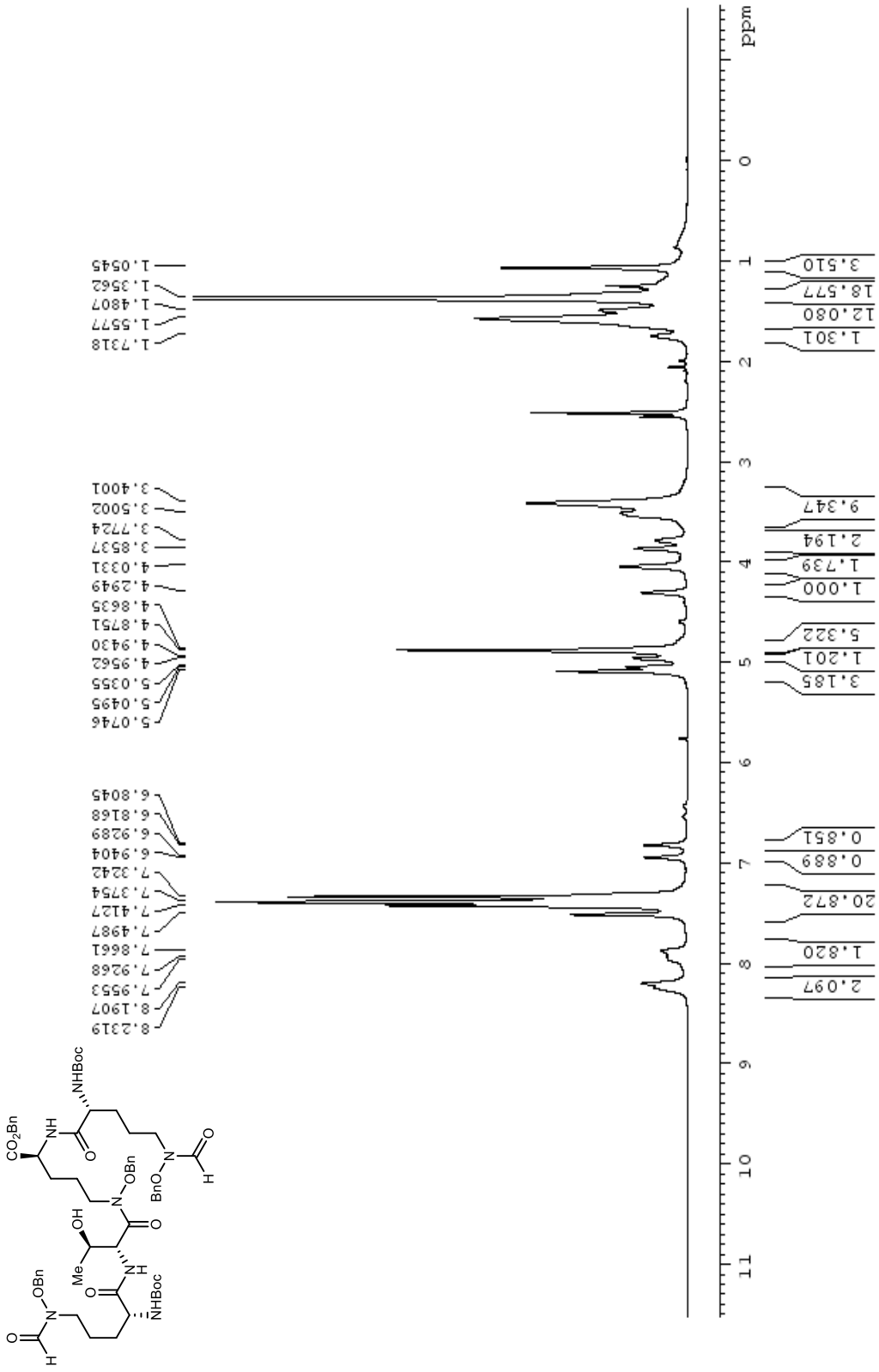

Figure 180. ^{13}C NMR (150 MHz, DMSO-d_6) spectrum of **1.118**.

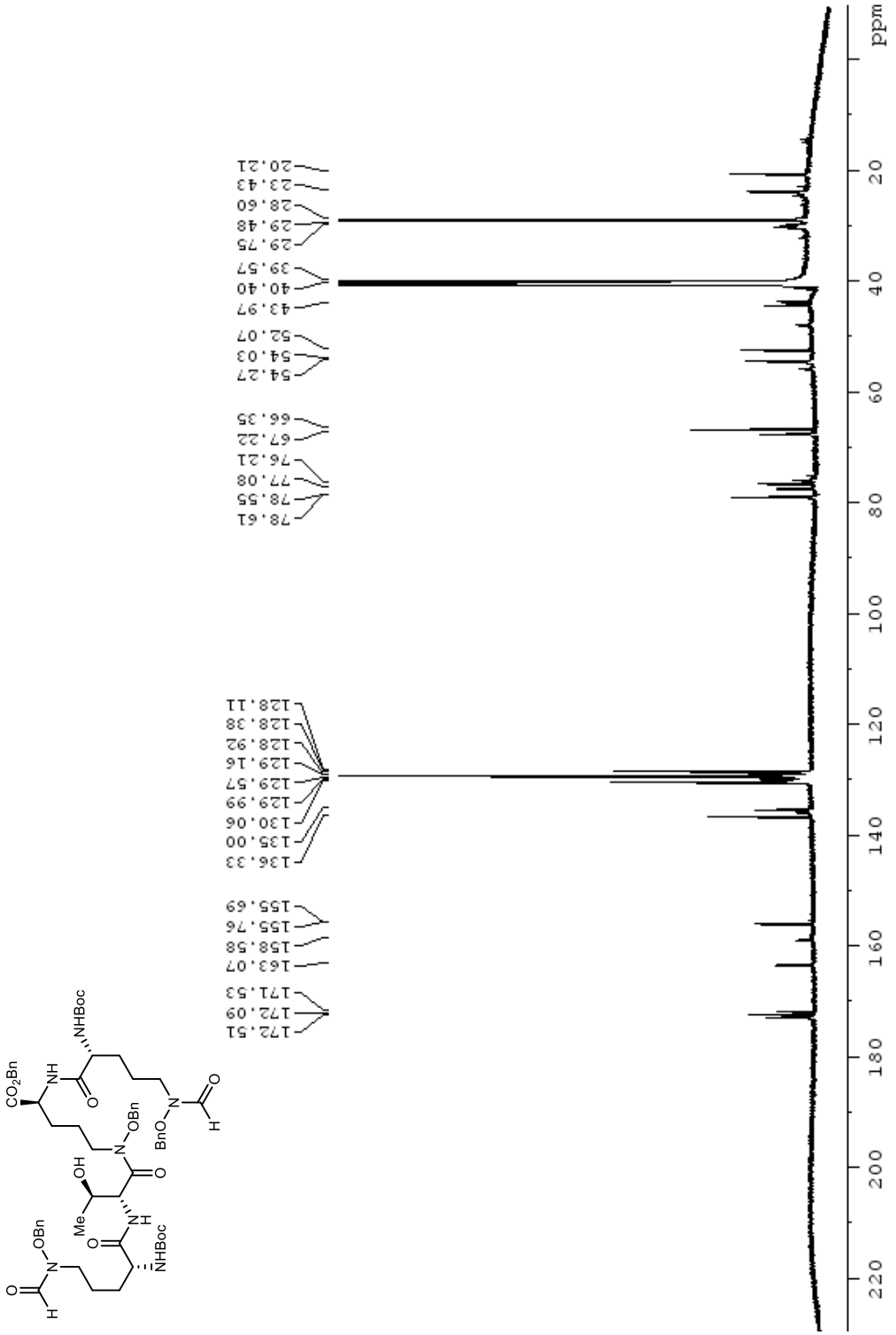

Figure 181. ^{1}H NMR (600 MHz, DMSO-d_6) spectrum of **1.119**.

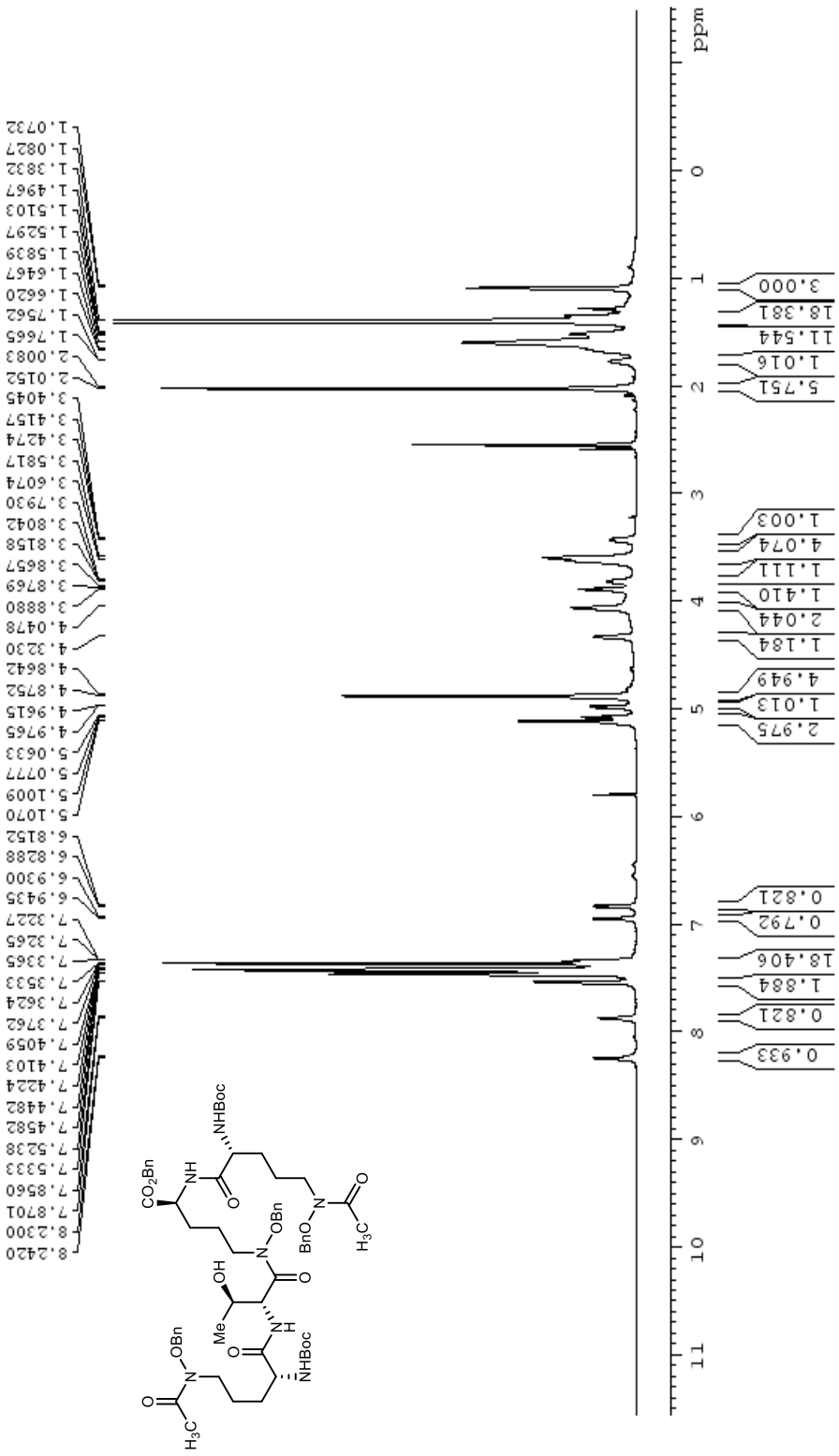

Figure 182. ^{13}C NMR (150 MHz, DMSO-d_6) spectrum of **1.119**.

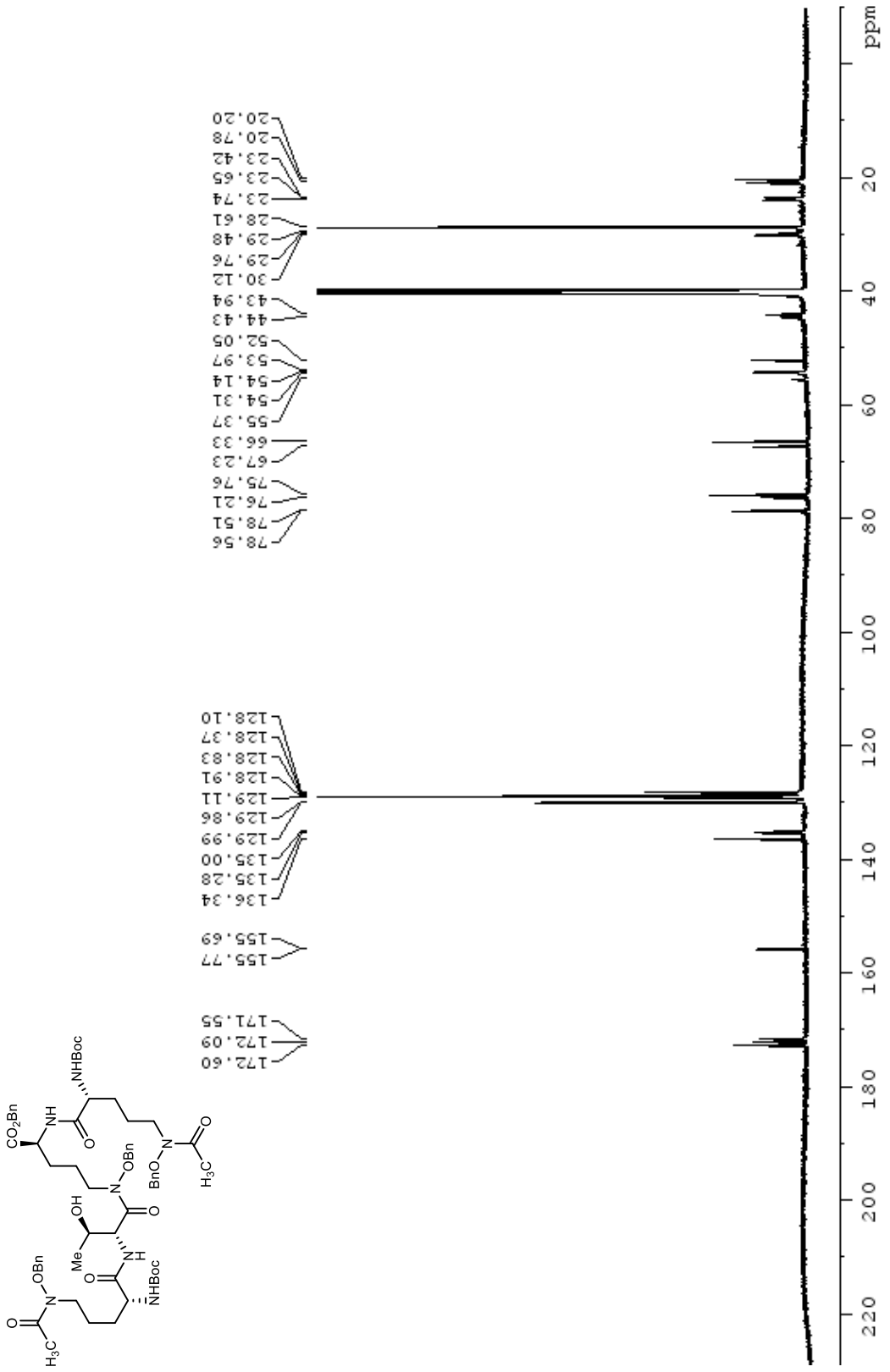

Figure 183. ^{1}H NMR (600 MHz, DMSO-d_6) spectrum of **1.120**.

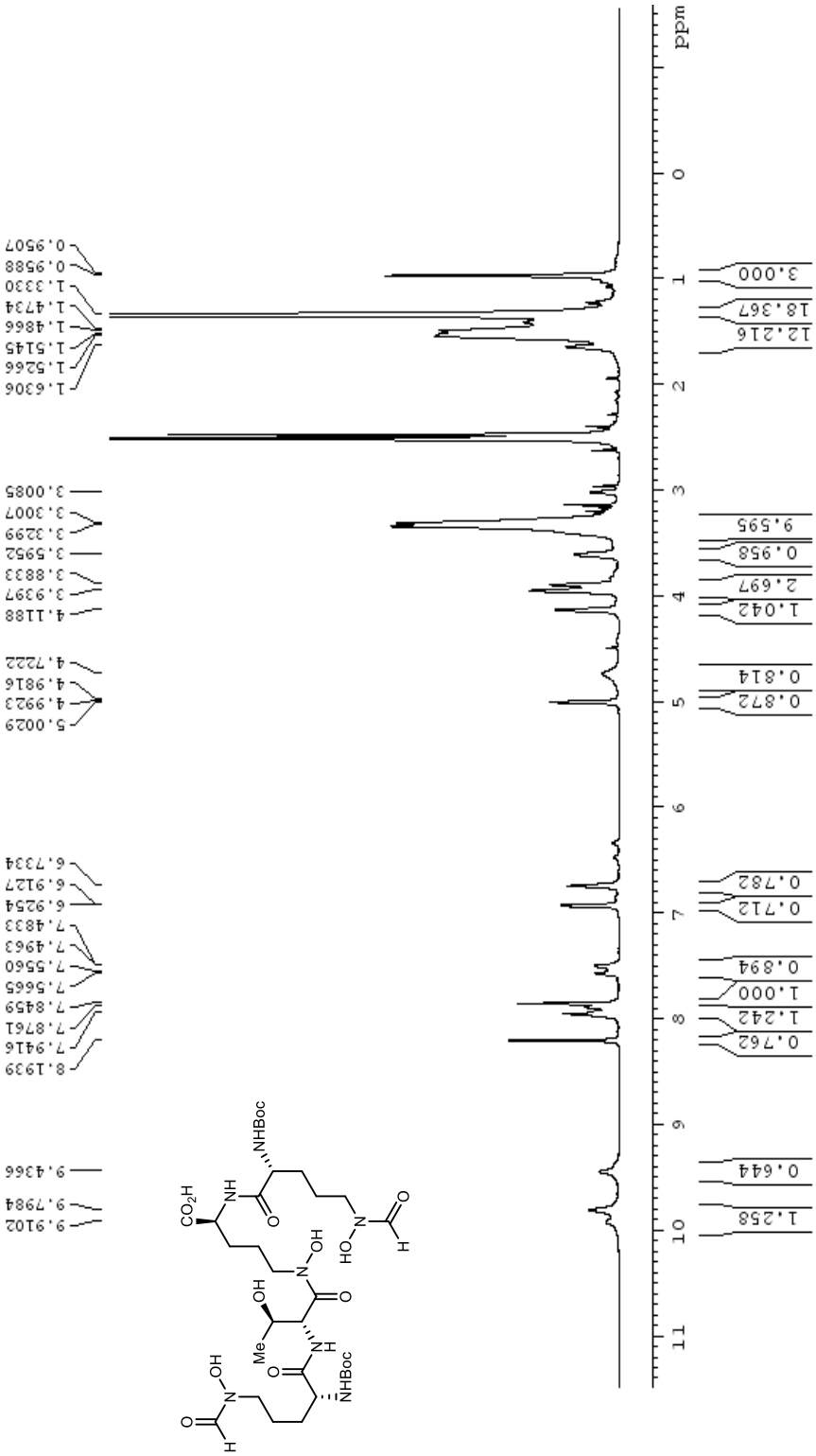

Figure 184. ^{13}C NMR (150 MHz, DMSO-d_6) spectrum of **1.120**.

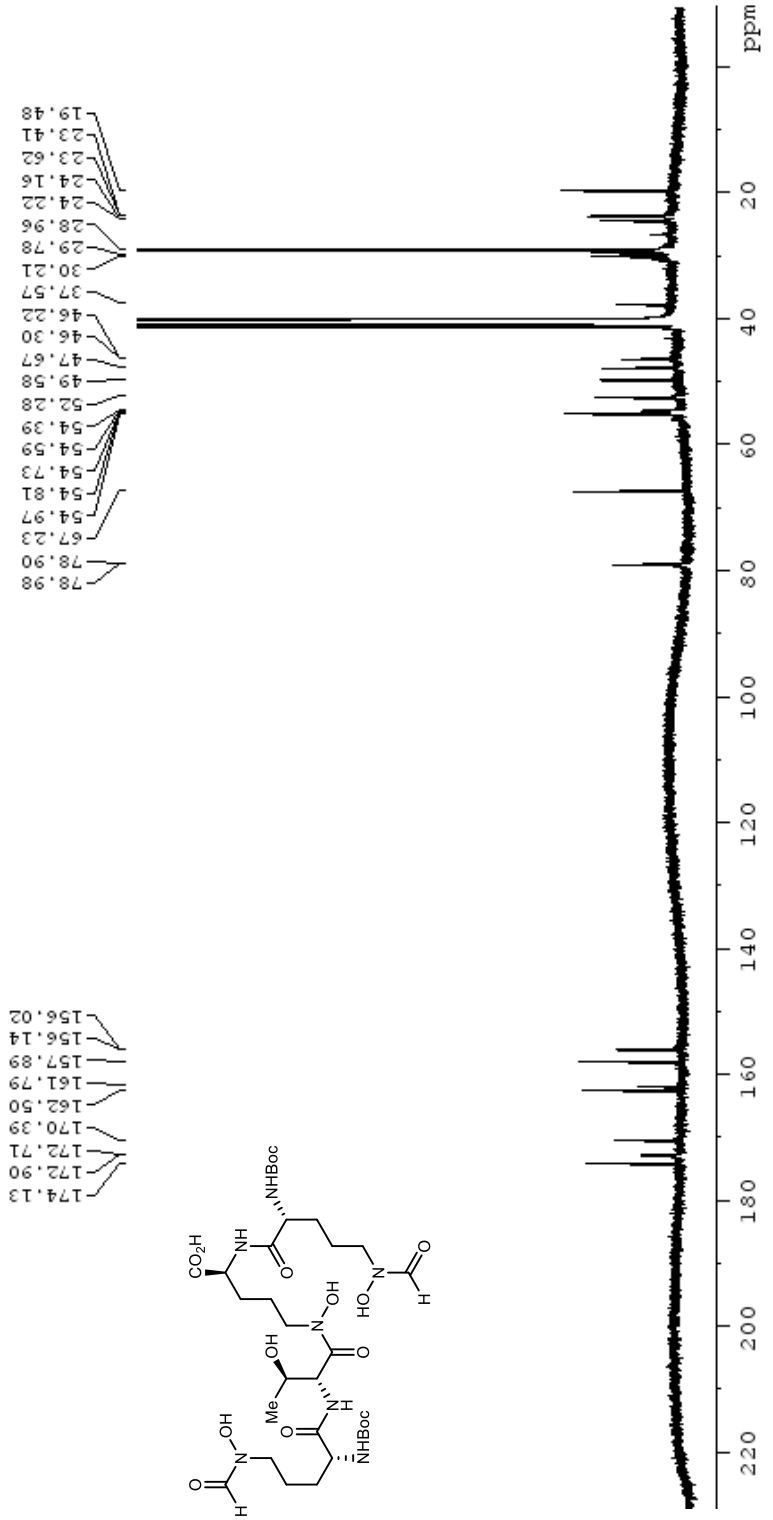

Figure 185. ^{1}H NMR (600 MHz, DMSO-d_6) spectrum of **1.121**.

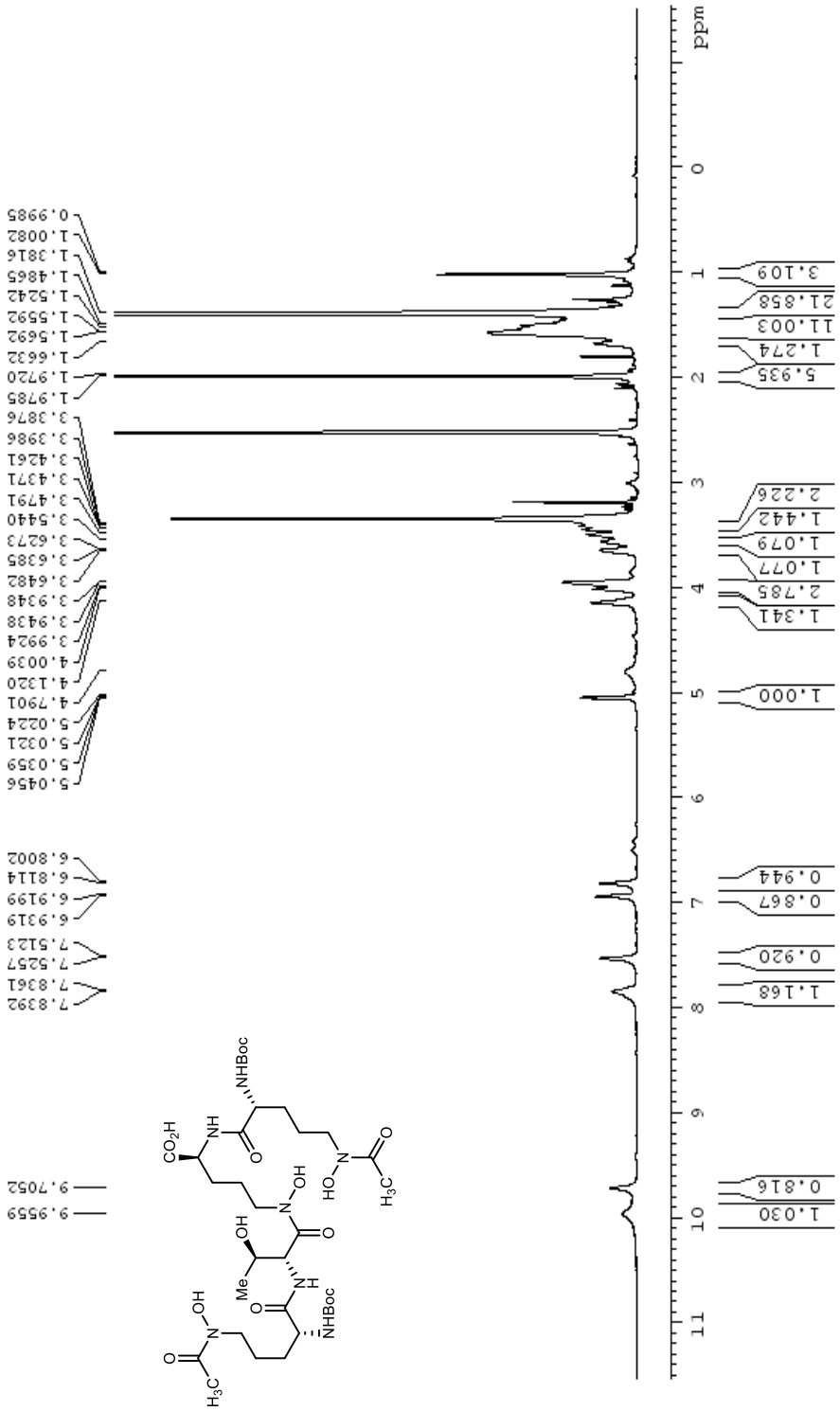

Figure 186. ^{13}C NMR (150 MHz, DMSO-d_6) spectrum of **1.121**.

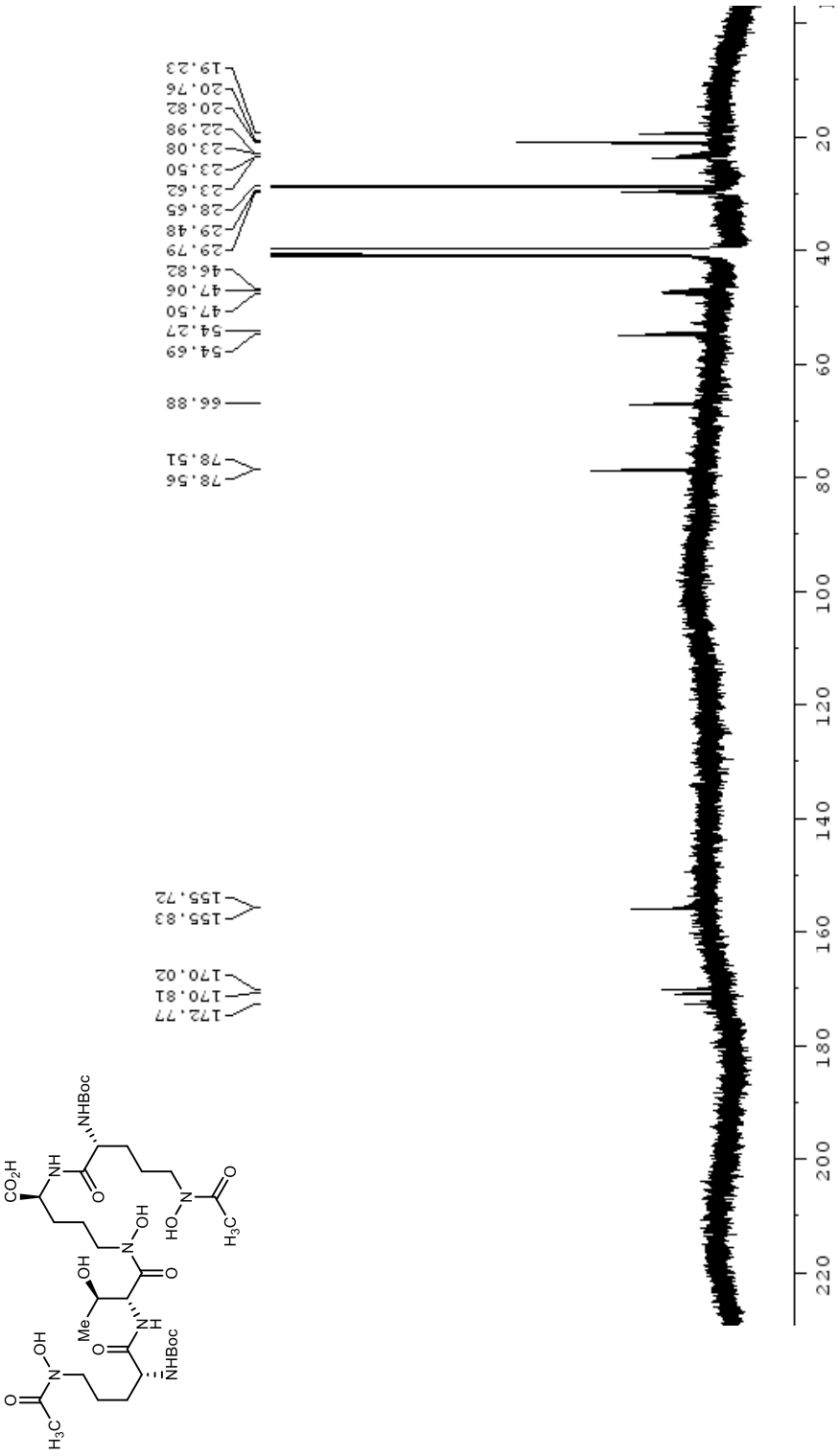

Figure 187. ^{1}H NMR (600 MHz, DMSO-d_6) spectrum of **1.90**.

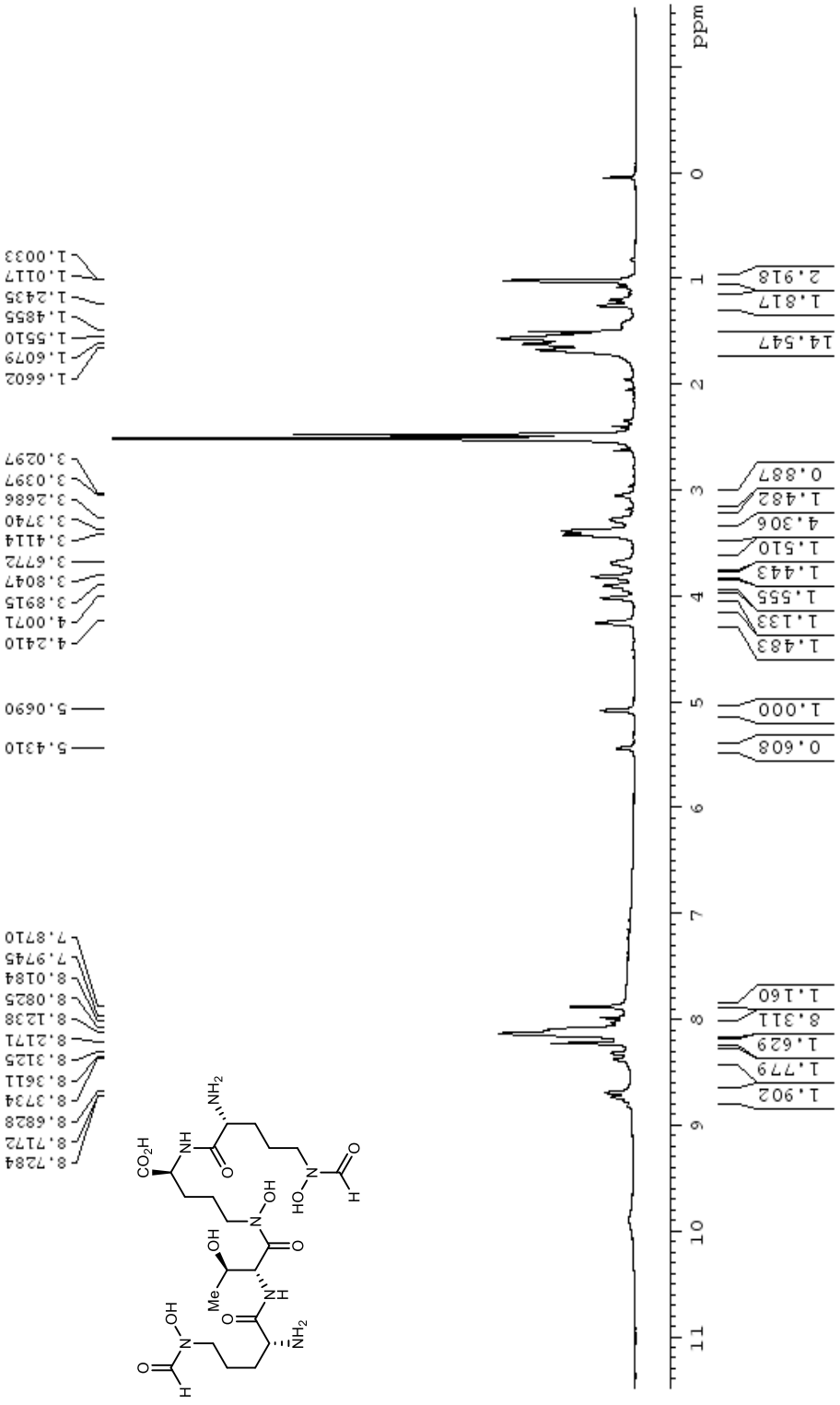

Figure 188. ^{13}C NMR (150 MHz, DMSO-d_6) spectrum of **1.90**.

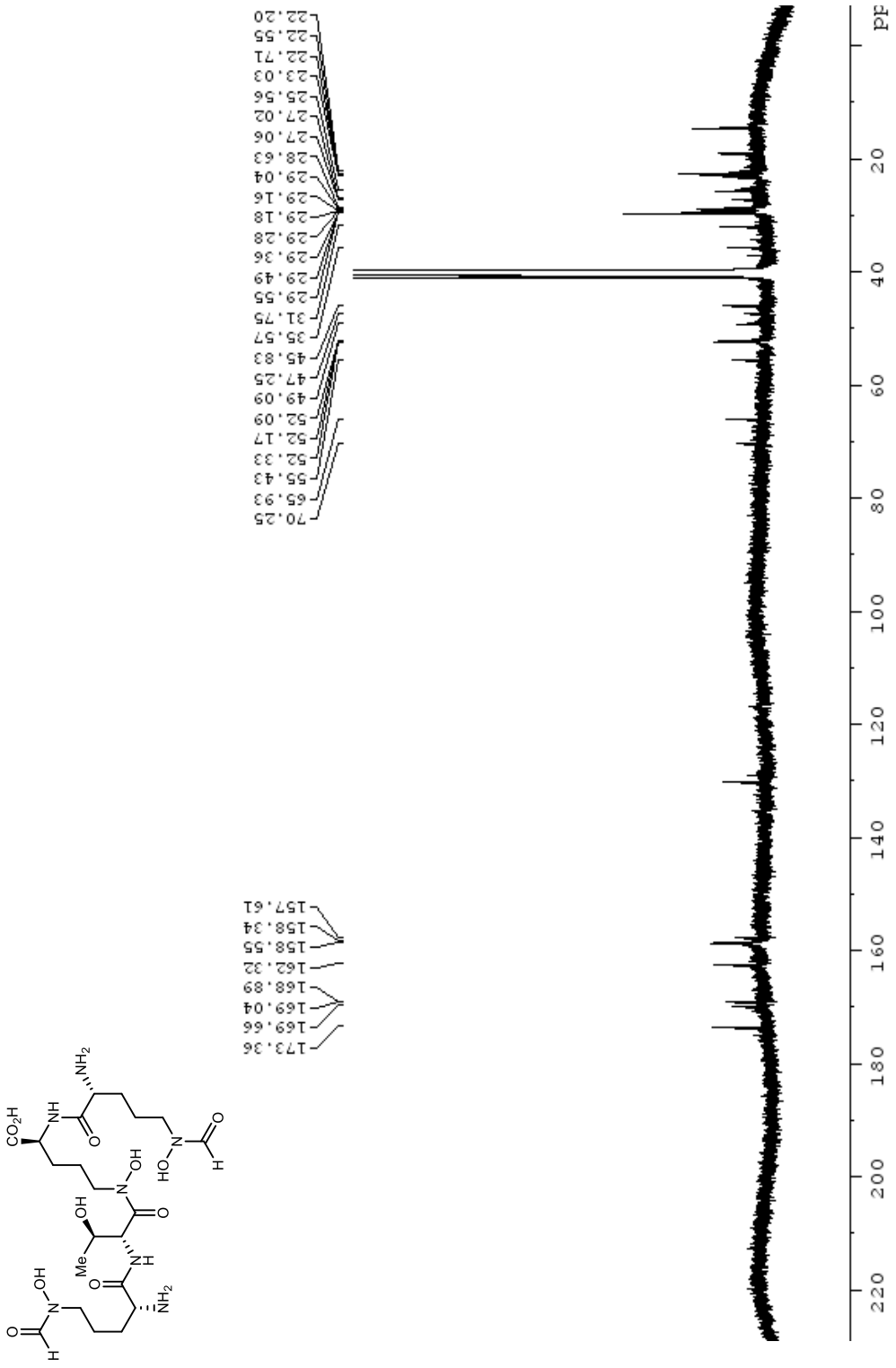

Figure 189. ^{1}H NMR (600 MHz, DMSO-d_6) spectrum of **1.91**.

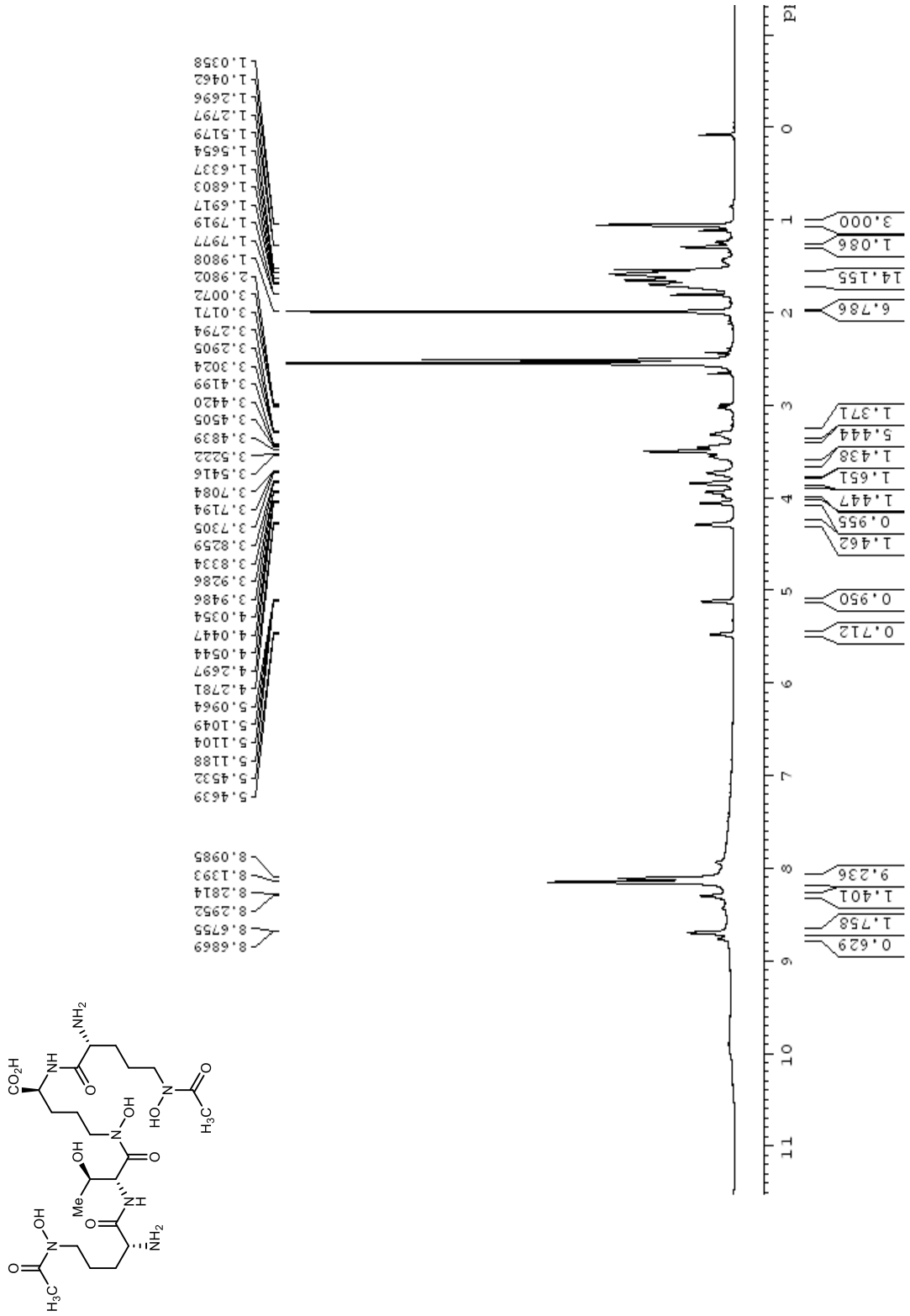

Figure 190. ^{13}C NMR (150 MHz, DMSO-d_6) spectrum of **1.91**.

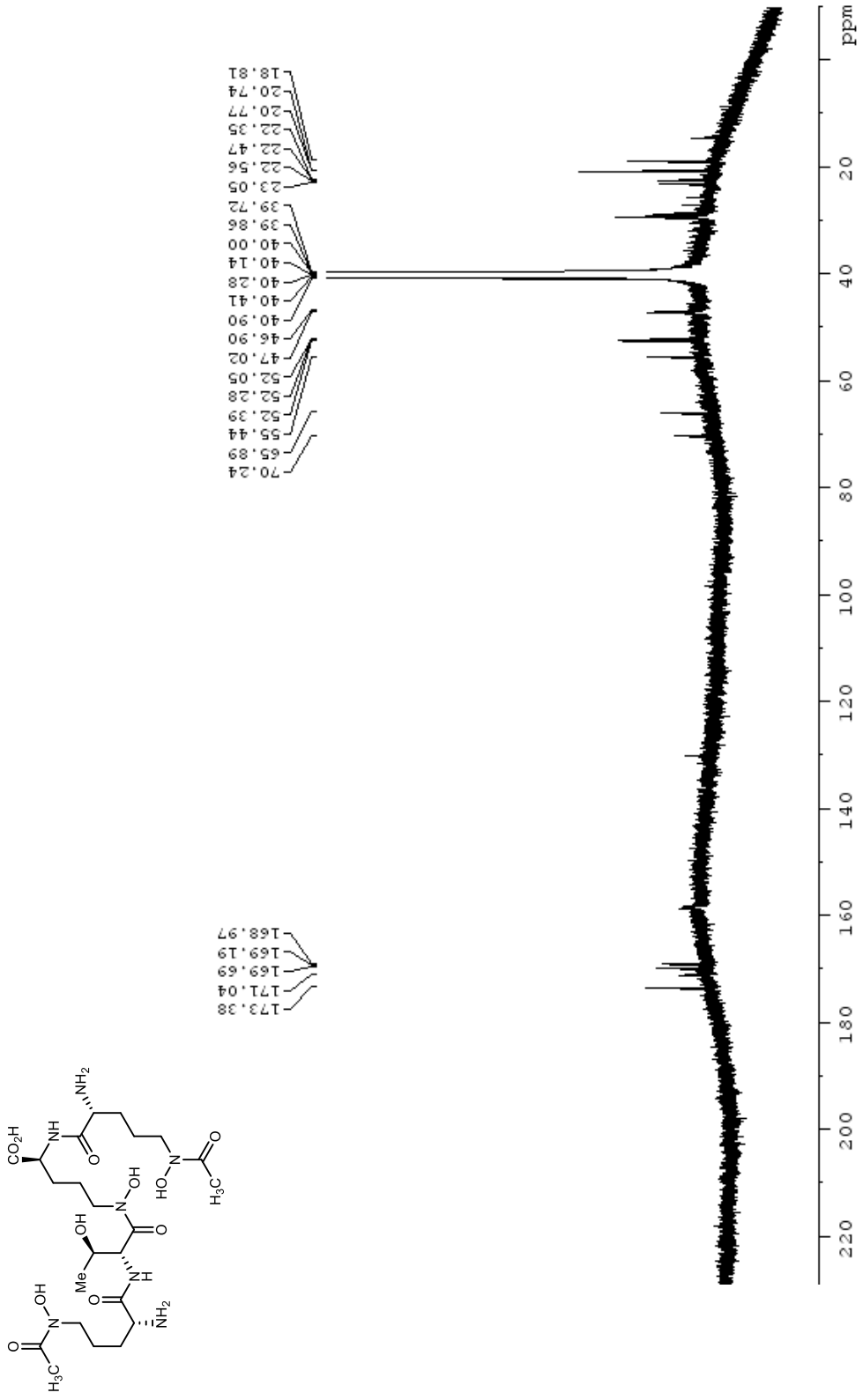

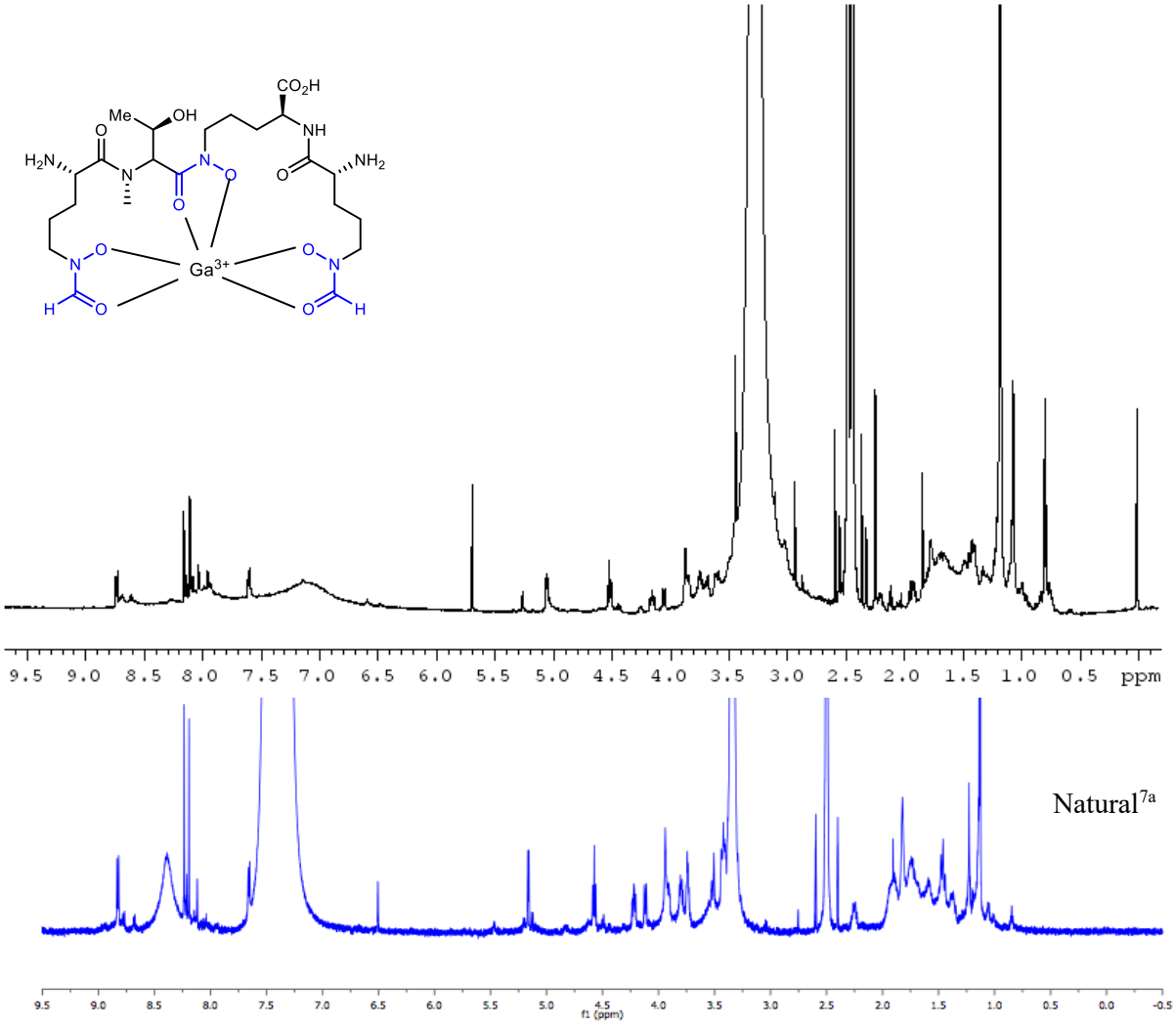

Figure 191. ^{1}H NMR spectra of synthetic coelichelin complexed to gallium (black) and ^{1}H NMR spectra7c of natural coelichelin provided by Challis and coworkers (blue).

Figure 192. ^{1}H NMR (400 MHz, MeOD) spectrum of **2.7**.

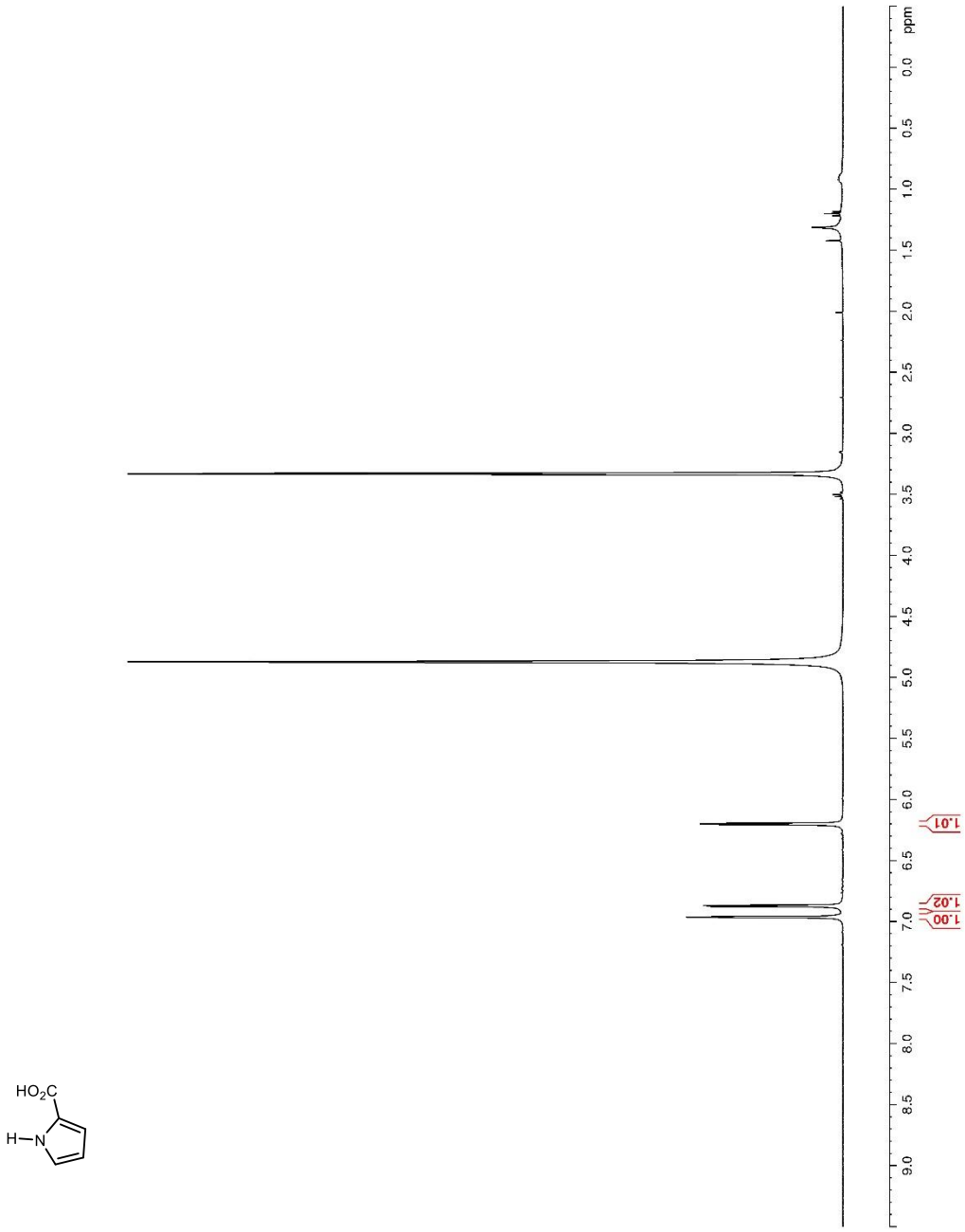

Figure 193. ^{1}H NMR (400 MHz, $CDCl_3$) spectrum of **2.8**.

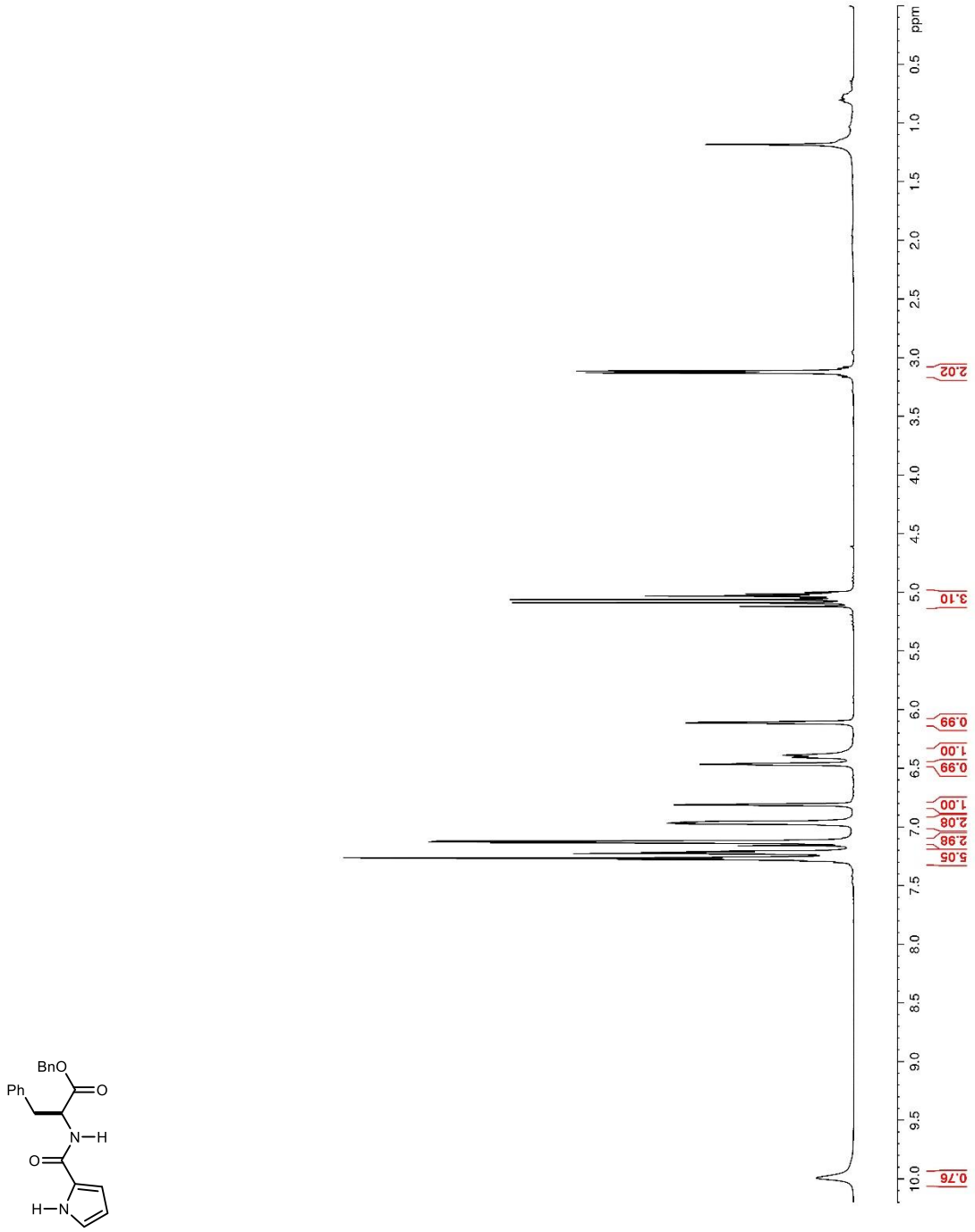

Figure 194. ^{13}C and DEPT-135 NMR (100 MHz, $CDCl_3$) spectra of **2.8**.

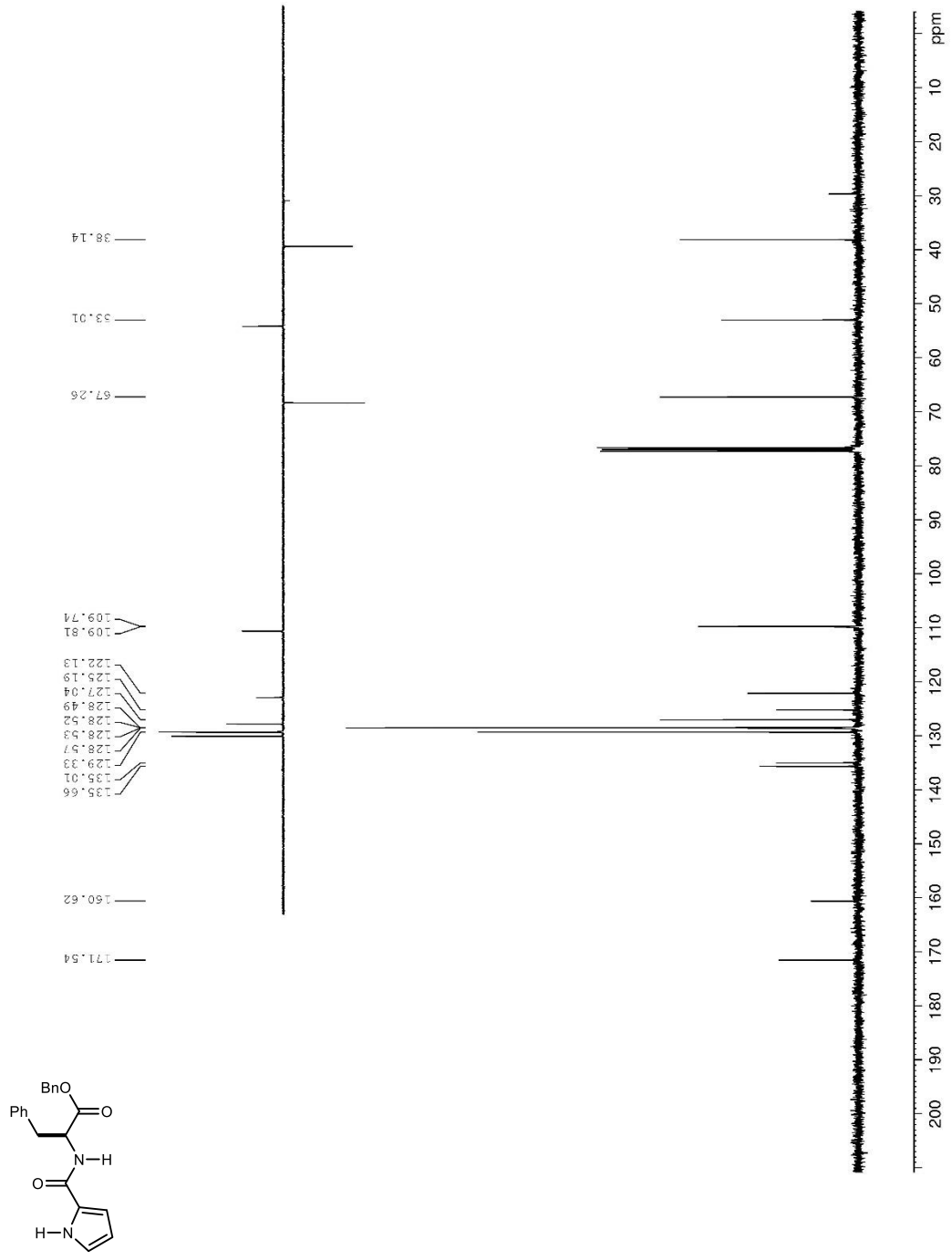

Figure 195. ^{1}H NMR (400 MHz, MeOD) spectrum of **2.5**.

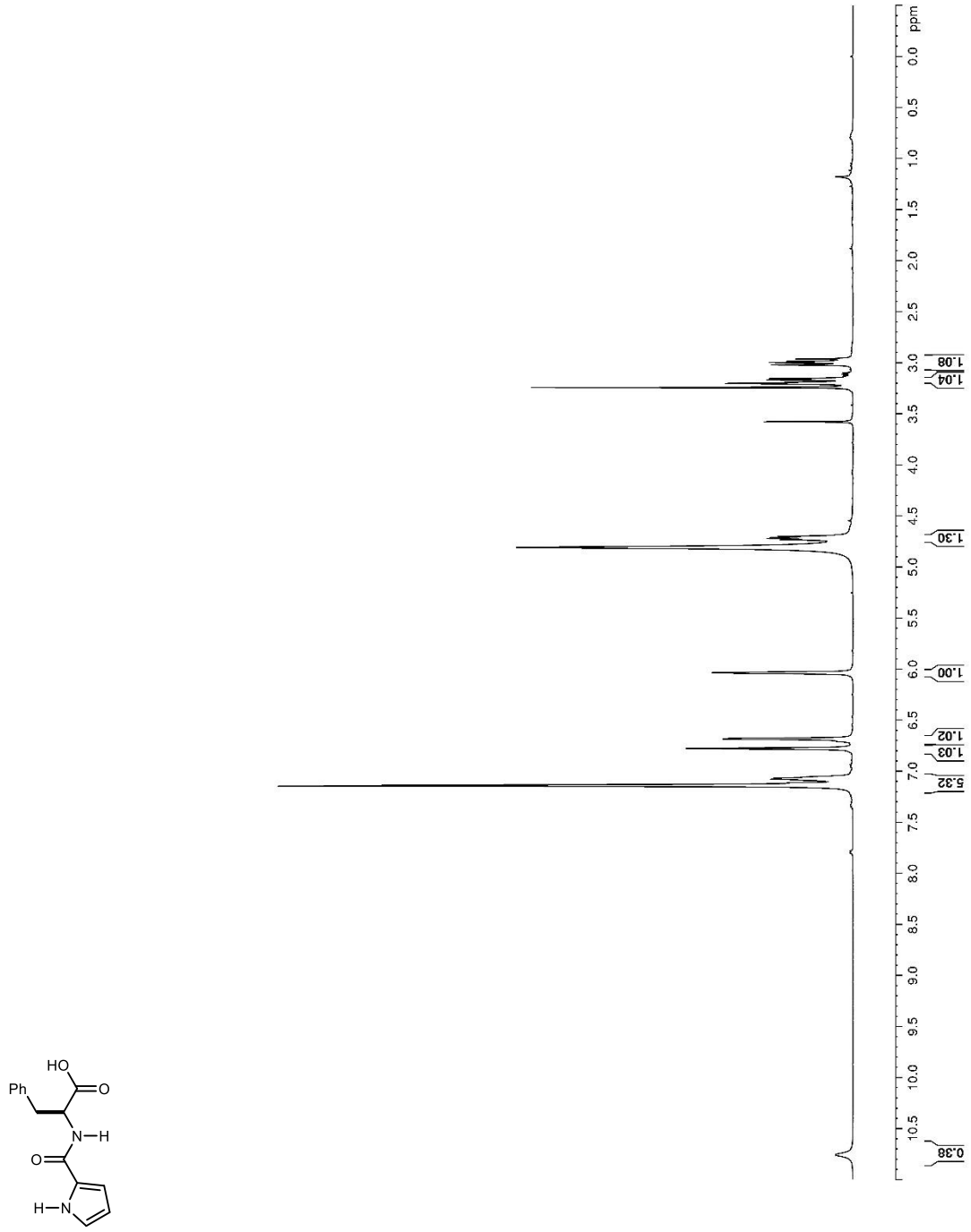

Figure 196. ^{13}C and DEPT-135 NMR (100 MHz, MeOD) spectra of **2.5**.

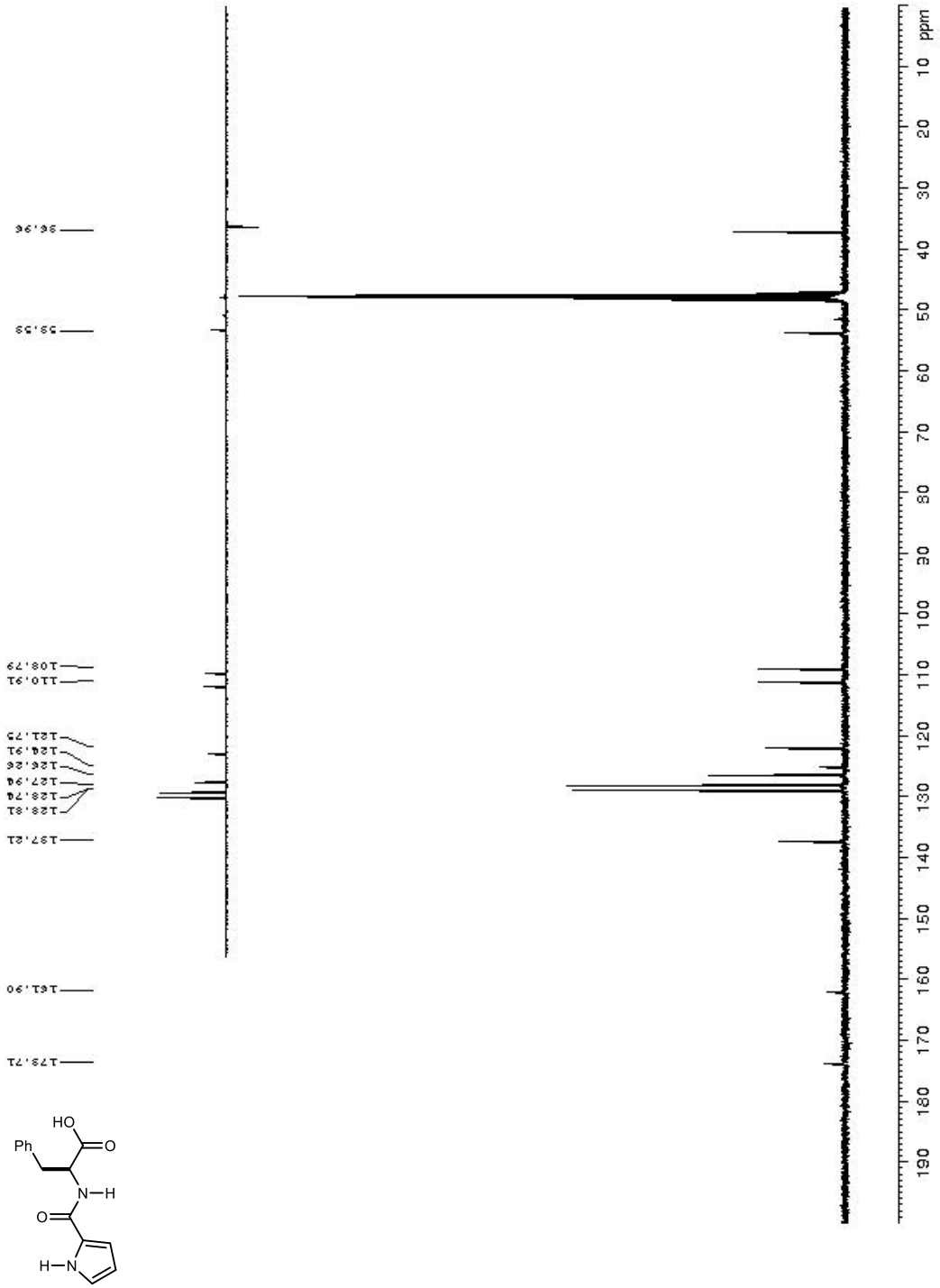

Figure 197. ^{1}H NMR (400 MHz, $CDCl_3$) spectrum of **2.10**.

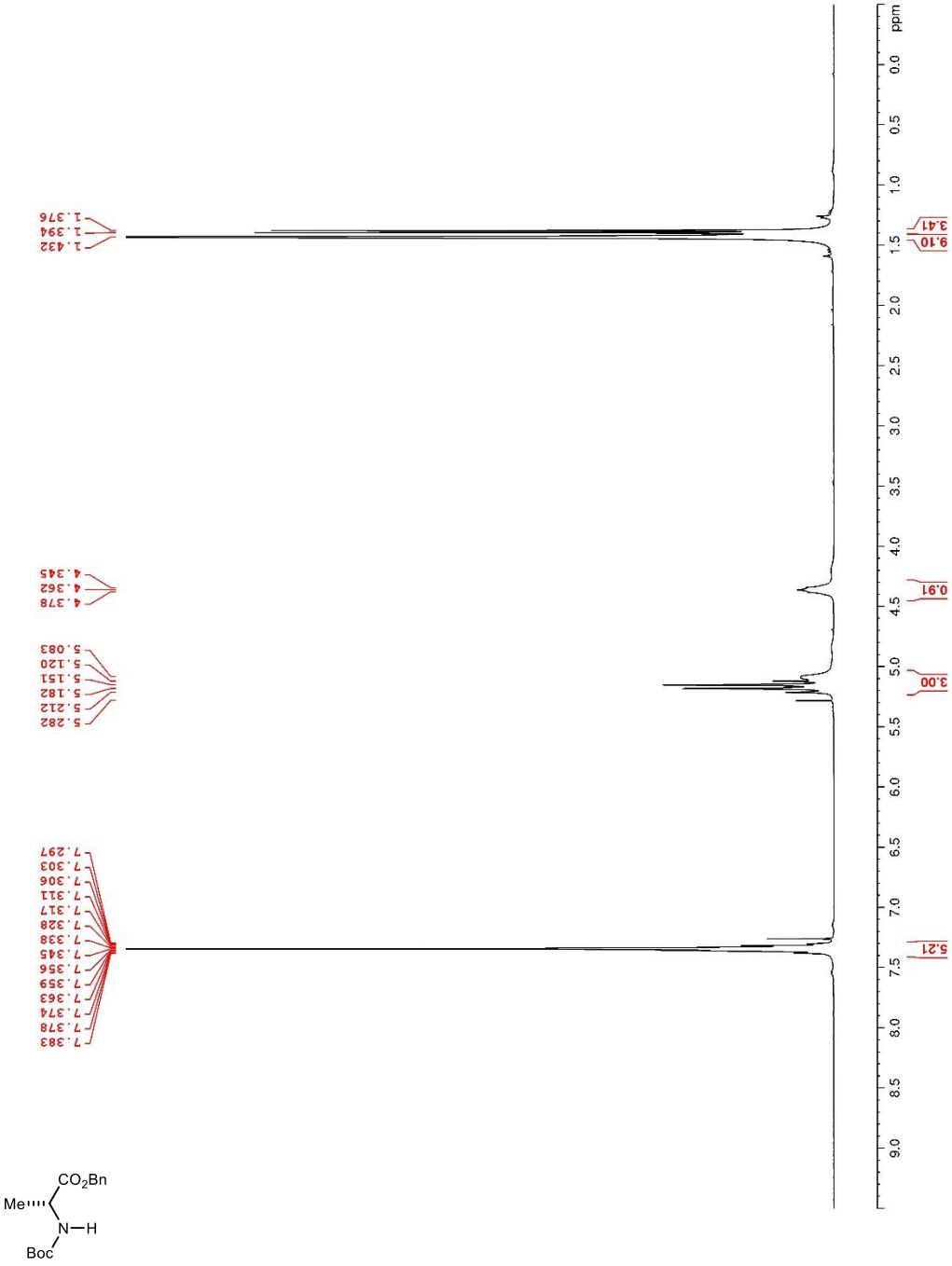

Figure 198. ^{13}C and DEPT-135 NMR (100 MHz, $CDCl_3$) spectra of **2.10**.

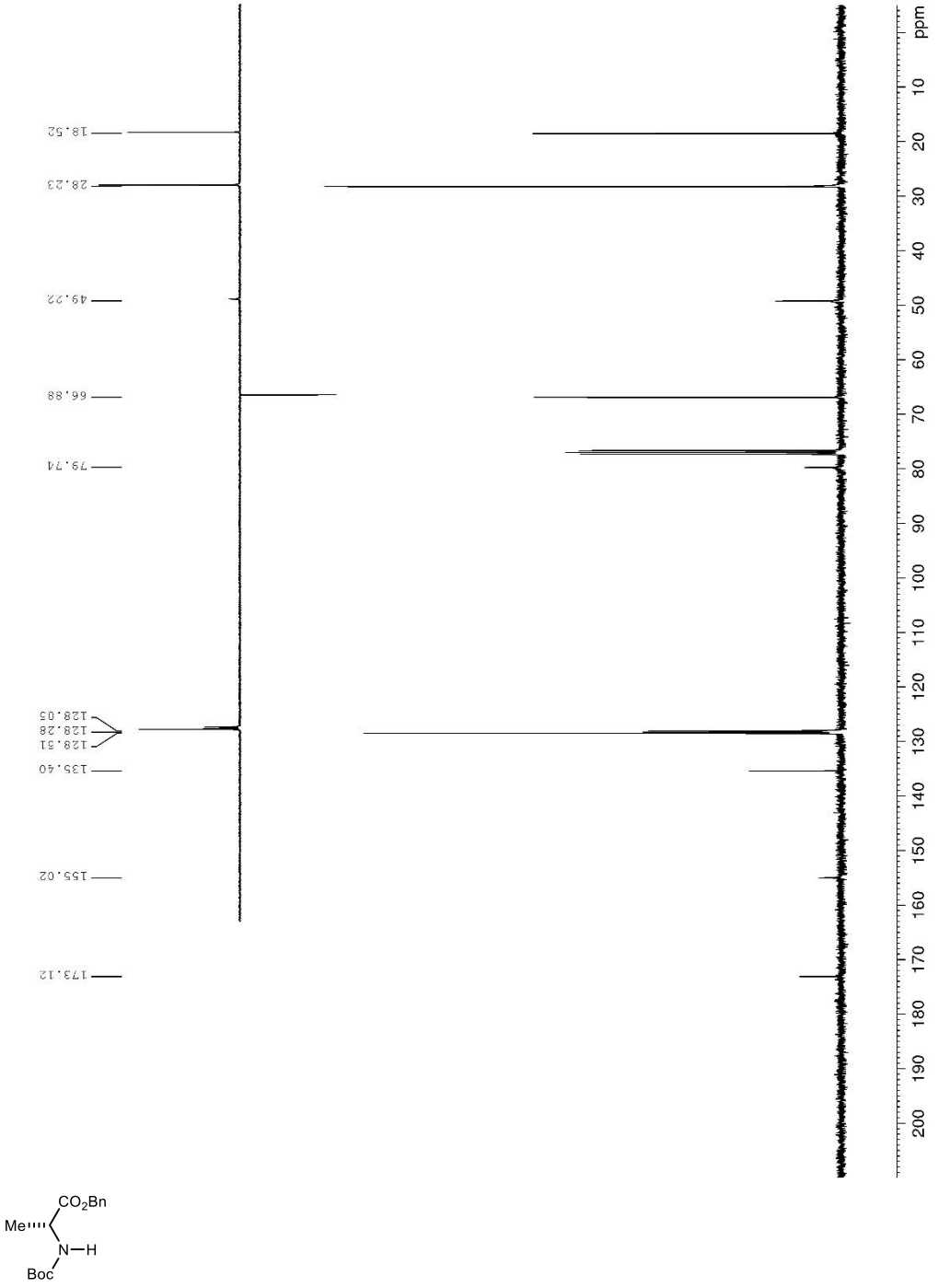

Figure 199. ^{1}H NMR (400 MHz, $CDCl_3$) spectrum of **2.11**.

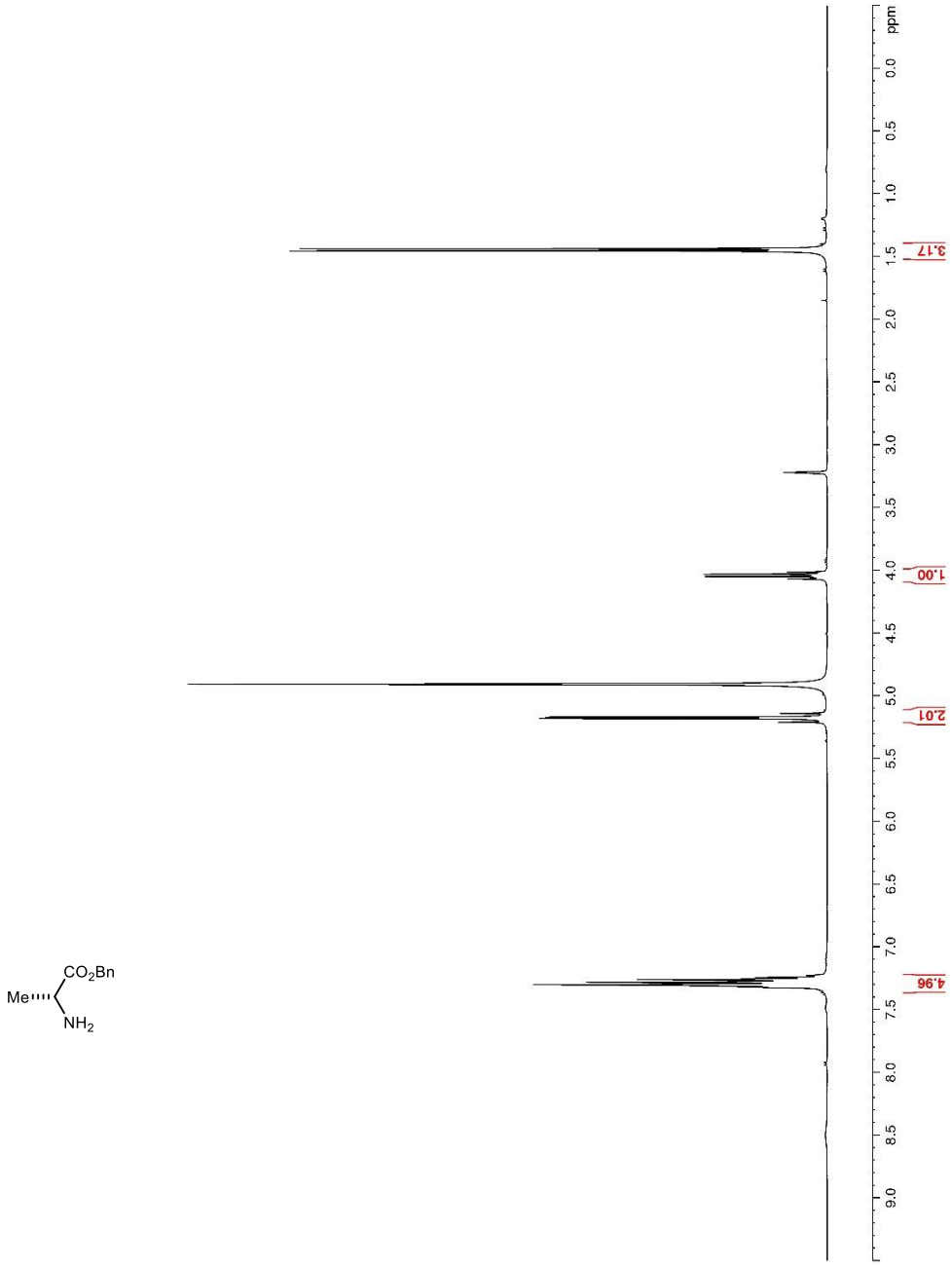

Figure 200. ^{1}H NMR (400 MHz, $CDCl_3$) spectrum of **2.12**.

Figure 201. ^{13}C and DEPT-135 NMR (100 MHz, $CDCl_3$) spectra of **2.12**.

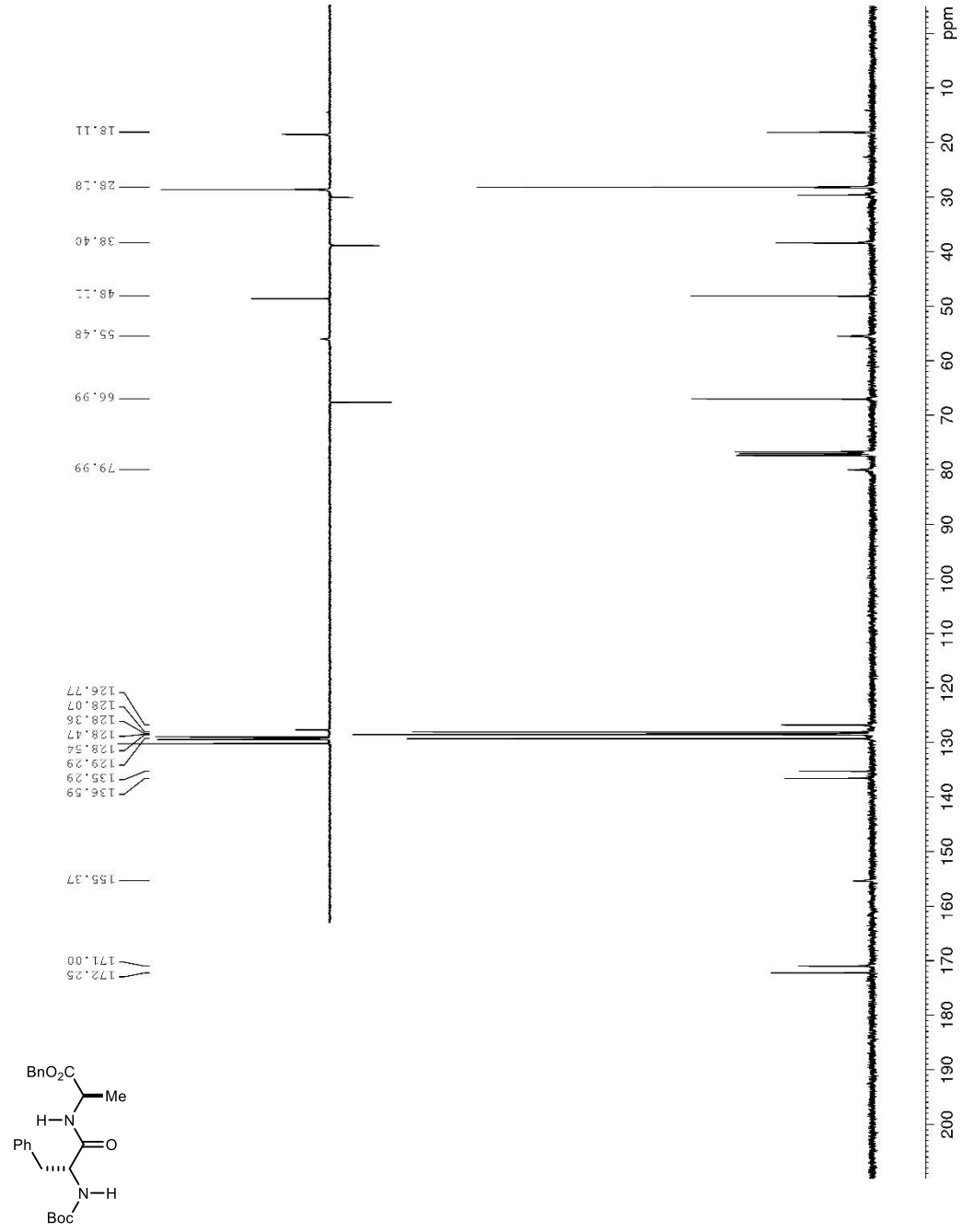

Figure 202. ^{1}H NMR (400 MHz, MeOD) spectrum of **2.13**.

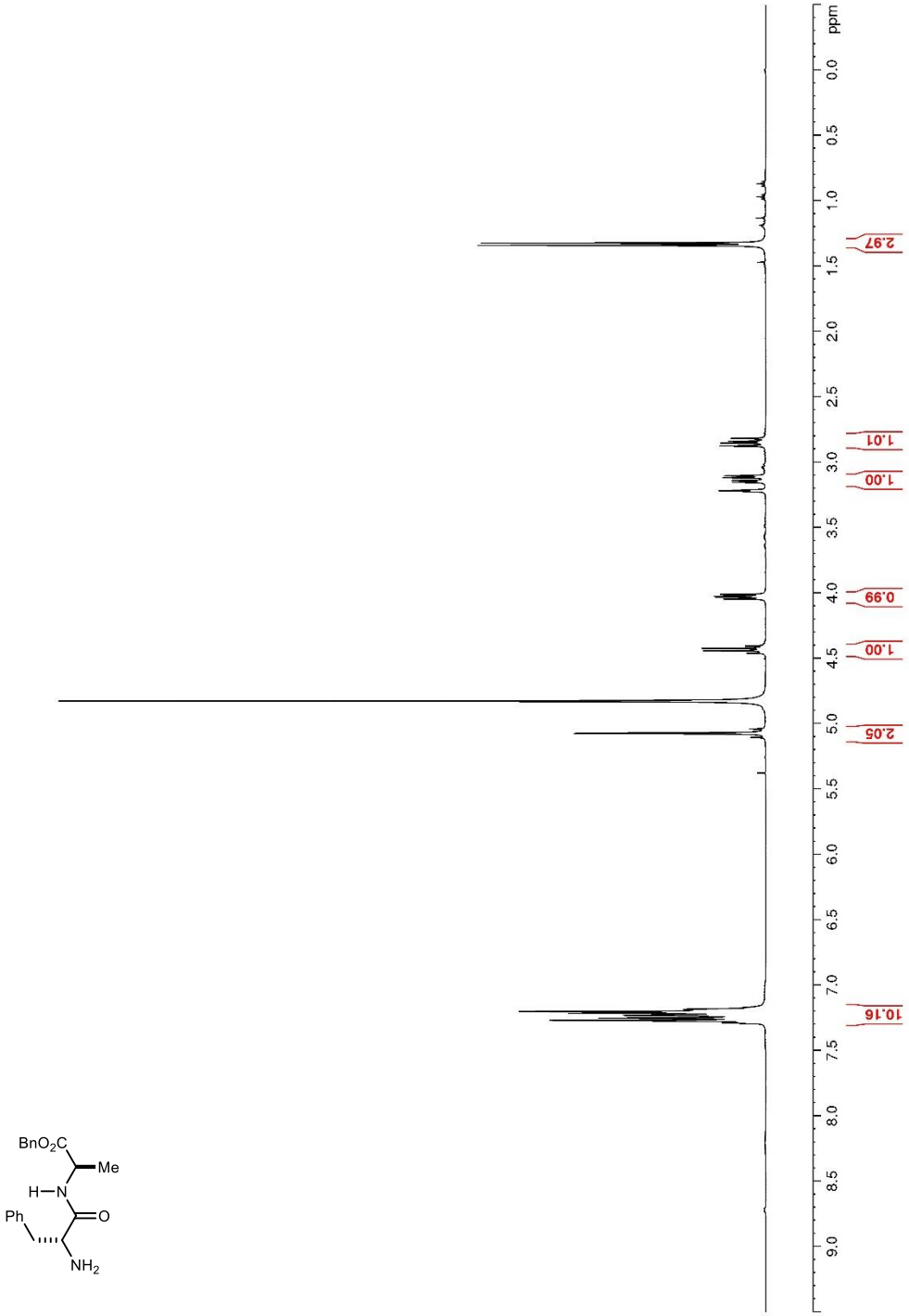

Figure 203. ^{13}C and DEPT-135 NMR (100 MHz, MeOD) spectra of **2.13**.

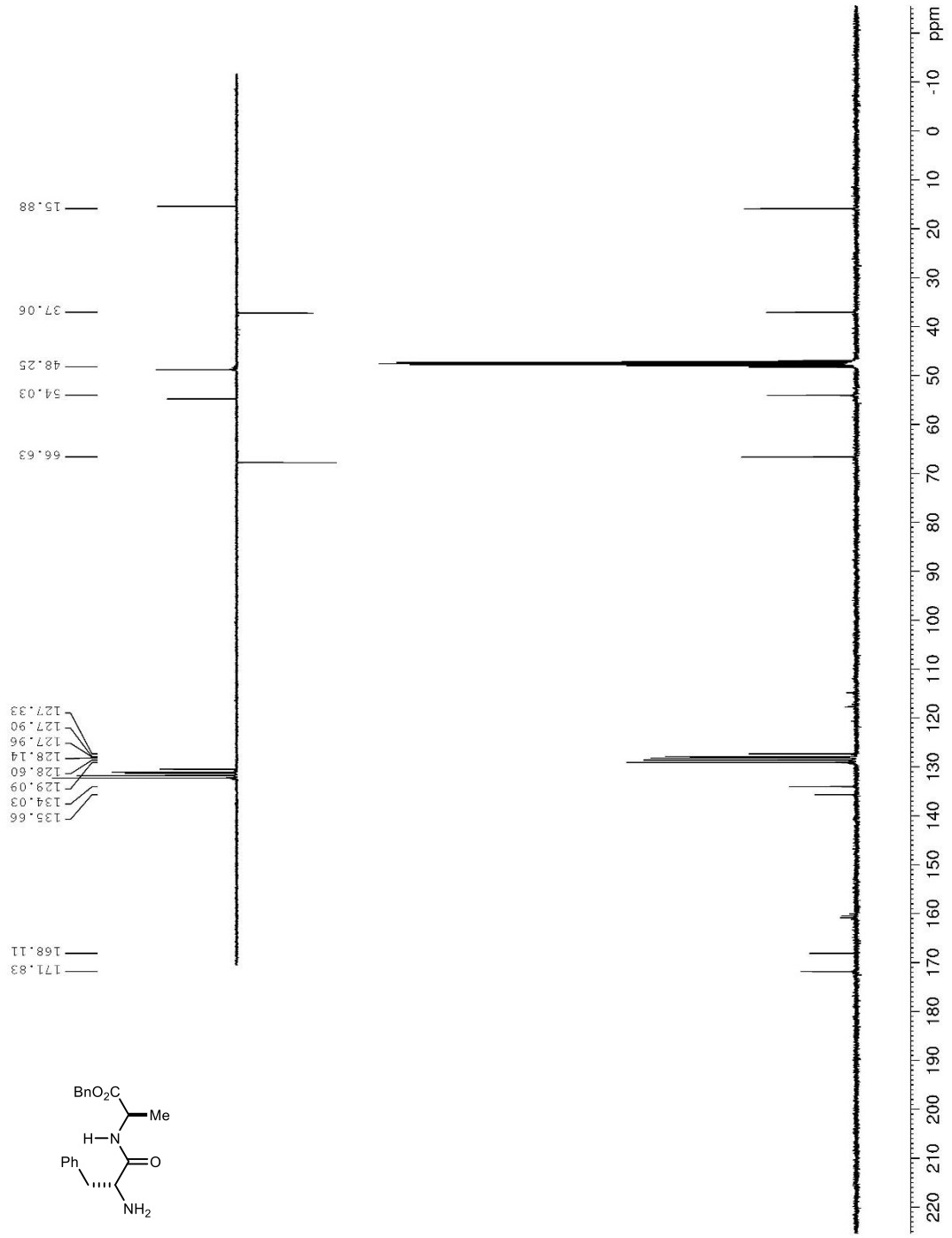

Figure 204. ^{1}H NMR (400 MHz, MeOD) spectrum of **2.94**.

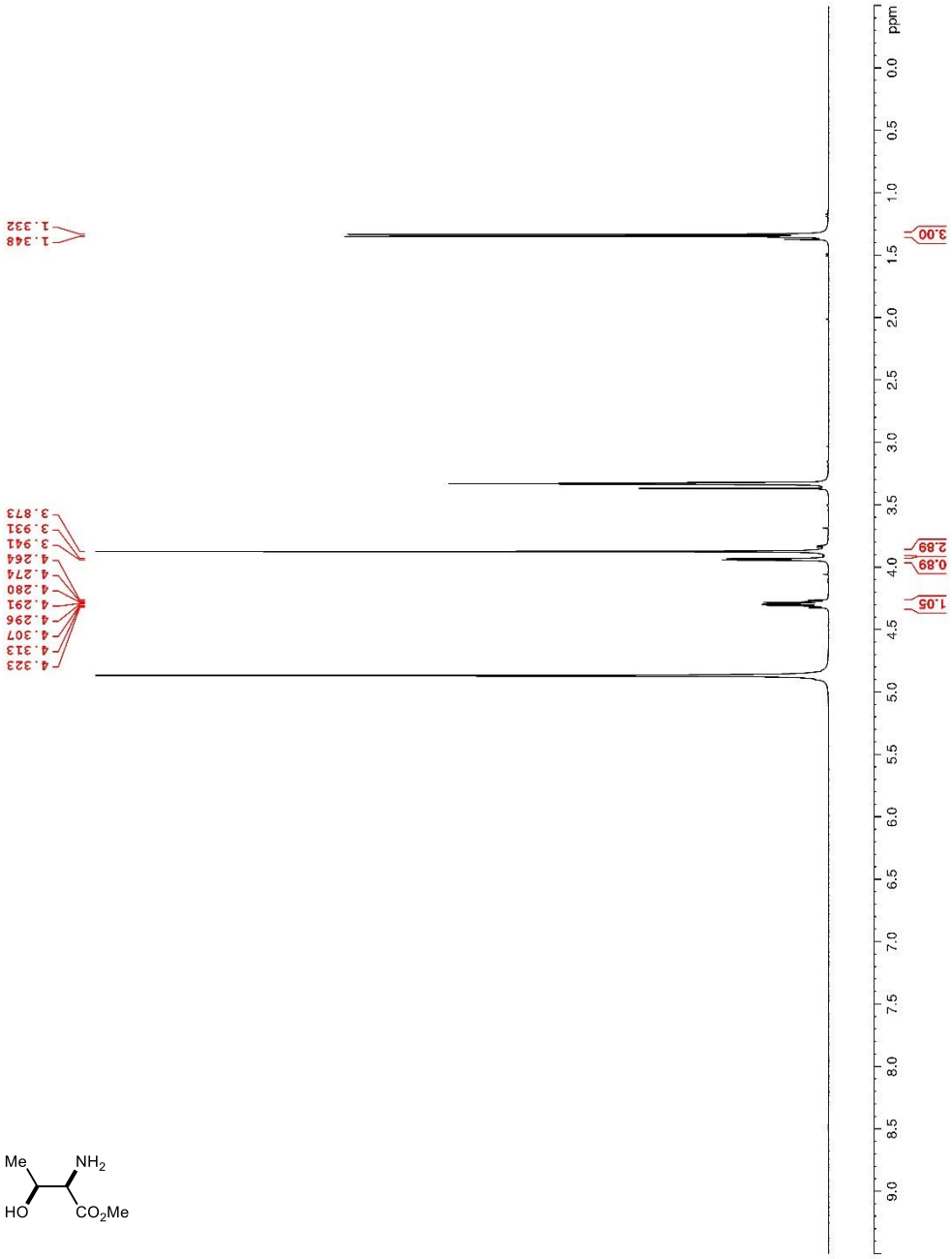

Figure 205. ^{1}H NMR (400 MHz, $CDCl_3$) spectrum of **2.95**.

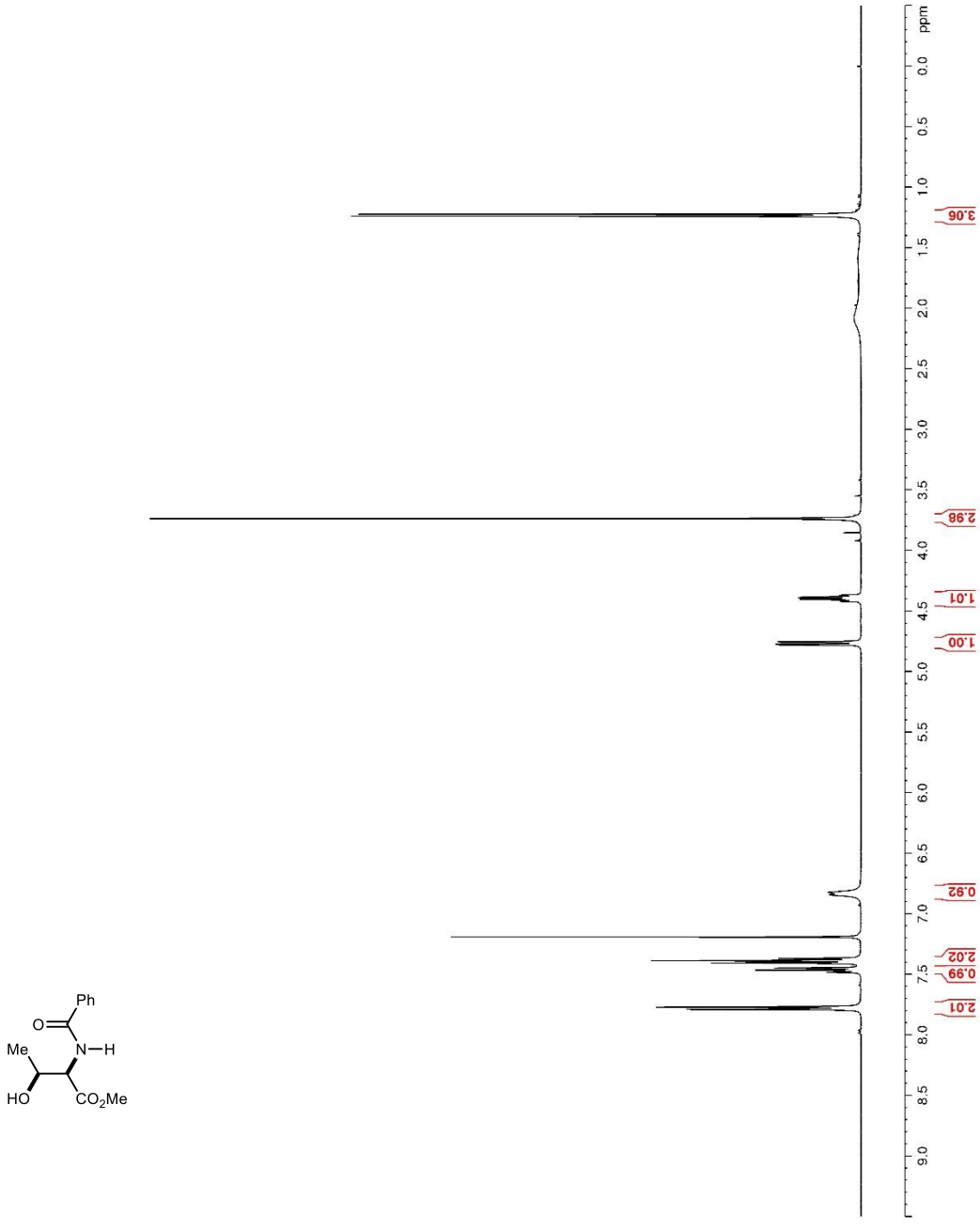

Figure 206. ^{1}H NMR (400 MHz, $CDCl_3$) spectrum of **2.96**.

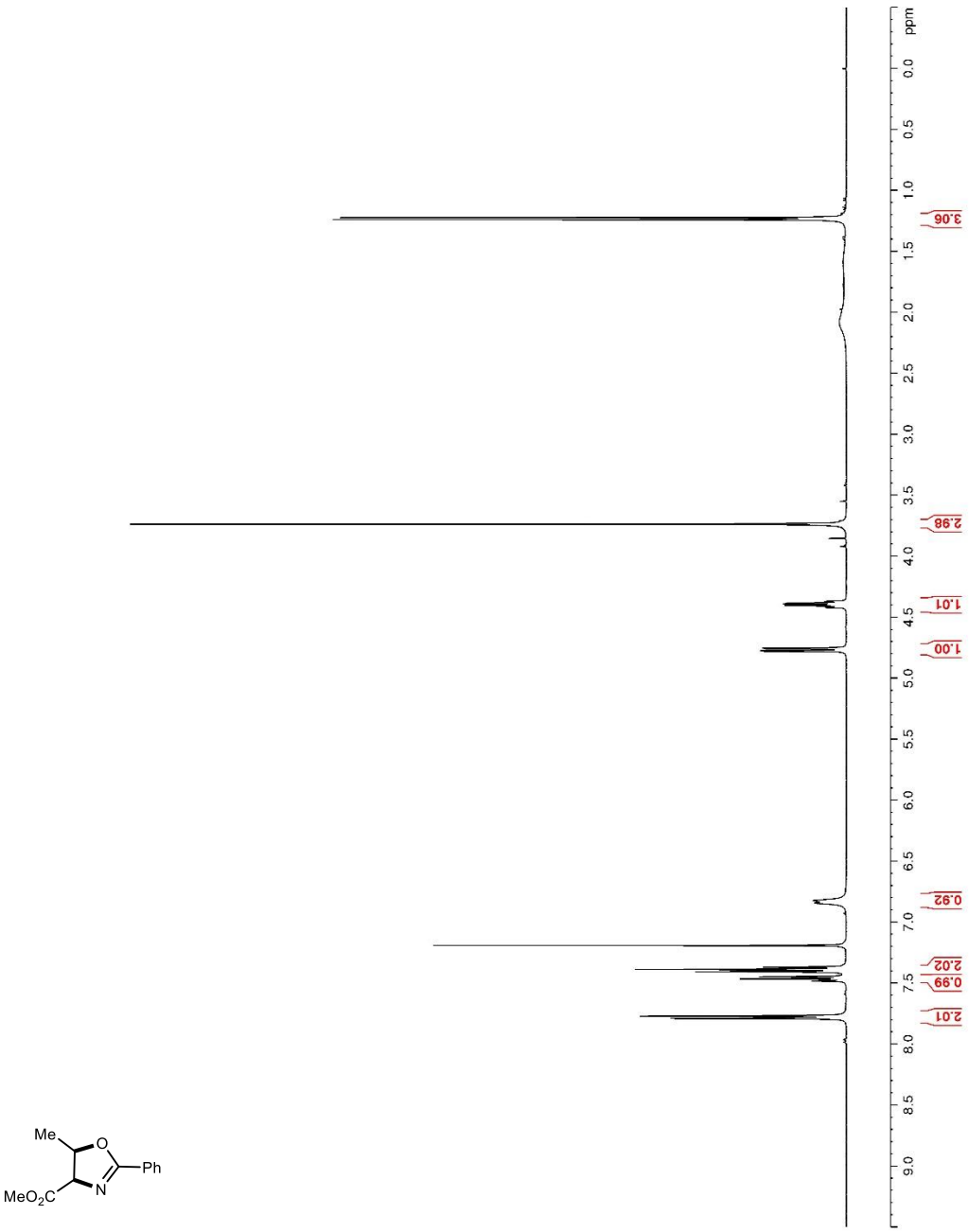

Figure 207. ^{1}H NMR (400 MHz, MeOD) spectrum of **2.97**.

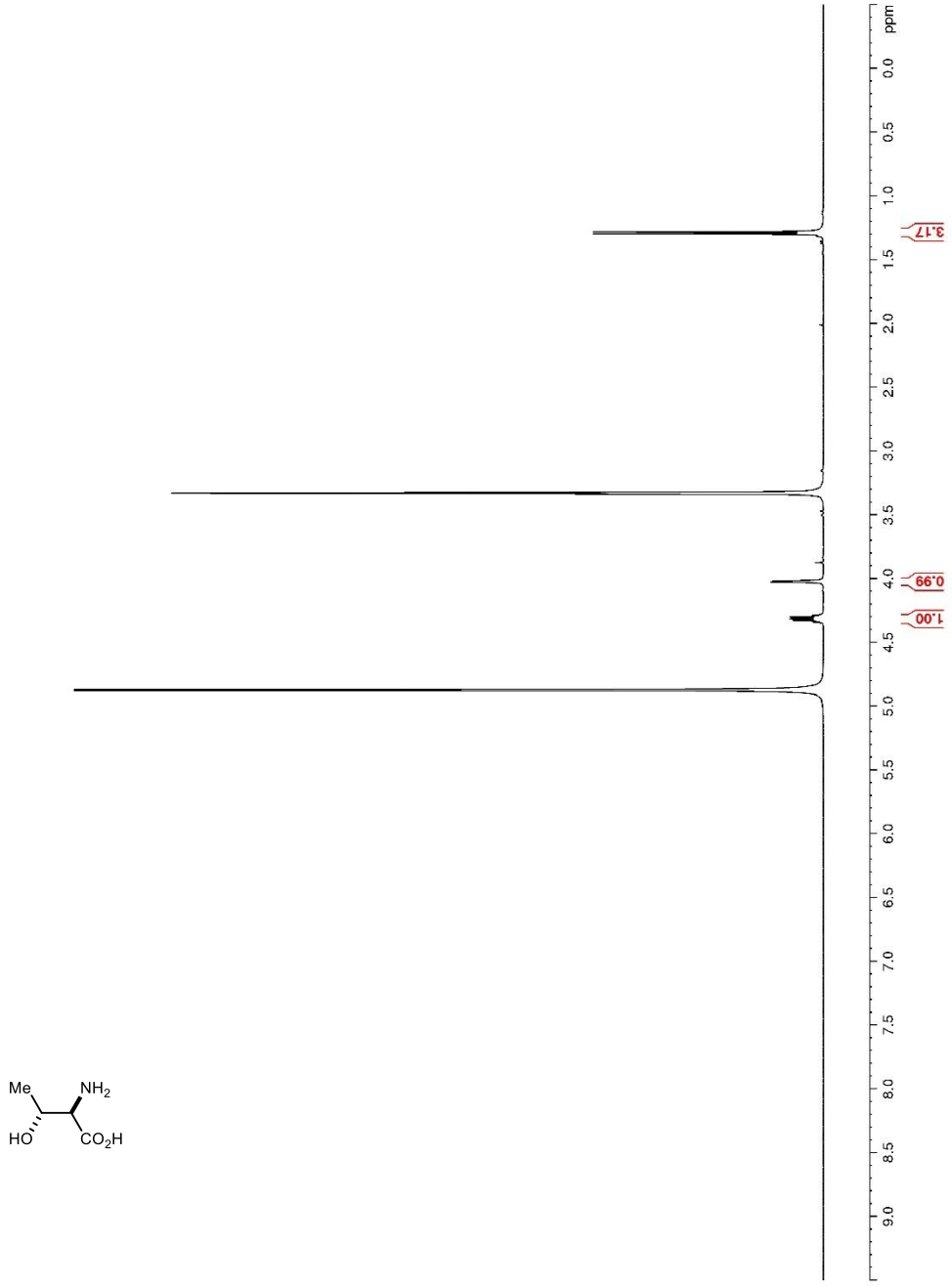

Figure 208. ^{1}H NMR (400 MHz, MeOD) spectrum of **2.98**.

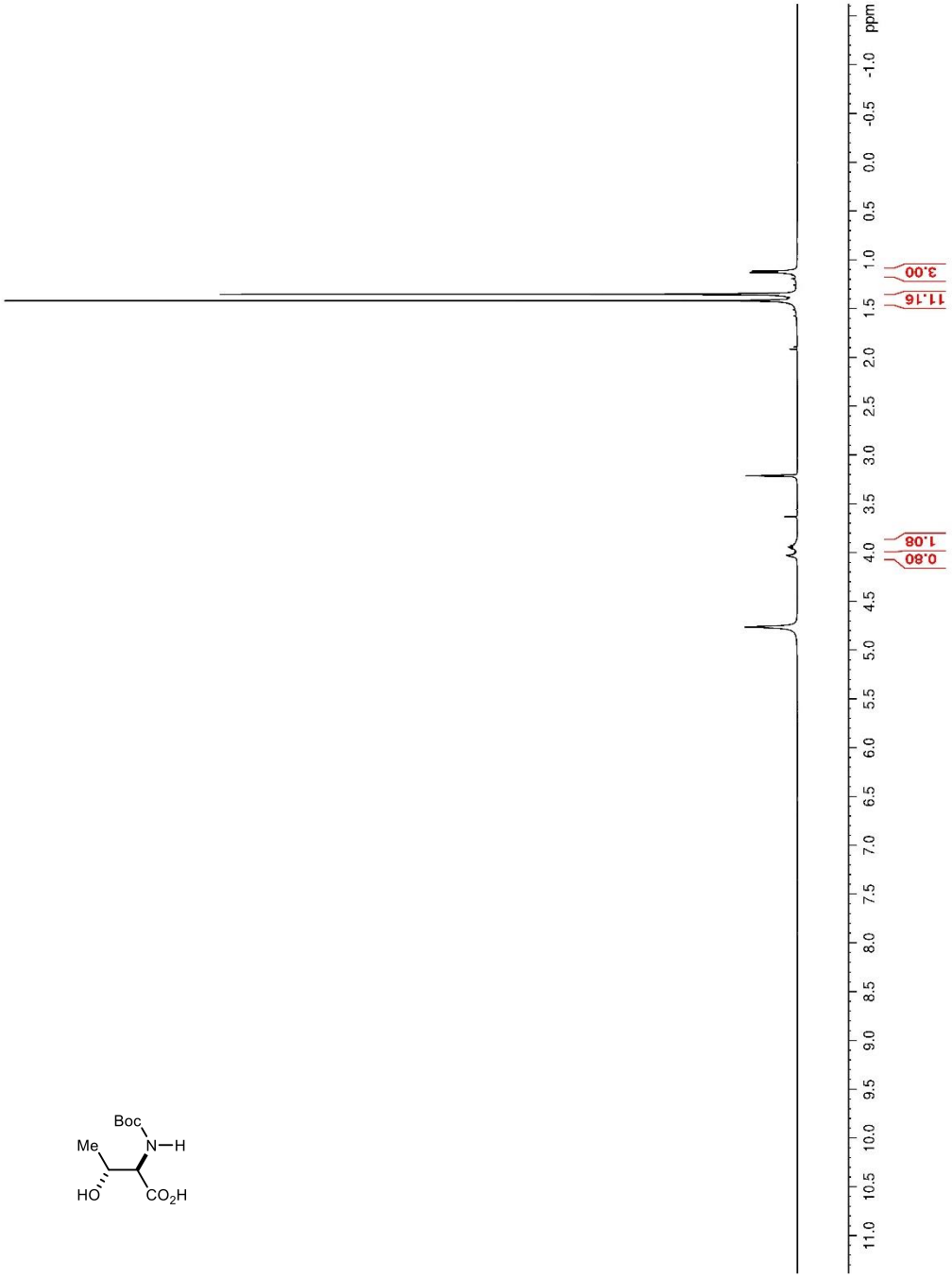

Figure 209. ^{1}H NMR (400 MHz, MeOD) spectrum of **2.14**.

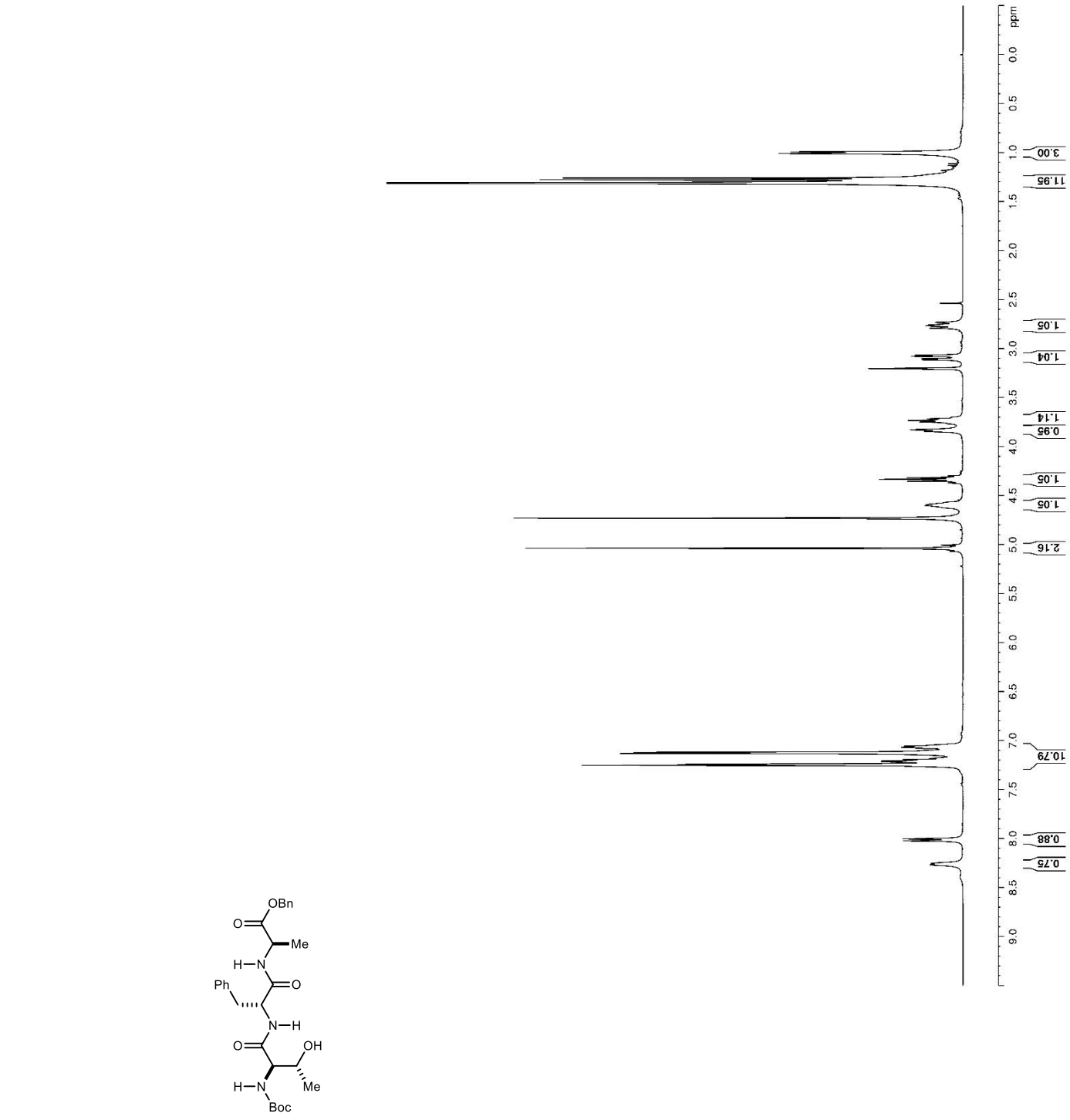

Figure 210. ^{13}C and DEPT-135 NMR (100 MHz, MeOD) spectrum of **2.14**.

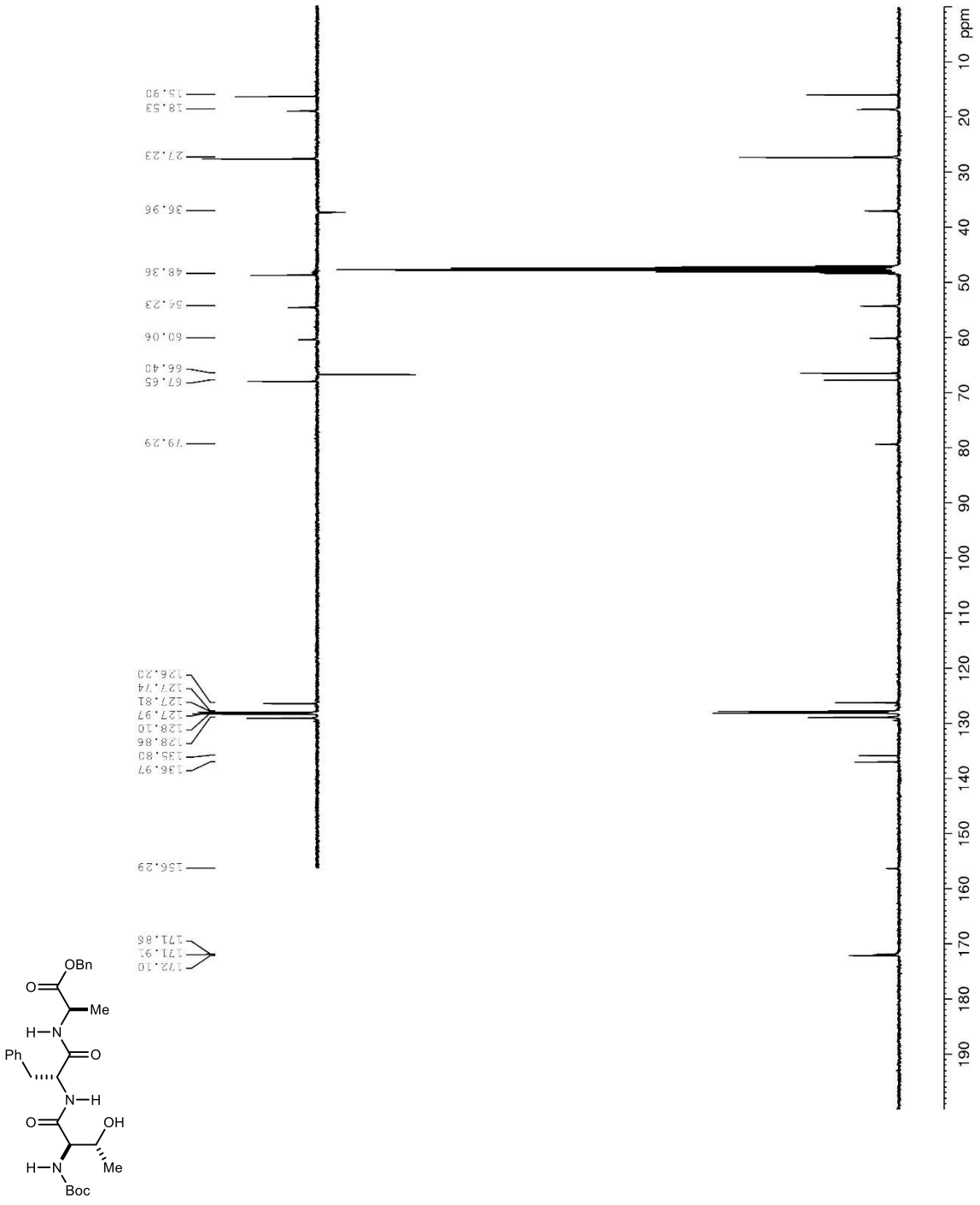

Figure 211. ^{1}H NMR (400 MHz, MeOD) spectrum of **2.15**.

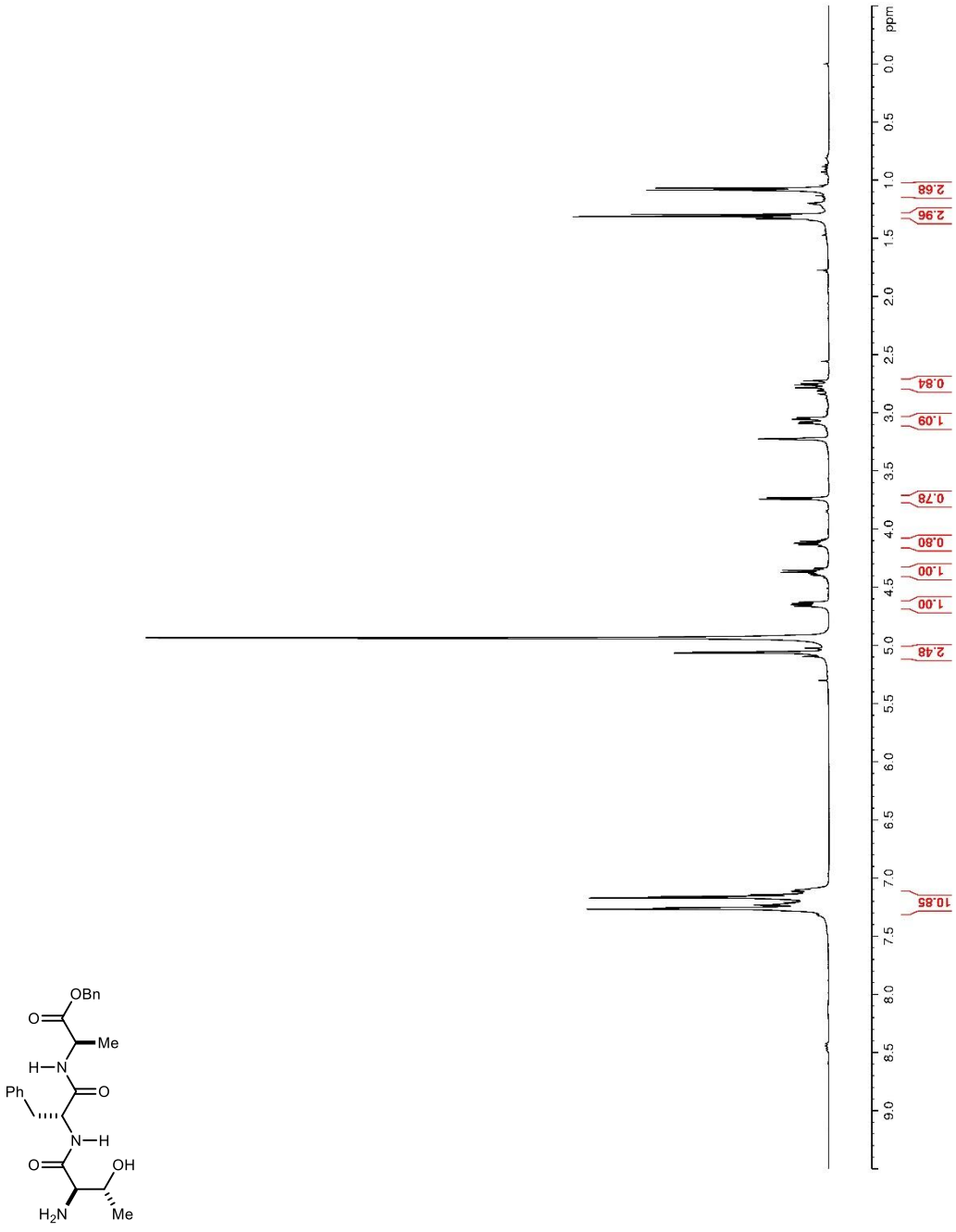

Figure 212. ^{13}C and DEPT-135 NMR (100 MHz, MeOD) spectrum of **2.15**.

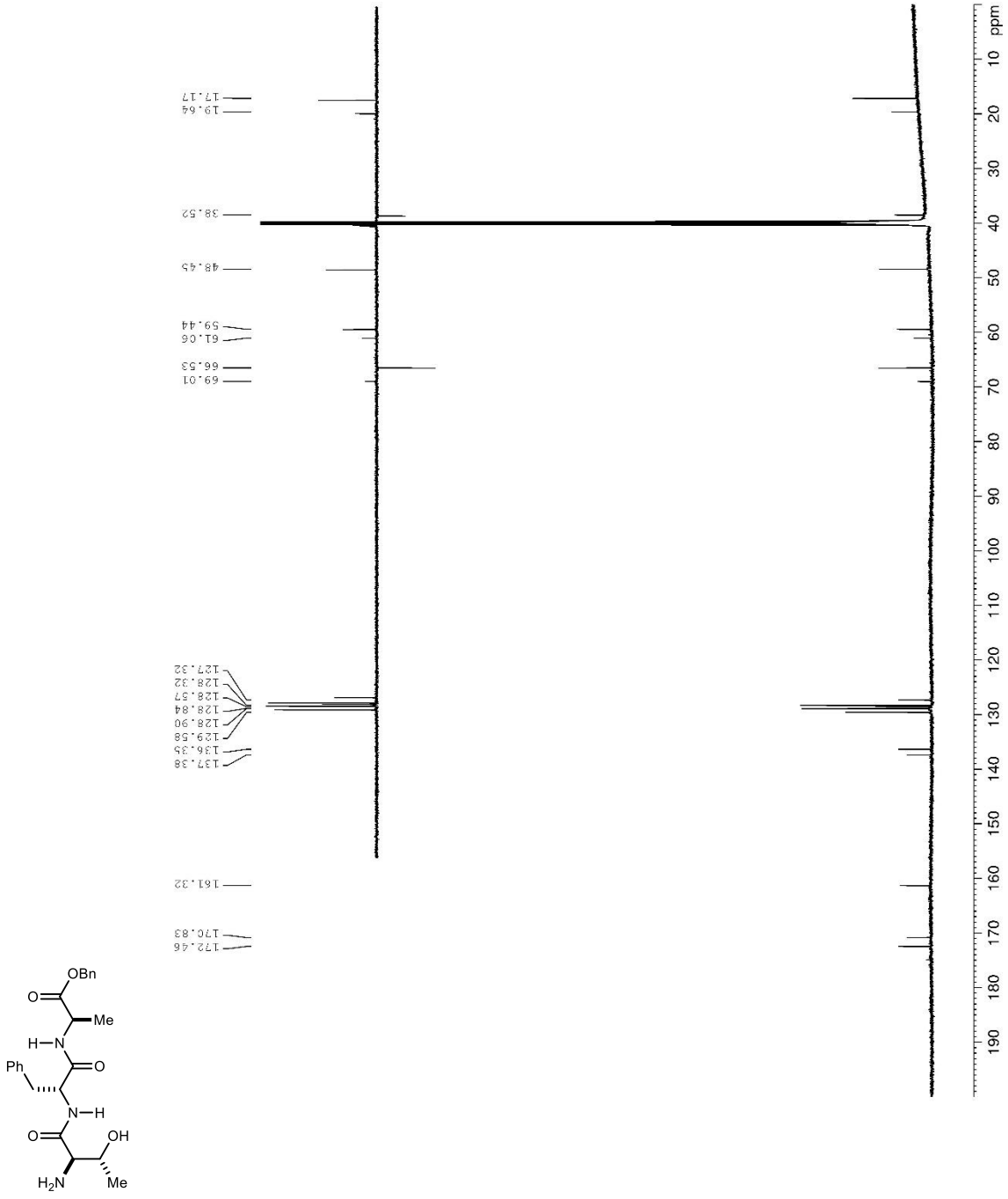

Figure 213. ^{1}H NMR (600 MHz, acetone-d_6) spectrum of **2.16**.

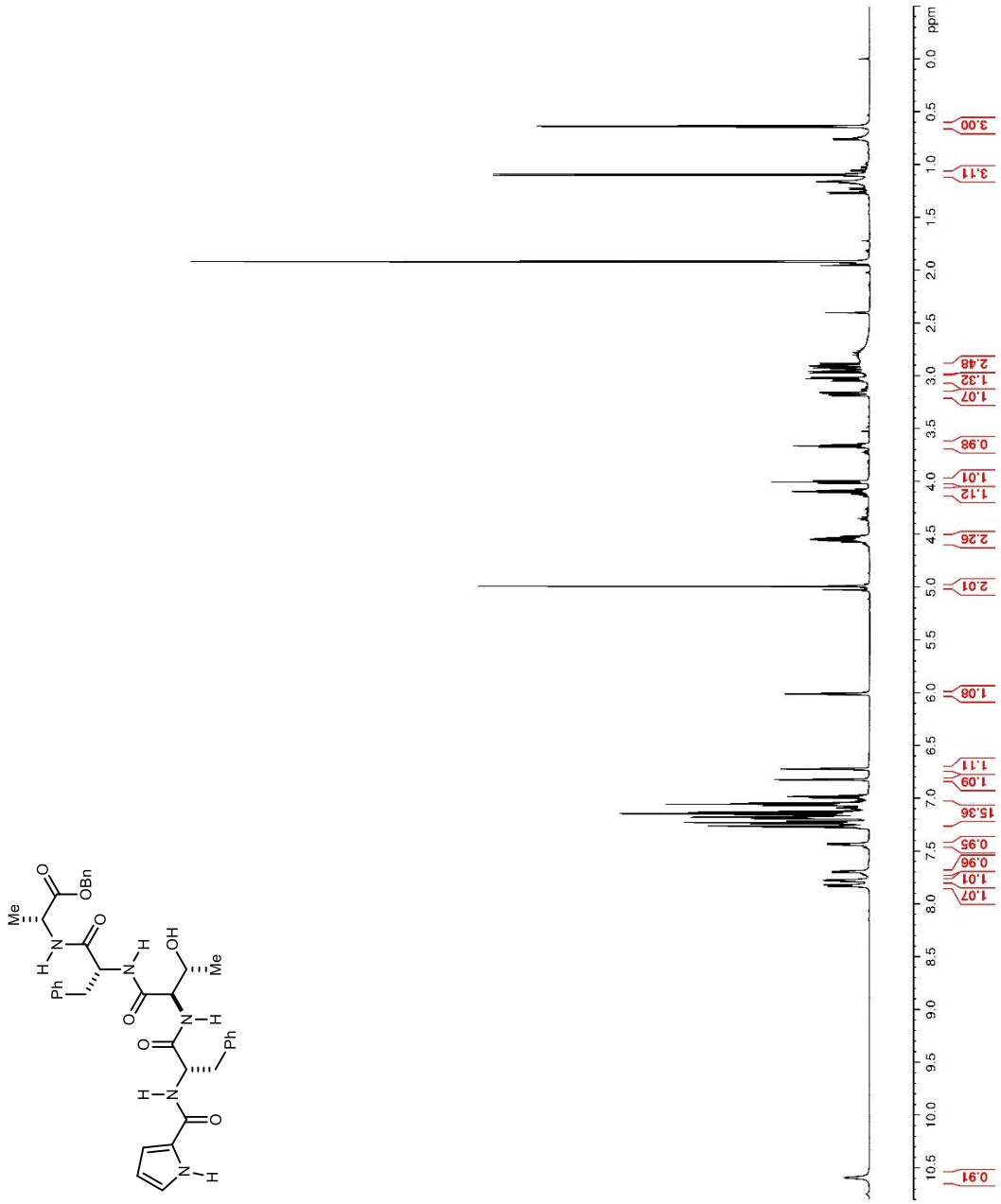

Figure 214. ^{13}C and DEPT-135 NMR (150 MHz, acetone-d_6) spectrum of **2.16**.

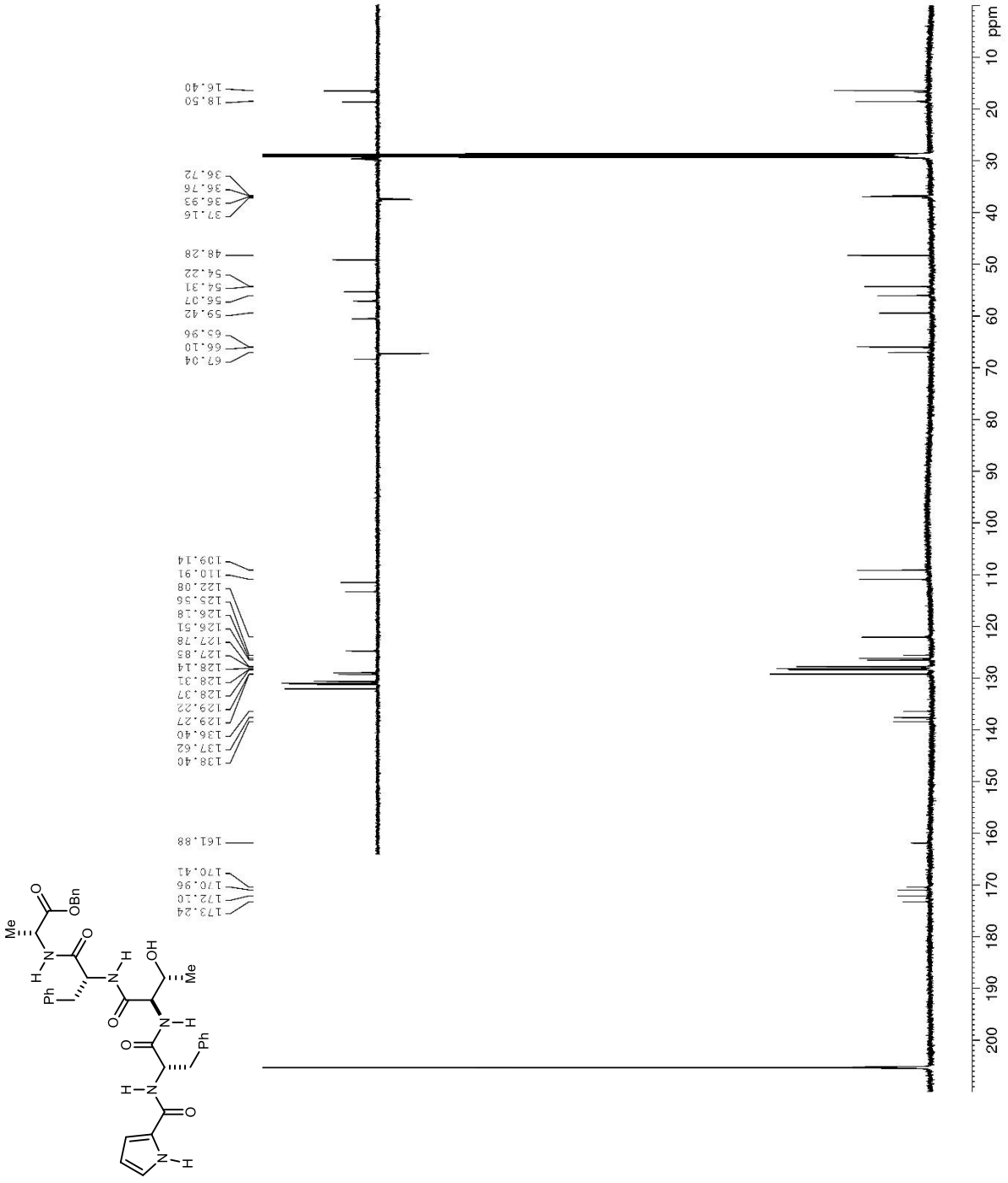

Figure 215. ^{1}H NMR (400 MHz, $CDCl_3$) spectrum of **2.24.**

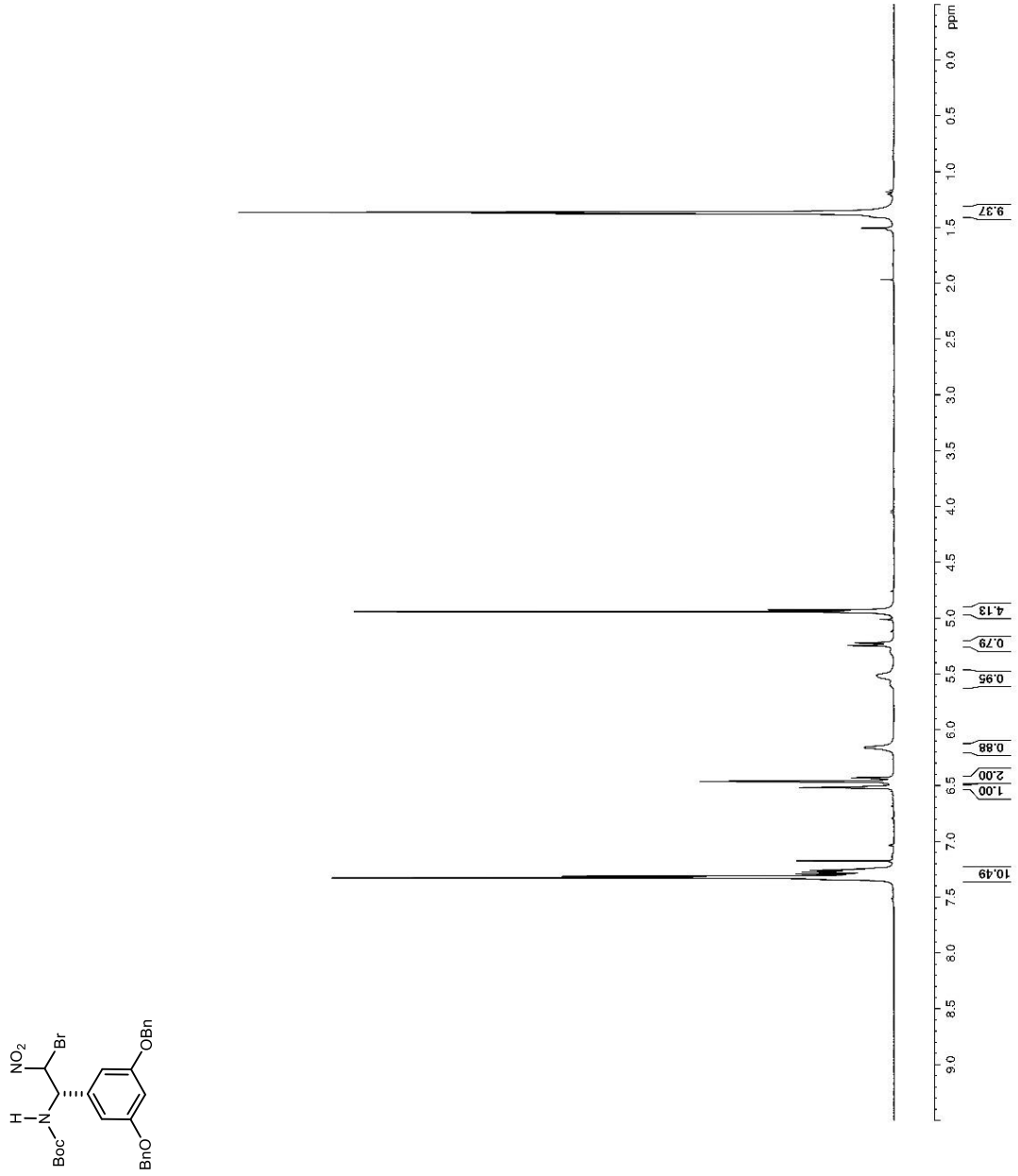

Figure 216. ^{13}C and DEPT-135 NMR (100 MHz, $CDCl_3$) spectra of **2.24.**

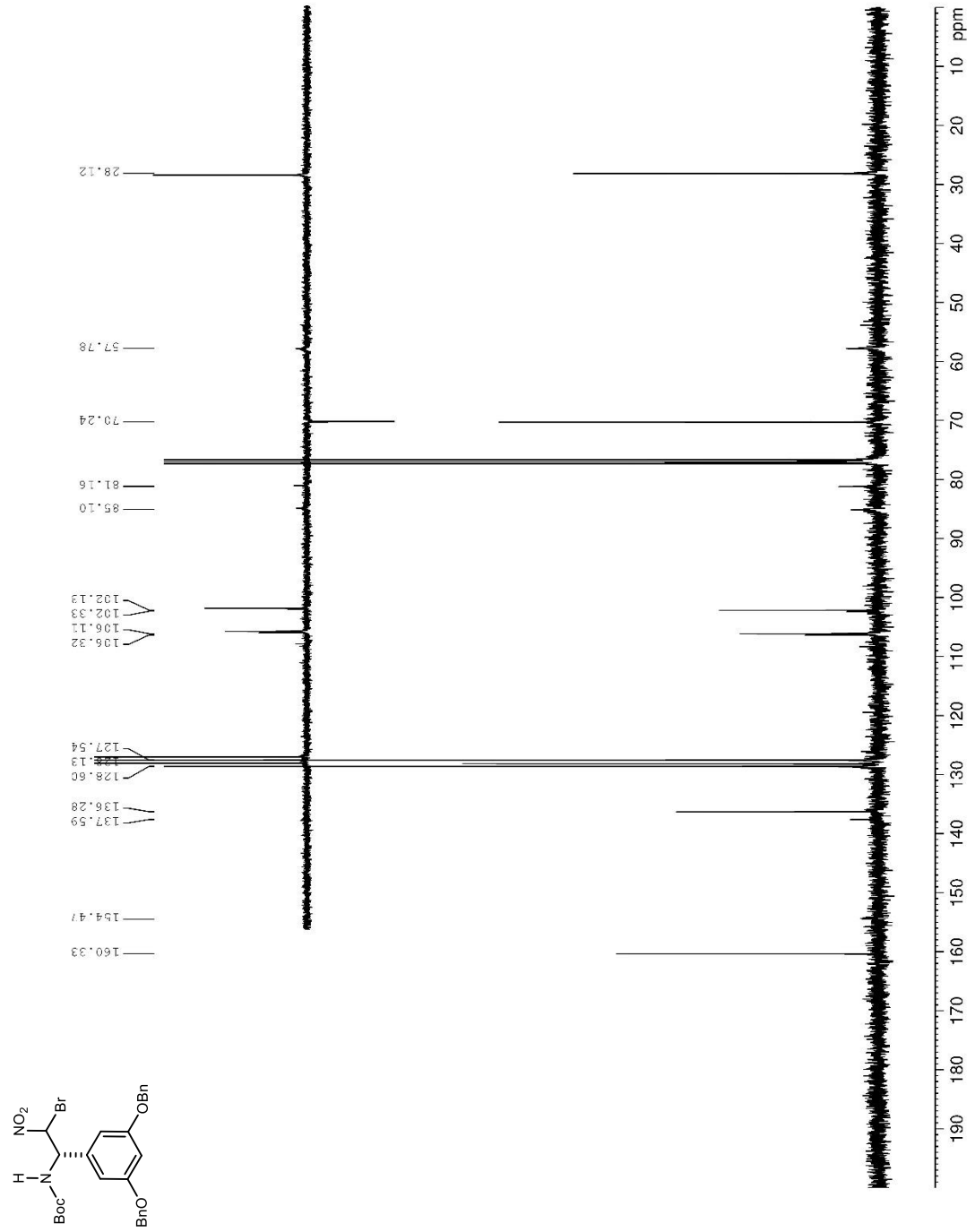

Figure 217. ^{1}H NMR (400 MHz, $CDCl_3$) spectrum of **2.28**.

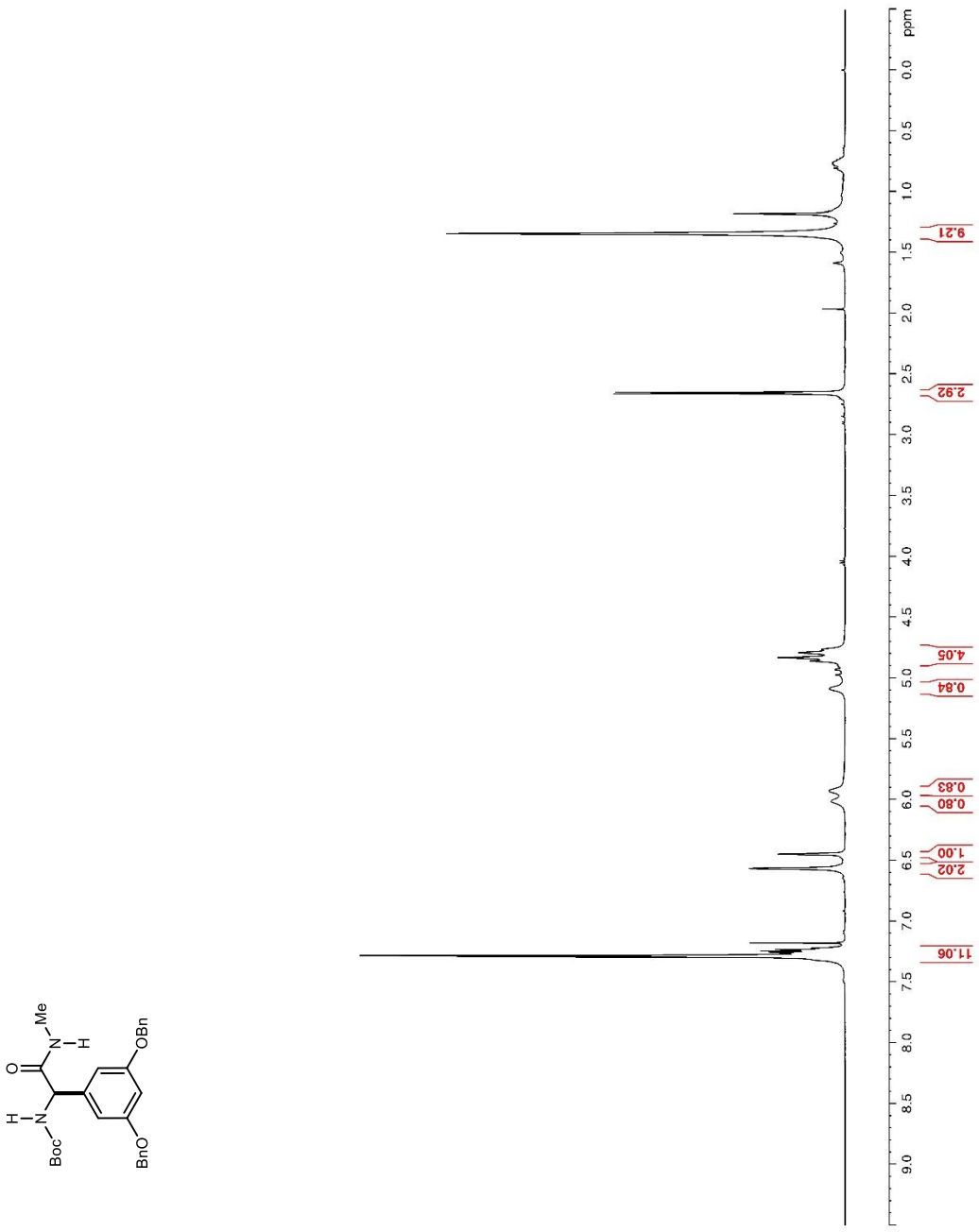

Figure 218. ^{13}C and DEPT-135 NMR (100 MHz, $CDCl_3$) spectra of **2.28**.

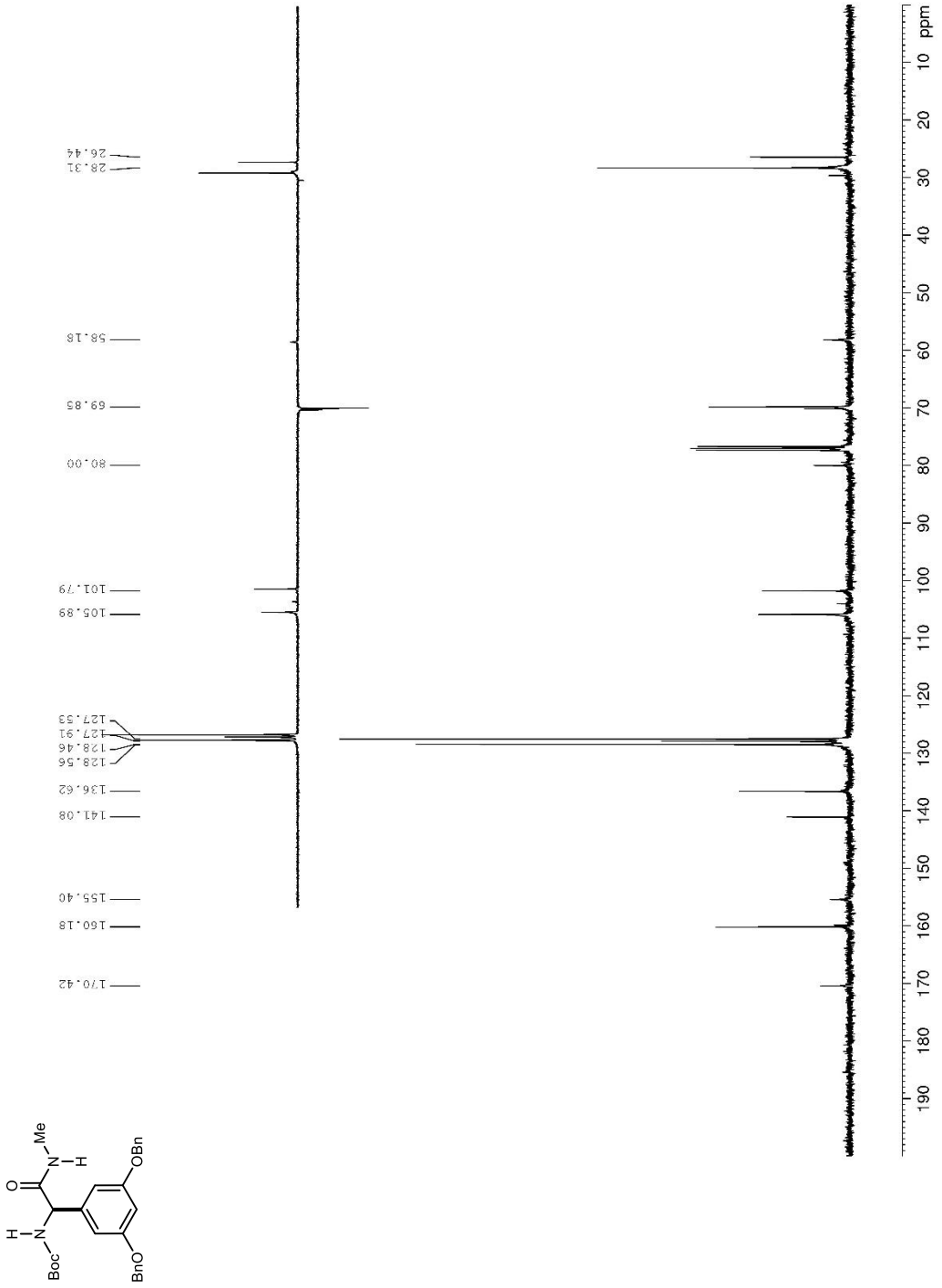

Figure 219. ^{1}H NMR (400 MHz, DMSO-d_6) spectrum of **2.27**.

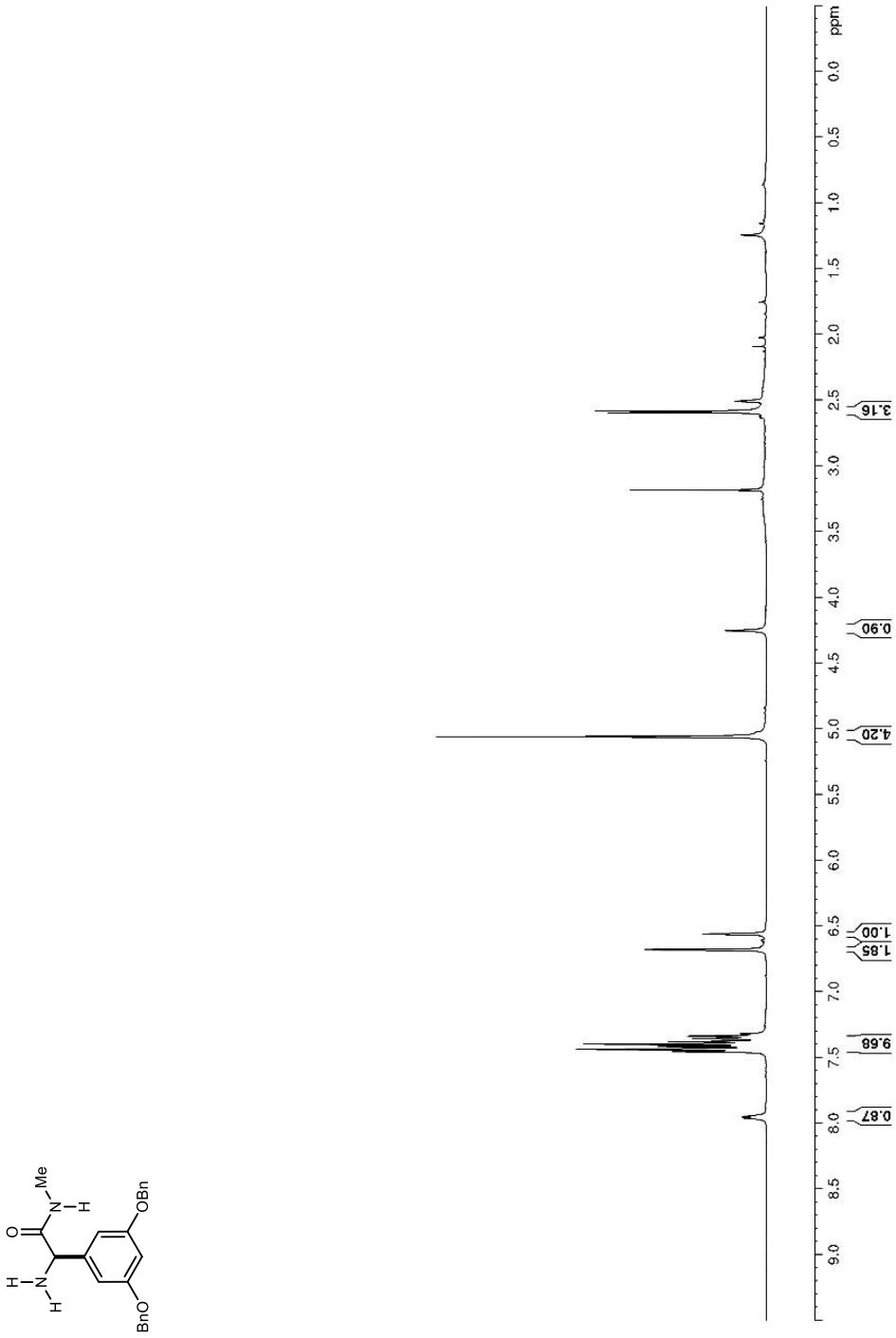

Figure 220. ^{13}C and DEPT-135 NMR (100 MHz, DMSO-d_6) spectrum of **2.27**.

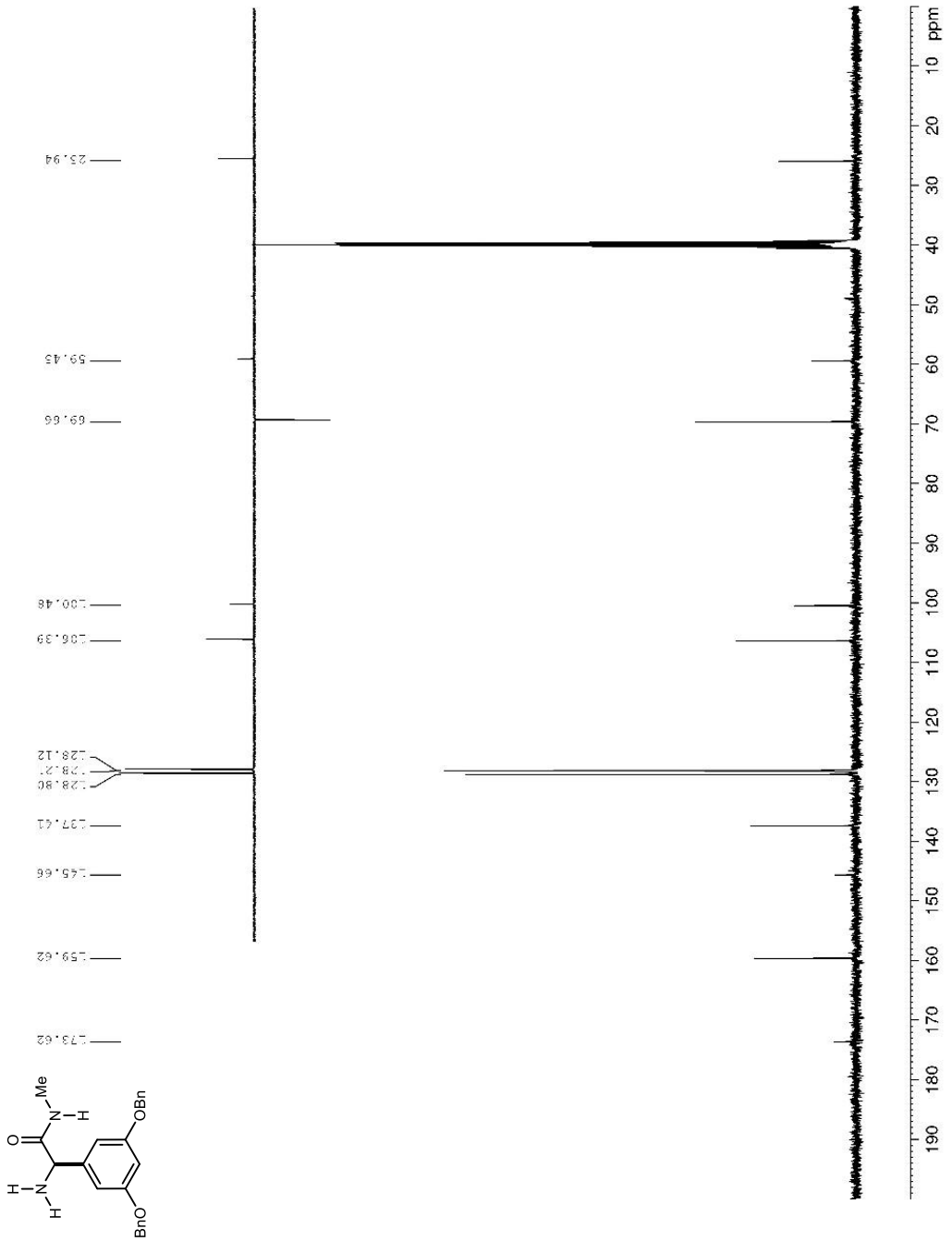

Figure 221. ^{1}H NMR (600 MHz, acetone-d_6) spectrum of **2.31**.

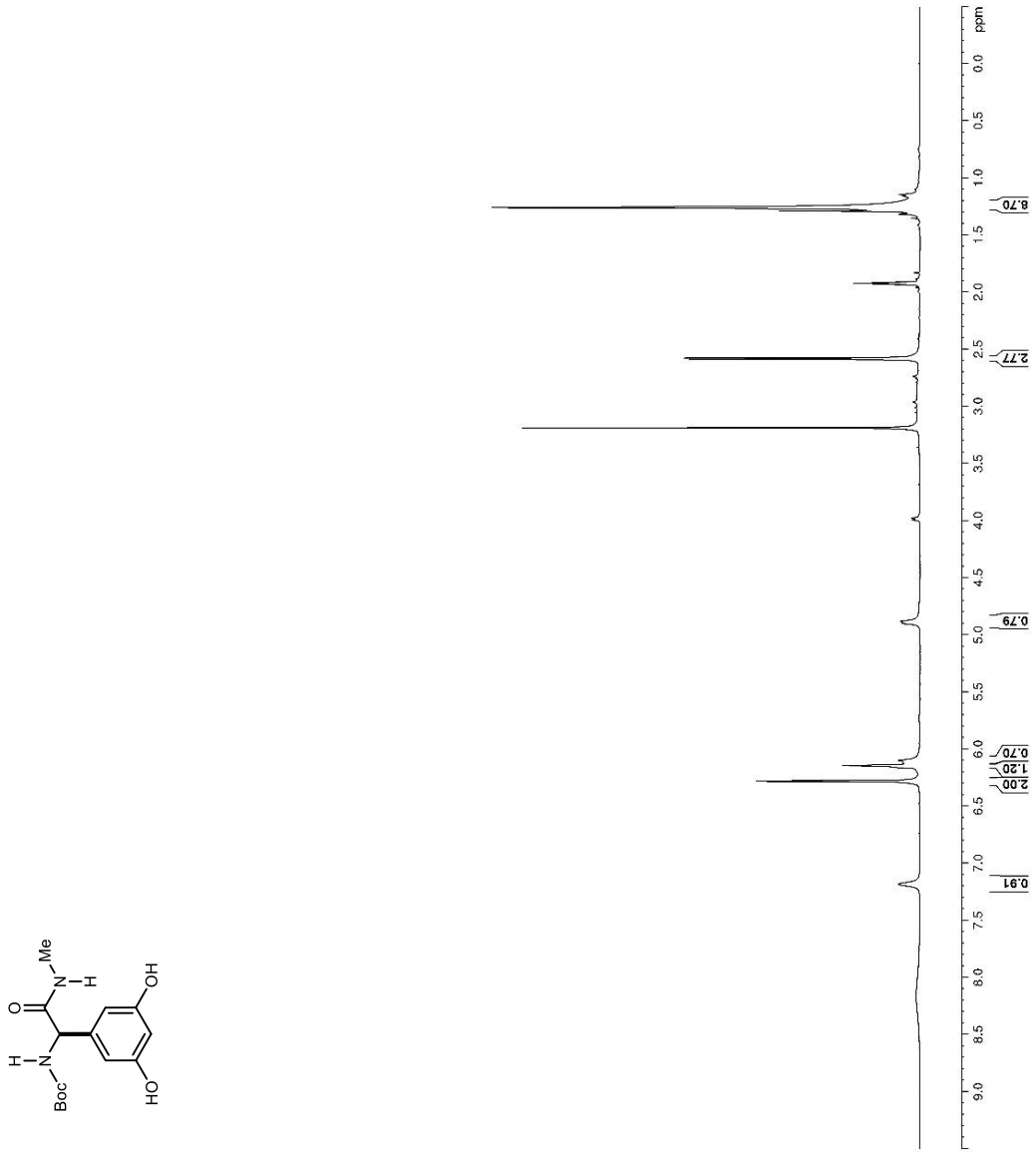

Figure 222. ^{13}C and DEPT-135 NMR (150 MHz, acetone-d_6) spectrum of **2.31**.

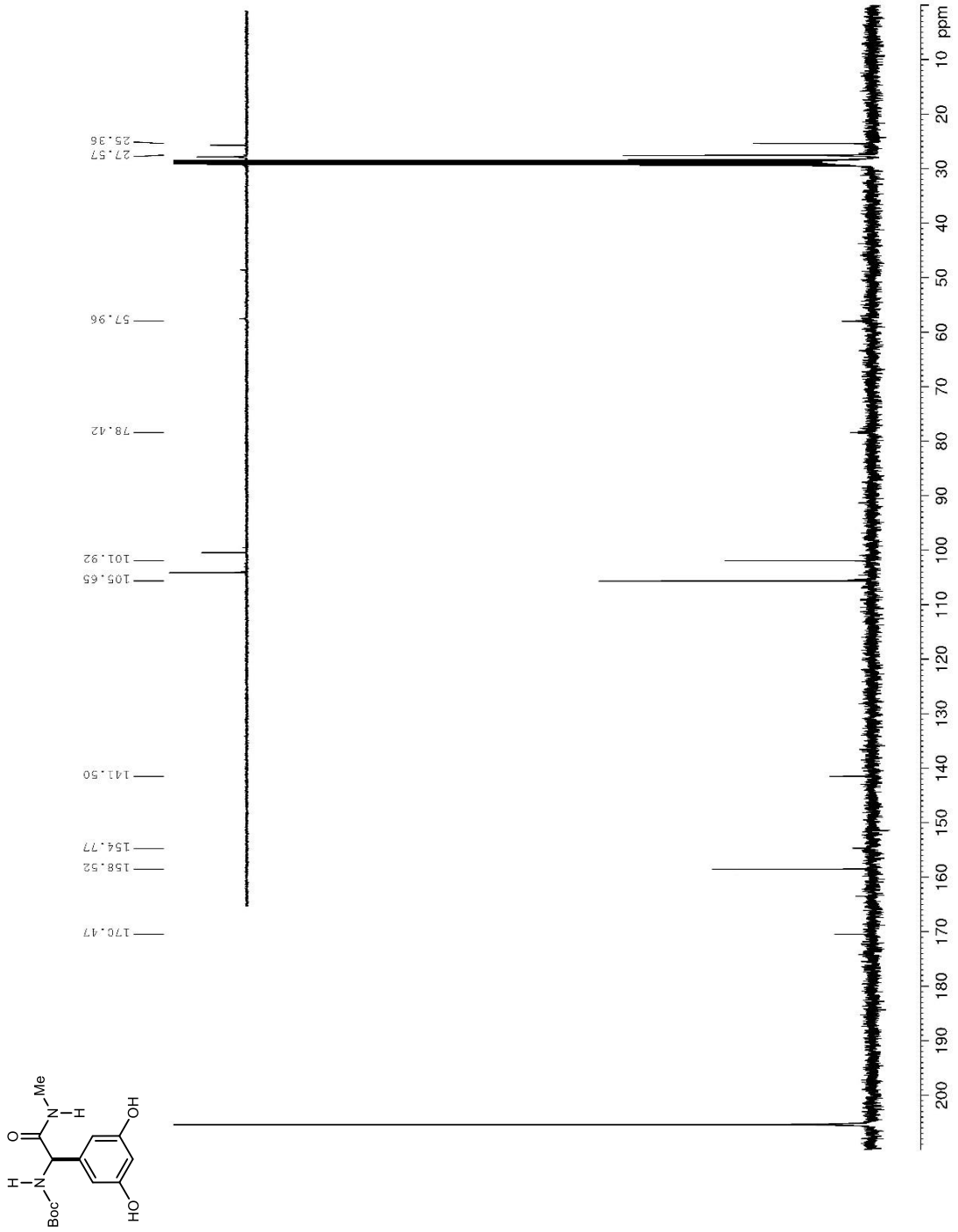

Figure 223. ^{1}H NMR (600 MHz, acetone-d_6) spectrum of **2.32**.

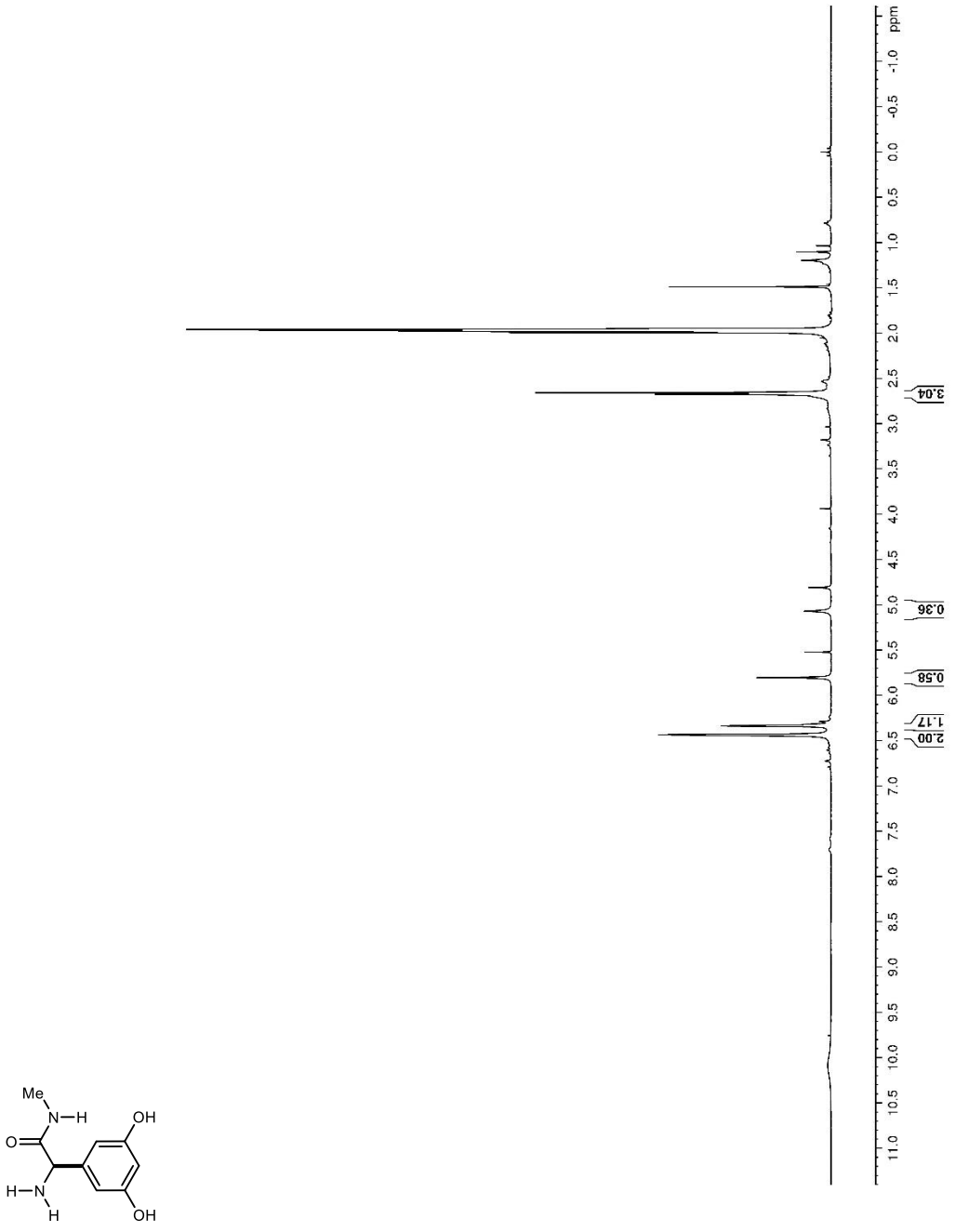

Figure 224. ^{1}H NMR (600 MHz, $CDCl_3$) spectrum of **2.39**.

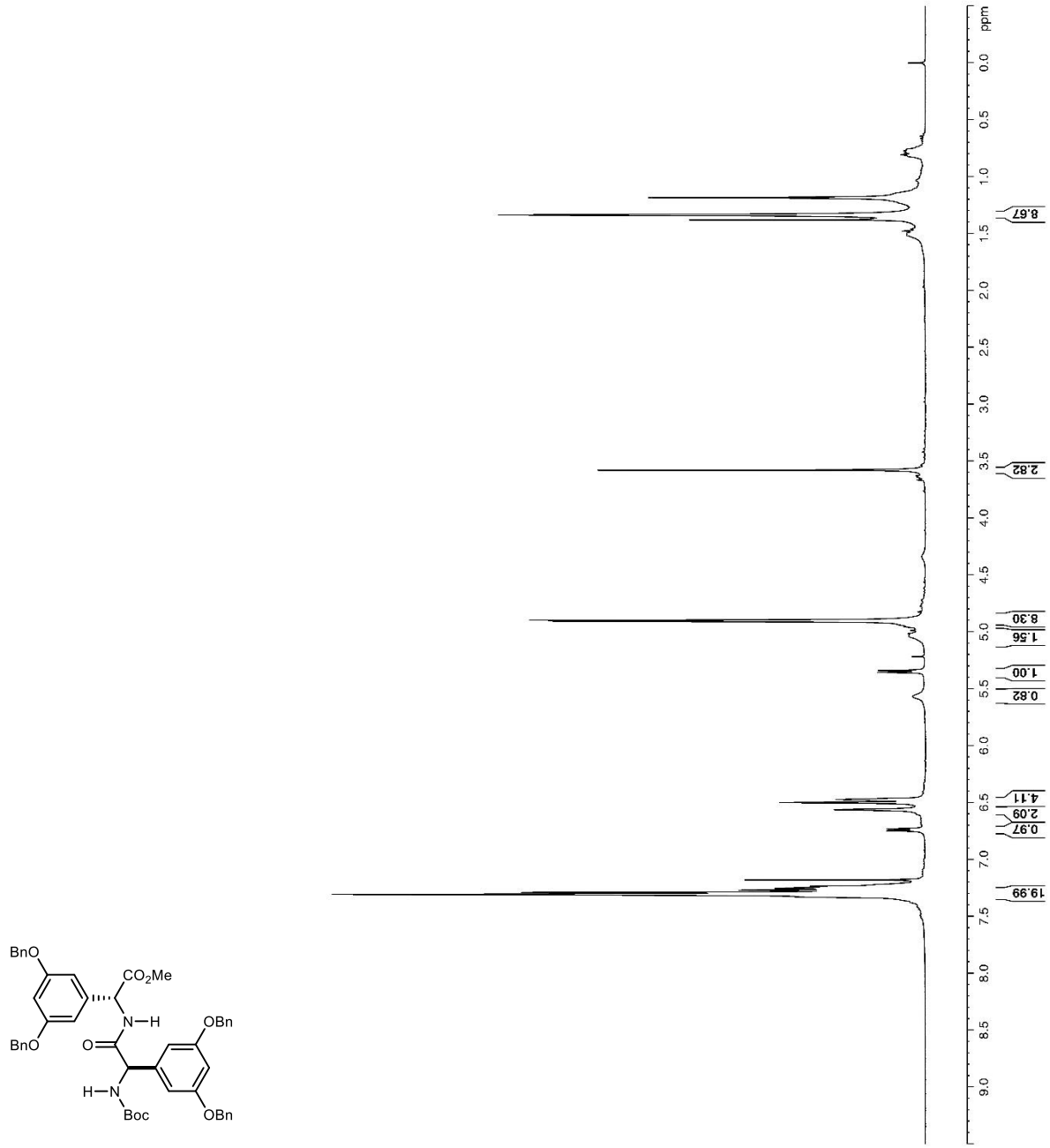

Figure 225. ^{13}C and DEPT-135 NMR (150 MHz, $CDCl_3$) spectra of **2.39**.

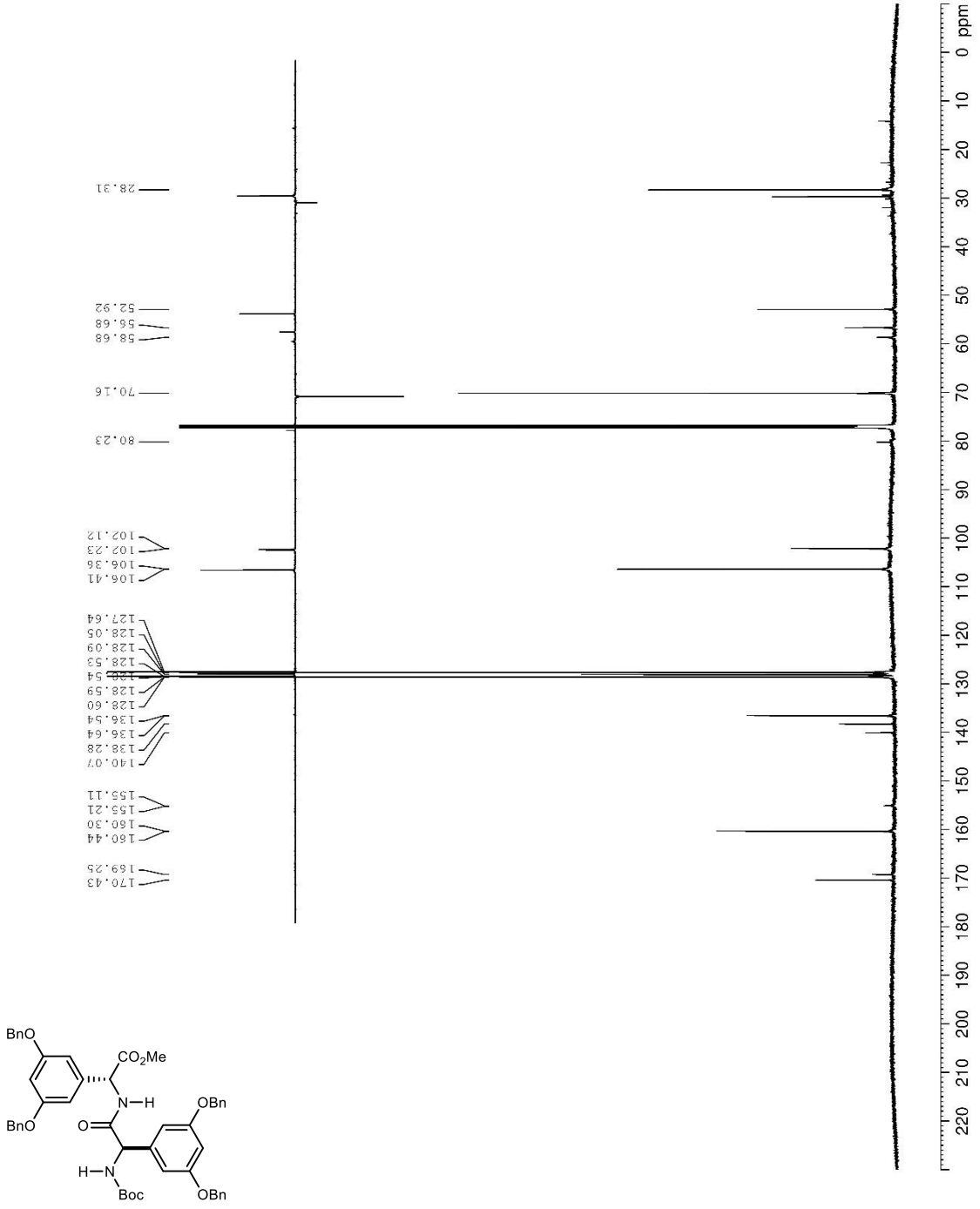

Figure 226. ^{1}H NMR (400 MHz, $CDCl_3$) spectrum of two epimers (**2.40**) formed in DEPBT coupling.

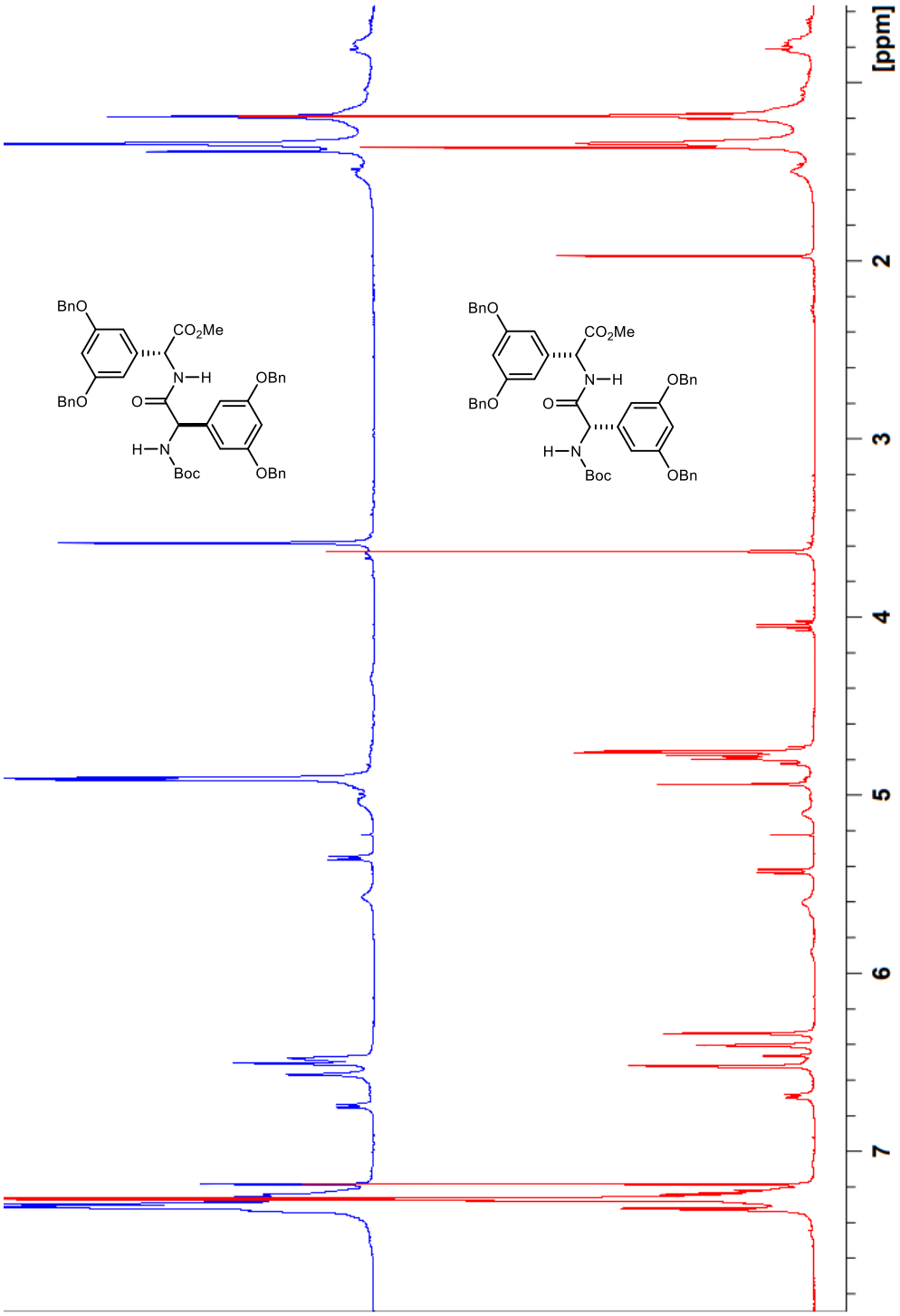

Figure 227. ^{1}H NMR (600 MHz, $CDCl_3$) spectrum of **2.43**.

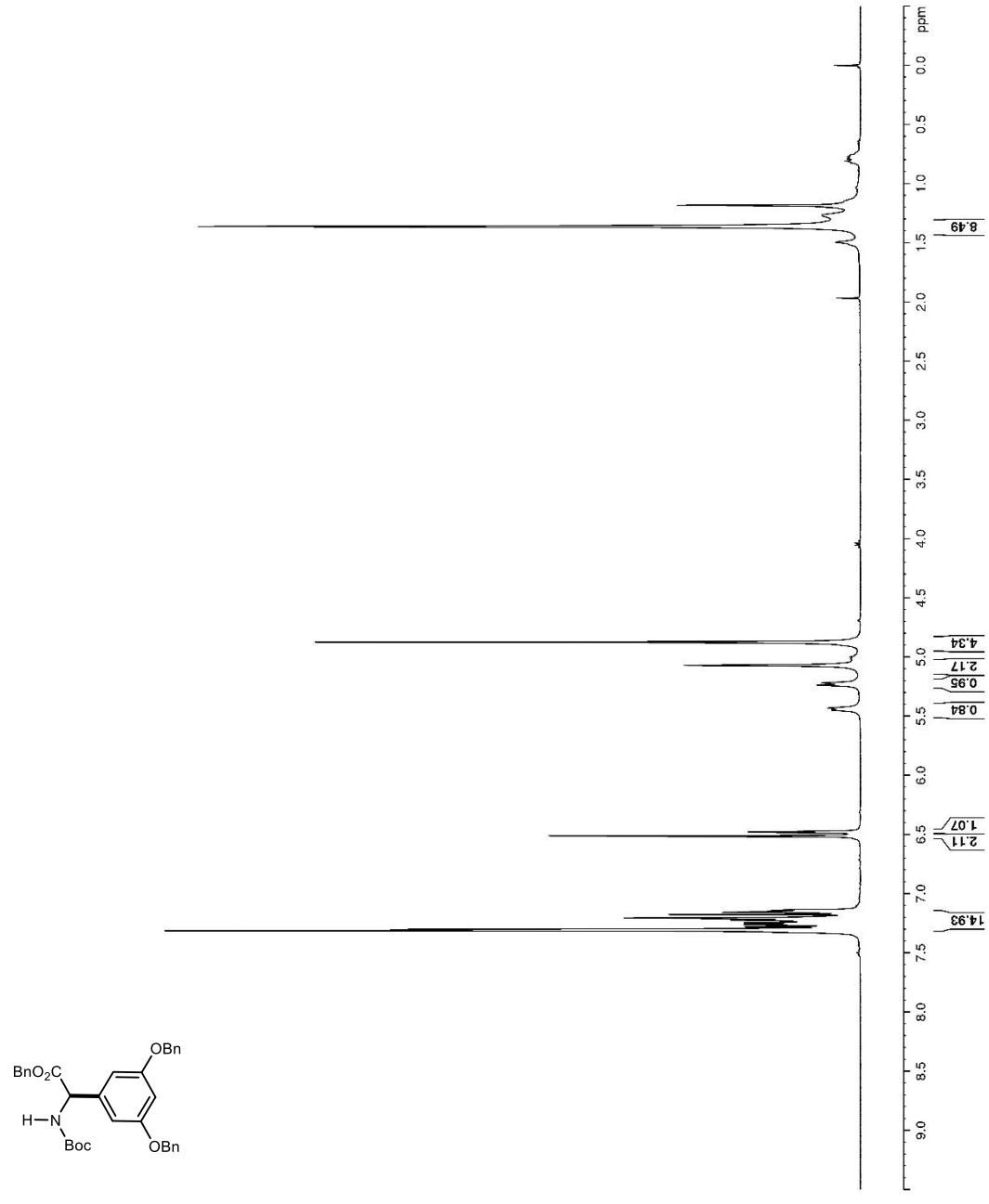

Figure 228. ^{13}C and DEPT-135 NMR (150 MHz, $CDCl_3$) spectra of **2.43**.

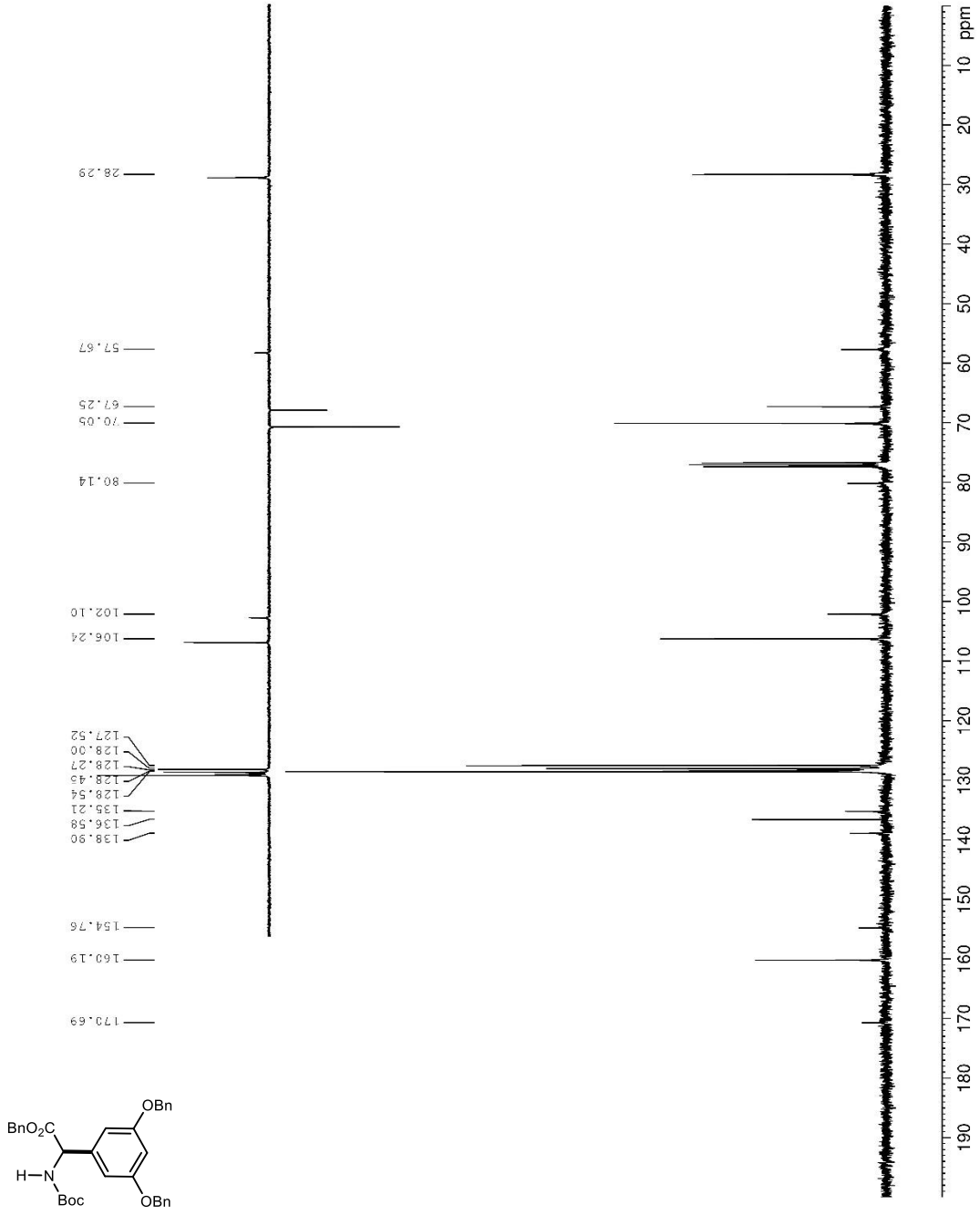

Figure 229. ^{1}H NMR (400 MHz, acetone-d_6) spectrum of **2.44**.

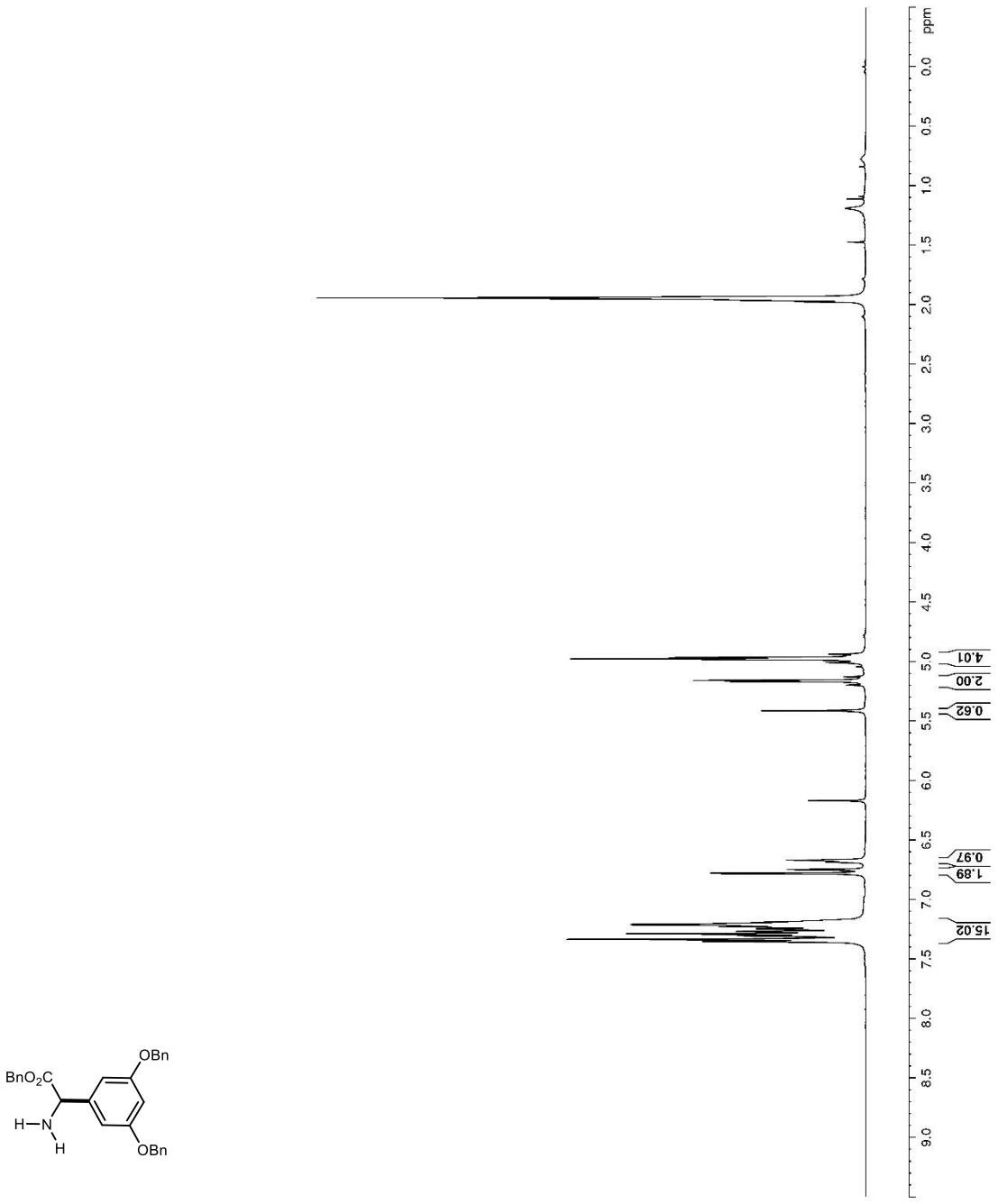

Figure 230. ^{13}C and DEPT-135 NMR (100 MHz, acetone-d_6) spectrum of **2.44**.

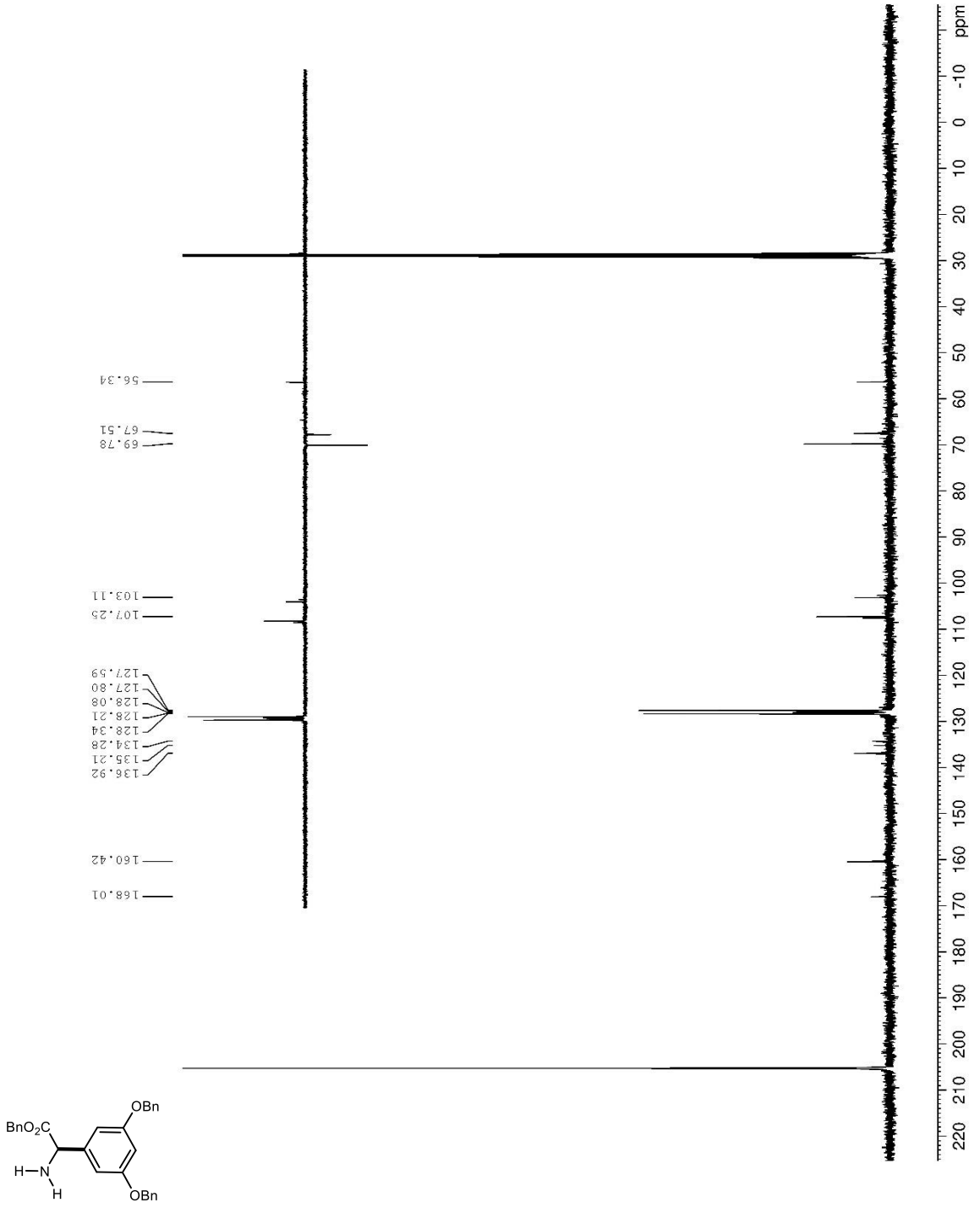

Figure 231. ^{1}H NMR (600 MHz, $CDCl_3$) spectrum of **2.45**.

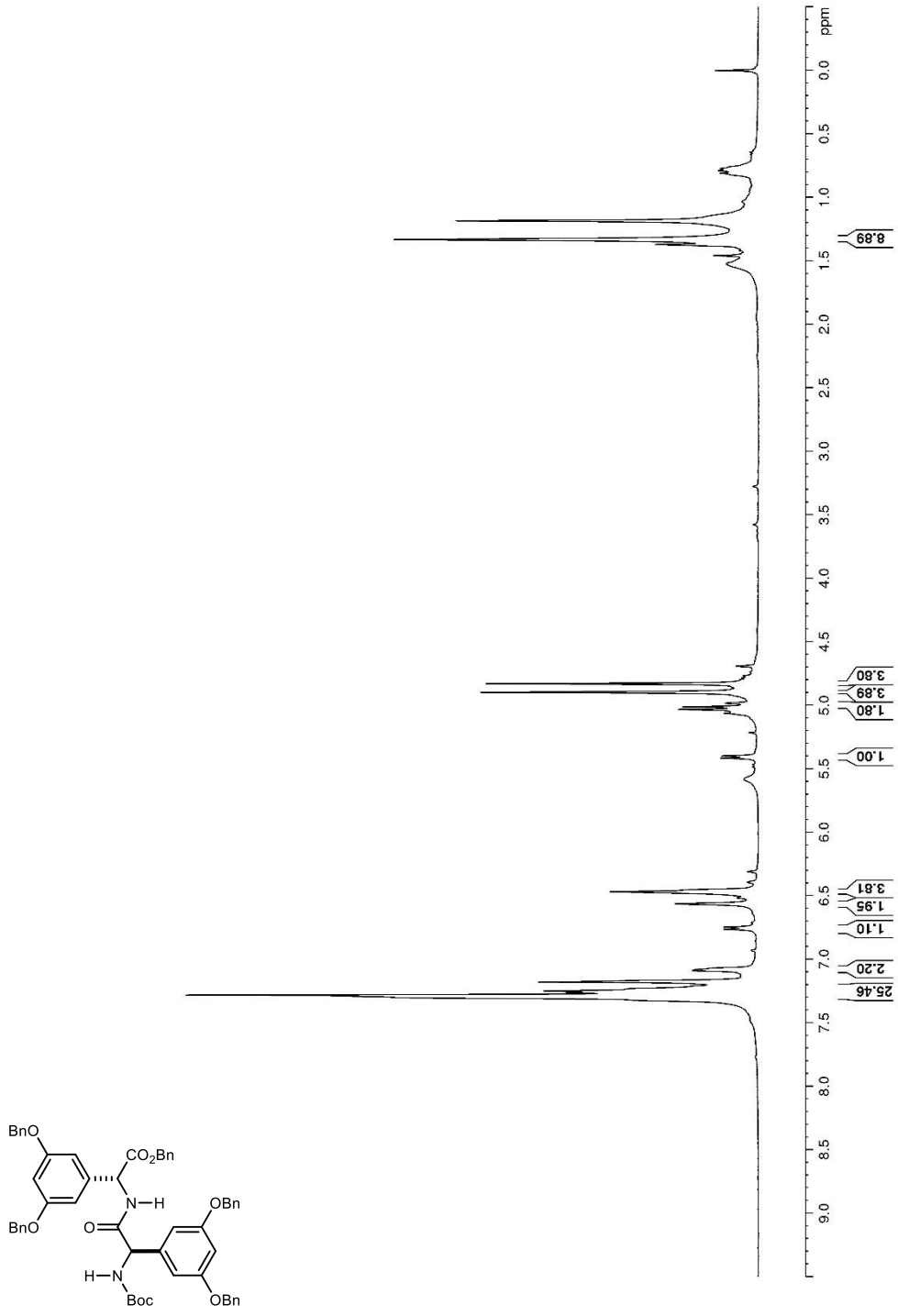

Figure 232. ^{13}C and DEPT-135 NMR (150 MHz, $CDCl_3$) spectra of **2.45**.

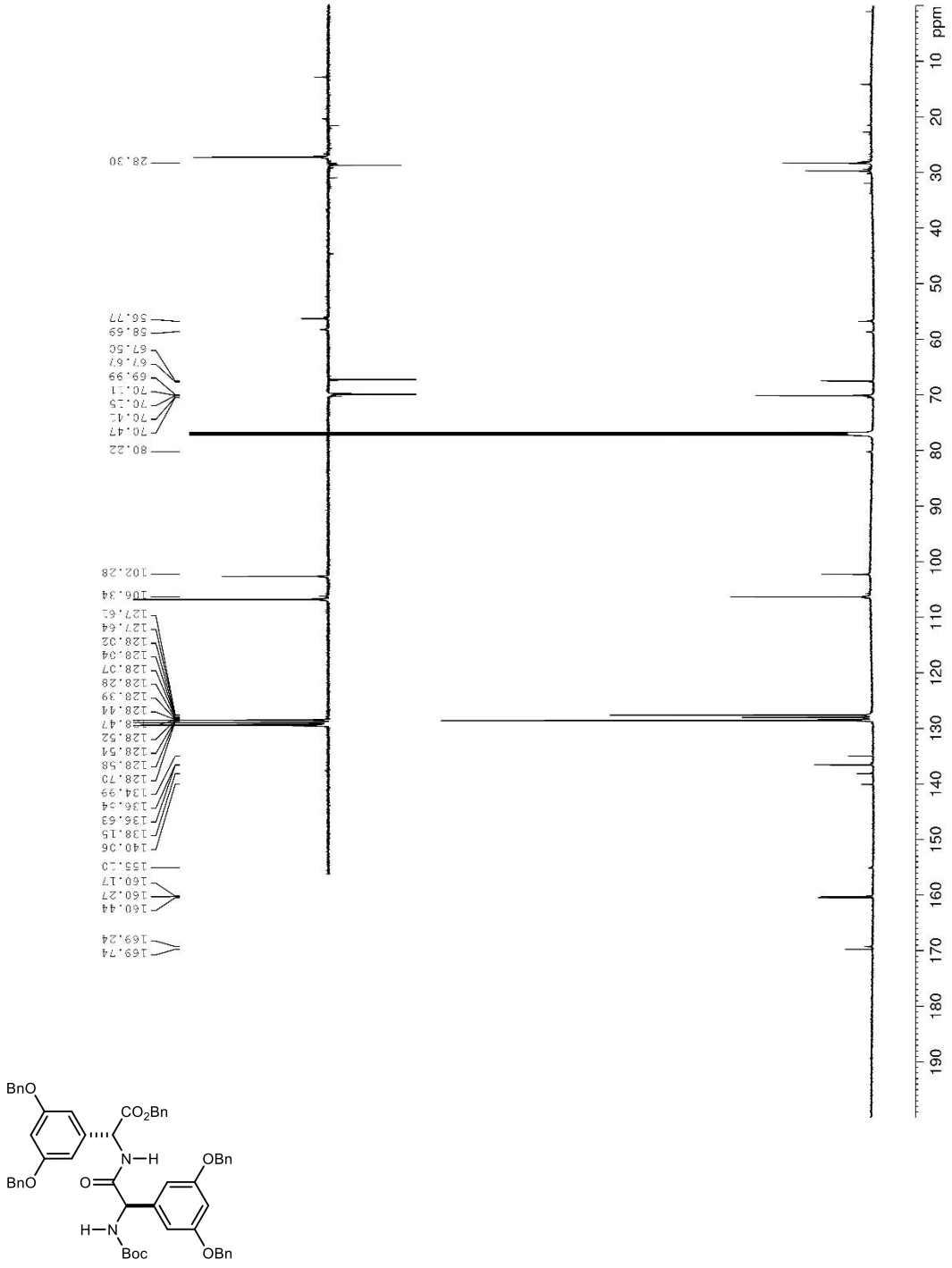

Figure 233. ^{1}H NMR (600 MHz, acetone-d_6) spectrum of **2.46**.

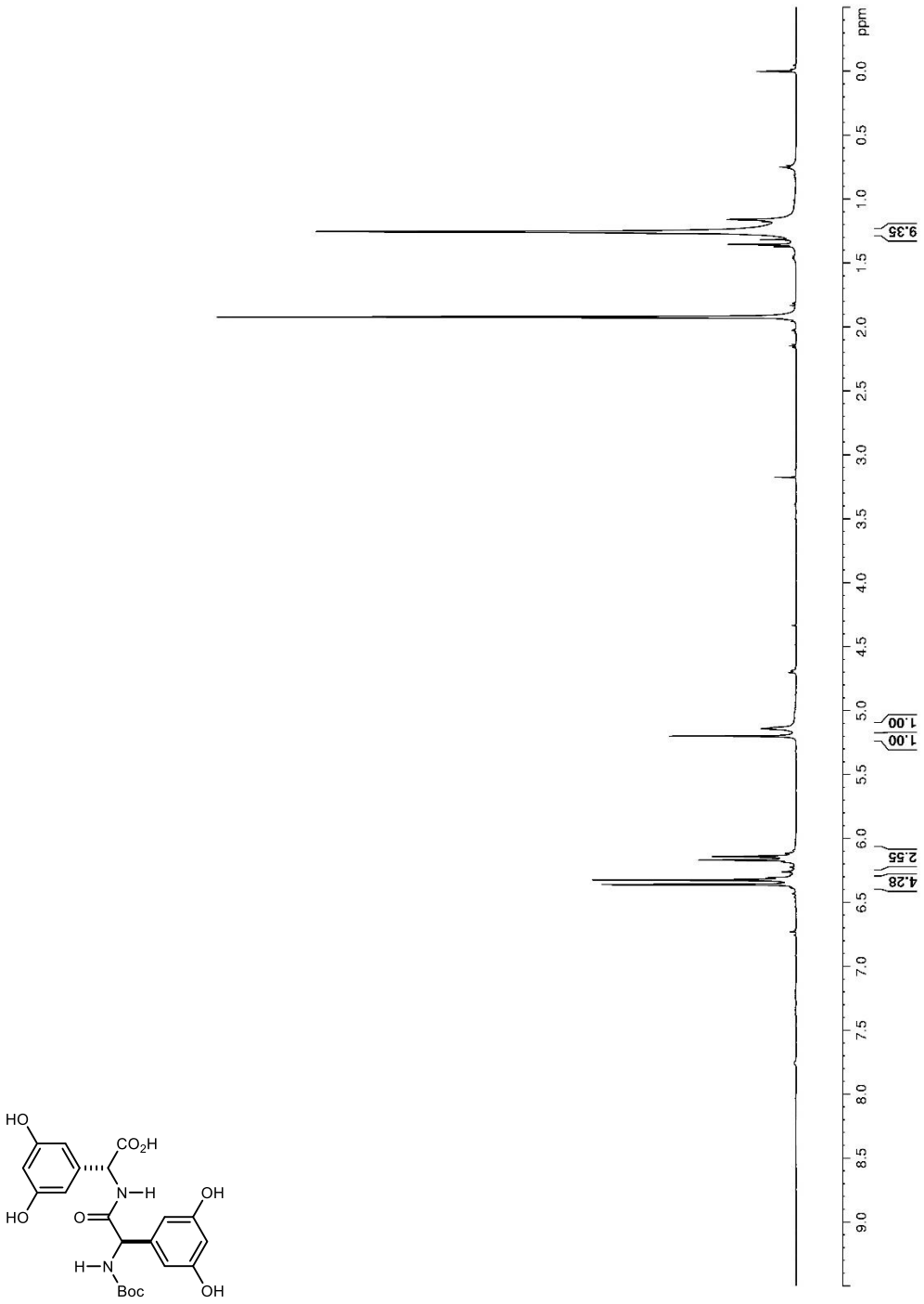

Figure 234. ^{1}H NMR (400 MHz, $CDCl_3$) spectrum of **2.47**.

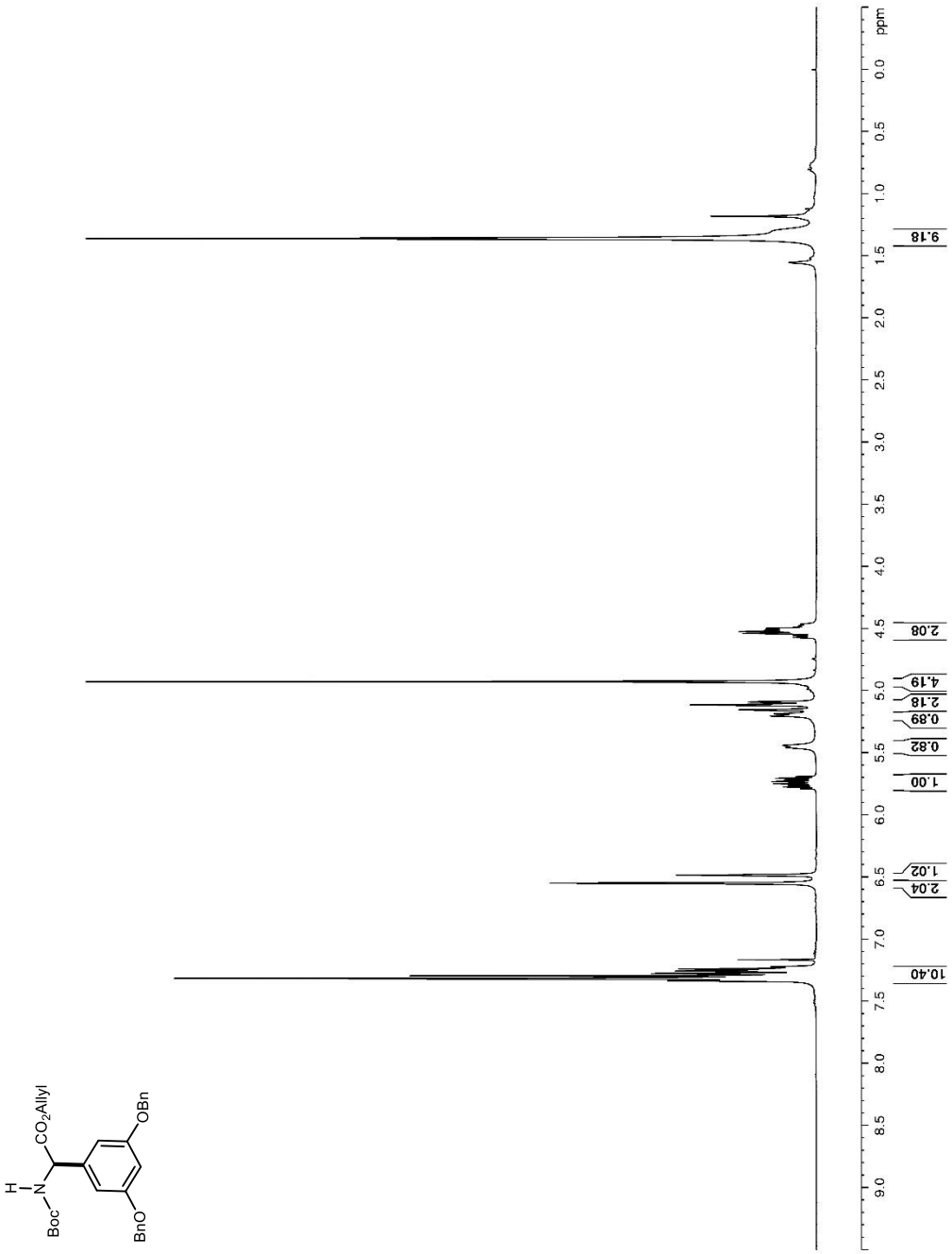

Figure 235. ^{13}C and DEPT-135 NMR (100 MHz, $CDCl_3$) spectra of **2.47**.

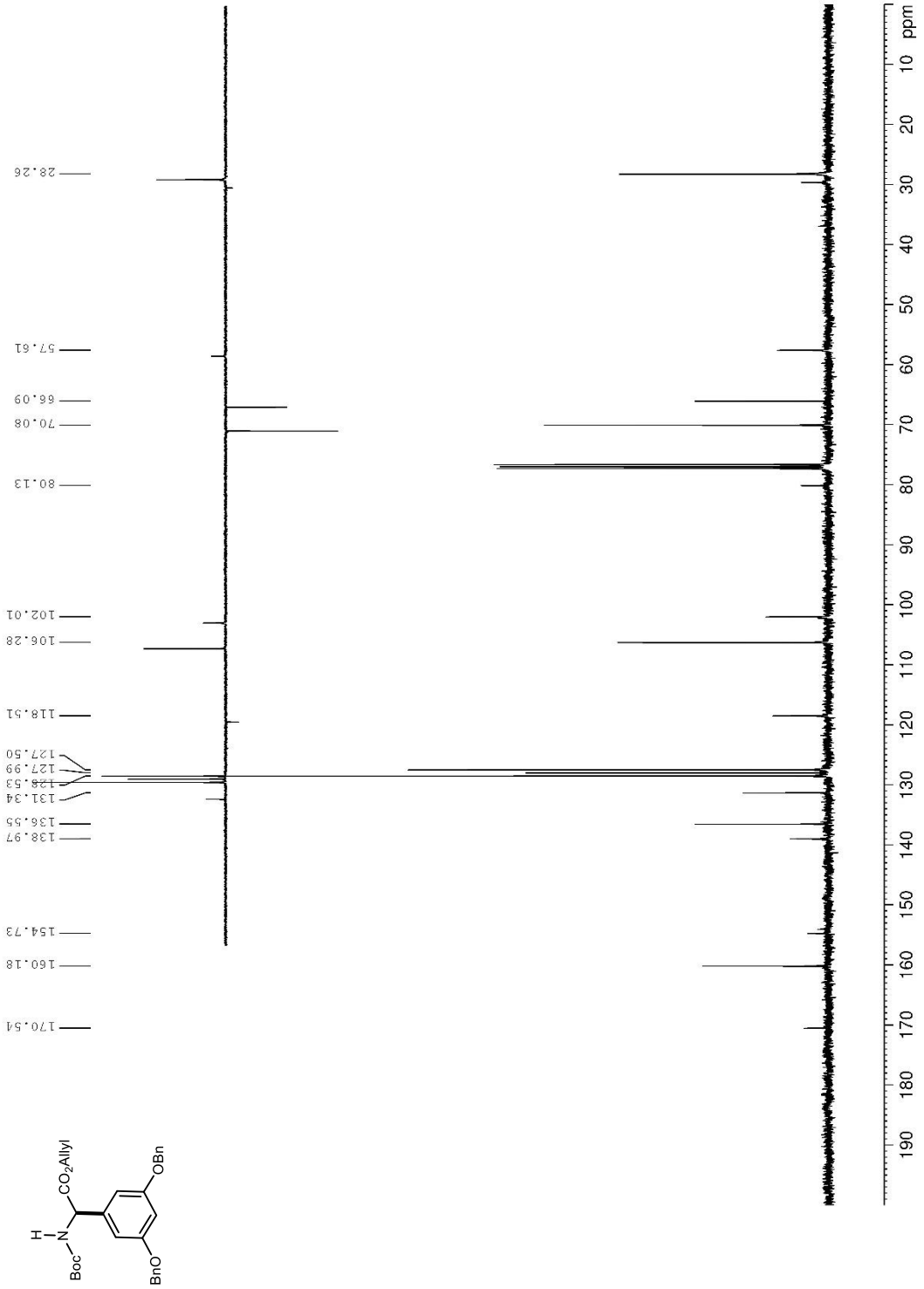

Figure 236. ^{1}H NMR (400 MHz, acetone-d_6) spectrum of **2.48**.

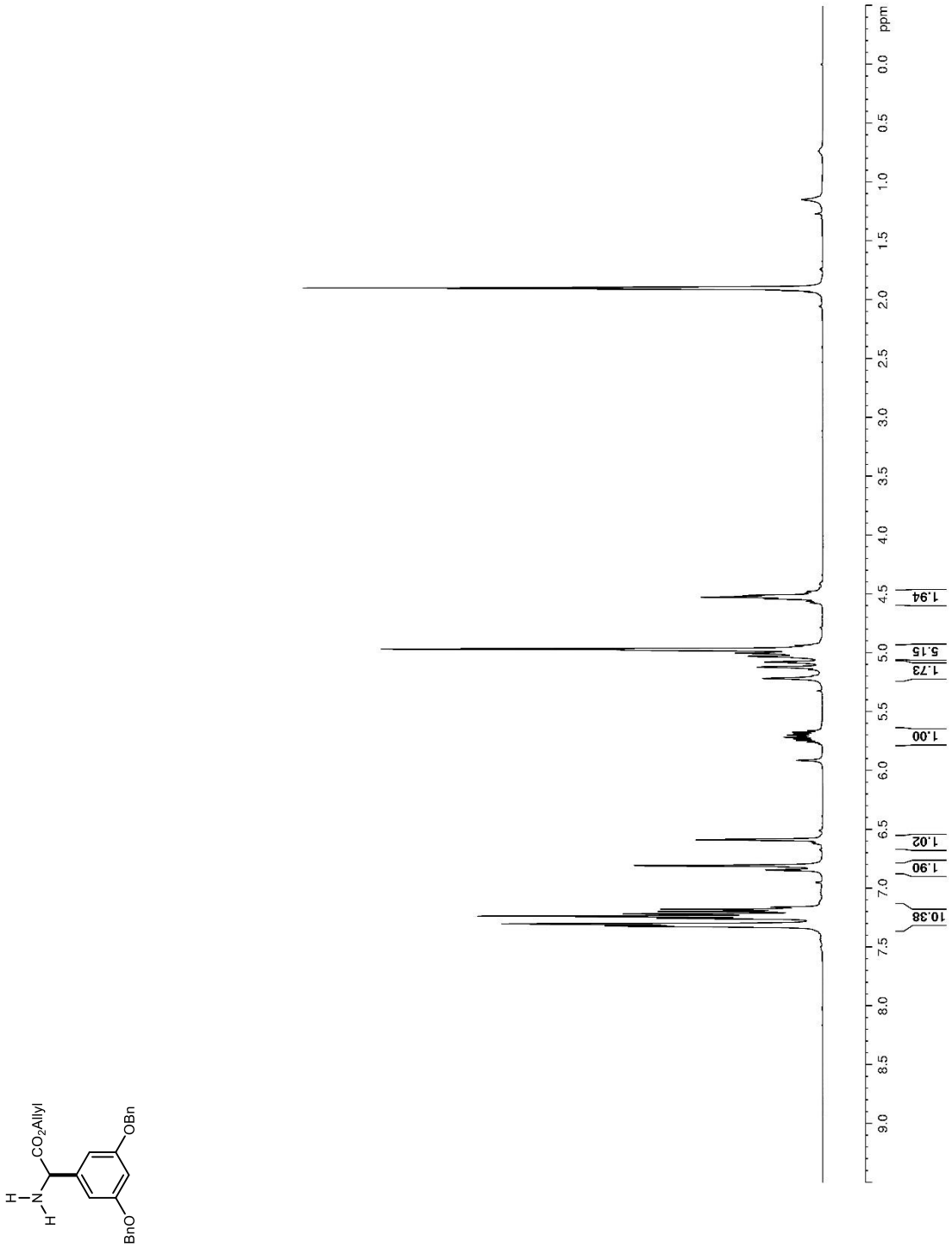

Figure 237. ^{13}C and DEPT-135 NMR (100 MHz, acetone-d_6) spectrum of **2.48**.

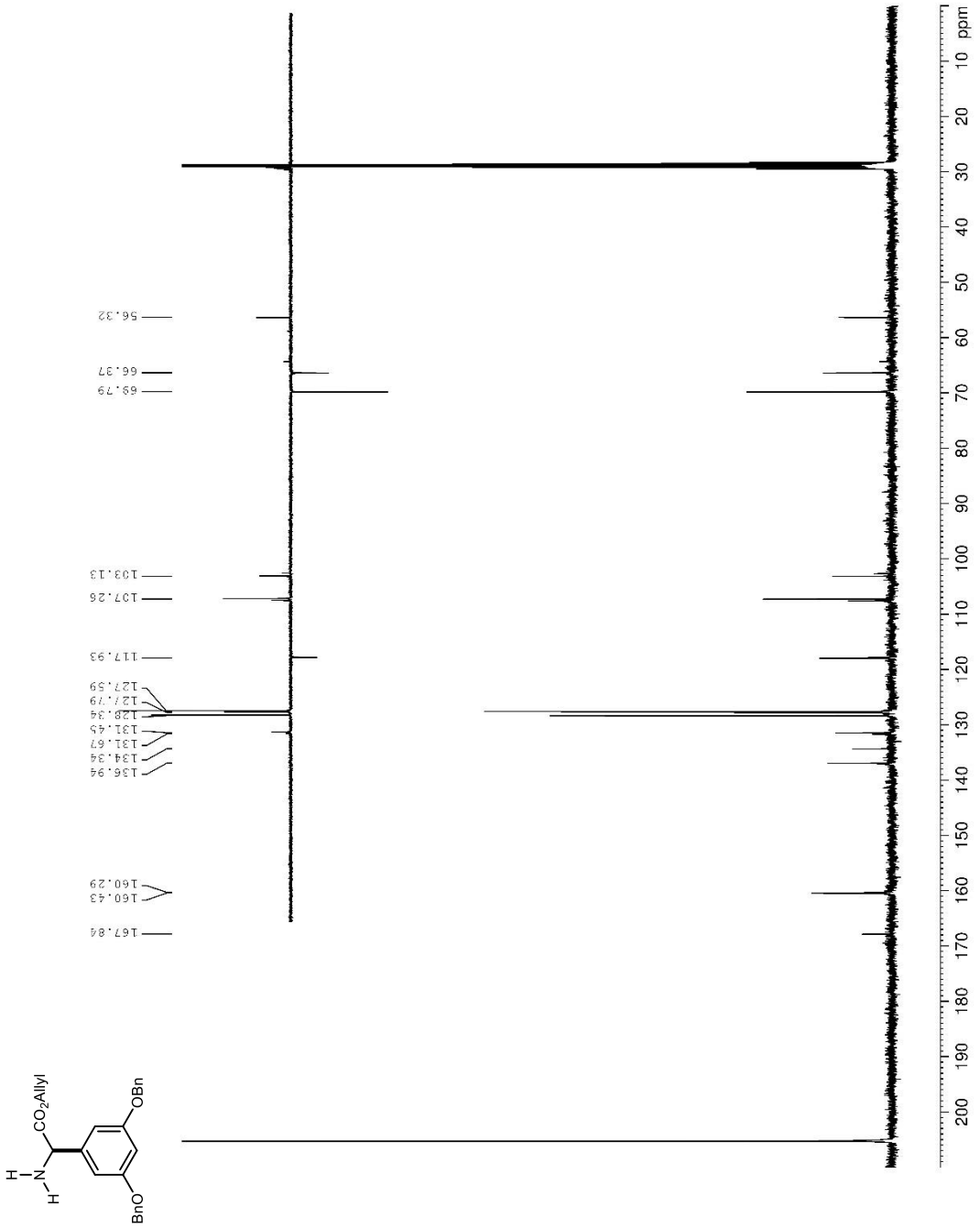

Figure 238. ^{1}H NMR (600 MHz, $CDCl_3$) spectrum of **2.49**.

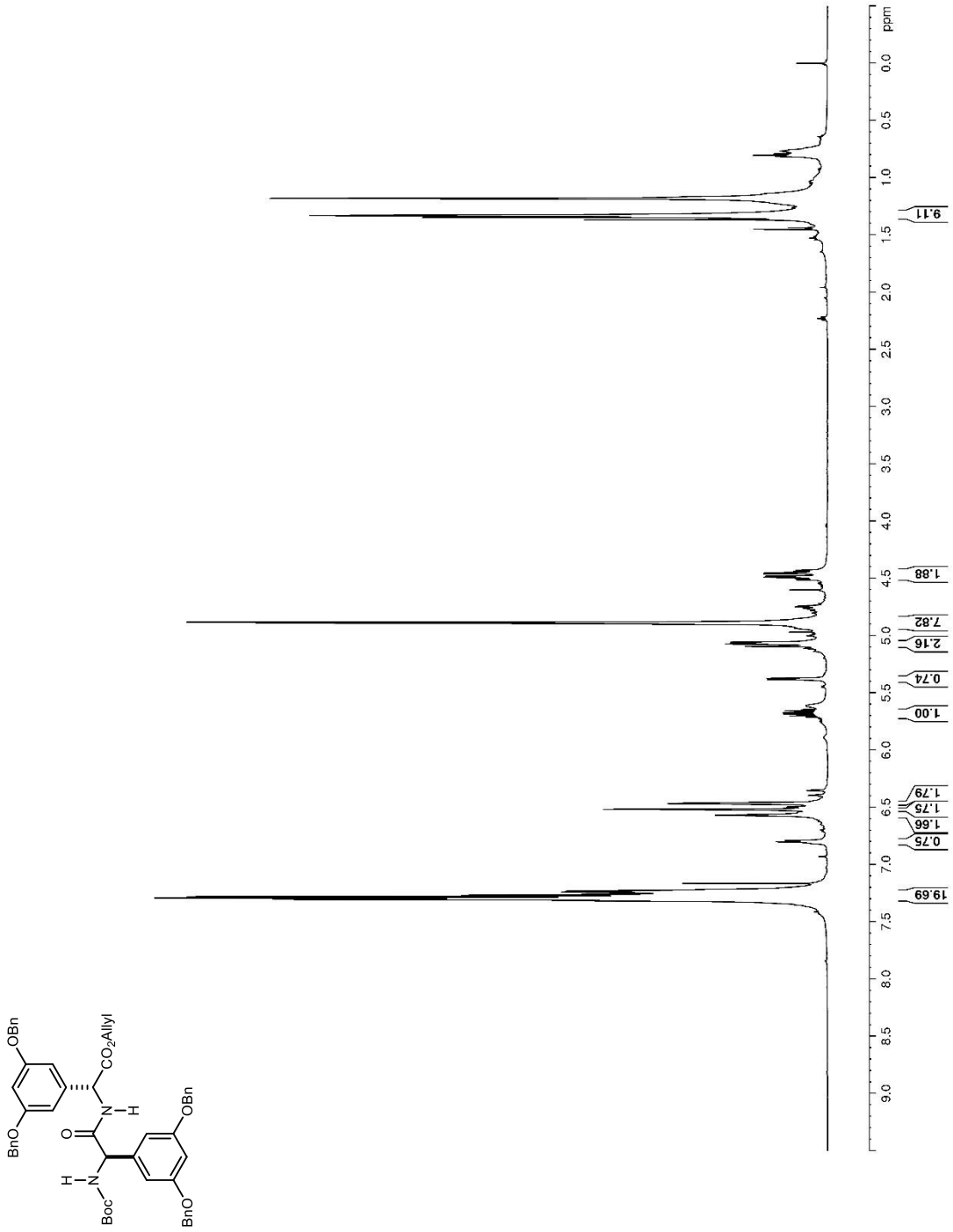

Figure 239. ^{13}C and DEPT-135 NMR (150 MHz, $CDCl_3$) spectra of **2.49**.

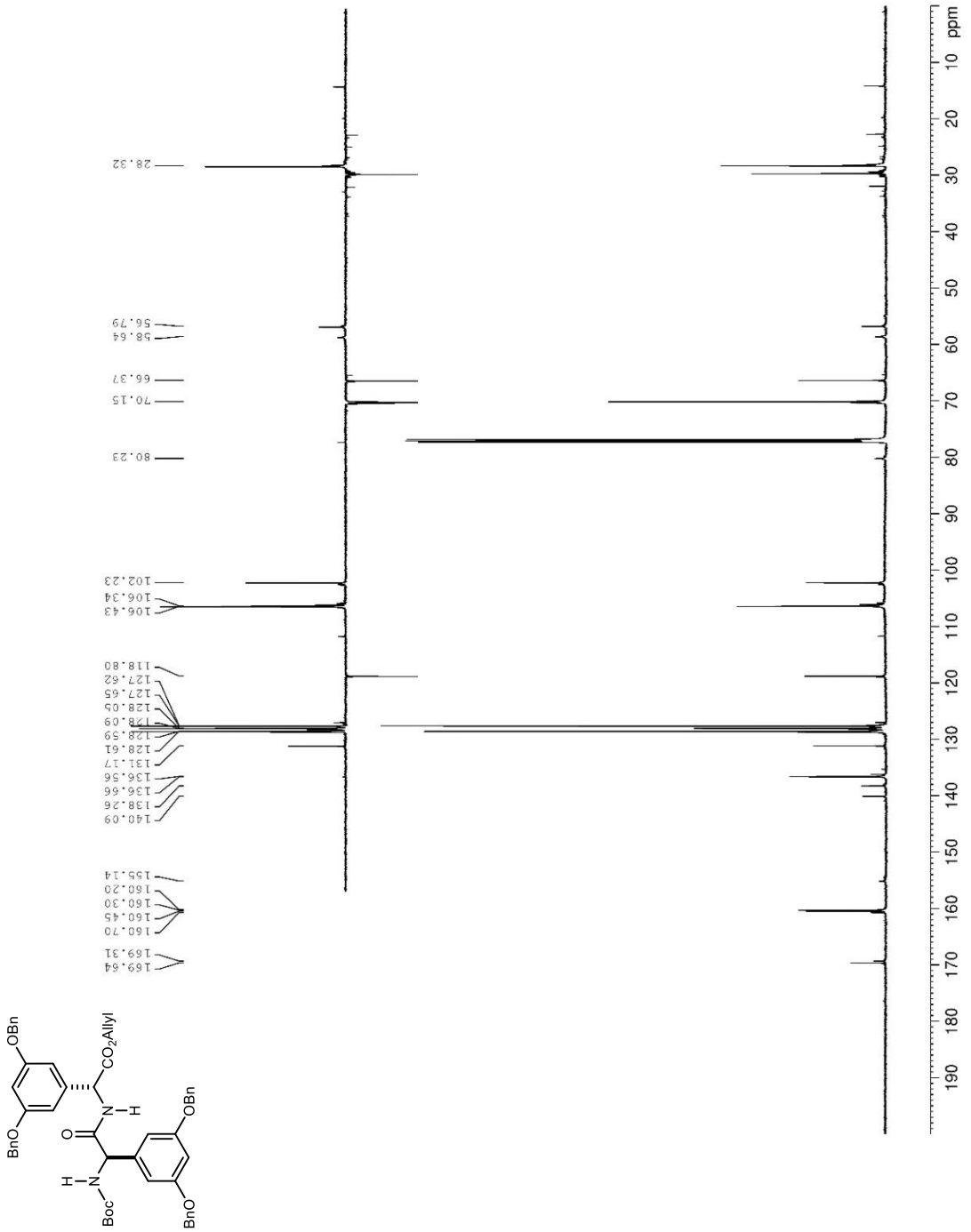

Figure 240. ^{1}H NMR (600 MHz, DMSO-d_6) spectrum of **2.41**.

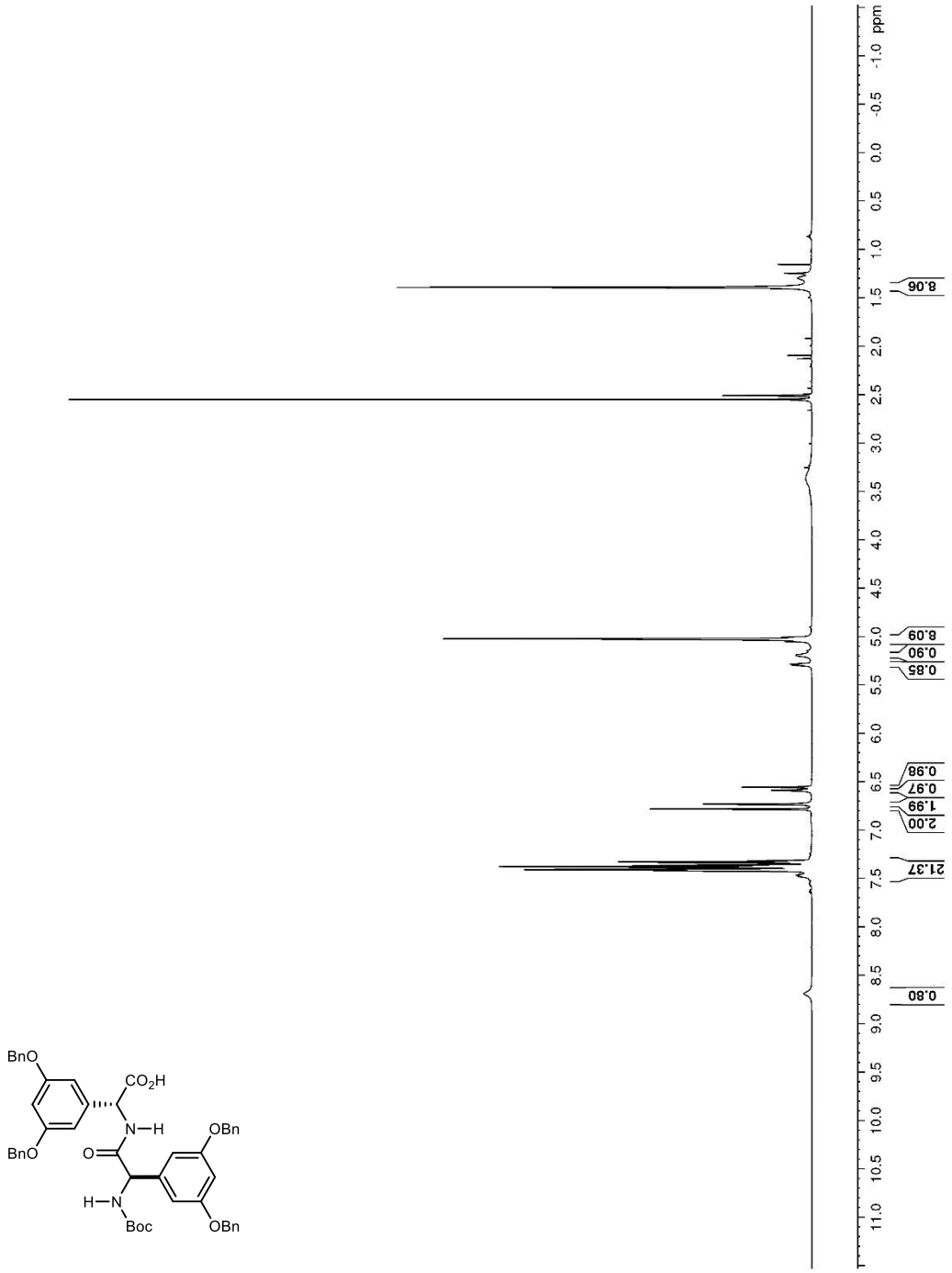

Figure 241. ^{13}C and DEPT-135 NMR (150 MHz, DMSO-d_6) spectra of **2.41**.

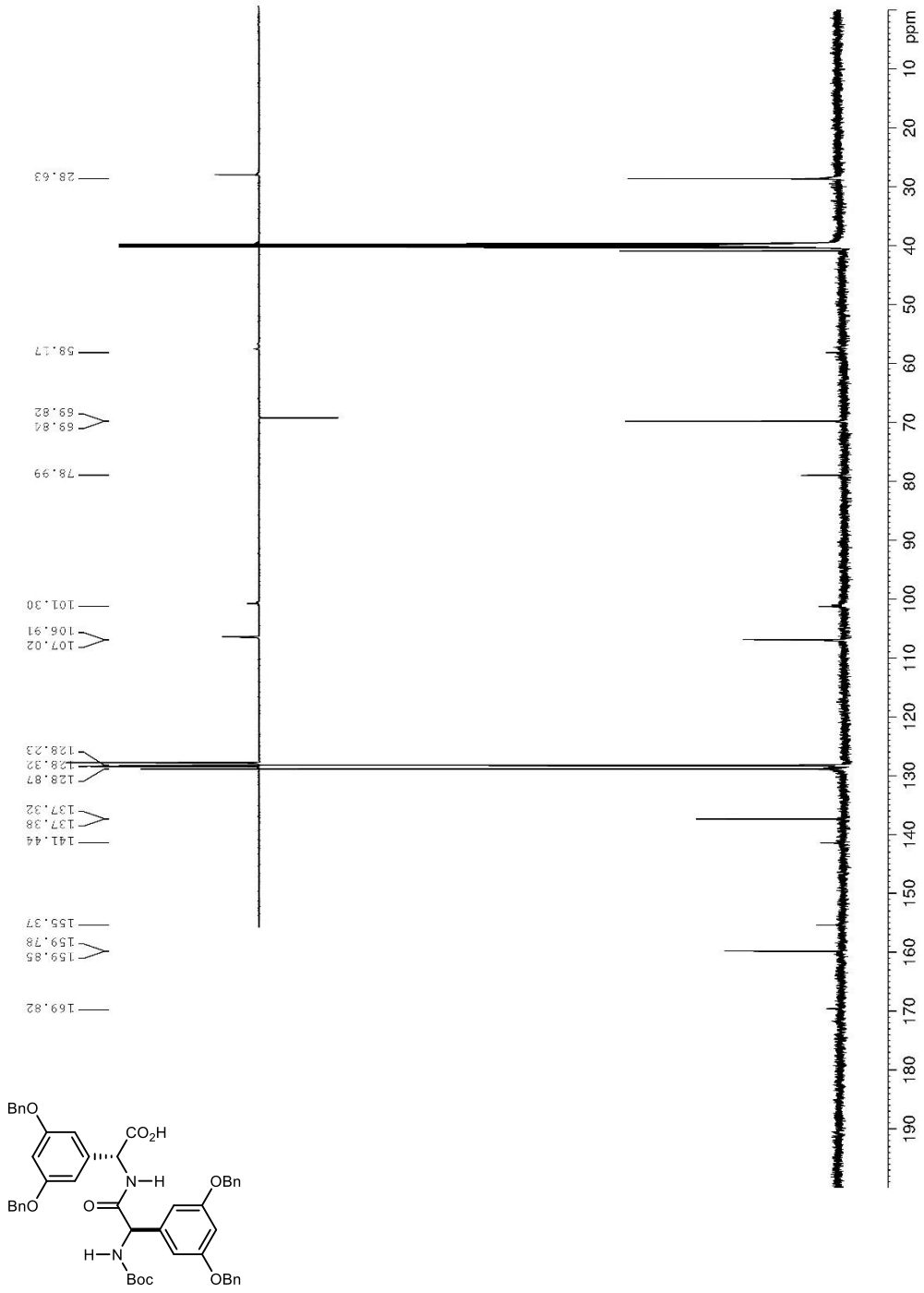

Figure 242. ^{1}H NMR (400 MHz, $CDCl_3$) spectrum of **2.50**.

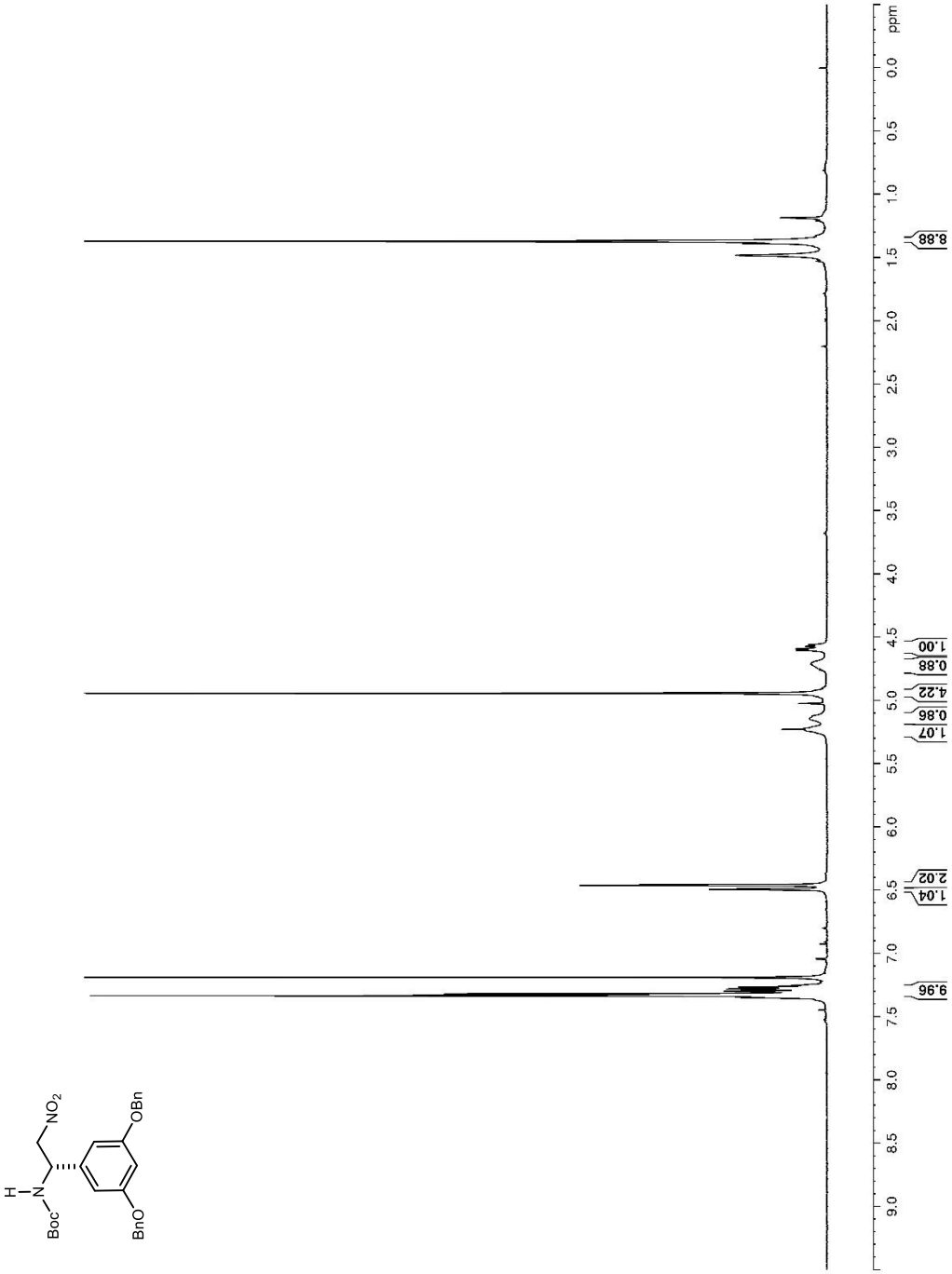

Figure 243. ^{13}C and DEPT-135 NMR (100 MHz, $CDCl_3$) spectra of **2.50**.

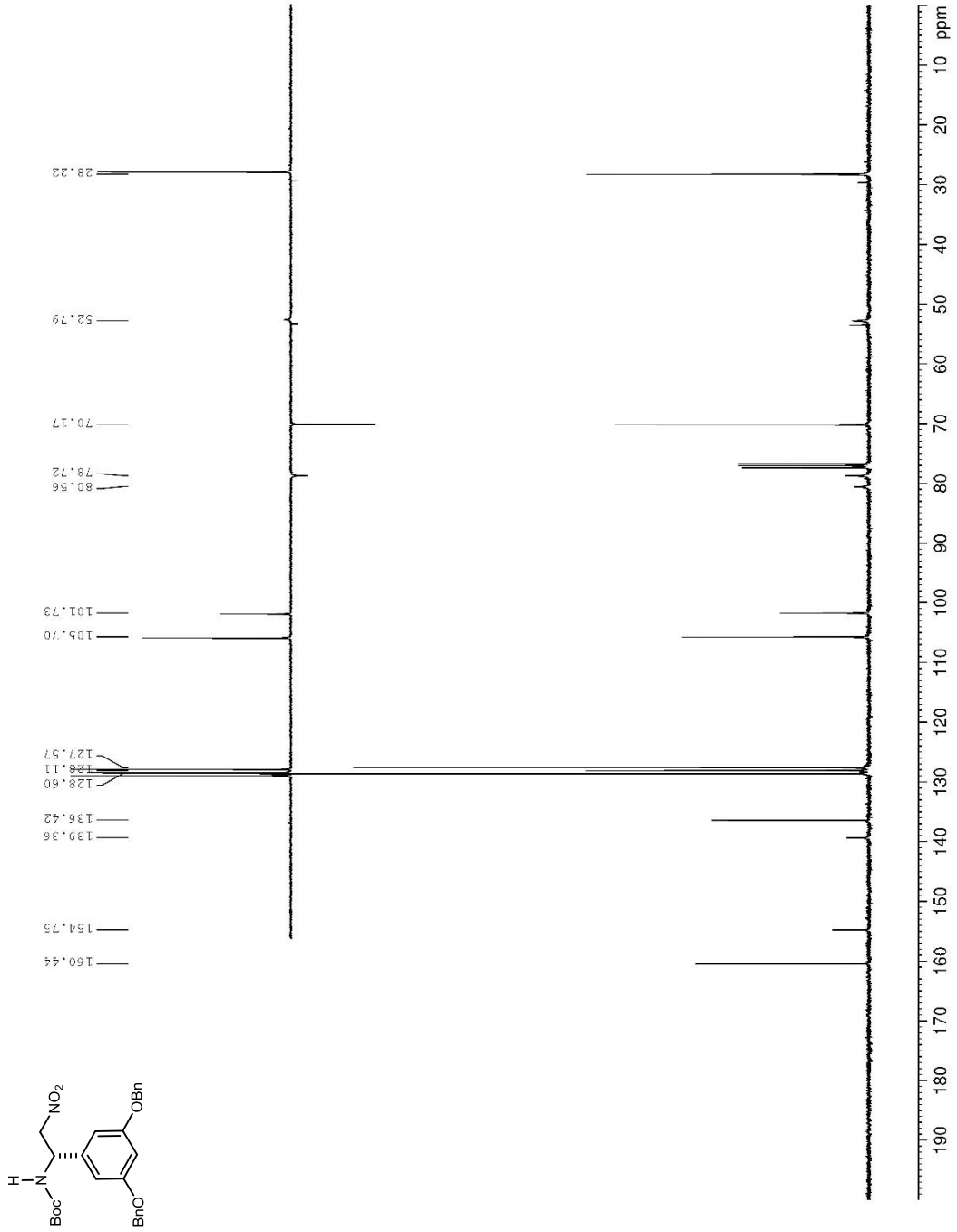

Figure 244. ^{1}H NMR (400 MHz, MeOD) spectrum of **2.51**.

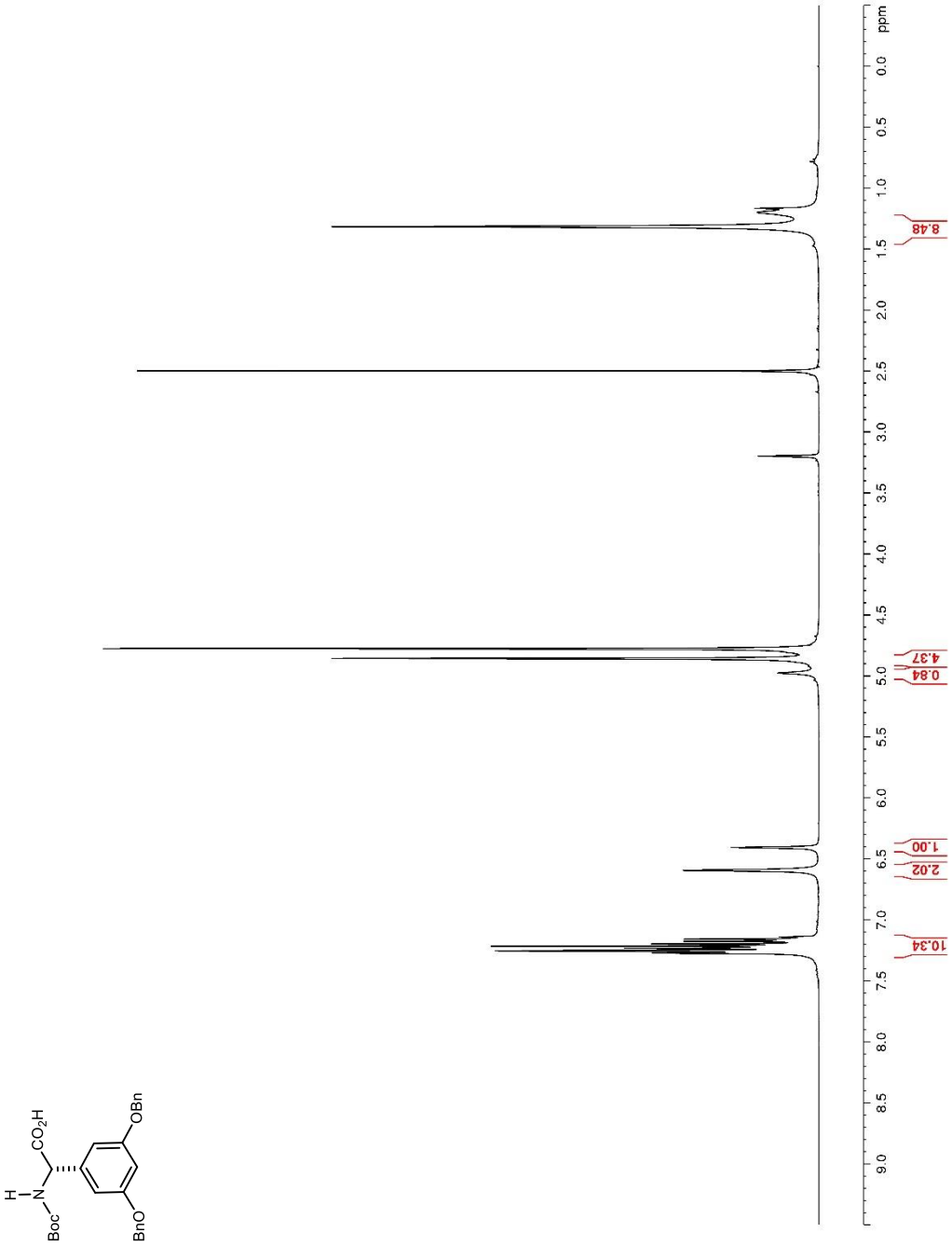

Figure 245. ^{13}C and DEPT-135 NMR (100 MHz, MeOD) spectra of **2.51**.

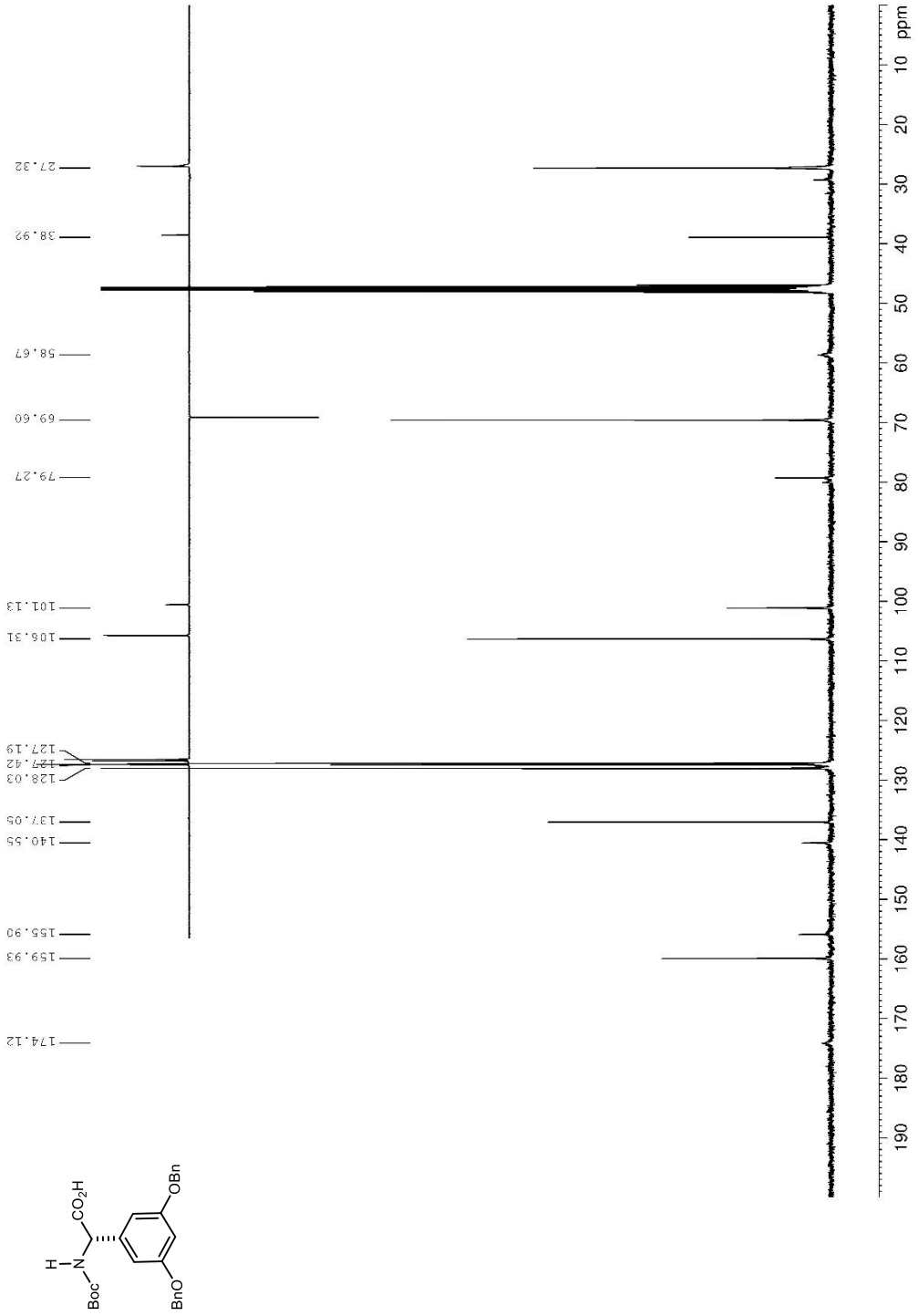

Figure 246. ^{1}H NMR (400 MHz, $CDCl_3$) spectrum of **2.52**.

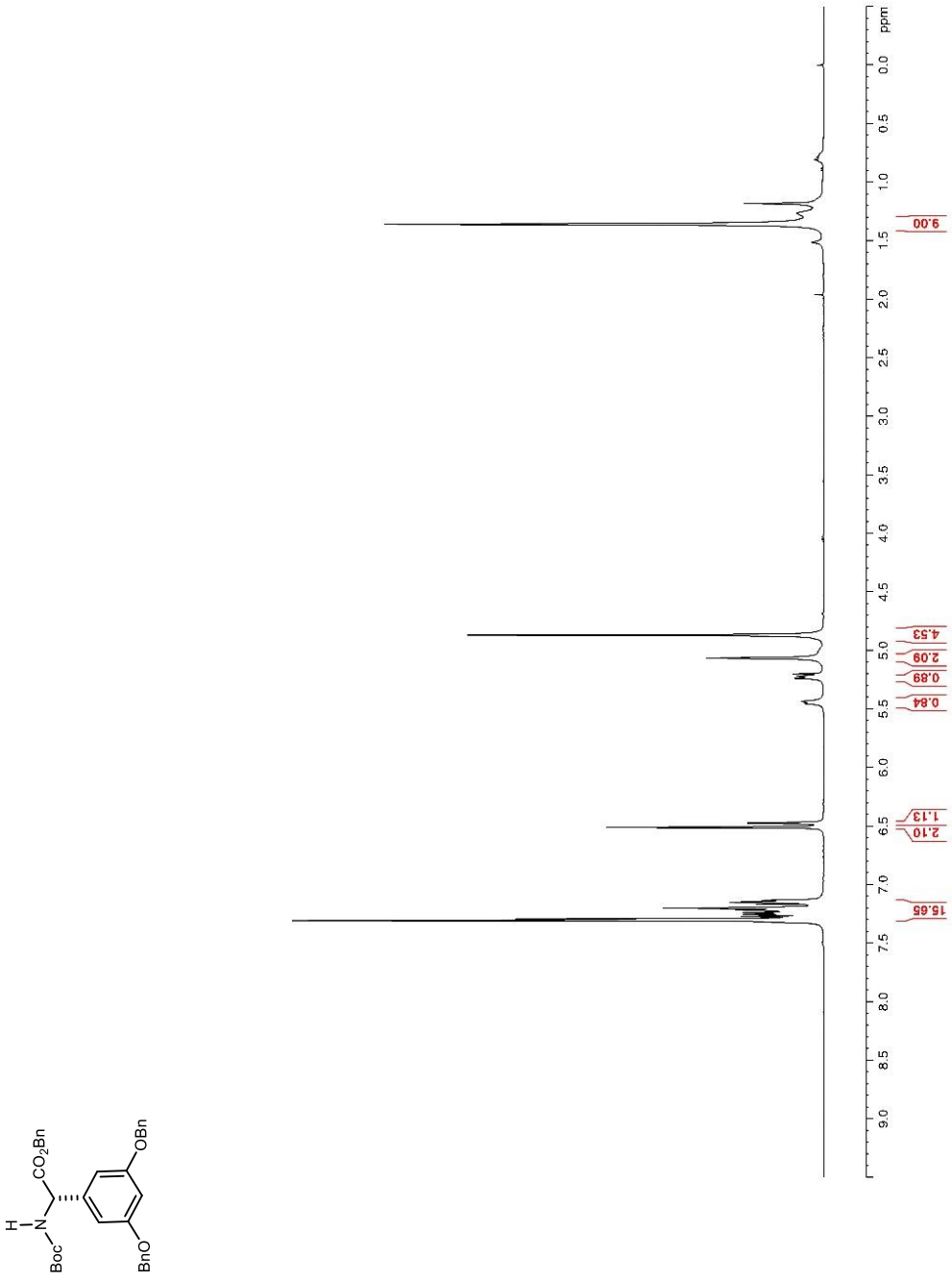

Figure 247. ^{13}C and DEPT-135 NMR (100 MHz, $CDCl_3$) spectra of **2.52**.

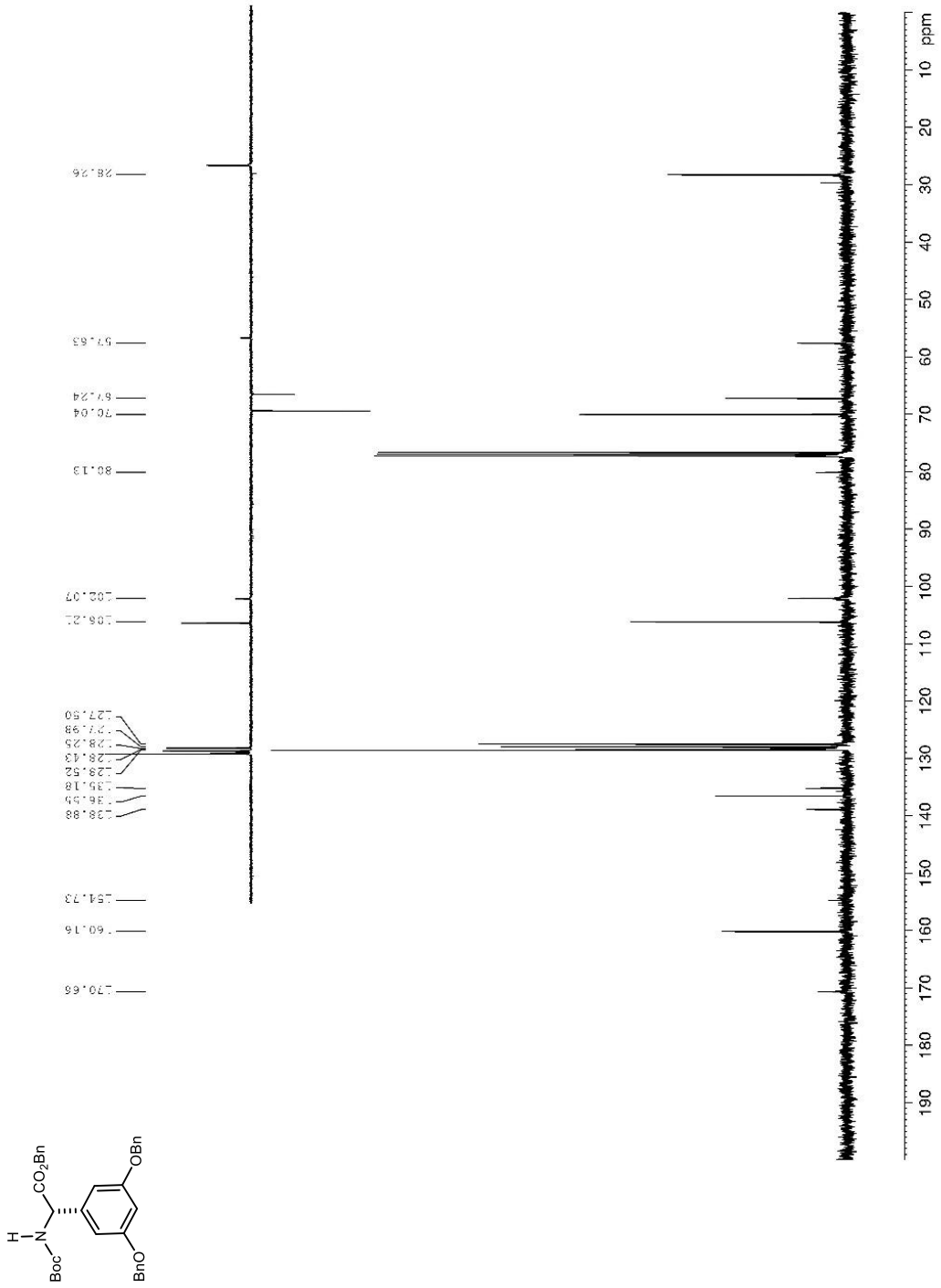

Figure 248. ^{1}H NMR (400 MHz, acetone-d_6) spectrum of **2.53**.

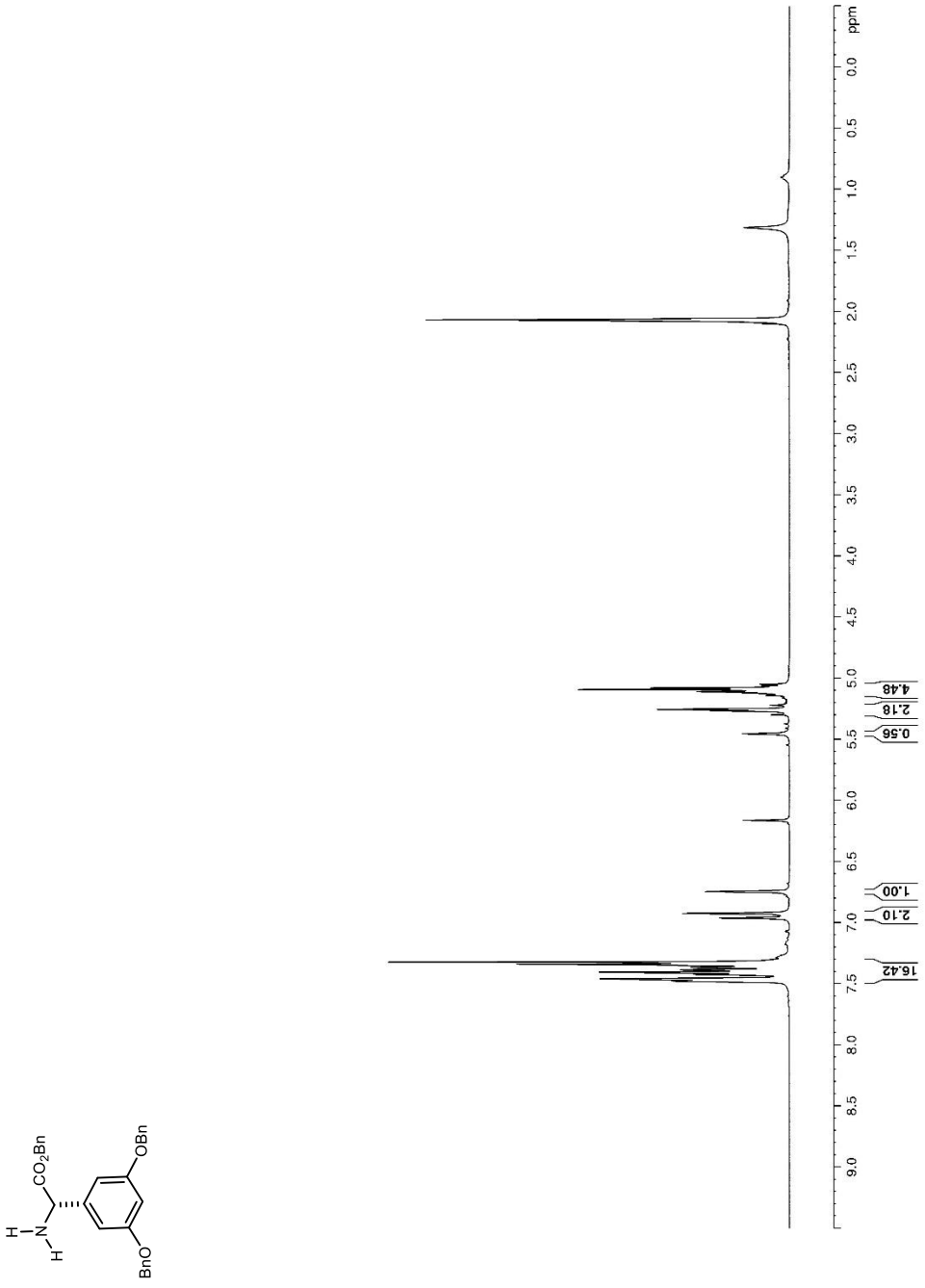

Figure 249. ^{13}C and DEPT-135 NMR (100 MHz, acetone-d_6) spectrum of **2.53**.

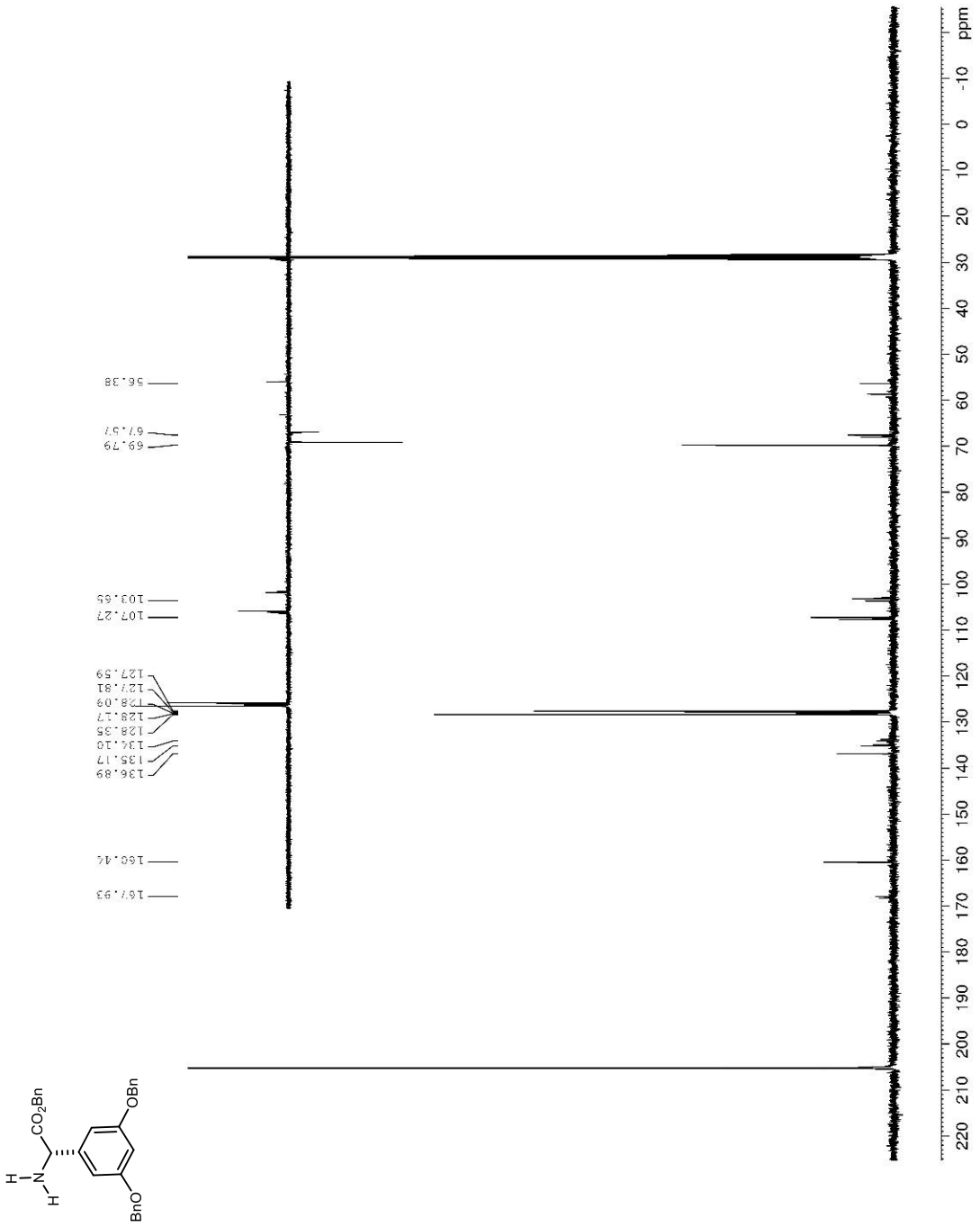

Figure 250. ^{1}H NMR (600 MHz, $CDCl_3$) spectrum of **2.55**.

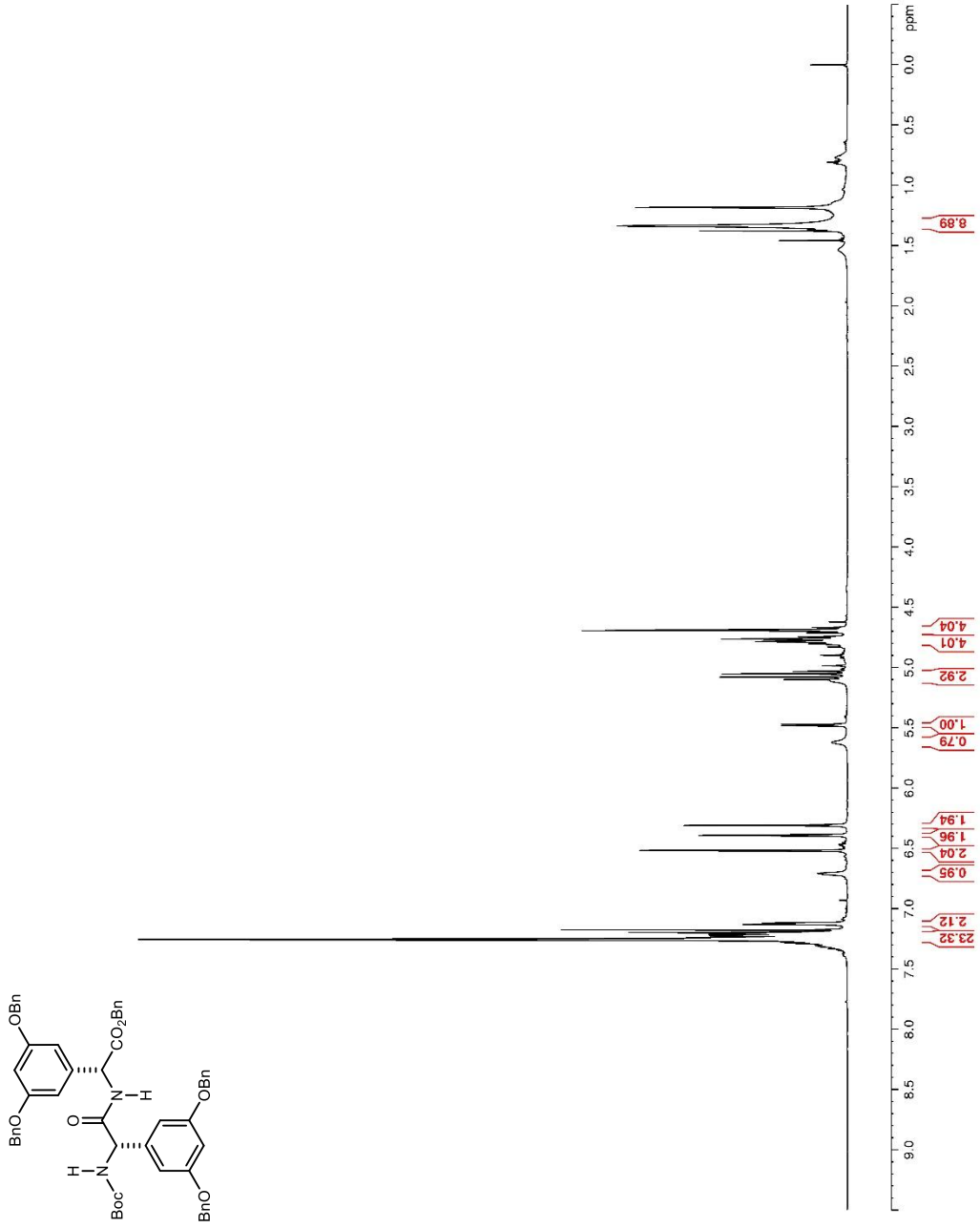

Figure 251. ^{13}C and DEPT-135 NMR (150 MHz, $CDCl_3$) spectra of **2.55**.

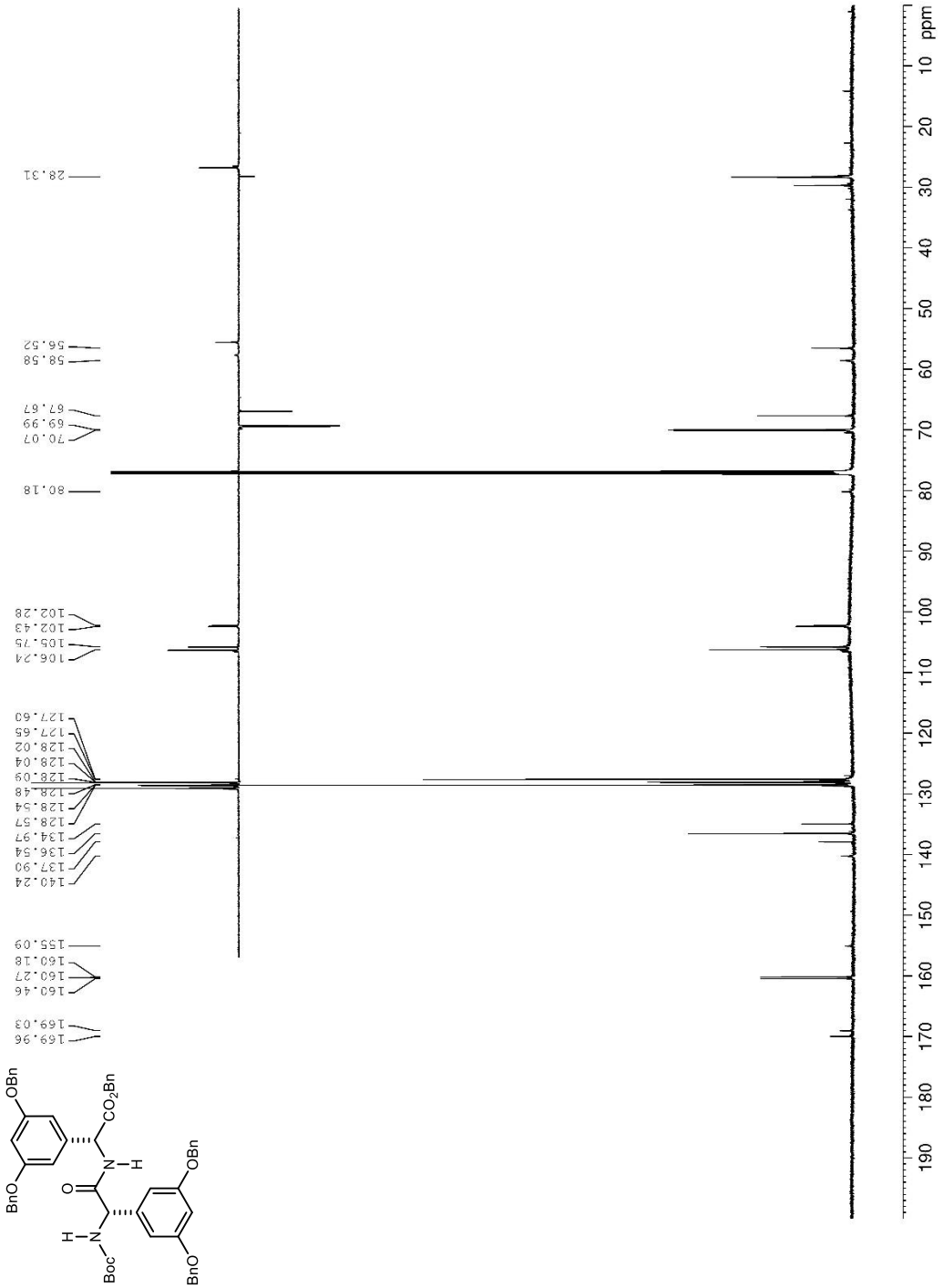

Figure 252. ^{1}H NMR (600 MHz, $CDCl_3$) spectrum of **2.56**.

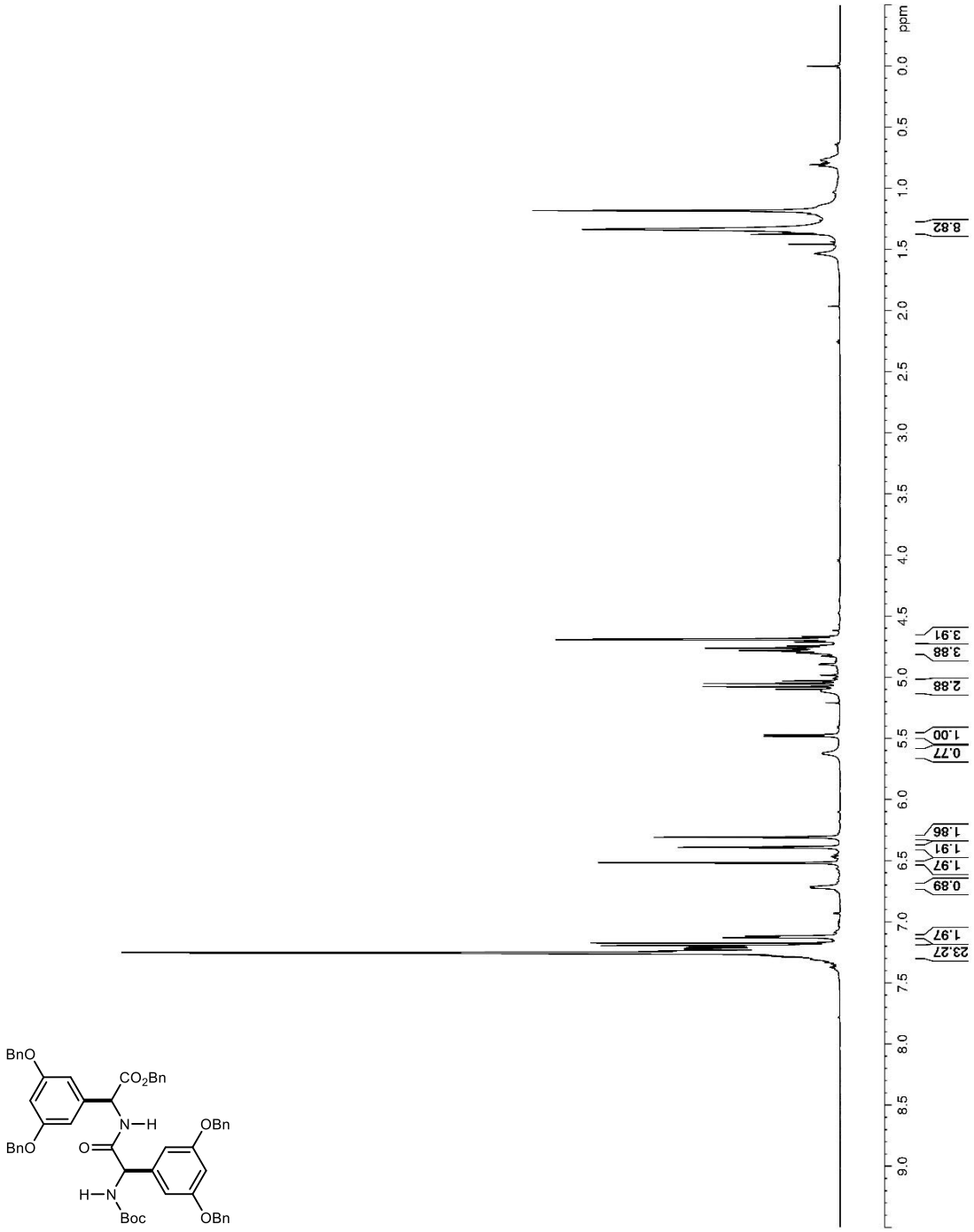

Figure 253. ^{13}C and DEPT-135 NMR (150 MHz, $CDCl_3$) spectra of **2.56**.

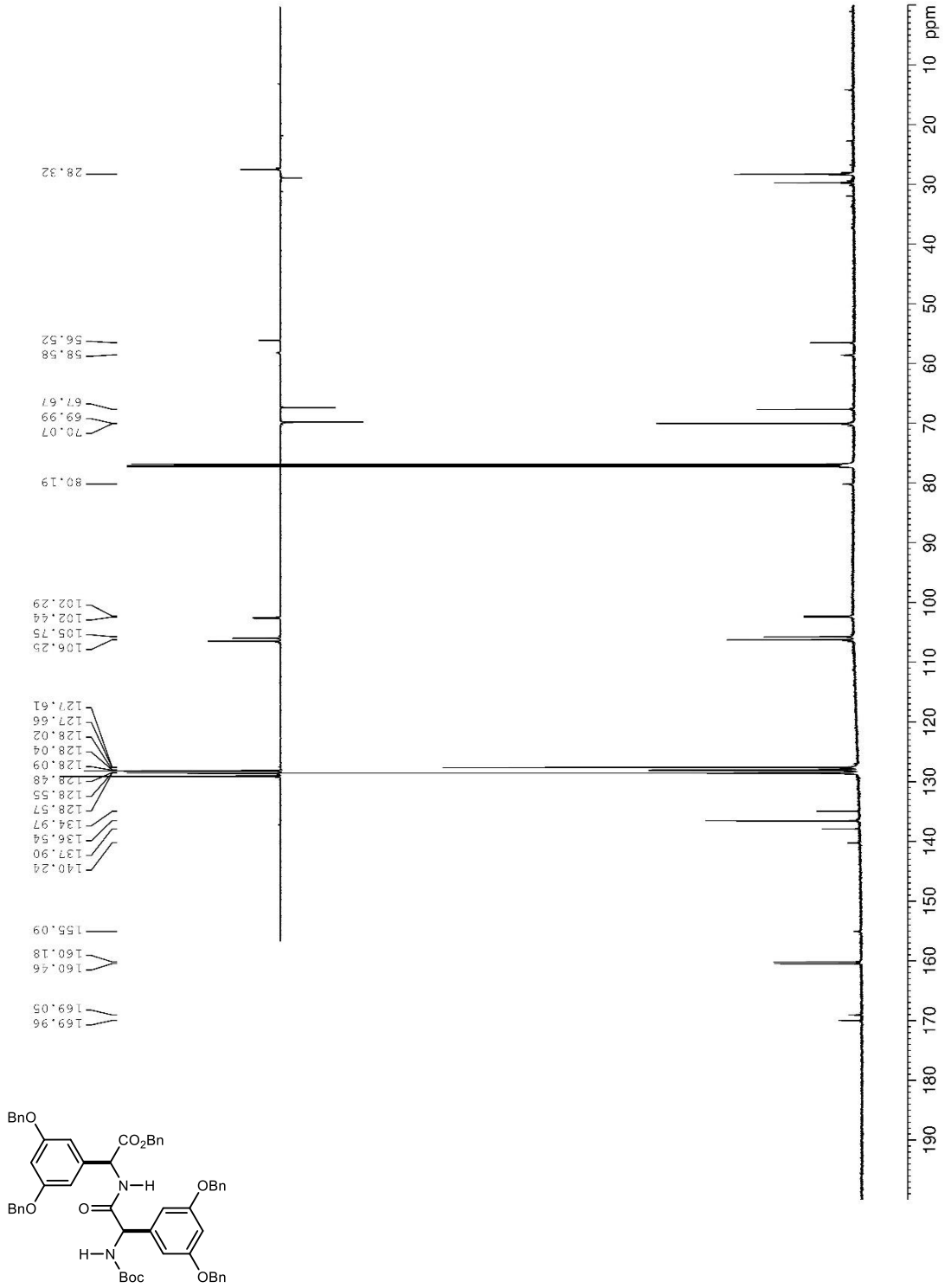

Figure 254. ^{1}H NMR (600 MHz, $CDCl_3$) spectrum of **2.57**.

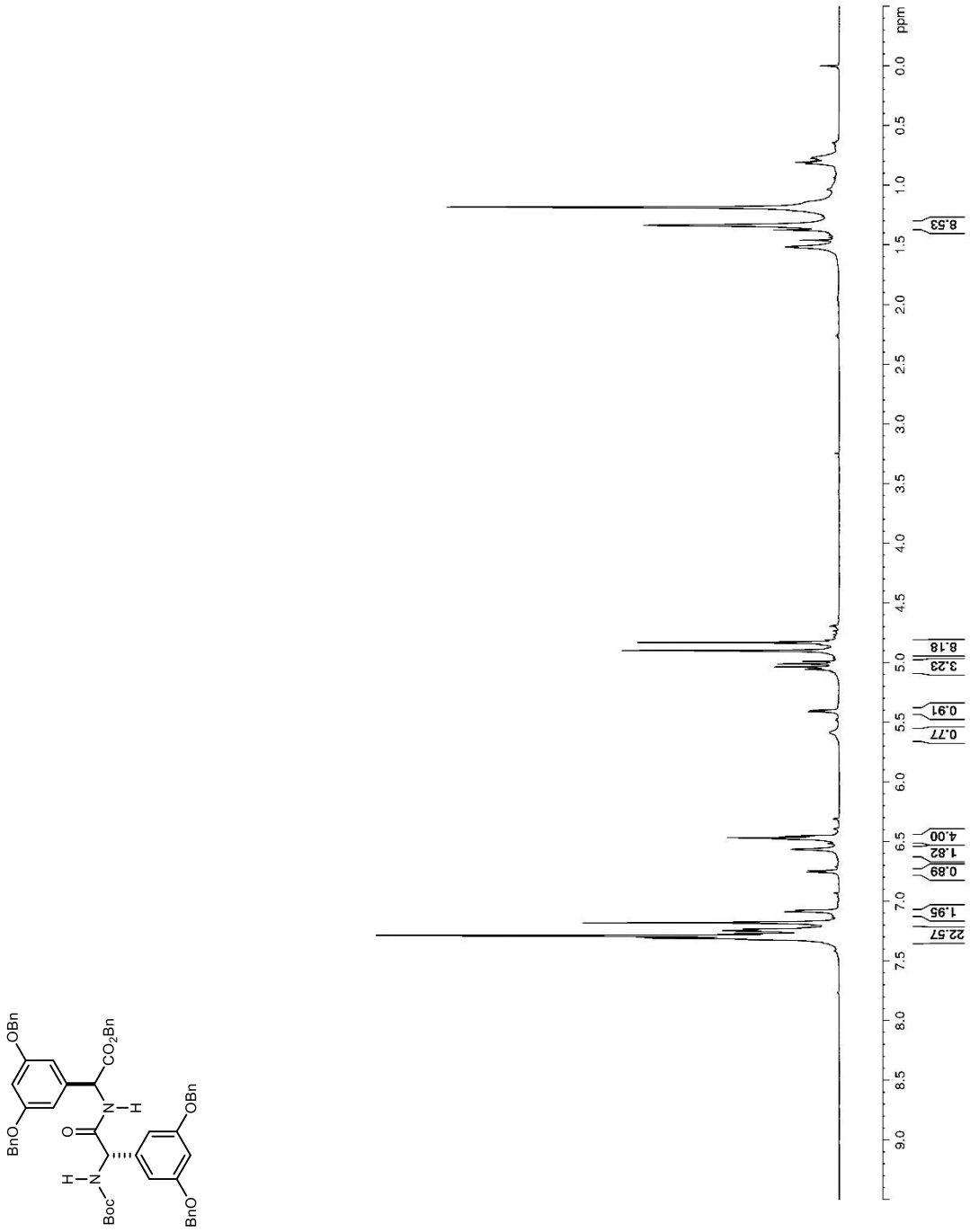

Figure 255. ^{13}C and DEPT-135 NMR (150 MHz, $CDCl_3$) spectra of **2.57**.

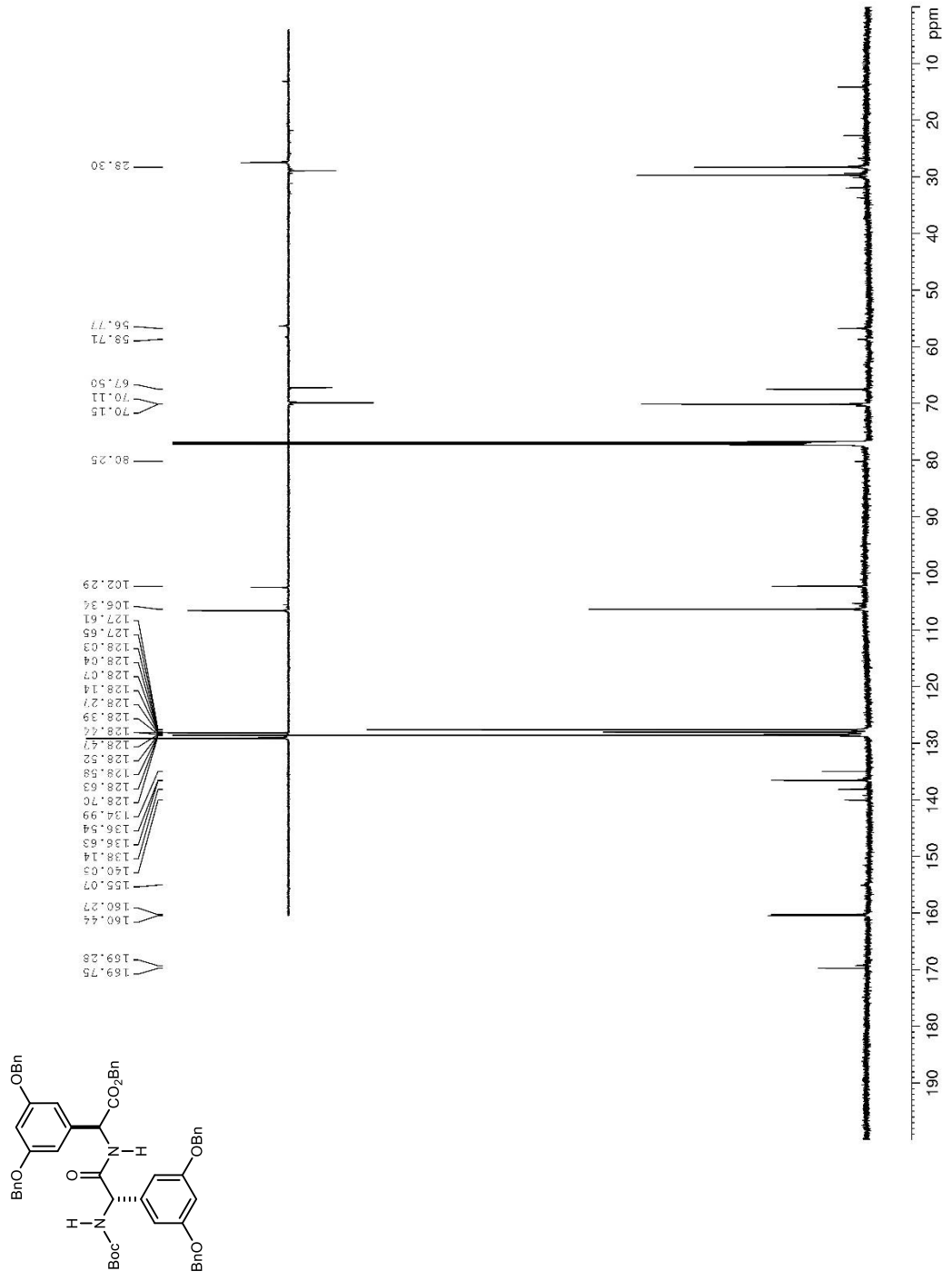

Figure 256. ^{1}H NMR (600 MHz, DMSO-d_6) spectrum of **2.59**.

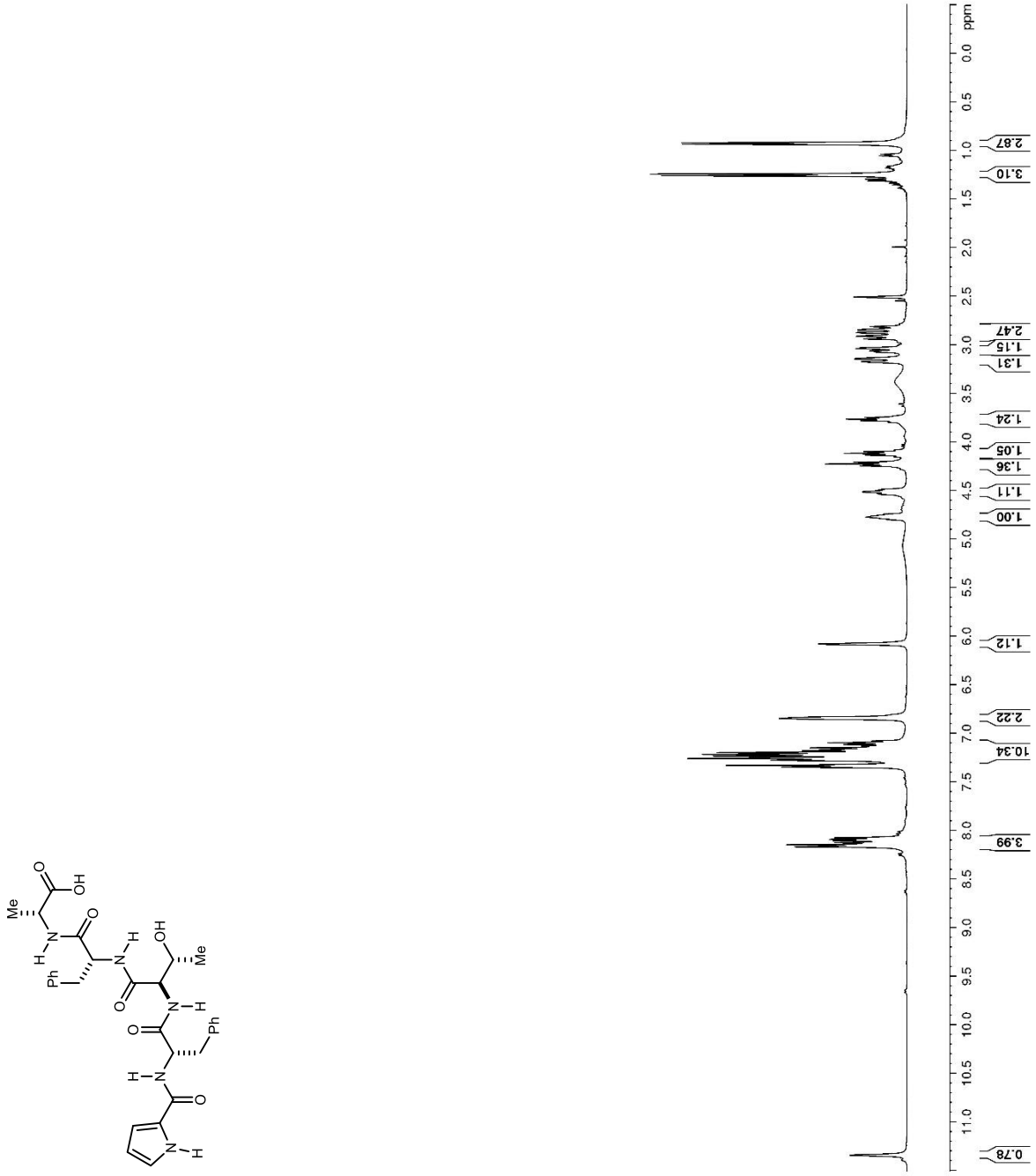

Figure 257. ^{13}C and DEPT-136 NMR (150 MHz, DMSO-d_6) spectrum of **2.59**.

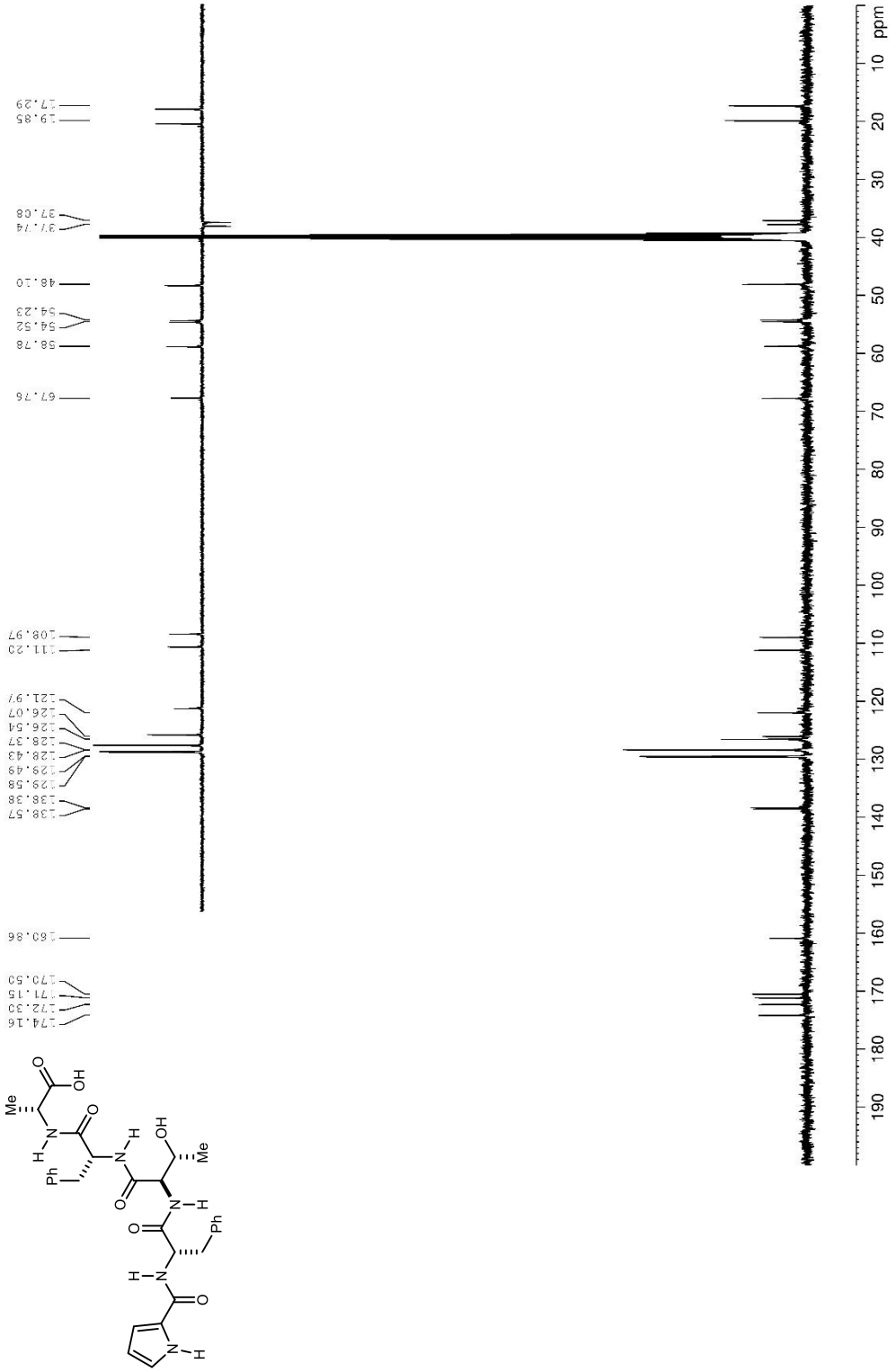

Figure 258. ^{1}H NMR (400 MHz, acetone-d_6) spectrum of **2.62**.

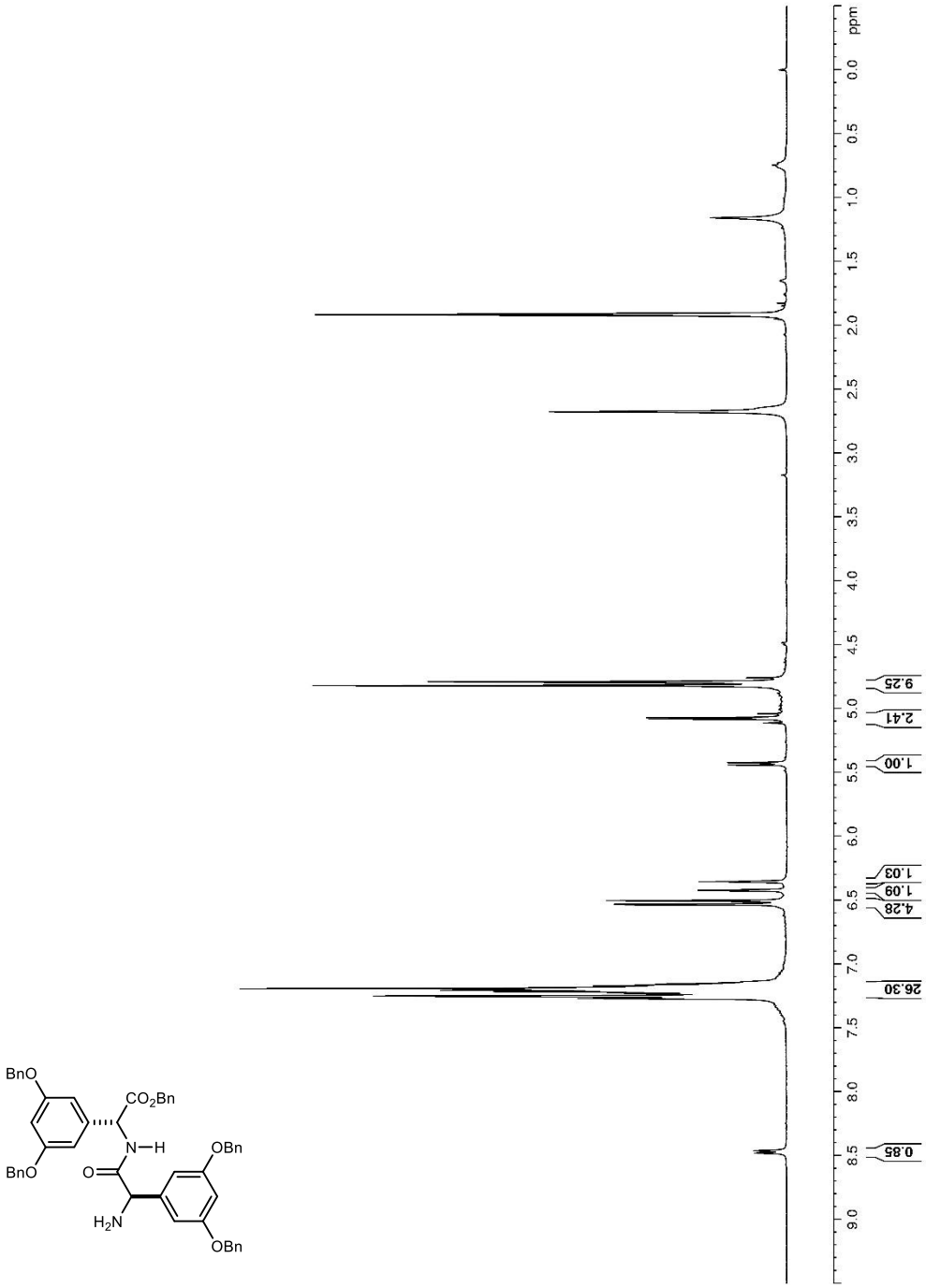

Figure 259. ^{1}H NMR (600 MHz, DMSO-d_6) spectrum of **2.61**.

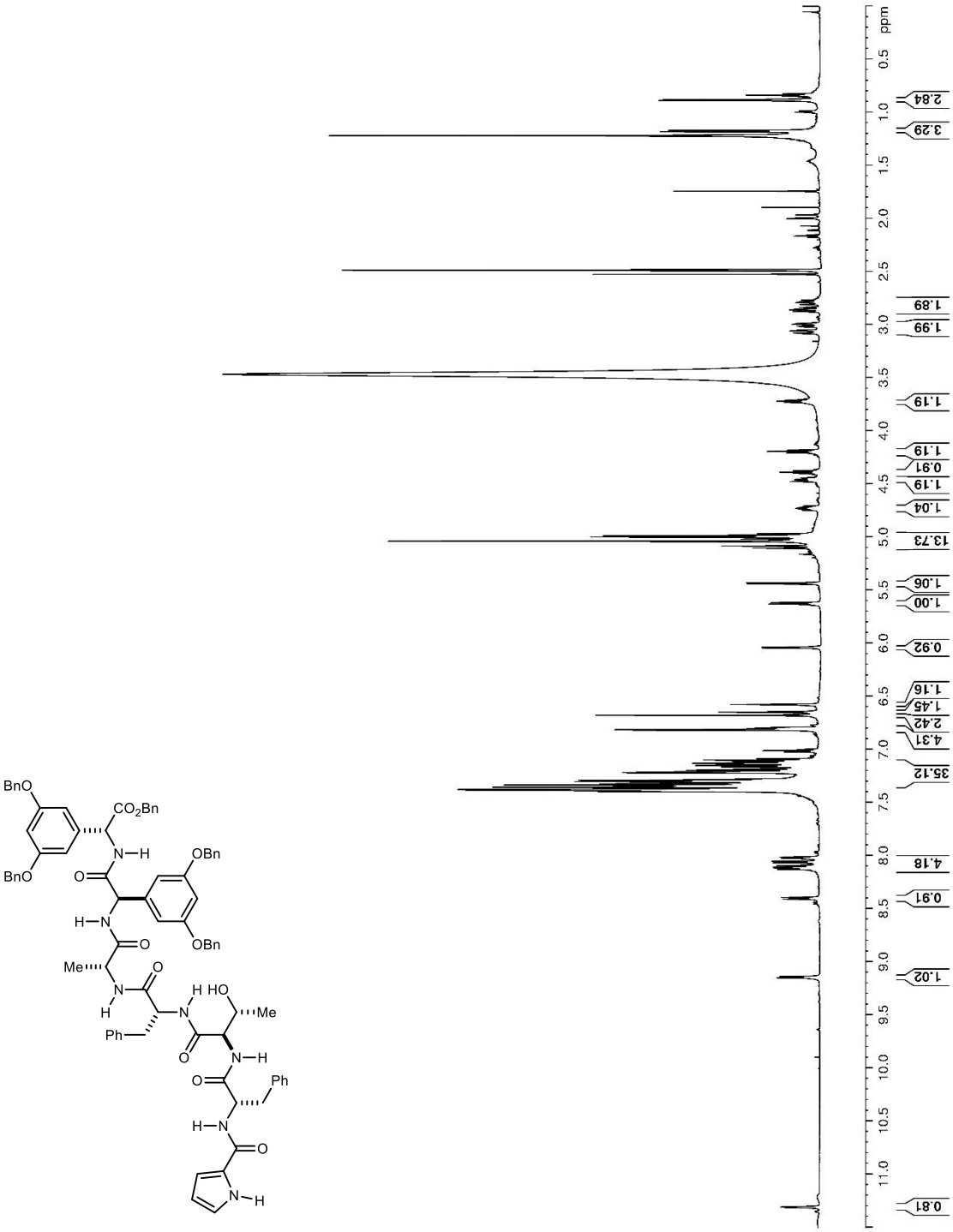

Figure 260. ^{13}C and DEPT-135 NMR (150 MHz, DMSO-d_6) spectrum of **2.61**.

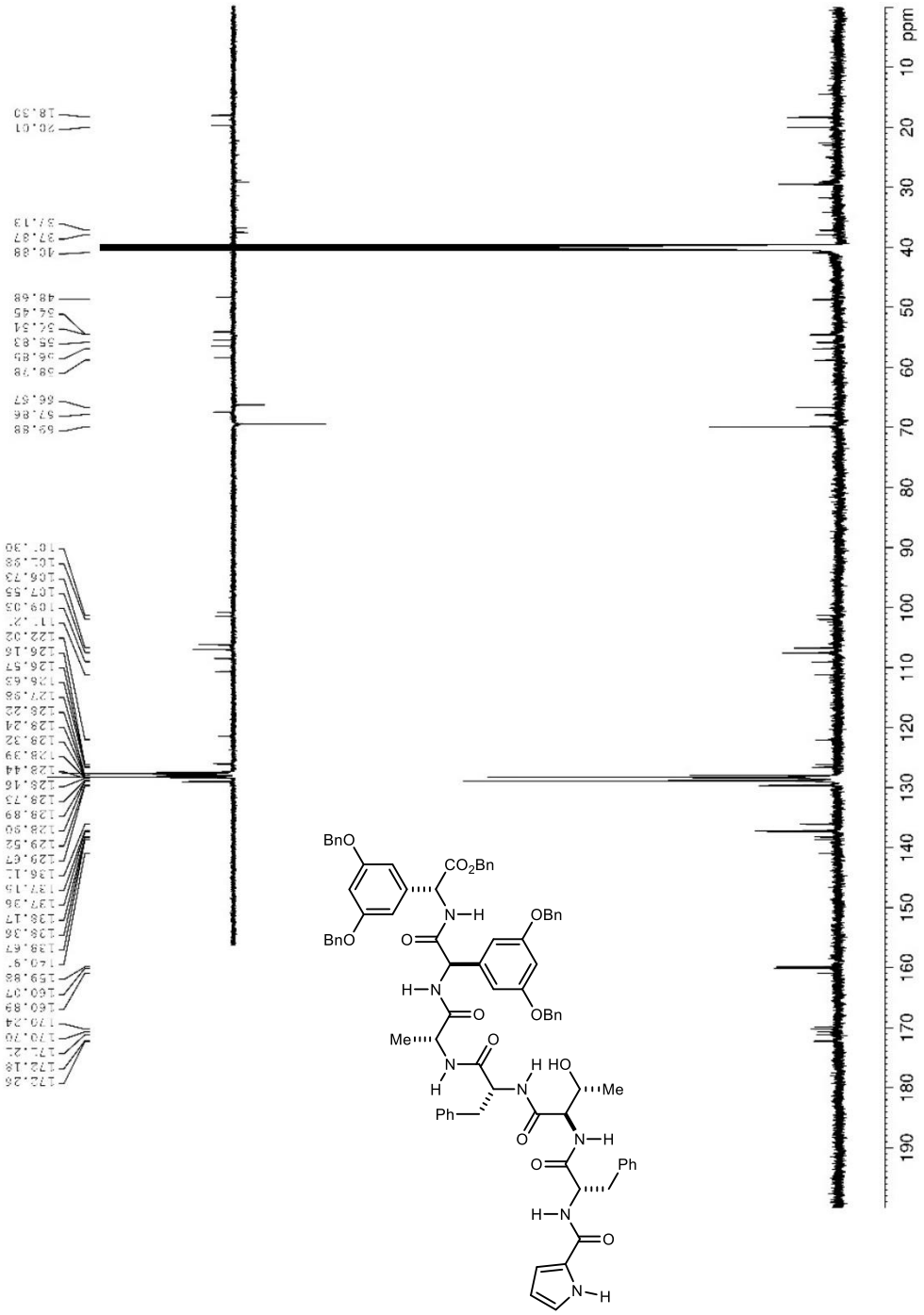

Figure 261. ^{1}H NMR (600 MHz, DMSO-d_6) spectrum of **2.64**.

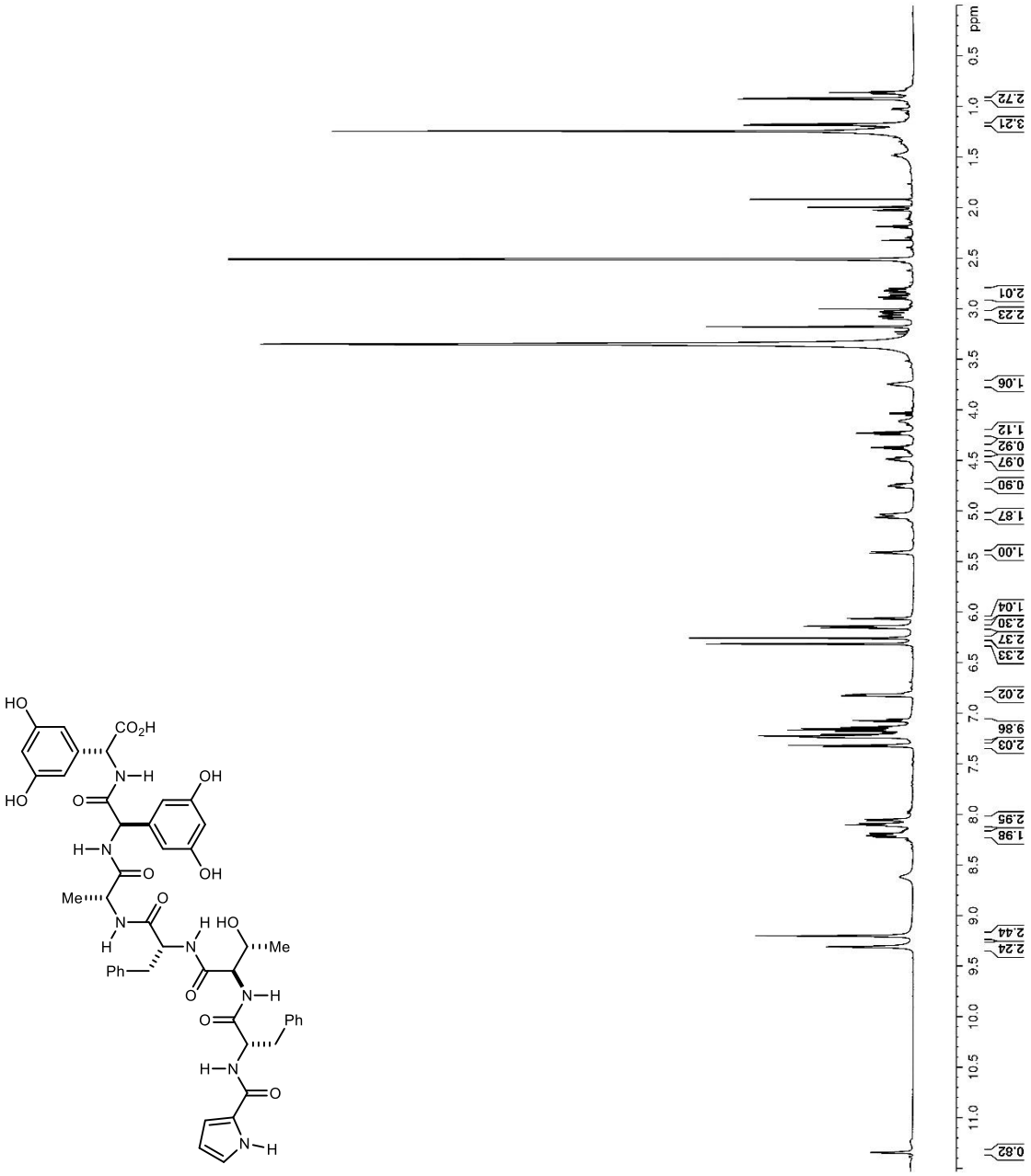

Figure 262. ^{13}C and DEPT-135 NMR (150 MHz, DMSO-d_6) spectrum of **2.64**.

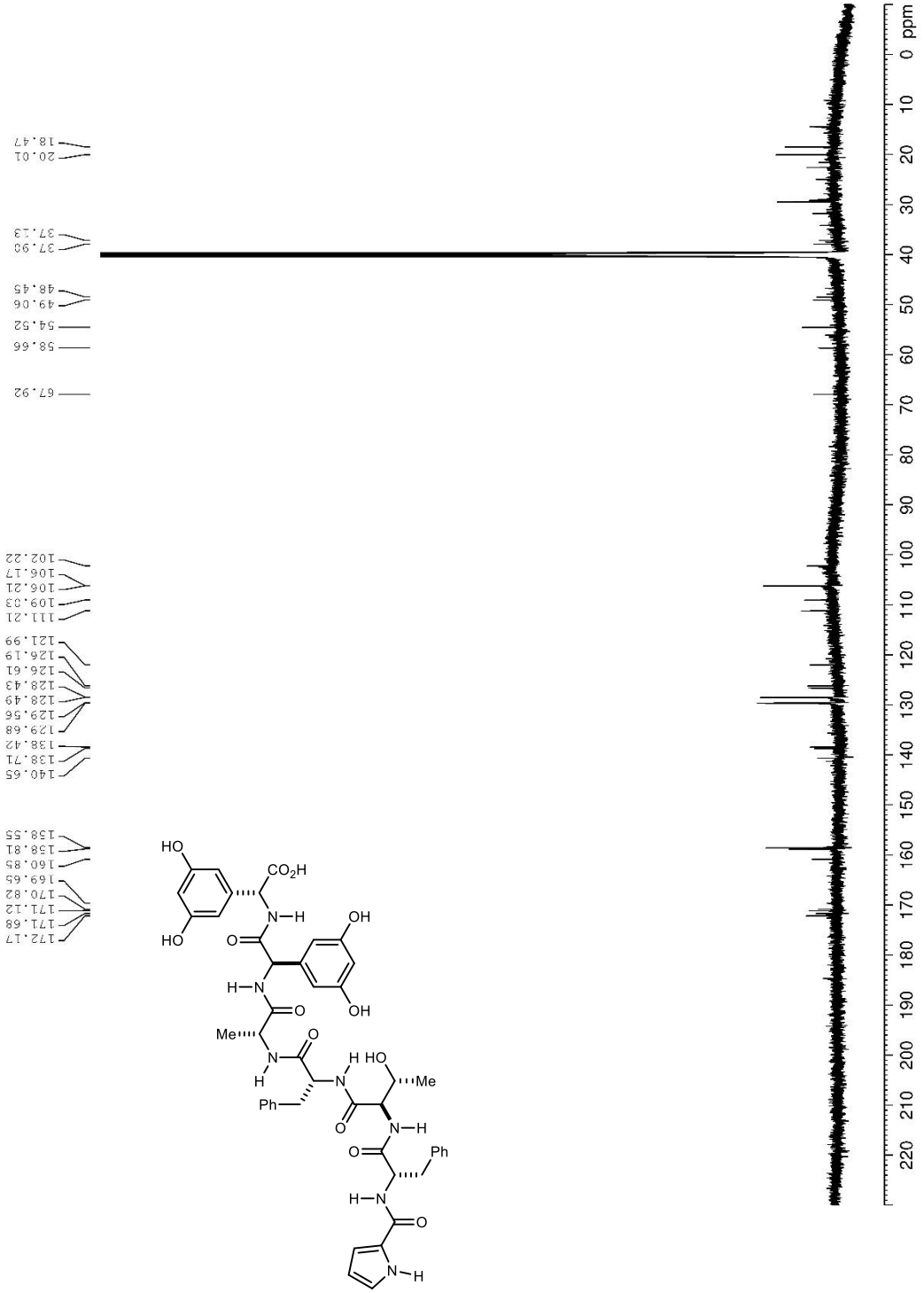

Figure 263. ^{1}H NMR (400 MHz, acetone-d_6) spectrum of **2.68**.

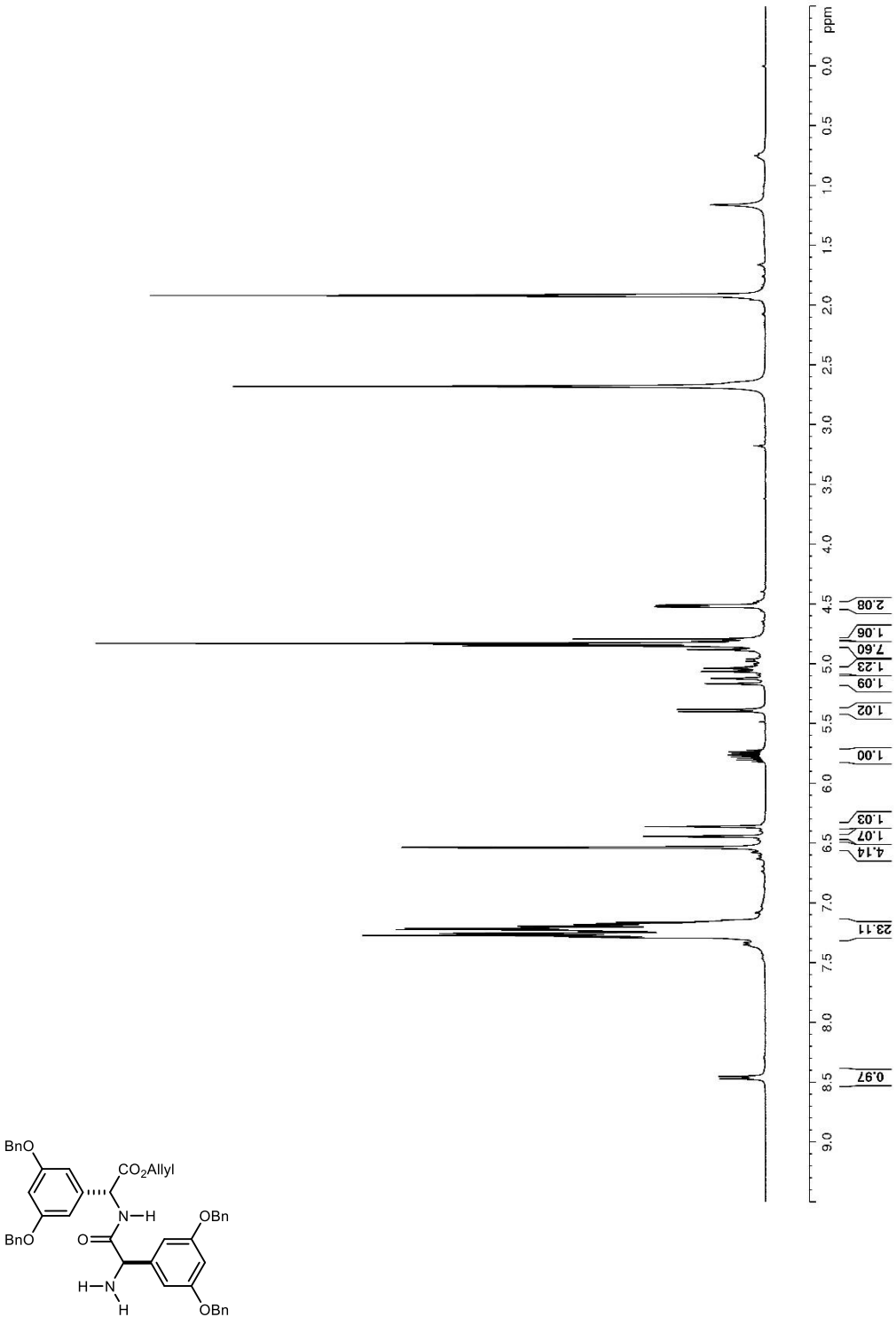

Figure 264. ^{13}C and DEPT-135 NMR (100 MHz, acetone-d_6) spectrum of **2.68**.

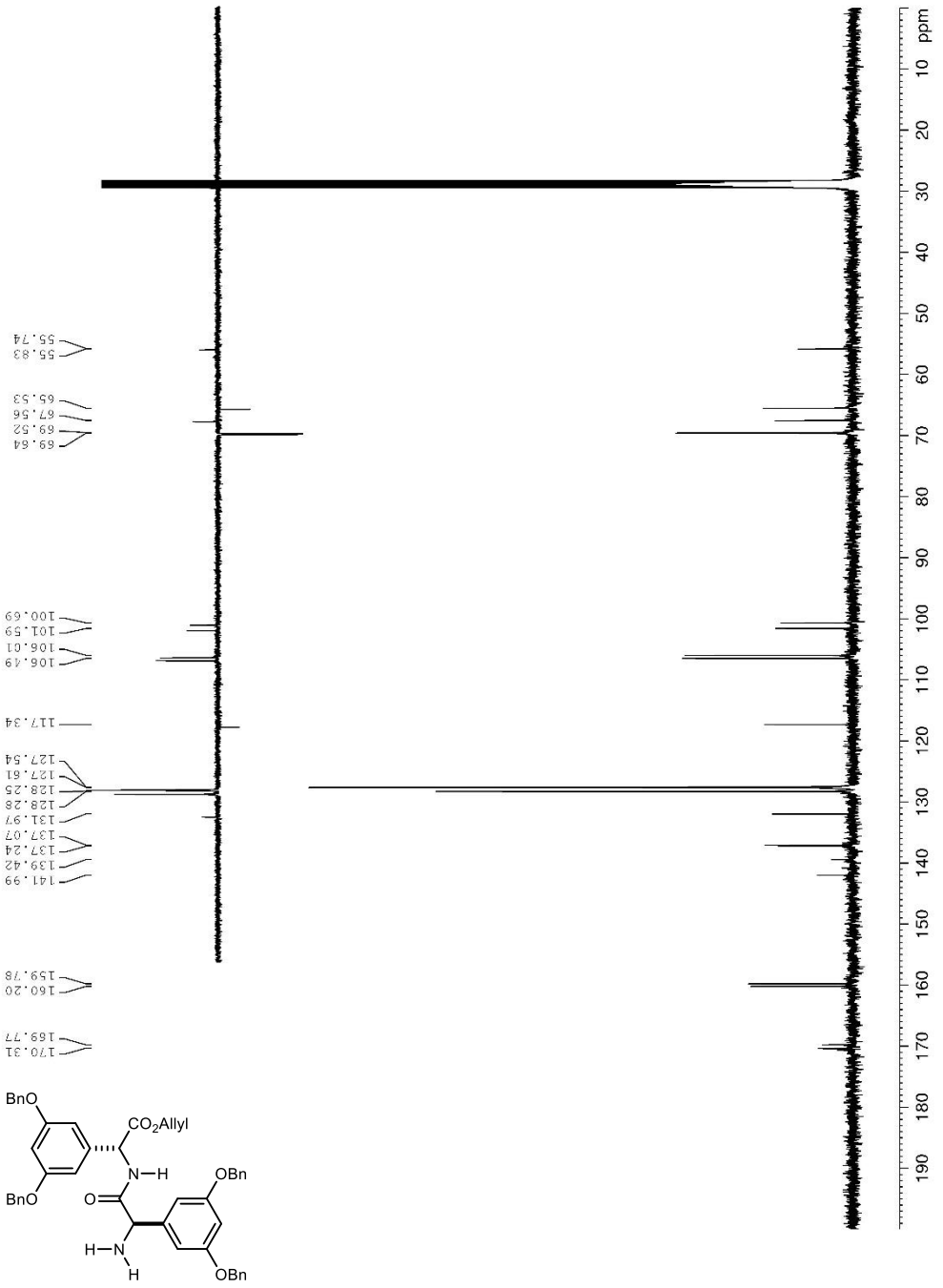

Figure 265. ^{1}H NMR (600 MHz, DMSO-d_6) spectrum of **2.66**.

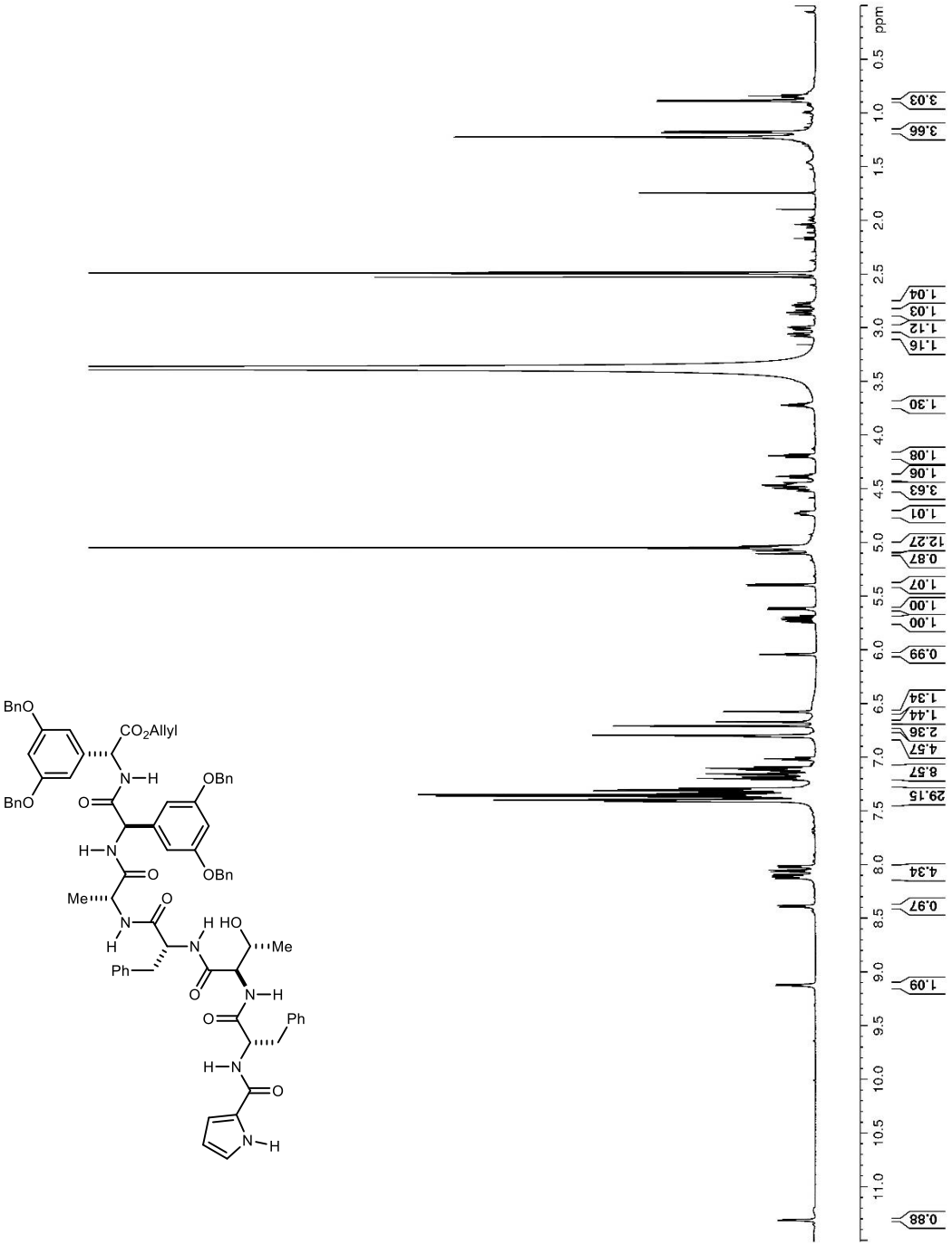

Figure 266. ^{13}C and DEPT-135 NMR (150 MHz, DMSO-d_6) spectrum of **2.66**.

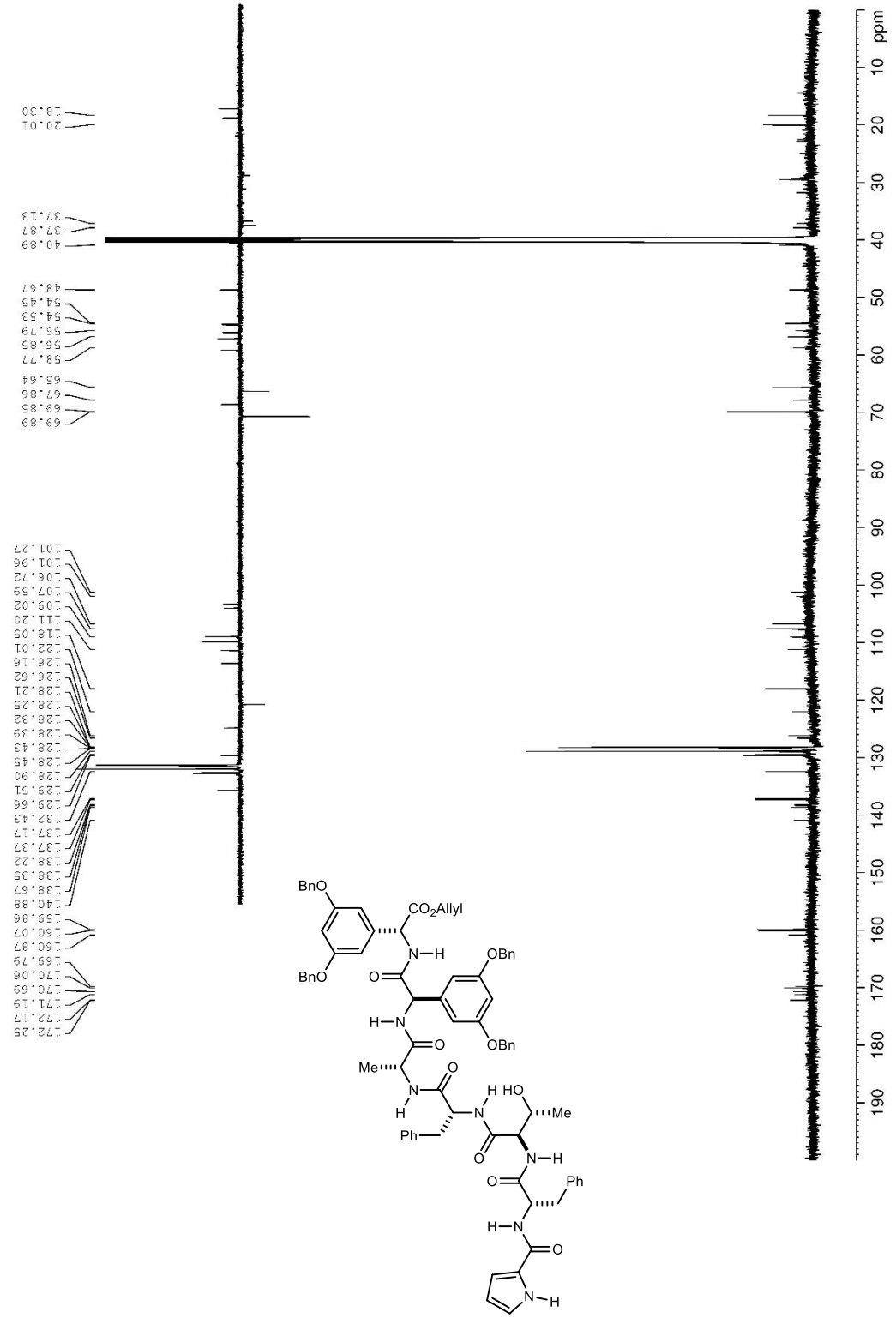

Figure 267. ^{1}H NMR spectrum (600 MHz, DMSO-d_6) of **2.69.**

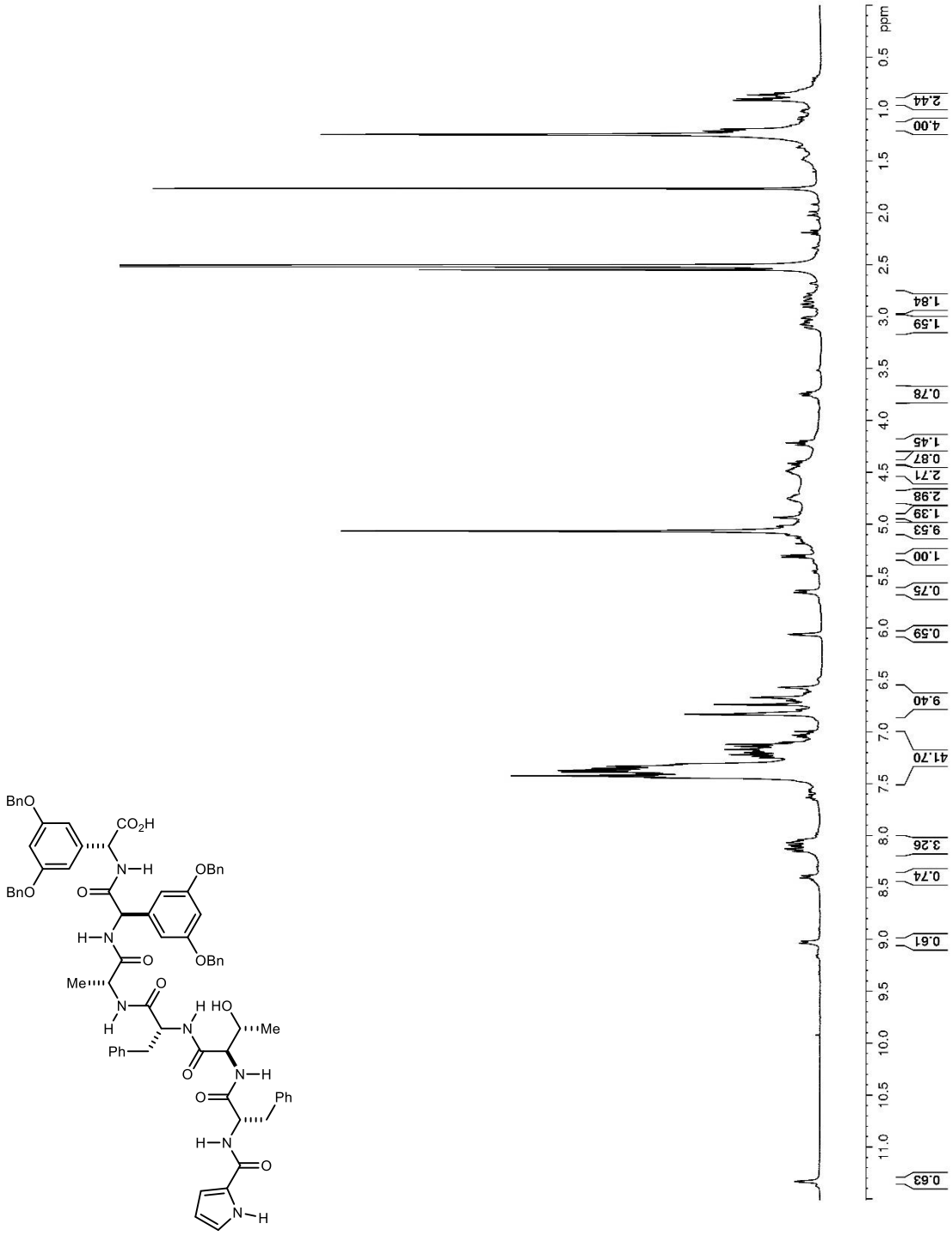

Figure 268. ^{1}H NMR (600 MHz, $CDCl_3$) spectrum of **2.79**.

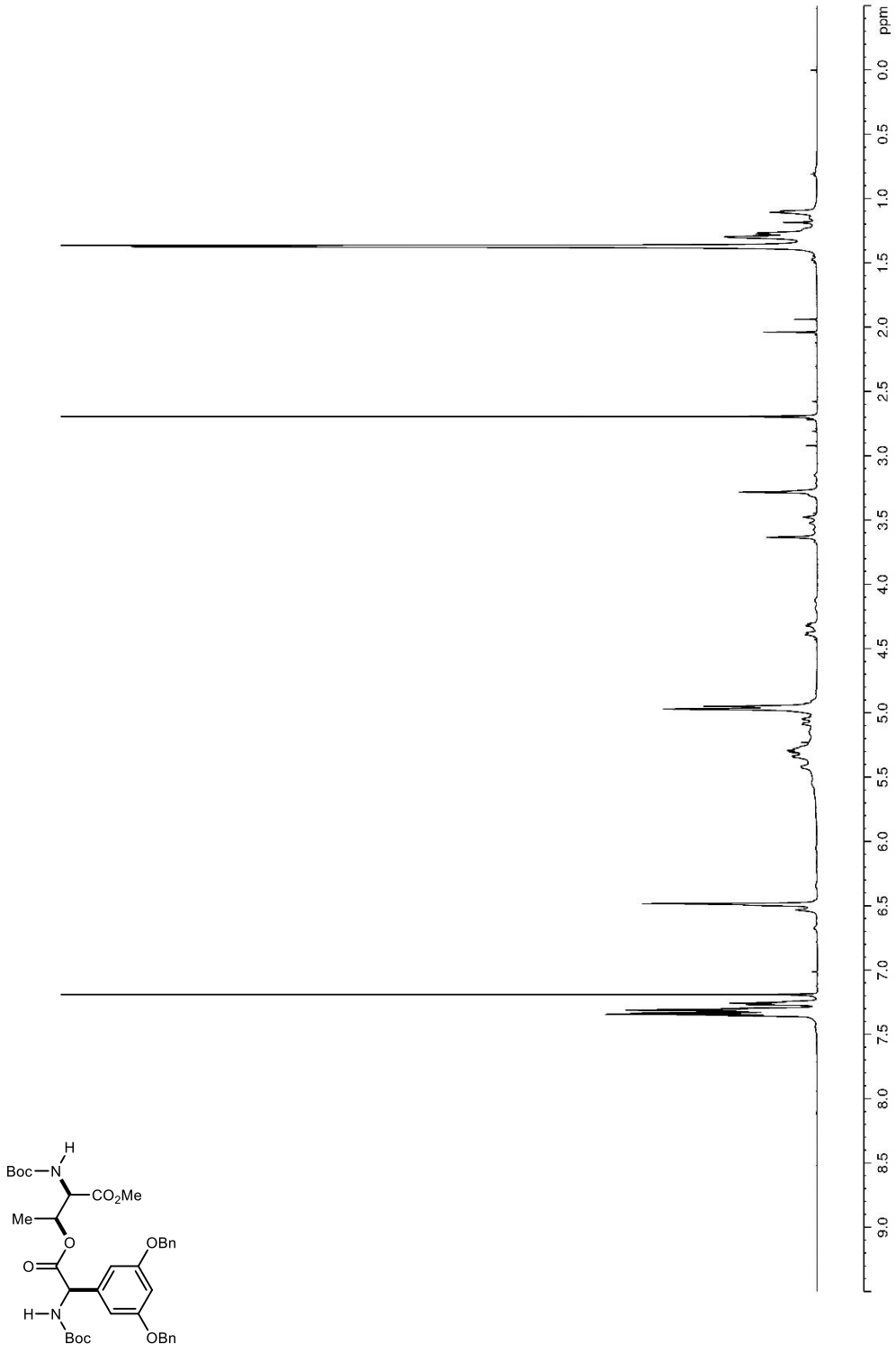

Figure 269. ^{1}H NMR (600 MHz, acetone-d_6) spectrum of **2.84** (14:1 mixture of epimers favoring major).

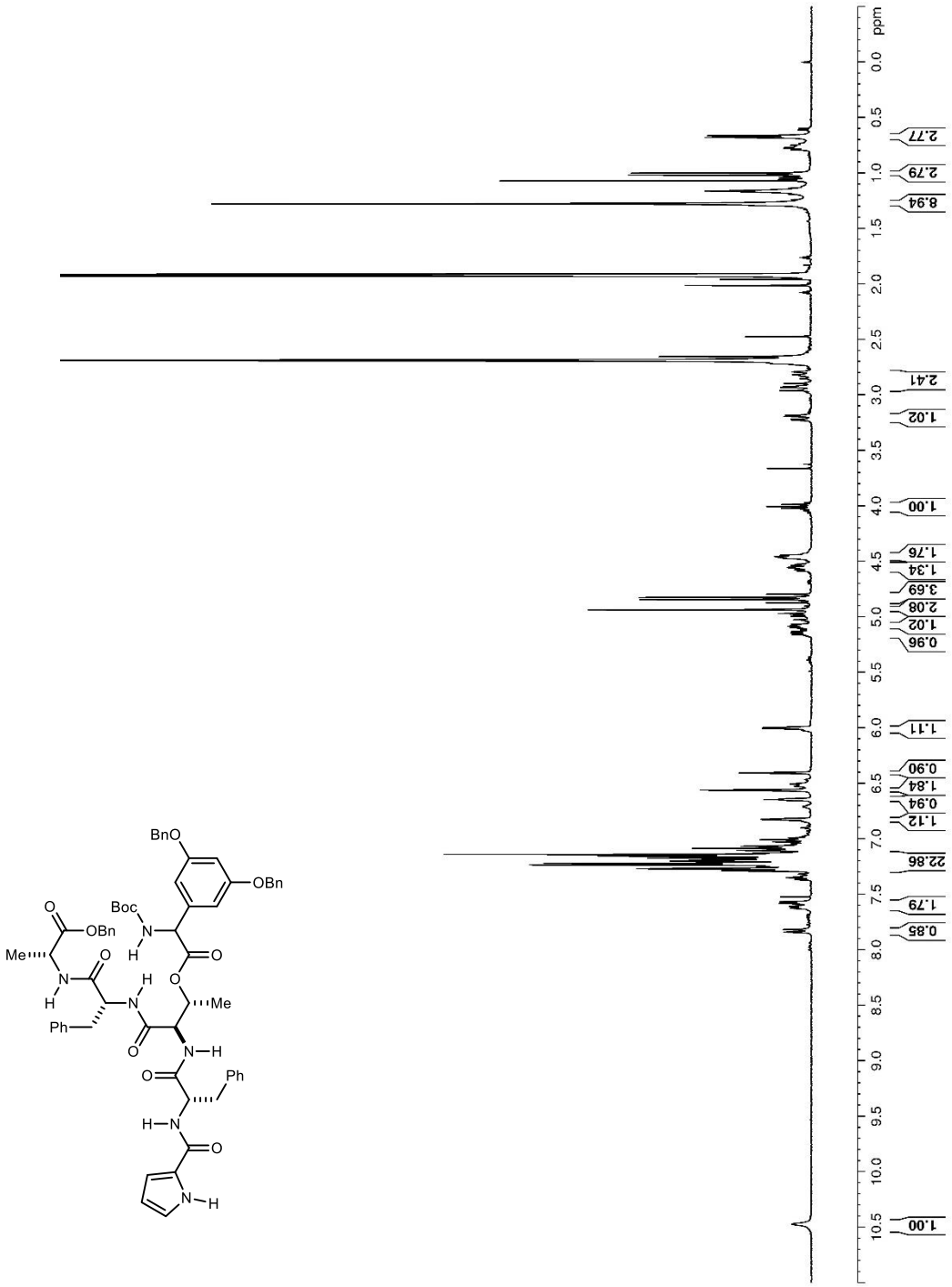

Figure 270. ^{1}H NMR (400 MHz, acetone-d_6) spectrum of **2.83**.

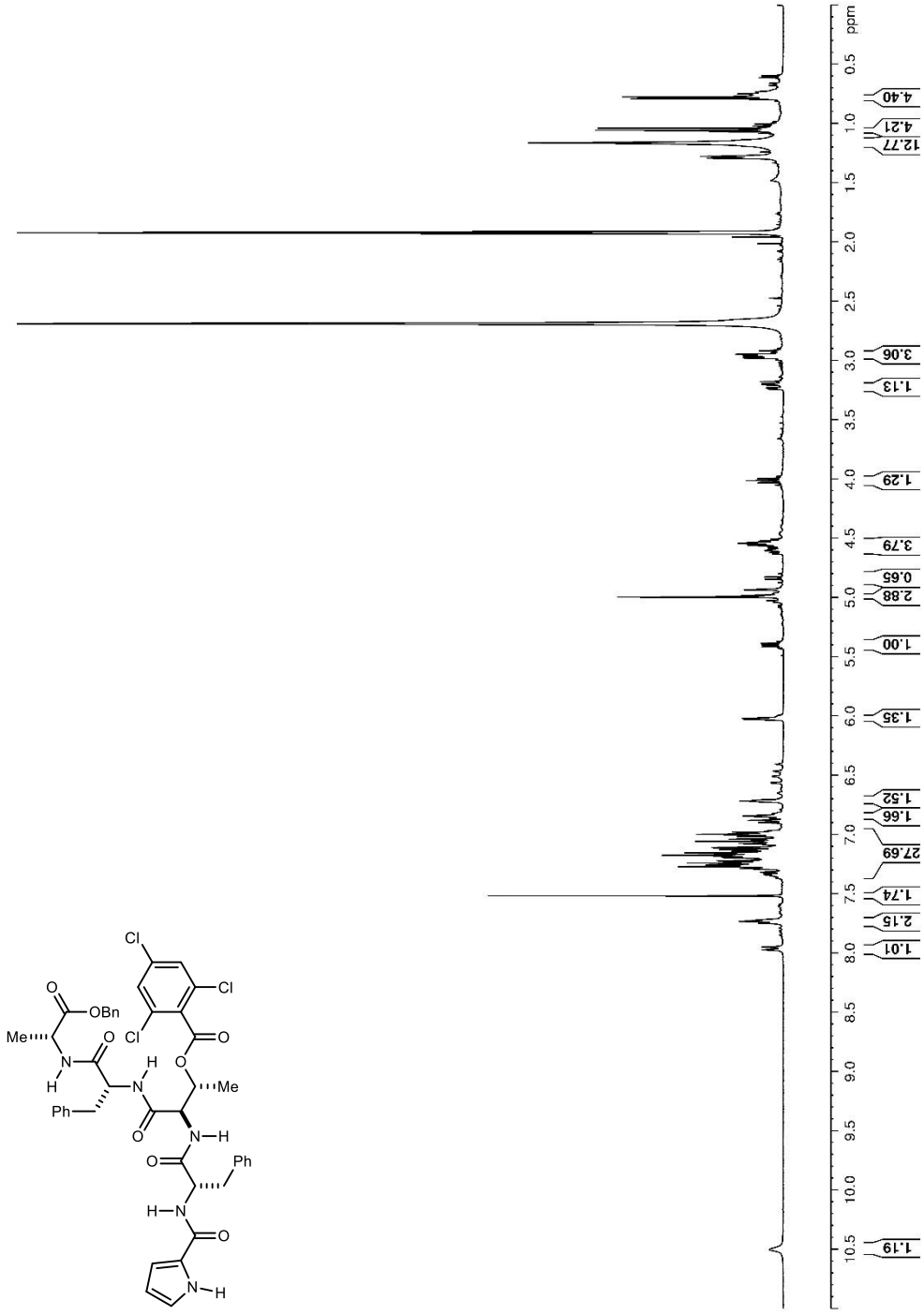

Figure 271. ^{1}H NMR (400 MHz, DMSO-d_6) spectrum of **2.89**. (mixture of epimers)

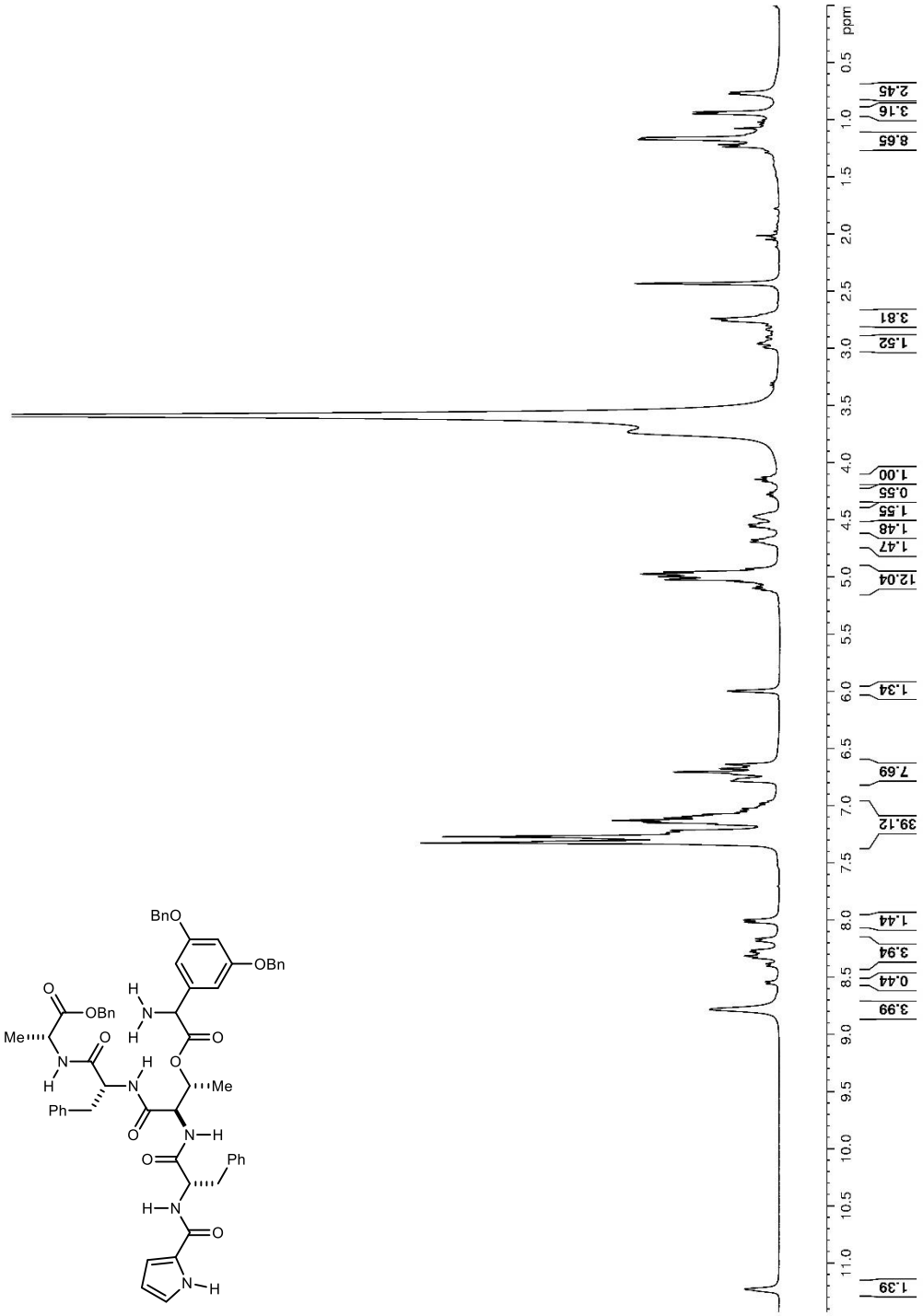

Figure 272. ^{1}H NMR (400 MHz, DMSO-d_6) spectrum of **2.90**. (mixture of epimers)

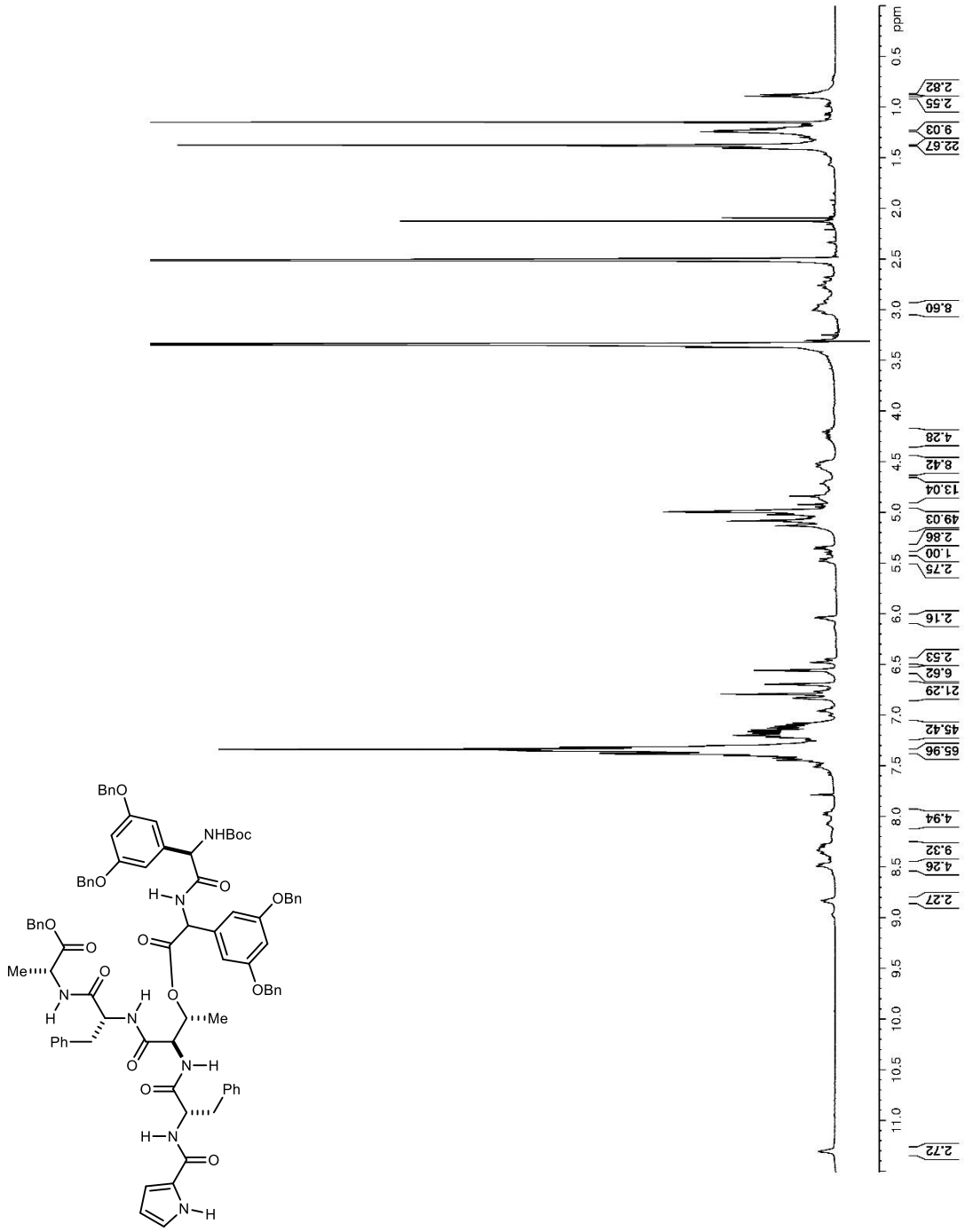

Figure 273. ^{1}H NMR (400 MHz, DMSO-d_6) spectrum of **2.91**. (mixture of epimers)

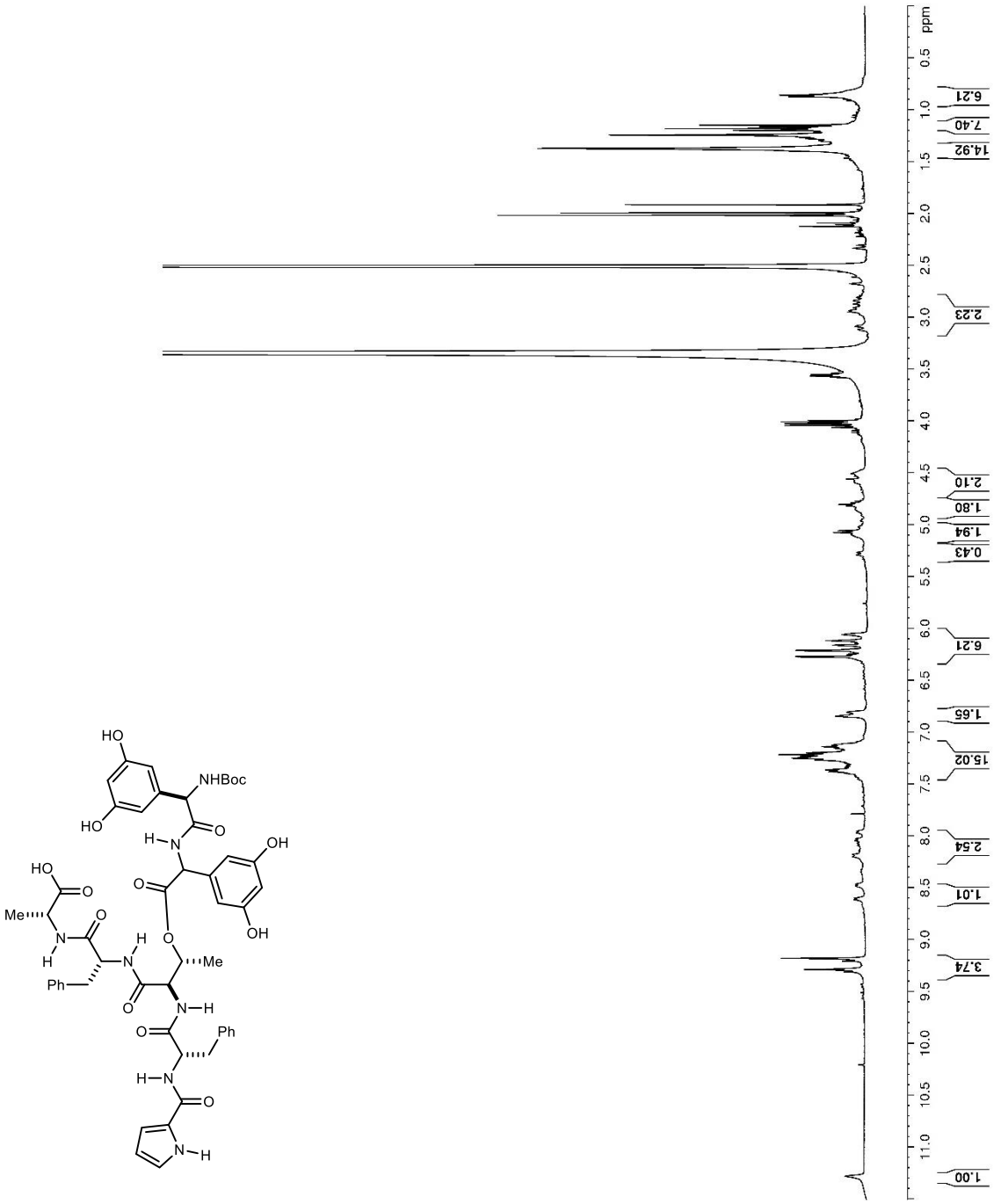

Figure 274. ^{1}H NMR (600 MHz, DMSO-d_6) spectrum of **2.92**. (mixture of epimers)

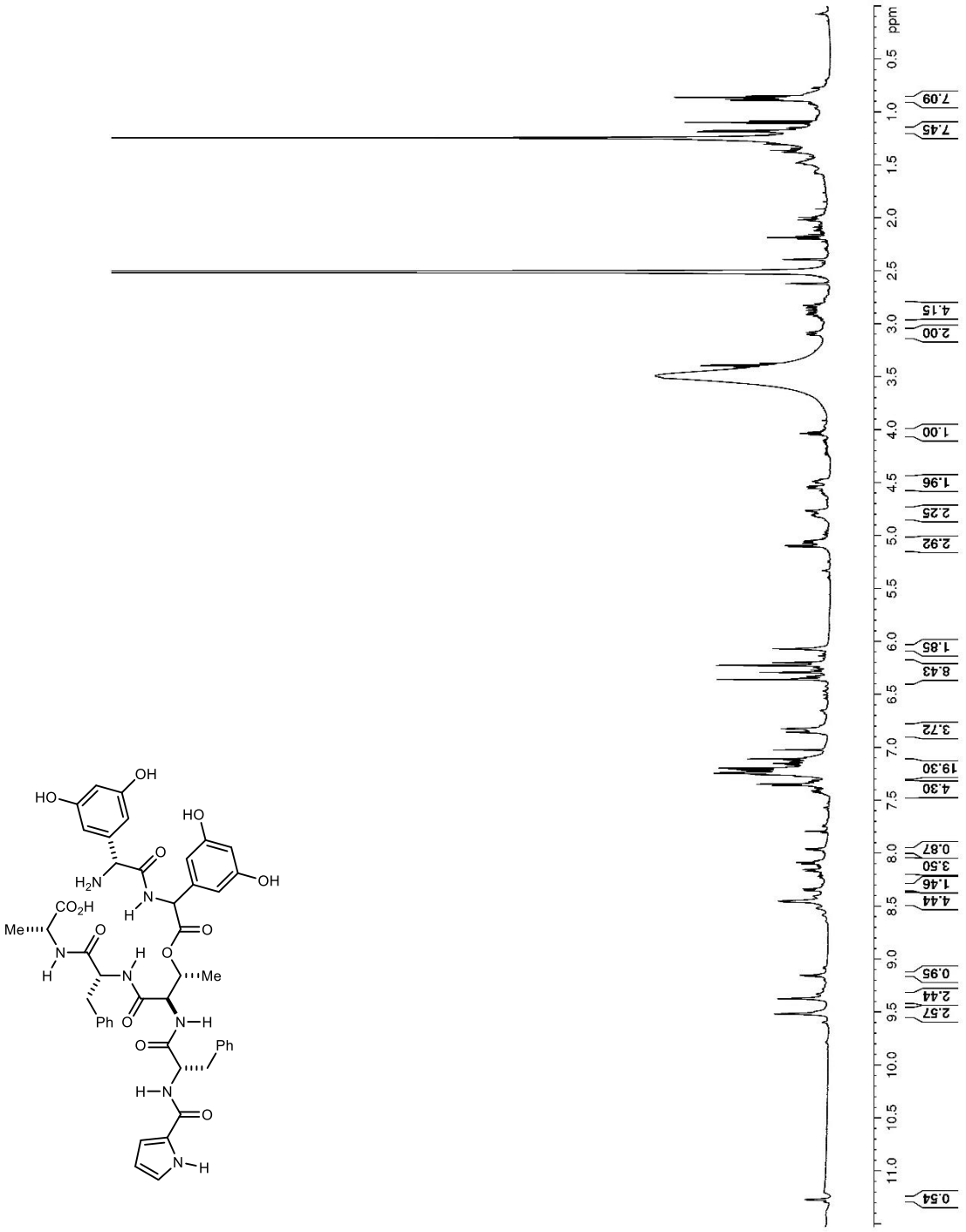

Figure 275. ^{1}H NMR (600 MHz, DMSO-d_6) spectrum of **2.93**. (mixture of epimers)

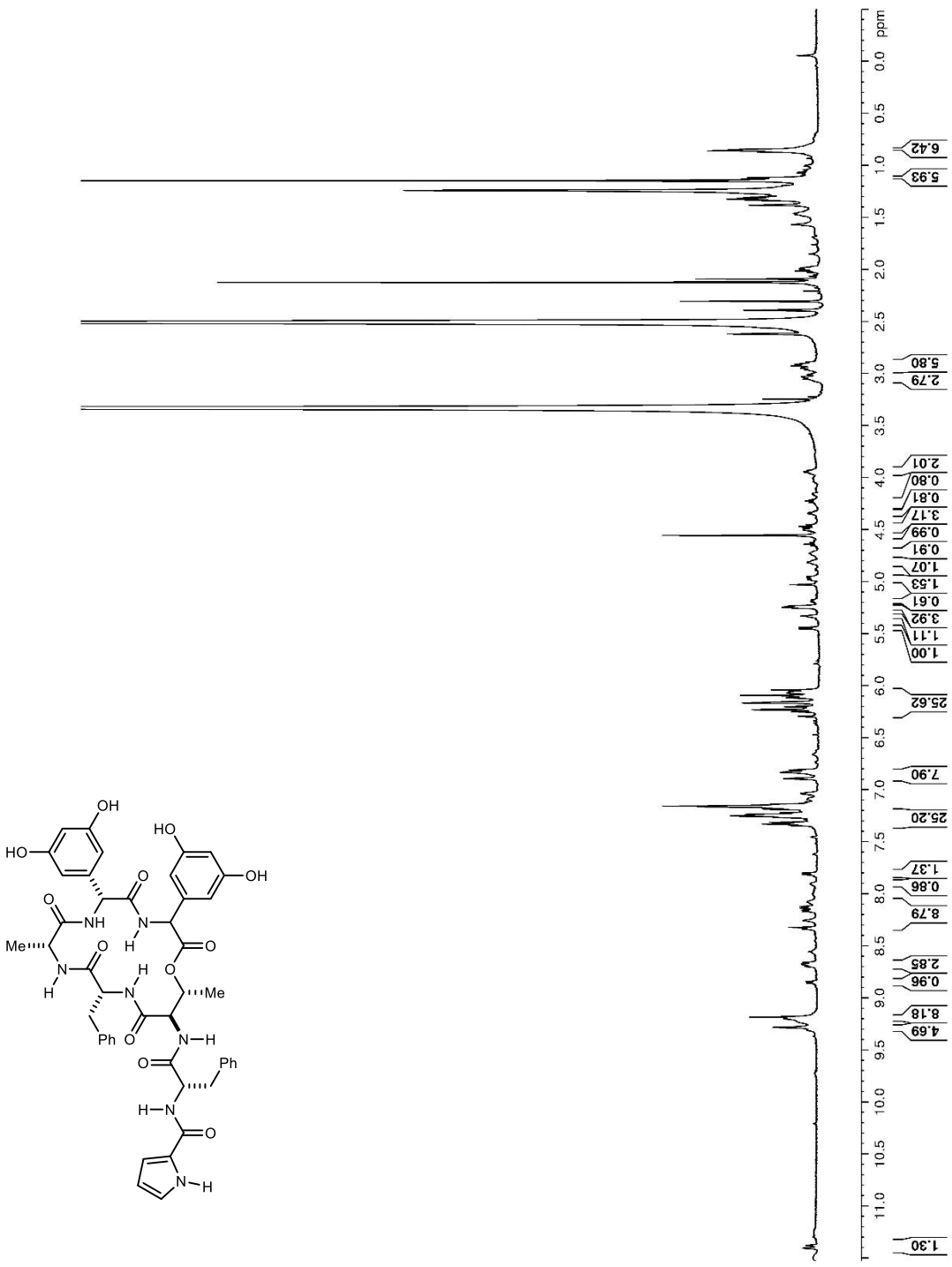

[1] Papanikolaou, G.; Pantopoulos, K., *Toxicol Appl Pharmacol* **2005,** *202*, 199-211.
[2] Koskenkorva-Frank, T. S.; Weiss, G.; Koppenol, W. H.; Burckhardt, S., *Free Radic Biol Med* **2013,** *65*, 1174-1194.
[3] Nairz, M.; Schroll, A.; Sonnweber, T.; Weiss, G., *Cell Microbiol* **2010,** *12*, 1691-702.
[4] Nairz, M.; Haschka, D.; Demetz, E.; Weiss, G., *Front Pharmacol* **2014,** *5*, 152.
[5] Skaar, E. P., *PLoS Pathog* **2010,** *6*, e1000949.
[6] Hood, M. I.; Skaar, E. P., *Nat Rev Microbiol* **2012,** *10*, 525-37.
[7] Nairz, M.; Schroll, A.; Sonnweber, T.; Weiss, G., *Cell Microbiol* **2010,** *12*, 1691-702.
[8] Skaar, E. P., *PLoS Pathog* **2010,** *6*, e1000949.
[9] Soares, M. P.; Weiss, G., *EMBO Rep* **2015,** *16*, 1482-500.
[10] Wilson, B. R.; Bogdan, A. R.; Miyazawa, M.; Hashimoto, K.; Tsuji, Y., *Trends Mol Med* **2016,** *22*, 1077-1090.
[11] Ibid.
[12] Miethke, M.; Marahiel, M. A., *Microbiol Mol Biol Rev* **2007,** *71*, 413-51.
[13] Nairz, M.; Schroll, A.; Sonnweber, T.; Weiss, G., *Cell Microbiol* **2010,** *12*, 1691-702.
[14] Nairz, M.; Haschka, D.; Demetz, E.; Weiss, G., *Front Pharmacol* **2014,** *5*, 152.
[15] Goetz, D. H.; Holmes, M. A.; Borregaard, N.; Bluhm, M. E.; Raymond, K. N.; Strong, R. K., *Molecular Cell* **2002,** *10*, 1033-1043.
[16] Skaar, E. P., *PLoS Pathog* **2010,** *6*, e1000949.
[17] Wilson, B. R.; Bogdan, A. R.; Miyazawa, M.; Hashimoto, K.; Tsuji, Y., *Trends Mol Med* **2016,** *22*, 1077-1090.
[18] Nairz, M.; Schroll, A.; Sonnweber, T.; Weiss, G., *Cell Microbiol* **2010,** *12*, 1691-702.
[19] Wilson, B. R.; Bogdan, A. R.; Miyazawa, M.; Hashimoto, K.; Tsuji, Y., *Trends Mol Med* **2016,** *22*, 1077-1090.
[20] Johnstone, T. C.; Nolan, E. M., *Dalton Trans* **2015,** *44*, 6320-39.
[21] Wilson, B. R.; Bogdan, A. R.; Miyazawa, M.; Hashimoto, K.; Tsuji, Y., *Trends Mol Med* **2016,** *22*, 1077-1090.
[22] Perry, R. D.; Balbo, P. B.; Jones, H. A.; Fetherston, J. D.; DeMoll, E., *Microbiology* **1999,** *145 (Pt 5)*, 1181-1190.
[23] Nairz, M.; Schroll, A.; Sonnweber, T.; Weiss, G., *Cell Microbiol* **2010,** *12*, 1691-702.
[24] Wilson, B. R.; Bogdan, A. R.; Miyazawa, M.; Hashimoto, K.; Tsuji, Y., *Trends Mol Med* **2016,** *22*, 1077-1090.
[25] Soares, M. P.; Weiss, G., *EMBO Rep* **2015,** *16*, 1482-500.
[26] Wilson, M. E.; Andersen, K. A.; Britigan, B. E., *Infection and Immunity* **1994,** *62*, 5133-5141.
[27] Ben-Othman, R.; Flannery, A. R.; Miguel, D. C.; Ward, D. M.; Kaplan, J.; Andrews, N. W., *PLoS Pathog* **2014,** *10*, e1003901.
[28] Skaar, E. P., ibid.**2010,** *6*, e1000949.
[29] Ratledge, C.; Dover, L. G., *Annual Review of Microbiology* **2000,** *54*, 881-941.
[30] Miethke, M.; Marahiel, M. A., *Microbiol Mol Biol Rev* **2007,** *71*, 413-51.
[31] Nairz, M.; Haschka, D.; Demetz, E.; Weiss, G., *Front Pharmacol* **2014,** *5*, 152.
[32] Arosio, P.; Levi, S., *Free Radical Biology and Medicine* **2002,** *33*, 457-463.
[33] Miethke, M.; Marahiel, M. A., *Microbiol Mol Biol Rev* **2007,** *71*, 413-51.
[34] Wandersman, C.; Delepelaire, P., *Annual Review of Microbiology* **2004,** *58*, 611-647.
[35] Miethke, M.; Marahiel, M. A., *Microbiol Mol Biol Rev* **2007,** *71*, 413-51.
[36] Wilson, B. R.; Bogdan, A. R.; Miyazawa, M.; Hashimoto, K.; Tsuji, Y., *Trends Mol Med* **2016,** *22*, 1077-1090.
[37] Saha, R.; Saha, N.; Donofrio, R. S.; Bestervelt, L. L., *J Basic Microbiol* **2013,** *53*, 303-17.
[38] Neilands, J. B., *J Biol Chem* **1995,** *270*, 26723-6.
[39] Ahmed, E.; Holmstrom, S. J., *Microb Biotechnol* **2014,** *7*, 196-208.
[40] Khan, A.; Singh, P.; Srivastava, A., *Microbiol Res* **2018,** *212-213*, 103-111.
[41] Bollmann, R., *Journal of Basic Microbiology* **1987,** *27*, 448-448.
[42] Ratledge, C.; Dover, L. G., *Annual Review of Microbiology* **2000,** *54*, 881-941.
[43] Traxler, M. F.; Seyedsayamdost, M. R.; Clardy, J.; Kolter, R., *Mol Microbiol* **2012,** *86*, 628-44.
[44] Saha, R.; Saha, N.; Donofrio, R. S.; Bestervelt, L. L., *J Basic Microbiol* **2013,** *53*, 303-17.
[45] Winkelmann, G., *Biometals* **2007,** *20*, 379-92.
[46] Ahmed, E.; Holmstrom, S. J., *Microb Biotechnol* **2014,** *7*, 196-208.
[47] Khan, A.; Singh, P.; Srivastava, A., *Microbiol Res* **2018,** *212-213*, 103-111.
[48] Devireddy, L. R.; Hart, D. O.; Goetz, D. H.; Green, M. R., *Cell* **2010,** *141*, 1006-17.
[49] Miethke, M.; Marahiel, M. A., *Microbiol Mol Biol Rev* **2007,** *71*, 413-51.
[50] Grunewald, J.; Marahiel, M. A., ibid.**2006,** *70*, 121-46.

[51] Kohli, R. M.; Trauger, J. W.; Schwarzer, D.; Marahiel, M. A.; Walsh, C. T., *Biochemistry* **2001,** *40*, 7099-108.
[52] Challis, G. L., *Chembiochem* **2005,** *6*, 601-11.
[53] Neilands, J. B., *J Biol Chem* **1995,** *270*, 26723-6.
[54] Miethke, M.; Marahiel, M. A., *Microbiol Mol Biol Rev* **2007,** *71*, 413-51.
[55] Johnstone, T. C.; Nolan, E. M., *Dalton Trans* **2015,** *44*, 6320-39.
[56] Ibid.
[57] Ibid.
[58] Chaturvedi, K. S.; Hung, C. S.; Crowley, J. R.; Stapleton, A. E.; Henderson, J. P., *Nat Chem Biol* **2012,** *8*, 731-6.
[59] Hood, M. I.; Skaar, E. P., *Nat Rev Microbiol* **2012,** *10*, 525-37.
[60] Wilson, B. R.; Bogdan, A. R.; Miyazawa, M.; Hashimoto, K.; Tsuji, Y., *Trends Mol Med* **2016,** *22*, 1077-1090.
[61] Bickel, H.; Bosshardt, R.; Gäumann, E.; Reusser, P.; Vischer, E.; Voser, W.; Wettstein, A.; Zähner, H., *Helvetica Chimica Acta* **1960,** *43*, 2118-2128.
[62] Bickel, H.; Hall, G. E.; Keller-Schierlein, W.; Prelog, V.; Vischer, E.; Wettstein, A., ibid., 2129-2138.
[63] Heilmeyer, L.; Woehler, F., *Dtsch Med Wochenschr* **1962,** *87*, 2661-7.
[64] Bannerman, R. M.; Callender, S. T.; Williams, D. L., *Br Med J* **1962,** *2*, 1573-7.
[65] Keberle, H., *Ann N Y Acad Sci* **1964,** *119*, 758-68.
[66] Ballas, S. K.; Zeidan, A. M.; Duong, V. H.; DeVeaux, M.; Heeney, M. M., *Am J Hematol* **2018,** *93*, 943-952.
[67] Miyajima, H.; Takahashi, Y.; Kamata, T.; Shimizu, H.; Sakai, N.; Gitlin, J. D., *Ann Neurol* **1997,** *41*, 404-7.
[68] Zeng, L.; Tan, L.; Li, H.; Zhang, Q.; Li, Y.; Guo, J., *PLoS One* **2018,** *13*, e0193615.
[69] Sayer, J. M.; Emery, T. F., *Biochemistry* **1968,** *7*, 184-90.
[70] Moore, R. E.; Emery, T., ibid.**1976,** *15*, 2719-23.
[71] Ledyard, K. M.; Butler, A., *JBIC Journal of Biological Inorganic Chemistry* **1997,** *2*, 93-97.
[72] Neilands, J. B., *Journal of the American Chemical Society* **1952,** *74*, 4846-4847.
[73] Konetschny-Rapp, S.; Jung, G.; Meiwes, J.; Zahner, H., *Eur J Biochem* **1990,** *191*, 65-74.
[74] Meiwes, J.; Fiedler, H. P.; Haag, H.; Zahner, H.; Konetschny-Rapp, S.; Jung, G., *FEMS Microbiol Lett* **1990,** *55*, 201-5.
[75] Haag, H.; Fiedler, H. P.; Meiwes, J.; Drechsel, H.; Jung, G.; Zahner, H., ibid.**1994,** *115*, 125-30.
[76] Smith, M. J.; Shoolery, J. N.; Schwyn, B.; Holden, I.; Neilands, J. B., *Journal of the American Chemical Society* **1985,** *107*, 1739-1743.
[77] Munzinger, M.; Budzikiewicz, H.; Expert, D.; Enard, C.; Meyer, J. M., *Z Naturforsch C J Biosci* **2000,** *55*, 328-32.
[78] Pollack, J. R.; Neilands, J. B., *Biochemical and Biophysical Research Communications* **1970,** *38*, 989-992.
[79] O'Brien, I. G.; Cox, G. B.; Gibson, F., *Biochimica et Biophysica Acta (BBA) - General Subjects* **1970,** *201*, 453-460.
[80] Dertz, E. A.; Xu, J.; Stintzi, A.; Raymond, K. N., *J Am Chem Soc* **2006,** *128*, 22-3.
[81] Moynie, L.; Milenkovic, S.; Mislin, G. L. A.; Gasser, V.; Malloci, G.; Baco, E.; McCaughan, R. P.; Page, M. G. P.; Schalk, I. J.; Ceccarelli, M.; Naismith, J. H., *Nat Commun* **2019,** *10*, 3673.
[82] Poole, K.; Young, L.; Neshat, S., *J Bacteriol* **1990,** *172*, 6991-6.
[83] Griffiths, G. L.; Sigel, S. P.; Payne, S. M.; Neilands, J. B., *Journal of Biological Chemistry* **1984,** *259*, 383-385.
[84] Cornish, A.; Page, W., *Biometals* **1995,** *8*.
[85] Perry, R. D.; Balbo, P. B.; Jones, H. A.; Fetherston, J. D.; DeMoll, E., *Microbiology* **1999,** *145 (Pt 5)*, 1181-1190.
[86] Perry, R. D.; Fetherston, J. D., *Microbes Infect* **2011,** *13*, 808-17.
[87] Francis, J.; Macturk, H. M.; Madinaveitia, J.; Snow, G. A., *Biochem J* **1953,** *55*, 596-607.
[88] Snow, G. A., *Journal of the Chemical Society (Resumed)* **1954**.
[89] Marks, J., *J Pathol Bacteriol* **1954,** *67*, 254-6.
[90] Wendenbaum, S.; Demange, P.; Dell, A.; Meyer, J. M.; Abdallah, M. A., *Tetrahedron Letters* **1983,** *24*, 4877-4880.
[91] Suenaga, K.; Kokubo, S.; Shinohara, C.; Tsuji, T.; Uemura, D., ibid.**1999,** *40*, 1945-1948.
[92] Kokubo, S.; Suenaga, K.; Shinohara, C.; Tsuji, T.; Uemura, D., *Tetrahedron* **2000,** *56*, 6435-6440.
[93] Fennell, K. A.; Mollmann, U.; Miller, M. J., *J Org Chem* **2008,** *73*, 1018-24.
[94] Ibid.
[95] Wu, C.; Miller, P. A.; Miller, M. J., *Bioorg Med Chem Lett* **2011,** *21*, 2611-5.
[96] Fennell, K. A.; Miller, M. J., *Org Lett* **2007,** *9*, 1683-5.
[97] Konetschny-Rapp, S.; Jung, G.; Meiwes, J.; Zahner, H., *Eur J Biochem* **1990,** *191*, 65-74.
[98] Meiwes, J.; Fiedler, H. P.; Haag, H.; Zahner, H.; Konetschny-Rapp, S.; Jung, G., *FEMS Microbiol Lett* **1990,** *55*, 201-5.

[99] Haag, H.; Fiedler, H. P.; Meiwes, J.; Drechsel, H.; Jung, G.; Zahner, H., ibid.**1994,** *115*, 125-30.
[100] Madsen, J. L.; Johnstone, T. C.; Nolan, E. M., *J Am Chem Soc* **2015,** *137*, 9117-27.
[101] Pandey, R. K.; Jarvis, G. G.; Low, P. S., *Tetrahedron Letters* **2012,** *53*, 1627-1629.
[102] Vértesy, L.; Aretz, W.; Fehlhaber, H.-W.; Kogler, H., *Helvetica Chimica Acta* **1995,** *78*, 46-60.
[103] Roosenberg, J. M., 2nd; Miller, M. J., *J Org Chem* **2000,** *65*, 4833-8.
[104] Sridhar, P. R.; Venkatesh, B. C.; Kalesha, S.; Sudharani, C., *Org Biomol Chem* **2018,** *16*, 3732-3740.
[105] Ino, A.; Murabayashi, A., *Tetrahedron* **2001,** *57*, 1897-1902.
[106] Ino, A.; Hasegawa, Y.; Murabayashi, A., ibid.**1999,** *55*, 10283-10294.
[107] Ino, A.; Murabayashi, A., ibid., 10271-10282.
[108] Bickel, H.; Hall, G. E.; Keller-Schierlein, W.; Prelog, V.; Vischer, E.; Wettstein, A., *Helvetica Chimica Acta* **1960,** *43*, 2129-2138.
[109] Keller-Schierlein, W.; Merterns, P.; Prelog, V.; Walser, A., *Helv Chim Acta* **1965,** *48*, 710-23.
[110] Prelog, V.; Walser, A., *Helvetica Chimica Acta* **1962,** *45*, 631-637.
[111] Bergeron, R. J.; Pegram, J. J., *The Journal of Organic Chemistry* **1988,** *53*, 3131-3134.
[112] Vértesy, L.; Aretz, W.; Fehlhaber, H.-W.; Kogler, H., *Helvetica Chimica Acta* **1995,** *78*, 46-60.
[113] Braun, V.; Günthner, K.; Hantke, K.; Zimmermann, L., *Journal of Bacteriology* **1983,** *156*, 308-315.
[114] Sackmann, W.; Reusser, P.; Neipp, L.; Kradolfer, F.; Gross, F., *Antibiot Chemother (Northfield)* **1962,** *12*, 34-45.
[115] Miller, M. J.; Malouin, F., *Accounts of Chemical Research* **2002,** *26*, 241-249.
[116] Page, M. G., *Ann N Y Acad Sci* **2013,** *1277*, 115-26.
[117] Gorska, A.; Sloderbach, A.; Marszall, M. P., *Trends Pharmacol Sci* **2014,** *35*, 442-9.
[118] Neumann, W.; Nolan, E. M., *J Biol Inorg Chem* **2018,** *23*, 1025-1036.
[119] Ghosh, M.; Miller, P. A.; Miller, M. J., *J Antibiot (Tokyo)* **2020,** *73*, 152-157.
[120] Miller, M. J.; Walz, A. J.; Zhu, H.; Wu, C.; Moraski, G.; Mollmann, U.; Tristani, E. M.; Crumbliss, A. L.; Ferdig, M. T.; Checkley, L.; Edwards, R. L.; Boshoff, H. I., *J Am Chem Soc* **2011,** *133*, 2076-9.
[121] Ghosh, M.; Miller, M. J., *Bioorganic & Medicinal Chemistry* **1995,** *3*, 1519-1525.
[122] McPherson, C. J.; Aschenbrenner, L. M.; Lacey, B. M.; Fahnoe, K. C.; Lemmon, M. M.; Finegan, S. M.; Tadakamalla, B.; O'Donnell, J. P.; Mueller, J. P.; Tomaras, A. P., *Antimicrob Agents Chemother* **2012,** *56*, 6334-42.
[123] Ito, A.; Nishikawa, T.; Matsumoto, S.; Yoshizawa, H.; Sato, T.; Nakamura, R.; Tsuji, M.; Yamano, Y., ibid.**2016,** *60*, 7396-7401.
[124] Bassetti, M.; Ariyasu, M.; Binkowitz, B.; Nagata, T. D.; Echols, R. M.; Matsunaga, Y.; Toyoizumi, K.; Doi, Y., *Infect Drug Resist* **2019,** *12*, 3607-3623.
[125] Stachelhaus, T.; Mootz, H. D.; Marahiel, M. A., *Chemistry & Biology* **1999,** *6*, 493-505.
[126] Challis, G. L.; Ravel, J.; Townsend, C. A., ibid.**2000,** *7*, 211-224.
[127] Ziemert, N.; Alanjary, M.; Weber, T., *Nat Prod Rep* **2016,** *33*, 988-1005.
[128] Zerikly, M.; Challis, G. L., *Chembiochem* **2009,** *10*, 625-33.
[129] Challis, G. L.; Ravel, J., *FEMS Microbiol Lett* **2000,** *187*, 111-4.
[130] Ziemert, N.; Alanjary, M.; Weber, T., *Nat Prod Rep* **2016,** *33*, 988-1005.
[131] Zerikly, M.; Challis, G. L., *Chembiochem* **2009,** *10*, 625-33.
[132] Konz, D.; Marahiel, M. A., *Chemistry & Biology* **1999,** *6*, R39-R48.
[133] Stachelhaus, T.; Mootz, H. D.; Marahiel, M. A., ibid., 493-505.
[134] Challis, G. L.; Ravel, J.; Townsend, C. A., ibid.**2000,** *7*, 211-224.
[135] Challis, G. L.; Ravel, J., *FEMS Microbiol Lett* **2000,** *187*, 111-4.
[136] Lautru, S.; Deeth, R. J.; Bailey, L. M.; Challis, G. L., *Nat Chem Biol* **2005,** *1*, 265-9.
[137] Ibid.
[138] Stephan, H.; Freund, S.; Meyer, J.-M.; Winkelmann, G.; Jung, G., *Liebigs Annalen der Chemie* **1993,** *1993*, 43-48.
[139] Lautru, S.; Challis, G. L., *Microbiology* **2004,** *150*, 1629-1636.
[140] Williams, J. C.; Sheldon, J. R.; Imlay, H. D.; Dutter, B. F.; Draelos, M. M.; Skaar, E. P.; Sulikowski, G. A., *Org Lett* **2019,** *21*, 679-682.
[141] Brendan Dutter PhD Thesis
[142] Liang, X.; Lee, C. J.; Chen, X.; Chung, H. S.; Zeng, D.; Raetz, C. R.; Li, Y.; Zhou, P.; Toone, E. J., *Bioorg Med Chem* **2011,** *19*, 852-60.
[143] Duranti, A.; Tontini, A.; Antonietti, F.; Vacondio, F.; Fioni, A.; Silva, C.; Lodola, A.; Rivara, S.; Solorzano, C.; Piomelli, D.; Tarzia, G.; Mor, M., *J Med Chem* **2012,** *55*, 4824-36.
[144] {, #20}
[145] Liang, X.; Lee, C. J.; Chen, X.; Chung, H. S.; Zeng, D.; Raetz, C. R.; Li, Y.; Zhou, P.; Toone, E. J., *Bioorg*

Med Chem **2011,** *19*, 852-60.
[146] Duranti, A.; Tontini, A.; Antonietti, F.; Vacondio, F.; Fioni, A.; Silva, C.; Lodola, A.; Rivara, S.; Solorzano, C.; Piomelli, D.; Tarzia, G.; Mor, M., *J Med Chem* **2012,** *55*, 4824-36.
[147] Gloanec, P.; Hervé, Y.; Brémand, N.; Lecouvé, J.-P.; Bréard, F.; De Nanteuil, G., *Tetrahedron Letters* **2002,** *43*, 3499-3501.
[148] Aggarwal, V. K.; Astle, C. J.; Rogers-Evans, M., *Org Lett* **2004,** *6*, 1469-71.
[149] Córdova, A.; Reed, N. N.; Ashley, J. A.; Janda, K. D., *Bioorganic & Medicinal Chemistry Letters* **1999,** *9*, 3119-3122.
[150] Hyun Lee, B.; Miller, M. J., *Tetrahedron Letters* **1984,** *25*, 927-930.
[151] Kishimoto, S.; Nishimura, S.; Hatano, M.; Igarashi, M.; Kakeya, H., *J Org Chem* **2015,** *80*, 6076-82.
[152] Rigo, B. t.; Lespagnol, C.; Pauly, M., *Journal of Heterocyclic Chemistry* **1988,** *25*, 49-57.
[153] Qu, S.; Chen, Y.; Wang, X.; Chen, S.; Xu, Z.; Ye, T., *Chem Commun (Camb)* **2015,** *51*, 2510-3.
[154] Brendan Dutter Ph.D. Thesis
[155] Williams, J. C.; Sheldon, J. R.; Imlay, H. D.; Dutter, B. F.; Draelos, M. M.; Skaar, E. P.; Sulikowski, G. A., *Org Lett* **2019,** *21*, 679-682.
[156] Alexander, D. B.; Zuberer, D. A., *Biology and Fertility of Soils* **1991,** *12*, 39-45.
[157] Schwyn, B.; Neilands, J. B., *Analytical Biochemistry* **1987,** *160*, 47-56.
[158] Ankenbauer, R. G.; Cox, C. D., *J Bacteriol* **1988,** *170*, 5364-7.
[159] Sheldon, J. R.; Laaskso, H. A.; Heinrichs, D. E. Iron Acquisition Strategies for Bacterial Pathogens. In Virulence Mechanisms of Bacterial Pathogens, 5th ed.; Cornick, N. A., Ed.; ASM Press: Washington, DC, 2016; p 43.
[160] Dumas, Z.; Ross-Gillespie, A.; Kummerli, R., *Proc Biol Sci* **2013,** *280*, 20131055.
[161] Miller, M. J.; McKee, J. A.; Minnick, A. A.; Dolence, E. K., *Biol Met* **1991,** *4*, 62-9.
[162] Miller, M. J.; Malouin, F., *Accounts of Chemical Research* **2002,** *26*, 241-249.
[163] Page, M. G., *Ann N Y Acad Sci* **2013,** *1277*, 115-26.
[164] Negash, K. H.; Norris, J. K. S.; Hodgkinson, J. T., *Molecules* **2019,** *24*.
[165] Kong, H.; Cheng, W.; Wei, H.; Yuan, Y.; Yang, Z.; Zhang, X., *Eur J Med Chem* **2019,** *182*, 111615.
[166] Schalk, I. J., *Clin Microbiol Infect* **2018,** *24*, 801-802.
[167] Bassetti, M.; Ariyasu, M.; Binkowitz, B.; Nagata, T. D.; Echols, R. M.; Matsunaga, Y.; Toyoizumi, K.; Doi, Y., *Infect Drug Resist* **2019,** *12*, 3607-3623.
[168] Ito, A.; Nishikawa, T.; Matsumoto, S.; Yoshizawa, H.; Sato, T.; Nakamura, R.; Tsuji, M.; Yamano, Y., *Antimicrob Agents Chemother* **2016,** *60*, 7396-7401.
[169] Stewart, P. S.; William Costerton, J., *The Lancet* **2001,** *358*, 135-138.
[170] Xu, K. D.; McFeters, G. A.; Stewart, P. S., *Microbiology* **2000,** *146 (Pt 3)*, 547-549.
[171] Harrison, F.; Buckling, A., *ISME J* **2009,** *3*, 632-4.
[172] Banin, E.; Vasil, M. L.; Greenberg, E. P., *Proc Natl Acad Sci U S A* **2005,** *102*, 11076-81.
[173] Singh, P. K., *Biometals* **2004,** *17*, 267-70.
[174] Ojha, A.; Hatfull, G. F., *Mol Microbiol* **2007,** *66*, 468-83.
[175] Carroll, A. R.; Copp, B. R.; Davis, R. A.; Keyzers, R. A.; Prinsep, M. R., *Nat Prod Rep* **2021,** *38*, 362-413.
[176] Dang, T.; Sussmuth, R. D., *Acc Chem Res* **2017,** *50*, 1566-1576.
[177] Taevernier, L.; Wynendaele, E.; Gevaert, B.; Spiegeleer, B., *Curr Protein Pept Sci* **2017,** *18*, 425-452.
[178] McKeown, S. R., *Br J Radiol* **2014,** *87*, 20130676.
[179] Torres, J. P.; Lin, Z.; Fenton, D. S.; Leavitt, L. U.; Niu, C.; Lam, P. Y.; Robes, J. M.; Peterson, R. T.; Concepcion, G. P.; Haygood, M. G.; Olivera, B. M.; Schmidt, E. W., *J Nat Prod* **2020,** *83*, 1249-1257.
[180] Han, F.; Liu, G.; Zhang, X.; Ding, Y.; Wang, L.; Wu, Y.; Chen, Y.; Zhang, Q., *Org Lett* **2021,** *23*, 4976-4980.
[181] Julia, V.; Macia, L.; Dombrowicz, D., *Nat Rev Immunol* **2015,** *15*, 308-22.
[182] Baxi, S. N.; Phipatanakul, W., *Adolesc Med State Art Rev* **2010,** *21*, 57-ix.
[183] Kim, G. J.; Li, X.; Kim, S. H.; Yang, I.; Hahn, D.; Chin, J.; Nam, S. J.; Nam, J. W.; Nam, D. H.; Oh, D. C.; Chang, H. W.; Choi, H., *Org Lett* **2018,** *20*, 7539-7543.
[184] Shabani, S.; Hutton, C. A., ibid.**2020,** *22*, 4557-4561.
[185] Katsuyama, A.; Yakushiji, F.; Ichikawa, S., *J Org Chem* **2018,** *83*, 7085-7101.
[186] Shoji, J.; Hinoo, H.; Katayama, T.; Matsumoto, K.; Tanimoto, T.; Hattori, T.; Higashiyama, I.; Miwa, H.; Motokawa, K.; Yoshida, T., *J Antibiot (Tokyo)* **1992,** *45*, 817-23.
[187] Shoji, J.; Hinoo, H.; Katayama, T.; Nakagawa, Y.; Ikenishi, Y.; Iwatani, K.; Yoshida, T., ibid., 824-31.
[188] Biel, M.; Wascholowski, V.; Giannis, A., *Angew Chem Int Ed Engl* **2005,** *44*, 3186-216.
[189] Ueda, H.; Nakajima, H.; Hori, Y.; Fujita, T.; Nishimura, M.; Goto, T.; Okuhara, M., *J Antibiot (Tokyo)* **1994,** *47*, 301-10.
[190] Li, K. W.; Wu, J.; Xing, W.; Simon, J. A., *Journal of the American Chemical Society* **1996,** *118*, 7237-7238.

[191] Greshock, T. J.; Johns, D. M.; Noguchi, Y.; Williams, R. M., *Org Lett* **2008,** *10*, 613-6.
[192] Chen, Y.; Gambs, C.; Abe, Y.; Wentworth, P., Jr.; Janda, K. D., *J Org Chem* **2003,** *68*, 8902-5.
[193] Wen, S.; Packham, G.; Ganesan, A., ibid.**2008,** *73*, 9353-61.
[194] Pettit, G. R.; Tan, R.; Pettit, R. K.; Smith, T. H.; Feng, S.; Doubek, D. L.; Richert, L.; Hamblin, J.; Weber, C.; Chapuis, J. C., *J Nat Prod* **2007,** *70*, 1069-72.
[195] Beveridge, R. E.; Batey, R. A., *Org Lett* **2014,** *16*, 2322-5.
[196] Valeria D'Auria, M.; Zampella, A.; Paloma, L. G.; Minale, L.; Debitus, C.; Roussakis, C.; Le Bert, V., *Tetrahedron* **1996,** *52*, 9589-9596.
[197] Zampella, A.; Randazzo, A.; Borbone, N.; Luciani, S.; Trevisi, L.; Debitus, C.; D'Auria, M. V., *Tetrahedron Letters* **2002,** *43*, 6163-6166.
[198] D'Auria, M. V.; Sepe, V.; D'Orsi, R.; Bellotta, F.; Debitus, C.; Zampella, A., *Tetrahedron* **2007,** *63*, 131-140.
[199] Krishnamoorthy, R.; Vazquez-Serrano, L. D.; Turk, J. A.; Kowalski, J. A.; Benson, A. G.; Breaux, N. T.; Lipton, M. A., *J Am Chem Soc* **2006,** *128*, 15392-3.
[200] Kikuchi, M.; Konno, H., *Org Lett* **2014,** *16*, 4324-7.
[201] Goodreid, J. D.; dos Santos Eda, S.; Batey, R. A., ibid.**2015,** *17*, 2182-5.
[202] Mukaiyama, T.; Izumi, J.; Miyashita, M.; Shiina, I., *Chemistry Letters* **1993,** *22*, 907-910.
[203] Ishihara, K.; Kubota, M.; Kurihara, H.; Yamamoto, H., *J Org Chem* **1996,** *61*, 4560-4567.
[204] Shiina, I.; Fujisawa, H.; Ishii, T.; Fukuda, Y., *Heterocycles* **2000,** *52*.
[205] Shiina, I.; Fukuda, Y.; Ishii, T.; Fujisawa, H.; Mukaiyama, T., *Chemistry Letters* **1998,** *27*, 831-832.
[206] Kurusu, K.; Ohba, K.; Arai, T.; Fukushima, K., *J Antibiot (Tokyo)* **1987,** *40*, 1506-14.
[207] Nomura, T.; Kuroda, J.; Fukai, T.; Konishi, M.; Uno, J.; Kurusu, K., *Heterocycles* **2000,** *53*.
[208] Cochrane, J. R.; Yoon, D. H.; McErlean, C. S.; Jolliffe, K. A., *Beilstein J Org Chem* **2012,** *8*, 1344-51.
[209] Hikota, M.; Sakurai, Y.; Horita, K.; Yonemitsu, O., *Tetrahedron Letters* **1990,** *31*, 6367-6370.
[210] Morino, T.; Shimada, K.; Masuda, A.; Yamashita, N.; Nishimoto, M.; Nishikiori, T.; Saito, S., *J Antibiot (Tokyo)* **1996,** *49*, 564-8.
[211] Morino, T.; Masuda, A.; Yamada, M.; Nishimoto, M.; Nishikiori, T.; Saito, S.; Shimada, N., ibid.**1994,** *47*, 1341-3.
[212] Alonso, A.; Saxena, M.; Williams, S.; Mustelin, T., *J Biol Chem* **2001,** *276*, 4766-71.
[213] Chakraborty, T. K.; Ghosh, S.; Laxman, P.; Dutta, S.; Samanta, R., *Tetrahedron Letters* **2005,** *46*, 5447-5450.
[214] Peterson, J. R.; Mitchison, T. J., *Chemistry & Biology* **2002,** *9*, 1275-1285.
[215] Disanza, A.; Steffen, A.; Hertzog, M.; Frittoli, E.; Rottner, K.; Scita, G., *Cell Mol Life Sci* **2005,** *62*, 955-70.
[216] Grieco, P. A.; Hon, Y. S.; Perez-Medrano, A., *Journal of the American Chemical Society* **2002,** *110*, 1630-1631.
[217] Waldmann, H.; Hu, T. S.; Renner, S.; Menninger, S.; Tannert, R.; Oda, T.; Arndt, H. D., *Angew Chem Int Ed Engl* **2008,** *47*, 6473-7.
[218] Hoffmann, H.; Kogler, H.; Heyse, W.; Matter, H.; Caspers, M.; Schummer, D.; Klemke-Jahn, C.; Bauer, A.; Penarier, G.; Debussche, L.; Bronstrup, M., ibid.**2015,** *54*, 10145-8.
[219] Krastel, P.; Roggo, S.; Schirle, M.; Ross, N. T.; Perruccio, F.; Aspesi, P., Jr.; Aust, T.; Buntin, K.; Estoppey, D.; Liechty, B.; Mapa, F.; Memmert, K.; Miller, H.; Pan, X.; Riedl, R.; Thibaut, C.; Thomas, J.; Wagner, T.; Weber, E.; Xie, X.; Schmitt, E. K.; Hoepfner, D., ibid., 10149-54.
[220] Liao, L.; Zhou, J.; Xu, Z.; Ye, T., ibid.**2016,** *55*, 13263-13266.
[221] Yang, Z.; Xu, X.; Yang, C. H.; Tian, Y.; Chen, X.; Lian, L.; Pan, W.; Su, X.; Zhang, W.; Chen, Y., *Org Lett* **2016,** *18*, 5768-5770.
[222] Pourvali, A.; Cochrane, J. R.; Hutton, C. A., *Chem Commun (Camb)* **2014,** *50*, 15963-6.
[223] Thombare, V. J.; Hutton, C. A., *Angew Chem Int Ed Engl* **2019,** *58*, 4998-5002.
[224] Shabani, S.; Hutton, C. A., *Chem Commun (Camb)* **2021,** *57*, 2081-2084.
[225] Batiste, S. M.; Johnston, J. N., *Proc Natl Acad Sci U S A* **2016,** *113*, 14893-14897.
[226] Monma, S.; Sunazuka, T.; Nagai, K.; Arai, T.; Shiomi, K.; Matsui, R.; Omura, S., *Org Lett* **2006,** *8*, 5601-4.
[227] Stephens, T. C.; Lawer, A.; French, T.; Unsworth, W. P., *Chemistry* **2018,** *24*, 13947-13953.
[228] Nagano, M.; Huang, Y.; Obexer, R.; Suga, H., *J Am Chem Soc* **2021,** *143*, 4741-4750.
[229] Vertesy, L.; Aretz, W.; Knauf, M.; Markus, A.; Vogel, M.; Wink, J., *J Antibiot (Tokyo)* **1999,** *52*, 374-82.
[230] Dettner, F.; Hanchen, A.; Schols, D.; Toti, L.; Nusser, A.; Sussmuth, R. D., *Angew Chem Int Ed Engl* **2009,** *48*, 1856-61.
[231] Nicolaou, K. C.; Estrada, A. A.; Zak, M.; Lee, S. H.; Safina, B. S., *Angewandte Chemie* **2005,** *117*, 1402-1406.
[232] Hanchen, A.; Rausch, S.; Landmann, B.; Toti, L.; Nusser, A.; Sussmuth, R. D., *Chembiochem* **2013,** *14*, 625-32.
[233] Fuse, S.; Mifune, Y.; Nakamura, H.; Tanaka, H., *Nat Commun* **2016,** *7*, 13491.
[234] Cavalleri, B.; Pagani, H.; Volpe, G.; Selva, E.; Parenti, F., *J Antibiot (Tokyo)* **1984,** *37*, 309-17.

[235] Pallanza, R.; Berti, M.; Scotti, R.; Randisi, E.; Arioli, V., ibid., 318-24.
[236] Ciabatti, R.; Kettenring, J. K.; Winters, G.; Tuan, G.; Zerilli, L.; Cavalleri, B., ibid.**1989,** *42*, 254-67.
[237] Kettenring, J. K.; Ciabatti, R.; Winters, G.; Tamborini, G.; Cavalleri, B., ibid., 268-75.
[238] Jiang, W.; Wanner, J.; Lee, R. J.; Bounaud, P. Y.; Boger, D. L., *J Am Chem Soc* **2002,** *124*, 5288-90.
[239] Rew, Y.; Shin, D.; Hwang, I.; Boger, D. L., ibid.**2004,** *126*, 1041-3.
[240] Shen, B.; Makley, D. M.; Johnston, J. N., *Nature* **2010,** *465*, 1027-32.
[241] Bo Shen, Ph.D. Dissertation, 2010
[242] Jessica Shackleford, Ph.D. Dissertation, 2012
[243] Shackleford, J. P.; Shen, B.; Johnston, J. N., *Proc Natl Acad Sci U S A* **2012,** *109*, 44-6.
[244] Kenneth Schweiter, Ph.D. Dissertation, 2016
[245] Jade A. Bing, Ph.D. Dissertation, 2021
[246] Suzanne Batiste, Ph.D. Dissertation, 2018
[247] Marasciulo, F. L.; Montagnani, M.; Potenza, M. A., *Curr Med Chem* **2006,** *13*, 1655-65.
[248] Dhaun, N.; Goddard, J.; Kohan, D. E.; Pollock, D. M.; Schiffrin, E. L.; Webb, D. J., *Hypertension* **2008,** *52*, 452-9.
[249] Ibid.
[250] Ibid.
[251] Schiffrin, E. L., *J Hypertens* **1998,** *16*, 1891-5.
[252]
[253] {, #4}
[254] {, #4}
[255] Al Toma, R. S.; Brieke, C.; Cryle, M. J.; Sussmuth, R. D., *Nat Prod Rep* **2015,** *32*, 1207-35.
[256] Shen, B.; Makley, D. M.; Johnston, J. N., *Nature* **2010,** *465*, 1027-32.
[257] Shackleford, J. P.; Shen, B.; Johnston, J. N., *Proc Natl Acad Sci U S A* **2012,** *109*, 44-6.
[258] Crocker, M. S.; Foy, H.; Tokumaru, K.; Dudding, T.; Pink, M.; Johnston, J. N., *Chem* **2019,** *5*, 1248-1264.
[259] Jade A. Bing, PhD Dissertation Vanderbilt 2020
[260] Jade Bing, Ph.D. Dissertation, 2021
[261] Evans, D. A.; Wood, M. R.; Trotter, B. W.; Richardson, T. I.; Barrow, J. C.; Katz, J. L., *Angewandte Chemie International Edition* **1998,** *37*, 2700-2704.
[262] Evans, D. A.; Carter, P. H.; Dinsmore, C. J.; Barrow, J. C.; Katz, J. L.; Kung, D. W., *Tetrahedron Letters* **1997,** *38*, 4535-4538.
[263] Yedage, S. L.; Bhanage, B. M., *J Org Chem* **2017,** *82*, 5769-5781.
[264] Jade A. Bing Dissertation, Vanderbilt University, 2020
[265] Jade A. Bing PhD Dissertation, 2020
[266] Ye, Y. H.; Li, H.; Jiang, X., *Biopolymers* **2005,** *80*, 172-8.
[267] Dettner, F.; Hanchen, A.; Schols, D.; Toti, L.; Nusser, A.; Sussmuth, R. D., *Angew Chem Int Ed Engl* **2009,** *48*, 1856-61.
[268] Rew, Y.; Shin, D.; Hwang, I.; Boger, D. L., *J Am Chem Soc* **2004,** *126*, 1041-3.
[269] Dettner, F.; Hanchen, A.; Schols, D.; Toti, L.; Nusser, A.; Sussmuth, R. D., *Angew Chem Int Ed Engl* **2009,** *48*, 1856-61.
[270] Nicolaou, K. C.; Estrada, A. A.; Zak, M.; Lee, S. H.; Safina, B. S., *Angewandte Chemie* **2005,** *117*, 1402-1406.
[271] Okuno, Y.; Isomura, S.; Nishibayashi, A.; Hosoi, A.; Fukuyama, K.; Ohba, M.; Takeda, K., *Synthetic Communications* **2014,** *44*, 2854-2860.
[272] Ibid.
[273] Zink, D.; Hensens, O. D.; Lam, Y. K.; Reamer, R.; Liesch, J. M., *J Antibiot (Tokyo)* **1992,** *45*, 1717-22.
[274] Johnson, A. L.; Price, W. A.; Wong, P. C.; Vavala, R. F.; Stump, J. M., *J Med Chem* **1985,** *28*, 1596-602.
[275] Aggarwal, V. K.; Astle, C. J.; Rogers-Evans, M., *Org Lett* **2004,** *6*, 1469-71.
[276] Jackson, R. F. W.; Moore, R. J.; Dexter, C. S.; Elliott, J.; Mowbray, C. E., *The Journal of Organic Chemistry* **1998,** *63*, 7875-7884.
[277] Liang, X.; Lee, C. J.; Chen, X.; Chung, H. S.; Zeng, D.; Raetz, C. R.; Li, Y.; Zhou, P.; Toone, E. J., *Bioorg Med Chem* **2011,** *19*, 852-60.
[278] Ibid.
[279] Ibid.
[280] Ibid.
[281] Duranti, A.; Tontini, A.; Antonietti, F.; Vacondio, F.; Fioni, A.; Silva, C.; Lodola, A.; Rivara, S.; Solorzano, C.; Piomelli, D.; Tarzia, G.; Mor, M., *J Med Chem* **2012,** *55*, 4824-36.
[282] Rigo, B. t.; Lespagnol, C.; Pauly, M., *Journal of Heterocyclic Chemistry* **1988,** *25*, 49-57.
[283] Adiguzel, E.; Yilmaz, F.; Emirik, M.; Ozil, M., *Journal of Molecular Structure* **2017,** *1127*, 403-412.

[284] Lautru, S.; Deeth, R. J.; Bailey, L. M.; Challis, G. L., *Nat Chem Biol* **2005,** *1*, 265-9.
[285] Stephan, H.; Freund, S.; Meyer, J.-M.; Winkelmann, G.; Jung, G., *Liebigs Annalen der Chemie* **1993,** *1993*, 43-48.
[286] Note: We were unable to acquire an authentic sample of coelichelin from the isolation chemists. Challis provided the attached spectra (highlighted in blue) for comparison. We also utilized the experimental data provided in the isolation paper.
[287] Ankenbauer, R. G.; Cox, C. D., *J Bacteriol* **1988,** *170*, 5364-7.
[288] Sebulsky, M. T.; Speziali, C. D.; Shilton, B. H.; Edgell, D. R.; Heinrichs, D. E., *J Biol Chem* **2004,** *279*, 53152-9.
[289] Schwyn, B.; Neilands, J. B., *Analytical Biochemistry* **1987,** *160*, 47-56.
[290] Alexander, D. B.; Zuberer, D. A., *Biology and Fertility of Soils* **1991,** *12*, 39-45.
[291] Dumas, Z.; Ross-Gillespie, A.; Kummerli, R., *Proc Biol Sci* **2013,** *280*, 20131055.
[292] Sun, Z. N.; Liu, F. Q.; Chen, Y.; Tam, P. K.; Yang, D., *Org Lett* **2008,** *10*, 2171-4.
[293] *Chem, Eur. J. Chem.* **2019**, *25*, 287.
[294] Zhu, S. F.; Xu, B.; Wang, G. P.; Zhou, Q. L., *J Am Chem Soc* **2012,** *134*, 436-42.
[295] Liang, X.; Lee, C. J.; Chen, X.; Chung, H. S.; Zeng, D.; Raetz, C. R.; Li, Y.; Zhou, P.; Toone, E. J., *Bioorg Med Chem* **2011,** *19*, 852-60.
[296] Duranti, A.; Tontini, A.; Antonietti, F.; Vacondio, F.; Fioni, A.; Silva, C.; Lodola, A.; Rivara, S.; Solorzano, C.; Piomelli, D.; Tarzia, G.; Mor, M., *J Med Chem* **2012,** *55*, 4824-36.
[297] Jade A. Bing, PhD Dissertation, Vanderbilt University, 2020
[298] Jade A. Bing, PhD Dissertation, Vanderbilt University, 2020
[299] Jade A. Bing, PhD Dissertation, Vanderbilt University, 2020
[300] Jade A. Bing, PhD Dissertation, Vanderbilt University, 2020
[301] Dettner, F.; Hanchen, A.; Schols, D.; Toti, L.; Nusser, A.; Sussmuth, R. D., *Angew Chem Int Ed Engl* **2009,** *48*, 1856-61.
[302] Nicolaou, K. C.; Estrada, A. A.; Zak, M.; Lee, S. H.; Safina, B. S., ibid.**2005,** *44*, 1378-82.
[303] Due challenging solubility profile, not all characterization data was acquired.
[304] Due challenging solubility profile, not all characterization data was acquired.
[305] Due challenging solubility profile, not all characterization data was acquired.
[306] Okuno, Y.; Isomura, S.; Nishibayashi, A.; Hosoi, A.; Fukuyama, K.; Ohba, M.; Takeda, K., *Synthetic Communications* **2014,** *44*, 2854-2860.
[307] Zink, D.; Hensens, O. D.; Lam, Y. K.; Reamer, R.; Liesch, J. M., *J Antibiot (Tokyo)* **1992,** *45*, 1717-22.